

AD 432931

134

Bulletin No. 33

1313

**SHOCK, VIBRATION
and
ASSOCIATED ENVIRONMENTS**

PART II

**TECHNICAL LIBRARY
REFERENCE COPY**

FEBRUARY 1964

**Office of
The Director of Defense
Research and Engineering**



Washington, D.C.



20020815047

AD432931

AD 432931

SHOCK, VIBRATION and ASSOCIATED ENVIRONMENTS

PART II

FEBRUARY 1964

**Office of
The Director of Defense
Research and Engineering**

The 33rd Symposium on Shock, Vibration and Associated Environments was held in Washington, D. C. on 3-5 December 1963. The Navy was host.

Washington, D.C.

DISTRIBUTION

<p>Aberdeen Proving Ground, Md. Att: Ballistic Research Lab. 1 Att: Development & Proof Services 1 Att: Physical Test Lab. 1</p> <p>Advisory Group on Electron Tubes Att: Secretary 1</p> <p>Aeronautical Standards Group, DC 1</p> <p>Aeronautical Systems Division, WPAFB Att: FDFE, C. A. Golueke 1 Att: FDD, H. A. Magrath 1 Att: ASNDSV, R. F. Wilkus 1 Att: ASTEVS, C. W. Gerhardt 1 Att: AFML(MAMD), J. R. Henderson 1</p> <p>Air Defense Command, Ent AFB Att: Deputy for Civil Engineering 1 Att: ADIRP 1</p> <p>Air Proving Ground Center, Elgin AFB Att: PGTRI, Technical Library 1</p> <p>Air Force Flight Test Center, Edwards AFB Att: FTRLG, A. J. Davies 1</p> <p>Air Force Headquarters, DC Att: AFCIN-3K2 1 Att: AFDRD-GW 1 Att: Ops. Analysis Off., Off VCOS, Library 2</p> <p>Air Force Logistics Command, WPAFB Att: MCTEP, G. P. Civile 1</p> <p>Air Force Missile Development Center, Holloman AFB Att: MDSGL-2, Mr. H. Dunbar 3</p> <p>Air Force Missile Test Center, Patrick AFB Att: Chief, Tech. Systems Lab. 2</p> <p>Air Force Office of Scientific Research, DC Att: Library 1</p> <p>Air Force Regional Civil Engineer Att: North Atlantic Region, AFRCE-NA-A 1 Att: South Atlantic Region, AFRCE-SA-E 1</p> <p>Air Force Systems Command, Andrews AFB Att: Technical Library 2</p> <p>Air Force Weapons Lab., Kirtland AFB Att: Development Test Division 1 Att: WLRS, Dr. W. E. Fisher 1 Att: SWOI 631-276 1</p> <p>Army Air Defense Center, Ft. Bliss Att: Technical Library 1</p>	<p>Army Chemical Center, Md. Att: Library 1</p> <p>Army Electronics R&D Lab., Ft. Monmouth Att: SELRA/SL-ADT 1 Att: SELRA/SL-PEE 1 Att: SELRA/SL-PRT 1 Att: SELRA/SL-G 1 Att: SELRA/SL-GTF 1 Att: J. J. Oliveri 1</p> <p>Army Engineer District, NY Att: NANGD 1</p> <p>Army Engineer R&D Labs., Ft. Belvoir Att: Director of Research 1 Att: Package Development Br. 1 Att: Mr. A. Carolla 1 Att: Chief, Spec. Proj. Branch 4</p> <p>Army Engineer Waterways Exp. Sta., Vicksburg Att: Mr. J. M. Strange 1</p> <p>Army Erie Ordnance Depot, Ohio Att: Chief Materiel Testing Div. 1</p> <p>Army Materiel Command, DC Att: AMCRD-RS-CM 1</p> <p>Army Materiel Command, Redstone Arsenal Att: Technical Library 4</p> <p>Army Missile Command, Redstone Arsenal Att: AMSMI-RB 1 Att: AMSMI-RG 1 Att: AMSMI-RL 1 Att: AMSMI-RS 1 Att: AMSMI-RT 1 Att: AMSMI-RTR, J. M. Taylor 1</p> <p>Army Mobility Command, Centerline Att: Otto Renius 1</p> <p>Army, Office Chief of Engineers, DC Att: ENGMC-EM 2</p> <p>Army, Office Quartermaster General, DC Att: Military Planning Division 1</p> <p>Army, Office Chief of Res. & Dev., Arlington Att: A. L. Tarr 1</p> <p>Army, Office Chief Signal Officer, DC Att: R&D Division 1</p> <p>Army, Office Chief of Transportation Att: Dir of Transportation Engrg. 1</p> <p>Army Ordnance Ammunition Command, Joliet Att: ORDLY-T 1 Att: NNSC/A 1</p>
---	--

Army Ordnance Arsenal, Detroit, Mich.		David Taylor Model Basin, Portsmouth	
Att: Tech. Library	2	Att: Code 281A	1
Att: Engrg. Standards Unit	1		
Att: Engrg. Design Div. ORDMX-N	1	David Taylor Model Basin, DC	
Army Security Agency, Md.	1	Att: Library	3
		Att: Harry Rich	1
Army Transportation Engrg. Agency,		Att: Contract Research Administrator,	
Ft. Eustis		513	1
Att: Library	1	Att: J. A. Luistra, Code 591L	1
Att: L. J. Pursifull	1	Dayton Air Force Depot, Gentile AFB	
Arnold Engineering Dev. Ctr., Tenn.		Att: MDMG	1
Att: AEOIM	1	Defense Atomic Support Agency, DC	
Atomic Energy Commission, Oak Ridge	6	Att: Technical Director	1
		Att: Weapons Development Div.	1
Atomic Energy Commission, DC		Att: John G. Lewis	1
Att: Library	1	Defense Atomic Support Agency, Livermore	
Att: Div. of Reactor Development,		Att: Administrative Officer	1
Tech. Evaluation Branch (Army			
Reactors)	1	Defense Documentation Center, Alexandria	20
Aviation Supply Office, Phila.		District Public Works Office, 14th ND	1
Att: TEP-1	1	Electronic Systems Div., L. G. Hanscom	
Ballistic Systems Div., AFSC, Norton AFB		Field	
Att: Technical Data Division	3	Att: Library	1
Boston Naval Shipyard		Electronics Supply Office, Great Lakes	1
Att: Library	1	Federal Aviation Agency, DC	
Bureau of Medicine & Surgery, DC		Att: Emergency Readiness Division	
Att: Research Division	1	Off. of Plans & Requirements	2
Bureau of Naval Weapons, DC		Frankfort Arsenal, Phila.	
Att: DLI-3	2	Att: Library Branch, CC 0270/40	1
Att: FWAA, C. H. Barr	1	Att: David Askin, CC 1730-230	1
Att: PREN-5	5		
Att: RRMA	1	Harry Diamond Laboratories, DC	
Att: RAAE-2	1	Att: B. M. Horton	1
Att: RM-3	2	Att: Chief, Lab. 700	1
Att: RM-2	1	Att: Branch 320, Miss Johnson	1
Att: RSSH	2	Att: Chief, Branch 850	1
Att: FWAE	1	Att: Ben Reznec	1
Att: RREN-8	1	Inspector of Naval Material, San Francisco	1
Bureau of Naval Weapons Rep., E. Hartford	2	Library of Congress, DC	
Bureau of Naval Weapons Rep., Pomona		Att: Exchange & Gift Div	
Att: Chief Engineer	1	(Unclassified Only)	1
Att: Metrology Dept., Code 60	1	Long Beach Naval Shipyard, Calif.	
Bureau of Naval Weapons Rep., Sunnyvale	1	Att: Code 240	1
Bureau of Ships, DC		Los Angeles Air Procurement District,	
Att: Code 423	20	Calif.	
Bureau of Supplies & Accounts, DC		Att: Quality Control Division	1
Att: Library	1	Los Angeles Ordnance District, USA,	
Bureau of Yards & Docks, DC		Calif.	
Att: Code D-440	1	Att: ORDEV	1
Att: Code D-220	1	Mare Island Naval Shipyard, Calif.	
Att: Code D-220 (Unclassified Parts)	6	Att: Library	1
Coast Guard Headquarters, DC	1	Marine Corps Equipment Board, Quantico	2

Marine Corps Headquarters, DC		Naval Ammunition Depot, Crane	
Att: Res & Dev Section	1	Att: Code 3540	1
Att: Code A04E	1	Att: Code 3400	1
Maxwell Air Force Base, Ala.		Naval Ammunition Depot, Earle	
Att: Air University Library	1	Att: Chief Engr., Materials Handling Lab.	1
Mobile Air Materiel Area, Brookley AFB		Naval Ammunition Depot, Oahu	
Att: MONRPPR	1	Att: Weapons Tech. Library	1
Att: MONE	1	Naval Applied Science Laboratory, Brooklyn	
NASA, Ames Research Ctr., Moffett Field		Att: Library	1
Att: S. J. DeFrance, Dir.	1	Naval Attache, Navy 100	
NASA, High Speed Flight Sta., Edwards AFB	1	Att: Logistics Division	1
NASA, Goddard Space Flight Ctr., Greenbelt		Naval Civil Engineering Lab., Pt. Hueneme	
Att: J. C. New, Code 320	1	Att: Library	2
Att: G. Hinshelwood, Code 623.3	1	Naval Construction Battalion Ctr., Pt. Hueneme	
Att: Elias Klein	1	Att: OIC, USN School, Civil Engineer Corps Officers	1
Att: K. M. Carr, Code 321.2	1	Naval Medical Field Research Lab., Camp Lejeune	
Att: F. Lindner, Code 321.2	1	Att: Commanding Officer	1
NASA, Langley Research Ctr., Va.		Naval Mine Engrg. Facility, Yorktown	
Att: Library	2	Att: Library	1
Att: S. A. Clevenson, Dynamic Loads Div.	1	Naval Missile Center, Pt. Mugu	
NASA, Lewis Flight Propulsion Lab., Cleveland		Att: Library, N-03022	1
Att: Library	1	Att: Environment Div., N314	2
NASA, Manned Spacecraft Center, Houston		Naval Operations, Office Chief of, DC	
Att: G. A. Watts	1	Att: Op 31	1
NASA, Marshall Space Flight Center, Huntsville		Att: Op 34	1
Att: Mr. R. M. Hunt, M-P&VE-S	1	Att: Op 75	1
Att: Mr. James Farrow, M-P&VE-ST	1	Att: Op 07T6, T. Soo-Hoo	1
Att: AMSMI-RBLD	1	Att: Op 725	1
NASA, Scientific & Tech. Info. Facility, Bethesda		Naval Ordnance Lab., Corona	
Att: S-AK/DL	1	Att: Quality Eval. Lab	1
National Bureau of Standards, DC		Att: Code 56, Sys. Eval. Div.	1
Att: B. L. Wilson	1	Naval Ordnance Lab., White Oak	
Att: S. Edelman, Mech. Div.	1	Att: Technical Director	1
National Security Agency, DC		Att: Library	3
Att: Engineering	1	Att: Environmental Simulation Div.	6
Naval Air Development Center, Johnsville		Att: G. Stathopoulos	1
Att: E. R. Mullen	1	Naval Ordnance Test Sta., China Lake	
Att: Aeronautical Instruments Lab.	1	Att: Technical Library	1
Att: NADC Library	2	Att: Code 3023	1
Naval Air Engineering Center, Phila.		Att: Code 3073	1
Att: Library	1	Att: Code 4062	1
Naval Air Station, Patuxent River		Naval Ordnance Test Sta., Pasadena	
Att: Weapons Systems Test (E. B. Hamblett)	2	Att: P8087	3
Naval Air Test Center, Patuxent River		Att: P8092	1
Att: Electronics Test Div.	1	Att: P8073	1
Att: VTOL/STOL Br.	1	Att: P80962	1
		Naval Postgraduate School, Monterey	
		Att: Library	1

Naval Propellant Plant, Indian Head		Off. Naval Research, DC	
Att: Library	1	Att: Code 439	6
		Att: Code 104	1
Naval Radiological Def. Lab., San Fran.		Off. Naval Research Branch Office, Boston	1
Att: Library	1		
Naval Research Laboratory, DC		Off. Naval Research Branch Office,	
Att: Code 6250	1	Pasadena	1
Att: Code 6260	1		
Att: Code 6201	1	Off. Naval Research Branch Office,	
Att: Code 4021	2	San Fran.	1
Naval Security Engrg. Facility, DC		Ogden Air Materiel Area, Hill AFB	
Att: R&D Branch	1	Att: Service Engr. Dept., OONEW	1
Naval Supply R&D Facility, Bayonne		Oklahoma City Air Materiel Area	
Att: Library	1	Att: Engineering Division	1
Naval Torpedo Station, Keyport		Pearl Harbor Naval Shipyard	
Att: QEL, Technical Library	1	Att: Code 264	1
Naval Training Device Ctr., NY		Philadelphia Naval Shipyard	
Att: Library Branch	1	Att: Ship Design Section	1
Att: Code 4211	1	Att: Naval Boiler & Turbine Lab.	1
Naval Underwater Ord. Sta., Newport		Picatinny Arsenal, Dover	
Att: Tech. Documents Library	1	Att: Library SMUPA-VA6	1
		Att: SMUPA-VP7, R. G. Leonardi	1
Naval Weapons Evaluation Facility,		Att: SMUPA-T, R. J. Klem	1
Albuquerque		Att: SMUPA-D, E. Newstead	1
Att: Library, Code 42	1	Att: SMUPA-VP3, A. H. Landrock	1
Naval Weapons Laboratory, Dahlgren		Portsmouth Naval Shipyard	
Att: Technical Library	1	Att: Code 246	1
		Att: E. C. Taylor	1
Navy Central Torpedo Office, Newport		Puget Sound Naval Shipyard	
Att: Quality Evaluation Lab.	1	Att: Code 251	1
Navy Electronics Lab., San Diego		Att: Material Labs.	1
Att: Library	1	Att: K. G. Johnson, Code 242	1
Navy Marine Engineering Lab., Annapolis		Quartermaster Food & Container Inst.,	
Att: Code 705	1	Chicago	
		Att: Dir., Container Lab.	1
Navy Mine Defense Lab., Panama City		Att: Technical Library	1
Att: Library	1		
Navy ROTC & Admin. Unit, MIT, Cambridge	1	Quartermaster R&E Airborne Test Activity,	
		Yuma	
		Att: QMATA	1
Navy Underwater Sound Lab., New London		Quartermaster Res. & Engrg. Ctr., Natick	
Att: Technical Director	1	Att: Technical Library	2
Att: J. G. Powell, Engrg & Eval. Div.	1	Att: Dr. W. B. Brierly	1
Navy Underwater Sound Ref. Lab., Orlando		Randolph AFB, Texas	
Att: J. M. Taylor, Code 120	1	Att: USAF School of Aviation Medicine	1
Norfolk Naval Shipyard, Va.		Rome Air Development Center, NY	
Att: Design Superintendent	1	Att: Dana Benson, RASSM	1
Norton AFB, Calif.		Rossford Ordnance Depot, Ohio	
Att: AFIMS-2-A	1	Att: Ordnance Packaging Agency	1
Off. Director of Defense R&E, DC		San Francisco Naval Shipyard	
Att: Technical Library	3	Att: Design Division	1
Att: Mr. Melvin Bell	1		
Att: Mr. Walter M. Carlson	1	Savanna Ordnance Depot, Illinois	
Off. of Naval Material, DC	1	Att: OASMS	1

Sheppard AFB, Texas		Supervisor of Shipbuilding, USN, Camden,	
Att: 3750th Tech. School (TC)	1	NJ	
		Att: Code 299	2
6511 Test Group (Parachute), El Centro			
Att: E. C. Myers, Tech. Dir.	1	Watertown Arsenal, Mass.	
		Att: R. Beeuwkes, Jr., Ord. Matls,	2
6570 Aerospace Med. Res. Labs., WPAFB		Res. Off.	1
Att: MRMAE	1	Att: Technical Information Sec.	1
		Att: ORDBE-LE	1
Special Projects, USN, DC			
Att: SP Tech. Library	1	Watervliet Arsenal, NY	
		Att: ORDBF-RR	2
Springfield Armory, Mass.			
Att: Library	2	White Sands Missile Range, NM	
		Att: Electro-Mechanical Div.	1
Strategic Air Command, Offutt AFB		Att: ORDBS-TS-TIB	3
Att: Operations Analysis Office	1		

CONTENTS

PART II

Distribution.	iii
RELIABILITY AND ENVIRONMENT ENGINEERING Leslie Ball, Boeing Company, Seattle, Washington	1
REFLECTIONS ON SHOCK AND VIBRATION TECHNOLOGY. C. T. Morrow, Aerospace Corporation	8
<u>Prediction of Flight Environment</u>	
AN ENERGY METHOD FOR PREDICTION OF NOISE AND VIBRATION TRANSMISSION R. H. Lyon, Bolt, Beranek and Newman, Inc.	13
A TECHNIQUE FOR PREDICTING LOCALIZED VIBRATION ENVIRONMENTS IN ROCKET VEHICLES AND SPACECRAFT R. E. Jewell, Marshall Space Flight Center, NASA	26
VIBRATION PREDICTION PROCEDURE FOR JET POWERED VEHICLES AND APPLICATION TO THE F-111. N. I. Mitchell and H. E. Nevius, General Dynamics/Fort Worth	34
COMPARISON OF PRE-LAUNCH AND FLIGHT VIBRATION MEASUREMENTS ON THOR VEHICLES S. A. Clevenson, Langley Research Center and W. B. Tereniak, Goddard Space Flight Center, NASA	47
VIBRATION STUDIES ON A SIMPLIFIED 1/2-SCALE MODEL OF THE (X64-10363) NIMBUS SPACECRAFT H. D. Carden and R. W. Herr, NASA Langley Research Center, Langley Station, Hampton, Virginia	57
DYNAMIC ENVIRONMENTS OF THE S-IV AND S-IVB SATURN VEHICLES. R. W. Mustain, Douglas Missiles and Space Systems	72
A PRACTICAL METHOD OF PREDICTING THE ACOUSTICAL DYNAMIC ENVIRONMENT FOR LARGE BOOSTER LAUNCH FACILITIES R. W. Peverley and E. B. Smith, Martin Company, Aerospace Division of Martin-Marietta Corp., Denver, Colorado	89
A COMPARISON OF THE VIBRATION ENVIRONMENT MEASURED ON THE SATURN FLIGHTS WITH THE PREDICTED VALUES G. D. Johnston, Marshall Space Flight Center, and T. Coffin, Chrysler Corp., Huntsville, Alabama	102
A COMPARISON OF THE FLIGHT EVALUATION OF THE VEHICLE BENDING DATA WITH THE THEORETICAL AND DYNAMIC TEST RESULTS FOR THE SATURN I VEHICLE. Everette E. Beam, Marshall Space Flight Center, Huntsville, Alabama	130
CORRELATION BETWEEN MEASURED AND PREDICTED TRANSIENT RESPONSE OF THE TALOS AIRFRAME (IN SHIPBOARD STOWAGE) WHEN SUBJECTED TO A NEARBY UNDERWATER EXPLOSION R. G. Alderson, The Bendix Corporation, Mishawaka, Indiana	150
PANEL SESSION - PREDICTION OF FLIGHT ENVIRONMENT.	161

COMPARISON OF PREDICTED AND MEASURED VIBRATION ENVIRONMENTS FOR SKYBOLT GUIDANCE EQUIPMENT	
J. M. Brust and H. Himmelblau, Nortronics (This paper appears in Part III of the 33rd Bulletin)	

Shock Data Analysis

DIGITAL SHOCK SPECTRUM ANALYSIS BY RECURSIVE FILTERING	173
D. W. Lane, Lockheed Missiles and Space Company, Sunnyvale, California	
AN ANALOG COMPUTER TECHNIQUE FOR OBTAINING SHOCK SPECTRA	182
J. J. Marous and E. H. Schell, Aeronautical Systems Division, Wright-Patterson Air Force Base, Ohio	
THE USE OF GRAPHICAL TECHNIQUES TO ANALYZE SHOCK MOTIONS OF LIGHTLY DAMPED LINEAR SPRING MASS SYSTEMS	195
R. O. Brooks, Sandia Corporation, Albuquerque, New Mexico	
SHOCK SPECTRA FOR A GENERAL FORCING FUNCTION	211
A. F. Todaro, Lawrence Radiation Laboratory, University of California, Livermore, California	
SOLUTION OF STRUCTURAL RESPONSE PROBLEMS BY ANALOG COMPUTERS . . .	216
R. Pittman and R. W. Wheeler, McDonnell Aircraft Corporation	
AN ANALYTICAL SIMULATION OF THE DYNAMIC RESPONSE OF AN IMPACTING ELASTIC SYSTEM	230
R. E. Hess and W. L. Kammer, North American Aviation, Inc., Columbus, Ohio	

Vibration Data Analysis

MODEL BASIN PROCEDURE FOR THE ANALYSIS AND PRESENTATION OF VIBRATION DATA	243
E. Buchmann and R. G. Tuckerman, David Taylor Model Basin, Washington, D. C.	
TECHNIQUES FOR ANALYZING NONSTATIONARY VIBRATION DATA	259
P. T. Schoenemann, Sandia Corporation, Livermore, California	
THE APPLICATION OF A COMPONENT ANALYZER IN DETERMINING MODAL PATTERNS, MODAL FREQUENCIES, AND DAMPING FACTORS OF LIGHTLY DAMPED STRUCTURES	264
F. E. Hutton, General Electric Company, Re-Entry Systems Department	
THE EFFECTS OF FILTER BANDWIDTH IN SPECTRUM ANALYSIS OF RANDOM VIBRATION	273
W. R. Forlifer, Goddard Space Flight Center, Greenbelt, Maryland	
RANDOM-SINE FATIGUE DATA CORRELATION	279
L. W. Root, Collins Radio Company, Cedar Rapids, Iowa	
THE DEVELOPMENT OF DIGITAL TECHNIQUES FOR THE STATISTICAL ANALYSIS OF RANDOM INFORMATION	286
C. L. Pullen, Martin Company	
RANDOMNESS TESTER FOR ACOUSTIC SIGNALS	291
E. D. Griffith, LTV Vought Aeronautics, Dallas, Texas	
RESPONSE OF A SINGLE-DEGREE-OF-FREEDOM SYSTEM TO EXPONENTIAL SWEEP RATES	296
P. E. Hawkes, Lockheed Missiles and Space Company, Sunnyvale, California	
THE INTEGRATED CORRELATION SYSTEM	305
B. K. Leven, Trials and Analysis Branch, U.S. Navy Marine Engineering Laboratory	

PAPERS APPEARING IN PART I

Part I - Confidential
(Titles Unclassified)

Prediction of Vibration Environment

A STATISTICAL APPROACH TO PREDICTION OF THE AIRCRAFT FLIGHT VIBRATION ENVIRONMENT

A. J. Curtis, Hughes Aircraft Company

THE USE OF MERCURY DATA TO PREDICT THE GEMINI VIBRATION ENVIRONMENT AND APPLICATIONS TO THE GEMINI VIBRATION CONTROL PROGRAM

J. A. Callahan, McDonnell Aircraft Corporation

Design Techniques

THE DERIVATION AND USE OF SHOCK AND VIBRATION SPECTRUM CHARTS COVERING A WIDE VARIETY OF ADVERSE ENVIRONMENTS

E. G. Fischer, C. R. Brown, and A. J. Molnar, Westinghouse Electric Corp.

Ship Shock

EXTENSION OF PERFORMANCE OF NAVY LIGHTWEIGHT HI SHOCK MACHINE

W. E. Carr, David Taylor Model Basin, Washington, D.C.

THE SHOCK ENVIRONMENT OF SUBMARINE PRESSURE-HULL PENETRATIONS UNDER EXPLOSION ATTACK

E. W. Palmer, Underwater Explosion Division, David Taylor Model Basin, Portsmouth, Virginia

THE USE OF MODELS TO DETERMINE SHOCK-DESIGN REQUIREMENTS FOR SHIPBOARD EQUIPMENT

R. L. Bort, David Taylor Model Basin, Washington, D. C.

Data Analysis

AN AUTOMATIC SYSTEM FOR SHIPBOARD VIBRATION DATA ACQUISITION AND INTEGRATED ANALOG-DIGITAL ANALYSIS

R. D. Collier, General Dynamics/Electric Boat

PAPERS APPEARING IN PART III

Instrumentation

EFFECT OF MOUNTING-VARIABLES ON ACCELEROMETER PERFORMANCE

B. Mangolds, Radio Corporation of America, Princeton, New Jersey

SURFACE FINISH EFFECTS ON VIBRATION TRANSDUCER RESPONSE

R. W. Miller, U.S. Navy Marine Engineering Laboratory

CALIBRATION OF WATER COOLED HIGH TEMPERATURE ACCELEROMETERS

W. R. Taylor and C. D. Robbins, LTV Military Electronics

A METHOD OF EMBEDDING ACCELEROMETERS IN SOLID PROPELLANT ROCKET MOTORS

R. L. Allen and L. R. Flippin, Thiokol Chemical Corporation, Wasatch Division, Brigham City, Utah

CALIBRATORS FOR ACCEPTANCE AND QUALIFICATION TESTING OF VIBRATION MEASURING INSTRUMENTS

R. R. Bouche and L. C. Ensor, Endevco Corporation

A PEAK SHOCK VELOCITY RECORDER FOR STUDYING TRANSPORTATION HAZARDS

M. Gertel, MITRON Research and Development Corporation

THE USE OF STRAIN GAGES TO DETERMINE TRANSIENT LOADS ON A MULTI-
DEGREE-OF-FREEDOM ELASTIC STRUCTURES

F. R. Mason, Lockheed Missiles and Space Company, Sunnyvale, California

AUTOMATIC ACCELEROMETER CHECK-OUT EQUIPMENT

G. M. Hieber and B. Mangolds, Radio Corporation of America, Princeton, New Jersey

THE CONDENSER MICROPHONE FOR BOUNDARY LAYER NOISE MEASUREMENT

W. T. Fiala and J. J. Van Houten, LTV Research Center, Western Division,
Anaheim, California

A TEST VEHICLE PROTECTION CIRCUIT

E. L. Gardner, Atomics International, Canoga Park, California

Shock Testing

THE DESIGN AND ADVANTAGES OF AN AIR-ACCELERATED IMPACT
MECHANICAL SHOCK MACHINE

L. F. Thorne, The Bendix Corporation, Kansas City, Kansas

SIMULATING FLIGHT ENVIRONMENT SHOCK ON AN ELECTRODYNAMIC SHAKER

G. W. Painter and H. J. Parry, Lockheed-California Company, Burbank, California

DYNAMIC MOORING TESTS OF ONE-QUARTER SCALE MODELS OF THE GEMINI
AND AGENA SPACECRAFT

N. E. Stamm and L. A. Priem, McDonnell Aircraft Corporation

Vibration Testing

PROBLEMS AND CONSIDERATIONS IN COMBINING SINE AND RANDOM VIBRATION IN
THE ENVIRONMENTAL TEST LABORATORY

A. R. Pelletier, Radio Corporation of America

FLEXURE STABILIZATION OF A REACTION VIBRATION MACHINE

R. H. Chalmers, Jr., U.S. Navy Electronics Laboratory, San Diego, California

AN ALTERNATE METHOD OF EXCITER SYSTEM EQUALIZATION

D. Scholz, McDonnell Aircraft Corporation

CORRELATION OF DAMAGE POTENTIAL OF DWELL AND CYCLING SINUSOIDAL
VIBRATION

E. Soboleski and J. N. Tait, U.S. Naval Air Development Center, Johnsville, Pa.

SIMULATION OF REVERBERANT ACOUSTIC TESTING BY A VIBRATION SHAKER

D. U. Noiseux, Bolt, Beranek, and Newman Inc., Cambridge, Mass.

Combined Temperature-Vibration Tests

COMBINED HIGH TEMPERATURE-VIBRATION TEST TECHNIQUES

H. S. Bieniecki and E. Kuhl, McDonnell Aircraft Corporation

COMBINING INDUCTION HEATERS WITH EXISTING ENVIRONMENTAL FACILITIES TO
CONDUCT TESTS AT RE-ENTRY TEMPERATURES

C. D. Robbins and E. L. Mulcahy, Ling-Temco-Vought, Inc.

THE NEL EXPERIMENTAL VIBRATION TEST STAND FOR USE IN CHAMBERS

A. A. Arnold, U.S. Navy Electronics Laboratory

A TECHNIQUE FOR PERFORMING VIBRATION TESTS AT HIGH TEMPERATURES IN
EXCESS OF 3500°F

C. F. Hanes and R. W. Fodge, Temco Electronics and Missiles Company

Vibration Test Specification

A PROCEDURE FOR TRANSLATING MEASURED VIBRATION ENVIRONMENT INTO LABORATORY TESTS

K. W. Smith, White Sands Missile Range

MEASUREMENT OF EQUIPMENT VIBRATIONS IN THE FIELD AS A HELP FOR DETERMINING VIBRATION SPECIFICATIONS

I. Vigness, U.S. Naval Research Laboratory

DETERMINATION OF AN OPTIMUM VIBRATION ACCEPTANCE TEST

G. J. Hasslacher, III and H. L. Murray, General Electric Company, Utica, New York

VIBRATION TESTS, AN ESTIMATE OF RELIABILITY

J. L. Rogers, Martin Company, Denver, Colorado

Standardization of Vibration Tests

SINUSOIDAL VIBRATION TESTING OF NONLINEAR SPACECRAFT STRUCTURES

W. F. Bangs, Goddard Space Flight Center, NASA, Greenbelt, Maryland

SOME PROBLEM AREAS IN THE INTERPRETATION OF VIBRATION QUALIFICATION TESTS

J. E. Wignot and M. D. Lamoree, Lockheed-California Company

TAMING THE GENERAL-PURPOSE VIBRATION TEST

J. P. Salter, War Office, Royal Armaments Research and Development Establishment,
Fort Halstead, England

PANEL SESSION - STANDARDIZATION OF VIBRATION TESTS

COMPARISON OF PREDICTED AND MEASURED VIBRATION ENVIRONMENTS FOR SKYBOLT GUIDANCE EQUIPMENT

J. M. Brust and H. Himelblau, Nortronics, A Division of Northrop Corporation,
Hawthorne, California

PAPERS APPEARING IN PART IV

Mechanical Impedance

THE APPLICATION OF IMPEDANCE TECHNIQUES TO A SHIPBOARD VIBRATION ABSORBER

R. M. Mains, General Electric Company, Schenectady, New York

VIBRATION ANALYSIS OF AN IDEAL MOTOR USING MECHANICAL IMPEDANCE TECHNIQUES

J. I. Schwartz, U.S. Navy Marine Engineering Laboratory

LOW-FREQUENCY HULL MOBILITY

D. C. Robinson and J. T. Cummings, David Taylor Model Basin, Washington, D.C.

A THEORETICAL BASIS FOR MECHANICAL IMPEDANCE SIMULATION IN SHOCK AND VIBRATION TESTING

F. J. On, Goddard Space Flight Center, Greenbelt, Maryland

MECHANICAL IMPEDANCE MEASUREMENTS IN FOUNDATION STUDIES

R. A. Darby, U.S. Navy Marine Engineering Laboratory

Pyrotechnic Shock

MECHANICAL SHOCK FROM FRANGIBLE JOINTS

V. R. Paul, Lockheed Missiles and Space Company

SHOCK ENVIRONMENTS GENERATED BY PYROTECHNIC DEVICES

H. J. Roberge and J. Rybacki, General Electric Company

Transportation Environment

TRACK-VEHICLE MISSILE SYSTEM DYNAMIC ENVIRONMENT DATA ACQUISITION AND APPLICATION

R. Eustace, Martin Company, Orlando, Florida

A SURVEY OF VIBRATION ENVIRONMENT IN VEHICLES TRAVELING OVER PAVED ROADS

J. E. Rice, Goodyear Aerospace Corp.

SHOCK AND VIBRATION DATA OBTAINED FROM TRUCK AND RAIL SHIPMENT

J. W. Lahood, Raytheon Company, Bedford, Mass.

THE DYNAMIC ENVIRONMENT OF THE S-IV STAGE DURING TRANSPORTATION

R. W. Trudell and K. E. Elliott, Saturn-Acoustics and Structural Dynamics Missiles and Space Systems Division, Douglas Aircraft Company, Inc.

Design Techniques

DAMPING CHARACTERISTICS OF ISOLATORS WHEN USED IN OTHER THAN CG MOUNTED CONFIGURATIONS

F. H. Collopy and R. H. Coco, AVCO Corporation, Wilmington, Mass.

THE EFFECTS OF A SPRING CLEARANCE NONLINEARITY ON THE RESPONSE OF A SIMPLE SYSTEM

J. P. Young, Goddard Space Flight Center, Greenbelt, Maryland

DETERMINATION OF THE RATE DEPENDENCE OF THE YIELD STRESS FROM IMPULSE TESTING OF BEAMS

S. R. Bodner, Brown University, Providence, R. I., and J. S. Humphreys, Avco, RAD Division, Wilmington, Mass.

REDUCTION OF VIBRATION FROM ROTOR UNBALANCE BY USE OF A FORCE-CANCELING SYSTEM (AN ACTIVE VIBRATION ABSORBER)

C. S. Duckwald and T. P. Goodman, Advanced Technology Laboratories, General Electric Company, Schenectady, New York

DYNAMIC MATHEMATICAL MODEL FOR EVALUATING AIRBORNE EXTERIOR LAMPS

David Ehrenpreis, Consulting Engineers Inc., New York, N. Y., and John DeJong, Naval Air Station, Patuxent River, Maryland

SOLID PROPELLANT DYNAMIC PROPERTIES AND THEIR EFFECT ON VIBRATION RESPONSE OF MODEL SOLID PROPELLANT STRUCTURES

G. J. Kostyrko, Aerojet-General Corporation

DESIGN CONSIDERATIONS OF LARGE SPACE VEHICLES DUE TO AXIAL OSCILLATIONS CAUSED BY ENGINE-STRUCTURAL COUPLING

D. McDonald, N. C. State College, Raleigh, North Carolina, and T. R. Calvert, Lockheed Missiles and Space Company, Sunnyvale, California

VIBRATION ENERGY LOSSES AT JOINTS IN METAL STRUCTURES

Eric E. Ungar, Bolt, Beranek and Newman Inc., Cambridge, Mass.

Application of Data to Design

DESIGN OF SPACE VEHICLE STRUCTURES FOR VIBRATION AND ACOUSTIC ENVIRONMENTS

C. E. Lifer, Marshall Space Flight Center, NASA

SUMMARY OF DESIGN MARGIN EVALUATIONS CONDUCTED AT THE U. S. NAVAL MISSILE CENTER

C. V. Ryden, U.S. Naval Missile Center, Point Mugu, California

PANEL SESSION - THE USE OF ENVIRONMENTAL DATA IN DESIGN

RELIABILITY AND ENVIRONMENTAL ENGINEERING*

Leslie W. Ball
Boeing Company
Seattle, Washington

In recent years increased complexity of military equipment has been accompanied by decreased reliability and maintainability. Environmental engineering potentially can contribute a great deal to reducing the total cost of owning and operating complex equipment. This paper outlines the technical and management steps that must be taken to exploit the potential contributions of environmental engineering to reliability and overall cost effectiveness.

INTRODUCTION

Seventeen years ago, I became responsible for the shock, vibration, and other environmental technologies at the Naval Ordnance Laboratory. At that time, our group asked these questions: "Why has the Navy spent millions of dollars in providing an outstanding environmental facility to support ordnance development," and "What are the obligations of those who earn their living as environmental engineers?" One somewhat facetious answer, was that our mission was to eliminate the need for our sister division, the Field Test Engineers. For example, in the case of Naval Mine Warfare, much of the existing reliability had been achieved by actually taking mines on trucks, trains, and ships, dropping them from aircraft, and recovering them by use of divers. It was our ambition to make such field tests unnecessary. We aimed to do so by discovering in the environmental laboratory, every scrap of information that could be obtained by the more time consuming and expensive field tests.

More generally, the objective of any environmental laboratory, in the research and development phase, is to discover every mode of failure inherent in the design, and to which environmental stress is a contributing factor. The objective in the production phase is to prevent use of any equipment that contains a strength discrepancy that could be converted into a failure by environmental stress.

Now what is the situation in environmental testing, as we contemplate the year 1964? The principles of discovery of inherent modes of failure and of elimination of strength discrepancies in production equipment are still vital. The cost of omitting laboratory tests and relying on discovery of design errors by field tests, however, has increased enormously. The cost of not discovering production discrepancies and thereby allowing failure during a mission has increased even more. For example, it is estimated that a single test launch of a Saturn Booster will cost \$50 million. The cost of a single failure during an Apollo moon-landing mission is awesome. Even if the life of the astronaut is saved, the cost of the flight equipment, ground and sea support operations, and the cost in national prestige make almost any amount of environmental testing cost fade into insignificance.

Have these changes in cost automatically brought full exploitation of every environmental and other technique that can discover and eliminate unreliability? The answer is no. The actual situation was illustrated by a lead article in a recent national magazine. It told how the recent solar eclipse provided a rare opportunity to obtain scientific data, but the rocket employed to obtain this data exploded. The article stated that it was known that radiography could have discovered and eliminated the cause of failure, but typically, a minute gain in schedule was preferred over a major gain in reliability assurance.

*Invited paper

RELIABILITY MANAGEMENT SYSTEM

In order to ensure proper application of the technical excellence developed by environmental engineers, it has become necessary to develop what we now call a "Reliability Management System." The general objective of this system is to achieve cost effectiveness by spending a little more money on development disciplines and thereby saving a great deal on weapon systems support or space objective attainment.

Although this system does have to be supported by top management of NASA, the Department of Defense, and the contractors, it cannot operate successfully without the understanding and support of environmental engineers. Consequently, our purpose today is to describe this system, to the extent that it is related to the interests of environmental engineers.

THE SCIENTIFIC METHOD

The Reliability Management System has been developed by applying the four steps of the scientific method to development and application of reliability technology. Reliability technology is concerned with prediction, control, and measurement of equipment failure rate. Ability to predict is essential to making decisions on the feasibility of a new system and for comparing the potential effectiveness of alternative systems. For example, one factor in the choice between land-based and sea-based missiles is a comparison between the predicted failure rates of the alternate systems. Also, in the case of space flight, one factor in decisions, such as the choice of an earth or lunar orbit, is a comparison between predicted failure rates.

The need to control failure rates by such disciplines as parts selection, design review, qualification test, and production environmental test is self-evident. It is through decisions on the amount of control that will be exercised on a particular project, that management can assure cost effectiveness. The need for measurement of failure rates likewise is self-evident. Measurement is required to check that the disciplines used were effective, and it is a factor in checking that a contractor has fulfilled his obligations.

In the general case, the steps of the scientific method are: Observe, Analyze, Hypothesize, and Test the Hypothesis. In the Reliability Management System, the corresponding steps are Data Acquisition, Discipline Analysis, Resources Development, and Resources Application. Each of these four steps will be discussed in relation to environmental engineering.

DATA ACQUISITION

In a science such as physics, the first step in the scientific method consists of Data Acquisition on natural phenomena or laboratory experiments. In a similar way, the first step in the Reliability Management System consists of acquiring data on problems in laboratory, factory, or field operations. This step includes reporting on failure modes, probabilities, and effects. By the term failure mode, we mean a description of symptoms and physical observations, including those obtained by dissection and microscopic observation.

Because failures occur only when some type of stress on a part exceeds the corresponding strength, it is important to include stress and strength information in the data acquisition system. This is particularly true in regard to observations made in an environmental laboratory during development testing.

For example, if during a vibration test of an electronic chassis a wire connection snaps, it is extremely important to report if, and the degree to which, the wire had been nicked during manufacturing. Nicked wires are a good example of what is meant by the term manufacturing strength discrepancy.

In regard to failure probability, the test engineer should examine every item tested and report a value for the frequency with which strength discrepancies such as nicked wires are occurring. Also, he should report on how practical it would be to use some method of production environmental testing to increase reliability. For example, a simple use of environmental testing to increase reliability was reported many years ago in connection with the Rascal Missile Program. It was known that cut O-rings were a major cause of unreliability in hydraulic actuators. The environmental laboratory established that about 50 cycles of operation at -40 degrees centigrade would discover most cut O-rings and thereby prevent their causing loss of a missile.

Because environmental laboratories are an important source of reliability data, it is appropriate to ask at this symposium how well have we been doing in acquiring such data. In regard to acquiring knowledge of modes of failure and organizing them for use by design, manufacturing, and inspection engineers, the situation is quite unsatisfactory.

In regard to failure probabilities, the situation is much better. Figures 1 and 2 illustrate the type of data that has been obtained and which

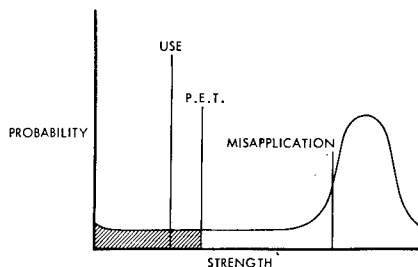


Fig. 1 - Environmental stress levels

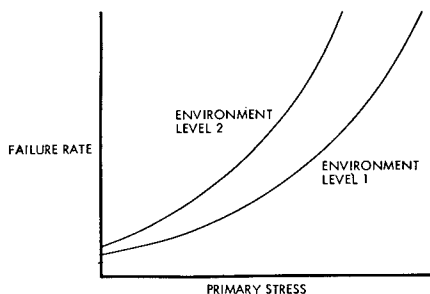


Fig. 2 - Failure rates of capacitors

is familiar to most of you. The type of data shown in Fig. 1 is typical of most electronic and many electromechanical equipments. The type of data illustrated in Fig. 2 is typical of the failure rates of capacitors. In this case, failure rates have been tabulated as a function of the ratio of circuit voltage to manufacturer's rated voltage and of ambient temperature.

The end product of this segment of the reliability management system consists of failure mode, probability, and effects data manuals. Every environmental test engineer has a responsibility to contribute to these manuals. To do so is in his own interest, because it informs program managers of the capability of environmental methods. It is in the national interest because such knowledge is essential to building reliability into new weapon and space systems. Unfortunately, many environmental laboratories are owned by or are subservient to the vendors of components who consider that failure information is proprietary. This is a clear case of a clash between the interest of the nation and the supposed interest of an individual vendor. It is my belief that programs should be so managed that the interest of the nation will prevail.

DISCIPLINE ANALYSIS

As with the general scientific method, the second step in the reliability management system is analysis. Because management cannot prevent failures from recurring by changing the laws of physics, they must do so by changing the actions of people. Consequently, failures are analyzed in terms of the actions of people and of the ability of management to modify these actions. This type of analysis is described by the term Reliability Discipline Analysis. Of the four steps in the management system, this is the most difficult to understand. This difficulty exists partly because engineers are accustomed to dealing with failures merely by taking corrective action. In teaching discipline analysis, we have found it helpful to state that there are three types of action required on each significant failure, namely, quick fix, corrective action, and experience retention.

A quick fix, such as replacing a failed part with an identical one, merely restores to operating condition the equipment in which the failure occurred. A corrective action, such as a design, manufacturing, or inspection change, prevents recurrence of the same type of failure in subsequent equipments produced from the same drawings and specifications. An experience retention action carries forward the lessons learned in such a manner that they will be applied to all future work done by any organization that receives the experience retention report. For example, if a long lead fails during a production vibration test and it is replaced by an identical lead, the action is a quick fix. If the drawings for that particular chassis are revised to provide for additional tying-down of the lead, that is a corrective action. If feedback is made into the training and motivation of the electronic packaging engineers, and into the electronic assembly process specifications, that is experience retention. Figure 3 illustrates the extreme importance of the experience retention principle to NASA's space programs. The lower curve illustrates a traditional situation in which a moderately reliable prototype can be built and then, through testing and corrective action, the required operational reliability can be achieved. The upper curve illustrates that, in the space program, disciplines based on experience retention must be used from the very beginning of the project in order to achieve high reliability in the prototype. This is obviously necessary in a program such as the Saturn Booster where the very first launch must have a very high probability of success.

Experience retention is achieved through Reliability Discipline Analysis, which involves

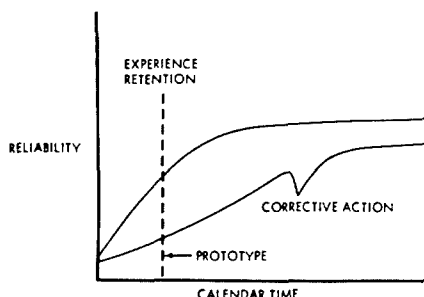


Fig. 3 - Corrective Action
vs Experience Retention

Activity Identification, Functional Responsibility, and Discipline Requirement. Incidentally, the word discipline is never used in science and technology to imply punishment; it is derived from the latin word disciplina which means the teaching of disciples. A modern definition is: "the training of scholars and subordinates to proper conduct and action by inducting and exercising them in the same mental and moral training." To establish engineering discipline, for the purpose of failure experience retention, the first step is to identify an activity that can and must be brought under formal control. Electronic packaging and test planning are examples of what is meant by the term activity.

The second step is to identify the executive who has the responsibility and the right to control the particular activity. In the Boeing Aero-Space Division, we have about 12 division functional executives with titles such as, Director of Engineering, Director of Contracts, and Director of Quality Control.

The third step in the discipline analysis process is for the test engineer or reliability specialists to convert the lesson learned from failure analysis into an addition to what we call a Discipline Requirement Checklist. The following two paragraphs are illustrative of checklist items:

"For high reliability electronic equipments that will be subject to transportation stresses, all wires and wire harnesses must be tied down at intervals not greater than 3 inches.

"All hydraulic actuators to be used on high reliability equipments must be subjected to 50 cycles of operation at -40 degrees centigrade prior to installation."

To facilitate operation of the complete system each checklist item must be assigned to a

particular functional executive and must be correlated with a particular activity. In the Boeing A-SD we provide our discipline analysts with an activity identification system that closes the gap from broad management concepts, such as design assurance, down to working level activities, such as integrated test planning.

RESOURCES DEVELOPMENT

The term resources is apt to bring to mind the factors of money, men, materials, and machines. For the reliability purposes, we recognize the five Reliability Resources—Reliability Technology, Directive Documents, Qualified Personnel, Variance Control Facilities, and Rated Suppliers. Technology includes know-how in the form of published papers and training and motivation curricula. Directive Documents include commands to apply the technology expressed in the form of policies, procedures, process specifications, or any other type of command media. Qualified Personnel include reliability specialists but it also includes design, manufacturing, inspection and all other functional skills that have been developed to create or assure reliable equipment. Variance Control Facilities include the strength variance control features of manufacturing equipment as well as inspection and test equipments that contribute to reliability assurance. Rated Suppliers include the resources that are available to increase the company's own resources through purchasing and sub-contracting.

Directive documents, or more familiarly procedures, are the key link between past experience and future applications. For example, by qualified people we mean people who have been trained to understand and motivated to apply the procedures. It is a curious thing that the engineer in college seeks technical excellence in the textbooks that he buys. He expects these textbooks to be written by the best technical experts of his generation, yet this same engineer, when he works on an aerospace program, is liable to regard all written materials as trash, just paperwork.

If it were possible to design, manufacture, inspect, and test weapon systems and space vehicles using only highly experienced personnel working with materials with which they had long familiarity, then in the real world in which we live, concise intelligent documentation would be vital to reliability. This is true whether we are dealing with advanced systems engineering or with a mundane manufacturing control. People who think that because a cause of failure is well known that there is no need to write it down

are constantly being proved wrong by test laboratory and operating experiences. These experiences show that without adequate documentation the same errors and discrepancies are repeated again, and again, and again. Many of them have been repeated for more than 30 years.

The feedback of a failure experience into the types of Reliability Resources can be illustrated by the case of a vibration failure of a nicked wire. In regard to technology, feedback is made into training and motivation curricula for manufacturing personnel. In regard to directive documents, feedback is made into an electronic assembly process specification. In regard to qualified personnel, manufacturing supervision must assure that wire stripping is done only by workers who have been trained and certified. In regard to facilities, manufacturing controls must eliminate use of mechanical strippers and specify an alternative such as thermal strippers. Also, the manufacturing plan must provide for production and vibration equipment to increase the probability of discovery of nicked wires. In regard to rated suppliers, purchasing of electronic assemblies must be limited to those suppliers who have the disciplines enumerated for the above four types of resources.

The Reliability Discipline Requirements Checklists provided by the Discipline Analysis part of the system are used by functional executives to develop all these resources. The end product of the Resources Development segment of the Reliability Management System is a catalogue of resources that are available for project application. This is illustrated in Fig. 4.

RESOURCES APPLICATION

During the past few years, most aerospace companies have reorganized to provide product line organizations. Each such organization is responsible for a single product such as a Saturn Booster or for a single product line such as boosters in general. It is the responsibility of the branch or product line managers to apply the resources developed by the functional executives.

The major connecting link between functional executives and branch managers is a project program plan. In the case of reliability, both NASA and the Defense agencies require comprehensive program plans. Each Boeing Aero-Space Division Reliability Program Plan

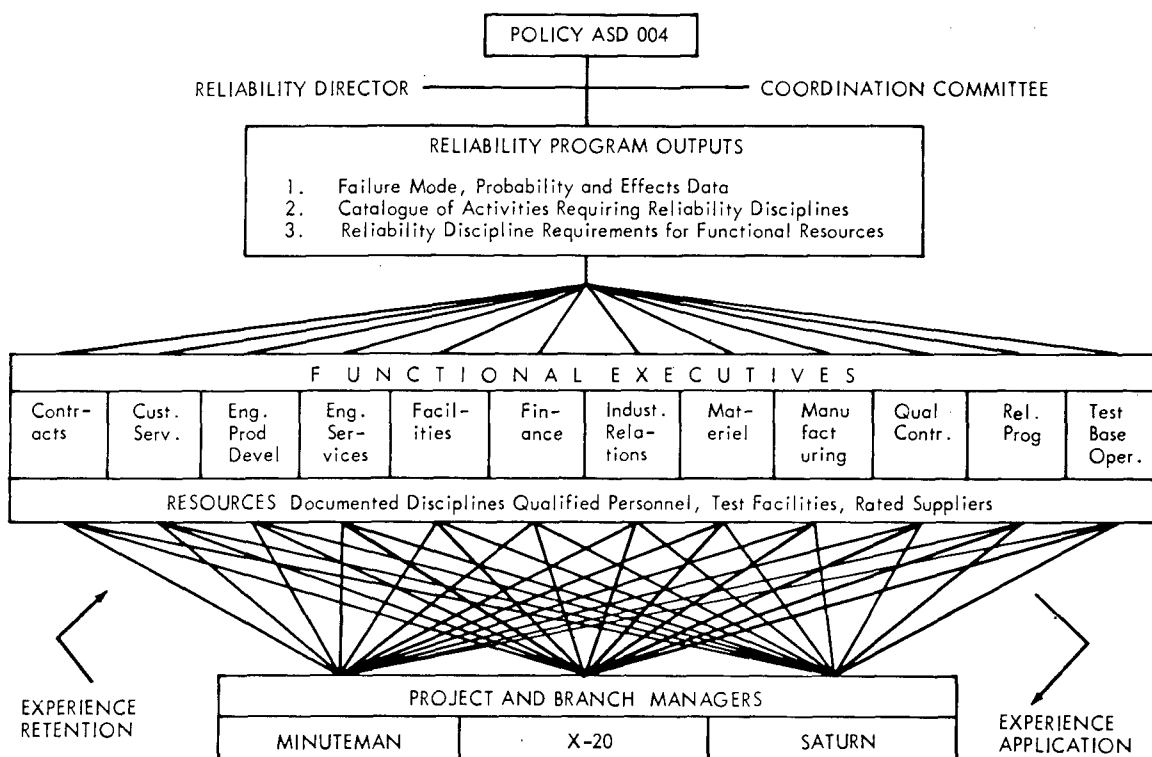


Fig. 4 - Aero-space Division reliability relationships

is prepared in two parts. The first part is a narrative that is highly responsive to customer requirements in that it shows that the division has available and will apply resources covering every aspect of the customers specifications and work statements. The second part is a tabulation which sets forth the disciplines that will be applied to a particular item of equipment or to a particular process. In addition, it shows the responsibility, the funding, and the results that will become considered as evidence of satisfactory task completion. Identification of program tasks is based on the same list of activities that was used for failure experience retention.

For an environmental engineer to ensure that his procedures and other resources will be properly used, these resources must be correlated with activities, such as, failure modes and

affect analysis, integrated test planning, design review, qualification testing, and production environmental testing. When such correlation is available, it is easier for project managers to decide how much time and money will be spent on using environmental techniques for particular items. These decisions have to be based on cost optimization so the environmental engineer should help to provide the necessary cost data. To perform a cost optimization study, an analyst must be able to estimate the cost of applying each discipline, its effect on reducing failure rates, and the reduction in operating cost that would come from a reduction in failure rates. In the case of the Minuteman Program, such studies have been and are being made in regard to the cost effectiveness of environmental screening of electronic parts.

Figure 5 illustrates that the four segments of the reliability management system provide

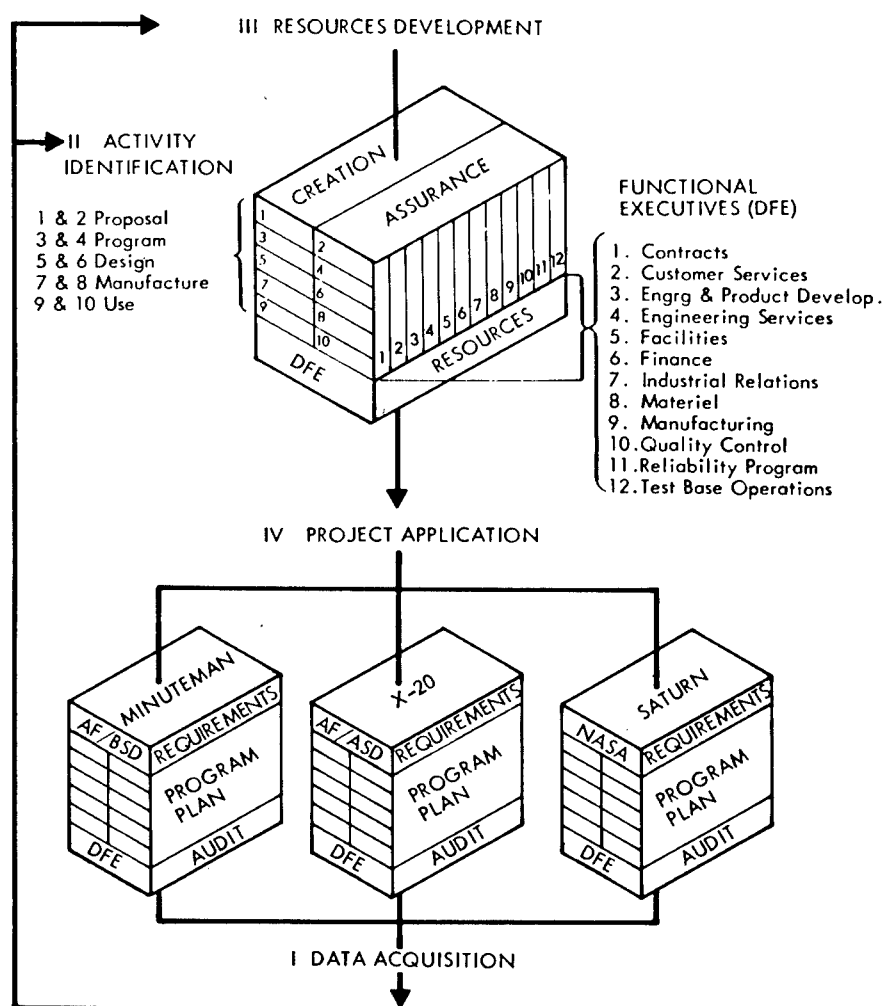


Fig. 5 - Experience retention and application system

a closed-loop for continuous improvement of weapon system and space system operations. Somewhat bitter experience has shown that it is not enough to develop good data, good discipline requirements, and good resources and to specify in reliability program plans that they will be applied. Project people are always under pressure to decide in favor of schedule when schedule and reliability requirements conflict. It follows, that the Reliability Management System must provide for closing of the loop through a system of audit.

The word audit may suggest a sterile, police-type action; this is not so. Audit in the form of Resources Evaluation is a research process which involves the following four types of questions:

The first type of question is to check with the project reliability program manager as to whether the resources that were available to him for callout in his program plan were adequate. For example, if he wanted to do a good job of integrated test planning, did he find procedures, personnel, and equipment adequate for his purposes? If he wanted to specify production environmental testing, did he find procedures ready and available to him?

The second type of question, is whether the line organization for the particular project converted customer specifications or company procedures into direct orders to their subordinates. Again, somewhat bitter experience has

shown that subordinates do what their immediate bosses tell them and it is not enough to bury requirements in relatively remote specifications, policies, or procedures.

The third type of question, is whether when adequate procedures were available and the line bosses ordered them followed, the level of compliance by product personnel was adequate.

The fourth type is whether when the best available procedures were considered to be adequate, their use was commanded by the line organization, and their requirements were complied with, the results were as predicted. Obviously when the results are disappointing, the research cycle starts all over again and goes through the four stages of the Reliability Management System. These stages are Data Acquisition, Discipline Analysis, Resources Development, and Resources Application.

SUMMARY

In summary, during the past decade, shock, vibration, and general environmental engineers have done a magnificent job of developing technology and facilities. The potential payoff to NASA and the Department of Defense from application of these resources is enormous. Realization of this potential depends upon a Reliability Management System. This paper has presented an account of such a system.

* * *

REFLECTIONS ON SHOCK AND VIBRATION TECHNOLOGY*

Charles T. Morrow
The Aerospace Corporation
Los Angeles, California

I am glad to talk to all of you on the subject of shock and vibration technology. This field has undergone many changes in the last decade. I have had the opportunity to assist in bringing some of them about and the opportunity to reflect at length on many of the developments. These symposiums have been invaluable in presenting and recording the thoughts of shock and vibration engineers over the course of time. I have attended nearly every one since I first concerned myself with shock and vibration problems, and have found them indispensable for understanding the engineering problems connected with shock and vibration.

CONCEPTS RECENTLY INTRODUCED

Perhaps I should start by reviewing some of the scientific concepts recently introduced or brought to more frequent application.

Power Spectral Density

The first of these is power spectral density, in terms of which, the results of data reduction and the excitations in a test specification are now frequently written. This is the most important single concept in the application of random noise theory to shock and vibration. The introduction of this concept was inevitable. Had it not come as it did, it would have come later or would be coming in another way. Eventually it became apparent that the bulk of the vibration in missiles and spacecraft, except for that associated with combustion instability, is induced by aerodynamic turbulence or by acoustic noise generated by it. Power spectral density is a powerful tool for the investigation of such turbulence and the associated sound field. It has been used for this purpose for many years. It could not continue in this way indefinitely without spilling over into shock and vibration engineering. As it happened, the power spectral density concept was introduced to shock and vibration engineers before they became generally aware of

acoustic noise as an environment. We are now further along in our thinking because of this early introduction and in a better position to appreciate what shock and vibration engineering is really about.

We can agree, I believe, on the sources of random vibration. Furthermore, the controversy over what is random and what is periodic appears to have settled down more or less in accordance with the intuitive ideas of those of us who were initially somewhat familiar with random noise theory. In the meantime, we ourselves have learned that the distinction that must be used in shock and vibration engineering is more subtle than we at first suspected. Of course, any finite sample of random vibration that has already occurred and been measured, can, theoretically, according to Fourier's theorem, be approximated by a collection of sinusoids. The limiting result is an exact description of the sample except for an artificial repetition, but not necessarily an accurate description of the next sample taken. The individual sinusoids are extremely variable with the timing and duration of the sample and provide an abundance of detail that does not correlate well with damage potential and does not serve the objectives of data reduction. Moreover, especially for wide-band vibration such a collection is extremely complicated and not particularly useful or informative. The power spectral density plot derived conceptually from the sinusoids by moderate smoothing in frequency and by normalization, is less dependent on the sample and is both a simpler and more useful description. It is a distillation of the predicatable from the unpredictable. Thus, the distinction in practice, as opposed to rigorous definitions for infinite ensembles of vibrations or for vibrations of infinite duration, becomes largely a matter of simplicity and utility.

But the real problem with random noise theory is not one of understanding concepts. Rather, it is a matter of our basic objectives in

*Invited Paper.

testing and how they are affected or brought open to question by the availability of the random vibration test. This test should certainly not be used indiscriminately. I recommend it primarily for completed airborne missile and space-vehicle equipment. Here we have more chance than usual to measure equipment excitations, but little opportunity to recover equipment after flight and analyze shock and vibration effects. We are more completely dependent on the laboratory. I do not necessarily recommend random vibration as a general-purpose test. I do not recommend it for smaller components, sub-assemblies and parts except when there is reason to expect some special interaction of the effects of vibration in different frequency bands, as might perhaps occur in relays, or when the phenomena to be studied may have a distinctly different character under random excitation, as with the drift of a gyroscope. It may appear that this involves a serious compromise of realism in testing. One answer to this is that whenever we consider general purpose specifications or the testing of subassemblies whose excitation is seldom measured, we must expect serious compromises of realism regardless of the potential refinement of the test method selected. We are constrained to treat an extremely complicated situation in a very simple way and with little or no specific excitation data. Compromise is inherent. Yet, in spite of uncertainties and compromises, testing at various levels of assembly is commonly a useful and essential procedure.

Shock Spectrum

A second concept of recently increased importance and application is the shock spectrum which has permitted a more refined comparison of shock severities. This has produced no more controversy in connection with testing than would be expected simply because of the introduction of a new term. A related concept, the Fourier Spectrum is more abstract, but in some respects simpler; it may in time supersede the shock spectrum for purposes of data reduction. It is, of course, more fundamental for the calculation of responses of a complex system, but, potentially more important, it is less confusing when the mechanical impedance of the airframe is less than that of the equipment (i.e., force rather than motion is a better measure of excitation). Under this circumstance the simple model for the one-degree-of-freedom vibrator is not so pertinent. However, the transition should not be so difficult as it may appear.

Residual Shock Spectrum

The residual shock spectrum differs from the magnitude of the Fourier spectrum only by

a factor of 2π times the frequency. The shock spectrum, being a measure of the response of a simple resonator to the Fourier spectrum, will continue to be helpful for auxiliary reference purposes by giving increased physical significance to the more abstract concept.

Mechanical Impedance

Finally, mechanical impedance, which permits the prediction of linear loading effects on the basis of measurements made entirely at the interface, has been explored to some degree in the last several years. This is a tremendously valuable concept both for calculation and for facilitating a qualitative understanding of vibrating systems. Our technology focusses at present, however, on the simulative test. I have seen numerous scholarly articles interpreting mechanical impedance for the shock and vibration engineer—many of them implying that as soon as we all get to understand this concept we will immediately begin to simulate it, in addition to motional excitation, with our shakers. So far, little has been attempted in this direction. Again, the real problem is not one of understanding the concept, but of determining what it means in terms of test apparatus, what refined techniques are actually feasible, and what generally they are likely to accomplish in improved rate of reliability improvement. In several respects, this appears to be more difficult than the question for random vibration tests. I neither recommend nor expect any elaborate attempts at precise simulation of impedance in the immediate future. But we should arrange to recognize those instances where the source (airframe) impedance is lower than the impedance of the equipment excited, rather than higher as commonly assumed. If these are common, we should develop techniques of low-rather than high-impedance testing. These limited objectives will not require precise measurement of airframe impedances nor elaborate setup procedures for simulative test.

These four are probably the most important new concepts to be discussed in the Symposia on Shock, Vibration and Associated Environments over the last decade. They have sharpened and refined shock and vibration theory. We have not finished learning to use them so as to obtain maximum rate of reliability improvement and minimum complication of test effort.

CORRECT AND EFFECTIVE USE OF SCIENTIFIC INFORMATION

In spite of such advances, a number of current practices and approaches can stand

improvement. We are still rating the shock resistance of parts in gs. These simple ratings, based often on acceleration levels of unspecified shock pulses, do much to confuse our fundamental insight into shock-induced failure. It would be better to refer to a standard test. It would be still better, as our shock and related testing becomes more refined, to talk in terms of a spectrum over a frequency range (even if it sometimes has to be inferred somewhat crudely from pulse shape data) preferably giving some idea of those interior frequency bands in which an item is particularly sensitive or insensitive, by virtue of its resonances.

A random vibration is more completely described by probability distributions in addition to power spectra. There has naturally been some interest in deviations from the Gaussian distribution. However, too much of this to date has been concerned with deviations at the mounting or excitation points of equipment because of nonlinearities of the source, and too little has been concerned with deviations at the failure point caused by nonlinearities associated with the failure mechanism. There has been too little recognition that a non-Gaussian distribution is a delicate thing, readily altered by filtering and phase shift, so that deviations at the excitation points are probably less significant than irregularities of spectrum that, for practical reasons, we may often be forced to ignore. Theoretical treatments have concentrated on effects of gentle nonlinearities. These treatments are worthwhile advances. However, there are more critical problems associated with abrupt nonlinearities out at the extreme tails of a distribution. In any event, there appears to be little justification for routine observation of distributions in addition to power spectra at excitation points of equipment.

This supports the thought that we should use more perspective in the reduction of data and be guided more by expected utility. I have heard of meticulous data reduction being carried out on low-level vibrations with overall rms accelerations less than 1 g. Especially in this period of cost sensitivity, there are dangers in too much reduced data; extremes of it divert attention from the more important problems and may serve only as published evidence that effort has been expended without expectation of beneficial effect on a program. The ultimate application may not always influence the form in which data are displayed; the immediate objective of data reduction is to describe an environment, not to arrive at a specification. But utility should influence the extent of data reduction.

Recently, we have become more aware of noise as well as vibration. There has been too

much tendency to treat them as independent environments and simulate both as a routine matter of policy. Crudely speaking, in missiles and space vehicles, noise and vibration are proportional. I have seen several exploratory papers showing experimentally that noise excitation and vibration produce somewhat different failures. But the conclusion that both must therefore be simulated is not necessarily valid and should be approached with caution. The state-of-the-art of vibration testing is still such that a change of test fixture will often result in significantly different failures. But it does not necessarily follow that both fixtures must be used. The difference in failures in noise excitation may be from problems analogous to that of a difference in fixtures. But, apart from the subtleties of test apparatus, there are inherent uncertainties in the realism of simulation of environment at the parts level. We should hesitate before doubling the effort.

Now let us consider a matter of even broader implications. It is important to distinguish between what is scientifically proved and what is convention or standardization. For example, the ways in which we measure tensile strengths and fatigue limits and in which we design to prescribed fractions of them is convention, not a matter of procedures that have been scientifically proved to be best. This should be accepted without any implication of stigma. The pioneers who established the procedures did something that was necessary before any effective approach to design could be possible and before any further progress could be made. They did what all good engineers should be able to do on occasion—use their best judgment and get on with the job. The fundamentals of fatigue and failure are under continuing study. The current design procedures will, however, continue to be used, perhaps eventually with slight modification.

Again, our use of specifications is a convention we have found empirically to be useful. The way in which we use them is convention. The idea that the test excitation should simulate the environment is convention. It may seem obvious that simulation is a necessary objective but the obvious should not be taken as entirely axiomatic. Great scientific advances have come from questioning the obvious, and science has repeatedly disclosed areas in which the obvious is not valid. Specifications serve ultimately as a motivation to people who influence design. The probable effect on design is potentially as fruitful a field for study as the problem of simulation. I do not suggest that we all rush out to make radical changes in our approach to specifications, but we should recognize a need for further gradual investigation, and we should

avoid too much wishful thinking that specifications are an exact science.

In some specific areas, we can make more immediate progress. For example, in shipping container design, the procedure by which we routinely compare equipment fragilities, cushion transmissibilities, and standard test conditions is to my mind wasteful of effort. The information used is not of sufficient precision to support the elegance of the concept. Smoothing of data tends to obscure the most important aspects. Engineering feeling for the problem to be solved tends to get lost in the formalities. The problem is simple enough to be attacked in a somewhat different way. It is more fruitful to think in terms of frequencies of resonance than in terms of conventional fragility.

WHAT ARE WE OVERLOOKING?

In the future, we hope to make even more significant advances than we have in the past decade. This will be easier if we recognize problem areas that need more attention.

Shock and vibration engineers have generated an extensive lore of qualitative design considerations: where to mount transformers and other heavy parts, methods of locking nuts and machine screws so they will not shake loose, and so on. I do not believe that as yet this has been satisfactorily gathered in one place. Such an effort would help design engineers to avoid the more obvious design errors. As the packaging of electronic equipment is undergoing rapid change, a loose-leaf book, permitting individual sections to be kept up to date, might be appropriate.

The interaction of specifications with equipment dynamics indirectly being controlled deserves more investigation. The shipping container cushion, already mentioned, and the vibration isolator represent relatively simple problems for initial study.

We need instrumentation for dynamical analysis of equipment. The bulk of the accelerometers manufactured are designed for measuring shock and vibration environments, not for investigation of dynamics inside equipment. This deficiency of instrumentation and associated techniques is probably the greatest immediate obstacle to our progress. However, the dynamics of equipment as designed at present are horribly complicated. It will be necessary to develop our techniques of measurement by first investigating some simple units or even simplified configurations assembled only for dynamical study, so that engineers will not become

hopelessly bewildered by the complexity of equipment under study.

We need a tabulation of resonance frequencies of standard parts, such as, vacuum tubes. This should start slowly, and we should learn to use the data as they accumulate. In some instances, it may be desirable to measure resonances both with infinite-impedance and zero-impedance excitation, or to make at least ball park measurements of impedance. In the designing of electronic equipment to perform its intended function, more information is demanded about the vacuum tubes than their maximum power output. In design for reliability under vibration, more information should be demanded than just the simple standard test condition the vacuum tubes have survived. We should begin, even more gradually, to accumulate data on typical equipment structures.

We need further conscious development of semi-quantitative design approaches. We are hampered by our tendency to believe that shock and vibration is or must become an exact science in the classical sense. We tend to believe that response calculation and stress analysis must be carried out with extreme accuracy, and that eventually the procedures will be refined and elaborated in keeping with the complexity of the dynamical problem. In the meantime, stress analysis is a useful but limited tool, because we almost never calculate interior dynamical responses of equipment. (In fact, if this were done meticulously, it would in principle be inefficient and too late. It cannot be done until after an equipment design is finished. Furthermore, the classical approaches if carried to an extreme generally require too much data, effort and time). We tend to believe that simulation must necessarily be carried out to a high degree of refinement in all shock and vibration tests, and that, in time, refinement and elaboration of test apparatus and technique will make this possible. In the meantime we do not achieve this at all except in a few special cases. Furthermore, there are reasons why we should not want to eliminate overdesign entirely. Our procedures do not lead to the design of equipment to precise safety factors such as 1.25 or 1.50. They merely decrease the probability of equipment failure, decrease the risk in the design, and more nearly approach an optimum. If we accept this qualitative, probabilistic objective as legitimate, and pursue it with some imagination, we may make more progress than by insisting on a more ambitious goal that is clearly out of reach.

A more comprehensive display of objectives is given in Table 1. They are not mutually

TABLE 1
Objectives of Shock and Vibration Engineering

Considerations	Objectives
Rate of improvement of reliability under shock and vibration excitation in the course of development and production	Maximize
Ultimate reliability	Maximize
Overdesign beyond what is needed for precautions against changes of application and associated environment, if there are trade-off penalties of weight, bulk, cost or schedule	Minimize
Overall design and test effort and cost	Minimize

independent, and one must make tradeoffs between the different objectives. Shock and vibration engineering is as much a matter of management-type techniques as it is of classical technical disciplines. In time, operations research may make its contribution in conjunction with those of the more purely technical disciplines that are applied now.

SHOCK AND VIBRATION AS AN INTERDISCIPLINARY ENGINEERING FIELD

As with most activities that have any connection with missiles or space, shock and vibration would certainly be considered an interdisciplinary field. What might at one time have been expected to develop purely as a matter of mechanical engineering has encompassed a tremendous variety of specialties.

Yet in some senses the term interdisciplinary is not adequate. There is an implication that the objectives can be achieved entirely by juxtaposing or fusing together several technical disciplines as taught at academic institutions. The academic disciplines are indispensable, but

they do have some limitations. They correlate in a framework of theory a tremendous scope of information. The orderly research and assimilation that bring a discipline to a particular state of progress are self-perpetuating. They facilitate the discovery and investigation of any voids of information that are apparent from logic alone. But each discipline tends to establish impenetrable external boundaries separating it from other disciplines and from considerations that are not as yet within any boundary. The specialist is under constant pressure to stay inside his boundary, look only inside his boundary, and confine his serious attention to the interior voids. Considerations that, because of their empirical, qualitative, ill-defined or controversial nature, or, because of lack of technical purity, have not become part of a recognized discipline, are commonly pressed aside as unworthy of the refined scientific intellect. Individually, out in the field, we see only part of the elephant, and, collectively, we seldom see the whole. By staring at part of the elephant, we proceed to prescribe cures for the whole animal. There are many ways that we as specialists, can and do contribute to shock and vibration engineering, but we should not let disciplinary boundaries restrict our vision.

Shock and vibration engineers should be objective-oriented as well as discipline-oriented. The ultimate objectives, apparent to everyone, should be general, like those of Table 1, and not stated entirely in the language of existing disciplines. We should focus our attention on the practical constraints of the overall engineering problem.

CONCLUSION

We have made great progress in the last decade, but it has resembled a succession of explorations by scouting parties, resulting in some changes of weaponry (i.e., test apparatus, instrumentation and data reduction techniques), but no large frontal advance. We should make greater progress in the next decade. I hope that the reflections I have shared with you this morning will be of some help.

* * *

Section I

PREDICTION OF FLIGHT ENVIRONMENT

AN ENERGY METHOD FOR PREDICTION OF NOISE AND VIBRATION TRANSMISSION

Richard H. Lyon
Bolt, Beranek, and Newman, Inc.
Cambridge 38, Massachusetts

The problem of malfunction in components at high frequencies is reviewed. The overall problem is one of environmental excitation, acoustic and vibration transmission paths, and establishment of criteria for noise reduction through component criteria. The source problem is being studied by several groups. Several aspects of the vibration path problem are described. Experimental studies of transmission effects and establishment of component criteria are hampered by a shortage of instrumentation capable of operating at the higher frequencies.

THE HIGH FREQUENCY NOISE AND VIBRATION ENVIRONMENT OF COMPONENTS

Introduction

Many of the current acoustic specifications extend over the range from a few cps to 20 kc or so, for both pure tone sweeps and bands of noise in a reverberant or travelling wave environment. Vibrational specifications, are frequently required over a range from 50 cps to 2 kc or so, using a uniform base excitation in the vertical or horizontal direction. The small size of modern-day components, the higher vehicle speeds and the consequent broad frequency range of the noise sources have produced serious component malfunction in the range from a few kc to over 100 kc. In this paper we shall discuss a method of vibration analysis and estimation which is particularly useful in the higher frequency multimodal vibration regime of structures and acoustic spaces.

It has been suggested that one reason that many vibration specifications do not go above 2 kc is that the instrumentation does not generally exist for the analysis and excitation of structures above this frequency range. Nevertheless the malfunctions that have occurred in the higher frequency ranges make it necessary to use instrumentation that is available and to

develop new instrumentation to cover this region if malfunction is to be understood and avoided. The vibration of component leads can lead to their fracture;¹ the vibration of cathodes of vacuum tubes can cause modulation and noise in the signal. In addition, many vibration reduction techniques which are useful at lower frequencies will not work effectively in this range. Vibration isolators are not designed to reduce vibration at higher frequencies because of internal wave effects in the mount structure.²

Sources of Environmental Vibration

In Fig. 1 we diagram some of the major elements in the environmental estimation problem for a component package in a spacecraft booster. The external frame and skin structure is the common element in all the sources of environmental excitation. It absorbs the longitudinal sources of vibration due to thrust fluctuations and aerodynamic resistance. These longitudinal loadings predominate at the lower frequencies. In addition the skin panels are

¹"Measurement of Acoustic and Vibration Response of Atlas Titan Guidance Computer," BBN Report No. 1010, submitted to Space Technology Laboratories April 22, 1963.

²Reference 1, section VI.

good transducers of the high frequency pressure loads and are set into transverse vibration by impinging sound fields and the loadings due to boundary layer and "dirty-flow" pressure fluctuations. The "dirty-flow" loads are the very complicated aerodynamic loads from wake impingement, buffeting, fluctuating separation, and so on, which can exist on the exterior of the booster.³

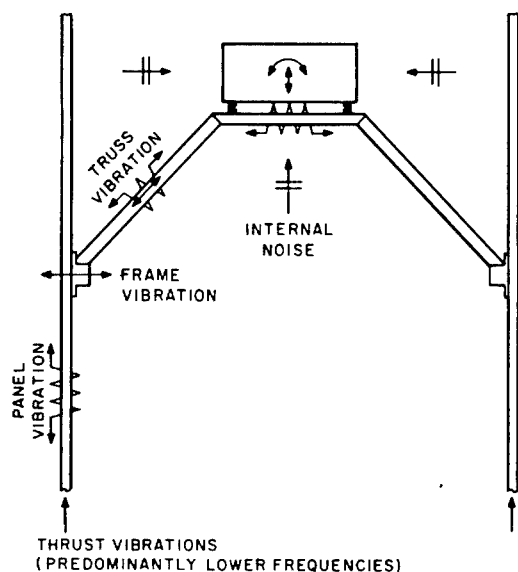


Fig. 1 - Supporting structure for component package

Energy Paths

The component package of Fig. 1 is mounted on vibration isolators and supported by a truss

³I. Dyer, "Aerodynamic Noise," contribution to Proceedings of the First Symposium on Engineering Applications of Random Function Theory and Probability, Ed. J. L. Bogdanoff and F. Kozin (John Wiley and Sons, New York, 1963), p. 204.

system attached to the frames of the external skin frame structure. We shall specify next the paths the energy takes in getting from the environment to the component. These paths have been made more explicit in Fig. 2. The acousto-mechanical path consists of the acoustic excitation of the skin, the internal re-radiation of the skin, and the absorption of acoustic energy by the box. This path was essentially described in a paper at the 31st Symposium by Franken and Lyon.⁴ In this paper we should like to emphasize the mechanical transmission aspects of the problem and demonstrate to what extent solutions for the properties of these paths are currently available.

The mechanical path consists of transmission of vibrational energy through the skin frame structure into the truss, through the vibration mounts, and into the box structure. If the component is mounted on a sub-assembly within the box, then the path includes an excitation of the component mounting and finally the transmission to the component itself. The large number of links in this chain represent a complication, but not an insuperable one. We are, in fact, closer to a solution of the vibration estimation in systems such as this than might be apparent at first glance. In the next section, we will describe several studies which pertain to different aspects of the general transmission problem.

Vibration Criteria and Specifications

One of the essential elements of the noise control problem is the establishment of criteria for acceptable noise levels.⁵ The phenomenon

⁴P. A. Franken and R. H. Lyon, "Estimation of Sound-Induced Vibrations by Energy Methods," Shock, Vibration, and Associated Environments Bulletin No. 31, Part III, Office of the Secretary of Defense (April 1963).

⁵L. L. Beranek, "Criteria for Noise and Vibration in Buildings and Vehicles," chapter 20 of Noise Control, Ed. L. L. Beranek (McGraw Hill Book Company, Inc., New York, 1960).

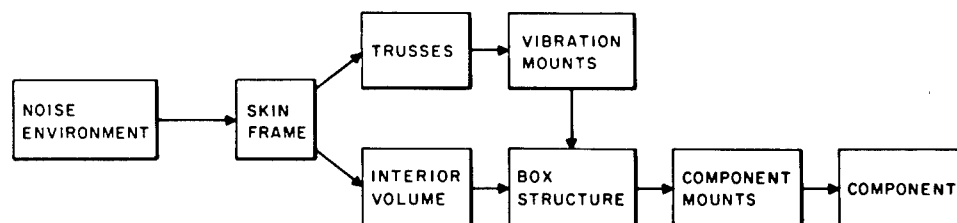


Fig. 2 - Energy paths from noise environments to component

of component malfunction is similar. Just as an individual's reaction to noise depends on his daily activities, the malfunction of a component will depend on its operating mode. It will have differing sensitivities to noise depending on whether it acts as a local oscillator, an amplifier, or a limiter, and the sensitivity of the signal processing to the form of the induced noise. The proper design of electronic and mechanical equipment for service in a high frequency vibration environment will depend upon a knowledge and understanding of the sensitivity to vibration of the individual component. This requires the ability to estimate vibration in complex structures and the experimental ability to generate and measure these vibrations.

Vibration Levels in Complex Systems

In Fig. 3 we have sketched the cross section of several structural sections of a panel frame booster structure. During the launch phase the power absorbed by the structure may be approximately as sketched, being higher toward the base and lower at the nose because of the higher acoustic levels in the proximity of the engine.⁶ Because of the different levels of the excitation, there will be a transport of the energy through the frame structure along the skin as shown, and a local dissipation of energy including both external and internal radiation loss which may vary as shown. In addition there will be energy transferred into the truss.

⁶P. A. Franken and F. M. Wiener, "Estimation of Noise Levels at the Surface of a Rocket-Powered Vehicle," Shock, Vibration, and Associated Environments Bulletin No. 31, Office of the Secretary of Defense (April 1963).

The resulting equilibrium levels of energy in the bays will depend on the balance between the power injected, that transferred from the bay, and locally dissipated. The structural dissipation can be affected by adding damping materials to that which exists naturally in the structure due to damping at the joints. This natural damping will be discussed later by Ungar.⁷ The action of applied damping treatments has been discussed by Kerwin, Ungar, and Ross.⁸ We shall not discuss the dissipation here except to point out some of the problems with its measurement at an appropriate time, but rather concentrate on the energy transmitted through the frame and into the truss members.

The vibration levels of a truss will depend on the vibration of the frame to which it is attached which in turn depends on the vibration level of the adjoining skin. We shall see that these vibration levels can be obtained from a rather simple analysis.

SPECIFIC STUDIES OF STRUCTURAL VIBRATION

Energy Sharing Between a Beam and a Plate

Suppose the panel shown in Fig. 4 has been excited into reverberant resonant vibration of

⁷E. E. Ungar, "Vibrational Energy Losses at Joints in Metal Structures," Shock, Vibration and Associated Environments Bulletin No. 33, Part IV, Office of the Secretary of Defense 1964.

⁸D. Ross, E. E. Ungar, and E. M. Kerwin, "Damping of Flexural Vibrations by Means of Viscoelastic Laminae," contribution to Structural Damping, E. J. Ruzicka (Am. Soc. Mech. Engrs., New York, 1959).

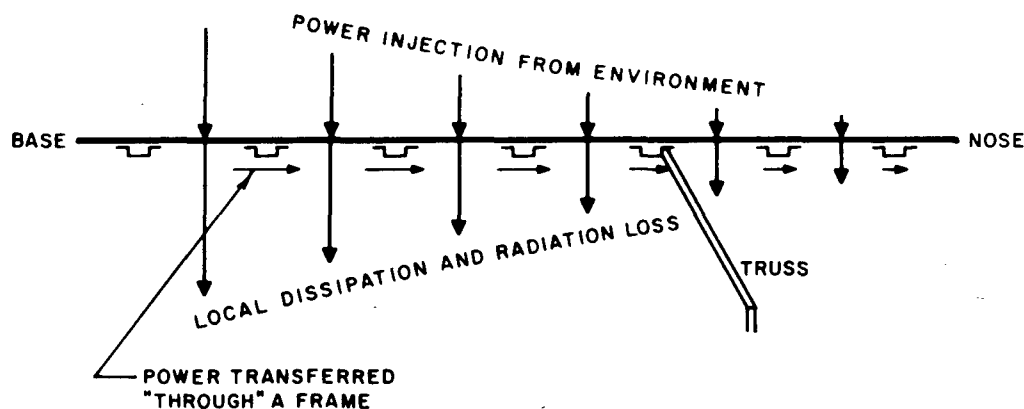


Fig. 3 - Distribution of injected, transferred, and dissipated power in extended structure

amplitude v_p by the applied point force f . The force f is assumed to be white noise over a band Δ . We should like to estimate the transverse vibrational level of the attached beam v_b . We shall do this by using a reciprocity argument.⁹

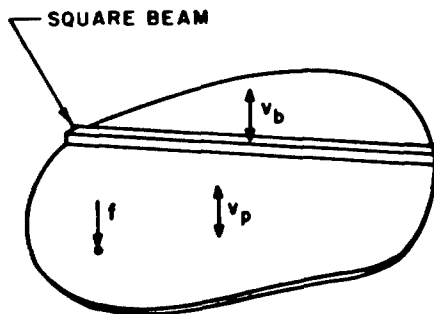


Fig. 4 - Beam-plate reciprocity experiment

The input power to the panel Π_{in} is given by

$$\Pi_{in} = f^2 G_p, \quad (1)$$

where G_p is the averaged input conductance over the bandwidth Δ . The resulting vibration of the plate is

$$v_p^2 = \frac{\Pi_{in}}{\omega \eta_p M_p} = \frac{f^2}{\omega \eta_p} \frac{G_p}{M_p}, \quad (2)$$

where ω is the radian center frequency of the band, η_p is the loss factor of the plate, and M_p is the mass of the plate. If the system is linear, the beam vibration velocity will be proportional to the plate velocity;

$$\frac{v_b^2}{v_p^2} = \alpha. \quad (3)$$

Next consider the reciprocal situation. At the point where the beam velocity was previously measured, we apply a force f' . The input power is

$$\Pi'_{in} = f'^2 G_b, \quad (4)$$

which results in a beam vibration amplitude v'_b

$$v'_b{}^2 = \frac{\Pi'_{in}}{\omega \eta_b M_b}, \quad (5)$$

where η_b is the beam loss factor and M_b is its mass.

A portion of the input power, Π'_{trans} , will be carried from the beam into the plate. This is measured by the coupling loss factor η_b^p :

$$\Pi'_{trans} = v'_b{}^2 \omega \eta_b^p M_b. \quad (6)$$

Since this power is related to the resulting mean square plate velocity v_p^2 by the same relation as shown in (2), one has

$$v_p^2 = \frac{\Pi'_{trans}}{\omega \eta_p M_p} = \frac{f'^2}{\omega \eta_p} \frac{G_b}{M_p} \frac{\eta_b^p}{\eta_b}. \quad (7)$$

If f and f' are white noise sources over the same frequency band, then one can write the reciprocal relationship

$$\frac{v_b^2}{f^2} = \frac{v_p^2}{f'^2}, \quad (8)$$

which results in a remarkably simple expression for the unknown ratio of beam to plate amplitude α ,

$$\alpha = \frac{G_b}{G_p} \frac{\eta_b^p}{\eta_b}, \quad (9)$$

involving the point conductances of the beam and plate and the coupling and total loss factors of the beam. It will frequently happen that the loss factor for the beam is determined almost completely by its losses to the structure to which it is attached. In this case α is simply the ratio of the two point conductances. One could experimentally determine this ratio by applying a mean square force in a noise band at the plate and on the beam and looking at the ratio of the power injected. The measurement of injected power over bands of noise will be discussed at this symposium by Noiseux and Dietrich.¹⁰

⁹The use of reciprocity for the derivation of response relationships in acoustics has been spearheaded by M. Heckl. For an acoustics example, see M. Heckl and E. J. Rathe, "Relationship between the Transmission Loss and the Impact-Noise Isolation of Floor Structures," J. Acoust. Soc. Am. 35, 11, 1825 (Nov. 1963).

¹⁰D. U. Noiseux and C. W. Dietrich, "Simulation of Reverberant Acoustic Testing by a Vibration Shaker," Shock, Vibration, and Associated Environments Bulletin No. 33, Part III, Office of the Secretary of Defense, 1964.

It can be shown¹¹ that the average conductance of a structure over a band will be given by

$$G = \frac{\pi}{2} \frac{n}{M}, \quad (10)$$

where n is the modal density of the structure and M is its mass. If we place (10) in (9) then we can rewrite (9) as

$$\frac{M_b v_b^2}{n_b} = \frac{M_p v_p^2}{n_p} \frac{\eta_b^p}{\eta_b}, \quad (11)$$

where the quantity on the left is the average modal energy of the beam and on the right we have the average modal energy of the plate times the loss factor ratio discussed above. When the internal losses of the beam become negligible, it achieves the same modal energy as the structure to which it is attached.

Frequently one can use the uncoupled point conductance for individual structures in estimating response ratios. For example, Lamb¹² has computed the input admittance of a beam connected to a plate and has shown that the first order effects on beam plate coupling are to change the input susceptance but not to affect the conductance of the beam. One should also note that in order for applied damping to be effective in reducing beam vibration, the internal loss factor of the beam must be made comparable to or greater than the coupling loss factor. In a tightly coupled system this may be difficult to achieve.

Transmission of Flexural Wave Energy Past a Frame

The transmission of bending wave energy from one of the panels shown in Fig. 5 to another depends on the coupling loss factor introduced by the restraining frames. This loss factor can be derived from expressions developed by Ungar¹³ for the transmission of a flexural wave

on a plate through an attached beam of specified bending and torsional rigidity. On one side of the beam one has an incident bending wave at an angle ϕ resulting in a reflected transverse wave, reflected and transmitted near fields, and a transmitted transverse wave. It is this transmitted wave that we are primarily concerned with here, since it carries energy from one side of the beam to the other. Ungar's formalism allows us to calculate the transmission quite generally but for the purposes of illustration we shall only consider the case where the beam has infinite bending rigidity but no torsional rigidity, corresponding to a supported line on the plate. If the incident amplitude is unity, then $|T|^2$ is proportional to the transmitted energy, and is given by $(1/2) \cos^2 \phi$. The transmitted bending energy per unit projected length of the beam introduces another $\cos \phi$. If we average this over all angles of incidence of the incoming energy, we have the result

$$\langle |T|^2 \cos \phi \rangle_\phi = \frac{1}{2} \langle \cos^3 \phi \rangle_\phi = \frac{2}{3\pi}. \quad (12)$$

Thus, a fraction $2/3\pi$ of the incident energy is transmitted giving an absorption coefficient for the beam as defined by Heckl¹⁴ of approximately 20 percent.

In a diffuse reverberant field the energy associated with propagation between angles ϕ , $\phi + d\phi$ is $\rho_s v_p^2 d\phi / 2\pi$, where ρ_s is the surface density of the panel. The intensity is this energy density times the energy velocity c_g . To compute the power falling on a unit length of the boundary we multiply this by the cosine of the angle of incidence and integrate over all angles of incidence. The resulting power per unit length of boundary is given by

$$I_{inc} = \frac{\rho_s v_p^2 c_g}{2\pi} \int_{-\pi/2}^{\pi/2} d\phi \cos \phi = \frac{2}{\pi} \rho_s v_p^2 c_p, \quad (13)$$

where ρ_s is the surface density of the panel and $c_p = (1/2) c_g$ is the bending wave speed. The transmitted intensity is then the fraction in (12) times the incident intensity in (13). The resulting transmitted power is the transmitted intensity times the perimeter, or,

$$P_{trans} = \frac{4}{3\pi^2} \rho_s v_p^2 c_p P, \quad (14)$$

where P is the perimeter of the panel.

¹¹R. H. Lyon, "A Review of the Statistical Analysis of Structural Input Admittance Functions," BBN Report 1068, in preparation for submission to the Bureau of Ships. See also, E. Skrudzyk, "Vibration of a System with a Finite or an Infinite Number of Resonances," J. Acoust. Soc. Am. **30**, 12, 1140 (Dec. 1958).

¹²G. Lamb, "Input Impedance of a Beam Attached to a Plate," J. Acoust. Soc. Am. **33**, 5, 628 (May 1961).

¹³E. E. Ungar, "Transmission of Plate Flexural Waves Through Reinforcing Beams; Dynamic Stress Concentrations," J. Acoust. Soc. Am. **33**, 5, 633 (May 1961).

¹⁴M. Heckl, "Measurements of Absorption Coefficients on Plates," J. Acoust. Soc. Am. **34**, 6, 803 (June 1962).

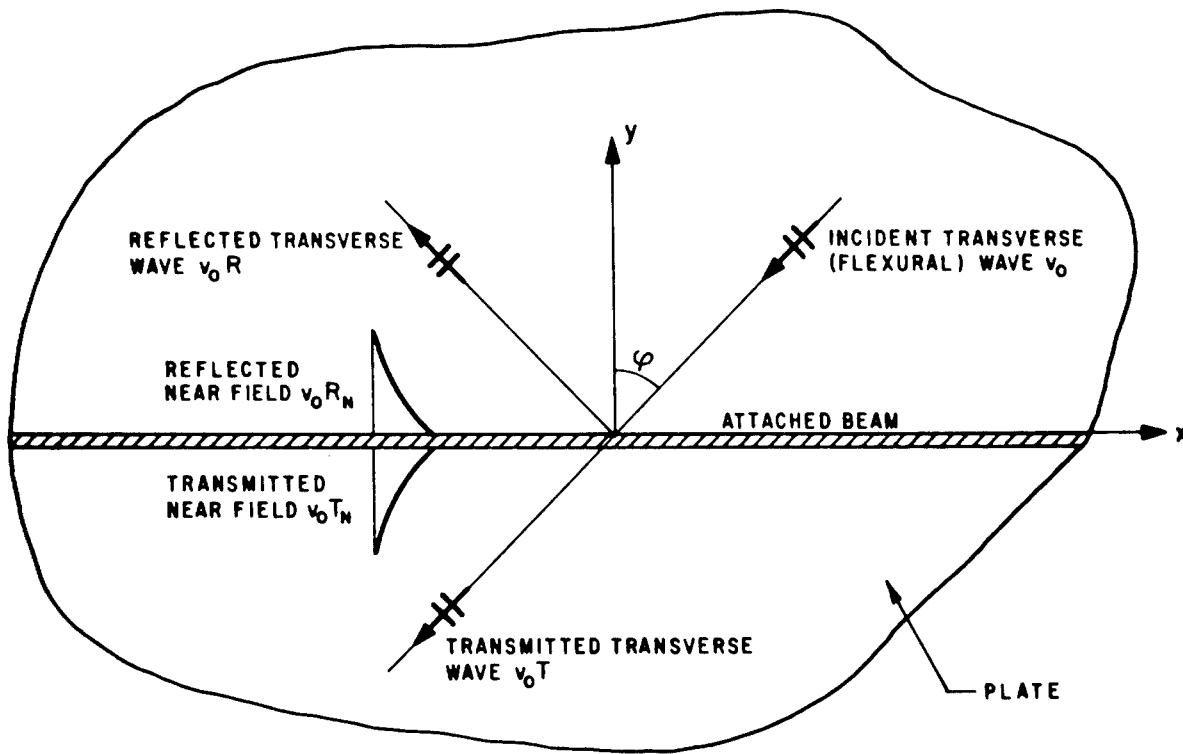


Fig. 5 - Transmitted and reflected plate waves through an attached beam

The coupling loss factor is

$$\eta_{\text{coup}} = \Pi_{\text{trans}} / \omega M_p v_p^2. \quad (15)$$

By using (14) one has

$$\eta_{\text{coup}} = 4/3\pi k_p d, \quad (16)$$

where k_p is the flexural wave number in the panel, $d = \pi A_p / P$ is the mean free path for bending waves,¹⁵ and A_p is the panel area. Since the structural loss factor generally is of the order of 10^{-2} , one sees that the coupling loss factor may be expected to dominate the panel losses for frequencies such that $k_p d < 10$. At higher frequencies the panels will be more effectively isolated from each other than at lower frequencies.

Energetics of Systems in Tandem

It is evident from Figs. 2 and 3 that there may be several structural elements interposed

between the vibration producing environment and the component or structural element whose vibration we wish to know. In the preceding sections we have studied energy transmission between two systems. Recently, Eichler¹⁶ has analysed several systems energetically connected. We shall follow a similar development in this section

The system we consider is shown in Fig. 6. A series of structural elements receive power $\Pi_{in}^{(n)}$, dissipate locally a power Π_n , and transfer amount of power $\Pi_{n,n+1}$ to their neighbor on the right. Each system is characterized by a modal density n_n , a mass M_n , and a mean square velocity v_n^2 . The power balance for a single system at equilibrium is

$$\Pi_{in}^{(n)} = \Pi_n + \Pi_{n,n+1} - \Pi_{n-1,n}. \quad (17)$$

The energy of the n^{th} system is $E_n = M_n v_n^2$. This equation, in fact, defines the velocity v_n .

¹⁵C. W. Kosten, "The Mean Free Path in Room Acoustics," *Acustica* 10, 4, 245 (1960), sec. 4.

¹⁶E. Eichler, "Energy Averages in Loosely Coupled Systems with Applications to Noise Reduction," submitted for publication.

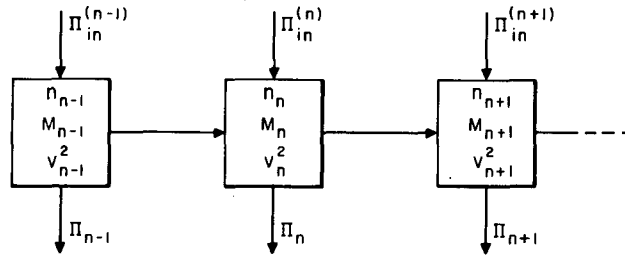


Fig. 6 - Power storage and transfer in multi-element system

The dissipated power, Π_n , is given by

$$\Pi_n = \omega \eta_n E_n, \quad (18)$$

where η_n is the loss factor for local dissipation.

It has been shown previously that the power flow between systems depends on the difference in the modal energies.¹⁷ Thus, the power flow $\Pi_{n,n+1}$ can be defined in terms of a coupling loss factor γ_n^{n+1} by

$$\Pi_{n,n+1} = \omega n_n \left[\frac{E_n}{n_n} - \frac{E_{n+1}}{n_{n+1}} \right] \gamma_n^{n+1}, \quad (19)$$

with a similar relationship for $\Pi_{n-1,n}$. Since the power flow must be the same whether we regard it as leaving system n or entering system $n+1$, one has the consistency relationship between the coupling loss factors

$$n_{n+1} \gamma_{n+1}^n = n_n \gamma_n^{n+1}. \quad (20)$$

Placing these in (17) one has two forms available for the power balance equation.

$$\begin{aligned} \Pi_{in}^{(n)} = & \omega \left[E_n (\eta_n + \gamma_n^{n+1} + \gamma_n^{n-1}) \right. \\ & \left. - E_{n+1} \gamma_{n+1}^n - E_{n-1} \gamma_{n-1}^n \right] \end{aligned} \quad (21)$$

or,

$$\begin{aligned} \frac{\Pi_{in}^{(n)}}{n_n} = & \omega \left[\frac{E_n}{n_n} (\eta_n + \gamma_n^{n+1} + \gamma_n^{n-1}) \right. \\ & \left. - \frac{E_{n+1}}{n_{n+1}} \gamma_{n+1}^n - \frac{E_{n-1}}{n_{n-1}} \gamma_{n-1}^n \right]. \end{aligned} \quad (22)$$

In this second form, one may represent the equations by the simple equivalent electrical circuit shown in Fig. 7, where the flow quantity is power per mode and the potential is modal energy. Such simple analog energy circuits can be useful in describing the distribution of energy through a complex structure and experimentally in demonstrating the effect of a change in certain parameters on this distribution.

Figure 7 also shows why it can be very difficult to measure the loss factor η_n by a simple decay measurement unless steps are taken to eliminate the transfer of energy from one structural element to another by establishing similar modal energies in each of the structural systems. This can be done by multiple excitation over the structure, or by a single excitation if the coupling is strong enough and the damping losses small enough so that the energy gets fairly uniformly distributed. Over a large structure this latter condition is unlikely and excitation damping measurements made on the single structure element usually will not give the correct loss factor.¹⁸

Studies of Average Power Flow Into Structures

In (9) we showed that the response ratio between two attached structures will depend on the input conductance averaged over a band of frequencies. In simulation studies also, one is concerned about the amount of power which one can inject into a structural element from a point shaker, particularly at the higher frequencies. This requires an understanding of the magnitude and frequency dependence of the average input conductance.¹⁰ For these reasons, the average value and variance of the input conductance averaged over bands of frequencies has been studied. The variances,

¹⁷R. H. Lyon and G. Maidanik, "Power Flow between Loosely Coupled Structures," J. Acoust. Soc. Am. 34, 5, 623 (May 1962).

¹⁸E. M. Kerwin, Jr., "Mechanisms and Measurement of Structural Damping," J. Underwater Acoustics, 13, 4 (Oct. 1963).

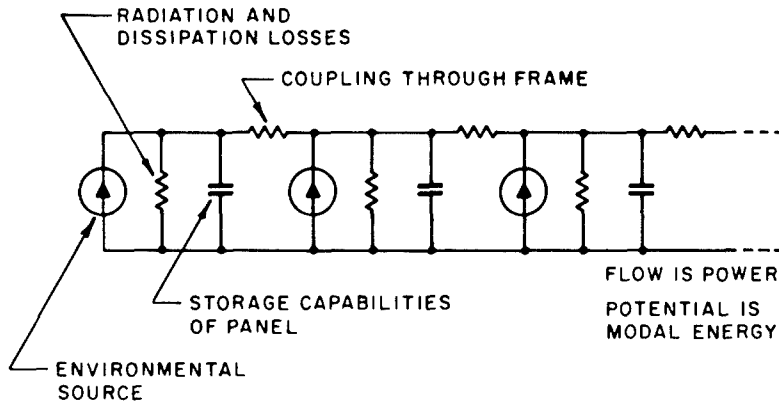


Fig. 7 - Energy circuit for multi-element system

along with an assumed probability distribution for the conductance amplitude has made it possible to compute confidence levels to be assigned to estimation intervals of the input power.

To compute the statistics of the power flow, we have assumed a statistical model of the structure comprising a group of resonant modes which occur randomly along the frequency axis and which have response amplitude depending on the relationship between their modal shape functions and the positions of excitation and observation on the structure. The average value of the input conductance is given by the infinite structure conductance and is simply related to the modal density and the mass as shown:

$$m_G = G_\infty = \frac{\pi}{2} \frac{n_s}{M_s} \quad (23)$$

It is this relationship that was previously to establish the quality of modal energies. The average value of the susceptance vanishes.

If one computes the variance of the conductance from the model, one obtains¹⁹

$$\frac{\sigma_G^2}{m_G^2} = \frac{\langle \psi^2 \rangle^2}{\langle \psi^4 \rangle} \frac{n_s \Delta}{F(N)} \xrightarrow{N \rightarrow 0} 2 \frac{\langle \psi^2 \rangle^2}{\langle \psi^4 \rangle} n_s \delta \omega, \quad (24)$$

where Δ is the bandwidth of the exciting noise source, and $N = \Delta/\pi\omega\eta$ is the ratio of the noise bandwidth to twice the modal bandwidth, which

we have called $\delta\omega$. The function $F(N)$ is plotted in Fig. 8. For narrow bands or large damping, one has the relationship shown as $N \rightarrow 0$. This displays the surprising behavior that the variance of the response increases as the damping increases, a result which is somewhat unexpected. Our usual idea is that increasing the damping tends to make the response smoother. The functions ψ are modal shape functions and for two-dimensional structures are essentially products of sine waves.

An estimation interval is a range of the unknown variable within which one wishes the experimental result to occur. The confidence level for the estimate is the probability with which one expects the measured or realized value of the variable to fall within that interval.²⁰ If the variable has a response or a probability density $p(G)$ then the confidence level CL is defined by

$$CL = \int_{G_1}^{G_2} p(G) dG. \quad (25)$$

We have computed the confidence levels based on the assumption that $p(G)$ is the Γ distribution²¹ for two types of estimation interval. In the first, one allows the variable to fall below some particular value \hat{G} .

In Fig. 9 we show the number of db by which \hat{G} must exceed the mean given in (23) in order to achieve various levels of confidence. This interval depends on the ratio of the square

¹⁹"Studies of Random Vibration of Coupled Structures," Parts I and II, BBN Reports 967 and 1061, submitted November 15, 1962 and October 15, 1963 to Aeronautical Systems Division.

²⁰A. M. Mood, Introduction to the Theory of Statistics (McGraw-Hill Book Company, Inc., New York, 1950), chapter 11.

²¹Reference 20, p. 112.

of the mean to the variance which is determined by (24). In Fig. 10 we show the estimation intervals required for a given confidence level when the mean value is the geometric mean of the upper and lower limits of the estimation interval. Such a definition of the interval is particularly convenient when one is dealing in decibel notation and would prefer to say that the interval is the mean plus or minus so many decibels.

The Γ distribution is convenient to use for response functions, particularly those proportional to energy or power. If one is willing to make the assumption that it is valid then all that one requires is the variance and the mean to establish confidence levels for any particular estimation interval. It has been applied to variations in response to attached substructures as well as input power, as we shall see in the following section.

Study of Energy Sharing in a Beam Plate Structure¹⁹

To see how the general ideas above are applied, it is instructive to review some experiments carried out on a simple beam cantilevered to a flat plate as shown in Fig. 11. The plate was excited in 8-percent and octave bands of noise and the response of free tip of the beam was measured for single mode response and in octave bands where more than one mode participated in the response. From (9) we see that a knowledge of the coupling loss factor and the internal damping is necessary to predict the beam response. When the beam is undamped its coupling is determined primarily by the coupling losses so that we have the equal energy condition (11).

The experimental results for the undamped beam are shown in Fig. 12. We see the close

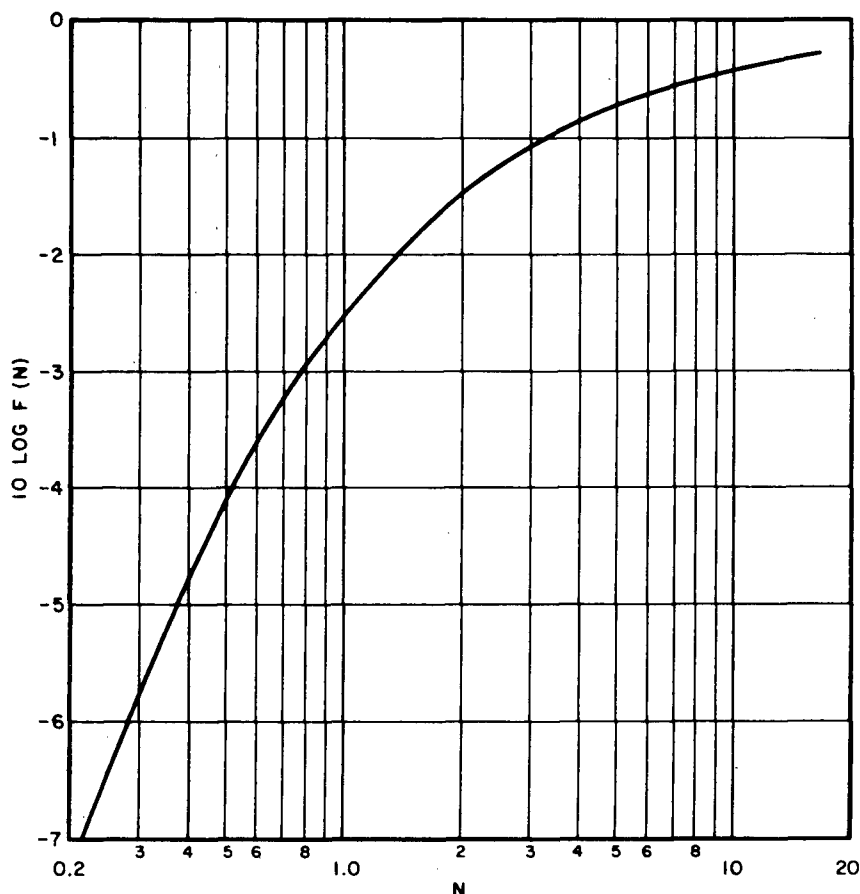


Fig. 8 - Graph of $10 \log F(N)$

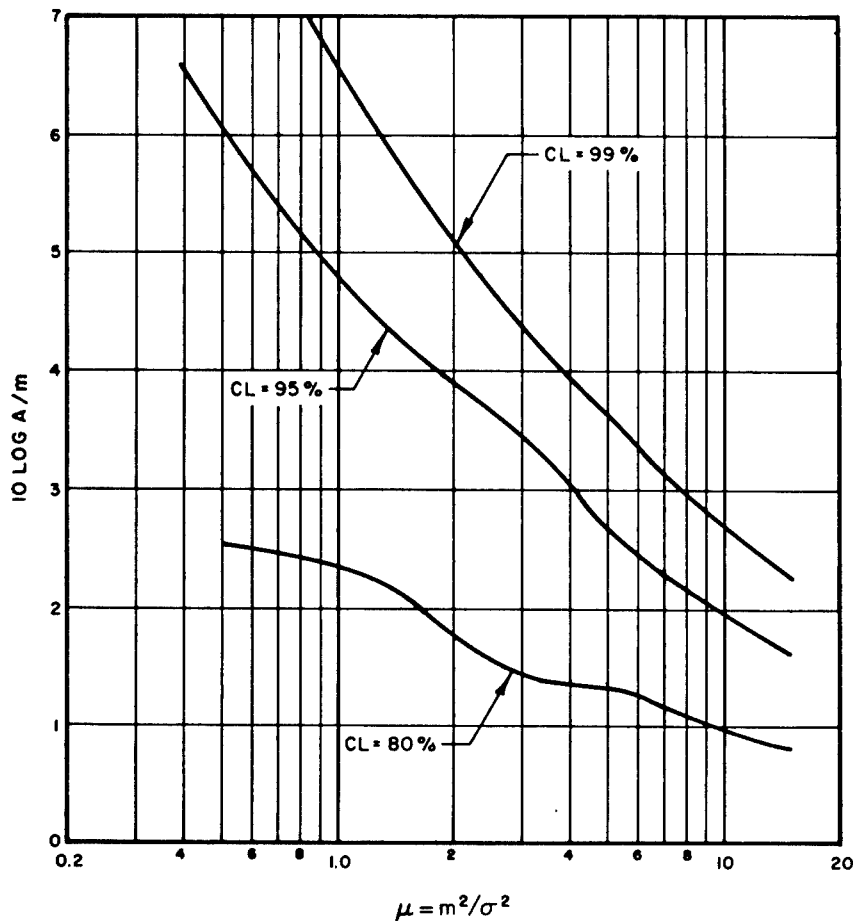


Fig. 9 - Semi-infinite estimation interval in decibels

agreement between the average modal energy of the beam and the plate as predicted by (9). In the equal energy case, the response variation that occurs is due to the unequal modal energy of the plate. This produces an uncertainty in the bar modal energy. The ratio of variance to square of mean is $\langle \psi^2 \rangle / \langle \psi \rangle^2 = 9/4$. If we use the interval estimation of Fig. 9, we see that this corresponds to an estimate approximately 2.5 db above the mean value. The individual model responses which are rather scattered are included within this interval at an 80-percent confidence level.

FURTHER DEVELOPMENTS

The moral of the preceding discussion has been that there exist, at the present time, methods which are able to give one considerable insight into the manner in which vibrational and acoustic energy is transferred throughout a structure and achieves its equilibrium levels. This is particularly so in the higher frequency

ranges where the statistical procedures of the estimation are likely to be somewhat tighter than they are at the lower frequencies where modes are fewer. There is a need for some improvement in the theoretical development. This would include a closer look at some of the statistical aspects of the structural model, the possibilities of making more realistic models on a large computer using Monte Carlo techniques,²² and the carrying out of further experiments on the vibration energy sharing with particular attention to the variations in the response.

A far more serious deficiency lies in the lack of instrumentation which will allow one to examine directly the vibration levels and the energy transfer through structures at the higher frequencies where malfunction is occurring

²²M. R. Schroeder, "Frequency-Correlation Functions of Frequency Responses in Rooms," J. Acoust. Soc. Am. 34, 12, 1819 (Dec. 1962).

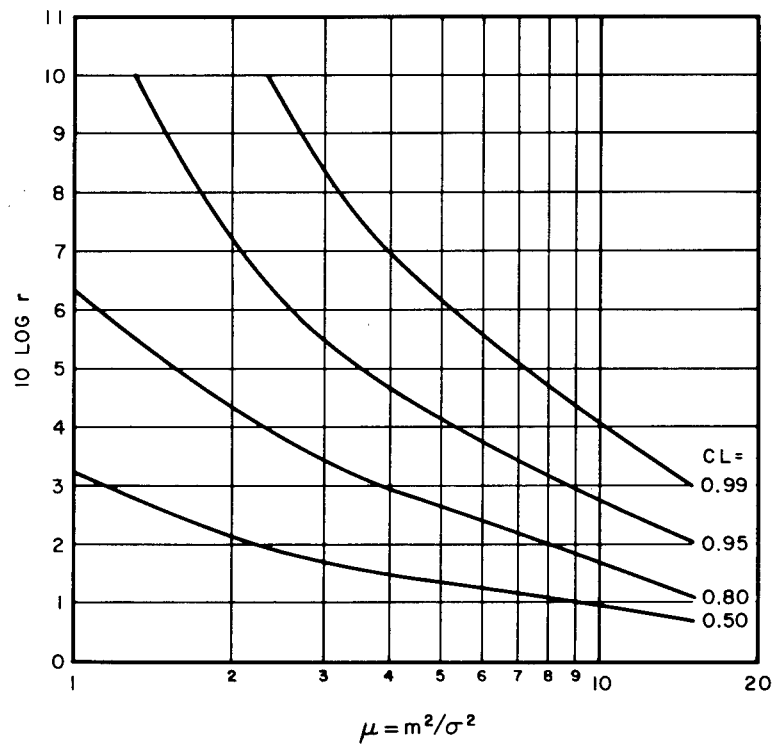


Fig. 10 - Half-width of estimation interval in decibels

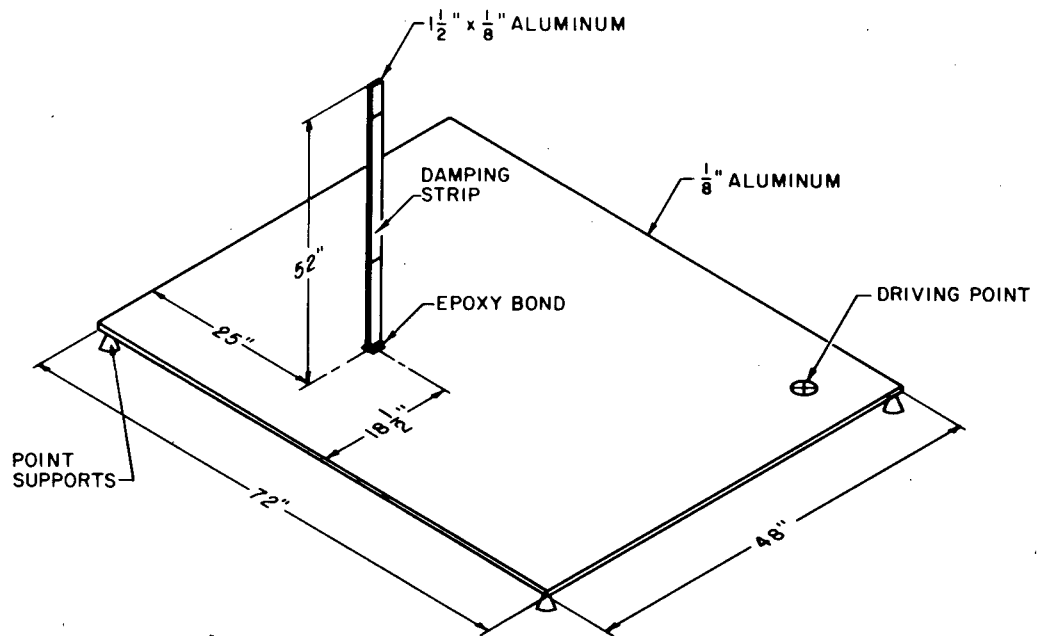


Fig. 11 - Experimental beam-plate structure

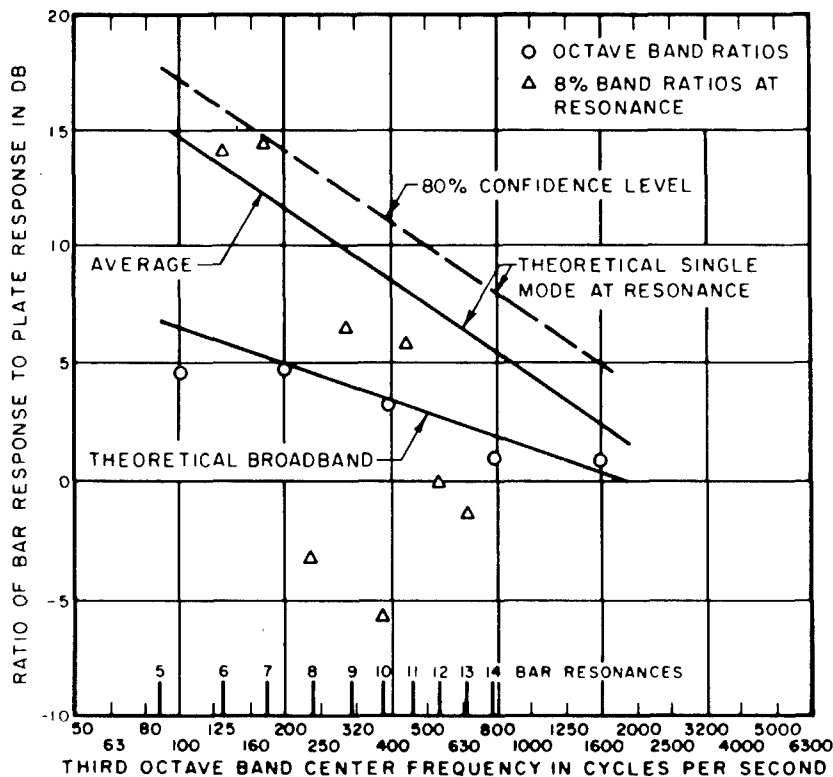


Fig. 12 - Response ratio for an undamped beam cantilevered to a plate

because of internal component vibration. Transducers for both excitation and sensing are required which will operate in the 100-kilocycle region. This would not only allow one to study response measurement, but to establish statistical criteria for component behavior in an intense high frequency vibration and acoustic environment.

ACKNOWLEDGMENTS

Portions of the work reported here have been supported by the National Aeronautics and Space Administration, the Bureau of Ships, and the Aeronautical Systems Division.

DISCUSSION

Mr. Bieber (Lockheed Missile and Space Company): In the experiment did you analyze the beam as a beam column or just as a beam?

Dr. Lyon: The analysis of the beam is that of a simple thin rod clamped at its lower edge. Simple bending equations are assumed to apply.

Mr. Bieber: Then you only include the bending of the beam, not the longitudinal vibration of it.

Dr. Lyon: The first mode of the beam would be at several thousand cycles, about

2-1/2 kc. We assume that there are no longitudinal modes in the range that we are studying here. The energy method will apply equally well to the longitudinal modes, but generally there are so few longitudinal modes compared to flexural or bending modes, that most of the energy of the structure is in the bending vibration.

Mr. Granick (NASA): Your analysis is based on uncoupled modes, that is, they are separated in frequency and they are purely linear. Some experience exists that there is a coupling due to damping between the modes. Have you thought about this as a possible reason

why your narrow bandwidth analysis differs so greatly from your octave band analysis on that last slide?

Dr. Lyon: That has not been the interpretation of the narrow band analysis. If you only have one mode of the responding system, it looks at only a very narrow frequency range, and therefore, it sees only very few modes of the plate. If it happens to be high or low on the

slope of that mode, it will receive a greater or lesser amount of excitation. Our interpretation is that the variance in the individual mode of response can be accounted for by how these things match up in mode response. Now, undoubtedly there are many complications which one can find in real systems. I think my tendency is to take the simplest approach first, and then only be forced to something more complicated if it is necessary.

* * *

A TECHNIQUE FOR PREDICTING LOCALIZED VIBRATION RESPONSE IN ROCKET VEHICLE STRUCTURE*

R. E. Jewell
Marshall Space Flight Center
Huntsville, Alabama

The objective of this paper is to develop a prediction technique which is not based solely upon data acquired from similar vehicles. The total available energy concept is utilized with the localized vehicle structure regarded as an energy absorber. Acoustically induced vibrations are specifically treated by this method.

In October of 1961 I presented a paper which discussed the general philosophy and method which was utilized to establish the vibration response environment of the Saturn, Block I vehicle. This prediction was made prior to an actual Saturn flight. Some of the significant information gained from four successful flights will be given in another paper at this Symposium. What I would like to direct my attention toward today is to recall briefly the basic prediction technique that was used on the Saturn I vehicle. It was simply the process of multiplying measured vibration levels from a previous vehicle, by the ratios of impinging sound pressures and characteristic masses. The latter quantity (mass) was about the only knowledge available during the preliminary design stages. The relationship is written in equation form as

$$\ddot{X}_n = \ddot{X}_r \frac{P_n}{P_r} \frac{M_r}{M_n}$$

where the subscripts denote reference or new vehicle as appropriate.

This technique was later modified to establish the reference environment (\ddot{X}_r) as a statistic of a collection of data. Further, it became necessary to separate the vehicle into zones or structural regions and to consider the structural types contained in each region. The reference environment had placed upon it a certain confidence limit which, hopefully, would carry through to similar vehicles and structures. Another technique which attempts to use existing data to categorize, in a general way, the response

characteristics of a structure is the method reported by Mahaffey and Smith in which airframe response was plotted against environmental sound pressure level (SPL), and a linear regression line fitted to the data. A typical graph is given in Fig. 1.

By using this technique, one may obtain an estimate of the new vibration environment by merely determining the SPL of the new vehicle and utilizing the appropriate curve. Both methods have obtained wide use for extrapolating to new configurations. However, each method leaves a great deal to be desired. The method of Mahaffey and Smith requires that an extreme similarity exist in airframe structures; and the method utilizing ratios merely considers, in a very crude way, the mass loading effects. Neither method is capable of considering any of the elastic, structural, or interface properties associated with real structures. What I will attempt to do in the presentation of this paper is to outline a more comprehensive prediction technique — one which will accept many more of the parameters required to describe adequately the vibration environment, and one which, in its simplest form, reduces to the very simple ratio method previously described. The technique will, in general, be applicable to the prediction of the vibration environment on an untested vehicle and will do so with a minimum use of reference data.

Consider the rocket vehicle structure as an energy absorber. The rate and amount of absorption is dependent upon the characteristics

*Invited Paper.

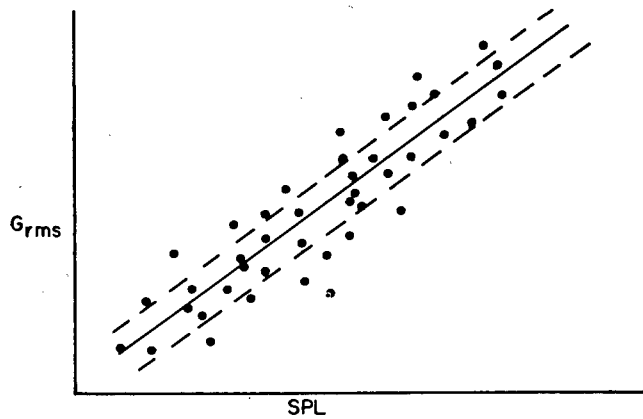


Fig. 1 - Airframe response as a function of SPL

of the structural system. Energy from several sources may be present to excite the system, and the total energy flux into the system will be some portion of the total available from N sources. That is

$$\bar{E}_v = \sum_{i=1}^N \phi_i \bar{E}_{avi}, \quad (1)$$

where

ϕ_i = the energy transfer efficiency of the i^{th} source, and

\bar{E}_{avi} = total available energy of the i^{th} source.

If the system were conservative it would dissipate no energy, and once set into oscillation would require no additional energy input to maintain the motion. In the practical case all systems are nonconservative and dissipate energy in the form of power losses directly proportional to the amount of damping in the system. For viscous damping forces proportional to velocity the power loss is proportional to the square of velocity. This is expressed from (1) as the rate of change of energy in the system. In terms of their time average values,

$$\frac{d\bar{E}_v}{dt} = \bar{P}_v = R \bar{\dot{X}}^2, \quad (2)$$

where

R = the total damping (resistance) in the system, and

$\bar{\dot{X}}^2$ = mean square velocity of the system mass.

In consideration of the right side of Eq. (1) the total vibrational power from all sources may be expressed as

$$\bar{P}_{v/T} = \sum_{i=1}^N \gamma_i \bar{P}_{avi}, \quad (2a)$$

where

γ_i = the efficiency of conversion to vibration power for the i^{th} source, and

\bar{P}_{avi} = the average power associated with the i^{th} source.

It is of interest to expand Eq. (2a) in order to indicate some of the more important sources available to cause system vibrations. Equation (3) is the expanded equation with the subscript (T) denoting total vibration power.

$$\begin{aligned} \bar{P}_{v/T} = & \gamma_a \bar{P}_a + \gamma_{ae} \bar{P}_{ae} + \gamma_{em} \bar{P}_{em} \\ & + \gamma_{aj} \bar{P}_{aj} + \dots + \gamma_N \bar{P}_N \end{aligned} \quad (3)$$

where

a = engine generated acoustics,

ae = aerodynamic pressure fluctuations,

em = engine mechanics, and

aj = adjacent structure.

By changing notation such that

$$\bar{P}_{v/a} = \gamma_a \bar{P}_a, \quad (3a)$$

we can rewrite equation (3) as

$$\begin{aligned}\bar{P}_{v/T} = & \bar{P}_{v/a} + \bar{P}_{v/ae} + \bar{P}_{v/em} \\ & + \bar{P}_{v/aj} + \cdots + \bar{P}_{v/N}.\end{aligned}\quad (4)$$

Now the total vibration power associated with a rocket vehicle structure is of interest. Assume a rocket vehicle whose exterior configuration is as shown in Fig. 2.

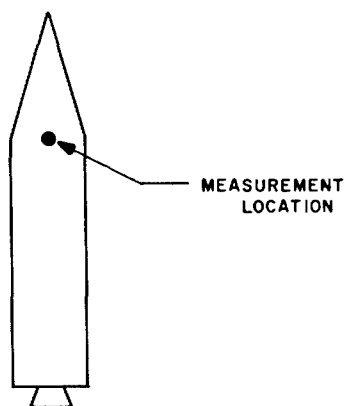


Fig. 2 - Typical measurement location

The total vibration environment for that location is given by Eq. (4), however, an exact solution to that equation consisting of contributions from all terms is not likely in the near future.

It would indeed be a difficult (but not impossible) task to separate that portion of the

total environment which is caused by engine combustion instabilities, local equipment, or acoustics. On the other hand it may be possible and of interest to attack each term separately in an effort to determine its contribution to the whole, and hence find that for certain structural types Eq. (4) may be controlled by the contribution of a single term.

Fortunately the single term which is dominant for much vehicle structure also is one which is easiest to handle, and one for which much work has been done. Smith, Lyon, Dyer, et. al., have reported on the response of structures to acoustic excitation. In so doing they have developed equations for the energy of a structure responding to random forces and have included an evaluation of the external damping associated with the boundaries of panels. It turns out that while all structures probably have some acoustic susceptibility, paneled structure is particularly susceptible, and it can be noted that a rocket vehicle's exterior profile indicates a high percentage of paneled structure; the consequence being that the treatment of acoustically induced vibration is of prime importance. The range of structural acoustic susceptibility is illustrated in Fig. 3.

Note that the time curve (A), a measurement on heavy internal structure is apparently not affected by the change in overall Sound Pressure Level indicated by curve (B). Conversely we note that curve (C) can hardly be differentiated from the acoustic curve. The excitation response comparison is remarkably close. One can even ascertain the magnitude of excitation from other sources by noting the vibration response when the acoustic level is a minimum. The middle curve is for a heavy gage honeycomb

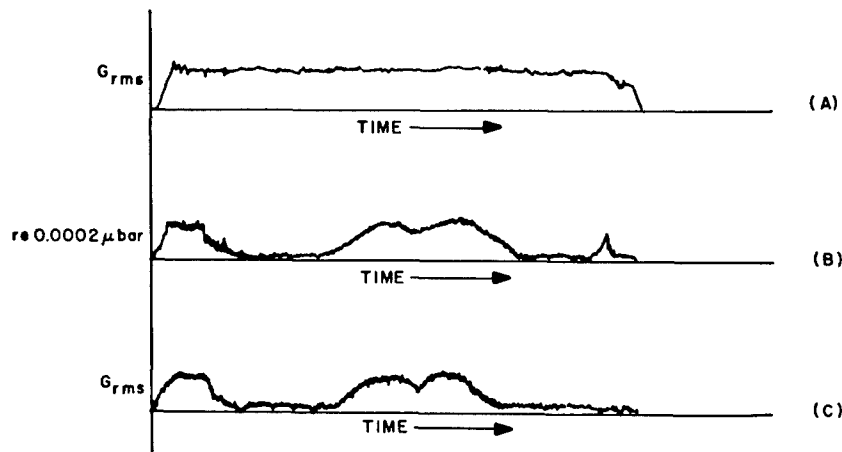


Fig. 3 - Range of acoustic susceptibility

panel mounted inside an equipment bay and attached directly to a skin panel. The curves of Fig. 3 are the extreme values that I have found. Most structures are acoustically susceptible to some degree. It was, in fact, difficult to find a structural element which showed no detectable response to acoustic excitation. It is then obvious that there is a direct proportionality between measured response and the impingement of sound pressures on the structure.

In order to equate the total vibrational power to the effects of an acoustic source we must find a structure whose response amplitude is related to impinging sound pressure in much the manner indicated by curves (B) and (C) of Fig. 3. If the summation of the effects of all other sources is considered negligible we may write

$$\bar{P}_{v/T} = \bar{P}_{v/a} = \gamma_a \bar{P}_a \quad (4a)$$

By recalling the form of vibrational power given in Eq. (2) and changing it to relate vibration accelerations rather than velocities, we have

$$\bar{P}_v = \frac{R}{\omega^2} \ddot{X}^2 \quad (5)$$

Assuming that the acoustic excitation is in general broadband and random, we expect that for the most selective mechanical systems the response would be within some practical bandwidth around ω rather than precisely at ω . In the event there are closely spaced modal frequencies, we assume that they are essentially uncoupled, and that a summation of modal responses would suffice. As an additional effort to establish the parameters in a form consistent with measured quantities we will multiply and divide the right side of Eq. (5) by both a bandwidth (Δf) and the acceleration constant due to gravity (g_o).

$$\bar{P}_v = \frac{R}{\omega^2} \ddot{X}^2 \frac{\Delta f}{\Delta f} \frac{g_o^2}{g_o^2} \quad (6)$$

which can be rewritten as

$$\bar{P}_v = \frac{R}{\omega^2} \text{PSD}_v \Delta f g_o^2 \quad (6a)$$

In accordance with Eq. (4a), the acoustic power is at most

$$\bar{P}_a = \frac{p^2 A}{\rho c} \quad (7)$$

where the usual cosine of the angle of incidence is assumed equal to unity for the maximum

case. Substituting Eqs. (6a) and (7) into (4a) yields

$$\frac{R}{\omega^2} \text{PSD}_v \Delta f g_o^2 = \gamma_a \frac{p^2 A}{\rho c} \quad (8)$$

Solving for the vibration power spectral density, we have

$$\text{PSD}_v = \frac{\gamma_a \text{PSD}_a A \omega^2}{R g_o^2 \rho c} \quad (8a)$$

In order to obtain solutions to Eq. (8a), we must determine the several parameters. The determination of most of the parameters is straightforward. The function γ_a must relate the conversion of acoustic energy to vibration energy. Intuitively we expect the conversion to vibration energy to be more efficient at or near resonances than at other positions in the spectrum. Further, γ_a should take into account the geometry and elastic characteristics of the structure. An analytic expression for γ_a which meets these requirements is developed as follows (see Fig. 4).

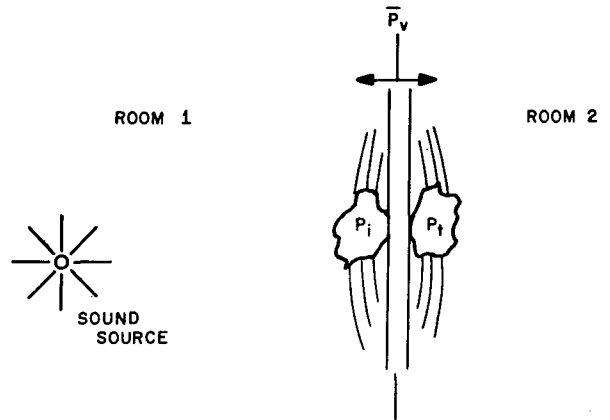


Fig. 4 - Sound transmission of single wall

The incident pressure P_i in room 1 will induce into the panel some vibration \bar{P}_v . This exchange should be governed according to Eq. (3a) as

$$\gamma = \frac{\bar{P}_v}{P_i} \quad (9)$$

The reconversion into sound pressure in room 2 will accordingly be

$$\gamma' = \frac{P_t}{\bar{P}_v} \quad (9a)$$

Now, if $\gamma = \gamma'$ as it should be, provided the acoustic impedances of the rooms are identical, we may combine (9) and (9a) into

$$P_t = \frac{\bar{P}_v^2}{P_i} \quad (9b)$$

The accepted expression for the ratio of P_i to P_t is given from transmission loss theory as

$$\frac{P_i}{P_t} = 1 + \left(\frac{Z_m}{2\rho c} \right)^2 \quad (10)$$

where

Z_m = the magnitude of the mechanical impedance of the plate per unit area, and

ρc = the specific acoustic impedance of the rooms.

It is immediately obvious that P_t may be eliminated from Eqs. (9b) and (10), and the result is an expression in terms of P_i , ρc , and Z_m . That expression is

$$\frac{\bar{P}_v}{P_i} = \left[1 + \left(\frac{Z_m}{2\rho c} \right)^2 \right]^{-1/2} \quad (11)$$

which is identical to the expression for γ given by Eq. (9).

Substitution of (11) for γ_a in Eq. (8a) yields

$$PSD_v = \frac{PSD_a A \omega^2}{\left[1 + \left(\frac{Z_m}{2\rho c} \right)^2 \right]^{1/2} R g_o^2 \rho c} \quad (12)$$

The calculation of the mechanical impedance (Z_m) to be used in Eq. (12) is of course a difficult task. One must estimate the values of spring rate (k) and mass (M) which is by no means straightforward. There are techniques, however, for estimating these parameters for the elements which make up the localized system. For example, one can determine the stiffness and the mass of the longeron stiffeners separately from the calculation of panel parameters. The optimum method for calculation of Z_m is yet to be determined. It does, however, seem that an attempt should be made to give numerical evaluation of this important parameter. For this paper the following technique was used.

With reference to Fig. 5 the ringframe element was considered as rigid or fixed. Both

the longeron and panel stiffnesses and masses were determined as separate elements.

The longerons were treated as beams and the relationship for their modal frequencies equated to the ratio of modal spring to modal mass. That is

$$K_{ns} = \omega_{ms}^2 m_n \quad (13)$$

where the modal mass (m_n) was taken as one-half the mass of the beam. In equation form

$$K_{ns} = \omega_{ms}^2 \frac{M_s}{2} \quad (13a)$$

The same technique was utilized to determine the spring and mass of the panel. The only exception being that for the panel the modal mass was one-fourth the actual panel mass. Hence, for panel parameters we have

$$K_{mp} = \omega_{mp}^2 \frac{M_p}{4} \quad (14)$$

Here it can be noted that the mass is not a function of mode which is an obvious error, but the result should be to hold the response prediction to a conservative value for the frequencies above and below resonance. Determining the mass and spring elements in this way made it necessary to devise a system from which to calculate the mechanical impedance. We chose a simple three-degree-of-freedom system from which we estimated the impedance of 12 selected modal combinations. The actual calculation of Z_m was to obtain solutions to the equation of motion for the system when subjected to a constant amplitude sinusoidal force applied to the mass of the panel. A sketch of the system is shown in Fig. 6.

The panel was assumed to have identical elements at the longeron boundaries, hence elemental parameters associated with mass one (M_1) and mass three (M_3) were combined and the system reduced to a two-degree-of-freedom system. The ratio of applied force to panel velocity gave values of impedance for particular modal combinations. An example of this impedance is given in Fig. 7.

The power spectral density of each individual impedance curve was calculated and a summation taken over all modal combinations. A conversion to G_{rms} for a 10-cps bandwidth was accomplished and the result is shown in Fig. 8.

From Fig. 8 we can note that the response is essentially bi-modal, as would be expected

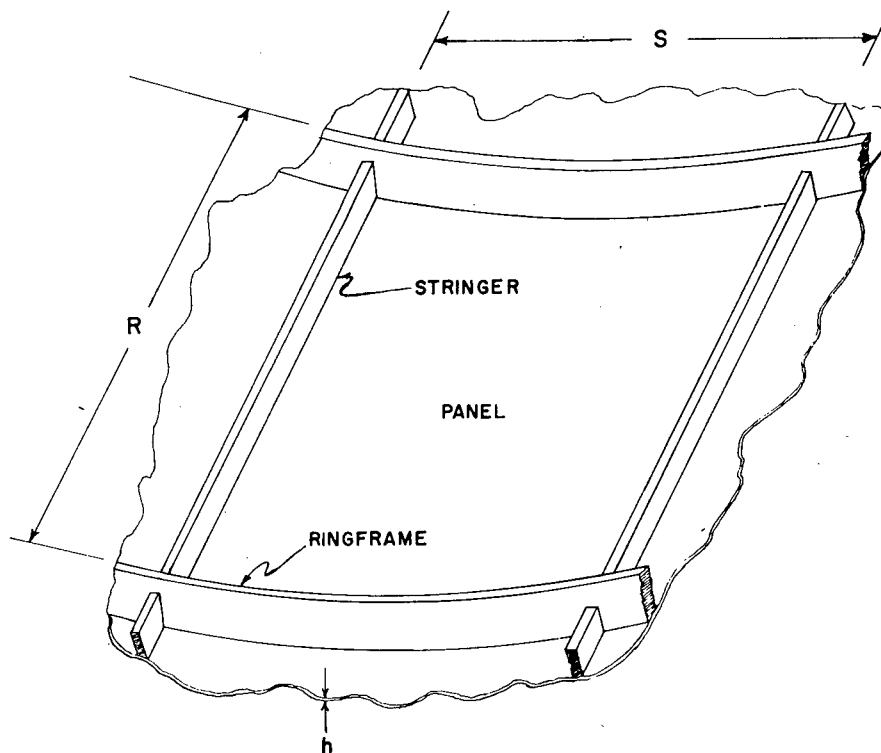


Fig. 5 - Typical structure

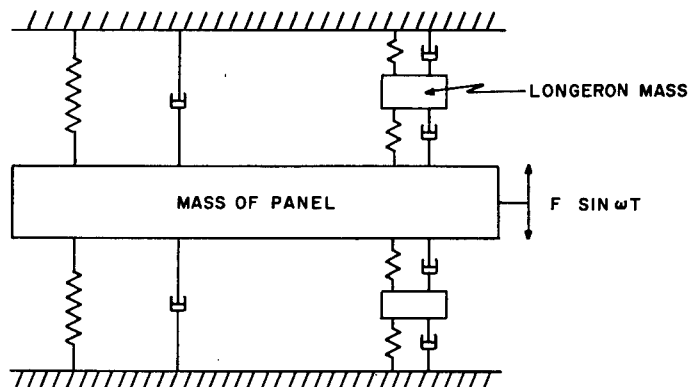


Fig. 6 - Spring-mass model of vibrating panel

from a two-degree-of-freedom system. The curve in Fig. 8 is shown as the envelope of peaks corresponding to a summation of modal response curves. It should also be noted that the responses and impedance in the frequency range beyond 1000 cycles has been indicated by dashed lines. The reason is that the calculation from the computer programs did not give reasonable answers beyond that point. It is realized, however, that there may not be significant

responses in that frequency range. The difficulty in the higher frequency range is being investigated.

Finally in Fig. 9, I have shown how the results from this analysis compare to a measured spectrum for the particular structure which was considered. This comparison is somewhat encouraging since the response prediction was carried out without knowledge of the measured

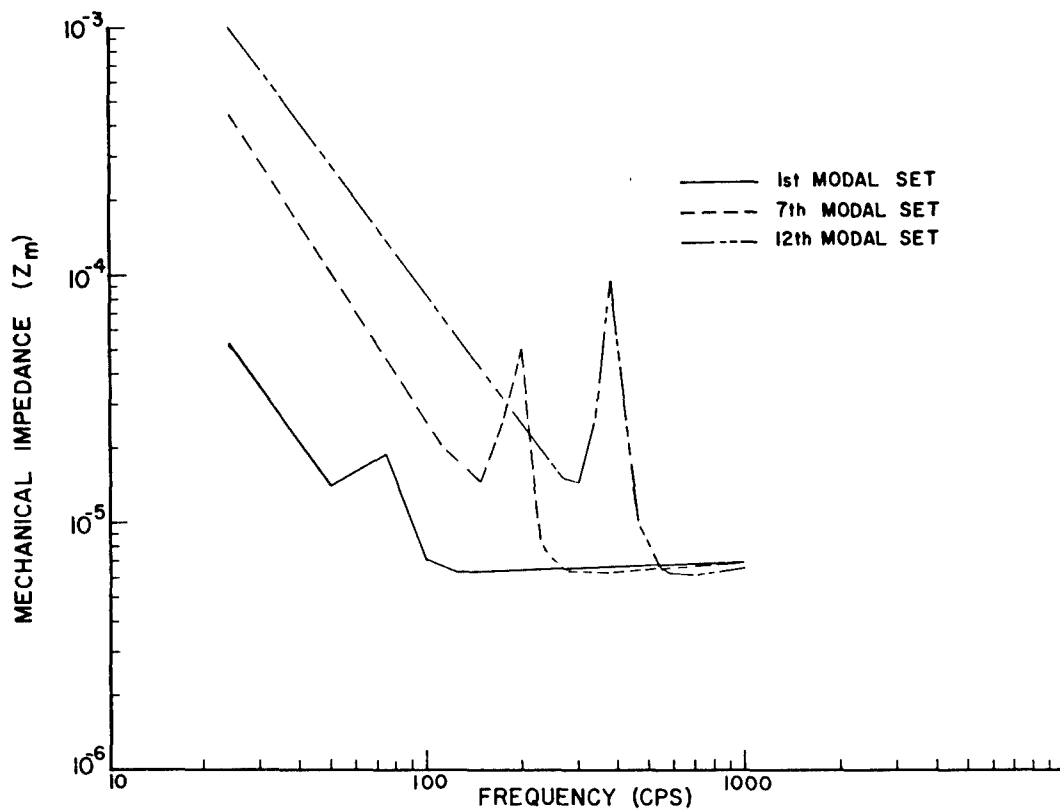


Fig. 7 - Calculated impedance

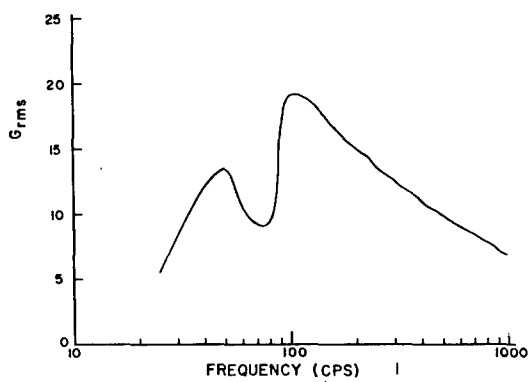


Fig. 8 - Predicted vibration response

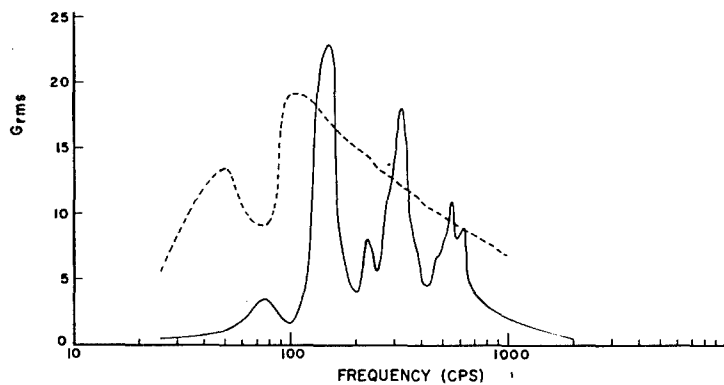


Fig. 9 - Comparison of measured and predicted vibrations

response. For this case, the application of the method to a specific structure was assigned to an engineer. He determined the impedance in the manner previously discussed, and the solution to Eq. (15) is plotted in Fig. 9. Contrary to

these results, attempts at other estimates for comparison to measured data have shown rather poor agreement. It is felt, however, that the method is general enough in the application to warrant further study and development.

DISCUSSION

Mr. Himmelblau (Nortronics): How did you determine damping from your impedance?

Mr. Jewell: I said in the beginning I would use a minimum of empirical data. The damping

value used in the calculation of impedance was the one empirical value that we did use. For this particular case we used the value 0.02. This was based upon panel studies done at Marshall on the Saturn vehicle.

BIBLIOGRAPHY

L. L. Beranek, editor, Noise Reduction, Chap. 13 (McGraw-Hill Book Company, Inc., New York, 1960).

S. H. Crandall, editor, Random Vibration, Vol. 1, Chap. 8 and 9 (Technology Press, M.I.T., 1958).

_____, editor, Random Vibration, Vol. 2, Chap. 7 (Technology Press, M.I.T., 1963).

K. Eldred, W. Roberts, and R. White, "Structural Vibrations in Space Vehicles," sections IV and V, WADD Tech. Rept. 61-62 (1961).

F. A. Fischer, Fundamentals of Electroacoustics (Interscience Publishers, Inc., New York, 1955).

C. M. Harris and C. E. Crede, editors, Shock and Vibration Handbook, Vol. 1, Chap. 10 (McGraw-Hill Book Company, Inc., New York, 1961).

M. A. Heckl, R. H. Lyon, G. Maidanik, and E. E. Ungar, "New Methods of Understanding and Controlling Vibrations of Complex Structures," Bolt, Beranek, and Newman, Inc., Tech. Note No. ASD-TW-61-122 (June 1962).

G. Maidanik, "Response of Ribbed Panels to Reverberant Acoustic Fields," J. Acoust. Soc. Am., Vol. 34 (June 1962).

* * *

VIBRATION PREDICTION PROCEDURE FOR JET POWERED VEHICLES AND ITS APPLICATION TO THE F-111*

N. I. Mitchell and H. E. Nevius
General Dynamics/Fort Worth
Fort Worth, Texas

A vibration prediction procedure which relates the structural vibration levels to external sound pressure levels on a jet powered vehicle is described. The application of this procedure to the F-111 program is presented, and other sources of vibration which must also be considered are discussed. Finally, possible improvements in the prediction procedure which are currently being studied are discussed.

INTRODUCTION

Early in the design stages of a new weapon system, the equipment designers need a realistic estimate of the environmental vibration levels. The practice in the past has been to use standard military vibration test specifications, regardless of the location of the equipment in the weapon system. This procedure is quite often more severe than necessary, and thus leads to over design, high costs, and excess weight. On the other hand, the standard environmental requirements are sometimes not severe enough. This leads to equipment which will not be satisfactory in the actual environment. Obviously, a weapon system will benefit from a realistic vibration estimation which will help to produce a reliable product without unduly penalizing any part of the system.

The purpose of this paper is to describe a vibration prediction procedure that has been developed at General Dynamics/Fort Worth, and to discuss its application to the F-111 Weapon System.

PREDICTION PROCEDURE

There are many sources of vibratory energy which must be considered in order to define vibration spectra for equipment mounted in complex weapon systems. Some of these are: jet or rocket engine exhaust noise, boundary layer turbulence, oscillating shock waves, buffet and

other flow separations, cavity resonances, mechanical equipment out-of-balance, and others depending on the design and use of the system. Of all these sources, however, the vibratory response to intense engine exhaust noise produces the most dominant excitation force in many present day, high-performance vehicles.

Thus, the basic thought in the vibration prediction procedure discussed in this paper is to seek a relationship between vibration levels and external acoustic noise levels at a point on the vehicle structure. If this relationship can be established, then it should be possible to estimate vibration levels from a knowledge of the jet exhaust noise levels. Studies at General Dynamics/Fort Worth several years ago established this relationship on statistical basis, and some of the results from these studies were presented in a paper by P. T. Mahaffey and K. W. Smith¹ at the 28th Symposium on Shock and Vibration. The procedure and results of the correlation study are described briefly below.

Statistical methods were used to correlate vibration levels on primary structural members in various areas of the B-58 with the external sound pressure levels in the same areas. The results are presented as curves of acceleration versus sound pressure level in octave bands

*Invited Paper.

¹P. T. Mahaffey and K. W. Smith, "A Method for Predicting Environmental Vibration Levels in Jet-Powered Vehicles," Shock, Vibration and Associated Environments Bulletin No. 28 (Aug. 1960).

from 20 to 2400 cps. Figure 1 illustrates the type of plot that is constructed for each octave band.

The measured data points are shown on the plot with the regression line giving the best fit of the data points. Upper and lower confidence limits are also shown. With a plot of this type for each octave and the octave band sound pressure level for a noise source, the vibration level in the frequency range of the octave can be estimated. Any degree of conservatism may be incorporated into the predicted vibration level by the use of the appropriate confidence limit.

To the vibration engineer, the data that falls in the interval between an upper and lower confidence limit is not as important as the confidence that the data falls below an upper limit. He must determine a satisfactory probability that the vibration environment will not be higher than a given level. For example, the upper 60-percent confidence limit will encompass the true accelerations during 80 percent of the prediction trials since 20 percent falls above the upper 60-percent confidence limit and 20 percent falls below the lower 60-percent confidence limit. In this paper, the 80-percent confidence level corresponds to the 60-percent confidence limit.

For each system, the level of confidence may be selected depending on the individual requirements of the system. Confidence levels of 80 to 90 percent, however, are believed to provide sufficient conservatism in most cases.

Summary curves of acceleration versus sound pressure level are shown for six octave bands in Figs. 2 and 3. In Fig. 2, the curves shown are for the 80-percent confidence that the levels will fall below the curves in each of the octaves. Figure 3 shows the same type of curves for 90-percent confidence that the levels will fall below the curves shown.

The vibration level prediction curves of Figs. 2 and 3 show vibration values in terms of rms acceleration for 1/3 octave filters. Similar curves could be developed for other filter bandwidths. In any case, proper use and evaluation of the curves requires a knowledge of the relationship between the rms levels and the peak levels. An evaluation of the B-58 data used in this study indicates that a Rayleigh distribution of peaks fits the test data very well except that peaks above three times the rms occur much less often than the Rayleigh distribution predicts. This apparent amplitude limiting may be a result of nonlinearities in the structure. It seems

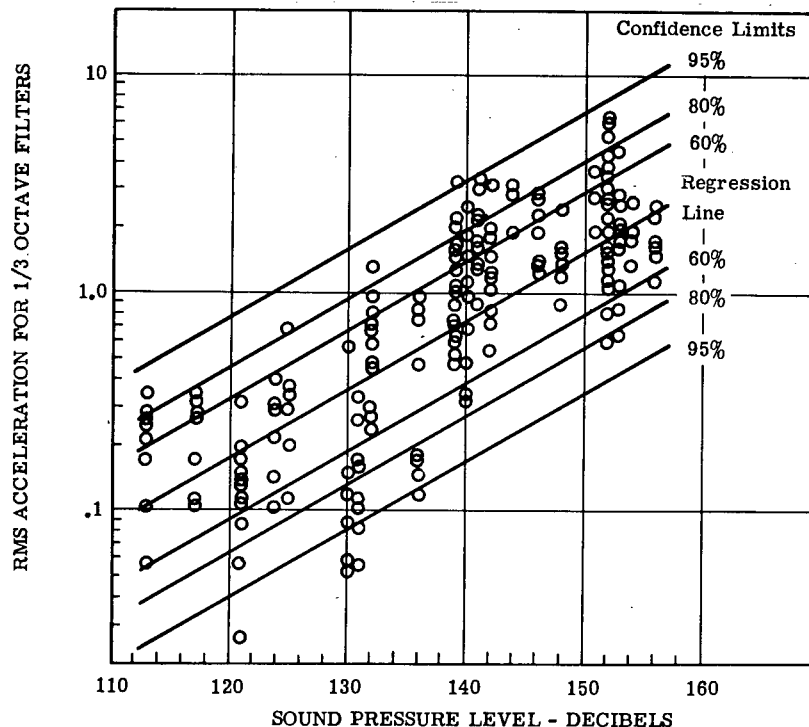


Fig. 1 - Acceleration vs sound pressure level in the 600- to 1200-cps octave band

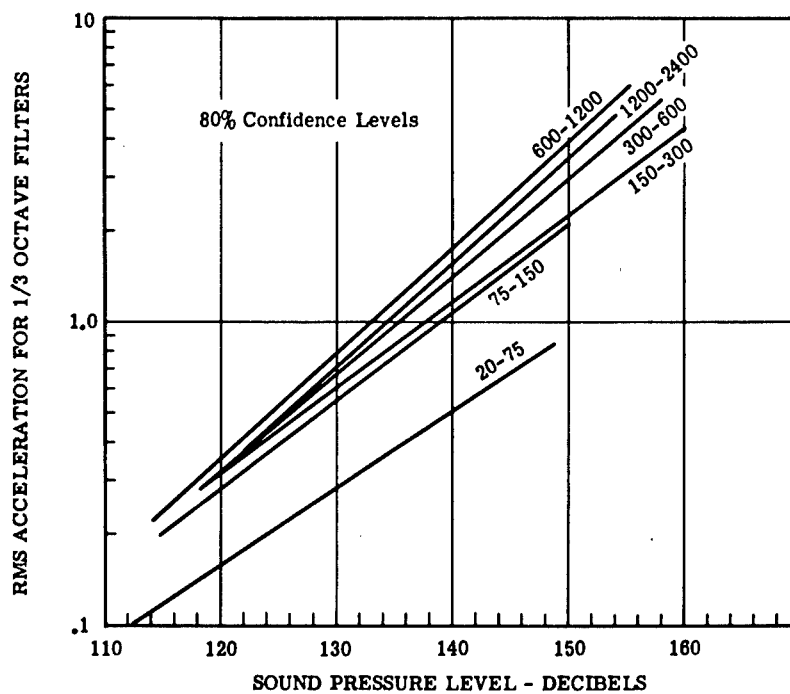


Fig. 2 - Confidence levels (80 percent) for acceleration vs octave band sound pressure levels

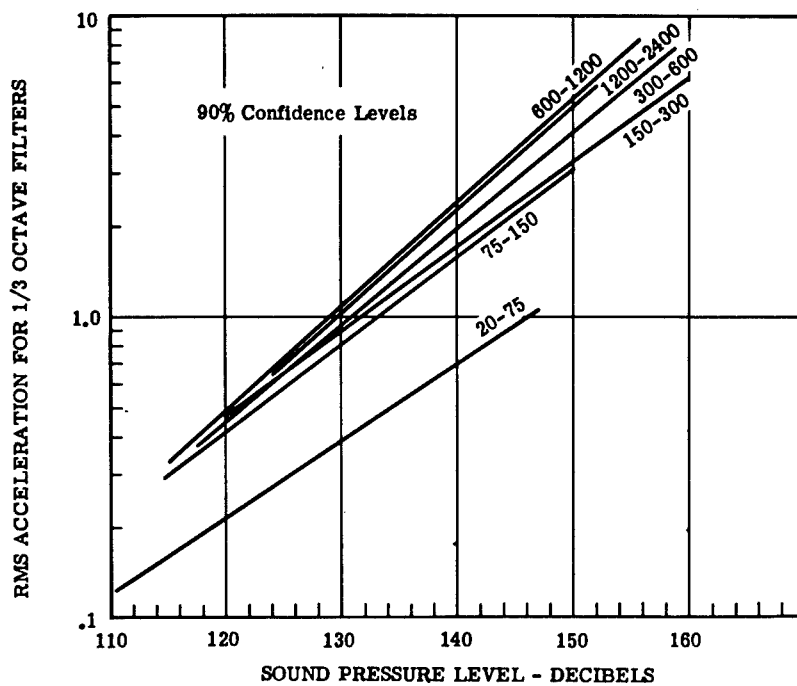


Fig. 3 - Confidence levels (90 percent) for acceleration vs octave band sound pressure levels

reasonable, therefore, to assume a maximum peak-to-rms ratio in the neighborhood of three.

TEST CASE: F-106 COMPARISON

The sound pressure level versus acceleration curves discussed above were developed by using data gathered on the B-58. It is of interest to apply the results to another design for which measured vibration data are available. The F-106 was chosen for this test case because of the aft location of the jet engine and similarity of structural parameters to the F-111.

The vibration prediction procedure may be broken down into the following steps:

1. Determine overall external sound pressure levels.
2. Determine the frequency spectrum of the noise field at selected locations on the airframe.
3. Determine octave band sound pressure levels using the frequency spectrum and the overall sound pressure levels.
4. Use the sound pressure level versus acceleration correlation curves to determine the vibration level in each octave.

To accomplish steps 1 and 2, it is necessary to know certain engine parameters. The F-106 is powered by a J-75 turbojet with a thrust rating of 16,000 pounds at military power and 24,500 pounds at maximum afterburner. The sea-level-static exhaust velocity in afterburner is approximately 2800 feet per second. The

reference sound pressure level contour lines² are then adjusted for the exhaust velocity and nozzle diameter of the J-75 engine, and the overall external sound pressure level contours are obtained. These are shown in Fig. 4 for the F-106 fuselage. In this case, the sound pressure levels were derived by using the North American Aviation procedure for estimating near field noise levels.³

The next step is to determine the frequency spectrum in the area of measured data. This is accomplished by adjusting the given frequency spectra data³ for the exhaust velocity and nozzle diameter of the J-75 engine. Figure 5 shows the resulting frequency spectra curves for two locations on the F-106.

At this point, it is necessary to decide what confidence level from the correlation curves will be used. Since this is a test case, both the 80- and 90-percent confidence levels shown in Figs. 2 and 3 are investigated.

The acceleration levels are then estimated by using the sound pressure level at the mid-frequency of the octaves in Fig. 5 with the appropriate curves in Figs. 2 and 3. The predicted vibration levels thus obtained are shown in Fig. 6 as an envelope in each octave for both the 80- and 90-percent confidence levels. Vibration levels measured on the F-106 during 23 flights, including ground afterburner operation,

²P. A. Franken and E. M. Kerwin, "Method of Flight Vehicle Noise Prediction," WADC Tech. Rep. 58-343, Vol. I (Nov. 1958).

³"Establishment of the Approach to, and Development of, Interim Design Criteria for Sonic Fatigue," ASD-TDR-62-26 (June 1962).

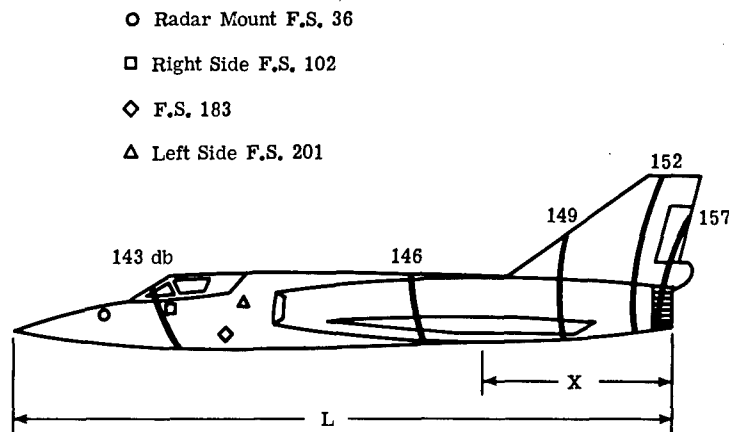


Fig. 4 - Predicted sound pressure level contours for the F-106

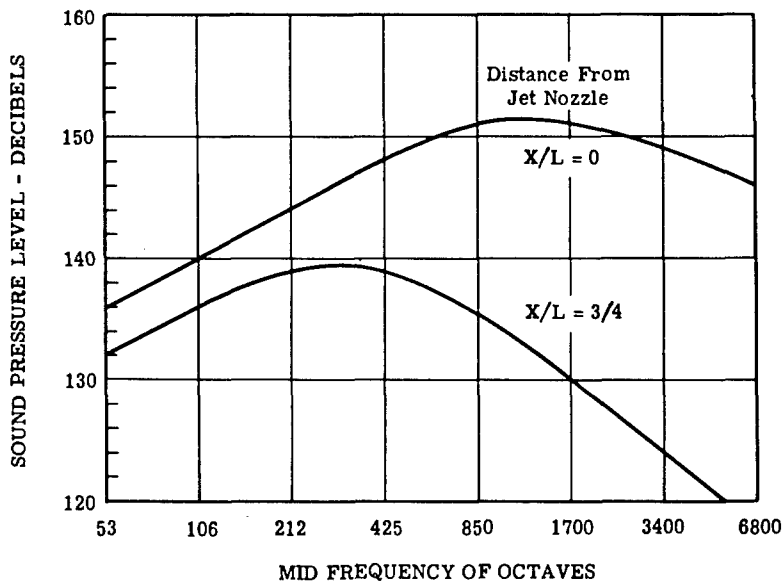


Fig. 5 - Frequency spectra for J-75 exhaust noise on the F-106

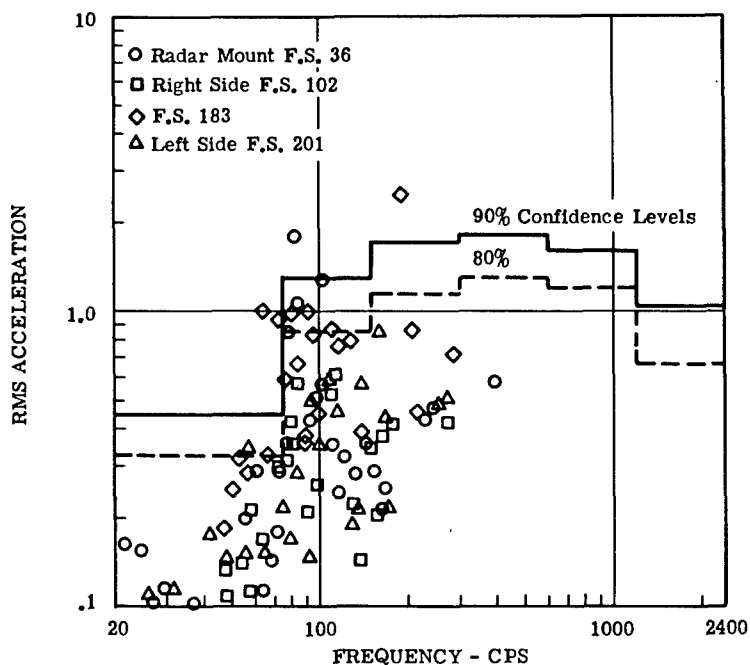


Fig. 6 - Comparison of predicted vibration envelope with measured vibration data in the F-106 forward electronics compartment

are plotted along with the predicted vibration envelope. The locations of the transducers from which the test data were obtained are illustrated in Fig. 4.

An interesting observation from Fig. 6 is that the B-58 correlation predicts more energy at the high frequency end than appears to be present in the F-106 data. This is possibly due to the wider filter bands used in reducing the B-58 data. Actually, there were some high frequency vibration levels recorded on the F-106. They were considered too low, however, to be of consequence and no data above 500 cps were included in the tabulated data available at this time.

It is concluded that the correlation procedure does a good job of estimating the F-106 vibration levels in the lower octaves and is overly conservative in the higher octaves.

PREDICTION OF F-111 VIBRATION LEVELS

The procedure for predicting the F-111 vibration environment is similar to the procedure outlined above for the F-106. At this stage, it would be nice to have measured noise data for the engine to be used. This is very seldom available, however, and the noise levels must be predicted from engine performance data. In this case, two methods for predicting the engine noise levels were investigated. These are discussed below.

Engine Noise Prediction

The sound pressure levels predicted in the F-111 proposal used the Bolt, Beranek, and Newman method.² This method uses the known

sound pressure level contours of a reference engine operating at military power. The contours are adjusted to alternate engine characteristics depending upon the exhaust velocity, nozzle diameter, thrust, and afterburner operation. The shape of the frequency spectrum is given for several locations down-stream of the jet exhaust nozzle.

In Ref. 3, published since the F-111 proposal work, North American Aviation has a slightly different approach for predicting the acoustic noise levels. Instead of using the exhaust velocity to the eighth power in calculating the change in sound pressure level contours, this method varies the velocity term, $10 \log (V/V_{ref})^n$, as a function of location relative to the exhaust nozzle. The value of n varies from $n = 4$ aft of the nozzle to $n = 7$ forward of the nozzle. A comparison of the overall sound pressure levels for the two methods is shown in Fig. 7. The NAA method predicts a 4- to 6-db higher level than the BB&N method for a low velocity jet exhaust.

The frequency spectra predicted by the two methods also changes. Figure 8 shows a comparison of the shape of the frequency spectra for three locations on the F-111. It can be seen that the spectrum sound pressure levels are higher (for a given overall level) in the low frequency region for the BB&N procedure at the aft end of the airplane. This is due to the lower velocity (military power) used in the procedure and shifting the spectrum one-half octave lower for afterburner operation. The NAA procedure uses the afterburner velocity. The frequency spectrum forward of the exhaust is not too different at low frequencies, but the BB&N procedure predicts much higher spectrum levels at the higher frequencies. The shaded area in Fig. 8 shows the range of values for the two methods near the exhaust plane.

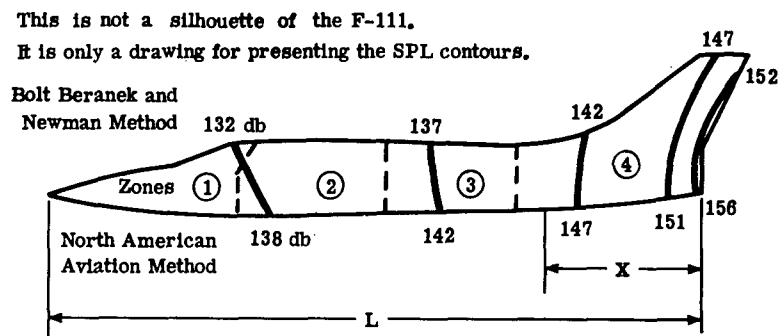


Fig. 7 - Comparison of sound pressure level contours in the F-111

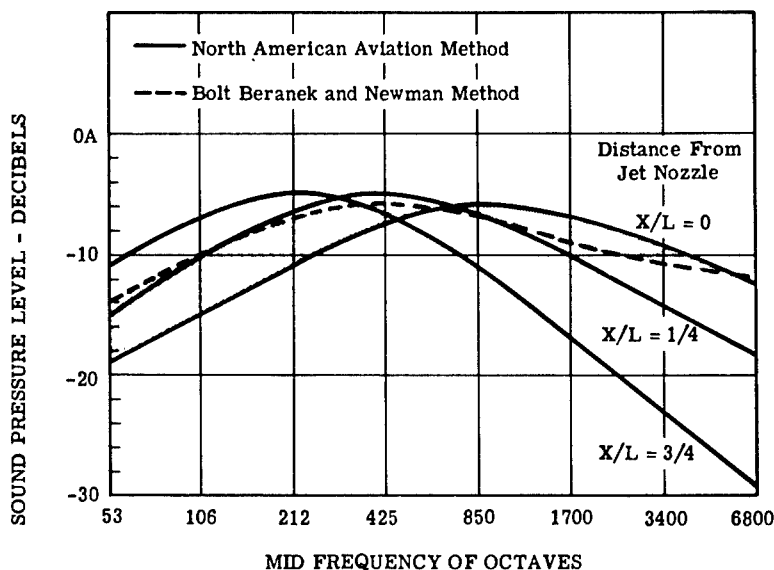


Fig. 8 - Frequency spectra of jet noise in the near field for the F-111

It is difficult to say which procedure is more accurate, particularly for afterburning fan engines. This unknown will be resolved only when measured data are available for the TF-30 fan engine.

Vibration Prediction

Early in the F-111 proposal stage, the vibration levels were estimated for a high exhaust velocity engine using the 80-percent confidence curves. Later in the proposal the engines were changed to lower exhaust velocity fan engines. Standard prediction methods indicate a 7-db decrease in the overall sound pressure levels for the fan engine. Little is known, however, about the noise characteristics of afterburning fan engines at this time. It is expected that the method used to mix the primary and secondary air will have considerable effect. Because of these unknown factors, the 7 db were left in the vibration predictions as an added margin of safety. A 7-db increase in sound pressure level will increase the vibration levels by a factor of approximately 1.7 when using the 80-percent confidence curves. On this basis, the predicted vibration levels for four fuselage zones are shown in Fig. 9.

As an added check on the predicted vibration levels following publication of Ref. 2, both methods for predicting the noise levels were used along with the 80-percent confidence correlation curves. The comparative results are shown in Fig. 10 for the forward and aft fuselage

zones. It is seen that the NAA engine noise prediction procedure leads to higher predicted vibration levels except in the highest frequency band in the forward zone. (The 7 db discussed in the preceding paragraph, however, adequately covers the NAA case too.) It is interesting also to note the change in the shape of the frequency spectrum from forward to aft zones seen in the curves for the NAA procedure. This follows, of course, from the spectrum shapes shown in Fig. 8.

As a result of this comparison, and based on the information available at this time, we recommend using the NAA method for near field engine noise prediction along with the 80-percent confidence level curves for estimating vibration levels.

Other Sources of Vibratory Energy

A good summary of major sources of vibratory energy and their relative importance in missiles and space vehicles has been prepared by Eldred and Roberts.⁴ Of these sources, those considered of most importance to the F-111 program are:

1. Boundary layer turbulence,
2. Cavity Resonance,
3. Fluctuating wake drag,

⁴K. Eldred, W. Roberts and R. W. White, "Structural Vibration in Space Vehicles," WADD Tech. Rep. 61-62 (Mar. 1961).

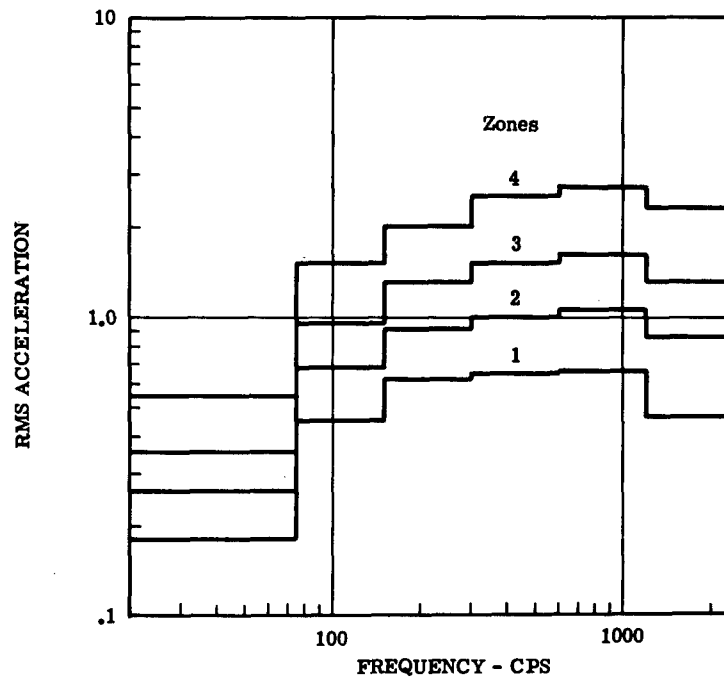


Fig. 9 - Estimated vibration levels using the Bolt, Beranek, and Newman method of acoustic prediction plus 7 db

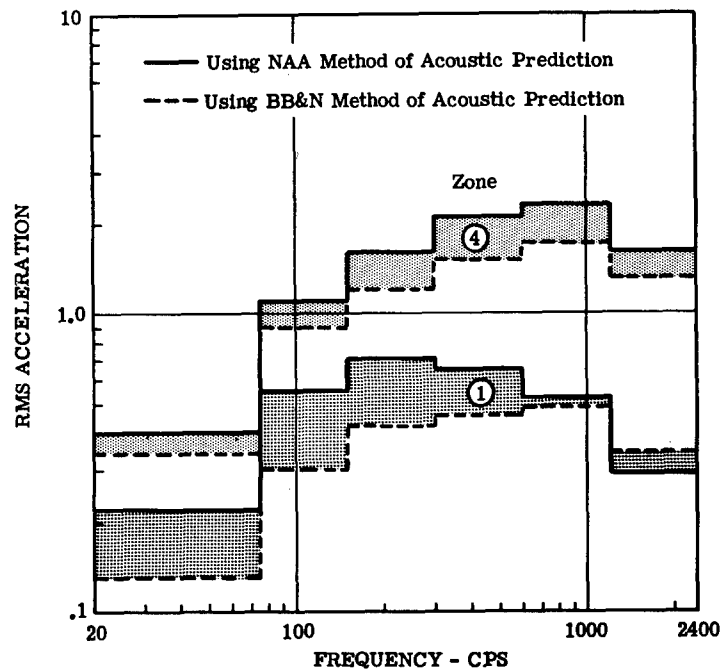


Fig. 10 - Comparison of estimated vibration levels in forward and aft zones of the F-111

4. Oscillating shock waves,
5. Buffet and other flow separations, and
6. Mechanical equipment unbalance.

The fluctuating pressure on the skin of a vehicle from the turbulent boundary layer is one of the most important aerodynamic sources of vibration. Some of the other aerodynamic sources can cause more severe vibration, but none occur for such a long period of time as does the boundary layer excitation. The generally accepted level of the rms fluctuating pressure is about 0.006 times the free stream dynamic pressure at subsonic Mach numbers. At supersonic Mach numbers, the ratio of boundary layer pressure to dynamic pressure seems to decrease as Mach number increases. Some investigators give a value of 0.003 times the free stream dynamic pressure at Mach 2.

Measured B-58 in-flight sound pressure levels and associated vibration levels were used as a guide in predicting problem areas on the F-111. Flush mounted external microphone data were recorded on the forward fuselage as shown in Fig. 11. Internal microphone data were also recorded at several locations.

The levels of pressure measured on the forward fuselage during subsonic flight are proportional to the free stream dynamic pressure as previously found by other investigators.

The ratio of overall rms pressure to q , however, is 0.009 which is somewhat higher than usually found. The reason why these readings are higher is not definitely known. One reason could be because the dynamic pressure at the microphone location is considerably higher than the free stream value. In any case, using this ratio should be conservative.

Pressure levels were also recorded during supersonic flight up to Mach 2. The sound pressure levels decreased with increasing Mach numbers, however, which is not consistent with some other investigations. It may be that the frequency spectrum shifts upward to a range not adequately covered by the instrumentation system, thus giving erroneous readings. There certainly is a need for additional investigations of external noise levels during flight, particularly at supersonic speeds.

An additional external microphone was installed on the lower surface of the wing inboard of the inboard engine exhaust nozzle. It was found, however, that engine noise overshadowed the boundary layer noise except during very high speed flight. This was substantiated by accelerometers located in the same region. The accelerometer data were directly related to engine power settings with very little indication that dynamic pressure caused any significant vibration.

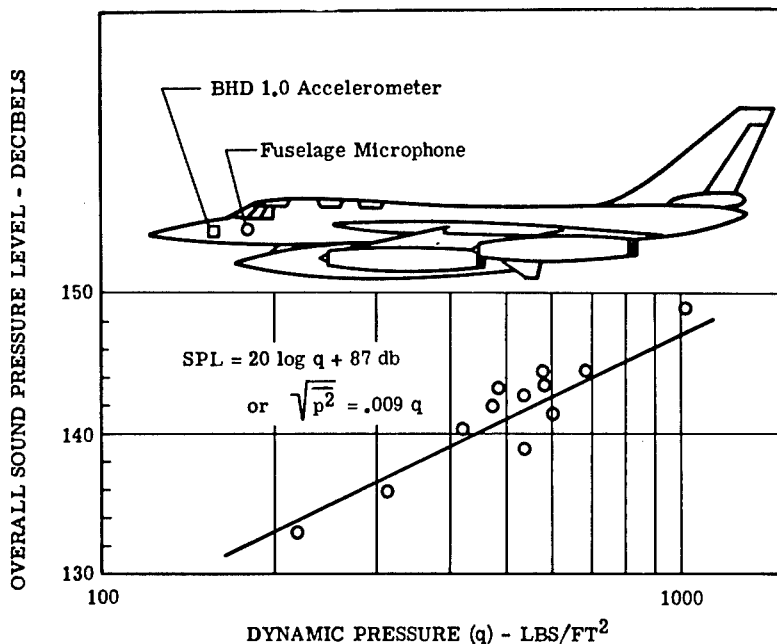


Fig. 11 - Overall sound pressure levels from aerodynamic turbulence on the B-58

The data from these microphones gave an indication of what to expect on the F-111 during high performance flight conditions. Aerodynamic noise levels at the aft end of the fuselage near the exhaust nozzles will exceed the engine exhaust noise only at very high dynamic pressures. These high dynamic pressures are associated with high speed flight which produces a shift in the acoustic energy to the high frequency range where structural resonances tend to be less significant.

The situation is different, however, in the forward fuselage area. Here, the overall sound pressure levels will be higher in flight than on the ground. This is illustrated in Fig. 12 from B-58 measured data. The sound pressure levels increase as engine power is increased from military to maximum afterburner, and then remain substantially constant during the takeoff roll up to the point of airplane rotation. At this point, an increase is obtained due to reflections of the jet exhaust from the runway. A decrease is noted immediately after lift-off. As the equivalent airspeed increases during the climb out, the sound pressure level due to boundary layer excitation begins to increase and soon becomes the major source of acoustic energy.

The vibratory levels, however, do not increase as the boundary layer noise levels increase. This is a very important point. The event-time-history of the output of an accelerometer located in the vicinity of the microphone is shown in Fig. 13. The vibration levels during ground engine run and takeoff are higher than

those obtained in flight, even though the overall sound pressure levels in flight are as much as 14 db higher than the ground levels.

This same phenomenon was found by British investigators⁵ for surface pressures and structural strains from a turbulent boundary layer. This investigation for their supersonic transport program indicates the overall strain due to boundary layer excitation was one-third to one-fifth that occurring when the panel was excited by jet noise of the same overall sound pressure level.

There are likely several factors which cause the difference in structural response to jet engine noise and boundary layer turbulence. Probably one of the most important is that the spatial correlation for boundary layer excitation is much less than for jet engine noise. The turbulent boundary layer is an assortment of randomly sized eddies or vortices which flow past a skin panel. The individual eddies lose their identity in a relatively short distance as a result of interaction with the skin or with other eddies. Therefore, the pressure fluctuations associated with these eddies are correlated for only short distances. These distances are much smaller for boundary layer excitation

⁵D. R. B. Webb, A. R. Keeler, and G. R. Allen, "Surface Pressure and Structural Strains Resulting from Fluctuations in the Turbulent Boundary Layer of a Fairey Delta 2 Aircraft," Ministry of Aviation, C. P. No. 638 (May 1962).

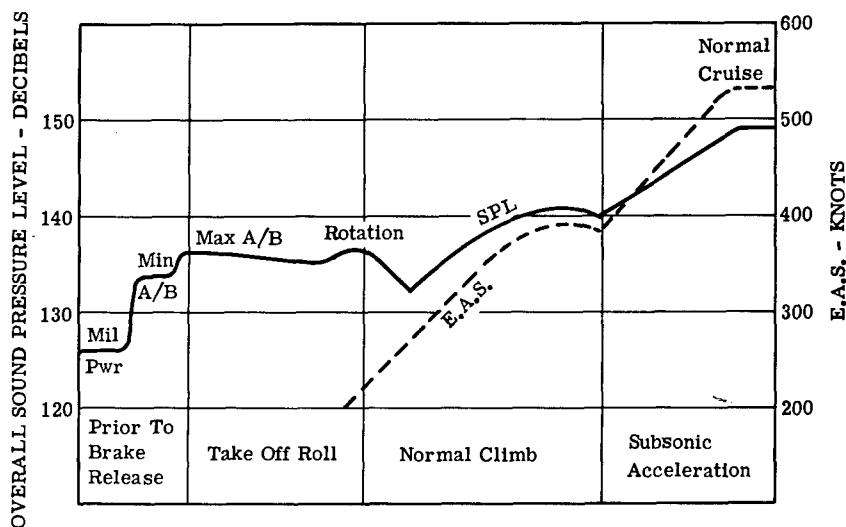


Fig. 12 - Event-time-history for external microphone forward of the jet exhaust on the B-58

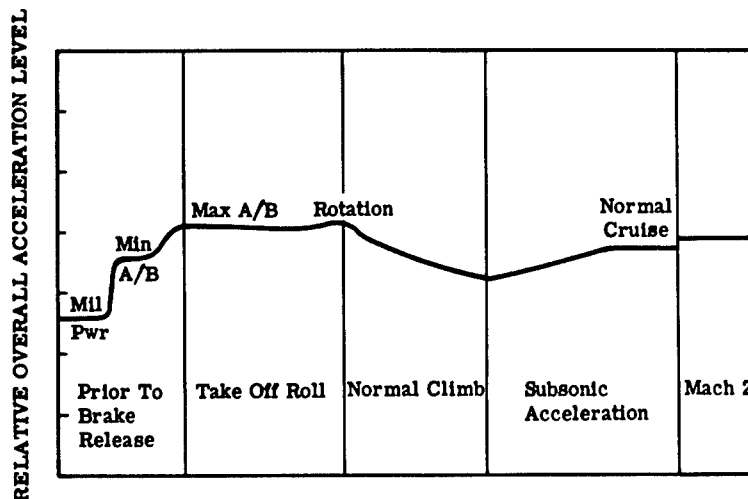


Fig. 13 - Event-time-history for BHD 1.0 accelerometer on the B-58

than those associated with jet exhaust acoustic pressures of similar frequency. With the pressure uncorrelated in flight, there is less excitation of the skin panels and less vibration is fed into the vehicle structure.

Perhaps an equally important reason for the reduction in response going from jet noise to boundary layer excitation is the shift in energy to higher frequencies. The resonances of an elastic structure represent a narrow band response with a transformation of the broad band acoustic input brought about by the filtering action of the structure. If the energy in the excitation source is largely at frequencies above the structural resonances, then the response will not be as large even though the total excitation energy may be greater.

It is concluded that even though the boundary layer noise levels will exceed the static engine noise levels for portions of the airframe, it is still reasonable to use the engine noise levels for vibration prediction due to the greater structural response obtained from this source.

The other aerodynamic sources outlined earlier are known problem areas on other aircraft. Opening the weapon bay doors can produce cavity resonances with sound pressure levels 20 db higher than the boundary layer excitation pressure. The weapon manufacturer for the F-111 is required to run acoustical tests on the weapon to include this effect even though the condition will exist for only short periods of time.

Base pressure fluctuations on speed brakes can produce levels twice as high as the boundary

layer pressure. Flow separation and oscillating shocks have caused failures in other aircraft, particularly in inlet duct structure. The excitation forces from these aerodynamic sources are very difficult to predict. Consequently, we must rely on early measurements to obtain information on these possible problem areas.

IMPROVING NOISE AND VIBRATION CORRELATION PROCEDURE

There is considerable scatter in the data points used to establish the correlation curves. These variations in acceleration level can be attributed partly to sound pressure level, partly to structural mounting points, partly to structural properties (mass, damping, and stiffness) and partly to chance. We should thus be able to assign parts of the total variation to the known factors. Most predictions of any nature can be improved by inclusion of additional parameters that are known to influence the results. We can usually expect to reach a saturation point, however, after which the addition of further information will no longer increase the accuracy of the predictions appreciably.

Several factors which can obviously influence the results (although how much they affect the results is not so obvious) are as follows:

1. Data reduction techniques,
2. Data recording and reduction errors,
3. Structural absorption of the acoustic excitation from the skin to the point of measurement,

4. Location of accelerometer with respect to modal response,
5. Nonlinear response of the structure,
6. Non-uniform structure throughout the vehicle, and
7. Structural transmission of vibration from high external noise level areas to those of lower external noise level.

There have been extensive improvements to data reduction systems since most of the B-58 data were analyzed. Much discussion in the past has been on the subject of constant bandwidth versus constant percentage filtering techniques. The primary argument against constant percentage type of amplitude versus frequency analysis is the lack of sharpness of the filters as compared to the sharp selectivity of the fixed crystal filter in the constant bandwidth analyzer. The selection of the analyzer filter bandwidth is always a compromise between measurement resolution and measurement quality. Some investigators believe that a reasonable criterion for proper resolution might be a filter bandwidth that is one fourth the bandwidth (between half power points) of the narrowest peak in the spectrum to be analyzed. The one-third octave filters used in the correlation procedure certainly would not meet this requirement, although for predicting vibration levels using one-third octaves will give a conservative level. Probably the first approach for improving the correlation would be to use a different type of data reduction system.

Of the other factors listed, probably the non-uniform structure throughout the vehicle will produce more scatter than any other factor. Separating the measurements as to types of structures would be an interesting undertaking.

The vibration prediction procedure cannot be used for in-flight estimations unless all of the noise source is due to the jet engine exhaust. If the excitation forces are a combination of boundary layer noise and jet noise or boundary layer noise alone, then the prediction procedure is not applicable because of the difference in

spatial correlation of the two sources of fluctuating pressure. Additional work needs to be done in this area.

Several investigators have suggested that vibratory response should be directly proportional to a change in pressure. The B-58 data for acoustic and vibration levels presented in Fig. 2, however, show the vibration levels to be proportional to the 0.6 to 0.8 power of pressure depending upon the octave band considered. An interesting conclusion in the strain versus fluctuating pressure investigation of Ref. 5 was that the strain was proportional to the 0.8 power of pressure over the range of 90 to 122 db. This agrees with the B-58 data. Therefore, trying to find reasons for vibratory response being less than pressure to the first power may not be a method of improving the correlation procedure.

CONCLUSIONS AND SUMMARY

The results of the F-106 comparison study indicated that the B-58 vibration prediction procedure can be used successfully on fighter type aircraft.

Two methods of predicting the acoustical environment were investigated to determine the difference in the methods. The North American Aviation procedure³ predicted 4 to 6 db higher acoustic levels than the Bolt, Beranek, and Newman procedure.² The shape of the frequency spectrum was the biggest difference, with more acoustic energy predicted by the NAA method at the lower end of the frequency spectrum for locations forward of the jet exhaust.

Aerodynamic boundary layer excitation measured on the B-58 indicates that vibration levels are lower in flight even though the sound pressure levels are as much as 14 db higher in flight than on the ground. The difference in vibratory response is attributed to the lack of spatial correlation of boundary layer pressure compared to jet exhaust noise on the ground and the shift of acoustical energy to the high frequency range where structural resonances are not as significant.

DISCUSSION

Dr. Burgess (United Technology Corporation): There seems to be a correlation between the acceleration level and what amounts to the mechanical impedance of the structure for which

you are making this correlation. Is there anything in the paper that you reference which can shed light on this correlation and its effect on the procedure you have described?

Mr. Mitchell: I am not sure that I understood your question. You mentioned that there seems to be an effect of the mechanical impedance?

Dr. Burgess: The impression I get from your paper is that it is restricted to aircraft structures. A specific example of a structure to which it would not apply would be, I believe, the Titan III solid motors where the skins are of the order of 1/4-inch thick and of solid steel. In this case there appears to be little correlation

between the acoustic environment and the experienced vibration level.

Mr. Mitchell: Yes, I think you are right. One point I do make in the paper that I possibly didn't bring out is that you would have to have a similar type of structure. There is another section in the paper regarding possible ways to improve this procedure which I felt that I didn't have enough time to go into in this oral presentation.

* * *

COMPARISON OF PRE-LAUNCH AND FLIGHT VIBRATION MEASUREMENTS ON THOR VEHICLES

S. A. Clevenson
Langley Research Center

and

W. B. Tereniak
Goddard Space Flight Center

A comparison of flight data for various nose fairings is presented. Results of a vibration survey on the forward equipment compartment of a Thor are compared with flight data, and the flight results are compared with payload environmental test specifications.

INTRODUCTION

One of the many obstacles that a spacecraft must overcome in order to operate successfully in space is the severe environment imposed during the launch and powered-flight phases. To assure that the spacecraft is capable of surviving such environments, it is subjected to extensive environmental testing. In order to establish adequate environmental simulation criteria, flight data must be obtained. Flight shock and vibration data were obtained during two suborbital flights of ECHO A-12 in which modified Thor launch vehicles were used (Fig. 1). Prior to the launching of the second vehicle, a vibration survey of the forward equipment compartment housing the flight vibration transducers was made while the Thor was on the launch pad at Cape Canaveral.

The purpose of this paper is to present measured flight data and to compare these data with measurements obtained during a vibration survey of the equipment compartment of a Thor launch vehicle. These data will also be compared to pre-flight environmental acceptance test specifications. The paper will be concluded with a discussion of flight data showing the effect of nose fairing shapes.

DESCRIPTION OF LAUNCH VEHICLE

Figure 2 shows a cutaway view of the launch vehicle used for the suborbital firings of the

ECHO A-12 passive communications satellite. These vehicles are designated AVT-1 and 2. The main booster was a modified DM-21 Thor missile. Mounted above the Thor forward compartment was the spacecraft equipment compartment to which the spacecraft adapter was secured. The spacecraft, in turn, was secured to the adapter with a marman clamp held together with explosive bolts. Three piezoelectric vibration accelerometers (transducers) were mounted at the base of the adapter on the outer ring stiffener of the equipment compartment (Fig. 3). The vibration system incorporated channels 13, A, and C of PDM/FM/FM (pulse duration modulation, frequency modulation, frequency modulation) telemeter to indicate accelerations along the yaw, pitch, and longitudinal axes, respectively. Additional information pertaining to the instrumentation may be found in Ref. 1.

OVERALL VIBRATION LEVELS

Figure 4 indicates how closely the overall rms vibratory levels measured on AVT-2 compare with those measured on AVT-1. The levels for the accelerations measured on AVT-1 and AVT-2 are given as one curve for the pitch axis and one curve for the yaw axis, since there was less than 10-percent difference in

¹W. B. Tereniak and S. A. Clevenson, "Flight Shock and Vibration Data of the ECHO A-12 Application Vertical Tests (AVT-1 and AVT-2)," NASA TN D-1908 (1963).

level between the two flights. The accelerations in the longitudinal direction closely agree except for the clipped region of AVT-1. Clipping of instantaneous peaks occurred during the flight time interval of 33 to 43 seconds of AVT-1. Time T is referred to ignition time of the

vehicle. During the AVT-1 flight there were two periods of radio-frequency signal dropout where no data were received; AVT-2 experienced no such dropouts. It is significant that at AVT-2 liftoff ($T = 2$ seconds) the value of acceleration measured on the longitudinal axis

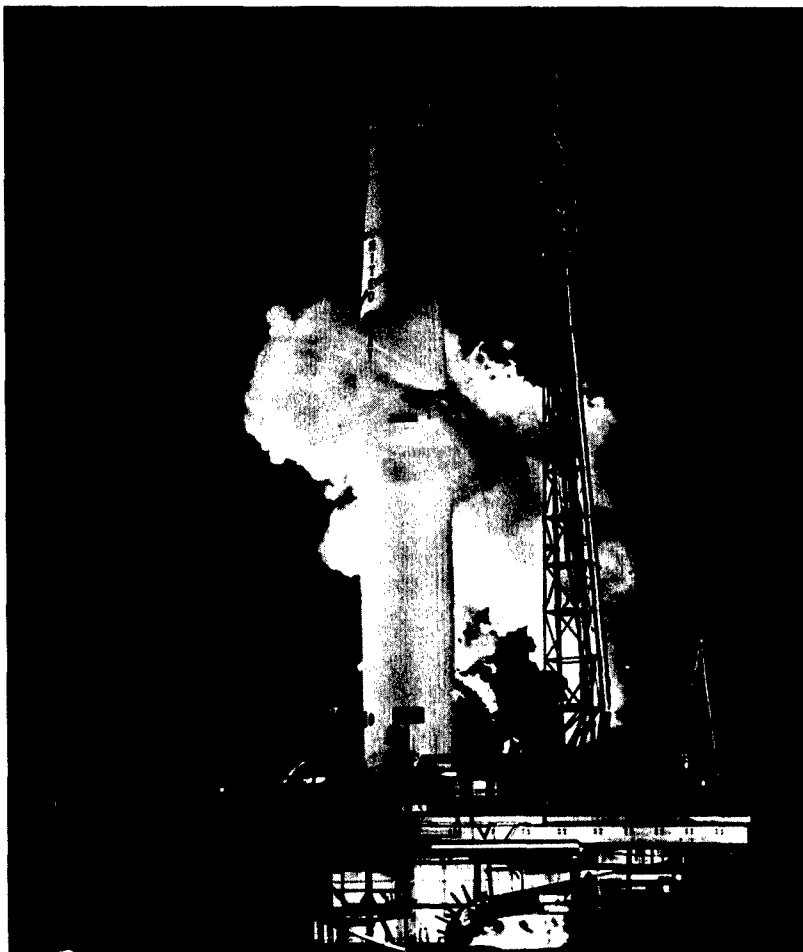


Fig. 1 - AVT vehicle on launch pad at AMR

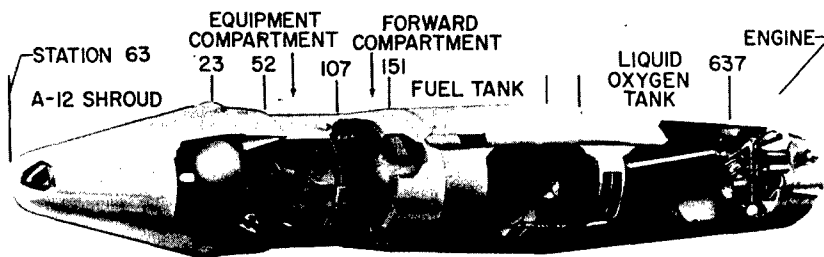


Fig. 2 - Cutaway view of AVT vehicle

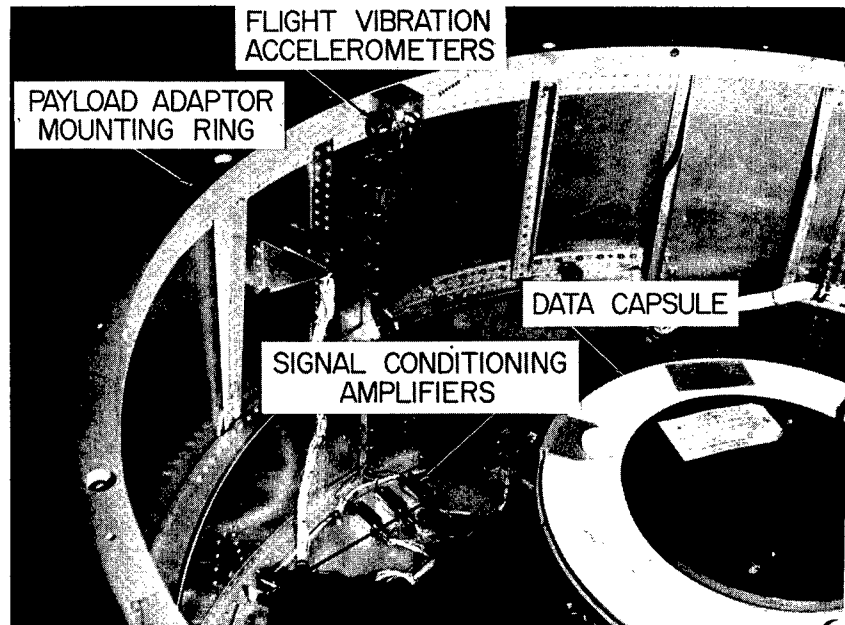


Fig. 3 - Instrumentation in equipment compartment

was 2.2 g-rms, whereas at approximately Mach 1 (T = 39 seconds) the acceleration level was 9.4 g-rms. The measured vibration level of 9.4 g-rms is somewhat greater than that indicated by previous measurements made in the forward compartment during flights of the Thor

booster. A comparison of AVT-1, AVT-2, and previous Thor flight data, at the main event times, is given in Table 1. A sketch showing the transducer locations and comparing the nose shapes of the AVT Thor with previous Thor's is shown in Fig. 5.

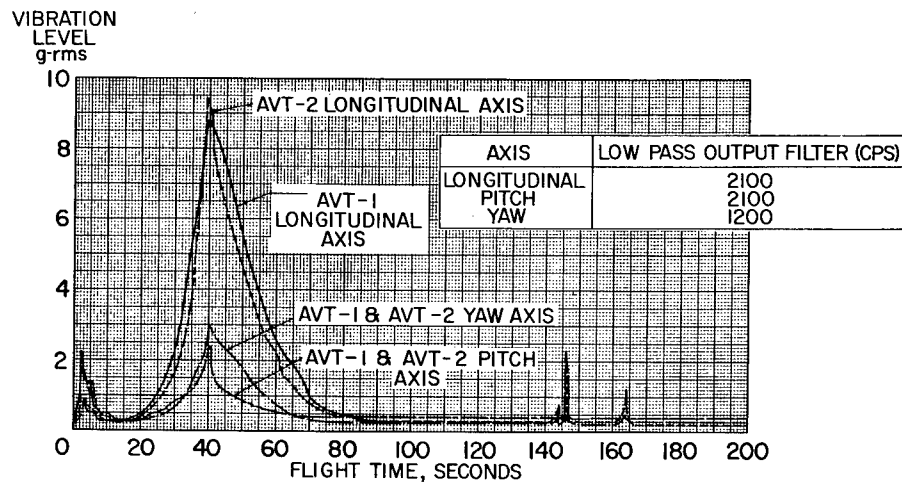


Fig. 4 - Overall in-flight vibrations, AVT-1 and 2

TABLE 1
Comparison of AVT-1, AVT-2, and Thor Flight Data at Main Event Times
[Vibration Level, g-rms]

Event	AVT-1 ^a		AVT-2 ^a		Previous Thor data ^b	
	Longitudinal axis	Pitch axis	Longitudinal axis	Pitch axis	Longitudinal axis	Pitch axis
Main engine ignition	1.8	0.93	2.2	0.8	1.7	3.7
Mach 1	8.8 ^c	3.2	9.4	3.0	-	-
Maximum dynamic pressure	3.5	1.6	4.7	1.6	1.7	3.2
Main engine cutoff	0.35	0.45	0.95	0.47	-	0.5

^aAVT low-pass output filters at 2.1 kc.

^bBandwidth unknown.

^cSignal clipped and level not considered valid.

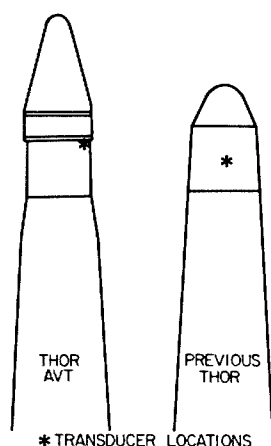


Fig. 5 - Comparison of AVT and previous Thor nose shapes and locations of the vibration transducers

Differences in flight-measured vibration levels between AVT and previous Thor flights may be accounted for by differences in transducer location, mass loading, and stiffness of the mounting structure, and by differences in the thrust output of the Thor booster (AVT-1 and AVT-2 had 10-percent greater thrust than previous Thor boosters). In general, the previous low values of measured vibration levels were obtained from transducers located on the central bulkhead in the Thor forward compartment, whereas on AVT-1 and AVT-2 the transducers were located on the inner circumference of the structural attach ring at the top of the spacecraft equipment compartment (see Fig. 3).

RANDOM VIBRATIONS

As shown in Fig. 4, the overall rms vibration level begins to build up again at about $T = 20$ seconds and reaches a peak at $T = 39$ seconds, at a level of 9.4 g-rms for AVT-2. This buildup in level, which occurs in the transonic region of flight, is attributed to the random excitation caused by aerodynamic buffeting.

Figure 6 shows a power spectral density (PSD) plot for the accelerations in the longitudinal direction using a 20-cps bandwidth filter at $T = 39$ seconds (Mach number ≈ 1). It is interesting to note that the predominant frequencies measured correspond to frequencies determined from transients occurring at lift-off, main engine cutoff, fairing separation, and spacecraft separation. The high PSD level ($0.488 \text{ g}^2/\text{cps}$) measured at 1030 cps is significant. The equivalent g-rms level in the region from 940 to 1120 cps is 6.62 g-rms, whereas the overall level at this time was 9.4 g-rms.

SHOCK OR TRANSIENT RESPONSE

The composite records indicated the vibrations excited by lift-off, MECO (Main Engine Cutoff), fairing separation, and spacecraft separation. These vibrations are short in duration and relatively high in level. Overall levels measured during fairing separation and

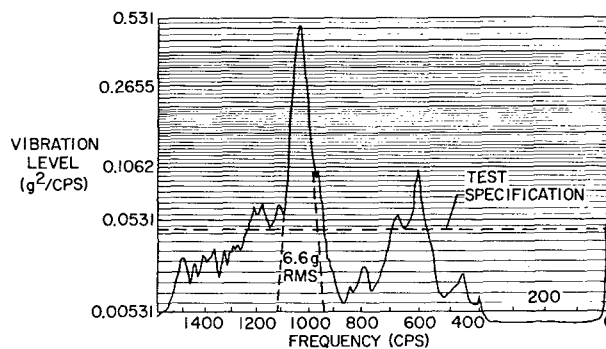


Fig. 6 - PSD of longitudinal vibration at $M = 1$ ($t = 38-40$ sec). Filter bandwidth - 20 cps, RC averaging time - 1 sec, sample length - 2 sec

spacecraft separation are beyond the optimum signal range of the measuring channels. These signals are in the nonlinear range of the system and may have been clipped by the limiter circuit in the charge amplifier. However, it was felt that a spectral analysis of these data would be enlightening.

A tabulation of the results of the qualitative analysis performed on the vibrations excited by the above-mentioned events of both flights is given in Tables 2 and 3. The data were analyzed by re-recording a continuous 1-second loop that included the transient vibration, and were then played back into a spectral wave analyzer that employed a 20-cps bandwidth filter. The levels presented are relative, since the time duration of the vibration signal was considerably shorter than the analyzer RC averaging time (1 second) used. The tables summarizing the predominant frequencies indicate that as a result of shocklike excitation certain resonant frequencies are excited. At lift-off these frequencies are excited by both shocklike and acoustic excitations. It is noteworthy that the frequencies are similar in value for these events. This similarity indicates that the high frequencies (greater than 200 cps) are due to a more localized response, that is, from the Thor spacecraft equipment compartment, and are not indicative of the response of the entire vehicle. The previous statement is based on the fact that the mass varies during powered flight and, in turn, varies the vibratory modes of the vehicle.

Figure 7 shows the predominant transient frequencies at lift-off for three Thor vehicles. A narrow band filter was used to obtain the response as a function of time. The upper sketch indicates the transient for the AVT

flights at 17 cps. The center sketch (Ref. 2) shows the filtered transient for the Thor-Delta vehicle at 16 cps. The bottom sketch (obtained from unpublished data by J. Nagy, GSFC, NASA) shows the filtered transient response for the Thor-Agena at 18 cps. It may be noted that ground resonance tests by Douglas Aircraft Company have indicated a resonance of the rocket engine on its hydraulic control actuators at about 17 cps. The data show that substantial vibrations at a frequency approximately equal

²L. A. Williams, "Flight Vibration Data from the Delta 9 Launch Vehicle," NASA TN D-1683 (1963).

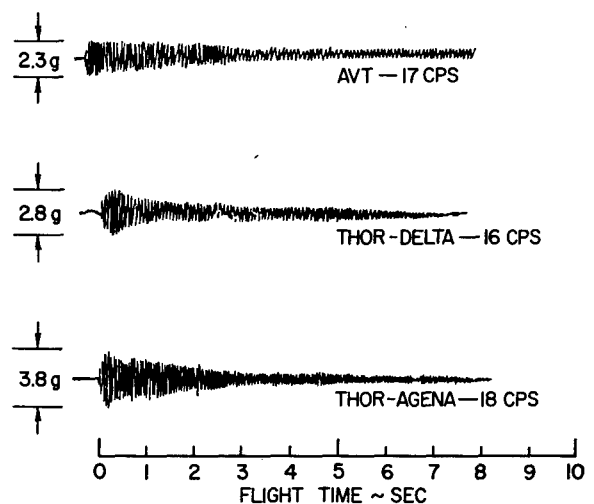


Fig. 7 - Discrete frequencies measured at lift-off on the AVT, Thor-Delta, and Thor-Agena vehicles. Narrow bandpass filters used

TABLE 2
Summary of Predominant High Frequencies and Relative Vibratory Levels Measured on the
AVT-1 and AVT-2 Principal Axes^a

Liftoff				Main Engine Cutoff				Fairing Separation				Spacecraft Separation			
AVT-1		AVT-2		AVT-1		AVT-2		AVT-1		AVT-2		AVT-1		AVT-2	
Freq. (cps)	Level	Freq. (cps)	Level	Freq. (cps)	Level	Freq. (cps)	Level	Freq. (cps)	Level	Freq. (cps)	Level	Freq. (cps)	Level	Freq. (cps)	Level
Longitudinal Axis															
130	0.05	130	0.09	170	0.02	140	0.13	-	-	-	-	-	-	-	-
-	-	-	-	230	0.02	280	0.04	225	0.04	230	0.15	-	-	-	-
300	.05	330	.09	330	.02	340	.04	-	-	350	.19	-	-	350	0.10
430	.08	430	.32	380	.04	400	.03	420	.04	420	.24	410	0.08	440	.12
510	.12	-	-	480	.01	500	.02	-	-	480	.30	-	-	520	.12
585	.15	580	.49	570	.01	-	-	575	.11	570	.58	580	.08	580	.11
-	-	640	.60	620	.02	-	-	-	-	650	.33	-	-	670	.48
-	-	680	.51	700	.02	-	-	-	-	-	-	710	.13	-	-
760	.10	780	.41	750	.01	-	-	770	.08	780	.43	790	.23	-	-
-	-	-	-	800	.03	800	.01	-	-	-	-	-	-	800	.36
-	-	830	.35	850	.02	-	-	-	-	850	.52	840	.25	850	.48
890	.15	-	-	920	.02	-	-	910	.05	-	-	-	-	-	-
970	.11	960	.43	990	.01	950	.01	-	-	960	.86	-	-	-	-
1070	.19	1030	.57	-	-	1040	.01	1060	.09	1020	.24	1060	.26	1010	.55
1200	.11	1160	.31	1190	.40	-	-	1170	.04	1120	.29	-	-	-	-
-	-	1260	.25	-	-	1240	.01	1270	.04	-	-	1280	.09	1220	.26
1320	.09	1340	.16	1350	.01	-	-	-	-	-	-	1310	.09	1340	.21
1420	.08	-	-	-	-	-	-	1400	.08	1450	.22	1420	.09	-	-
-	-	1490	.27	-	-	-	-	1510	.05	-	-	1500	.09	1490	.14
1580	.07	1600	.05	-	-	-	-	-	-	-	-	-	-	-	-
1710	.04	1700	.05	-	-	-	-	-	-	1700	.11	-	-	-	-
-	-	1780	.10	-	-	-	-	1800	.02	-	-	1770	.06	1800	.07
Pitch Axis															
-	-	-	-	-	-	110	0.08	-	-	-	-	133	0.12	110	0.12
-	-	-	-	180	0.05	150	.07	-	-	-	-	-	-	170	.11
200	0.06	210	0.08	-	-	210	.05	220	0.20	220	0.22	210	.11	-	-
240	.09	260	.16	-	-	280	.03	-	-	260	.28	-	-	260	.08
310	.06	340	.10	330	.04	330	.07	340	.08	-	-	-	-	310	.09
-	-	-	-	380	.03	-	-	390	.10	360	.14	-	-	-	-
460	.09	470	.12	470	.02	-	-	440	.13	440	.10	440	.07	440	.09
-	-	540	.11	-	-	500	.02	550	.08	-	-	-	-	520	.05
-	-	-	-	580	.02	-	-	-	-	600	.17	-	-	620	.09
650	.06	640	.04	-	-	680	.01	-	-	650	.15	650	.08	650	.07
-	-	700	.09	-	-	-	-	-	-	-	-	-	-	-	-
-	-	-	-	740	.03	-	-	-	-	-	-	-	-	740	.04
-	-	790	.04	-	-	800	.01	780	.10	780	.14	810	.08	820	.11
830	.05	860	.10	860	.03	-	-	920	.09	-	-	-	-	-	-
900	.05	-	-	-	-	-	-	-	-	-	-	-	-	-	-
980	.04	970	.08	960	.04	-	-	-	-	-	-	990	.07	1000	.05
1050	.04	1030	.07	1030	.04	-	-	1060	.08	1030	.01	1060	.07	-	-
1100	.03	-	-	1080	.04	1100	.01	-	-	1100	.23	-	-	1100	.10
-	-	1160	.07	1170	.09	-	-	-	-	-	-	-	-	-	-
-	-	-	-	1210	.05	-	-	-	-	-	-	-	-	1220	.06
1290	.04	1260	.07	1205	.05	-	-	1260	.07	-	-	-	-	-	-
-	-	-	-	-	-	-	-	1340	.08	1370	.19	1350	.07	1340	.06
1440	.03	-	-	-	-	1470	.02	1500	.06	-	-	1480	.05	1460	.05
1650	.03	-	-	-	-	-	-	1680	.06	1650	.12	1640	.06	1650	.06
-	-	1810	.04	-	-	1880	.02	1800	.05	1850	.06	1830	.05	1850	.04
Yaw Axis															
-	-	130	0.05	-	-	140	0.04	170	0.17	-	-	140	0.12	130	0.18
220	0.12	-	-	180	0.09	200	.03	210	.39	-	-	200	.12	-	-
260	.10	230	.13	-	-	-	-	-	-	250	0.04	250	.07	250	.18
-	-	300	.14	-	-	270	.02	280	.08	-	-	280	.07	-	-
-	-	350	.18	330	.11	330	.05	320	.09	340	.03	320	.05	340	.24
-	-	-	-	-	-	-	-	420	.14	420	.03	410	.04	430	.12
440	.09	-	-	450	.06	-	-	450	.08	460	.02	-	-	-	-
490	.07	480	.12	500	.08	-	-	-	-	530	.02	520	.04	-	-
-	-	600	.10	620	.09	600	.01	560	.05	600	.02	-	-	620	.09
650	.05	-	-	680	.09	-	-	-	-	670	.02	650	.04	670	.10
780	.05	770	.07	750	.10	-	-	770	.06	-	-	-	-	780	.06
820	.05	-	-	-	-	800	.01	-	-	800	.01	810	.03	-	-
-	-	840	.07	850	.12	-	-	830	.05	850	.02	850	.03	-	-
980	.04	-	-	950	.12	-	-	-	-	-	-	-	-	-	-
-	-	1000	.04	1000	.10	-	-	-	-	-	-	-	-	-	-
1040	.03	1080	.03	-	-	1070	.01	-	-	1030	.01	-	-	1030	.04
-	-	-	-	1120	.10	-	-	-	-	-	-	-	-	-	-
-	-	-	-	1160	.19	-	-	-	-	-	-	-	-	-	-
-	-	1270	.02	1280	.08	-	-	-	-	-	-	-	-	1280	.02
-	-	1380	.01	1390	.07	-	-	-	-	-	-	-	-	-	-
-	-	1740	.01	-	-	-	-	-	-	-	-	-	-	-	-

^aAll levels are relative; analysis filter bandwidth, 20 cps.

TABLE 3
Summary of AVT Low Frequencies at Their Maximum Level

Longitudinal Axis				Pitch Axis				Yaw Axis ^a			
AVT-1		AVT-2		AVT-1		AVT-2		AVT-1		AVT-2	
Freq. (cps)	Level (g-pk)	Freq. (cps)	Level (g-pk)	Freq. (cps)	Level (g-pk)	Freq. (cps)	Level (g-pk)	Freq. (cps)	Level (g-pk)	Freq. (cps)	Level (g-pk)
Liftoff											
17	1.8	17	1.0	8	0.70	8	0.5	11	1.4	11	1.1
22	2.0	-	-	-	-	9	.80	22	.70	-	-
33	1.6	-	-	-	-	11	1.0	33	.50	-	-
44	1.3	45	1.0	22	.40	-	-	-	-	45	.30
57	1.8	-	-	33	.40	-	-	57	.70	-	-
-	-	-	-	-	-	45	.90	-	-	-	-
-	-	-	-	57	.80	-	-	-	-	-	-
Main Engine Cutoff											
-	-	32	0.76	-	-	52	0.3				
-	-	42	.65	-	-	58	1.1				
55	0.4	55	.65	87	0.69	-	-				
95	.2	-	-	116	.87	-	-				
122	.91	-	-								
-	-	137	2.8								

^a Yaw axis has no significant levels in the 5-150 cps range during main engine cutoff.

to this ground measured resonant frequency appear in many flights of Thor vehicles.

VIBRATION SURVEY OF EQUIPMENT COMPARTMENT

The vibration survey was performed on the fully assembled AVT-2 vehicle prior to fueling on its launch pad at Cape Canaveral. Low-level sinusoidal vibration inputs (15 to 2000 cps) into the equipment compartment were accomplished by attaching two 25-pound electromagnetic shakers to the nose fairing dummy explosive bolts located 180 degrees apart at station 52.05. Responses to sinusoidal excitations were measured by the flight transducers and by transducers mounted at various external locations on the equipment compartment. Figure 8 shows a physical arrangement of the test setup. In addition to the sinusoidal test, the equipment compartment natural frequencies were excited by striking the vehicle at various locations and directions at station 52.05 with a rubber mallet. A comparison of the AVT-2 flight data, vibration survey data, and the AVT payload vibration

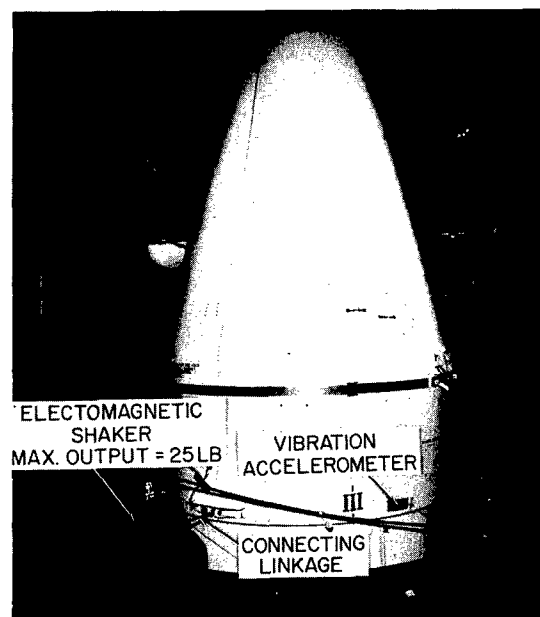


Fig. 8 - Equipment arrangement for vibration survey

TABLE 4
Comparison of Flight Vibration Data with Ground Vibration Survey
Frequencies and Test Specification Levels^a

Ground Vibration Data, Thrust			AVT-2 Flight Vibration Data, Power Spectral Density ^a				Flight Test Levels, Sinusoidal	
Tapping	Forced Vibration							
Freq. (cps)	Freq. (cps)	Response (± g)	Freq. (cps)	Yaw (g ² /cps) ^b	Pitch (g ² /cps) ^c	Thrust (g ² /cps) ^d	Freq. Range (cps)	Level
210	-	-	-	-	-	-	5-14	1/4 inch D.A.
400	390	3.3	340	0.0171	0.0071	-	14-400	4 g-rms
435	490	5.8	470	.0169	.0098	0.02	400-2000	6 g-rms
-	585	4.6	575-625	.0114	.0065	.102		
-	-	-	675-710	.0168	.0088	.058		
-	795	5.3	775-825	.0148	.0076	.024		
915	915	8.3	900	-	-	.028		
-	970	8.8	950	-	-	.102		
-	1040	10	1030	.0098	.0066	.488		
1100	1120	7.4	1100	.0133	.0062	.066		
1180	-	-	1180	-	-	.069		
1250	1200	6.4	1220	.0060	.0063	.065		
-	-	-	1280	-	-	.035		
-	-	-	1320	-	.0012	.032		
-	-	-	1380	-	-	.033		
-	-	-	1440	-	-	.026		
1570	1550	5.7	1500	-	.014	.029		
-	-	-	1630	-	.0067	-		
							Gaussian Random	
							15-2000 ₁	0.045 g ² /cps (9.5 g-rms)

^aData sample measured at maximum flight vibration level, T + 38 to T + 40 seconds.

^bFilter bandwidth, 50 cps.

^cFilter bandwidth, 50 cps.

^dFilter bandwidth, 20 cps.

flight-acceptance-test specification levels is given in Table 4. The comparison indicates that resonant frequencies excited manually by mallet and those excited by the electromagnetic shakers were the same predominant frequencies determined from the PSD analyses of the flight vibration data. It may be remembered that similar predominant frequencies occurred during lift-off, MECO, fairing separation, and spacecraft separation.

COMPARISON WITH PRE-FLIGHT ACCEPTANCE TEST LEVELS

A comparison of the flight-measured values with the flight test specification (Table 4) indicates that the previously written test specification is both adequate and not overly severe. The flight-measured overall level of 9.4 g-rms,

at transonic speeds, is slightly below the test specification of 9.5 g-rms random excitation. However, since the predominant excitation occurred in the frequency band of from 940 to 1120 cps with an overall excitation level of 6.62 g-rms over this bandwidth (corresponds to a PSD of 0.488 g²/cps), it is felt that the sinusoidal sweep at the level of 6 g-rms adequately simulates the flight vibration environment.

EFFECTS OF NOSE FAIRING SHAPES

One of the effects of buffeting is the acoustical excitation of random vibrations in the vehicle and payload structures. Buffeting is usually defined as the result of unstable flow over the body and generally occurs as the vehicle approaches transonic speeds. The flow instability

is essentially independent of body motions but is directly related to the vehicle nose shape. References 3, 4, and 5 report recent studies of buffeting forces on certain types of vehicle nose shapes. Figure 9 shows the nose shapes of three vehicles used to launch the S-51 (Thor-Delta),² Transit BI (Thor-Able-Star),⁶ and AVT (Thor); from a study of the references it might be expected that the highest vibration levels due to buffeting would be measured on the Thor-Able-Star vehicle and the lowest on the Thor-Delta vehicle. Figure 10, which compares the overall rms flight vibration levels for these three vehicles, confirms that the vibration levels at transonic speeds were highest on the Thor-Able-Star and lowest on the Thor-Delta.

³P. Woods and L. E. Ericsson, "Aeroelastic Considerations in a Slender, Blunt-Nose, Multistage Rocket," Aerospace Eng. 21(5):42-51 (May 1962).

⁴C. F. Coe, "Steady and Fluctuating Pressures at Transonic Speeds on Two Space-Vehicle Payload Shapes," NASA TM X-503 (1961).

⁵C. F. Coe, "The Effects of Some Variations in Launch-Vehicle Nose Shape on Steady and Fluctuating Pressures at Transonic Speeds," NASA TM X-646 (1962).

⁶D. G. Douglas, "Measurement and Analysis of Missile Vibration, Shock, and Noise Environments," Proc. Instrum. Soc. Am., 17(2), Paper No. 38.1.62 (1962).

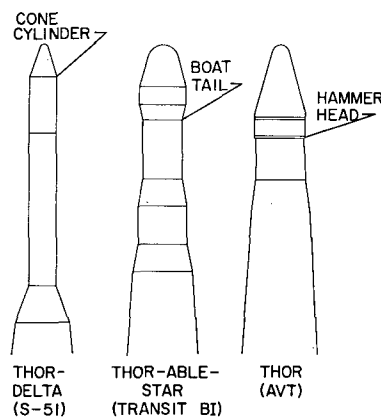


Fig. 9 - Comparison of Thor-Delta, Thor-Able-Star, and AVT nose shapes

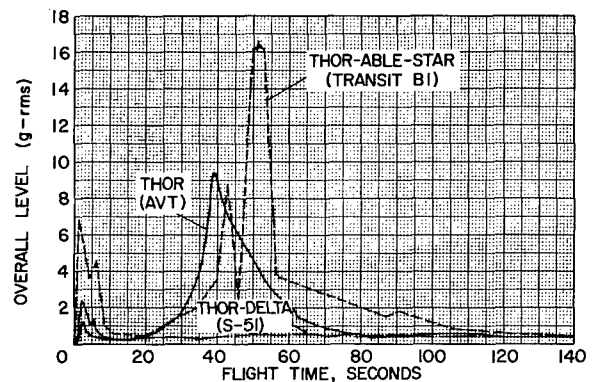


Fig. 10 - Longitudinal vibration-time history comparison of AVT, Thor-Delta, and Thor-Able-Star flights

CONCLUDING REMARKS

The flight data presented in this report indicate that (1) the major vibration levels measured during the AVT flights occurred during lift-off, Mach 1, fairing separation, and payload separation; (2) the composite levels of both flights measured during these occurrences are in close agreement; (3) the spectra (level and frequency) are similar for comparative time data samples; and (4) the frequencies measured during flight were similar to those measured during the ground vibration survey.

Payload vibration data measured during a recent Thor-Delta flight show that no increase in level was measured during Mach 1 or maximum dynamic pressure; in contrast, high vibration levels were measured on the AVT flights. Also, high vibration levels were measured at Mach 1 and maximum dynamic pressure during flights of the Thor-Able-Star. The differences in the vibration levels of these vehicles measured at transonic speeds are attributed mainly to the vehicle nose shape.

A comparison of the flight-measured vibration levels with the environmental flight acceptance test specification indicates that the previously written test specification is both adequate and not overly severe.

DISCUSSION

Mr. Condos (Martin Company): Do you agree with me that the use of a Q dependent function for the prediction of inflight vibration levels doesn't look very satisfactory?

Mr. Clevenson: I can only agree with that if you make other limitations. On something such as the Able Star possibly it would have been satisfactory, but certainly on the Delta

vehicle with a smooth nose and a smooth fairing it quite obviously would not be satisfactory. In other words, it certainly would not be satisfactory at all times.

Mr. Condos: On your wind tunnel data, were your measurements over a very broad frequency range or were these just simply low frequency measurements? In other words, you showed the reverse situation from that which one would expect between the wind tunnel data and the vibration data, and I am trying to find out whether it is due to a difference in bandwidth.

Mr. Clevenson: Possibly I stated it wrong about the wind tunnel data. If so, let me correct it. I tried to give the impression that the wind tunnel data showed the same as the flight data. I hope that is what I said. Namely, that the boat tail configuration showed the greatest turbulence in the wind tunnel at transonic speeds, and the cone cylinder nose fairing showed the least amount of turbulence of the three kinds of configurations.

Mr. Condos: OK. I thought that one configuration had the maximum level occurring at max Q which I didn't understand.

Mr. Clevenson: Yes, in the last figure, the Thor Able Star vehicle showed the maximum vibration level at max Q whereas the AVT vehicle showed the maximum level much closer to Mach 1 and considerably lower at max Q. I did not mean to imply that the maximum vibration level would always occur at max Q. It usually occurs during the transonic flight regime, and this wasn't on the Thor Delta in the data I just showed. There, the maximum levels occurred at lift off.

Mr. Condos: OK. This led to my question. Are you measuring over the same bandwidth in the wind tunnel as you were in the flight test

program and trying to make a correlation, or were you looking at a narrow bandwidth in one case and a broad band, 2000 cycles, in the other case?

Mr. Clevenson: Generally speaking, we are using the wide bandwidth in both cases. In the report you will find references to the wind tunnel tests which were done at NASA Ames Laboratory. The tests did not break down the turbulence levels into spectra, but in general they used wideband pickups to determine that the turbulence was not just the low frequency turbulence. It was both low and high frequency turbulence.

Voice: Could we see your last slide again? Is that possible?

Mr. Clevenson: It is if the projectionist will put it on for us.

Voice: In the slide, I believe that your Thor Able Star of course showed the highest level during the transonic max Q regime, but it also appeared to show the highest level on lift off. I couldn't understand that.

Mr. Clevenson: Well, you are perfectly right. I didn't make any particular point of that. You are referring to that level which does definitely show considerably higher vibration level at lift off. Exactly why it should do so, I am not sure. I can see that your reasoning says that if it is three times as high at lift off, maybe it should be three times as high at max Q also, and perhaps it should be. But generally speaking the high level at lift off is due to an acoustic coupling more than to just the engine firing up. The acoustic coupling ties the spacecraft into the ground through the resonance effect of the engine blasting into the ground. I have no good explanation of why it is so high. We do our best to make the data as accurate as possible and present it as we see it.

* * *

VIBRATION STUDIES ON A SIMPLIFIED 1/2-SCALE MODEL OF THE NIMBUS SPACECRAFT

H. D. Garden and R. W. Herr
NASA Langley Research Center
Langley Station, Hampton, Va.

Results of experimental investigation of the effectiveness of various isolation and damping methods in reducing the dynamic response of a simplified scale model of the Nimbus spacecraft to vibratory inputs are presented.

INTRODUCTION

The high reliability demanded of spacecraft requires that these complex structures be capable of operation during and after exposure to many hostile environments. Earliest of the flight environmental hazards encountered, and in many cases the most severe, are the extreme vibration levels through which these payloads pass during the launch and boost phases of the flight sequence.

At the present time, onboard instrumentation of a variety of spacecraft is being designed and developed to operate on power generated by solar cells mounted on large flexible panels. Vibration tests of prototype spacecraft of this type, at levels well below anticipated flight levels, have resulted in damage to the payloads and instrumentation. It is anticipated that future payloads of like design will experience similar vibration problems; therefore, it becomes necessary that means and techniques be explored for reducing the severity of the many resonant conditions which exist in the spacecraft and its component parts.

The purpose of this paper is to present the results of an experimental investigation which utilized a 1/2-scale dynamic model of a spacecraft typical of the solar panel category for evaluating the effectiveness of damping and isolation in reducing the dynamic response of the spacecraft to vibratory inputs.

DISCUSSION

Description of Model

The configuration of the half-scale model utilized is shown in Fig. 1. The model was a simplified version of the full-scale Nimbus weather satellite. The bending stiffness of the solar panels, panel shaft, and struts, as well as the mass of the major components in the model, were approximately scaled. Two sets of simulated solar panels were fabricated. Both consisted of two sheets of 0.016-inch aluminum attached to a tapered balsa wood core. The taper of the wood core from the center of the panel along the length to the panel tips made it possible

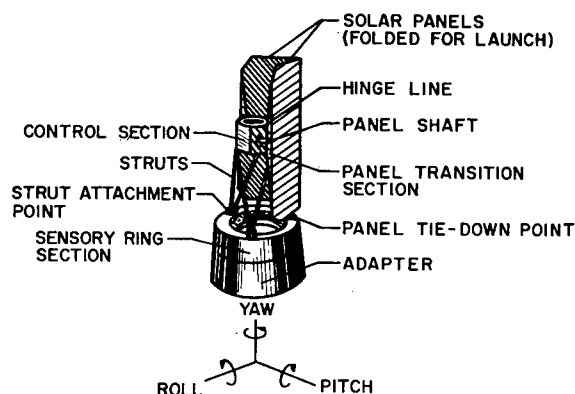


Fig. 1 - General configuration and elements of the 1/2-scale Nimbus model

to obtain the desired stiffness distribution. In one set the aluminum sheets were bonded to the wood core with an epoxy cement, while in the other set the sheets were bonded with a visco-elastic adhesive to provide shear damping. The principal dimensions of the components of the 1/2-scale Nimbus model are presented in Fig. 2.

PRINCIPAL DIMENSIONS

	INCHES
CONTROL BOX WIDTH	A- 11
SOLAR PANEL WIDTH	B- 192
SOLAR PANEL LENGTH	C- 48
LENGTH, OVERALL (ADAPTER INCLUDED)	D- 69
SENSORY RING HEIGHT	E- 6.5
SPACECRAFT ADAPTER HEIGHT	F- 12
SENSORY RING DIAMETER	G- 27.5
SPACECRAFT ADAPTER DIAMETER (BOTTOM DIAMETER)	H- 30

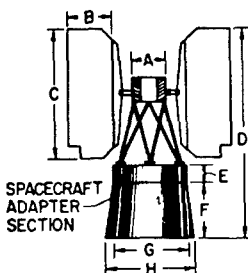


Fig. 2 - Principal dimensions of the 1/2-scale Nimbus model

Test Procedure

For tests involving excitation along the pitch and roll axes, the 1/2-scale model was mounted on a platform which was suspended on steel flexure springs to provide essentially planar motions. For excitation along the yaw axis the model was suspended by nylon ropes attached at the center of gravity of the control section, struts and solar panels combination, and at the center of gravity of the sensory system-adapter combination. Excitation of the model was provided by an electromagnetic shaker. Input accelerations and the response of the model were measured with lightweight accelerometers while the excitation frequency was measured by a frequency-period counter. Responses of the model to input accelerations along the roll, pitch, or yaw axis were measured on the solar panels, control section, and sensory section for the basic model configuration and for cases for which damping or isolation, or both, had been incorporated in the structure.

ANALYTICAL AND EXPERIMENTAL RESULTS

Panel Frequencies and Mode Shapes

Concurrent with the experimental determination of the structural amplification factors

of the 1/2-scale Nimbus model, an analytical technique for calculating the modes and frequencies of the simulated solar panels was employed. The technique utilizes a general finite-difference method for calculating the simple harmonic flexures of plates. The basis of the technique along with the procedure for application of the method to plate vibration problems is discussed fully by Walton.¹ Additional information needed for calculating the modes and frequencies of the simulated solar panels using the technique is included in appendix A.

Computed frequencies and node locations for the first 10 modes are compared with experimental results in Fig. 3 where it can be seen that the agreement, in general, is good. The largest discrepancies occurred for modes four, five, and six. Closer correspondence between all computed and experimental frequencies could possibly be realized by more sophisticated assumptions on the edge conditions, more refined panel stiffness distribution for input into the computing machine procedure, and taking panel-cutouts into consideration.

The dashed lines in Fig. 3 indicate the computed node lines for the panel considered as completely rectangular in form. The actual planform, however, had panel cutouts as indicated by the small shaded areas at three corners. Substantial agreement, nevertheless, is shown between computed and experimental (solid lines) nodes.

Comparison of Model Response to Full-Scale Vehicle Response

In order to assess the degree of simulation obtained with the 1/2-scale dynamic model of Nimbus, a comparison between the 1/2-scale model response and the response of the full-scale spacecraft was made at the base of the control assembly for input along the pitch axis. In Fig. 4 the 1/2-scale model response is given by the dashed line and open symbols; the solid symbols denote the peak values of the measured resonance. Input accelerations to the model were limited by the available shaker force to approximately 83 percent of the desired 0.6 g input level. Shown in the figure as a solid line

¹W. C. Walton, Jr., "Applications of a General Finite-Difference Method for Calculating Bending Deformations of Solid Plates," NASA TN D-536 (1960).

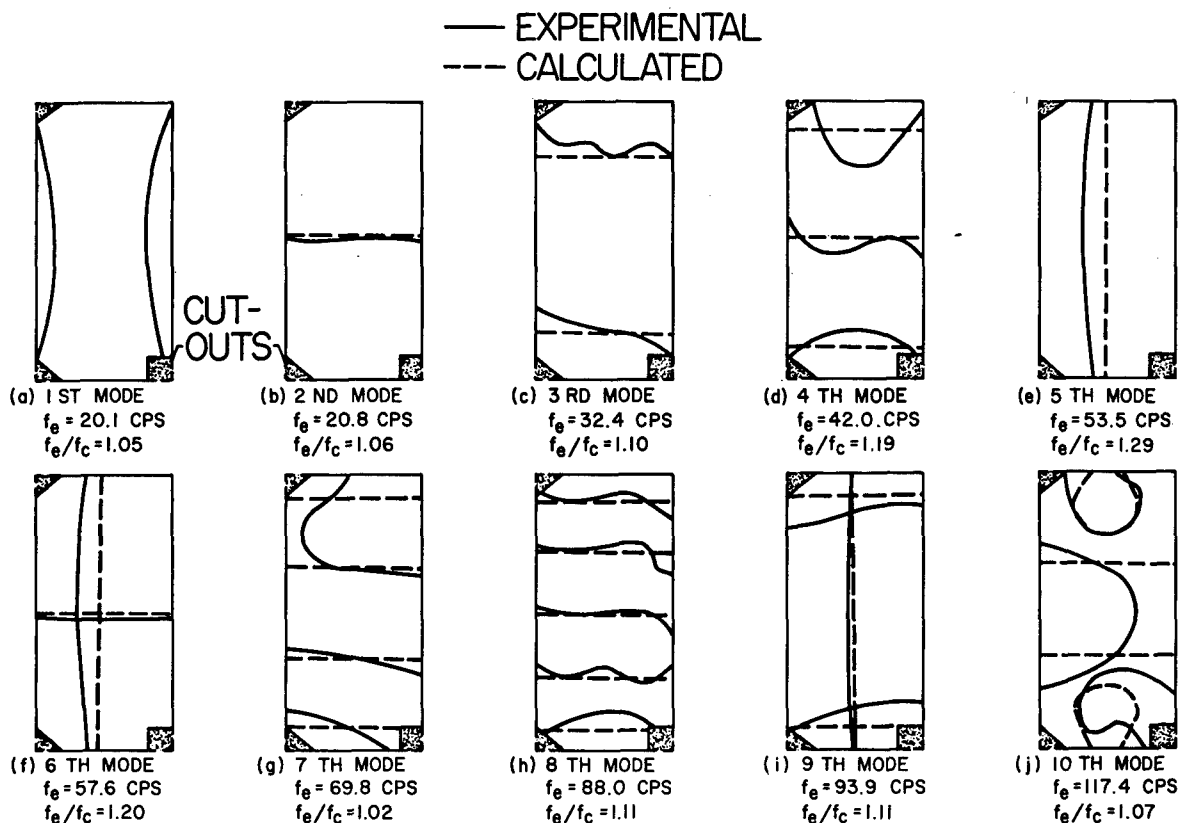


Fig. 3 - Comparison of experimental and calculated modes and frequencies of the simulated solar panel

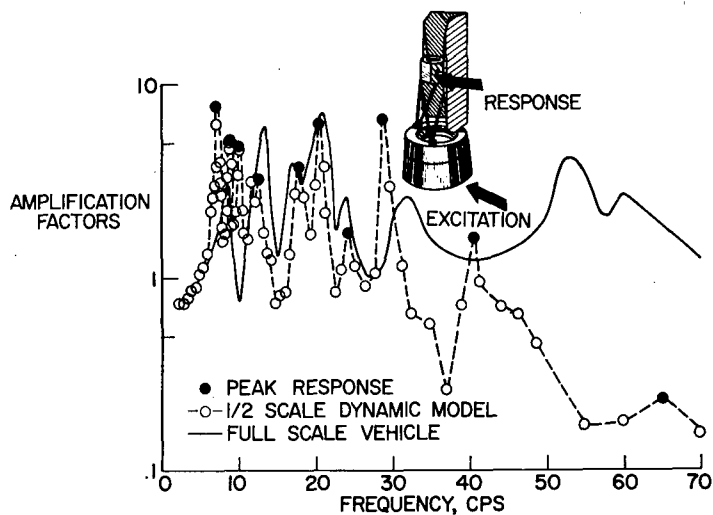


Fig. 4 - Comparison of responses at the base of control section on 1/2-scale model and full-scale spacecraft. Excitation along pitch axis. Model frequencies divided by 2.

is the corresponding experimentally measured full-scale vehicle response.²

The figure shows that general agreement exists between the model and full-scale vehicle resonances in the frequency range up to approximately 35 cps. However, two low-frequency resonant responses were measured on the 1/2-scale model which were not noted on the full-scale Nimbus. It is probable that the compromises and trade-offs necessitated in the construction of the model struts and strut attachments may have introduced these additional responses. But it is also possible that the inherent damping in these modes on the full-scale spacecraft was sufficiently high to mask out the individual modal responses.

In an elastic structure the response of the structure is dependent on the input accelerations and the amplification factors which relate the response of the structure to the input accelerations. For the 1/2-scale model under consideration, the primary interest was the determination of the amplification factors for the

spacecraft and the evaluation of the effectiveness of certain damping and isolation techniques for attenuating these amplifications.

Effects of Damping

One of the more significant elements affecting the amplification factors is the damping of the structure. In general, any increase in the damping of the structure is beneficial, but the use of damping can be made more effective by distribution of viscoelastic materials in areas of maximum relative shear displacement between two sandwich faces.³ Thus for minimum structural response to a given input spectrum, every attempt should be made to incorporate damping in the structure and to distribute the damping in areas as indicated by the critical modes.

The results of the study of the effects of distributed damping in the solar panels of the 1/2-scale model are given in Figs. 5-11. The measured damping, expressed as C/C_c , for the epoxy cement bonded panels and the damping adhesive bonded panels was approximately 0.003 and 0.020, respectively, for the first mode of

²These data were supplied by the Goddard Space Flight Center and were obtained during Nimbus vibration analysis performed by the General Electric Co., Missile and Space Vehicle Department, Valley Forge, Pa., under contract to GSFC.

³C. M. Harris and C. E. Crede, editors, *Shock and Vibration Handbook*, Vol. 2 (McGraw-Hill Book Company, Inc., New York, 1961), section 32, pp. 40-41, sections 36-37.

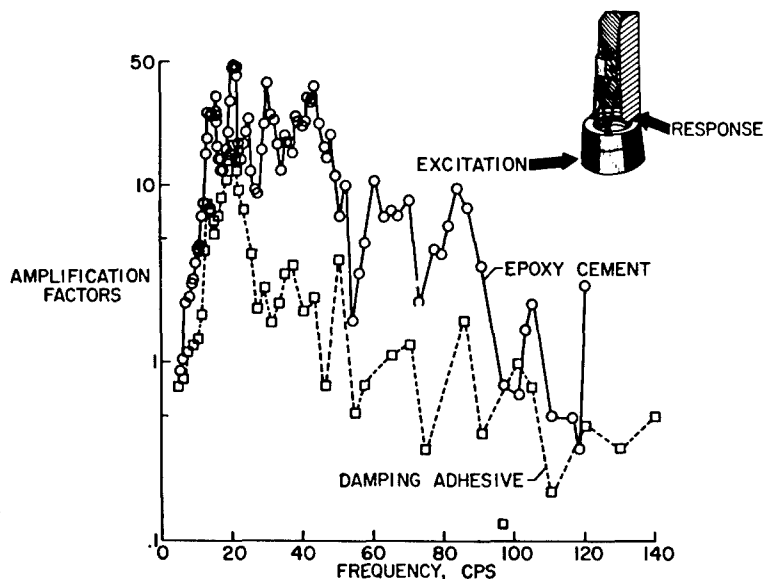


Fig. 5 - Dynamic amplification as a function of excitation frequency. $k = 15,250$ lb/in. Excitation along roll axis. Response at bottom-center of solar panel.

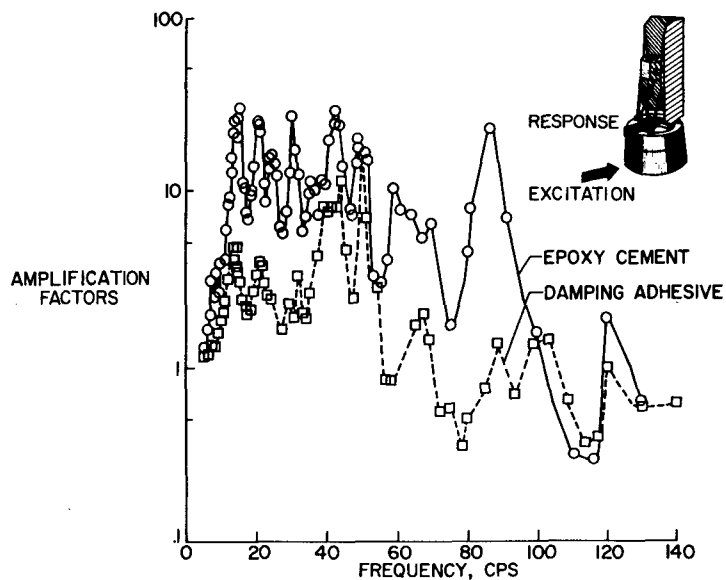


Fig. 6 - Dynamic amplification as a function of excitation frequency. $k = 15,250$ lb/in. Excitation along roll axis. Response at bottom of hinge line on panel transition.

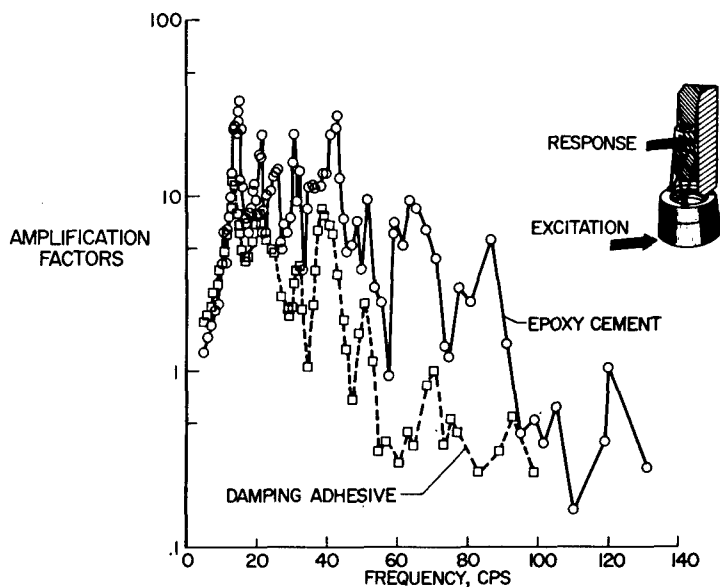


Fig. 7 - Dynamic amplification as a function of excitation frequency. $k = 15,250$ lb/in. Excitation along roll axis. Response at end of panel shaft.

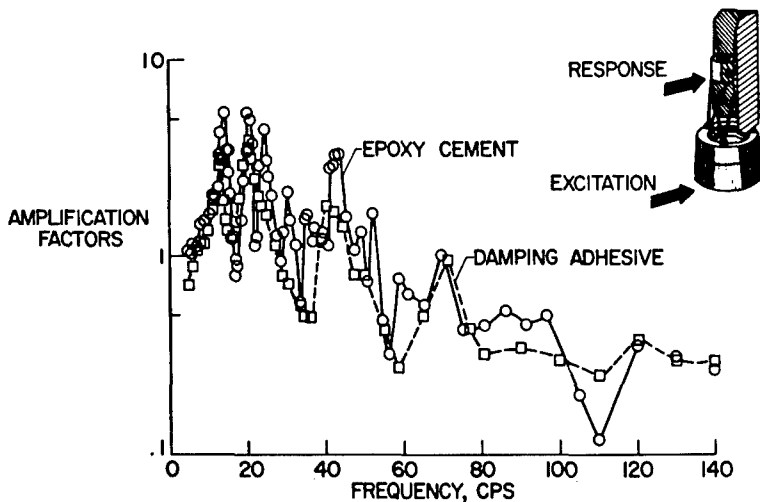


Fig. 8 - Dynamic amplification as a function of excitation frequency. $k = 15,250$ lb/in. Excitation along roll axis. Response at base of control section.

the panel. In Figs. 5-8 amplification factors are given as a function of excitation frequency for locations and directions as indicated by the arrows on the inserted sketch of the model. Excitation in each case was along the roll axis, and the spring stiffness between the control section and the sensory section was $k = 15,250$ lb/in. Figures 9-11 present amplification factors for the case of excitation along the pitch axis at three of the same locations as those chosen for the cases in the roll direction. The

test results shown in the figures emphasize three significant points. The first is that very high amplifications exist in such structures. Values as high as 30, 40, or 50 may be noted on the panels for the locations indicated. Secondly, the many structural resonances were associated mainly with panel natural modes. This suggests that proper design of the solar panels may be a means of locating the natural frequencies of the structure in certain areas of the frequency spectrum. In this manner significant reductions in

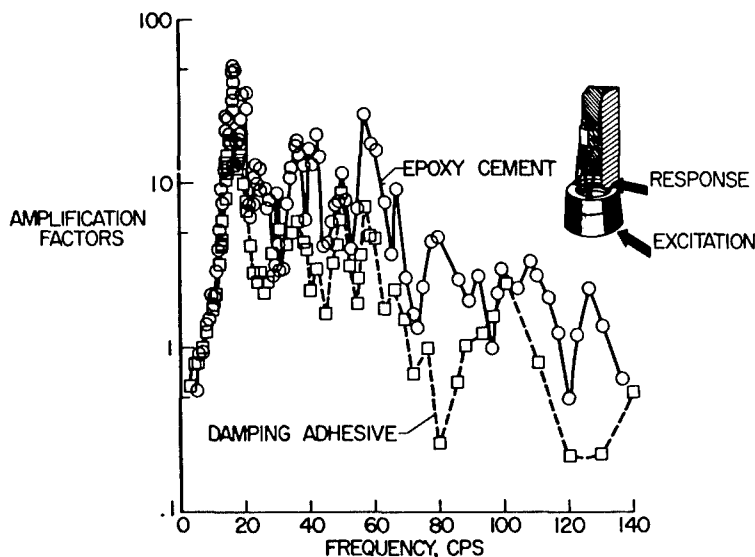


Fig. 9 - Dynamic amplification as a function of excitation frequency. $k = 15,250$ lb/in. Excitation along pitch axis. Response at bottom-center of solar panel.

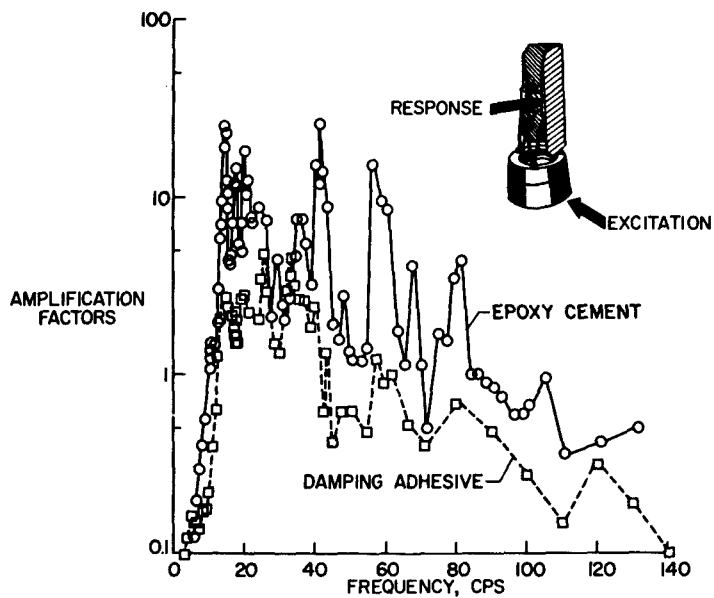


Fig. 10 - Dynamic amplification as a function of excitation frequency. $k = 15,250$ lb/in. Excitation along pitch axis. Response at end of panel shaft.

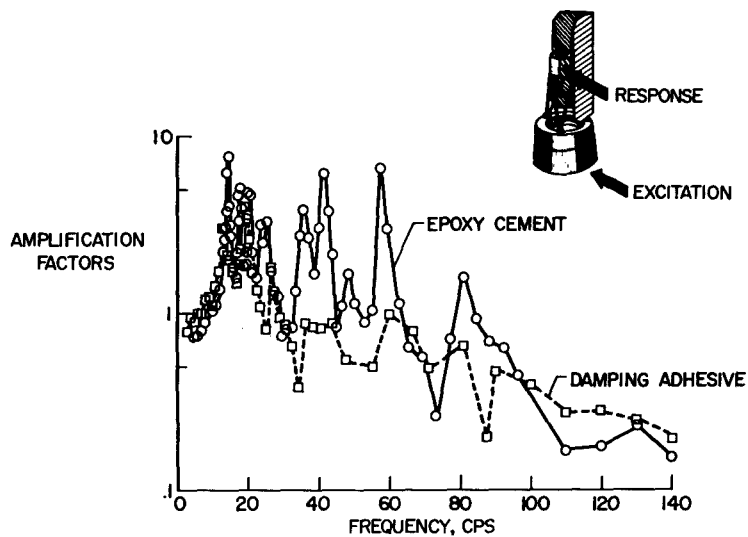


Fig. 11 - Dynamic amplification as a function of excitation frequency. $k = 15,250$ lb/in. Excitation along pitch axis. Response at base of control section.

conditions of resonance between the spacecraft panels and the booster inputs may be feasible. The third point is that the response of such a structure to unsteady forces can be substantially reduced, in most instances, by the use of damping materials at suitably chosen points. A comparison of the levels of the solid curves to the dashed curves in Figs. 5-11 indicates the relatively high degree of energy dissipation that was attained in the sandwich construction panels. The added damping was least effective at the base of the control section, particularly for excitation along the roll axis, Fig. 8.

Effects of Isolation and Damping

As an additional phase of the investigation of the 1/2-scale Nimbus model, a study of the effects of a combination of isolation and damping on the response of the vehicle to vibratory inputs was conducted. Commercially available isolators were utilized at the strut attachment points during the tests. The effective maximum radial capacity of the combination was experimentally determined as approximately 15-1/2 pounds. Two mounts had radial load capacities of 12-1/2 pounds each and the other had a radial load capacity of 20 pounds maximum. Typical results of the tests are presented in Fig. 12 for excitation along the pitch axis for which both damping and isolation were utilized. The results indicate that the isolation mounts were more effective in reducing the magnitudes of

structural amplifications of the epoxy-bonded panels than the inherently damped sandwich panels. The combination of both isolation mounts and the damping adhesive bonded panels was extremely effective in reducing the magnitude of detectable structural amplifications.

For excitation along the yaw axis, amplification factors were determined for locations on the base of the control section and on the bottom center of the solar panel. The response of the model for a spring stiffness between the control and sensory section of $k = 60,000$ lb/in. was used for comparison with the response for cases in which the isolation mounts were used. The results of these tests are presented in Figs. 13 and 14. For the location on the control section (Fig. 13), the amplification factors as a function of frequency were the typical mass-on-isolator response curve with attenuation occurring at frequencies above approximately 1.4 times the natural frequency of the mass-isolator system. As shown in Fig. 13, the measured attenuations on the control section are essentially unity for $k = 60,000$ lb/in. Presented in Fig. 14 are the responses on the bottom-center of the epoxy-bonded panels. Appreciable, but somewhat less effectiveness was obtained through the use of the isolation mounts for responses at this location on the model.

Although the results indicate that reductions in the structural amplifications can be obtained

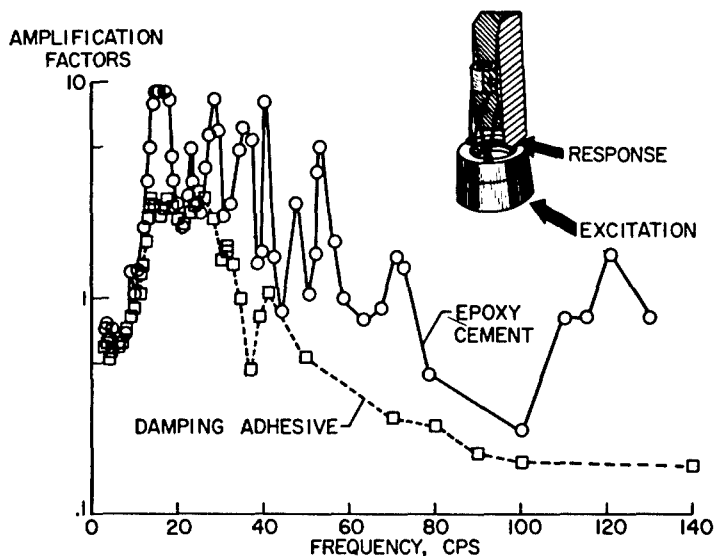


Fig. 12 - Dynamic amplification as a function of excitation frequency. Isolators $\begin{cases} 2:5-1/2 - 12-1/2 \text{ lb} \\ 1:20 \text{ lb} \end{cases}$. Excitation along pitch axis.

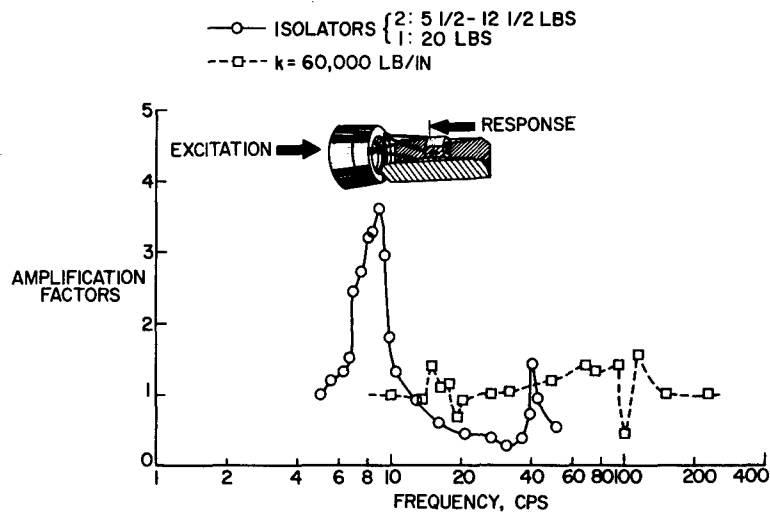


Fig. 13 - Dynamic amplification as a function of excitation frequency. Excitation along yaw axis. Response at base of control section.

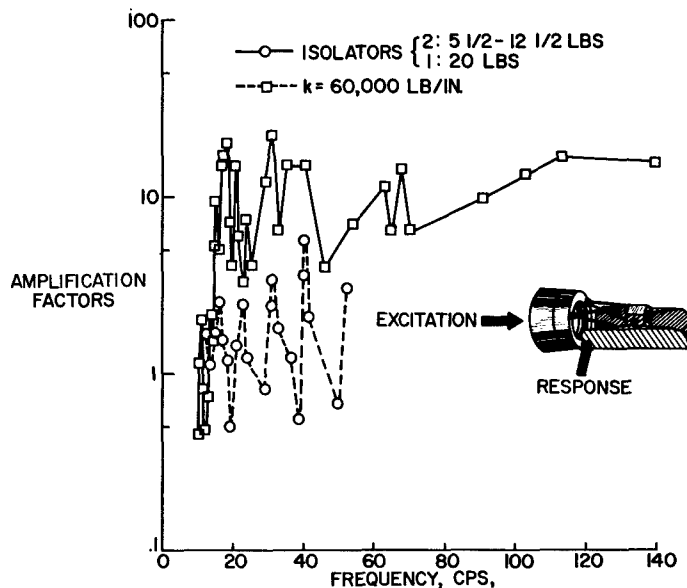


Fig. 14 - Dynamic amplification as a function of excitation frequency. Excitation along yaw axis. Response at bottom-center of solar panel.

by utilizing isolation mounts, several disadvantages are also presented. One such undesirable feature is that large lateral movements because of rocking action of the panels, control section, and struts on the isolators can occur at the isolator natural frequency. This presents the additional complication of possible interference of the model or vehicle panels with the launch-vehicle shroud. Further, for omnidirectional

isolators to provide desired isolation large deflections are often necessary. The deflections are needed to prevent bottoming out of the isolators under the loading imposed by the increasing acceleration of the launch vehicle during the flight. Sacrifice of omnidirectional isolation for unidirectional isolation could possibly overcome some of the disadvantages.

Effects of Stiffness Between Control and Sensory Sections

To assess the effects of stiffness between the control and the sensory section on the response of the model, structural amplifications as a function of frequency were determined for values of k equal to 60,000 and 15,250 lb/in. Typical results of this study are presented in Fig. 15 which shows the measured model response to inputs along the pitch axis for the bottom-center of the solar panel. The results indicate that increased stiffness between the two sections leads to only slight increases in panel amplifications at somewhat increased frequencies.

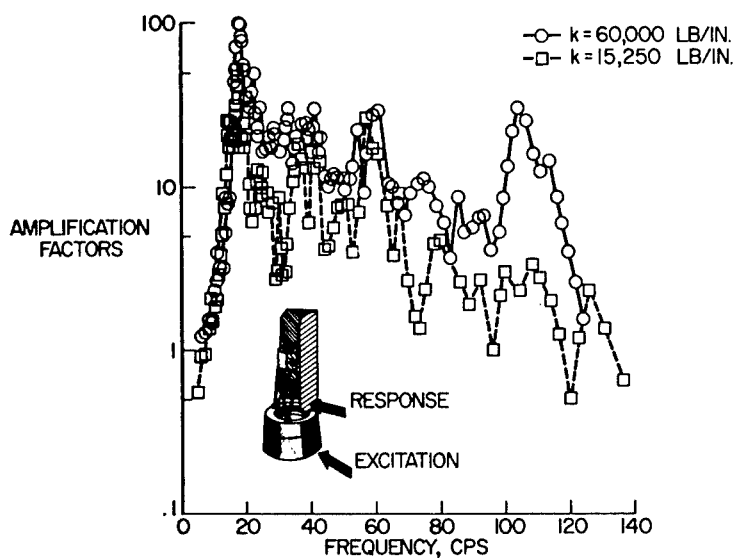


Fig. 15 - Effects of stiffness between control and sensory sections on dynamic amplification. Response at bottom-center of epoxy-bonded solar panel. Excitation along pitch axis.

Sensory Section Response

As might be intuitively expected, little, if any, reductions in the measured response in the compartments of the sensory section were noted when changes were made in the structure above the sensory section. As an illustration of the responses that occurred around the sensory section, peak values of the amplifications in several compartments were measured and are presented in Fig. 16. Maximum structural amplifications were found to occur at or near the compartment panel natural frequencies with the overall amplification magnitude being less severe than these maximums.

CONCLUDING REMARKS

An investigation has been conducted to evaluate the effectiveness of damping and isolation methods in reducing the structural amplifications of vibratory inputs on a simplified scale model of the Nimbus spacecraft. The results are summarized in the following paragraphs.

1. Experimental frequencies for the first 10 modes of the solar panels on the 1/2-scale model were compared with calculated values using a finite-difference method. In general, good agreement between the calculated and experimental frequencies was found. Fair

agreement was also shown between the computed and experimental node locations.

2. A comparison of the model response to full-scale vehicle response at the base of the control section for inputs along the pitch axis indicated that general agreement existed between model and full-scale vehicle resonances in the frequency range up to approximately 35 cps.

3. In the evaluation of the effects of distributed damping in the solar panels the results emphasized (a) that very high amplifications exist in such structures, (b) that the many

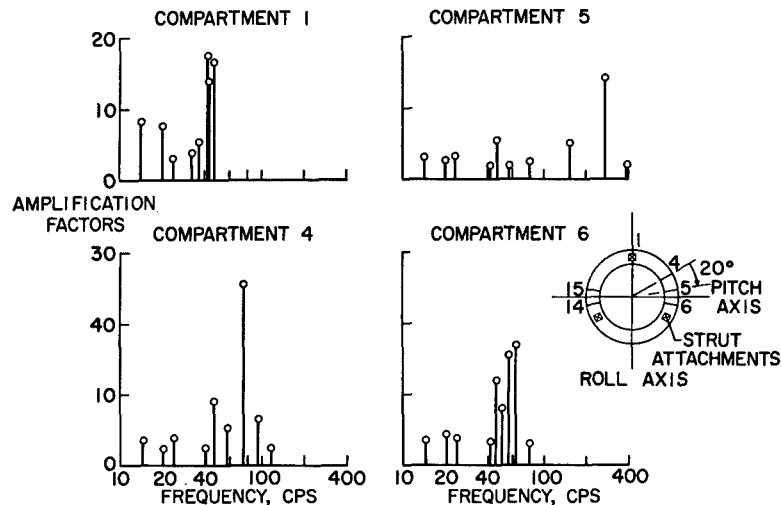


Fig. 16 - Peak values of dynamic amplification as a function of excitation frequency. Response in sensory section compartments. Excitation along roll axis.

structural resonances were associated mainly with the natural modes of the panels, and (c) that the response of such a structure to unsteady forces can be substantially reduced, in most instances, by the use of damping materials at suitably chosen points.

4. Isolation mounts were more effective in reducing the magnitude of structural amplifications on the epoxy bonded, lightly damped, solar panels than the inherently damped panels. The combination of both isolation mounts and damped

panels was extremely effective in reducing the magnitude of detectable structural resonances.

5. Increased stiffness between the control section and the sensory section resulted in only slight increases in panel amplifications at somewhat increased frequencies.

6. Little, if any, reductions in the measured response in the compartments around the sensory section were noted when changes were made in the structure above the sensory section.

Appendix A

PLANFORMS AND COMPUTING MACHINE INPUTS FOR CALCULATING MODES AND FREQUENCIES OF THE SOLAR PANEL

This appendix is included to present information required in conjunction with the procedure given in Ref. 1 for calculating the modes and frequencies of the simulated solar panels. Figure A1 presents the planform of the solar panel for the case of hinged-hinged edge conditions assumed along the length of the panel. Included in Table A1 are the computing machine inputs necessary for calculating the modes and frequencies of the panel with these assumed edge conditions.

Symbols included in Fig. A1 and Table A1 are:

D panel flexural rigidity,

$$E \left[\frac{(2h+t)^3 - t^3}{12} \right], \quad \text{in.} - \text{lb}$$

E Young's modulus of elasticity, lb/in.²

h panel skin thickness, in.

K number of moving mass points on the solar panel planform

L length of solar panel, in.

m mass per unit area of panel, lb-sec²/in.³

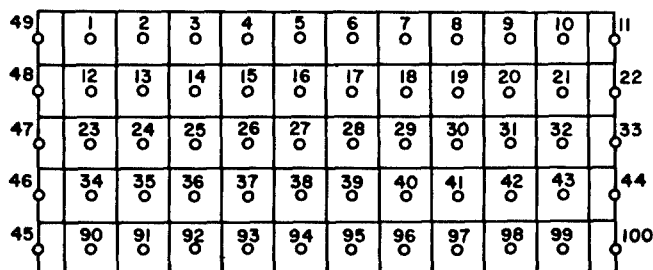
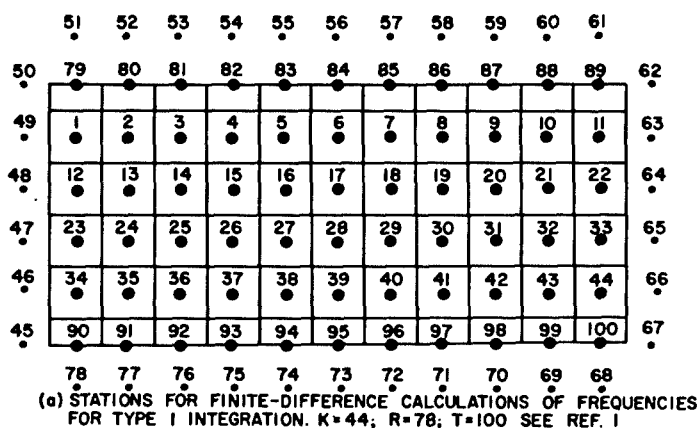


Fig. A1 - Planform assumed for panel for calculating frequencies and mode shapes by method of Ref. 1

R number of unknown deflections left in the expression for energy after conditions of constraint have been applied

T total number of points on the solar panel planform

t core thickness of panel section, in.

ϵ horizontal distance between vertical grid lines on panel planform

λ vertical distance between horizontal grid lines on panel planform

μ Poisson's ratio

Subscript:

r denotes any convenient reference of a quantity.

Computing machine outputs of particular interest include deflections in the natural mode shapes at the mass stations which move, and the dimensionless eigen-values, Ω , which are related to the natural frequencies of the plate by the formula

$$f_c = \frac{1}{2\pi\epsilon^2} \sqrt{\frac{D_r \Omega}{2m_r}}, \text{ cps.}$$

TABLE A1
Computing-Machine Input for Calculation of Modes and Frequencies of
Solar Panel for Hinged-Hinged Edges Along Panel Length

[L = 48 in.; $\epsilon/\lambda = 1.136$; $\mu = 0.333$; K = 44; R = 78; T = 100; D_r = 428 in.-lb;
 $m_r = 0.00083 \text{ lb-sec}^2/\text{in.}^3$ (see Ref. 1)]

①	②	③	④	⑤	⑥	⑦	⑧	⑨	⑩	⑪	⑫	⑬	⑭	⑮	⑯	⑰
Grid-point number	$\bar{D}_0 \alpha_0$	$\bar{D}_{NE/2} \alpha_{NE/2}$	N _{NN}	N _{NW}	N _{NN}	N _{NE}	N _{NW}	N _{NW}	N _O	N _E	N _{EE}	N _{SW}	N _S	N _{SE}	N _{SS}	$\bar{m}_0 \alpha_0$
1	0.297	0.297	51	50	79	80	0	49	1	2	3	48	12	13	23	1
2	.474	.474	52	79	80	81	49	1	2	3	4	12	13	14	24	1
3	.650	.650	53	80	81	82	1	2	3	4	5	13	14	15	25	1
4	.827	.827	54	81	82	83	2	3	4	5	6	14	15	16	26	1
5	1	1	55	82	83	84	3	4	5	6	7	15	16	17	27	1
6	1	1	56	83	84	85	4	5	6	7	8	16	17	18	28	1
7	1	.827	57	84	85	86	5	6	7	8	9	17	18	19	29	1
8	.827	.650	58	85	86	87	6	7	8	9	10	18	19	20	30	1
9	.650	.474	59	86	87	88	7	8	9	10	11	19	20	21	31	1
10	.474	.297	60	87	88	89	8	9	10	11	12	20	21	22	32	1
11	.297	.1485	61	88	89	90	9	10	11	12	13	21	22	23	33	1
12	.297	.297	79	49	1	2	0	48	12	13	14	47	23	24	34	1
13	.474	.474	80	1	2	3	48	12	13	14	15	23	24	25	35	1
14	.650	.650	81	2	3	4	12	13	14	15	16	24	25	26	36	1
15	.827	.827	82	3	4	5	13	14	15	16	17	25	26	27	37	1
16	1	1	83	4	5	6	14	15	16	17	18	26	27	28	38	1
17	1	1	84	5	6	7	15	16	17	18	19	27	28	29	39	1
18	1	.827	85	6	7	8	16	17	18	19	20	28	29	30	40	1
19	.827	.650	86	7	8	9	17	18	19	20	21	29	30	31	41	1
20	.650	.474	87	8	9	10	18	19	20	21	22	30	31	32	42	1
21	.474	.297	88	9	10	11	19	20	21	22	23	31	32	33	43	1
22	.297	.1485	89	10	11	12	20	21	22	23	24	32	33	34	44	1
23	.297	.297	1	48	12	13	0	47	23	24	25	46	34	35	90	1
24	.474	.474	2	12	13	14	47	23	24	25	26	34	35	36	91	1
25	.650	.650	3	13	14	15	23	24	25	26	27	35	36	37	92	1
26	.827	.827	4	14	15	16	24	25	26	27	28	36	37	38	93	1
27	1	1	5	15	16	17	25	26	27	28	29	37	38	39	94	1
28	1	1	6	16	17	18	26	27	28	29	30	38	39	40	95	1
29	1	.827	7	17	18	19	27	28	29	30	31	39	40	41	96	1
30	.827	.650	8	18	19	20	28	29	30	31	32	40	41	42	97	1
31	.650	.474	9	19	20	21	29	30	31	32	33	41	42	43	98	1
32	.474	.297	10	20	21	22	30	31	32	33	34	42	43	44	99	1
33	.297	.1485	11	21	22	23	31	32	33	34	35	43	44	45	100	1
34	.297	.297	12	47	23	24	0	46	34	35	36	45	90	91	78	1
35	.474	.474	13	23	24	25	46	34	35	36	37	90	91	92	77	1
36	.650	.650	14	24	25	26	34	35	36	37	38	91	92	93	76	1
37	.827	.827	15	25	26	27	35	36	37	38	39	92	93	94	75	1
38	1	1	16	26	27	28	36	37	38	39	40	93	94	95	74	1
39	1	1	17	27	28	29	37	38	39	40	41	94	95	96	73	1
40	1	.827	18	28	29	30	38	39	40	41	42	95	96	97	72	1
41	.827	.650	19	29	30	31	39	40	41	42	43	96	97	98	71	1
42	.650	.474	20	30	31	32	40	41	42	43	44	97	98	99	70	1
43	.474	.297	21	31	32	33	41	42	43	44	45	98	99	100	69	1
44	.297	.1485	22	32	33	34	42	43	44	45	46	99	100	67	68	1
45	0	.1485	47	0	46	34	0	0	45	90	91	0	0	78	0	
46	0	.1485	48	0	47	23	0	0	46	34	35	0	45	90	0	
47	0	.1485	49	0	48	12	0	0	47	23	24	0	46	34	45	
48	0	.1485	50	0	49	1	0	0	48	12	13	0	47	23	46	
49	0	.1485	0	0	50	79	0	0	49	1	2	0	48	12	47	
50	0	0	0	0	0	51	0	0	50	79	80	0	49	1	48	

TABLE A1 (Continued)
Computing-Machine Input for Calculation of Modes and Frequencies of
Solar Panel for Hinged-Hinged Edges Along Panel Length

[L = 48 in.; $\epsilon/\lambda = 1.136$; $\mu = 0.333$; K = 44; R = 78; T = 100; $D_r = 428$ in.-lb;
 $m_r = 0.00083$ lb-sec²/in.³ (see Ref. 1)]

(1)	(2)	(3)	(4)	(5)	(6)	(7)	(8)	(9)	(10)	(11)	(12)	(13)	(14)	(15)	(16)	(17)
Grid-point number	$\bar{D}_0 \alpha_0$	$\bar{D}_{NE/2} \alpha_{NE/2}$	N_{NN}	N_{NW}	N_N	N_{NE}	N_{WW}	N_W	N_O	N_E	N_{EE}	N_{SW}	N_S	N_{SE}	N_{SS}	$\bar{m}_0 \alpha_0$
51	0	0	0	0	0	0	0	0	51	52	53	50	79	80	1	
52	0	0	0	0	0	0	0	51	52	53	54	79	80	81	2	
53	0	0	0	0	0	0	51	52	53	54	55	80	81	82	3	
54	0	0	0	0	0	0	52	53	54	55	56	81	82	83	4	
55	0	0	0	0	0	0	53	54	55	56	57	82	83	84	5	
56	0	0	0	0	0	0	54	55	56	57	58	83	84	85	6	
57	0	0	0	0	0	0	55	56	57	58	59	84	85	86	7	
58	0	0	0	0	0	0	56	57	58	59	60	85	86	87	8	
59	0	0	0	0	0	0	57	58	59	60	61	86	87	88	9	
60	0	0	0	0	0	0	58	59	60	61	0	87	88	89	10	
61	0	0	0	0	0	0	59	60	61	0	0	88	89	90	11	
62	0	0	0	61	0	0	88	89	90	0	0	11	63	0	64	
63	0	0	0	89	62	0	10	11	63	0	0	22	64	0	65	
64	0	0	62	11	63	0	21	22	64	0	0	33	65	0	66	
65	0	0	63	22	64	0	32	33	65	0	0	44	66	0	67	
66	0	0	64	33	65	0	43	44	66	0	0	100	67	0	0	
67	0	0	65	44	66	0	99	100	67	0	0	68	0	0	0	
68	0	0	44	99	100	67	70	69	68	0	0	0	0	0	0	
69	0	0	43	98	99	100	71	70	69	68	0	0	0	0	0	
70	0	0	42	97	98	99	72	71	70	69	68	0	0	0	0	
71	0	0	41	96	97	98	73	72	71	70	69	0	0	0	0	
72	0	0	40	95	96	97	74	73	72	71	70	0	0	0	0	
73	0	0	39	94	95	96	75	74	73	72	71	0	0	0	0	
74	0	0	38	93	94	95	76	75	74	73	72	0	0	0	0	
75	0	0	37	92	93	94	77	76	75	74	73	0	0	0	0	
76	0	0	36	91	92	93	78	77	76	75	74	0	0	0	0	
77	0	0	35	90	91	92	0	78	77	76	75	0	0	0	0	
78	0	0	34	45	90	91	0	0	78	77	76	0	0	0	0	
79	.1485	0														
80	.237	0														
81	.325	0														
82	.4135	0														
83	.5	0														
84	.5	0														
85	.5	0														
86	.4135	0														
87	.325	0														
88	.237	0														
89	.1485	0														
90	.1485	.297														
91	.237	.474														
92	.325	.650														
93	.4135	.827														
94	.5	1														
95	.5	1														
96	.5	.827														
97	.4135	.650														
98	.325	.474														
99	.237	.297														
100	.1485	.1485														

DISCUSSION

Mr. Otts (Sandia Corporation): When you compared the full scale and the half scale model, did you use the same input?

Mr. Carden: We were limited to about 83 percent of the desired input for comparison at that point. In other words, the full scale input was approximately 0.3 g which meant that in our case we would have to put in 0.6 g, but we were only able to get about 0.5 g.

Mr. Rice (Goodyear Aerospace): On your curves you showed an epoxy cement and then below that you showed a curve marked damping adhesive. What were the construction details in your model?

Mr. Carden: Both sets of panels were constructed by attaching two sheets of 0.016-inch aluminum to a tapered balsa wood core. The

sheets were bonded to the core with an epoxy cement in one case, and in the other case with a damping adhesive.

Mr. Forlifer (NASA - Goddard): I noticed in a lot of your slides that the amplification factor was well below one at almost zero frequency. I wonder how this is physically possible?

Mr. Carden: I think probably the explanation of that is in the way we define the amplification factor. On most of the slides that I have shown, the response was measured on the solar panels and the input was at an angle to them.

Mr. Forlifer: The input and response are not parallel?

Mr. Carden: That's right.

* * *

DYNAMIC ENVIRONMENTS OF THE S-IV AND S-IVB SATURN VEHICLES

R. W. Mustain
Douglas Missiles and Space Systems

A brief review of techniques used to predict the dynamic environments of the S-IV and S-IVB vehicles is presented, and these environments are summarized. This review includes discussions on the prediction of rocket exhaust noise, boundary layer noise, sinusoidal vibrations, and random vibrations for the S-IV and S-IVB vehicles. In addition, sine-random vibration conversions are given.

INTRODUCTION

A primary design consideration for the Saturn S-IV and S-IVB stages is the effect of acoustical and vibrational excitations on the vehicle structure and on delicate airborne equipment. The importance of this consideration is enhanced by noting the severe dynamic environments which are produced by the high-thrust rocket systems of the Saturn vehicle. In addition, attention must be given to the possible damaging effects of aerodynamic noise which results from turbulence in the boundary layer; this noise approaches its highest level during the maximum Q (dynamic pressure) phase of the flight mission. In view of the high-thrust rocket systems and the boundary layer noise excitations, there exists a fundamental requirement for an adequate definition of the dynamic environments of the S-IV and S-IVB stages of the Saturn vehicle. The definition of these environments is continually being up-dated; therefore, this paper presents only an interim report. The definition of the S-IV and S-IVB dynamic environments is being modified and improved progressively by field measurements and more refined prediction studies.

The acoustic and vibrational environments of the S-IV and S-IVB stages of the Saturn vehicle are discussed in this paper. Predictions and measurements of these dynamic environments are presented. Predicted acoustic time histories are given for the early phases of the S-IV and S-IVB missions. These time histories are compared with acoustic measurements from two flights of the Saturn I vehicle. Prediction techniques for rocket exhaust noise and

boundary layer noise are discussed briefly. Predictions of acoustic spectra for six S-IV engines (RL-10), without diffuser attenuation, are given. Measurements of acoustic levels during firings of the S-IVB engine are presented and compared with predicted levels.

Different methods of acoustic-vibration correlativity are utilized to provide environmental vibration levels for both the S-IV and S-IVB stages. Various correlation techniques are compared and evaluated. A curve of classical vibration response to acoustic loading is given for use in the correlation of acoustic levels with structural vibration levels. Acoustic-vibration correlation methods are used to determine both sine and random vibration environments. Also, sine-random vibration conversions are used to establish random vibration levels for the S-IVB stage.

SATURN CONFIGURATIONS

The S-IV, powered by six RL-10 engines, is the second stage of the Saturn I; and the S-IVB, powered by one J-2 engine, is (1) the second stage of the Saturn IB, and (2) the third stage of the Saturn V (See Fig. 1). The primary mission of the Saturn I configuration is unmanned orbital flights around the earth. The Saturn IB configuration has as its primary mission the support of the basic Apollo mission by early testing of Apollo spacecraft modules in earth orbital environments. The Saturn V is a three-stage vehicle whose primary mission is lunar manned operations.

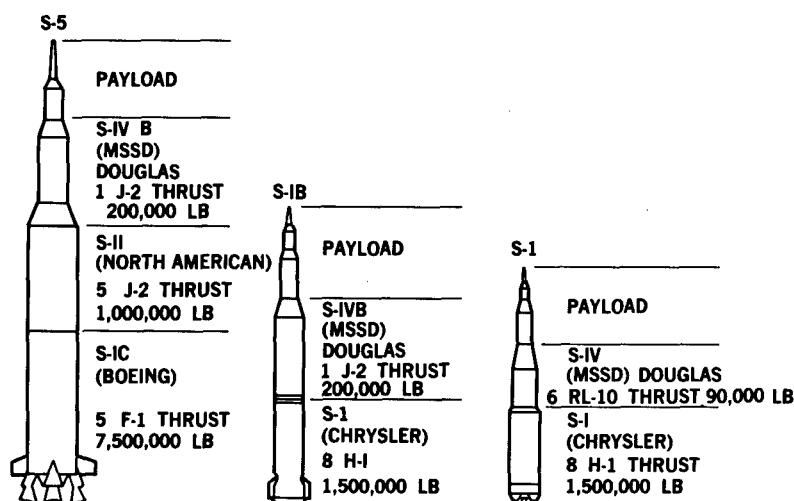


Fig. 1 - Saturn configurations

THE ACOUSTIC ENVIRONMENTS

The structure and the equipment on the S-IV and S-IVB stages will be exposed to acoustic forcing functions that are variant with time and the mission profile. The following list of forcing functions presents some of the acoustic sources that must be considered during the Saturn program:¹

1. Rocket engine noise,
2. Ancillary equipment,
3. Laminar boundary layer noise,
4. Turbulent boundary layer fluctuations,
5. Turbulent wakes (protuberated),
6. Base pressure fluctuations,
7. Cavity resonances, and
8. Secondary acoustic sources.

Usually, the sound field of the rocket engine is the most important source of vibration, and the boundary layer noise ranks second in source severity; however, preliminary data show that the boundary layer noise on the S-IV and S-IVB stages is equal to or greater than the rocket engine noise at some locations. This condition is being investigated; additional measurements will be made during Saturn flights. During the launch phase of the Saturn vehicle, the tremendous noise generated by the rocket engines is transmitted through the atmosphere and reflected by the ground plane around the space vehicle. Since the rocket noise is essentially

random and "white" in nature, it creates resonant responses of skin panels and structures. The magnitude of this excitation depends upon the frequency spectrum, the amplitude, the space correlation of the noise, and the mechanical impedance of the structure. The resulting vibrational energy is transferred throughout the vehicle to substructure and equipment. Some of the panels act as secondary noise sources and radiate acoustic energy into the vehicle's compartments. In turn, some of these bays become semi-reverberant chambers to maintain fairly high acoustic levels. Rocket engine noise, reflected from the ground plane, dominates the Saturn environment for the first few seconds of flight until the Saturn vehicle rises a distance equivalent to approximately 50 exit nozzle diameters. After the Saturn vehicle leaves the launch pad, it begins to gain velocity; and then the effect of vehicle motion becomes apparent until, on approaching Mach 1, the rocket noise does not propagate to the vehicle. As the Saturn vehicle moves with increased velocity through the atmosphere, boundary layer noise becomes the dominant forcing function. Originally, the boundary layer noise is extremely low and is masked during the launch phase by the intense rocket engine noise, and is not propagated in any degree until the sonic speed range is reached. The boundary layer noise is a function of dynamic pressure and other related aerodynamic parameters such as the vehicle's attitude and configuration; this noise reaches its highest level during the maximum Q phase of the flight mission.

Figure 2 summarizes the acoustic environment of the S-IV and S-IVB stages during the first 160 seconds of the flight mission. This

¹R. W. Mustain, "Prediction of Random Environments," SAE National Aeronautic and Space Engineering and Manufacturing Meeting, September 23-27, 1963 at the Ambassador, Los Angeles, California.

OVERALL SOUND PRESSURE LEVEL, db (re. 0.0002 dynes/cm²)

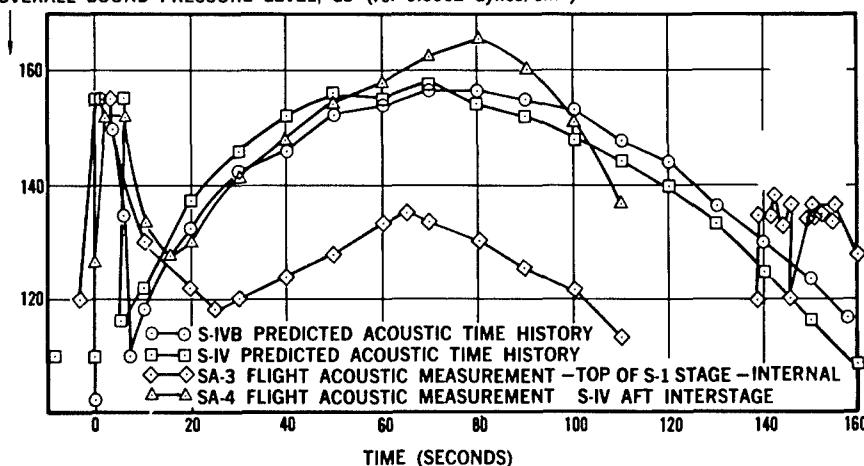


Fig. 2 - S-IV and S-IVB acoustic time histories

chronological history of the major acoustic sources depicts (1) the sound pressure levels predicted for the S-IV and S-IVB stages, and (2) the sound pressure levels measured during Saturn I flights SA-3 and SA-4. The launch phase, the diminution immediately after launch, the increase in level to the maximum dynamic pressure, and the final decline to negligible noise levels are included in this summation. This set of curves shows that the boundary layer noise is equal to or greater than the rocket engine noise during the flight mission. These boundary layer noise levels are indicative of local flow conditions with large protuberances and may be much less (approximately 14 db) on cleaner areas of the S-IV and S-IVB stages where undisturbed boundary layer flow occurs. Four individual time history curves are displayed in Fig. 2:

1. The predicted S-IV acoustic time history,
2. The predicted S-IVB acoustic time history,
3. Acoustic measurements obtained during the Saturn SA-3 flight internally on the SI stage, and
4. Acoustic measurements obtained during the Saturn SA-4 flight externally on the S-IV aft interstage.

All of these curves show a reasonable likeness during the launch phase. With the logical exception of the SA-3 data, the curves also show good agreement during the maximum Q phase of the mission. That is, the SA-3 microphone was located on the lower SI stage, was an internal measurement, and consequently, the SA-3 data should not correlate well with the

other data during the maximum Q phase. Since the microphone on the SI stage is the closest acoustic measurement to the S-IV stage, the SA-3 data are presented only for general interest. The microphone on the fourth Saturn flight (SA-4) was mounted flush with the skin of the S-IV aft interstage in a disturbed flow region. Incidentally, the S-IV stages on the SA-3 and SA-4 flights were dummy stages. The highest boundary layer noise levels on Fig. 2 are those measured during the SA-4 flight. As a first approximation, these fluctuations are assumed proportional to the freestream pressure:

$$\text{OAFPL or OASPL} \cong 20 \log Q + K \text{ db}, \quad (1)$$

where OAFPL is the level of the overall pressure fluctuations at the surface, Q is the freestream dynamic pressure in lb/sq ft, and K is a factor which varies with aerodynamic flow parameters. K is a function of the vehicle's altitude, attitude, velocity, and configuration. The value of K will be approximately 86 for an aerodynamically clean configuration with a zero angle of attack. As drag increases, the value of K increases. Recent wind tunnel tests performed at Douglas indicate that space vehicles, such as the Saturn, with large protuberances, have related K factors as great as 110. A K value of 100 was used to determine the S-IV and S-IVB predictions on Fig. 2. The protuberances are external vehicle items such as wiring ducts, fuel ducts, ullage rockets, and the like.

Predictions of rocket engine noise from six RL-10 engines, without diffusers, are shown in the three-dimensional display of Fig. 3. The sound pressure levels are given as a function of octave bands and location forward of the engine

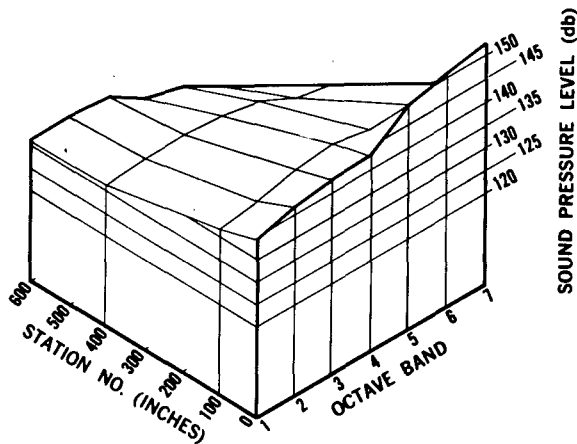


Fig. 3 - Predicted acoustic spectra; 6 RL-10 engines without diffuser attenuation

nozzles. These levels are extremely conservative since the S-IV stage is static (or acceptance) fired with 27-foot diffusers which exhaust against a deflector plate; therefore, these levels should be lowered considerably for S-IV static firings. Two different prediction methods² were used to calculate the noise from the RL-10 engine. The 15,000-pound-thrust engine produces a sound power level of approximately 181 db overall (re 10^{-13} watts). The value of 181 db was found by using an empirical equation which was based on data from rockets in the 1000 to 130,000-pound-thrust range:³

$$\text{OAPWL} = 78 + 13.5 \log_{10} W_m, \quad (2)$$

where W_m = mechanical power of jetstream in watts,

$$W_m = 0.676 \text{ tV} = 0.676 (t^2 g)/w,$$

with $V = (tg)/w$ = gas velocity at nozzle exit in fps,

t = thrust in pounds,

g = acceleration due to gravity = 32.2 ft/sec², and

w = weight flow in lb/sec;

then

²R. W. Mustain, "On the Prediction of Dynamic Environments," Vibration, and Associated Environments Bulletin No. 28, Part IV, Office of the Secretary of Defense (Aug. 1960).

³WADC Technical Report 57-354, "Noise Radiation from Fourteen Types of Rockets in the 1000 to 130,000-Pound Thrust Range" (Dec. 1957).

$$\text{PWL} = 78 + 13.5 \log 0.676 \frac{t^2 g}{w}.$$

The empirical relationship of Eq. (2) remains a fairly reliable prediction of the total acoustical power of conventionally fueled rockets at sea-level operations.⁴

Acoustic data obtained during test stand firings of the S-IVB engine, the J-2, at Rocketdyne are summarized in Fig. 4. The average sound pressure levels from four test firings are plotted as a function of octave bands and distance forward of the nozzle exit plane. Acoustic data, from Fig. 4, for the aft skirt are replotted in Fig. 5 and compared with acoustic levels which were determined by four different prediction methods:

1. WADC TR 58-343 (Ref. 5),
2. WADC TR 57-354 (Ref. 3),
3. Modified WADC TR 58-343 (Ref. 6), and
4. Scaled Thor data.

The highest levels on Fig. 5 are displayed by the measured J-2 data, especially in the second through fifth octave bands. The scaled Thor data and the modified WADC data show a reasonable agreement with the measured data at the higher frequencies. Following are the original measured data on the Thor booster:

Octave Band	Sound Pressure Level (db)
1	141
2	144
3	146
4	147
5	146
6	145
7	144
8	143
overall	154

By using Eq. (2), the sound power levels were found to be 199 db re 10^{-13} watt for the Thor and 198 db re 10^{-13} watt for the J-2 engine at sea level. Then, the sound power level differential of 1 db was subtracted from the original Thor data. These lower levels are plotted on Fig. 5 as the scaled Thor data.

⁴Northrop Report NOR-60-26, "Structural Vibration in Space Vehicles," Phase I Report, "Investigation of Structural Vibration Sources and Characteristics."

⁵WADC Technical Report 58-343, "Methods of Space Vehicle Noise Prediction" (Sept. 1960).

⁶P. A. Franken and F. M. Wiener, "Estimation of Noise Levels at the Surface of a Rocket-Powered Vehicle," Bolt, Beranek, and Newman Inc., Los Angeles, California and Cambridge, Massachusetts.

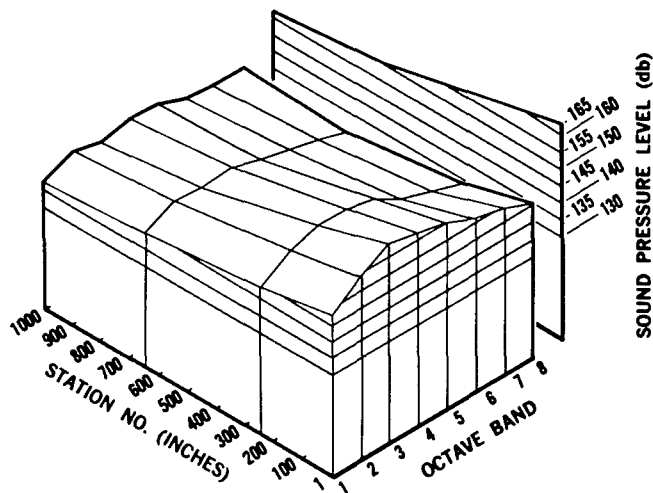


Fig. 4 - Measured S-IVB engine acoustic spectra

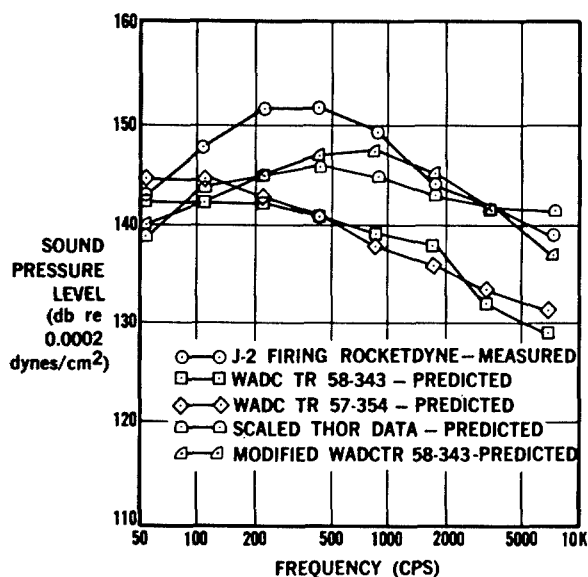


Fig. 5 - S-IVB static firing acoustic spectra at AFT skirt

S-IV VIBRATION PREDICTIONS AND MEASUREMENTS

Saturn rocket engine and boundary layer noise has, in general, a random distribution with broad spectra. As these acoustic excitations impinge on the S-IV stage they induce random vibrations (with variant bandwidths) on the vehicle structure. This condition of randomness varies throughout the vehicle as the spectra are influenced by structural filters that create dominant peaks at response frequencies.

Also, the random vibrations are assumed to have instantaneous accelerations (in any frequency band) that exhibit normal or Gaussian distributions. Perhaps, the most severe vibration environment occurs during the maximum Q phase of flight for a relatively short period of time. Lower vibration levels occur on the S-IV stage during the acceptance (static) firings which are conducted on each S-IV stage at the Sacramento, California facility of the Douglas Aircraft Company, Inc. The vibration levels during the S-IV acceptance firings are greatly reduced by the use of 27-foot diffusers which attenuate the acoustic excitations from the RL-10 engines. In addition, the S-IV stage is supported by isolators during the acceptance firings to minimize the dynamic feedback from the test stand. Hence, the vibration environment of the S-IV stage during the acceptance firings is primarily mechanically induced. Furthermore, it is highly probable that the vibration environment of the acceptance firings closely simulates the vibration environment during flight when the RL-10 engines are firing. In order to establish the vibration environment of the S-IV acceptance firings, vibration measurements were recorded during static firings of the S-IV-5 stage at Sacramento. Some of these data are presented in this report and compared with vibration predictions based on the conservative acoustic levels of Fig. 3.

Prior to discussing these vibration comparisons, a brief description is given of acoustic-vibration correlation techniques which are used in this paper to predict some of the S-IV vibration levels. Several investigators have attempted to establish the relationship between the acoustic

forcing function and the resultant vibratory response. This has led to the establishment of vibration prediction techniques which are founded on acoustic-vibration correlativity. These prediction methods have used empirical information as their basis. Much remains to be desired on the accuracy of these various methods. The fault lies in the fact that these prediction methods are based on general data; consequently, these methods may not provide optimum predictions for specific cases.

Another drawback of most prediction techniques is the failure to account for structural resonances caused by structural filters. To explain further, predictions of random vibrations should display dominant peaks at response frequencies. Most predictions, however, show broad spectra which are in general agreement with typical vibration test specifications. This leads to conservative vibration test levels which may or may not be justified; this depends on the structural configuration. Relatively soft structures with many response frequencies should be tested to conservative specifications with broad spectra. In contrast, strong primary structure with a high natural frequency will have a dominant response peak. Then, the environmental vibrations on such a structure are best represented or estimated by a peaked vibration spectrum. Thus, ideal predictions should be based on actual knowledge of the structure being investigated. First, analytical techniques can be used to determine response spectra of structures. Secondly, response frequencies of structures can be determined by actual measurements. Finally, it can be expected that, within this decade, mechanical admittance or impedance measurements will be widely used to define structural

response spectra and to determine transfer functions.

One of the popular empirical methods used to predict vibration levels is described in Ref. 7, which provides curves for predicting vibrations induced by acoustic excitations. Predictions using Ref. 7 data can be determined for different confidence levels. These resulting vibration spectra, however, are broad band such as those found in typical test specifications. Two additional curves for predicting acoustically induced vibrations are given in Figs. 6 and 7. The correlation data of Fig. 6 are based on Minuteman, Jupiter, Titan, and Skybolt measurements collected by E. F. Winter.⁸ The acoustic-vibration correlativity of Fig. 7 was compiled by the author of this paper. The data in Fig. 7 are representative of rigid primary structure with a dominant and high (say approximately 700 to 1200 cps) response frequency. These data tend to follow a classical transmissibility curve.

A large quantity of useful vibration data was obtained during two acceptance firings of the S-IV-5 stage. The presentation of all the vibration data from the S-IV-5 firings is beyond the scope of this paper. The accelerometer locations during the S-IV-5 acceptance firings at

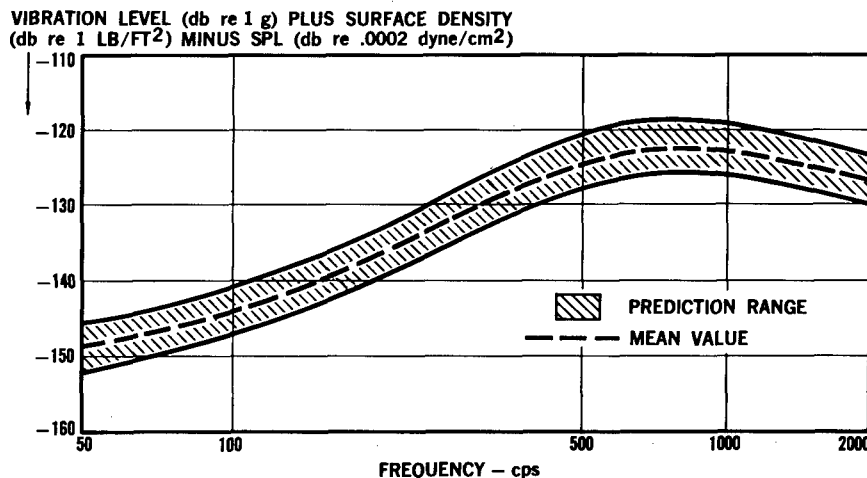


Fig. 6 - Structural response to acoustic loading

⁷P. T. Mahaffey and K. W. Smith, "A Method for Predicting Environmental Vibration Levels in Jet-Powered Vehicles," Shock, Vibration, and Associated Environments Bulletin No. 28, Part IV, Office of the Secretary of Defense (Aug. 1960).

⁸Personal communication E. F. Winter, Douglas Missile and Space Systems Division, to R. W. Mustain.

ACCELERATION IN DB - SPL IN DB
RE 0.1g (PEAK) & .0002 MICROBARS

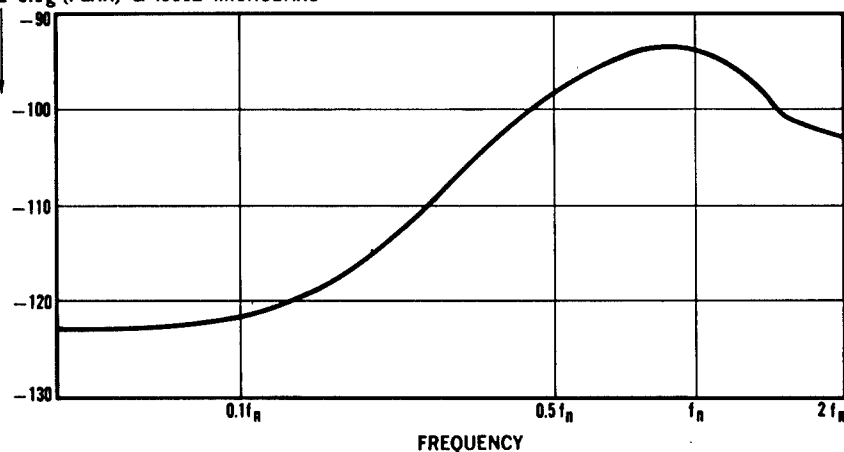


Fig. 7 - Classical response to acoustic loading

Sacramento are shown in Fig. 8. Data from only three accelerometer locations are given in this report. Acceptance firing vibrations at the gimbal point, the thrust cone, and the base of the telemetry rack are displayed in Figs. 9, 10, and 11. In these three figures, the acceptance firing vibrations are compared with predictions of acoustically induced vibrations which are based on the RL-10 engine data of Fig. 3. These predictions were established by using data from Figs. 3, 6, and 7 of this paper and data from Ref. 7. Four curves are shown in each of the graphs of Figs. 9, 10, and 11:

1. Vibration levels determined by the method of Smith and Mahaffey⁷ (95 percent confidence),

2. Vibration levels determined by using the data in Fig. 6 of this paper,

3. Vibration levels determined by using the data on the classical curve of Fig. 7, and

4. Measured vibration levels from the acceptance firings of the S-IV-5 stage at Sacramento, California.

Three tables showing typical data for each of the prediction methods are given in addendum A, which accompanies this paper.

The predicted vibration levels in Figs. 9, 10, and 11 are based on the acoustic levels shown in Fig. 3; consequently, these predicted vibrations are much greater than the actual

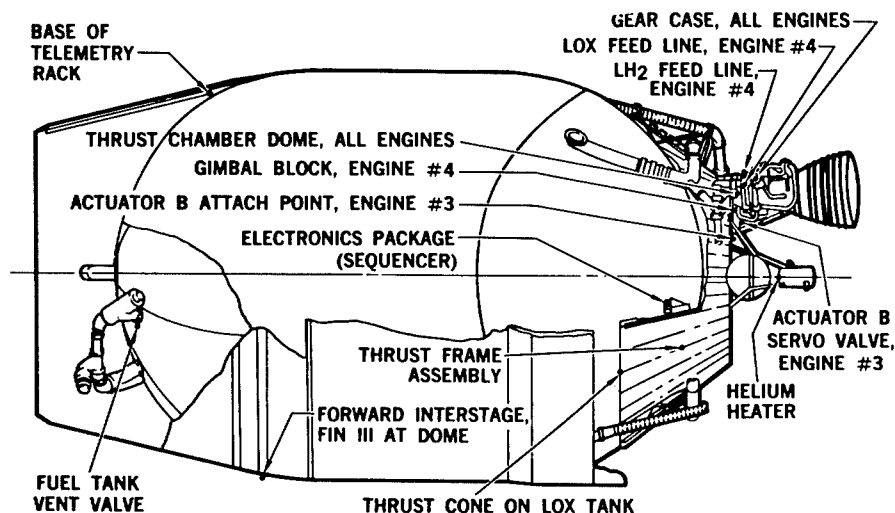


Fig. 8 - Accelerometer locations; acceptance firings S-IV-5

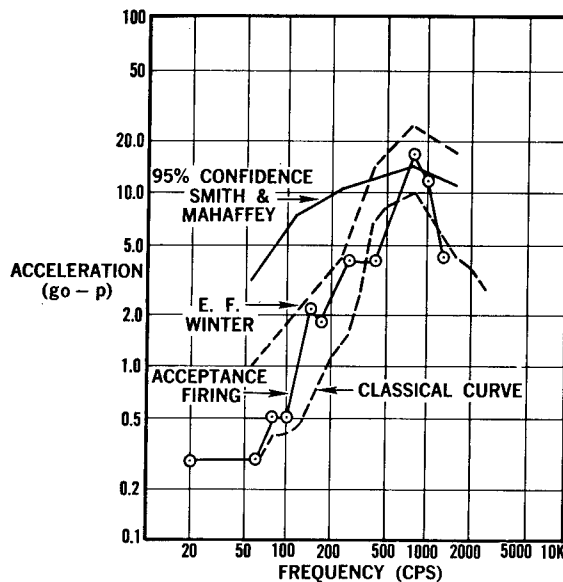


Fig. 9 - Comparison of S-IV-5 acceptance firing vibrations with predicted vibrations based on data from Fig. 3 (gimbal point)

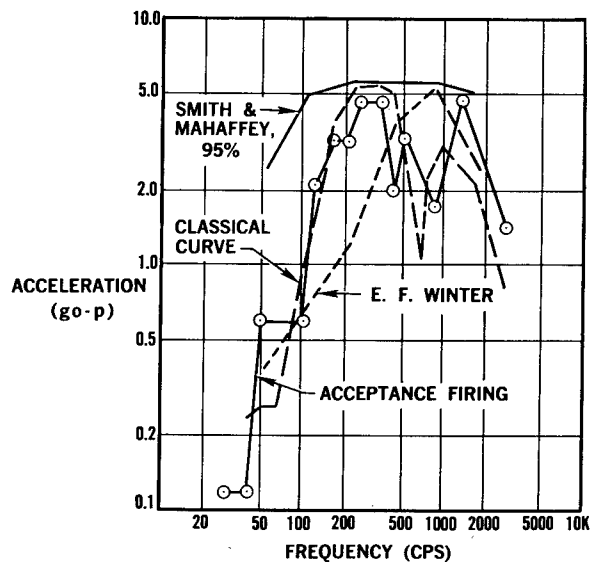


Fig. 11 - Comparison of S-IV-5 acceptance firing vibrations with predicted vibrations based on data from Fig. 3

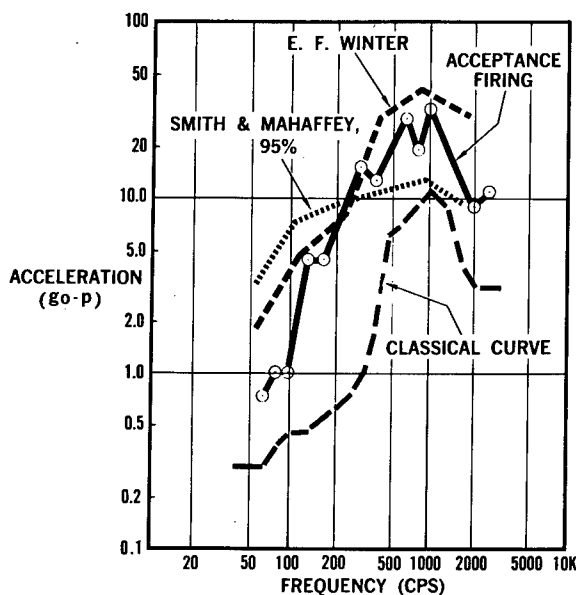


Fig. 10 - Comparison of S-IV-5 acceptance firing vibrations with predicted vibrations based on data from Fig. 3 (thrust cone)

acoustically induced vibrations on the S-IV acceptance firings. Since the actual S-IV acceptance firings are made with diffusers, the static firing acoustic levels are much lower than the levels of Fig. 3. In turn, the acoustically induced vibrations during the static firings are much

less than the predictions in Figs. 9, 10, and 11. Whereas the S-IV acceptance firings are made with diffusers which attenuate most of the sound, the vibrations on the S-IV stage during the acceptance firings are almost entirely mechanically induced. A study of Figs. 9, 10, and 11 shows that the mechanically induced vibrations during the acceptance firings are approximately equal to predicted acoustically induced vibrations from six unattenuated RL-10 engines. Originally, these figures were prepared to show the differential between mechanically induced vibrations (acceptance firing data) and acoustically induced vibrations (the predicted vibrations). However, the predicted and the measured vibrations show an unexpected agreement which indicates that the S-IV engine-vehicle transfer function results in relatively high mechanically induced vibrations. This transfer function includes the effects of multiple engine dynamics on the S-IV structure. Also, some of the mechanically induced vibrations may be attributed to accessories on the six RL-10 engines. This subject of mechanically and acoustically induced vibration on the S-IV stage is an interesting one that requires further analysis. This relationship will be better defined as microphone measurements and additional vibration measurements become available from future S-IV acceptance firings.

The next four figures (Figs. 12-15) show predictions of the acoustically induced vibrations during launch and flight of the S-IV

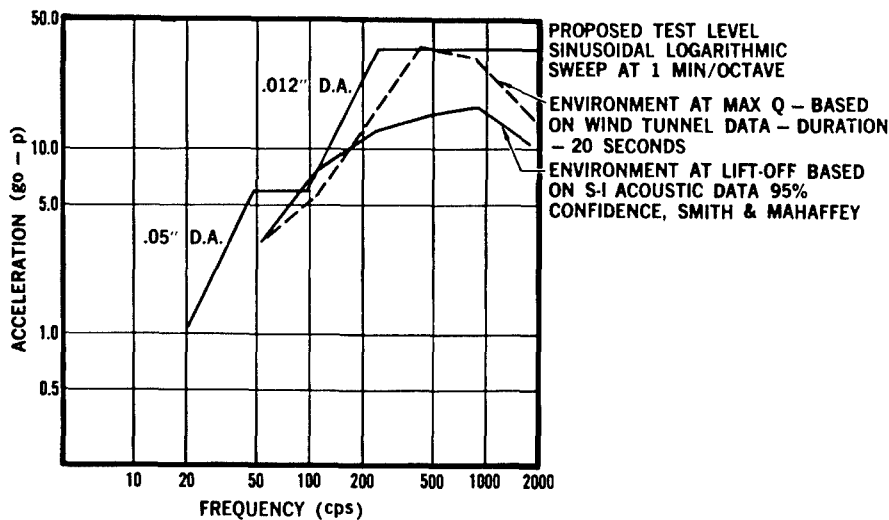


Fig. 12 - Prediction of acoustically and pressure fluctuation induced vibration-extreme aft of S-1/S-IV interstage

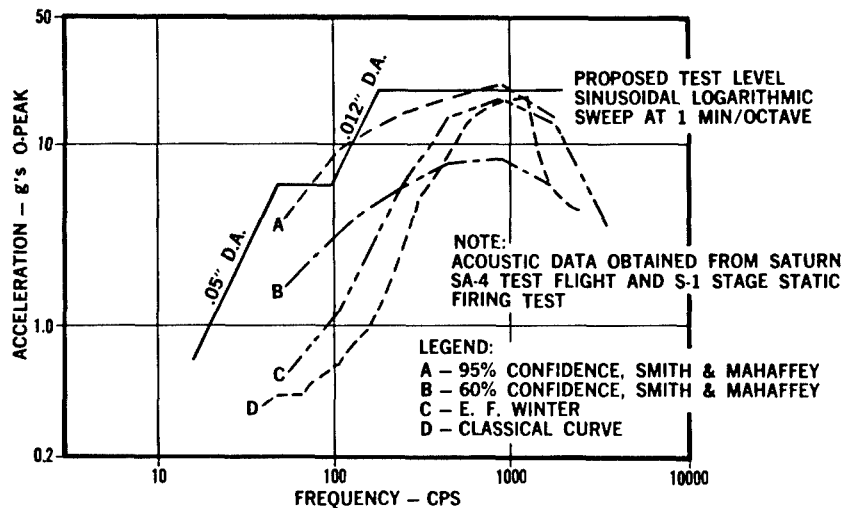


Fig. 13 - Predictions of acoustically induced vibration, aft interstage of S-IV

stage.⁹ In each figure, an envelope has been drawn over the 95-percent confidence level (Smith and Mahaffey) to provide a conservative test level. This test level is applied as a 1 minute per octave sinusoidal logarithmic sweep. With this sweep rate, a test specimen is exposed to each resonance for approximately 35 seconds (Ref. 9). Predicted vibrations on the extreme aft S-IV interstage are plotted on

⁹J. C. McClymonds and J. W. Lew, "Proposed Deviation from MSFC Vibration Specification IN-P&VE-S-62-7," Douglas Missile & Space Systems Division (Sept. 4, 1963).

Fig. 12. The vibration environment of Fig. 12 is based on wind tunnel data for the maximum Q phase and on SI acoustic data for the lift-off phase. Both the maximum Q and the lift-off predictions of Fig. 12 were determined by using the data from Ref. 7. The vibration environments of the aft interstage (Fig. 13), the thrust structure (Fig. 14), and the forward interstage (Fig. 15) are based on acoustic data which were obtained from the Saturn SA-4 flight and from SI stage static firings. Figures 13, 14, and 15 display comparative vibration levels which were obtained by using the data of Figs. 6 and 7 of this paper and the data from

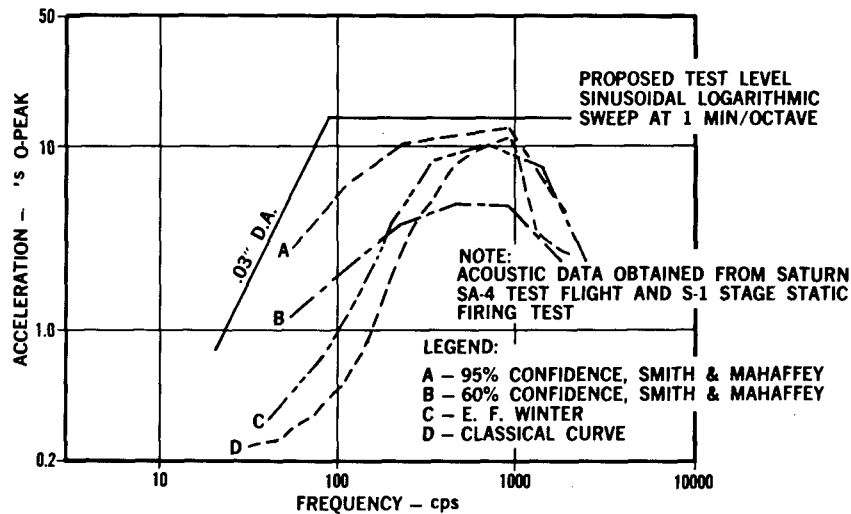


Fig. 14 - Predictions of acoustically induced vibration, thrust structure of S-IV

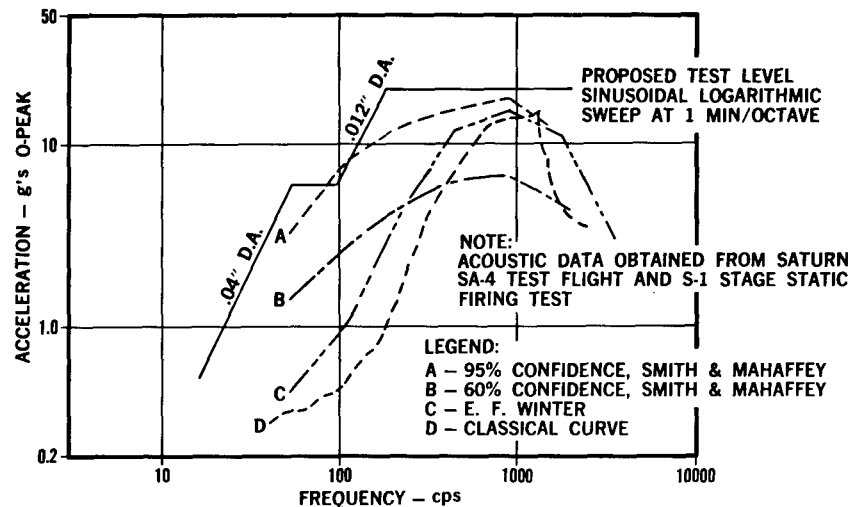


Fig. 15 - Predictions of acoustically induced vibration, forward interstage of S-IV

Ref. 7. Curves A, C, and D display a reasonable agreement. The best agreement is noted near the response frequency of the structure where curves C and D peak. The poorest correlation can be found at the lower frequencies where the broad spectrum of curve A exists. Curve A is typical of specifications which provide overly conservative test levels. The reason for the difference in the low frequency levels is probably due to the fact that curve A is an envelope of vibration levels of light components attached to light flexible structure. Curves B, C, and D are considered to envelope vibration levels measured on heavy primary structure.

S-IVB VIBRATION PREDICTIONS

An exploded view of the Saturn S-IVB stage is presented in Fig. 16. Similar to the S-IV dynamic environment, the S-IVB vibration environment has, in general, a random distribution with broad spectra. The bandwidth of these random vibrations varies throughout the vehicle as the spectra are influenced by structural filters that create dominant peaks at response frequencies. Furthermore, the instantaneous accelerations are assumed to have normal distributions or slight modifications of the normal distribution, and the corresponding peaks are

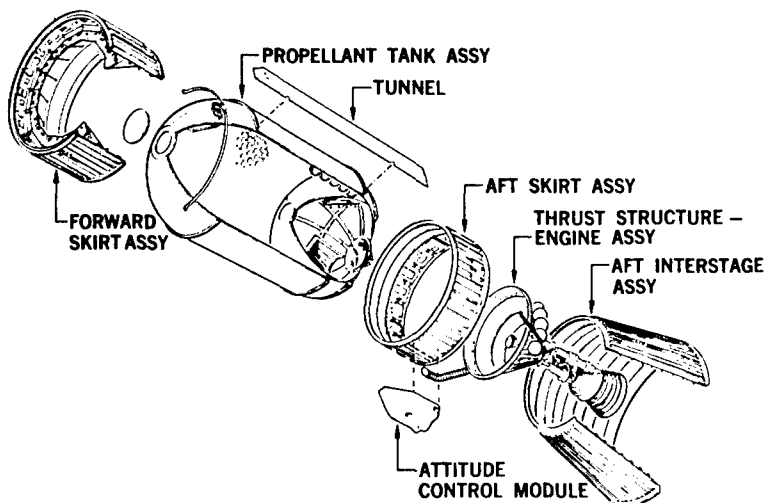


Fig. 16 - Saturn S-IVB stage, exploded view

assumed to be distributed according to the Rayleigh law. The S-IVB vibrations will be significant during the lift-off phase, the maximum Q phase, and the J-2 engine firing phase. The lift-off vibrations and the maximum Q vibrations of the S-IVB stage will be similar in severity to the S-IV lift-off and maximum Q vibrations. The vibrations during the S-IVB acceptance firings will be greater than the vibrations during the S-IV acceptance firings because of the more severe acoustical environment. Likewise, the mechanically induced vibrations from the J-2 engine during S-IVB flight will be greater than the flight vibrations from the RL-10 engines on the S-IV stage because of the increased engine size and thrust. Since the vibrations during the S-IVB acceptance firings will rank high in importance, predictions have been made of acoustically induced vibrations on the S-IVB static firings.

These predictions were established by using data from Figs. 4, 6, 7, and 17 of this paper and data from Ref. 7. Figure 17 of this paper was originally presented in Ref. 10. This figure is useful in proposal stages and early design stages where little is known about a vehicle. To use this figure, only an overall sound pressure level is required; this technique provides a reasonable "ball-park" estimation. Random vibration spectra are given for five different overall sound pressure levels in Fig. 17. Only random vibration predictions are given for the S-IVB acceptance firings. Predicted random vibration levels for the S-IVB acceptance firings

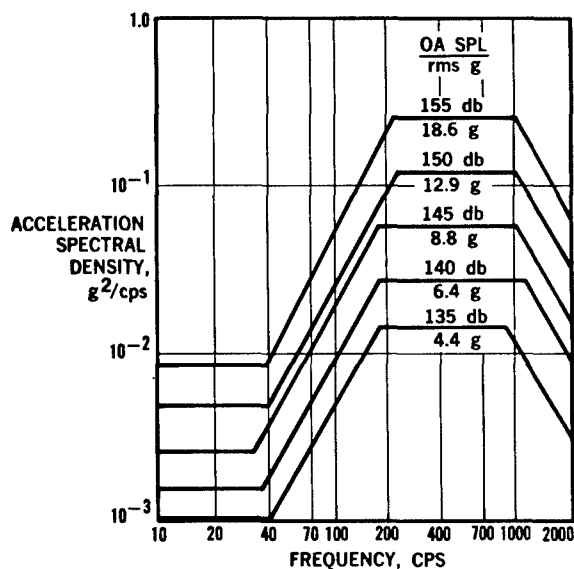


Fig. 17 - Test requirement envelopes for various acoustic noise levels

are given in Figs. 18 and 19. Five curves are shown in each of the graphs of Figs. 18 and 19:

1. Vibration levels determined by the method of Smith and Mahaffey⁷ (95-percent confidence),
2. Vibration levels determined by the method of Smith and Mahaffey⁷ (60-percent confidence),
3. Vibration levels determined by using the data in Fig. 6 of this paper,
4. Vibration levels determined by using the data on the classical curve of Fig. 7, and

¹⁰H. Himelblau and A. G. Piersol, "Summary of Nortronics Modification of Mahaffey Smith Procedure" (Oct. 1963).

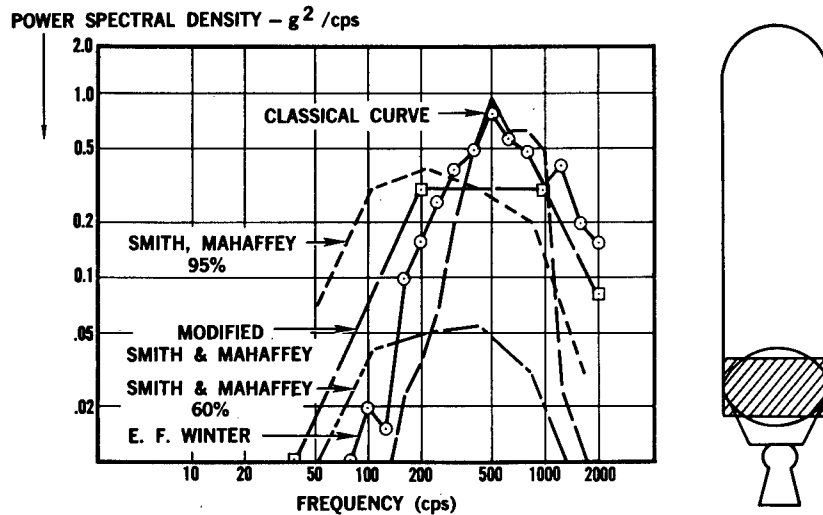


Fig. 18 - Predicted random vibration levels S-IVB, aft skirt static firing

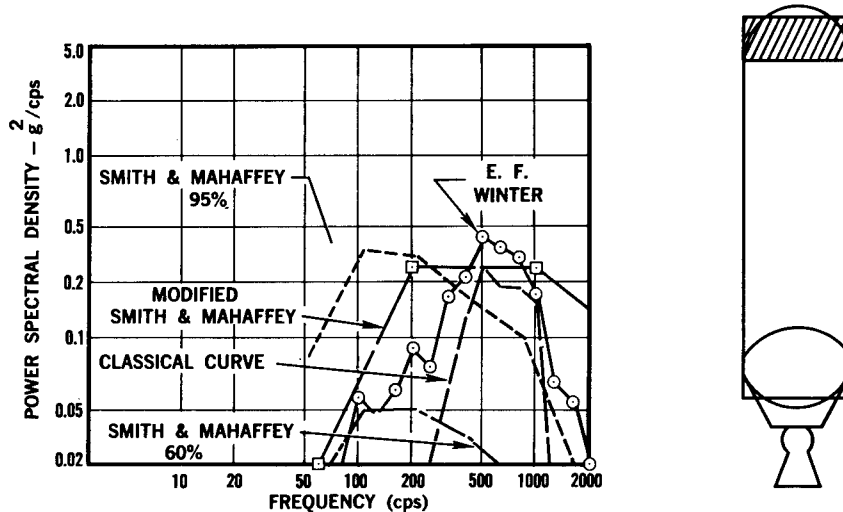


Fig. 19 - Predicted random vibration levels S-IVB, forward skirt static firing

5. Vibration levels determined by using the data of Fig. 17.

Three tables showing typical data on three of the prediction methods are given in addendum B of this paper. For additional information on predicting random vibration levels from Fig. 7 and on sine-random conversions, the reader is referred to Ref. 1. All of the curves labeled "Smith and Mahaffey" and "E. F. Winter" were determined by first finding sinusoidal vibration levels and then converting to random vibration levels by using the following equation from Ref. 1:

$$G = \frac{0.174 (A_p)^2}{f}, \quad (3)$$

where G = mean squared acceleration density or power spectral density in g^2/cps , A_p is the peak applied sinusoidal vibration, and f is the frequency of resonance.

A reasonable correlation is noticed on Figs. 18 and 19. In Fig. 18, the classical curve and the E. F. Winter curve display an excellent agreement. Also, the Smith and Mahaffey 95-percent curve and the Modified Smith and Mahaffey

curve are in good agreement. The main difference is in the frequency range; this difference is a natural result of the two different techniques. The predicted random vibration levels of the S-IVB forward skirt (Fig. 19) are less than the predicted vibration levels on the aft skirt. In Figure 19, all of the curves, except the Smith and Mahaffey 60-percent curve, compare very well. The predictions in Figs. 18 and 19 provide useful vibration levels which establish a vibration gradient for the S-IVB stage, and which are currently being used to determine S-IVB vibration test levels.

CONCLUSION

This paper has presented a brief review of the acoustic and vibration environments of the S-IV and S-IVB stages of the Saturn vehicle. Only a fragment of the available data was covered in this interim paper. Predictions and measurements of the acoustic and vibration environments were given. Predicted acoustic time histories for the early phases of the S-IV and S-IVB missions were presented. These acoustic predictions were compared with Saturn I flight data. Predictions of acoustic spectra for six S-IV engines (RL-10), without diffuser attenuation, were given. This presentation included a summary of acoustic data from J-2 engine firings.

Environmental vibration levels for both the S-IV and S-IVB stages were determined by using different methods of acoustic-vibration correlativity. Comparisons were made of the results obtained by the different correlation techniques. These methods were used to determine both sine and random vibration environments. Vibration data measured during the S-IV-5 acceptance firing were presented and discussed.

Much work remains to be done in the definition of the S-IV and S-IVB acoustical and vibrational environments. More vibration measurements will be acquired during static firings and flights of both the S-IV and S-IVB stages. In addition, microphone measurements will be obtained. A continuous and necessary effort is underway to adequately define the acoustical and vibrational environments of the S-IV and S-IVB stages.

ACKNOWLEDGMENT

The writer is greatly indebted to K. E. Elliot, J. W. Lew, P. M. Lewis, J. C. McClymonds, T. D. Schoessow, P. F. Spas, and E. F. Winter of the Douglas Missile and Space Systems Division for their contributions to this paper.

Addendum A

ACOUSTIC-VIBRATION CORRELATIVITY

VIBRATION LEVELS DETERMINED BY THE METHOD OF SMITH AND MAHAFFEY⁷

The basic data for the curve (95-percent confidence, Smith and Mahaffey) in Fig. 9 are given in Table A1. These curves have been drawn through points which were plotted at the geometric mean frequencies ($GMF = \sqrt{f_1 \times f_2}$) of the octave bands. Octave bandwidths were used in agreement with the method of Ref. 7.

VIBRATION LEVELS DETERMINED BY USING THE DATA IN FIG. 6 OF THIS PAPER

The calculations for the E. F. Winter curve in Fig. 9 are given in Table A2 for the gimbal point of the S-IV stage. This curve was determined by using the data in Fig. 6 and the following basic relationship:

$$20 \log_{10} g_{rms} = SPL + TF - 20 \log_{10} W \text{ (in db re 1 g),}$$

where W = surface density in lb/ft²,

TF = transfer function (ordinate of Fig. 6),

SPL = sound pressure level (db), and

$20 \log g_{rms}$ is in db re 1 g.

VIBRATION LEVELS DETERMINED BY USING THE DATA IN THE CLASSICAL CURVE OF FIG. 7

The calculations for the (classical) vibration levels in Fig. 9 are listed in Table A3. These vibrations display a dominant peak which is characteristic of rigid primary structure. In this case, a response frequency of approximately 800 cps was assumed. Since the correlation data in Fig. 7 were obtained from actual

TABLE A1

Octave Bands	GMF	SPL (db)	60% g's (o-peak)	95% g's (o-peak)
37.5 - 75	53	137.6	1.4	3.2
75 - 150	106	138.9	2.5	7.2
150 - 300	212	140.2	3.7	10.0
300 - 600	425	140.6	5.0	11.5
600 - 1200	850	139.0	5.2	13.3
1200 - 2400	1700	139.5	4.4	10.8

TABLE A2

$$20 \log_{10} W = -0.72$$

1	2	3	4	5	6	7	8
Octave Bands	GMF	SPL	TF	3 + 4	Col. 5-20 log W in db re 1g	g_{rms}	g (o-peak)
37.5 - 75	53	137.6	-148	-10.4	-9.7	.32	1.0
75 - 150	106	138.9	-143	-4.1	-3.4	.68	2.0
150 - 300	212	140.2	-138	2.2	2.9	1.40	4.2
300 - 600	425	140.6	-128	12.6	13.3	4.70	14.1
600 - 1200	850	139.0	-122	17.0	17.7	7.80	23.4
1200 - 2400	1700	139.5	-125	14.5	15.2	5.75	17.3

TABLE A3

1	2	3	4	5	6
f 1/3 Octave Band	TF	1/3 Octave SPL (db)	Column 2 plus Column 3 in db	Ratio g peak/0.1g Equivalent to db of Col. 4	Col. 5 x 0.1 in g's (o-peak)
40	-123	132.6	9.6	3.0	.3
50	-123	132.6	9.6	3.0	.3
63	-123	132.6	9.6	3.0	.3
80	-121	133.9	12.9	4.5	.45
100	-121	133.9	12.9	4.5	.45
125	-120	133.9	13.9	5.0	.5
160	-117	135.2	18.2	8.15	.815
200	-115	135.2	20.2	10.2	1.02
250	-112	135.2	23.2	14.5	1.45
315	-108	135.6	27.6	24.0	2.40
400	-99	135.6	36.6	67.5	6.75
500	-97	135.6	38.6	85.0	8.50
630	-95	134.0	39.0	89.0	8.90
800	-94	134.0	40.0	100.0	10.0
1000	-97	135.0	37.0	71.0	7.10
1250	-100	134.5	34.5	53.0	5.30
1600	-103	134.5	31.5	38.0	3.80
2000	-104	134.5	30.5	34.0	3.40
2500	-106	134.5	28.5	26.6	2.66

1/3-octave acoustic and vibration measurements, they are applicable to 1/3-octave predictions. The octave-band sound pressure levels listed in Tables A1 and A2 were converted to 1/3-octave-band sound pressure levels by simply subtracting 5 db from the octave-band sound pressure levels. Table A3 used the relationship:

$$20 \log_{10} (g_{\text{peak}}/g_{\text{ref}}) = \text{SPL} + \text{TF} \text{ (in db re 0.1 g),}$$

where SPL = sound pressure level in 1/3 octave bands (db) and

TF = transfer function (ordinate of Fig. 7).

Addendum B

RANDOM VIBRATION PREDICTIONS

RANDOM VIBRATION LEVELS DETERMINED BY THE METHOD OF SMITH AND MAHAFFEY⁷ AND THE USE OF EQ. (3)

The basic data for the Smith and Mahaffey 95-percent curve in Fig. 18 are given in Table B1. These curves have been drawn through points which were plotted at the geometric mean frequencies ($\text{GMF} = \sqrt{f_1 \times f_2}$) of the octave bands. Octave band widths were used in agreement with the method of Ref. 7.

RANDOM VIBRATION LEVELS DETERMINED BY USING THE DATA IN FIG. 6 AND BY USING EQ. (3)

The calculations for the E. F. Winter curve in Fig. 18 are given in Table B2. The data in Fig. 6 and the following basic relationship are used:

$$20 \log_{10} g_{\text{rms}} = \text{SPL} + \text{TF} - 20 \log_{10} W$$

(in db re 1 g),

where W = surface density in lb/ft²,

TF = Transfer function (ordinate of Fig. 6), and

SPL = sound pressure level (db);

$$W = 1 \text{ lb/ft}^2; 20 \log W = 0.$$

RANDOM VIBRATION LEVELS DETERMINED BY USING THE DATA IN THE CLASSICAL CURVE OF FIG. 7

The calculations for the classical curve of Fig. 18 are listed in Table B3. These vibrations display a dominant peak which is characteristic of rigid primary structure. In this case, a response frequency of approximately 900 cps was assumed. Since the correlation data in Fig. 7 were obtained from actual 1/3-octave acoustic and vibration measurements, they are applicable to 1/3-octave predictions. Table B3 uses the relationship:

$$20 \log_{10} (g_{\text{peak}}/g_{\text{ref}}) = \text{SPL} + \text{TF}$$

(in db re 0.1 g),

where SPL = sound pressure level in 1/3 octave bands and

TF = transfer function (ordinate of Fig. 7).

TABLE B1

Octave Bands	GMF	SPL (db)	95% g's (o-p)	95% \dot{g}^2/cps
37.5 - 75	53	143	4.4	.07
75 - 150	106	148	13.5	.30
150 - 300	212	152	21.8	.39
300 - 600	425	152	27.0	.30
600 - 1200	850	149	29.5	.20
1200 - 2400	1700	144	15.7	.03

TABLE B2

1	2	3	4	5	6	7	8	9	10
f CPS	SPL db	TF db	Col. 2 + Col. 3	Col. 4 - 20 log W	g_{rms}	$g_{(o-p)}$	g^2	$.174g^2$	g^2/cps
40	138	-150	-12	-12	0.25	0.75	0.565	.098	.0025
50	138	-148	-10	-10	0.32	0.96	0.925	.161	.0032
63	138	-147	-9	-9	0.55	1.65	2.72	.473	.0075
80	143	-146	-3	-3	0.71	2.17	5.08	.885	.0111
100	143	-144	-1	-1	1.1	3.3	10.95	1.91	.0191
125	143	-142	1	1	1.1	3.3	10.95	1.91	.0153
160	149	-139	10	10	3.17	9.5	90.4	15.75	.0985
200	149	-136	13	13	4.47	13.3	177	30.8	.154
250	149	-133	16	16	6.32	19.0	361	62.7	.251
315	149	-130	19	19	8.80	26.4	700	122	.387
400	149	-128	21	21	11.2	33.6	1134	197.5	.494
500	149	-125	24	24	15.8	47.4	2260	395	.779
630	146	-122.5	23.5	23.5	14.95	44.8	2020	351	.557
800	146	-122	24	24	15.8	47.4	2260	395	.493
1000	146	-123	23	23	14.1	42.2	1790	312	.312
1250	139	-124	15	15	5.62	16.9	286	49.7	.397
1600	139	-126	13	13	4.47	13.3	177	30.8	.193
2000	139	-126	13	13	4.47	13.3	177	30.8	.154

TABLE B3

1	2	3	4	5	6	7	8	9
f 1/3 Octave Band	TF	SPL db	Spectrum Level Conversion	20 Log $g_{peak}/0.1 g$	$g_{peak}/0.1 g$	g_{peak}	g_{rms}	g^2/cps
40	-123	138	-9.6	5.4	1.86	.19	.06	.004
50	-122.5	138	-10.6	4.9	1.78	.18	.06	.004
63	-122	138	-11.6	4.4	1.66	.17	.06	.004
80	-122	143	-12.6	8.4	2.63	.26	.09	.008
100	-121.5	143	-13.6	7.9	2.51	.25	.08	.006
125	-120.5	143	-14.6	7.9	2.51	.25	.08	.006
160	-118.5	147	-15.6	12.9	4.5	.45	.15	.023
200	-116	147	-16.6	14.4	5.3	.53	.18	.033
250	-112	147	-17.6	17.4	7.4	.74	.25	.063
315	-106	147	-18.6	22.4	13.3	1.33	.44	.194
400	-101	147	-19.6	26.4	20.9	2.1	.70	.49
500	-97	147	-20.6	29.4	29.5	2.95	.98	.96
630	-95	144	-21.6	27.4	23.5	2.35	.78	.61
800	-94	144	-22.6	27.4	23.5	2.35	.78	.61
1000	-94	144	-23.6	26.4	20.9	2.1	.70	.49
1250	-101	139	-24.6	13.4	4.65	.465	.15	.023
1600	-103	139	-25.6	10.4	3.31	.33	.11	.012
2000	-105	139	-26.6	7.4	2.35	.23	.08	.006

DISCUSSION

Mr. Himelblau (Nortronics): When you were working with the peak criteria, what bandwidth did you use for comparison? You were comparing the flight environment with the specification, and also with some of the predictions on a peak basis. It was one of the slides in the middle, in fact there were three or four like that. You were plotting g's, zero to peak, versus frequency.

Mr. Mustain: Do you mean the g's that were actually measured? Static firing information? That was third octave.

Mr. Himelblau: Now if you selected a tenth octave or a full octave, wouldn't this produce completely different conclusions?

Mr. Mustain: Yes it would.

Mr. Himelblau: Well, I guess I'm trying to pick up the gauntlet laid down by Dr. Mains, and trying to figure out what we are justifying when we are comparing, say, a test specification level with field data on the basis of peak only, when this can vary all over the map as a function of bandwidth.

Mr. Mustain: This is one of the drawbacks of all test specifications. Whenever a test specification is applied in the laboratory it is very seldom used with a vibration system in the same way that flight measurements or predicted values are obtained. This is a problem that is always there. I hope that it will get better, but we will certainly have to live with it for quite a while.

* * *

A PRACTICAL METHOD OF PREDICTING THE ACOUSTICAL DYNAMIC ENVIRONMENT FOR LARGE BOOSTER LAUNCH FACILITIES

R. W. Peverley and E. B. Smith
Martin Company
Aerospace Division of Martin-Marietta Corporation
Denver, Colorado

A review of prediction methods and their applicability to large booster systems is presented. The power spectrum, propagation constants, source location, and directivity are calculated for Titan and Saturn and the results compared to measured data. In addition, it is shown how this method was used to calculate Titan III and Saturn V launcher environments. It is suggested that this method, though only an approximation, will yield estimates which are within reasonable engineering limits.

INTRODUCTION

The problems associated with the intense noise generated by a large rocket engine during the initial stages of flight are an important parameter in the design of a space booster launch facility. These problems have increased as booster engine thrust levels have become larger. On early missile and space booster programs, acoustics were seldom, if ever, considered in the design of the launch facility, and the acoustically induced vibration environment of the vehicle was considered to be the major acoustical problem. Later, much time and money was devoted to the study of far field rocket engine noise and its effect on a community surrounding a launch site. The first program where rocket engine noise was considered to be a major factor in facility design was the Titan and Minuteman launch silos. In the Titan silo, for example, a considerable facility modification was required to reduce rocket engine noise so that an acceptable environment resulted. Launch facility acoustic environments were also considered to be major design factors on Titan III and Saturn V. Protection was required for fragile electronic checkout equipment, which was located within 100 feet from the multimillion-pound-thrust engines. The launch facility acoustic problems may be further increased on Nova, where engine thrust ratings are in excess of 20×10^6 pounds and where high chamber pressure, nonconventional engines are used. Acoustic environments will play a major role in the

design of the Nova launch facilities and may, in some cases, possibly determine the design that is finally chosen.

The purpose of this discussion is to examine the method of predicting launch facility acoustic environments. Several authors^{1,2,3,4} have presented methods of predicting rocket-engine noise levels. These methods are empirical relationships and are somewhat similar. These equations are combined, and Titan and Saturn data are used to establish mid-field values to provide an empirical method of predicting launch-facility acoustic environments. In addition, the effect of launcher design on the vehicle noise environment and how either the vehicle or facility design may be compromised in favor of the other are discussed.

¹J. N. Cole, et al., "Noise Radiation from Fourteen Types of Rockets in the 1000- to 130,000-Pound-Thrust Range," WADC TR 57-354 (Dec. 1957).

²I. Dyer, "Sound-Induced Missile Vibration," Random Vibration (John Wiley & Sons, New York, 1958), chapter 9.

³W. V. Morgan, et al., "The Use of Acoustic Scale Models for Investigating Near Field Noise of Jet and Rocket Engines, WADD T12 61-178 (Apr. 1961).

⁴G. A. Wilhold, et al., "A Technique for Predicting for Field Acoustic Environments Due to a Moving Rocket Sound Source," NASA TN D-1832.

NOTATION AND SYMBOLS

The following symbols and notations are used in this report, either in the text or the figures.

Near field — Region outside of the hydrodynamic pressure field, but within the area where the acoustic pressure is out of phase with particle velocity and the sound originates from a number of sources.

Mid-field — Region outside of the near field where pressure and particle velocity are in phase, finite amplitude effects must be considered, atmospheric and ground attenuation effects are negligible, and a point source may be assumed.

Far field — Region outside of mid-field where pressure and particle velocity are in phase, finite amplitude effects are negligible, atmospheric and ground attenuation effects must be considered, and a point source may be assumed.

DI	Directivity index (db)
NFI	Near field index (db)
FAI	Finite amplitude index (db)
RI	Radiation index (db)
DF	Distribution factor (db)
EA	Excess attenuation (db)
SPL	Sound pressure level (db re. 0.0002 dynes/cm ²)
OBSPL	Octave band sound pressure level (db)
p	Pressure (psi)
PWL	Sound power level (db re. 10 ⁻¹³ watts)
W _a	Acoustic power (watts)
W _m	Jet stream power (watts)
A _d	Divergence area = $2\pi r^2$ or $4\pi r^2$ (ft ²)
A _e	Area of nozzle at exit plane (ft ²)
A _s	Cross section area of launch silo
S(f)	Mean square pressure spectral density

A(f)	Spectrum function
$\beta^2(\phi, f)$	Angular function
G ₁ (θ)	Directivity factor
G ₂ (Kr)	Near field factor
G ₃ (a)	Finite amplitude factor
R or r	Distance from source to observer (ft)
ρ	Density of a gas (psi)
ρ_0	Density of air at ambient temperature & pressure (psi)
U _c	Source velocity (ft/sec)
c	Speed of sound (ft/sec)
C ₀	Speed of sound in air (ft/sec)
β	Angle of radiation
a	Radius of a sphere (ft)
V _e	Exit velocity of a jet (ft/sec)
w	Weight flow of a jet (lb/sec)
d _e & D _e	Nozzle diameter (ft)
T	Thrust (lb)
g	Gravity = 32.2 ft/sec ²
N	Number of engines
H	Height (ft)
f ₀	Frequency at source
η	Conversion efficiency
P _e	Rocket engine exit pressure, absolute (lb/in. ²)
P ₀	Ambient absolute pressure (lb/in. ²)

NOISE PREDICTION REQUIREMENTS

Space booster and R&D missile launch facility concepts have undergone few major changes except for the most recent programs. One would need only to examine the launch stands at the Atlantic Missile Range at Cape Canaveral to find only minor design changes from the earliest Redstone to Saturn I. Basically,

the launch vehicle is erected at the launch site by some type of erector, which also serves as a work platform. After all checks have been completed, the erector is moved and the launch is completed. Electronic checkout equipment is generally located in a concrete blockhouse so that long separation distances or massive walls provide the required protection from the noise environments. The first significant change in launcher design concepts was made on Titan III and Saturn V. The high cost of launch facilities and the lack of available real estate made it necessary to reduce the number of launch pads. The mission requirements, however, provided for a high launch rate which then necessitated a minimum on-pad time for each vehicle at the launch site. These requirements were fulfilled by the use of a transporter system, such as the one being employed by Titan III and Saturn V.

The vehicle is assembled on a transporter in a vertical assembly building and all checkout functions completed. The vehicle, in an upright position, its umbilical tower, and the ground checkout equipment are then moved to the launch site, which may be as much as 3 miles away. As an example, the Saturn V, its launcher and umbilical tower, and transporter are shown in Figs. 1 and 2. The vehicle will be launched from this assembly at the launch site. The major facility acoustic effort was concerned with the design of the ground equipment rooms for protection of fragile ground support equipment. From Fig. 3 it can be seen that the jet exhaust passes directly under the equipment rooms, A through D. The present planning for Nova provides two possible launcher concepts. One concept utilizes a transporter and is similar to that described above. The other concept

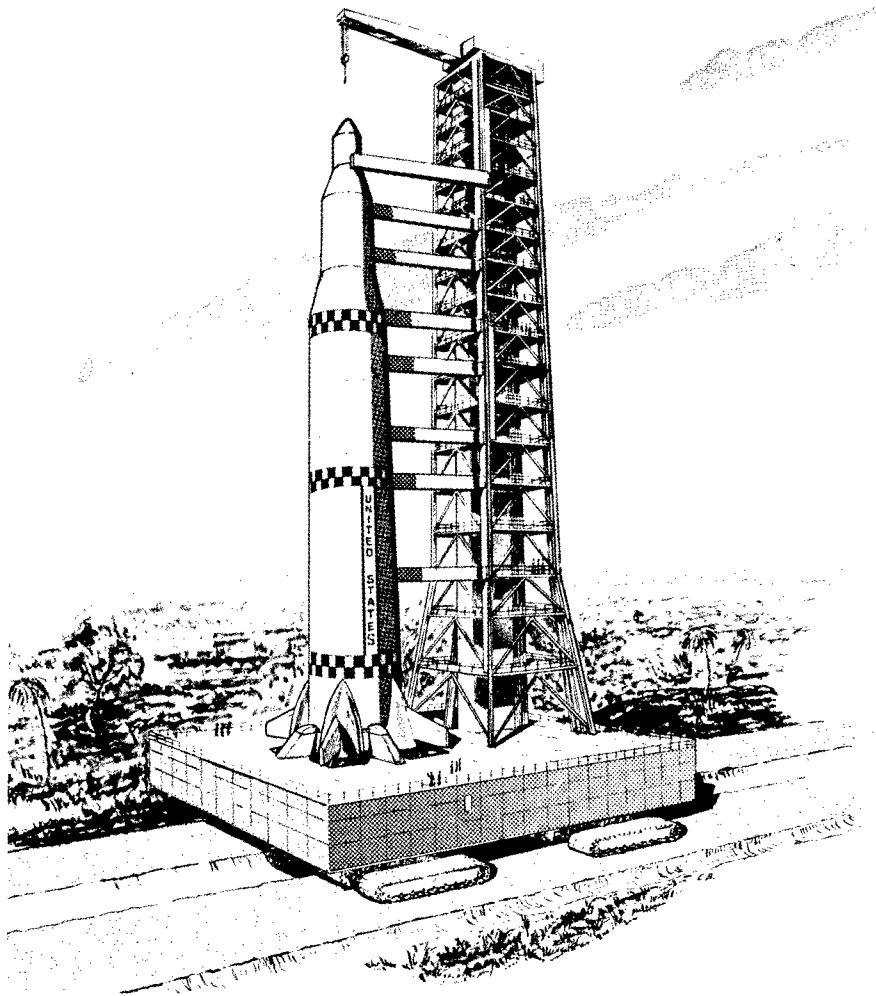


Fig. 1 - Saturn V transporter

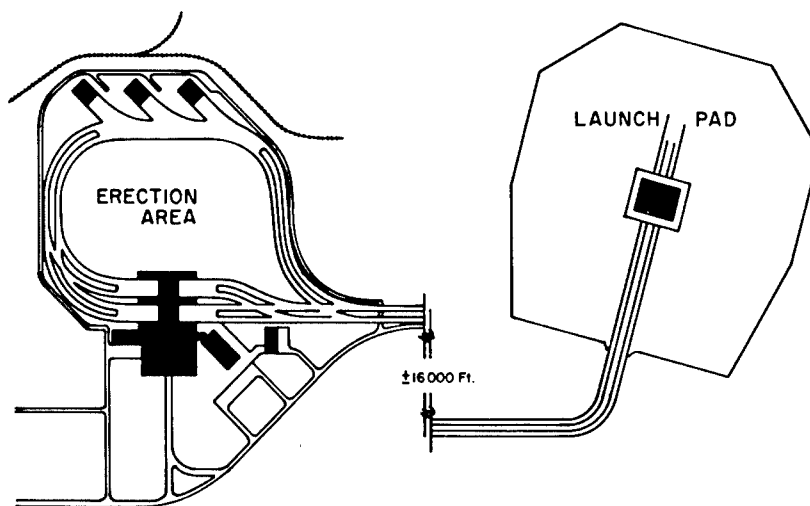


Fig. 2 - Saturn V basing

provides the launch of the Nova booster from the vertical assembly building. After checkout, the top of the building is opened and the Nova vehicle is then launched. The vertical assembly building then resembles an above-ground launch silo.

The prediction of launch facility acoustic environments involves the mid-field and, to a limited extent, the near field. Ordinarily, the sound pressure level at any point on a launch facility must be predicted twice during a launch. Predictions of the noise levels occurring after ignition but before liftoff must be made, since many critical ground support items are connected to the vehicle through umbilical connectors and are still performing critical check-out functions. Thus, an acoustically induced malfunction of the ground support equipment could result in an abrupt termination of the flight. Prediction of the noise levels following liftoff must also be made, since the maximum amplitudes will usually occur at this time. Each facility usually presents a unique problem in acoustic prediction that may strain the upper limit of existing knowledge. For example, the exhaust of both Titan III and Saturn V is confined to a trench. As a result, the radiation pattern is not well defined. In such cases, the resulting sound pressure levels must be estimated or scale model test data acquired. Another example is the Nova launch building, where over 1000 megawatts of acoustic power will be confined within the building. To predict the acoustic levels in any launcher, the basic parameters of power spectrum level, source location, directivity index, near field index, and radiation index must first be determined. Once the sound pressure level has been predicted, the

necessity and methods of noise control may be ascertained.

ACOUSTIC PREDICTION METHOD

Methods of predicting the sound pressure produced by a rocket engine jet have been published by various authors. The basic equations are summarized below.

J. N. Cole, et al.,¹

$$\text{SPL} = \text{PWL} - 10 \log_{10} A_d + \text{DI}; \quad (1)$$

I. Dyer,²

$$p^2 = \int_0^\infty S(f) df = \int_0^\infty \frac{A(f) B^2(\varphi, f) G_2^2(K_r)}{R^2} ; \quad (2)$$

W. V. Morgan, et al.,³

$$p_{r,\theta}^2 \sim \left[\frac{\rho_o}{\rho} \right] \times [\rho U_c]^2 \times \left[\frac{U_c}{C_c} \right]^4 \times \left[\frac{C_c}{C_o} \right]^4 \times \left[\frac{4\pi}{\beta} \right] \times \left[\frac{a}{r} \right]^2 \times G_1 \left(\frac{V_c}{C_c}, \frac{C_c}{C_o}, \theta \right) \times G_2(K_r); \quad (3)$$

G. A. Wilhold, et al.,⁴

$$\begin{aligned} \text{OBSPL} &= 10 \log (\text{DSF}) - 10 \log \left[\frac{2V_e \dot{w}}{\rho_o C_o D T^2 q N} \right] \\ &- 10 \log R(R+H) - \text{EA} + \text{DF} \\ &+ 10 \log f_o + 126 \text{ db.} \end{aligned} \quad (4)$$

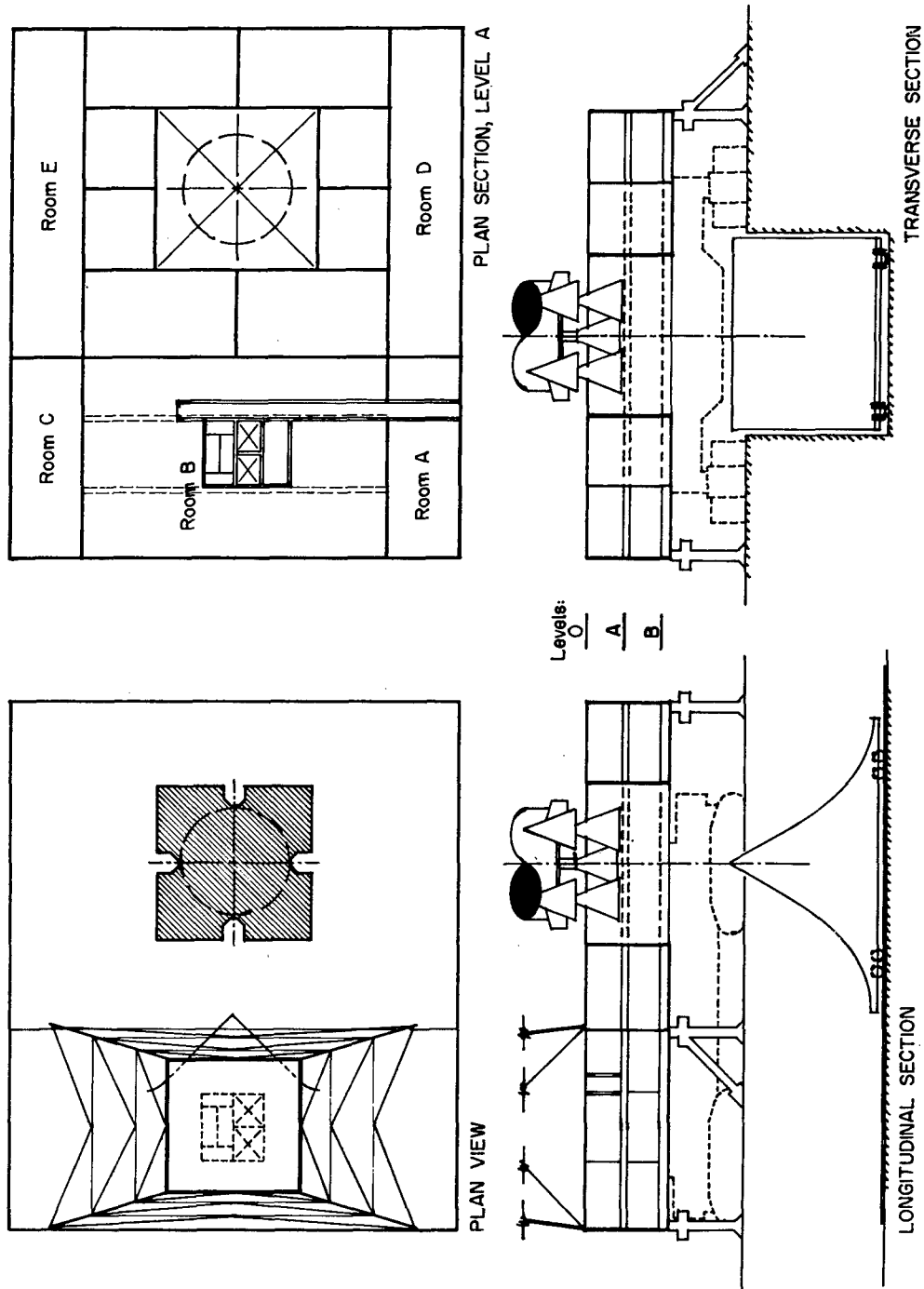


Fig. 3 - Saturn V L-UT

Equations 1 and 4 were primarily derived for far field noise but Eq. (2) applies to the pressure field along the surface of a vehicle. Equation (3) is a more general expression for either near or far field sound. The essential elements for prediction of the sound pressure in the launch facility area are contained in Eqs. (1) through (4). Assuming the facility area to be in either the mid-field or near field region, one can derive a general expression for sound pressure levels:

$$p^2 \sim \frac{W_a \cdot G_1(\theta) \cdot G_2(Kr)}{G_3(a) \cdot R^2}, \quad (5)$$

or, more conveniently,

$$SPL = PWL + DI + NFI - FAI - RI, \quad (6)$$

where

PWL = power level generated by the engines,

DI = directivity index,

NFI = near field index,

FAI = finite amplitude index,⁵ and

RI = radiation index.

We will now attempt to identify numerical values to each of these parameters.

⁵For far field calculations, excess attenuation would be substituted for the finite amplitude effects.

The acoustic power produced by a rocket engine can be expressed in terms of the total power produced by the engines, as follows:

$$KE(\text{acoustic}) \approx \eta \times KE(\text{engine}) \approx (\eta/2)(MV^2), \quad (7)$$

where η is the acoustic conversion efficiency. The value of η has been found to vary with the size of the engine. Von Gierke, et al.,¹ found the acoustic efficiency to vary, or

$$KE(\text{acoustic}) \approx 7.8 [KE(\text{engine})]^{1.35}, \quad (8)$$

for engines with thrust varying from 1000 to 130,000 pounds. This relationship is shown as the straight line part of the curve of Fig. 4. Obviously, the 1000 to 130,000-pound thrust relationship cannot be infinitely extended. The power curve has been extended by Cole, et al. as shown in Fig. 4. The overall acoustic power level as found from Titan⁶ and Saturn⁷⁻⁹ measurements is also shown in Fig. 4. The curve seems to indicate a decrease in conversion efficiency as the engine power level increases past 7×10^9 watts.

⁶J. N. Cole, et al., "Acoustic and Vibration Studies at Cape Canaveral Missile Test Annex, Atlantic Missile Range," ASD TR 61-608 (1) (Dec. 1962).

⁷W. D. Dorland and R. N. Tedrick, "Results of Acoustical Survey of SA-1 Launch," MTP-Test-62-2 (Mar. 1962).

⁸W. D. Dorland and R. N. Tedrick, "Results of Acoustical Survey of SA-2 Launch," MTP-Test-62-5 (Aug. 20, 1962).

⁹N. Cummings, et al., "Results of Acoustical Survey of SA-3 Launch," MTP-Test-63-2 (Feb. 7, 1963).

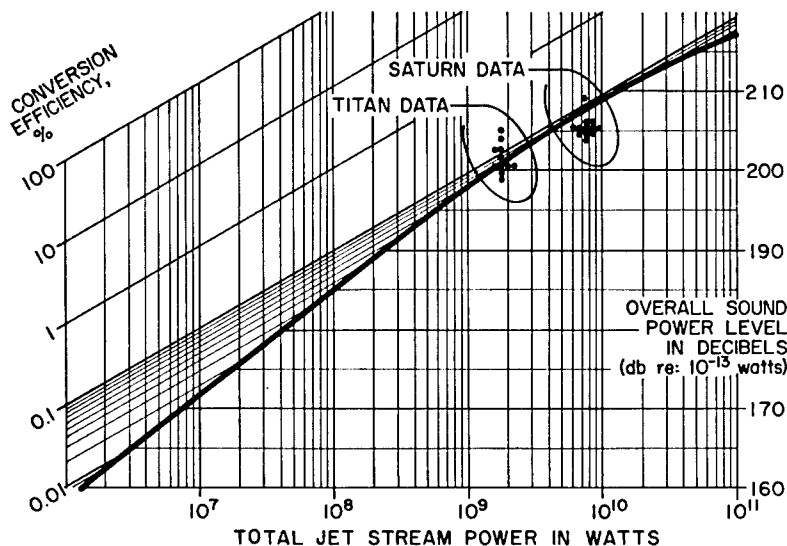


Fig. 4 - Overall acoustic power vs jet stream mechanical power

The Saturn data seem to lie below the curve, indicating that the slope of the curve may change sooner. The apparent decrease in conversion efficiency may be due to the fact that finite amplitude effects have not been considered in computing the acoustic power level from measured sound pressure levels. At the present time, there is too little data to provide a method of computing or allowing for the non-linear damping of the high amplitude sound waves from such large power sources. Thus, the use of the curve of Fig. 3 should provide some adjustment for finite amplitude losses until such a time that they may be computed. The finite amplitude index is included with the power level term in Eq. (6).

In many previous documents, rocket engine jet stream power has been defined in terms of full rated thrust. On many future vehicles, however, engines may be used that are overexpanded at liftoff. Thus, it may be more meaningful to express the jet stream power in terms of specific impulse and thrust at liftoff:

$$\begin{aligned} \text{PWL} &= 10 \log_{10} \frac{\eta \times w}{10^{-13}} \\ &= 10 \log_{10} \frac{0.676 \eta (T \times I_{sp})}{10^{-13}} \end{aligned} \quad (9)$$

$$\text{PWL} = 10 \log_{10} \frac{0.676 \eta \left[\frac{V_e^2 \dot{w}}{g} + (P_e - P_o) A_e V_e \right]}{10^{-13}} \quad (10)$$

A nondimensional power spectrum was also derived by Von Gierke¹ and is shown in Fig. 5. This spectrum was derived from far field data acquired from rocket engines with thrusts up to 130,000 pounds. The applicability of this spectrum for large booster engine mid-field noise can be determined with the use of Titan and Saturn data. The spread of these data is also shown in Fig. 5. The Saturn data seem to agree more closely than Titan data. In general, the use of the generalized curve as recommended by Cole, et al. for far field prediction, should also be applicable to the mid-field of large boosters.

When a large number of engines are used, multiple-nozzle effects may be observed. One may assume that two peaks in the sound pressure level produced by a multiple-nozzle booster may be measured. One peak would be produced by the combined effect of all engines, and the other peak produced by the single engines. The result would be a lower frequency peak produced by combined engines and a higher frequency peak produced by the single engines. An example of this effect is shown in Fig. 6. The second peak in the Saturn data is much lower than would be predicted. In addition, not all the Saturn data show the higher frequency peak. There has been some speculation that the apparent notch is the result of "grass attenuation." The data in Fig. 6, however, were acquired when the vehicle was airborne. More data are required on this phenomenon before an accurate prediction of its

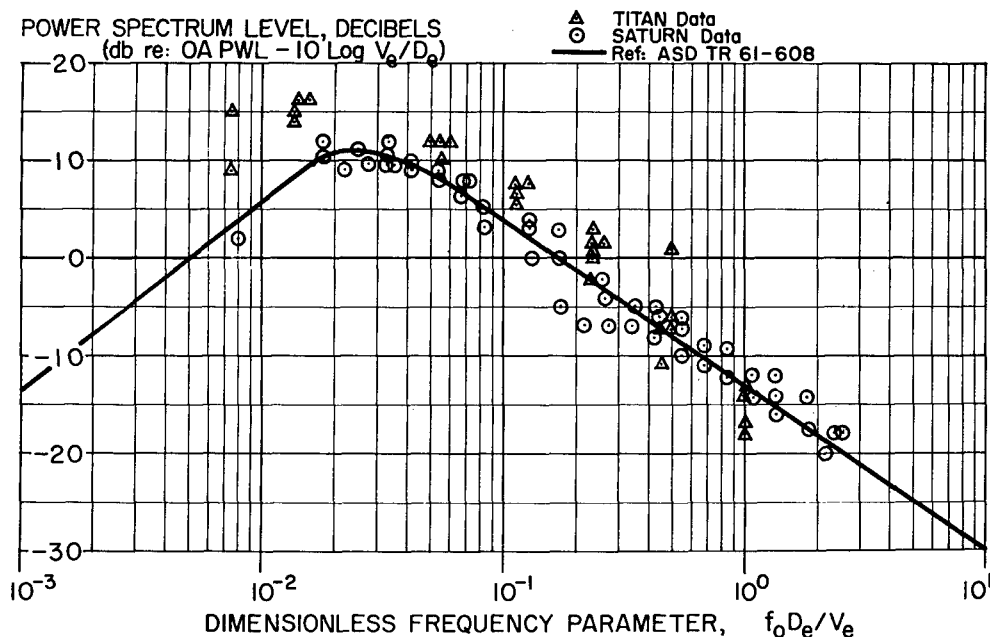


Fig. 5 - Generalized power spectrum of rocket noise sources

OCTAVE BAND SOUND PRESSURE
LEVELS IN DECIBELS
(db re: 0.0002 microbar)

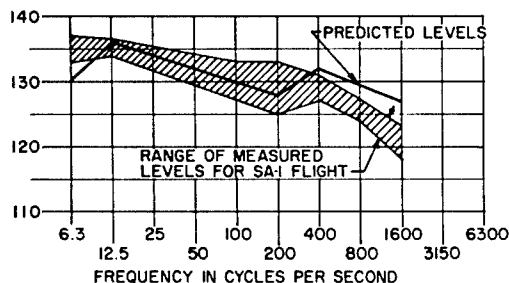


Fig. 6 - Apparent multiple nozzle effect from predicted and measured Saturn data

effects can be made. Consideration of multiple nozzles, such as shown in Fig. 6, would yield conservative estimates, and should probably be used.

The near field function has been described by Dyer.² This function was found to apply for lateral quadrupoles and was, for all practical purposes, negligible. On a launch facility design, however, much of the near field noise could originate from longitudinal quadrupoles. The boundary of the near field can be estimated at 5 wavelengths from the source. At this distance and for a simple source, the impedance is almost purely resistive, and the pressure and particle velocity are in phase. Morgan, et al.³ have shown that at these distances a monopole and quadrupole source exhibit similar characteristics. Thus, in the mid-field the near field function can be ignored. As an example, the mid-field for all frequencies above 100 cps is beyond 56 feet. It can therefore be concluded, that the near field function is equal to 1 in large launch facility design.

The radiation index can be defined as reduction of acoustic intensity due to the divergence of sound waves. When the noise source is in the air, the noise will radiate through a sphere, and the reduction in sound pressure level will be proportional to the area of a sphere whose radius is equal to the distance between the noise source and the observer. When the noise source is on the ground, such as during the time between ignition and liftoff, the radiation pattern is ordinarily hemispherical. An exception would occur if the jet exhaust were confined to a trench, such as Saturn V. The exhaust jet (see Fig. 3) is primarily confined to the trench. Thus, the acoustic energy will be radiated through the top of the trench and will therefore be highly directive.¹⁰ The computation of the sound pressure level would then depend on either a conservative estimate or scale-model data.

The propagation of rocket engine noise in the mid-field has been found to be highly directive. An example of measured Saturn and Titan data is shown in Fig. 7. The directivity of several rocket engines was plotted by Cole, et al.¹ Directivity curves were then plotted using Cole's data, Saturn data, and Titan data, as shown in Fig. 8. The directivity index can be directly added or subtracted from the power level in predicting sound pressure level.

Thus, the launch facility sound pressure level of a large booster can be predicted. As an example, assume that the launch facility sound pressure levels must be predicted for a

¹⁰R. Peverley, et al., "Saturn C-5 Launcher and Umbilical Tower Acoustic Design Considerations," Martin Company, Denver, Colo., RSH-CR-62-1 (Dec. 1962).

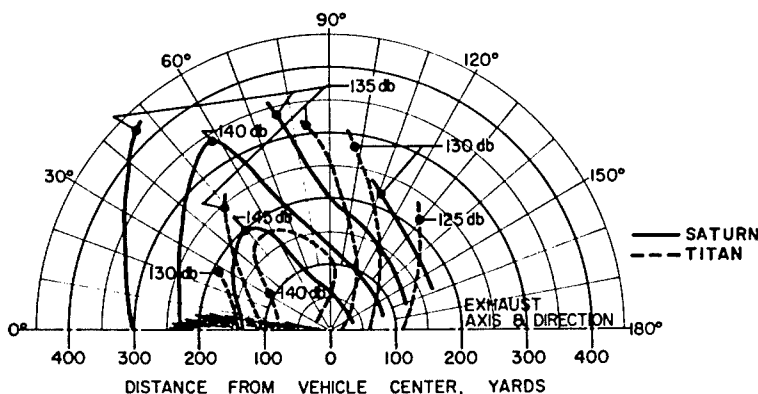


Fig. 7 - Directivity -- J-type deflector OASPL contours

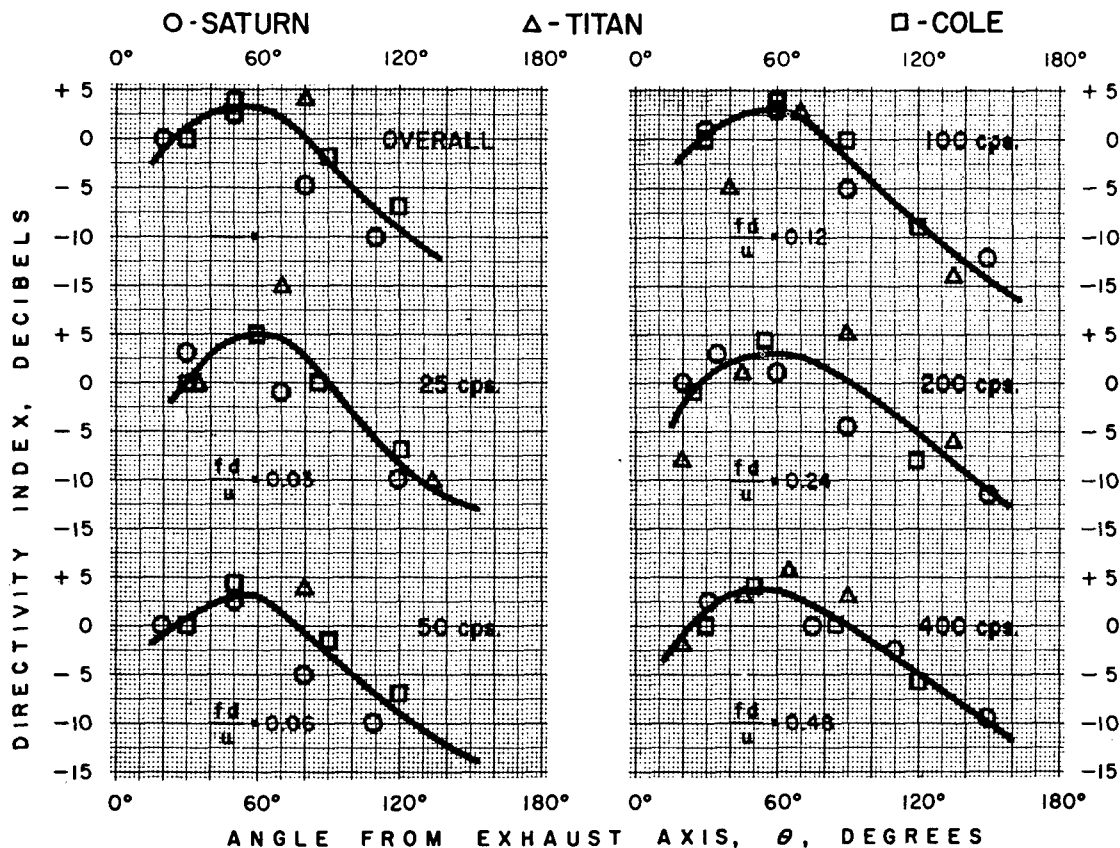


Fig. 8 - Generalized directivity indices, distances less than 600 feet

hypothetical 1.5×10^6 -pound thrust booster. From the previous discussion and Figs. 4, 5, 6, and 8, the predicted levels as shown in Fig. 9 were found. Spectrum levels could also be obtained for any point on the facility.

In some cases, it may be convenient to verify sound pressure level calculations by scaling data from other similar vehicles. Scaling laws have been well defined^{3,11} and can be summarized as follows:

$$\text{Amplitude scale factor} = \sqrt{\frac{\eta_p T_p V_p}{\eta_m T_m V_m}}$$

and

$$\text{Frequency scale factor} = \frac{f_m [S_m(f_m)]}{f_p [S_p(f_p)]}$$

Thus, if facility conditions and engine conditions are similar enough, scaling of data can produce a reasonably accurate estimate of

sound pressure levels. An example is shown in Fig. 10. Data acquired at the base of Titan and Saturn I during static firings were scaled to verify calculations of the acoustic environments near the base of the Saturn V on the launcher. The Saturn I data would be considered to be more accurate because of the smaller scale factor and greater similarity in deflector configurations. If only Titan data were available, however, it would give a reasonable verification of calculated levels.

EFFECTS OF THE LAUNCH FACILITY DESIGN ON THE VEHICLE ACOUSTIC ENVIRONMENT

The launcher configuration exerts considerable influence on the booster acoustic environment, affecting both the generated acoustic power and the propagation phenomenon. The flame deflector, in particular, produces a number of measurable effects with the deflector shape, distance from the engine exhaust plane, and the amount of cooling water being important parameters. Working with JATO rockets,

¹¹D. Bies and P. Franken, "Notes on Scaling of Jet and Rocket Noise," J. Acoust. Soc. Am., 33:1171 (1961).

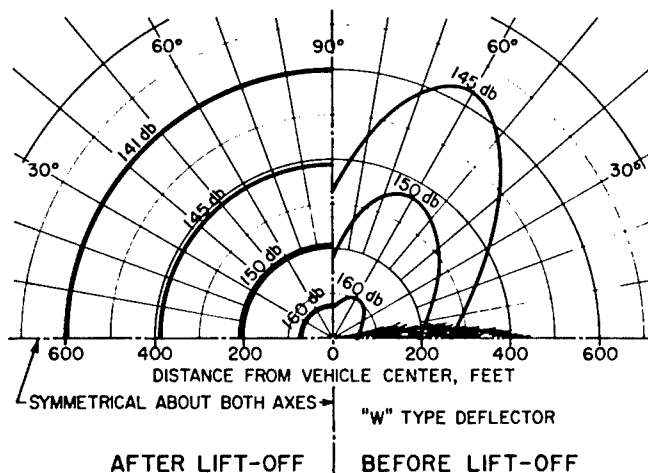


Fig. 9 - Hypothetical 1,500,000-lb-thrust booster, SPL contours

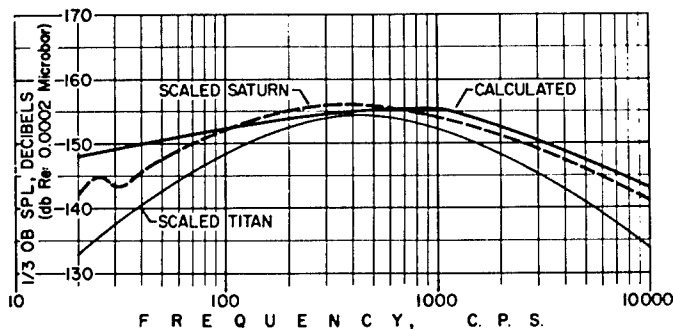


Fig. 10 - Comparison of noise levels for Saturn V configuration

Cole¹² at WADC has shown that deflectors which diffuse the flow rapidly also produce lower power levels, with a conical deflector showing the lowest PWL. Recent Saturn I static and flight tests confirm these results. The static tests used a water-cooled bucket deflector, and the flights were made with a dry wedge deflector. The power level measured during the on-pad conditions of the flight tests is about 3 db lower than the static measurement. It can also be seen in Fig. 11, that this decrease in the overall power level has taken place mainly in the lower frequency bands. This effect is favorable to the vehicle acoustic environment, since the lower frequencies tend to excite the natural frequencies of the structure and the vehicle.

¹²J. N. Cole, "Effects of Various Exhaust Blast Deflectors on the Acoustic Noise Characteristics of 1000-Pound-Thrust Rockets," WADD TR 60-6 (Sept. 1960).

The directivity pattern is also a function of deflector shape, becoming more uniform as the deflector approaches circumferential symmetry. The deflector, then, can either concentrate or diffuse the acoustic sources. The apparent location in the stream of the noise sources is an important parameter in calculating the acoustic levels close to the booster. Using full-scale Titan I and 1/33-scale Titan III tests, the apparent source location has been determined by amplitude correlation methods. Figure 12 shows the results plotted as Strouhal number vs distance from the engine exhaust plane in nozzle diameters. Source locations determined from Jupiter firings show a significant change, with deflector spacing and model measurements indicating that the sources in an undeflected stream are much further from the exit. The action of the deflector, thus, is to move the sources closer to the booster and launcher. Cole¹² has shown that the presence of the

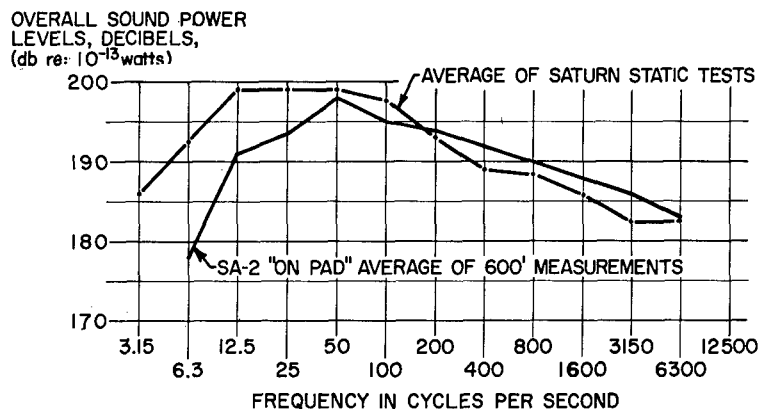


Fig. 11 - Saturn acoustic power spectra comparison

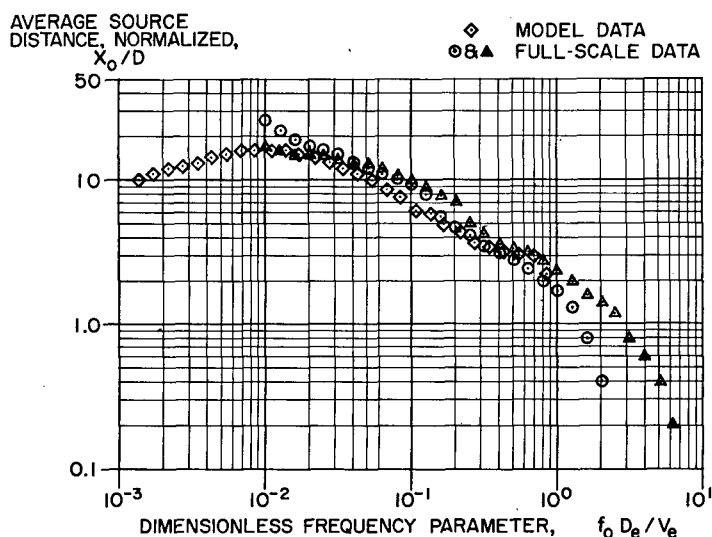


Fig. 12 - Rocket noise source locations

deflector reduces the overall sound power but increases the near field sound pressure levels. This phenomenon may be explained by the reduction in source-to-receiver distances brought about by the deflector.

The Saturn V launcher includes an exhaust trench to contain and direct the exhaust flow. This trench should actually increase the generated PWL by the presence of the rigid boundary and also by the reduction in mixing of the stream. Past experience would indicate that greater source distances would also result from the presence of the trench. The radiation pattern of the source in the trench is different from the uncontained stream. As an example, a trench that encloses the jet stream can be considered to be similar to an exhaust duct of a launch silo.

From experience on the Titan Silo Launch program, the acoustic intensity can be estimated by considering the total acoustic power uniformly distributed across the duct. Thus, the acoustic intensity at the top of the duct can be found. The radiation can then be considered hemispherical.

Some launcher configurations make use of a platform for the booster, with the flame deflector underneath. This means that part of the exhaust stream and therefore some of the noise sources lie under the platform with respect to the booster. These are usually high-frequency sources, and since the SPL reduction effect of a barrier between source and receiver is strongly a function of frequency, some shielding would occur. This shielding would result

in lower sound pressure levels than would be experienced without the platform.

A special case of how the launcher design can affect the overall acoustic environment is offered by the case of a launch silo. When a missile or space vehicle is launched from the confines of a silo, the rocket engine noise is increased over that encountered on a conventional launch stand. This point is illustrated in Fig. 13. Curve I shows measured sound pressure level vs missile height for Titan I on a conventional static test stand with a J-type deflector. Curve II also shows sound pressure level vs height, except that the missile is in an unlined silo. These data were acquired from a 1/6-scale model. The acoustic environment in a silo whose walls are lined with a sound absorbing material is shown as Curve III. An almost constant 7-db difference is maintained between the lined silo and the static test stand, except near the top, where exhaust duct noise is leaking back in the top of the silo. Sound pressure level vs height for the static firing of a second stage is shown as Curve IV. Thus, the maximum acoustic environment of at least part of the second stage may be encountered during the static firing of that stage.

It has been found that the acoustic environment of a rocket engine in a confined silo, where the jet gases are not exhausted in the same duct that is occupied by the vehicle, is a direct function of the duct area. Since the structural vibration is a function of not only the acoustic environment, but also of the structural mass, damping, and stiffness, the acoustic limitations on the size of a launch silo are a function of the vehicle's fragility and can therefore be estimated. Because of their inherent differences in structural

design, Minuteman and Titan possibly represent the upper and lower extremes in vibration fragility. Assuming that each vehicle is now functioning in its maximum acoustic environment, the upper and lower acceptable limits of acoustic intensity can be estimated for a ducted launch silo as shown in Fig. 14. A duct lined with acoustic liner is assumed. Further reductions in launch duct acoustic environments are possible with such methods as water injection, but at an added cost burden to the facility design. From Fig. 14, it is obvious that some reasonable estimate of the vehicle's fragility must be obtained before the launch silo can be designed for a satisfactory acoustic environment.

Several new engine configurations are being considered for future boosters, including the plug engine and the ring engine. The plug engine is composed of a number of modules in a circular array, firing onto a plug. The plug is part of the nozzle expansion system. The ring engine has a large diameter, annular opening, and a continuous annular sheet of flame leaves the engines. In both of these engine configurations, the chamber pressures may be as high as 2000 or 3000 psia. These engines will most probably require a circumferentially uniform deflector like a spike or cone. These deflectors will produce uniform radiation patterns and a distributed source of sound. The higher chamber pressures will result in high exit Mach numbers and extremely long exhaust plumes. For static firings or on-pad conditions of flight tests, the sources will be located further from the vehicle due to the high exit Mach number. The launcher will be subjected to high pressures during flight tests for a longer time because of the extended exhaust plume.

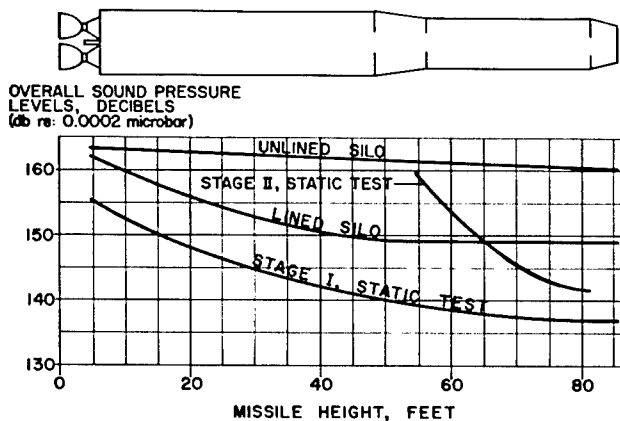


Fig. 13 - Titan missile acoustic levels

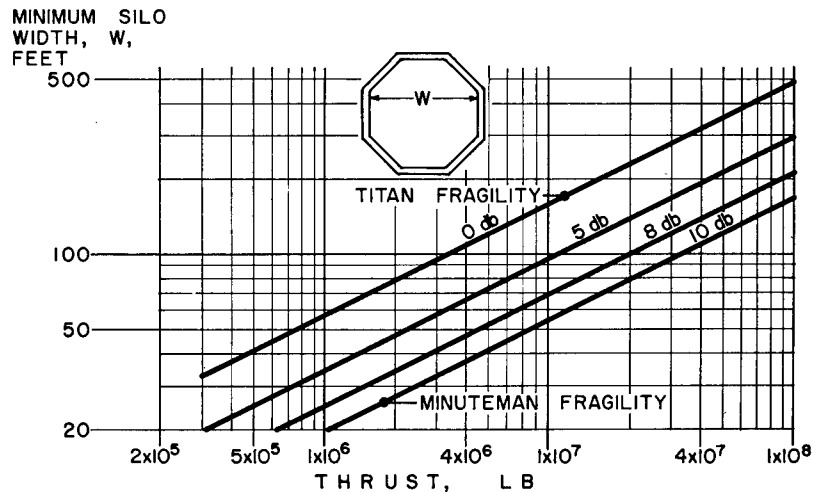


Fig. 14 - Launch silo acoustics, lined duct

CONCLUSIONS

A significant amount of additional effort is required to provide accurate methods of predicting noise levels of large booster rocket engines at a launch facility. Three areas of effort that have previously been mentioned are: effects of high pressure ring, plug, and clustered engines; effects of finite amplitude, and effects of multiple nozzles. Perhaps the most critical problem at this time is the evaluation of finite amplitude effects. These effects are not a problem in the prediction of far field acoustic levels, since a conversion efficiency (determined from far field sound pressure level measurements) accounts for this phenomenon. Using the far field power level for prediction of near

field pressure levels would be in error if the nonlinear loss of energy is not accounted for, and predicted levels would be lower than actually existing. This research will, however, require a significant amount of time. Meanwhile, the development of large boosters and large booster launch facilities will continue. During this time, the prediction of launch facility acoustic environments and the subsequent design of launch facilities will also continue. By using the methods outlined in this paper, a conservative estimate of the acoustic environment can be made. When the high cost of existing boosters and launch facilities are considered, the small amount of money required for a slight acoustic overdesign may be considered a good investment in added reliability.

DISCUSSION

Mr. Joe Young (NASA - Goddard Space Flight Center): In the generation of this Strouhal number which determines the shape of your spectrum, what is the latest thought on what is to be used as the effective diameter for clustered engines?

Mr. Pevery: We have used the combined diameter as effective diameter. It is just the square root of the number of engines times the diameter of one engine. At the present time we

are about ready to start a series of model engine tests and this is one of the things that we hope to be able to answer a little bit better. Looking at the one slide where we showed the scatter of data, particularly from Saturn around Cole's spectrum curve, it appears that using this effective diameter seems to give a pretty good result. The spectrum shape was very close. There are eight engines on this, and this is probably the maximum number that we will see according to present plans.

* * *

A COMPARISON OF THE VIBRATION ENVIRONMENT MEASURED ON THE SATURN FLIGHTS WITH THE PREDICTED VALUES*

G. D. Johnston
Marshall Space Flight Center
Huntsville, Alabama

and

T. Coffin
Chrysler Corporation
Huntsville, Alabama

Preliminary vibration levels which would provide information to be used in equipment design for the Saturn vehicles were predicted from available Jupiter data and a limited amount of data from Saturn static firings. Actual data have now been obtained from recent Saturn launchings and static firings. A comparison of the actual versus predicted vibration environment is presented.

This paper represents an extension to one presented at the 30th Symposium on Shock, Vibration, and Associated Environments. The previous paper, entitled "Acoustic and Vibration Environment for Saturn," discussed the early methods of vibration prediction used for Saturn and the use of data obtained from the Jupiter vehicle. It is very interesting for one to review the techniques and procedures of just a few years ago and compare them with today's methods. The recent growth of our knowledge of vibration environments is reflected by this statement from a Space Technology Laboratory report entitled "The Vibration Environment of the Thor, Atlas, and Titan Missiles," dated December 1959: "----the intensity levels in compartments other than the engine section can generally be said to reach their maximum values during the time when the missile is held down on the launch stand prior to lift-off. This maximum is believed to be due to the contribution of the acoustic field, which is enhanced by ground reflection effects while the missile is on the stand." The statements were quite accurate, but it has been only within the last few years that we have obtained reliable data in sufficient quantity to do much more than believe there is considerable influence from ground acoustics not to mention boundary layer noise.

We feel there has been a vast improvement during the last 2 years in the techniques or methods used throughout the industry to predict vibration and acoustic environments of space vehicles. This is evident in the fine papers on this subject being presented during this Symposium. One of the latest prediction techniques to be developed at Marshall Space Flight Center was given in Session D of this Symposium by Mr. R. E. Jewell.

The methods used for predicting vibration, acoustic, and shock environments have changed radically at Marshall Space Flight Center, but our use of the predictions for design analysis and component testing has not changed significantly. We still require sinusoidal testing to evaluate bracketry and component structural design. Random testing was performed on electrical components, valves, actuators, and the like, for the Saturn I, Block I vehicle, but it was not a general test requirement for all components.

The addition of random testing as a general requirement for evaluation of a component's function integrity began with the Saturn I, Block II vehicles. The sinusoidal vibration test will continue to be the primary requirement for

*Invited Paper.

qualification of structures and subassemblies in the Saturn I, Saturn IB, and Saturn V vehicles. Before we get into a comparison of data, it is appropriate at this point to provide some background on the Saturn program.

The Saturn vehicle we are concerned with in this paper is called the Saturn I vehicle. Figure 1 shows the family of vehicles that are playing a major role in this nation's space program. The vehicles shown here are modeled to the same scale. The Saturn I vehicle can be compared in size to the familiar Redstone, Jupiter, Atlas, and Titan vehicles. Figure 1 also gives you some idea of what the Saturn IB and Saturn V vehicles will be like.

The research and development program for the Saturn I vehicle consists of 10 flight vehicles, 1 S-I stage booster for static tests, 1 S-IV second stage for static tests, and 1 vehicle for dynamic studies. The program divides the 10 flight vehicles into what we term Block I and Block II. Figure 2 shows the Block I configuration. Four such vehicles have been launched; these flights were basically booster development flights. This configuration consists of a flight booster, dummy second stage, Jupiter aft section, and Jupiter nose cone. All four of these vehicles have been flown, and all were completely successful. Figure 3 shows the Block II configuration. This configuration consists of the S-I stage booster, second stage S-IV,

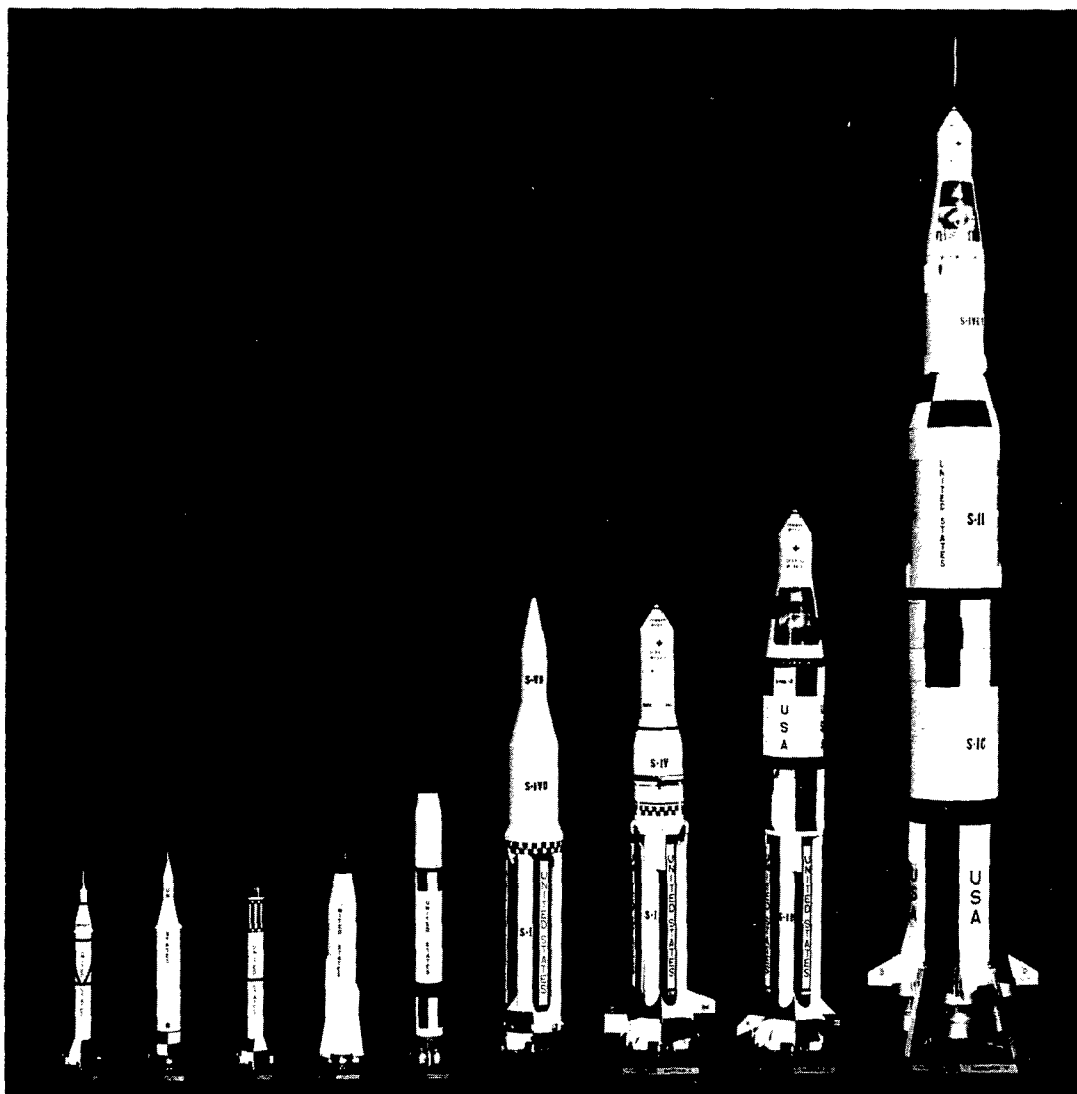


Fig. 1 - Family of NASA vehicles

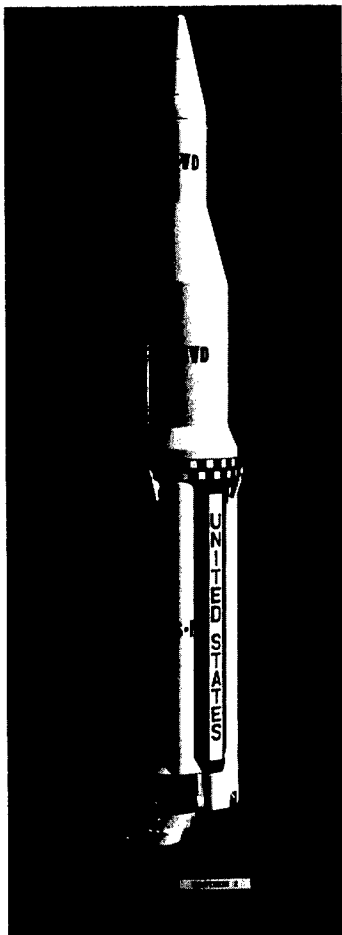


Fig. 2 - Saturn I,
Block I vehicle

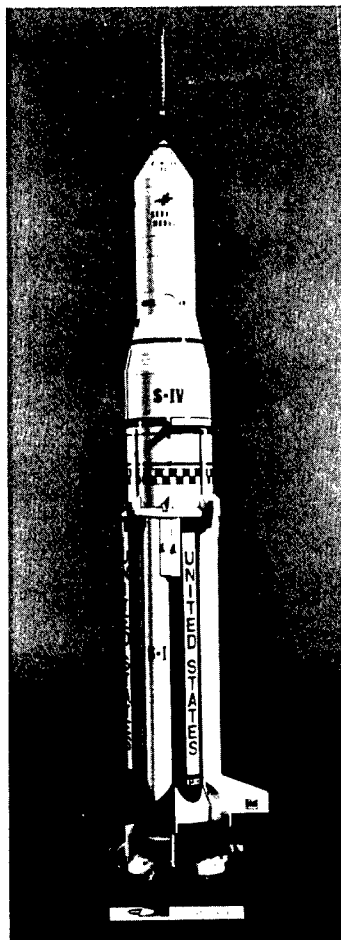


Fig. 3 - Saturn I,
Block II vehicle

instrument unit, and payload. The first flight of a Block II vehicle is scheduled for this month.

Since the Saturn I Research and Development Program divided the 10 flight vehicles into Block I and Block II, it was decided that separate specifications would be issued for each block. The Block I specification was issued using the established procedures from the Jupiter program since they had proven successful. This specification formed the outline for the Block II specification. The data from static tests and flight tests of Block I vehicles provided the environmental levels for the Block II specification.

The predicted vibration environment for the Saturn I, Block I presented in the reference paper was issued as the official analysis and test criteria in DSF-TM-7-59, dated 27 May 1959. The vibration environment was presented

in terms of "transient" and "steady-state" sinusoidal test levels. The terms transient and steady-state evolved during the development of the Redstone and Jupiter vehicles. The transient level was associated with the periods of engine ignition, lift-off, Mach 1, and maximum dynamic pressure, and provided data for sine sweep test. The steady-state level was associated with period of mainstage during captive firings and flight. Figure 4 shows a composite vibration level versus flight time for a typical Jupiter measurement on the tail section structure. The measurement indicates that this particular structure is very sensitive to the events of flight. The composite level time history of this measurement during a Jupiter captive firing would remain relatively constant after engine ignition and would be either slightly higher or lower in magnitude than the time increment referred to as mainstage in Fig. 4. Its orientation with respect to the lobes of maximum acoustic intensity would determine whether its

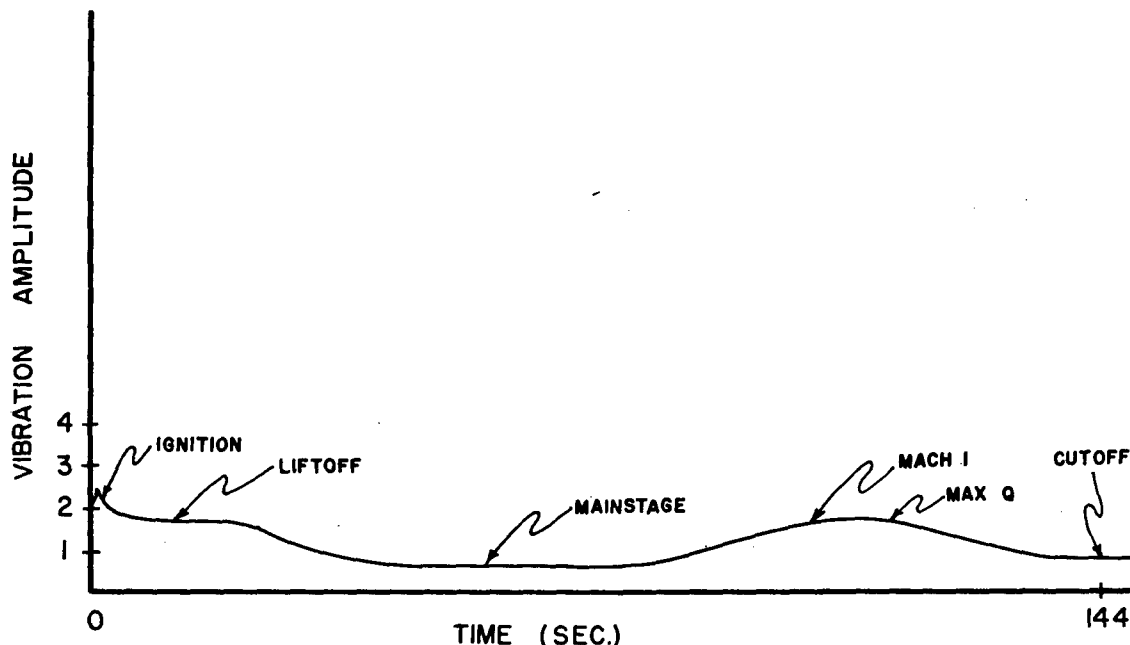


Fig. 4 - Flight history of a Jupiter composite vibration measurement

magnitude would be higher or lower. The Jupiter data also indicated that the power plant measurements were insensitive to these events in flight which means that their composite time history remained relatively constant throughout a captive firing or flight. It was assumed that the flight vibration time history of various Saturn structures would, in general, be similar to that indicated by the Jupiter measurements. The ratios of transient levels to mainstage levels established in the Jupiter program were used in the Saturn program.

The data from the first four flights of Saturn verified these assumptions. Before illustrating the general trend of the flight data we will discuss one phenomenon of a Saturn launch we were quite concerned about. We call this phenomenon the "hydro-dynamic" effect (for lack of a better name) which can be understood by viewing Figs. 5, 6, and 7. During the hold-down period, the booster builds up to full thrust. At this time a jet pump effect exists that causes a large volume of surrounding air to be sucked into the circular opening at the top of the launch pedestal. This causes a significant static loading on the shroud of the tail section. So far, this has not been a serious problem, but we are gathering as much data as possible to determine the potential effects it will have on the Saturn V vehicle.

Figures 8 and 9 are typical measurements selected to demonstrate the time history response

of various Saturn structures. These data were obtained during the boost flight phase of the fourth Saturn flight vehicle (SA-4). Figure 8 shows three measurements in the spider beam area. Measurement E1-11 was mounted directly to the spider beam and had its axis of sensitivity in the flight direction. Measurement E2-11 was located at the same point and had its axis of sensitivity in the pitch direction. Measurement E4-15 was a response measurement on a component in one of the instrument canisters. The three measurements in Fig. 8 show the structural response of different type structure and their sensitivity to the events in flights. They bear a very close resemblance to the Jupiter time history shown in Fig. 4. Figure 9 shows four measurements that were mounted directly on engines one, two, and four. These measurements remain relatively constant throughout the boost flight period. This is true to varying degrees for most of the basic load carrying structure in the thrust section area.

The general environmental zone breakdown for the Saturn I, Block I vibration specifications is illustrated in Fig. 10. As you can see, only three major zones were defined; the tail section, the center section, and the top section. The major zone defined as the tail section was divided into environmental subzones, as shown in Fig. 11, for components mounted on the engines, thrust frame, and thrust structure. The thrust frame and thrust structure were defined separately since the thrust frame consists of built-up



Fig. 5 - Saturn SA-3 vehicle at ignition

beam outriggers whereas the thrust structure consists mainly of the massive center thrust barrel.

The original environmental test levels for the tail section are illustrated in Fig. 12. As stated earlier the specification was defined in terms of transient and steady-state sinusoidal test levels. Only general environmental zone levels were specified for components located in the center and top sections of the Saturn booster as illustrated in Fig. 13. The center section test levels were mainly for the many components located in the fore and aft LOX and fuel tank skirts. The top section specification was for components located in the spider beam area, in the instrument canisters, or on the dummy upper stages.

Since static firing of vehicle stages is an integral part of any vehicle development program under the cognizance of MSFC, the

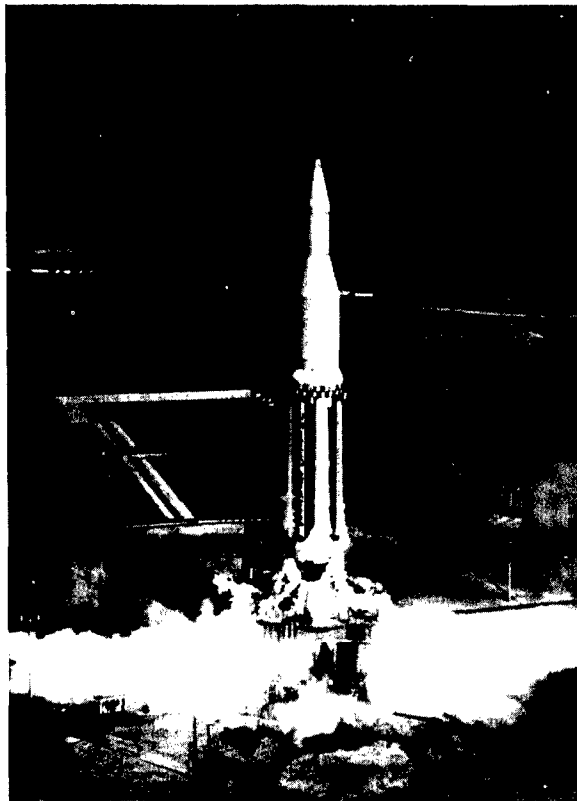


Fig. 6 - Saturn SA-3 vehicle during holddown

vibration and acoustic measurements obtained during static firing constitute a major criterion for the development of vibration specifications. It seems appropriate, therefore, to compare the early predicted environmental test levels with data obtained from booster static tests.

To date we have conducted 48 static firings of Saturn I ground test and flight-rated boosters at Marshall Space Flight Center. From these test firings approximately 4000 vibration measurements and 150 vehicle acoustic measurements have been obtained. Figure 14 illustrates a firing at the Marshall Space Flight Center static test tower. Modifications of the data obtained on this stand at MSFC must be made in order to permit prediction of the launch environment because of the difference in geometry between the static test tower and the launch pedestal at the Atlantic Missile Range. The most significant of these modifications apply to structure which is predominantly excited by the acoustic field. The bucket-type deflector used at the MSFC facility causes a relatively unidirectional acoustic field to be generated by the engine exhaust, whereas the wedge type deflector

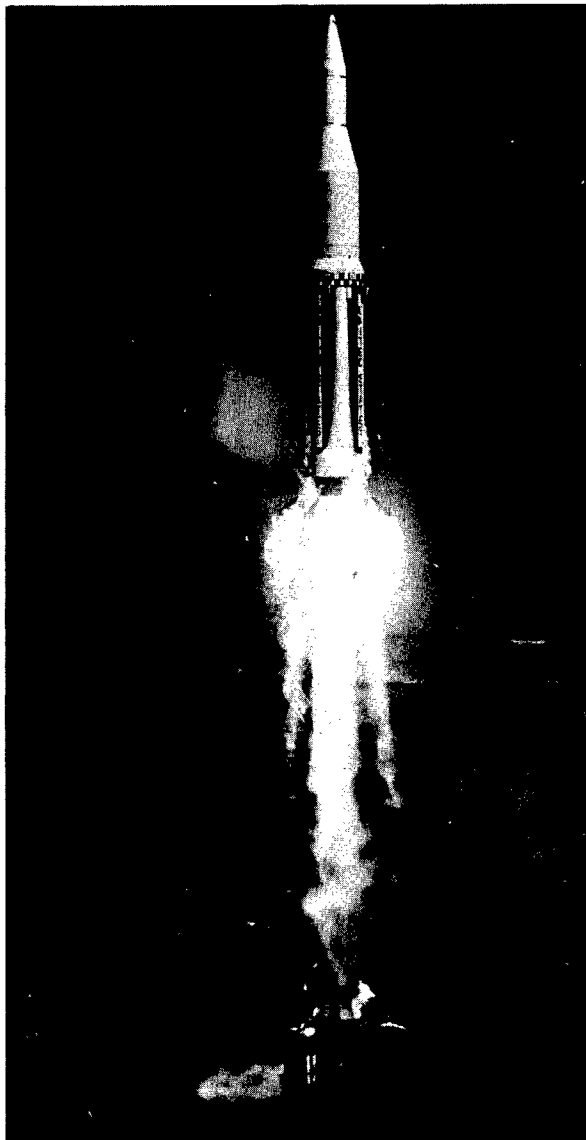
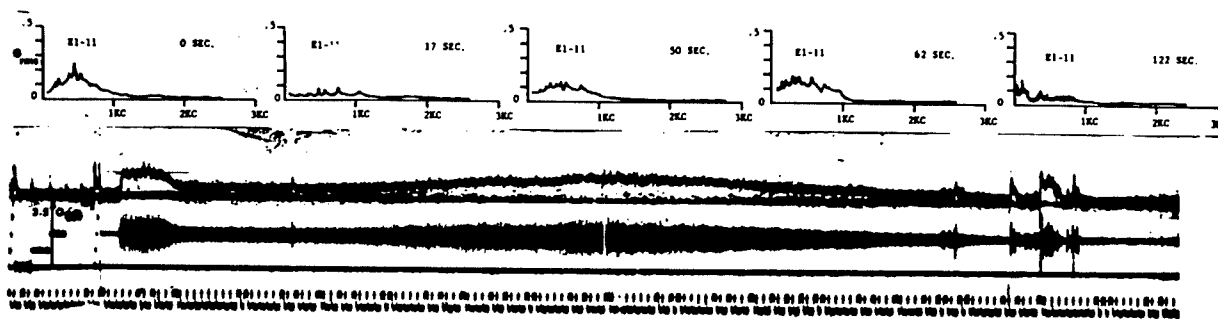
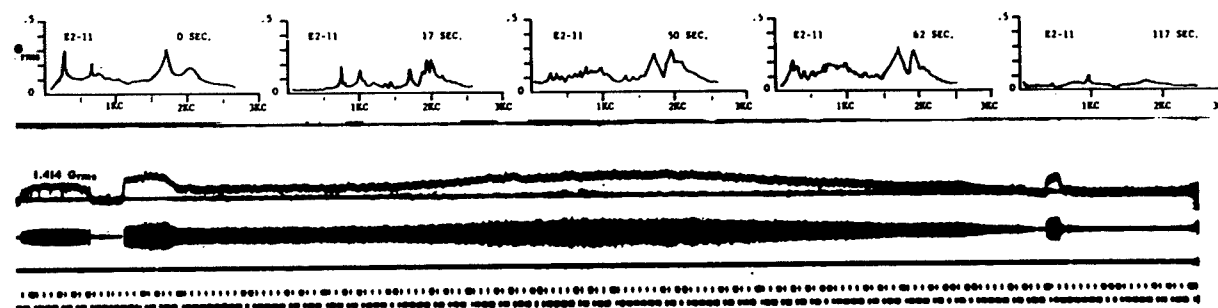


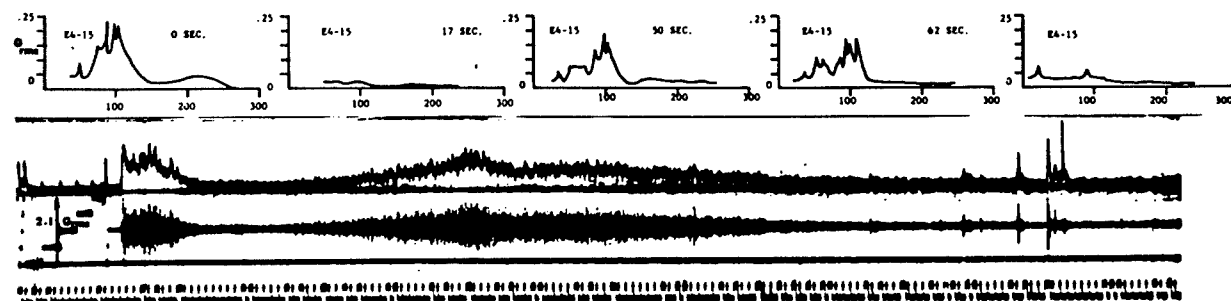
Fig. 7 - Saturn SA-3 vehicle in flight



E1-II UPPER STRUCTURE

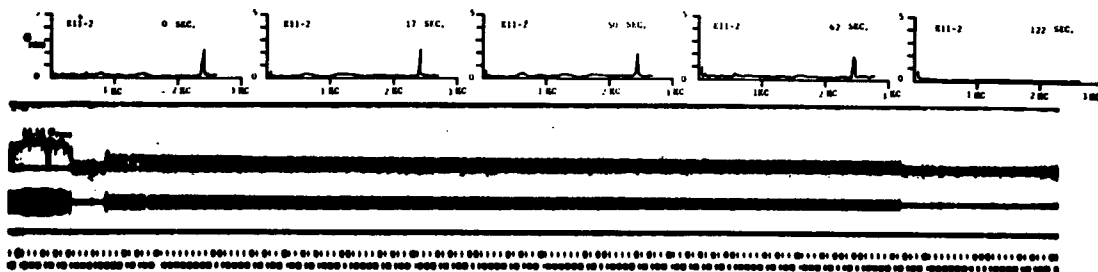


E2-II UPPER STRUCTURE

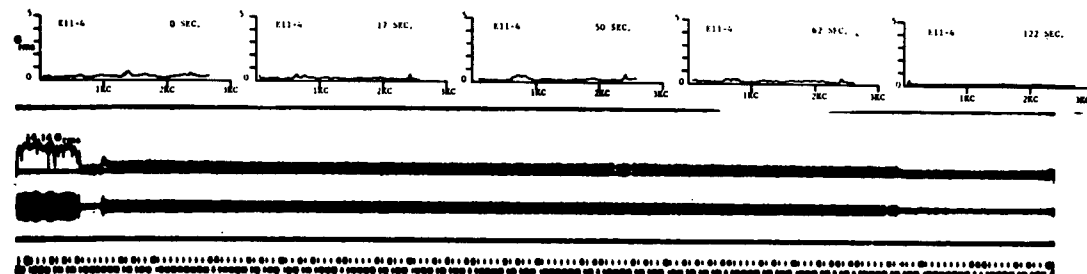


E4-15 ST-90

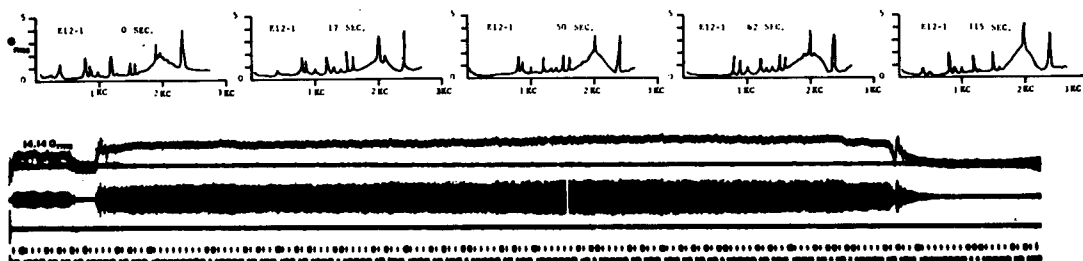
Fig. 8 - Flight-time-history of three upper structure measurements from SA-4 flight



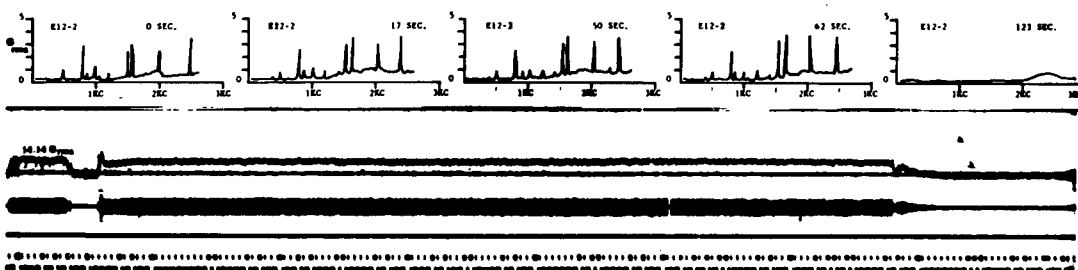
E11-2 THRUST CHAMBER DOME



E11-4 THRUST CHAMBER DOME



E12-1 TURBINE GEAR BOX



E12-2 TURBINE GEAR BOX

Fig. 9 - Flight-time-history of four engine-mounted measurements from SA-4 flight

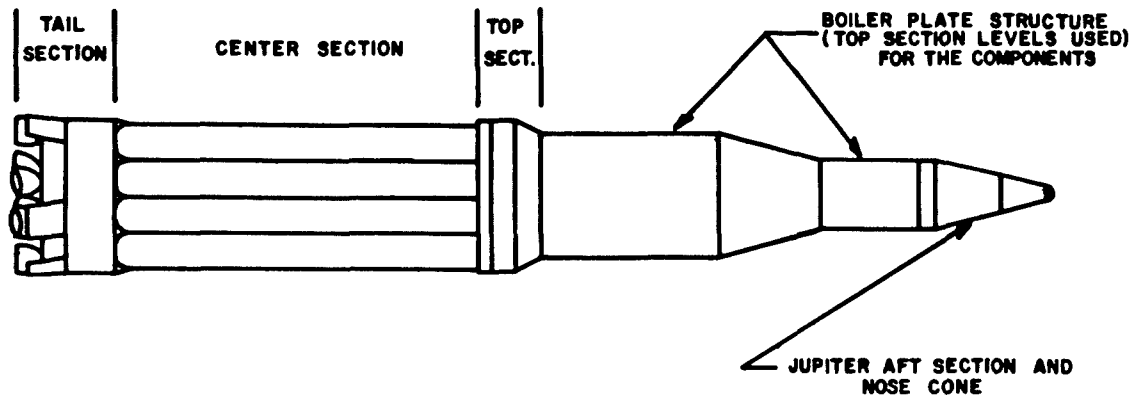


Fig. 10 - General zoning for Saturn I, Block I (original)

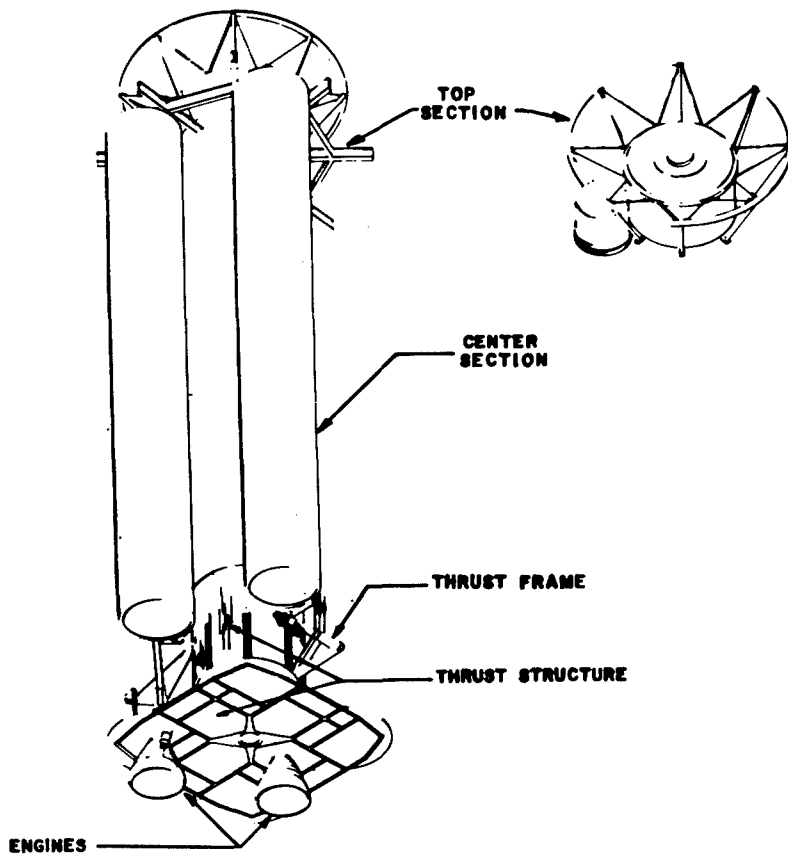


Fig. 11 - General zoning for Saturn I, Block I (original)

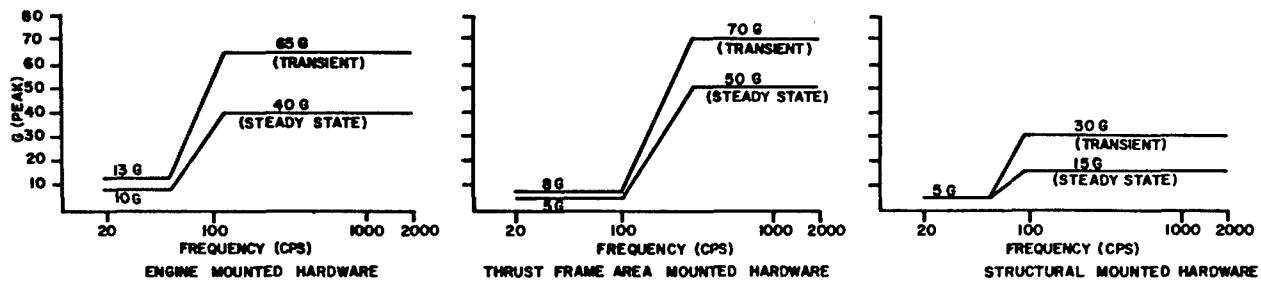


Fig. 12 - Tail section component vibration test levels, Saturn I, Block I

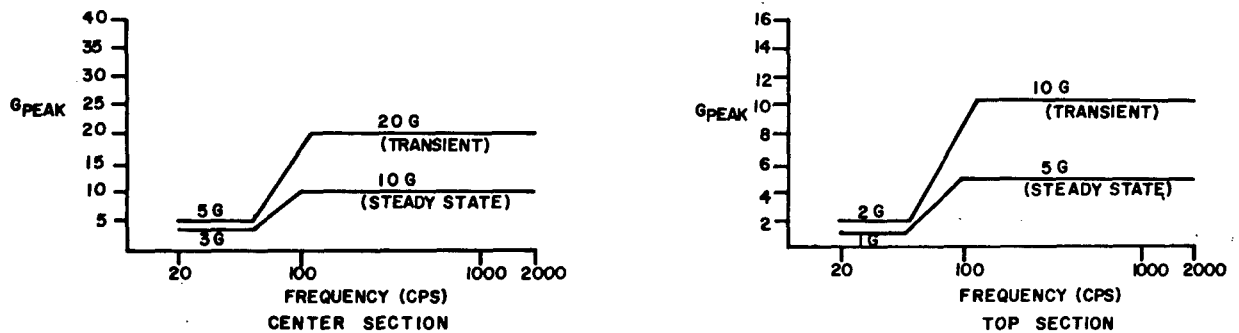


Fig. 13 - Center and top section component vibration test levels, Saturn I, Block I

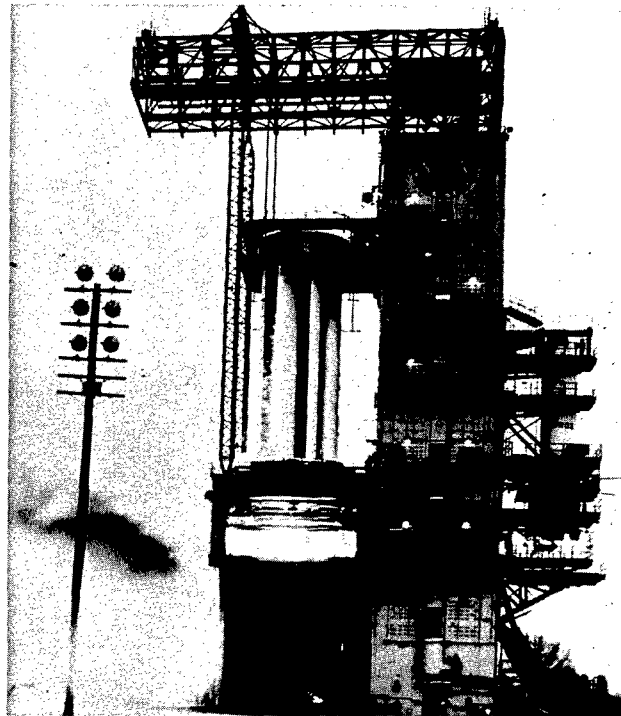


Fig. 14 - Typical S-I stage static firing at MSFC

at the Atlantic Missile Range launch facility yields a more uniform acoustic field. Also, the static test tower causes certain areas of the booster to be shielded from the acoustic field. Figure 15 illustrates the orientation of the deflected thrust axis for each case. The next two figures illustrate the influence of the static test facility on the engine generated sound pressure field. Figure 16 shows the space average of test stand overall sound pressure levels as a function of length along the vehicle. Station number 100 corresponds to the engine gimbal plane. Note the significant influence on the sound pressure level caused by the engine

holddown platform. Figure 17 illustrates the variation in overall sound pressure level at various angles around the vehicle from the major exhaust direction. This curve is to be used with the previous curve in Fig. 16. By selecting the space average sound pressure level at a particular vehicle station number in Fig. 16, the user can determine the more exact overall sound pressure level at any particular angle on booster by use of Fig. 17. Much more data has been obtained since these curves were determined in order to better define this effect and will be published at a future date. The static firing data to be next compared with the original

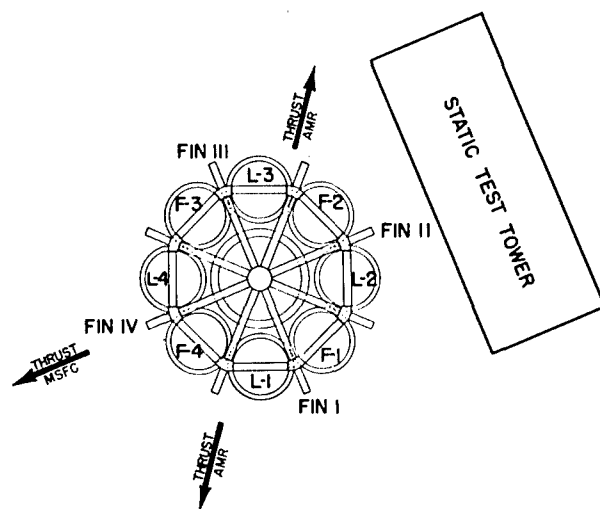


Fig. 15 - Thrust deflector; booster orientation at MSFC and AMR

predicted levels has been corrected where necessary for the above mentioned tower effects. In order to permit a comparison with the original test specifications we have reduced the static test data to a sinusoidal test level by the analysis technique described in NASA Technical Note D-1836. This technique is based on spectra obtained by constant bandwidth analysis of vibration measurements. The static firing test levels were derived from the 97-1/2-percent confidence spectra of measurements obtained within the respective vehicle zones. For this comparison the constant bandwidth analyses were extracted from measurements during the mainstage period of static firings. These data are therefore compared with the steady-state levels of the original specification. The next four slides illustrate this comparison. Figure 18 indicates the steady-state vibration level specified for engine-mounted hardware and data which was an input to H-1 engine turbo-pump components. As you can see, the test specification level appears overly conservative in this case. Some conservation is warranted, however, since the specification applies to all engine-mounted hardware. The vibrations experienced by hardware mounted to the turbo-pump are predominately caused by rotating impellers, bearings, and gears and the passage of fluid, and therefore is quite unique. Figure 19 shows a comparison between the specified vibration test level for structural-mounted hardware in the booster tail section and the envelope of static firing data obtained from the thrust structure. These levels compare more favorably than those of Fig. 18, yet are still quite conservative, especially at the extreme

ends of the test spectrum. The specification level for components located in the booster center section is next compared with the static firing envelope from measurements in the aft LOX and fuel skirts as illustrated in Fig. 20. These static firing measurements were obtained from ringframe and stringer type structure. Here for the first time the measured envelope exceeds the specified level at several frequencies, although the specification is again conservative over most of the spectrum. Our last comparison between the specification and static firing data, Fig. 21, shows the specification level for the booster top section and an envelope of measurements obtained from the spider beam area. These spectra indicate a fairly good correlation over a relatively wide band of frequencies.

Our conclusions from the above comparison is that considering the data available when the original predictions were made, the correlation between the predicted environment and the levels obtained during static firings is better than we had anticipated. In general, however, the data indicates our specifications were overly conservative at the extreme ends of the test spectra. A point should be made here concerning the low frequency vibration environment, which is not apparent from the above comparison. Our data indicates that the low frequency contribution to the vehicle vibration environment approaches a maximum not during mainstage operation but during the transition periods associated with engine ignition, booster release, high Q, engine cutoff, and retro-rocket firing. These extremely non-stationary periods

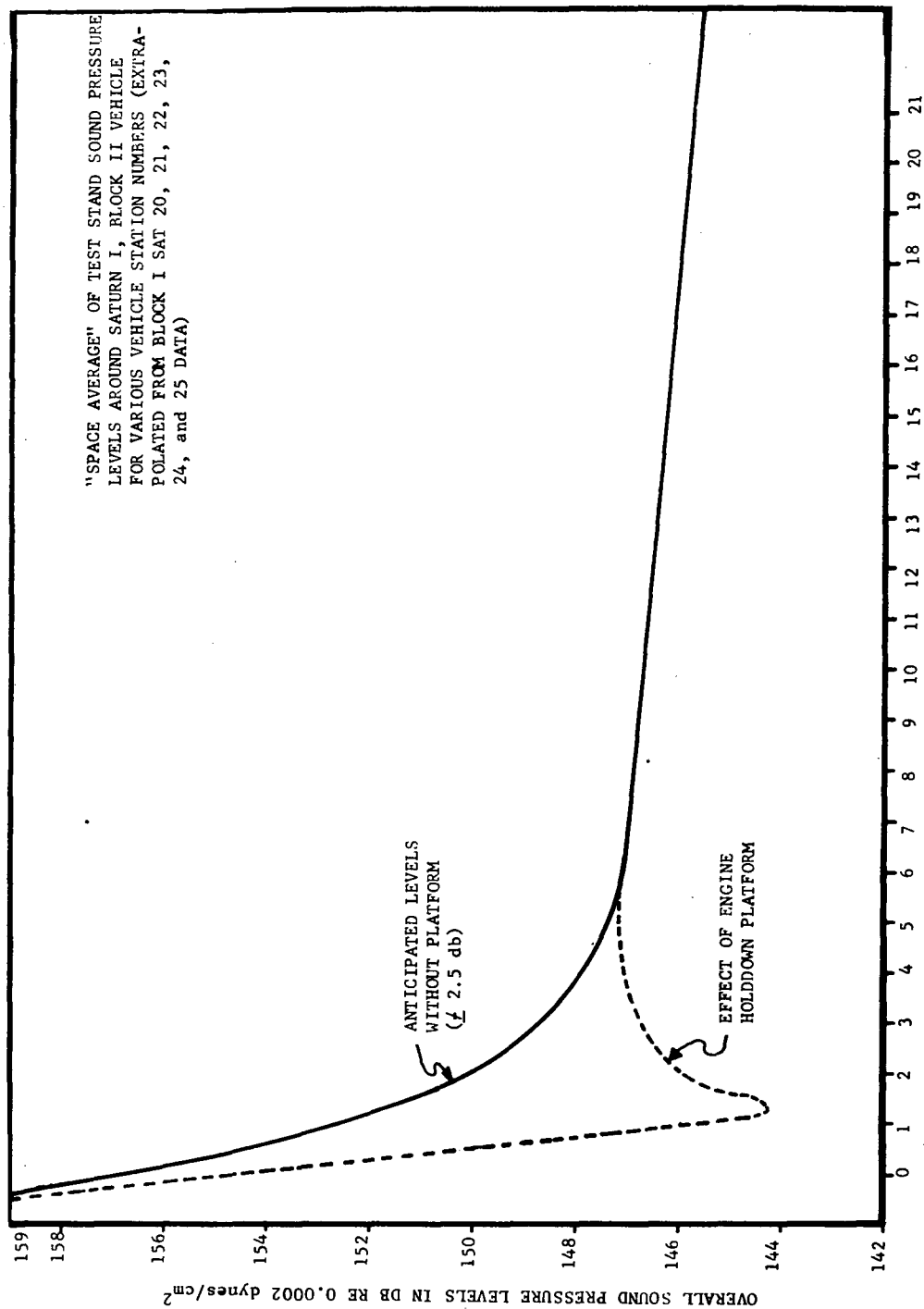


Fig. 16 - Space average overall sound-pressure-level vs vehicle length for static test stand at MSFC

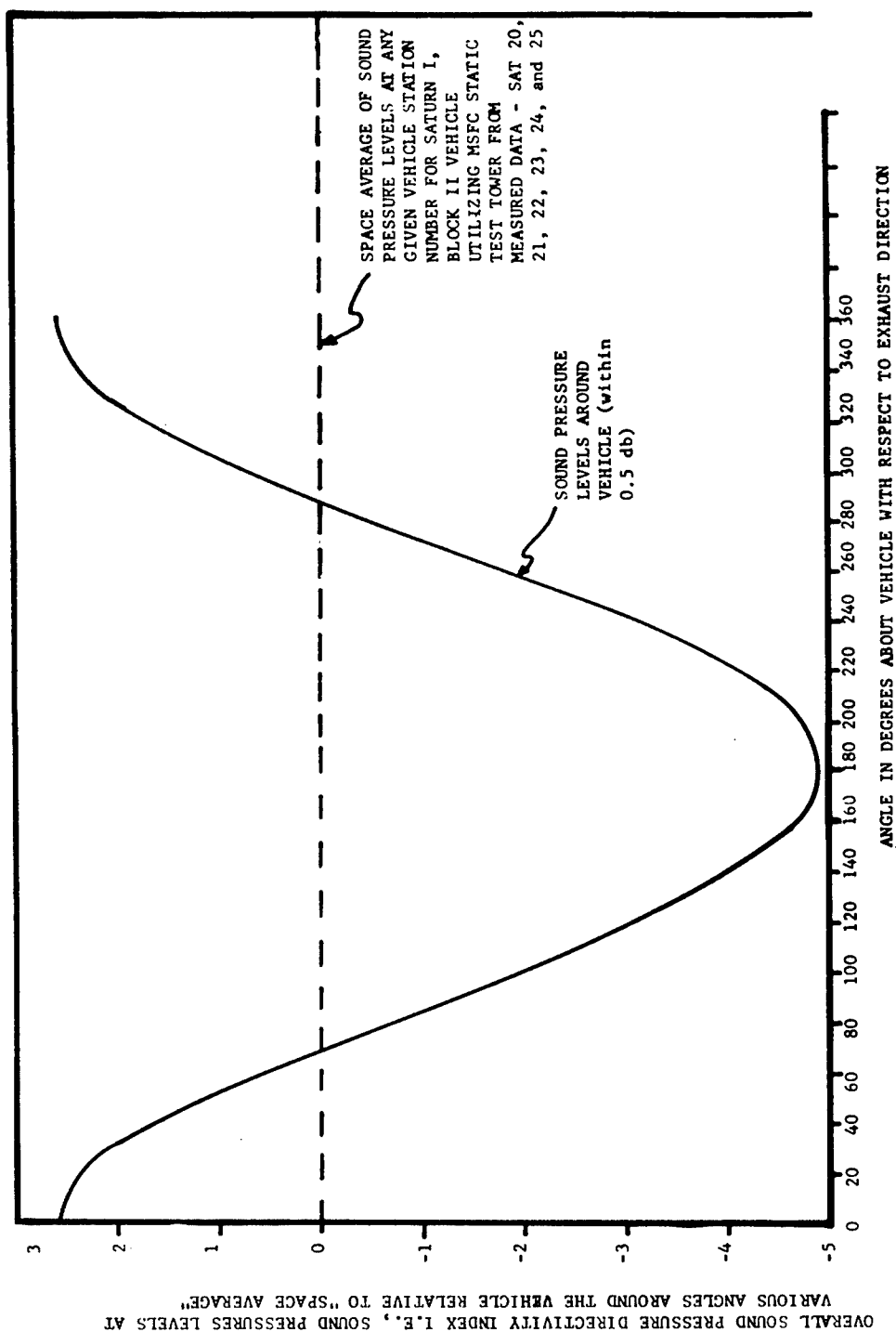


Fig. 17 - Angular correction curve for space average overall sound-pressure-level for static test stand at MSFC

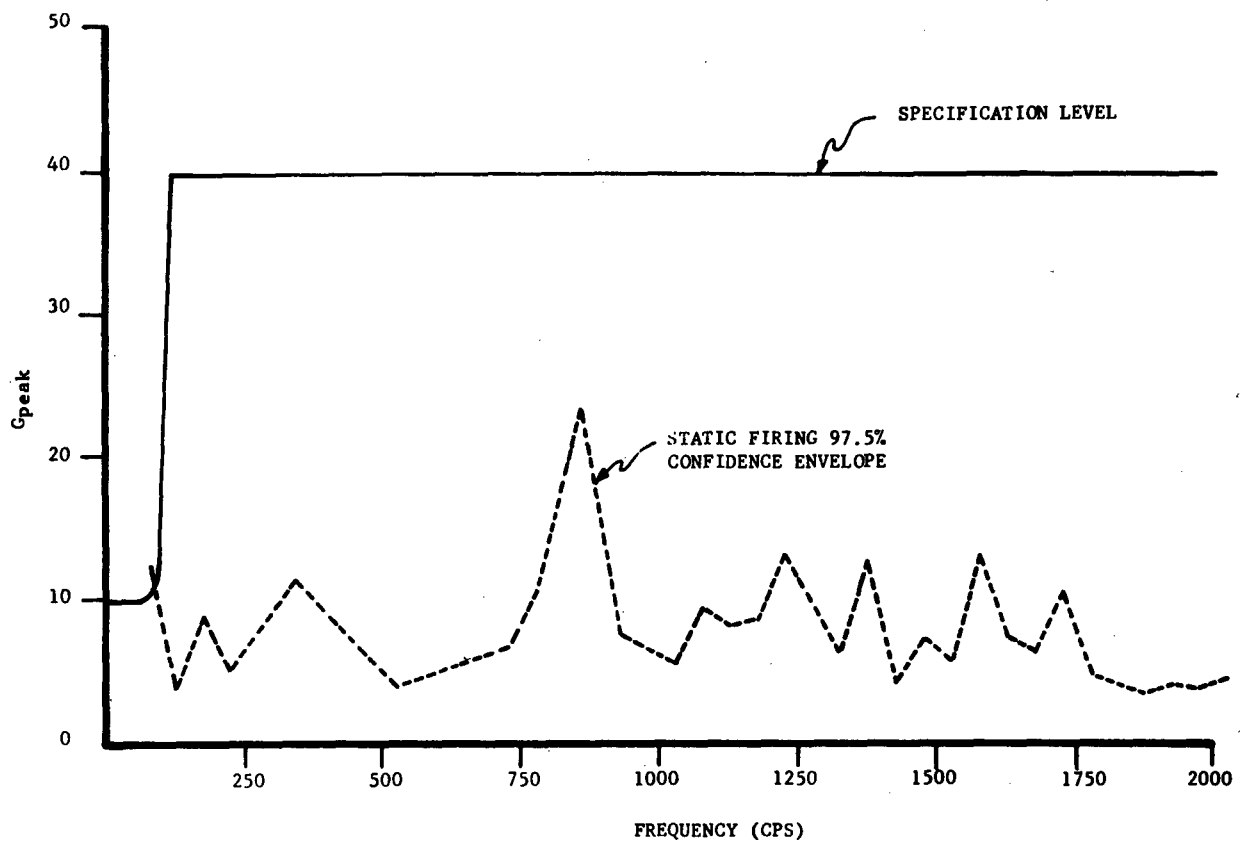


Fig. 18 - Comparison between the specified vibration test level for engine-mounted hardware and the 97-1/2-percent confidence envelope of data obtained from turbo-pump hardware during booster static firing

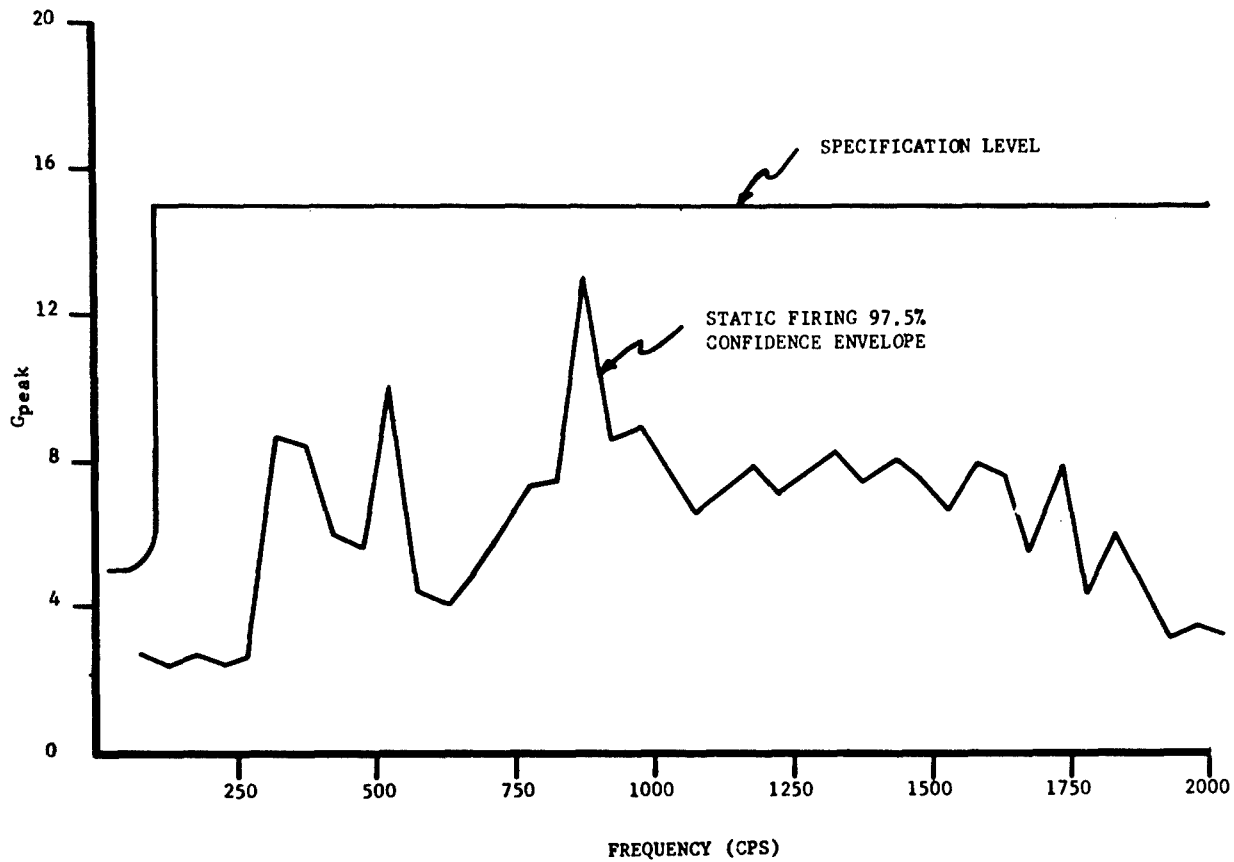


Fig. 19 - Comparison between the specified vibration test level for structural-mounted hardware in the booster tail section and the 97-1/2-percent confidence envelope of data obtained from the thrust structure during booster static firing

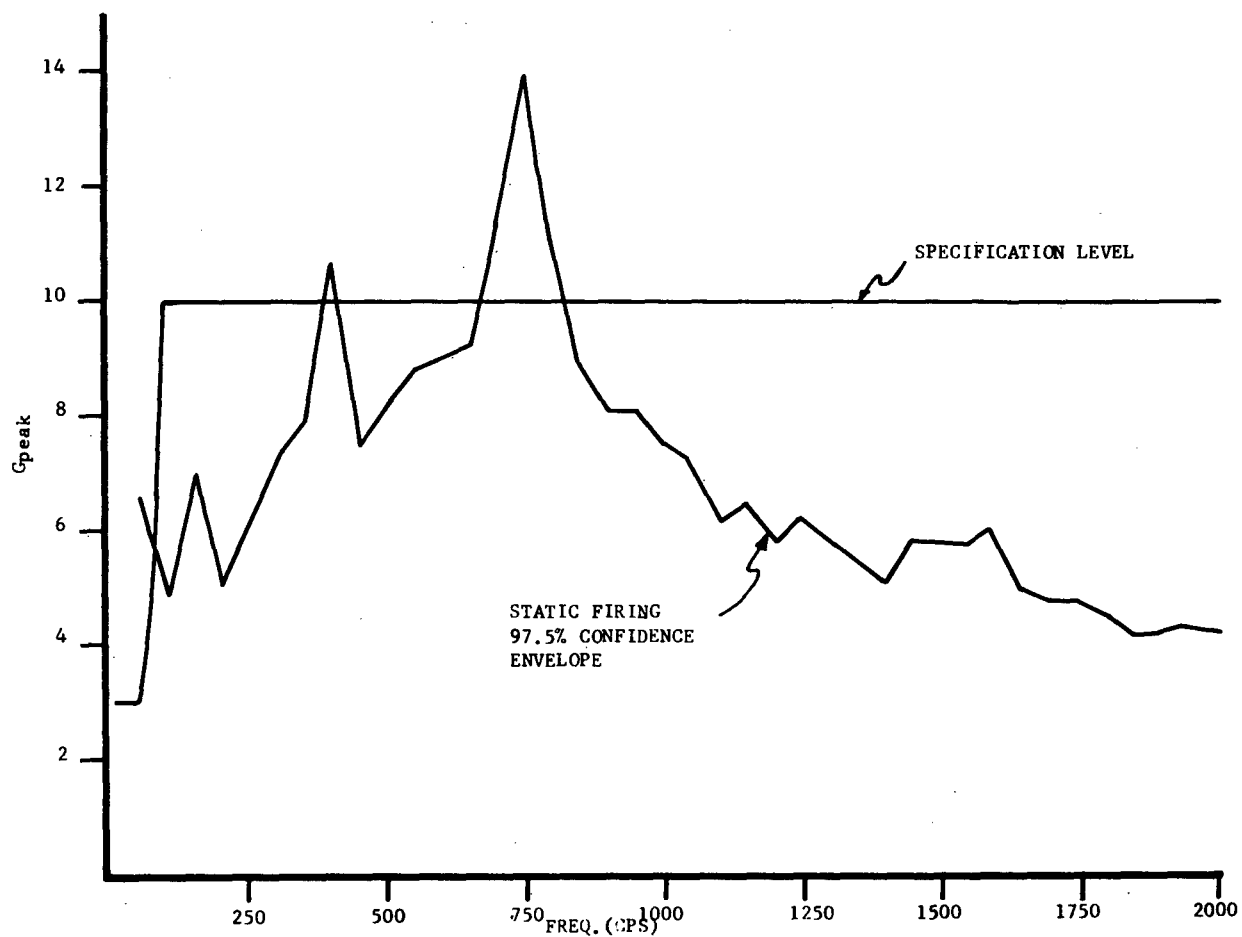


Fig. 20 - Comparison between the vibration level specified for testing components mounted in the booster center section and the 97-1/2-percent confidence envelope of data measured in the aft LOX and fuel skirts during static firing

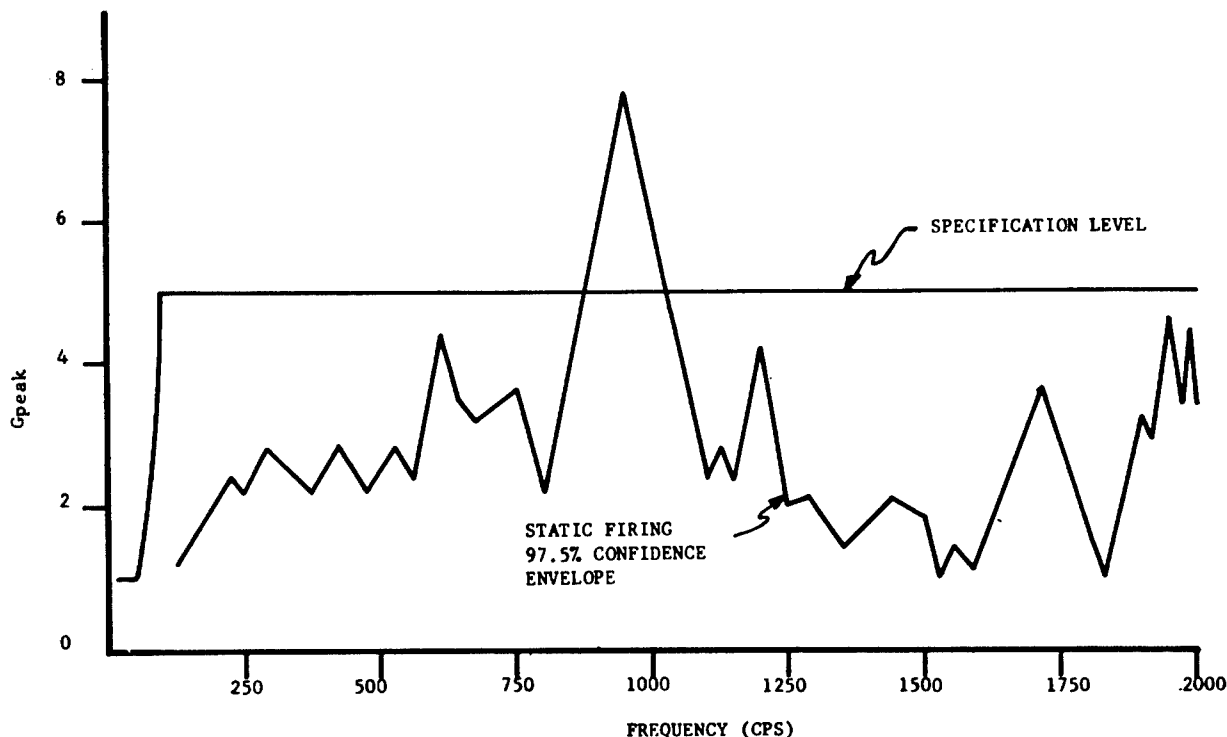


Fig. 21 - Comparison between the vibration test level specified for components located in the booster top section and the 97-1/2-percent confidence envelope of data obtained from the spider beam area during static firing

of vehicle operation must also be considered in the derivation of test specifications. We would like to emphasize that the static test data has been compared here to DSF-TM-7-59 which was issued in 1959.

We shall next show a comparison between static firing data and measurements obtained during the mainstage period of flight for the four Saturn I, Block I launches. The acceleration level for the comparisons is expressed as G_{rms} . This value is the root-mean-square acceleration as measured at the center frequency of a nominal 10-cps band-pass filter. The static firing data are presented as 97-1/2-percent confidence spectra of measurements obtained from the respective zones. The flight data represent the maximum envelope of constant bandwidth analyses obtained from measurements in the respective vehicle zones during flight.

Maximum levels are presented since we have, as of yet, too few flight measurements from the various zones from which to obtain a significant statistical description. The static firing measurements were obtained with land-wire instrumentation which had a linear frequency response beyond the 2 kc we are

comparing here. The flight measurements, however, were transmitted over telemetry channels with different bandwidths. For the first Saturn flight (SA-1) the vibration measurements were all transmitted by standard I.R.I.G. FM/FM telemetry with channel bandwidths varying up to a maximum of 1050 cps. Most of the measurements on the remaining three flights were transmitted by SSB/FM telemetry with a linear frequency range of approximately 50 cps to 3 kc. In view of the limited number of flight measurements no effort was made to normalize or adjust the data for telemetry channel bandwidth characteristics.

Figure 22 indicates a comparison of static firing and flight data from H-1 engine gear cases. The flight levels nowhere exceeded the statistical envelope from static firings. A close look at turbo gear case data would indicate harmonics associated with gear train and impeller blade-pass frequencies. A comparison of measurements obtained from the H-1 engine combustion chamber is shown next in Fig. 23. As you can see the statistical envelope was not exceeded during the flights and the general trend of the two curves show quite good correlation.

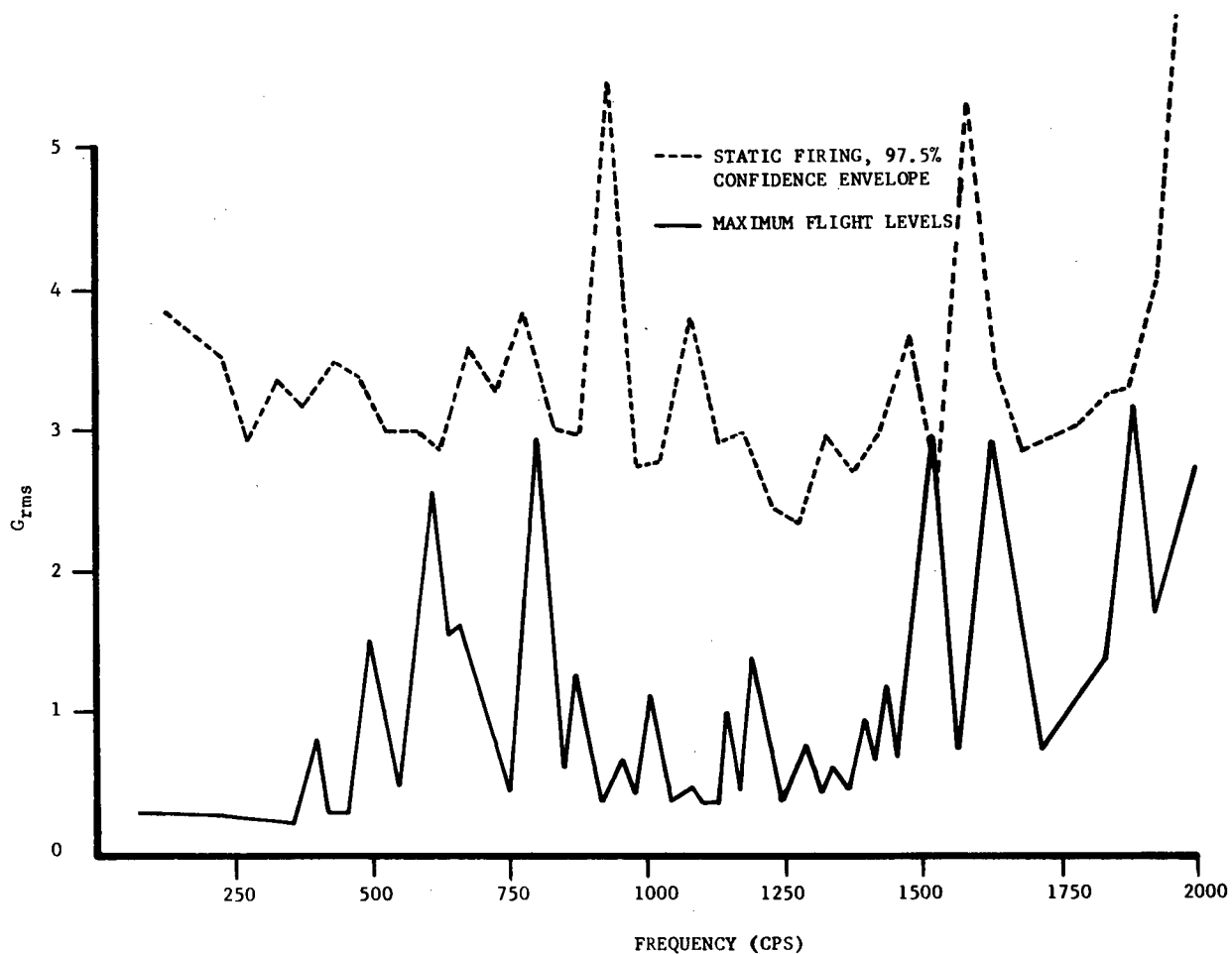


Fig. 22 - Maximum envelope of H-1 engine gear case measurements obtained during Block I flights and the 97-1/2-percent confidence envelope of measurements obtained from the same location during booster static firing

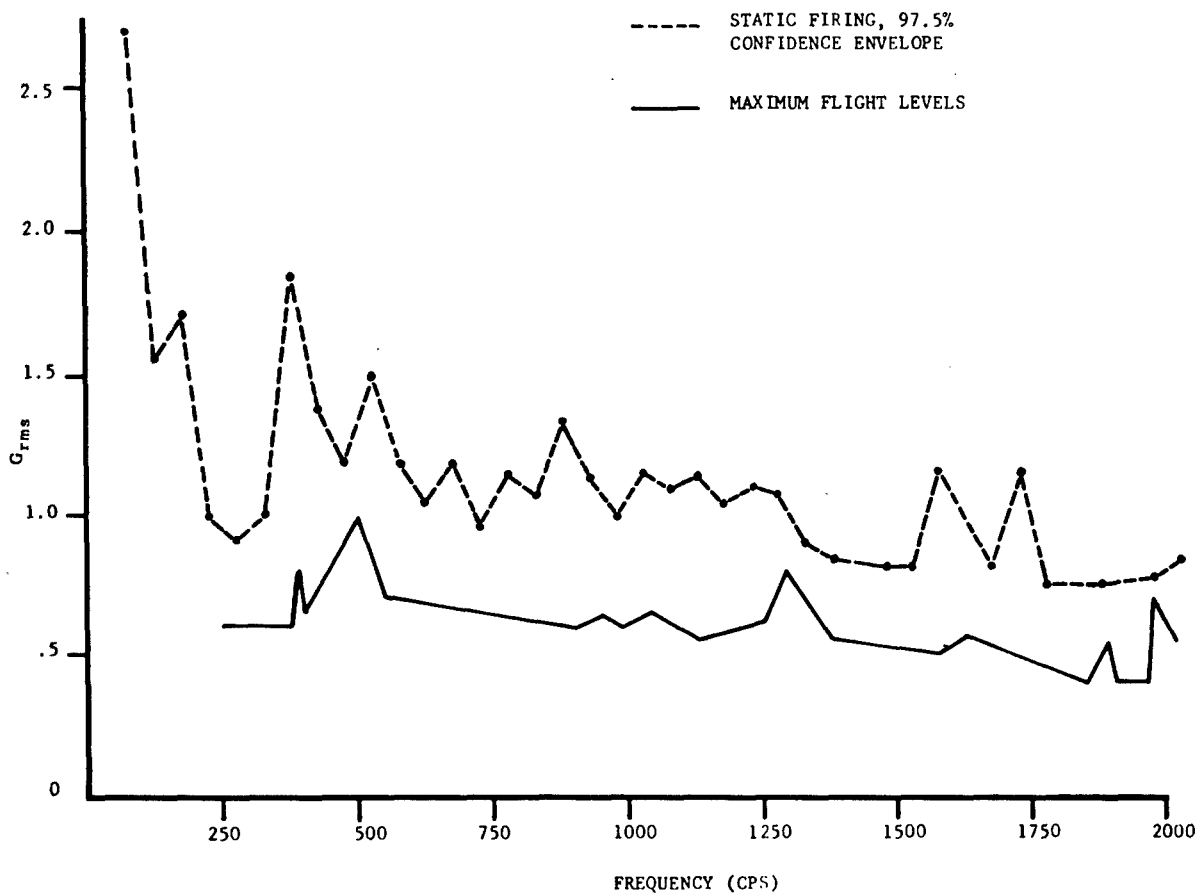


Fig. 23 - Maximum envelope of combustion chamber measurements obtained during Block I flights and the 97-1/2-percent confidence envelope of measurements obtained from the same location during booster static firing

Figure 24 illustrates a comparison of measurements from the thrust structure. In this area the maximum flight levels exceeded the statistical envelope in two frequency increments. Our final comparison shown in Fig. 25 shows the static firing and flight spectra for vibration measurements in the spider beam area. These curves indicate a significant point which must be considered in the derivation of test specifications from static firing data. Note the significant peak which appears in the flight envelope and not the statistical data. We conclude that the lack of correlation shown here is, at least in part, due to differences in the fixity conditions at the spider beam associated with the static test tower alignment and the launch configuration.

This ends our comparison of Saturn I, Block I vibration data. For all practical purposes, the books have been closed on the Saturn I, Block I vehicles, but the experience and data gained from these vehicles still linger on. We have utilized the data and prediction techniques

derived from the development of the Block I vehicle to determine the vibration, acoustic, and shock environments for Saturn I, Block II, Saturn IB, and Saturn V. The documents stating the vibration, acoustic, and shock criteria for each of these vehicles can be found in the list of references.

Figure 26 illustrates the more detailed zoning of the Block I booster data that was used for determining the Block II environments. This figure lists the number of measurements used to statistically define each major zone and sub-zone. Figure 27 is shown for the purpose of better defining the location of the engine sub-zones listed in Fig. 26.

The next three figures give you a more detailed description of the environmental zone breakdown for the Saturn I, Block II vehicles. Figure 28 illustrates the basic vehicle system with the S-I stage booster, S-IV second stage, instrument unit, and payload.

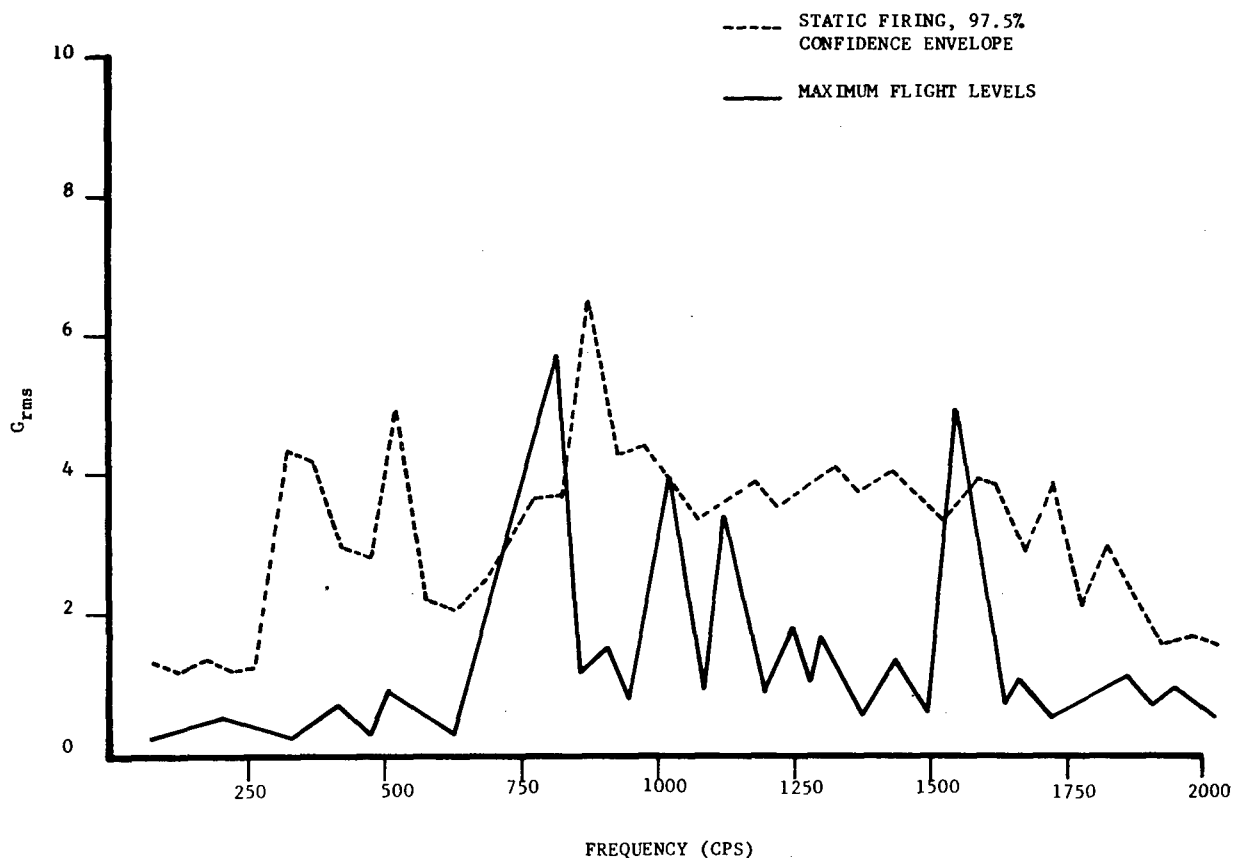


Fig. 24 - Maximum envelope of thrust structure measurements obtained during Block I flights and the 97-1/2-percent confidence envelope of data obtained from the same area during booster static firing

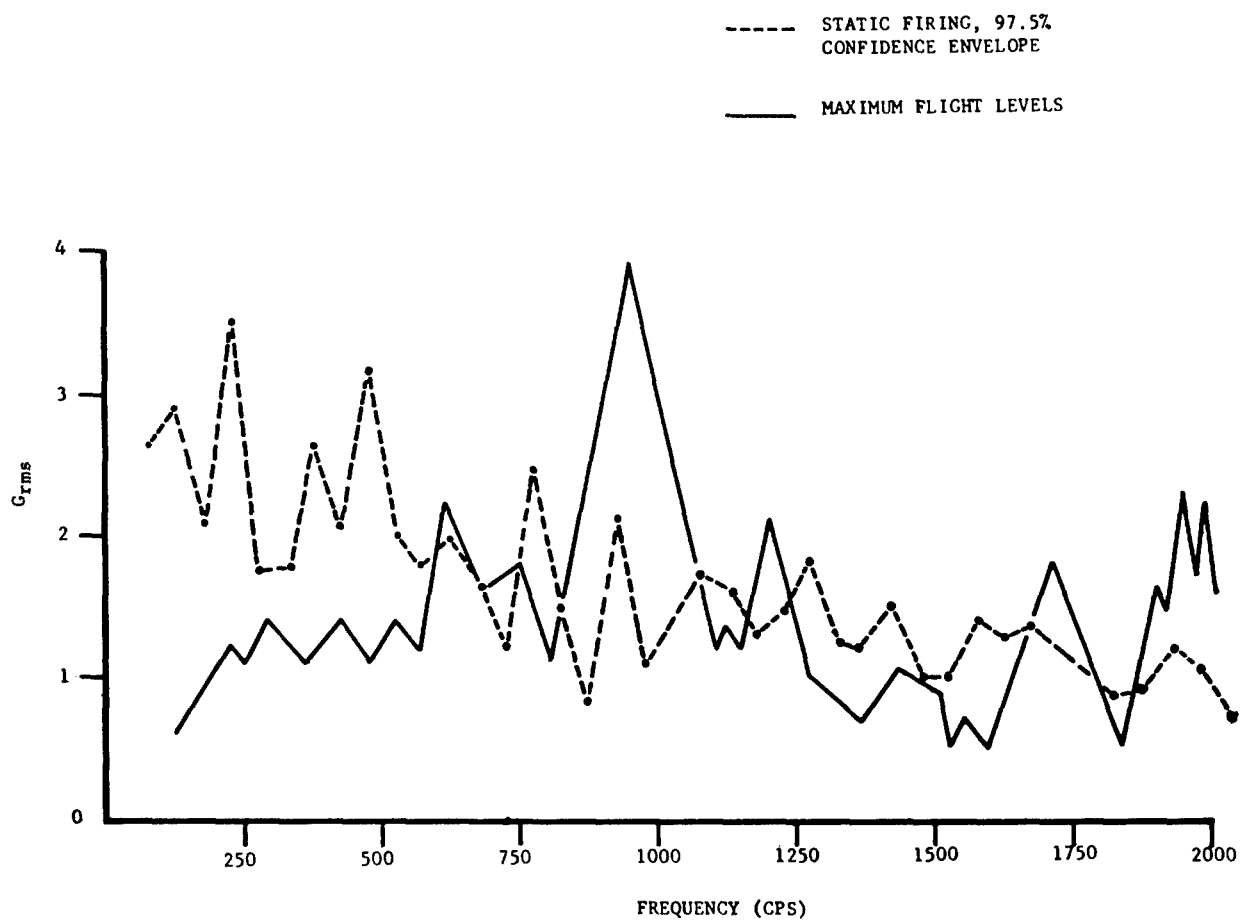


Fig. 25 - Maximum envelope of spider beam measurements obtained from Block I flights and the 97-1/2-percent confidence envelope of data obtained from the same area during booster static firing

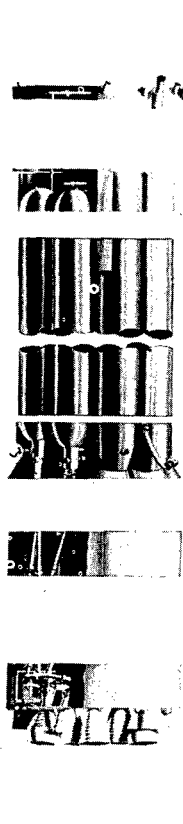
	ZONE	DESCRIPTION	NO. OF MEAS. USED IN EVALUATION
	7	SPIDER BEAM	60
	6-LOX	FWD. LOX SKIRTS (DATA OBTAINED FROM SKIN PANELS ONLY)	20
	6-FUEL	FWD. FUEL SKIRTS (DATA OBTAINED FROM SKIN PANELS ONLY)	20
	6-4-FUEL	FWD. FUEL BULKHEAD	15
	5-LOX	PRESSURIZED LOX TANK (LIQUID & NON-LIQUID LOADED RESPONSES TREATED SEPARATELY)	20
	5-FUEL	PRESSURIZED FUEL TANK (LIQUID & NON-LIQUID LOADED RESPONSES TREATED SEPARATELY)	20
	3-LOX	AFT LOX SKIRTS (DATA OBTAINED FROM RING FRAMES & STRINGERS ONLY)	30
	3-FUEL	AFT FUEL SKIRTS (DATA OBTAINED FROM RING FRAMES & STRINGERS ONLY)	60
	3-4-FUEL	AFT FUEL BULKHEAD	15
	2	THRUST STRUCTURE	132
	1-1	H-1 ENGINE TURBOPUMP (COMPONENTS)	136
	1-1-0	H-1 ENGINE TURBOPUMP (GEAR CASE ONLY)	180
	1-2	H-1 ENGINE COMBUSTION CHAMBER (COMPONENTS)	155
	1-2-0	H-1 ENGINE CHAMBER DOME ONLY	188
	1-2-C	ACTUATOR ASSEMBLY	174

Fig. 26 - Saturn I, Block I zonal statistics
breakdown from static test data

RESULTS OF H-1 ENGINE VIBRATION STATISTICAL
ANALYSIS INDICATING THE 97½% CONFIDENCE SPECTRA

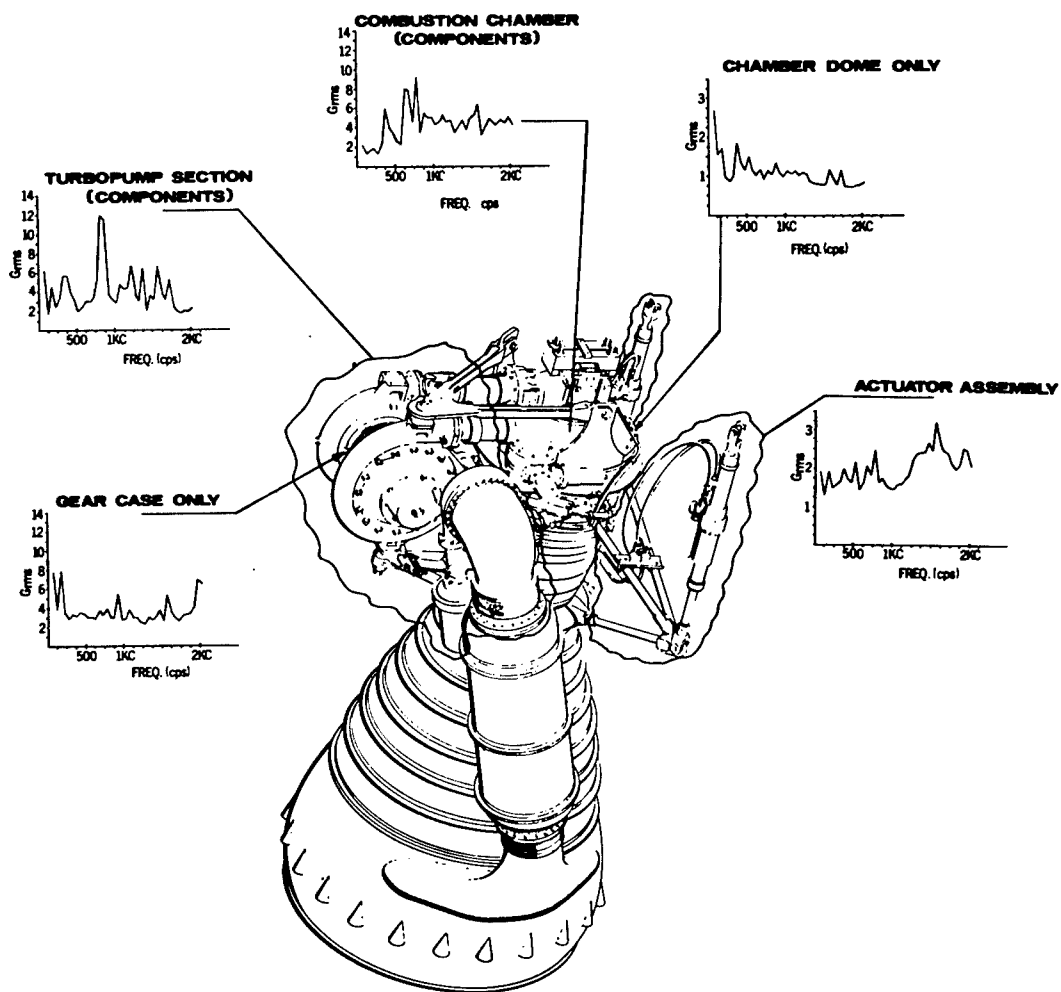


Fig. 27 - H-1 engine vibration statistics

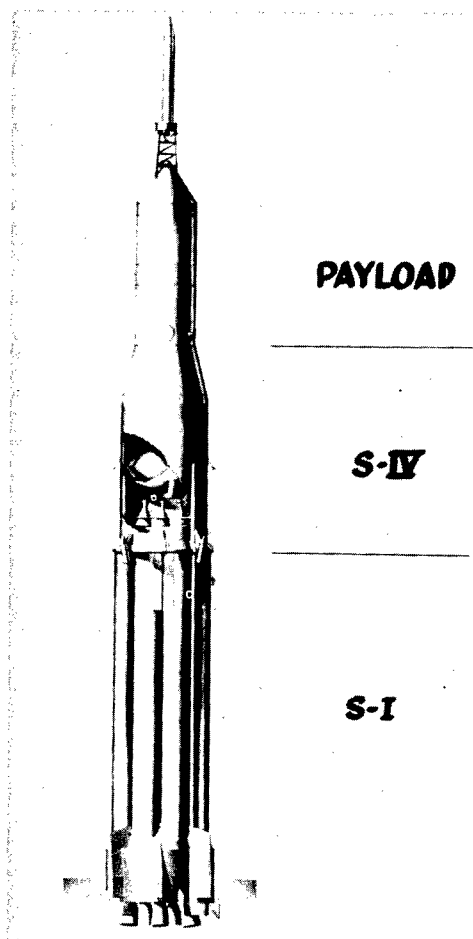


Fig. 28 - Typical Saturn I, Block I vehicle configuration

The major environmental zones for the S-1 booster are illustrated in Fig. 29. Figure 30 shows the major zone breakdown of the S-IV stage, instrument unit, and payload. This zoning represents a vast improvement over the environmental zone breakdown defined in the original Saturn vibration specification as can be seen by reviewing Fig. 10. The original Saturn vibration test specification was divided into three environmental zones and three sub-zones, whereas the specification for the Saturn I, Block II is defined in terms of 15 major environmental zones and 94 sub-zones.

Marshall environmental test specifications may appear overly conservative when compared with the flight data just presented. It should be

noted, however, that the first four Saturn flights were made under ideal conditions: no severe winds aloft, no rough combustion, no hard-over gimbaling, and no engine out other than one programmed engine shut-down 10 seconds prior to cutoff on SA-4. Also, many considerations other than mainstage operation must be considered in the derivation of test specifications. These include the transition periods of flight mentioned earlier as well as the dynamic environment associated with transportation and handling.

Marshall feels very strongly about rigid laboratory qualification test requirements. Our business is the development of man-rated vehicles and we cannot afford to base our philosophy on assumed flight failures.

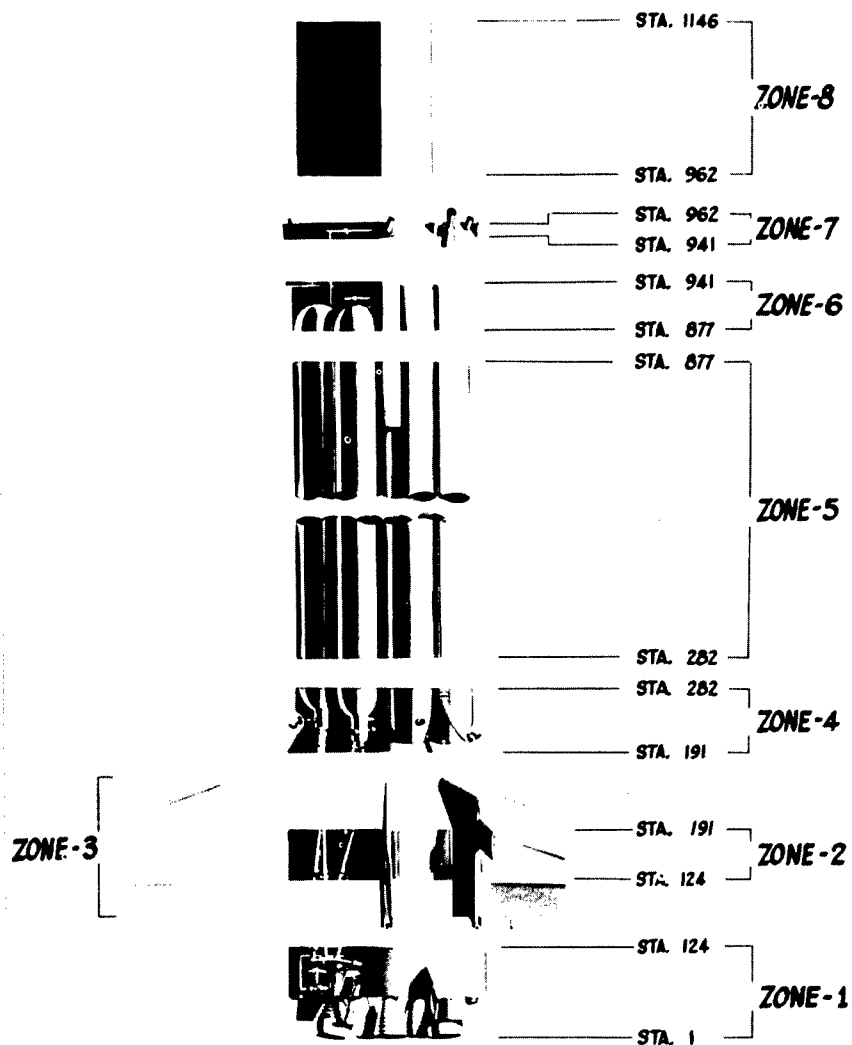


Fig. 29 - Environmental zone breakdown for
S-I stage of Saturn I, Block II vehicle

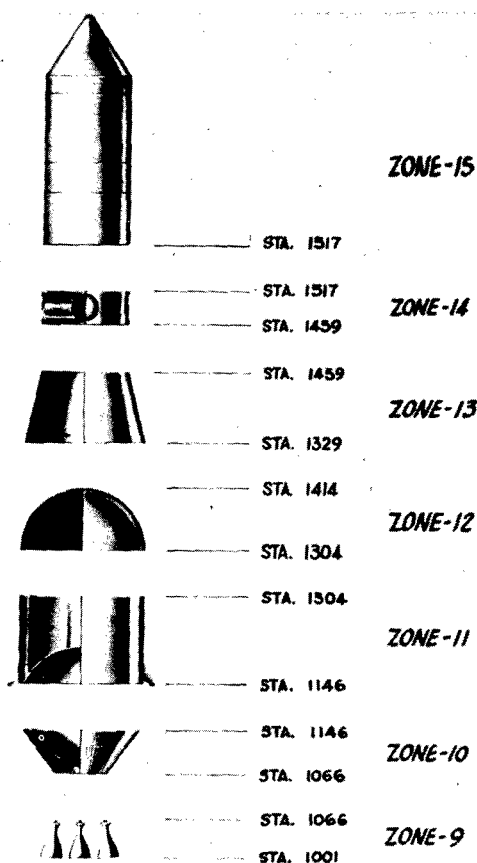


Fig. 30 - Environmental zone breakdown for S-IV stage and payload of Saturn I, Block II vehicle

BIBLIOGRAPHY

1. MTP-P&VE-S-62-1, "Comparison of Saturn Vibration Data - Static and Flight" by Environmental Vibration and Acoustic Analysis Unit (Feb. 28, 1962).
2. MTP-P&VE-S-62-6, "Vibration and Acoustic Analysis of Saturn SA-2 Flight," by Environmental Vibration and Acoustic Analysis Unit (Aug. 17, 1962).
3. IN-P&VE-S-63-6, "Vibration and Acoustic Analysis of Saturn SA-3 Flight," by Vibration and Acoustics Unit.
4. IN-P&VE-S-63-52, "Vibration and Acoustic Analysis of Saturn SA-4 Flight," by the Vibration and Acoustics Branch.
5. R. E. Barrett (MSFC), "Techniques for Predicting Localized Vibratory Environments of Rocket Engines," NASA Technical Note, NASA TN-D1836 (Oct. 1963).
6. MSFC Document, IN-P&VE-S-62-7, "Vibration, Acoustic, and Shock Specification for Components on Saturn I (Block II) Vehicle," by Structures Evaluation and Dynamics Section (May 10, 1963).
7. MSFC Document, IN-P&VE-S-63-1, "Preliminary Vibration, Acoustic, and Shock Specifications for Components on Saturn IB Vehicle," by Structures Evaluation and Dynamics Section.
8. MSFC Document, IN-P&VE-S-63-2, "Preliminary Vibration, Acoustic, and Shock Specifications for Components on Saturn V Vehicle," by Structures Evaluation and Dynamics Section (Nov. 5, 1963).

9. J. H. Farrow, "Preliminary Saturn Shock and Vibration Specifications," Report No. DSF-TM-7-59 (May 1959).

10. R. E. Jewell and G. D. Johnston, "Acoustic and Vibration Environment for Saturn," paper presented at the 30th Symposium of Shock, Vibration, and Associated Environments (Oct. 1961).

DISCUSSION

Mr. Judd (MB Electronics): I notice that all of your data cut off at 2,000 cycles. Did you make measurements to find out what was happening above 2,000 cycles, and, if so, what do you consider the significance of the energy contained above 2,000 cycles?

Mr. Johnston: Within the limitation of the tape recorder, all of the data from the static firing measurements taken on the tower go at least to 5 kc and higher if we so specify. The fundamental analysis that we do for each tape from the tower goes to 2,500 cps. The comparison here is to 2 kc because our specs go only to 2 kc. Of course, the limitation in the past has been mostly the laboratory equipment, not the analysis itself. We do have the data to 2,500 cps. Generally speaking, the only concern we have had for energy above 2 kc has been on the power plant measurements themselves. The structural measurements do not indicate a significant high frequency energy content.

Mr. Rice (Goodyear Aerospace): You stated that you felt sine wave testing was more important than random wave testing. Have you found that the sine wave testing is in general more severe?

Mr. Johnston: This is always brought up to us by most of the people we deal with on the stages in the power plant. There is always an argument. We continue to use this because it is an established, reliable procedure for developing good hardware. We feel that the random test definitely has its place. We are using the sine test to evaluate design and structural integrity. We are using the random test as a functional check on equipment. I don't think that we have enough experience right now to say that we are fully qualified in random testing for structural qualifications.

Dr. Vigness (NRL): In slides 15, 16, and 17, you gave a comparison in terms of the maximum amplitude of vibration, in which you compared the structural responses with the specifications. I would be interested in knowing what the peak values of the structural responses would be, as this is a random vibration and one

would have to know how you are going to determine the peak response in this case. Is it some rms value, is it three times the signal, or what is the peak response?

Mr. Johnston: Of course, that is what all of us are wondering. Each of us has his own way of getting from the measurements to what I have shown. I will tell you what we have done. The data are based on a 97-1/2 percent confidence level derived from the first free moment of the statistical distribution. We take 50-cycle bandwidths to a spectrum data and, for the measurements you saw on this chart, the different zones break down anywhere from 20 to 132 in each zone. We can determine the mean, the mean square, or standard deviation, and the skewness for each 50-cycle bandwidth. We don't assume any normal distribution within any of the bands. We take the two sigma value for each one of these bandwidths, and that is where the spectrum comes from for our comparison to the q-peak values. Does that answer the question?

Dr. Vigness: Yes, thank you.

Mr. Mutter (Boeing Co.): I believe you stated that your static firing levels were approximately the same as the in-flight steady-state level, yet most of your comparisons have indicated that the static test firing levels are considerably higher. Can you explain that?

Mr. Johnston: On a static test tower on the exhaust side, the deflector side, where maximum load intensities occur, the main stage level will be higher than during flight. The space average, however, around the vehicle is somewhat less. Now, if we look at it as the space average, not the maximum or not the minimum, then it is perhaps slightly higher in the case of the tail section area. Here is where we have pretty much garbage in the vehicle during the main stage portion of the flight.

Mr. Mutter: Do your comparisons average your on-pad conditions, or are they just the maxima? Your comparison between the static tests and the flight had indicated your static

test was considerably higher in most cases. Does your static test data average around the vehicle include the effect of the tower, or was it just the highest level?

Mr. Johnston: The static test data considers the tower effect on the distribution of the acoustic field. That's what we have

attempted to do with the curves here, with the space average and the angular correlation. We have tried to, in effect, get an average value and use this in our statistical data along with weighting factors for the number of measurements for each zone.

Mr. Mutter: Thank you.

* * *

A COMPARISON OF THE FLIGHT EVALUATION OF THE VEHICLE BENDING DATA WITH THE THEORETICAL AND DYNAMIC TEST RESULTS FOR THE SATURN I VEHICLE*

Everette E. Beam
Marshall Space Flight Center
Huntsville, Alabama

A flight evaluation of the bending mode accelerometer data has been conducted for several Saturn I vehicles. The evaluation was conducted in order to determine the frequency trends of the vehicle bending modes during powered flight. In addition, mode shapes and actual amplitudes of deflection were desired for the periods of maximum response.

In order to accomplish this data reduction, a digital program was developed using correlation and power spectral relationships. The program computes amplitude of response and phase relationships for the predominant frequencies in two or more accelerometer measurements. The results depend mainly upon the type and number of measurements available, and the magnitude and type of response measured. The results to date have been satisfactory, even on low level response.

This paper is an attempt to show the comparison of results obtained from flight data with the results of theoretical calculations and dynamic ground vibration tests for the Saturn I vehicle. The digital program is described and some examples of the significance and application of the results are also discussed.

INTRODUCTION

It is desirable in the development program of a vehicle system to have sufficient data from the research and development flights to conduct a post flight evaluation of the behavior of the vehicle. The systems that make up the vehicle have been designed on the basis of analytical studies and past experience, and redesigned as necessary after ground testing of component systems and subsystems. This preflight testing and evaluation is necessary to improve the possibility of a successful flight.

The development flight, however, is the first and only real test of the vehicle in the total performance of its mission. These flight tests provide the opportunity to evaluate the design criteria, analytical methods, and test methods used in order to improve the future vehicles. To accomplish this flight evaluation it is

necessary to determine the necessary instrumentation and evaluation methods that will provide the desired information.

The bending mode instrumentation on the Saturn vehicles to date has been used to provide information on the frequencies and amplitudes of response throughout the powered flight. This information can be of importance to help determine the causes in case of a malfunction or failure. The side benefits of instrumentation of this type are also present. It could be used for a study of an emergency detection system, evaluation of guidance and control data, determination of instability, evaluation of dynamic loads, and other studies associated with structural response.

The Saturn I vehicle under consideration here is the Block I vehicle which includes SA-1 through SA-4. The booster stage, as shown in

*Invited paper.

Fig. 1 is made up of a 105-inch-diameter center LOX tank and eight 70-inch-diameter outer tanks attached at each end to the center tank. The outer tanks consist of four fuel tanks and four LOX tanks attached to the center tank at the top by a spider beam assembly and at the bottom by the thrust structure outriggers. The upper stages are a dummy S-IV stage with a water ballast tank, a dummy S-V stage, and the payload.

took the form of a nonuniform single beam with an equivalent stiffness for the booster stage. The equivalent stiffness for this clustered tank booster was determined based on a structural deflection analysis on the total booster. Careful consideration was given to the weight distribution of the outer tanks.

The weight distribution of the outer tanks to the overall model would affect the beam

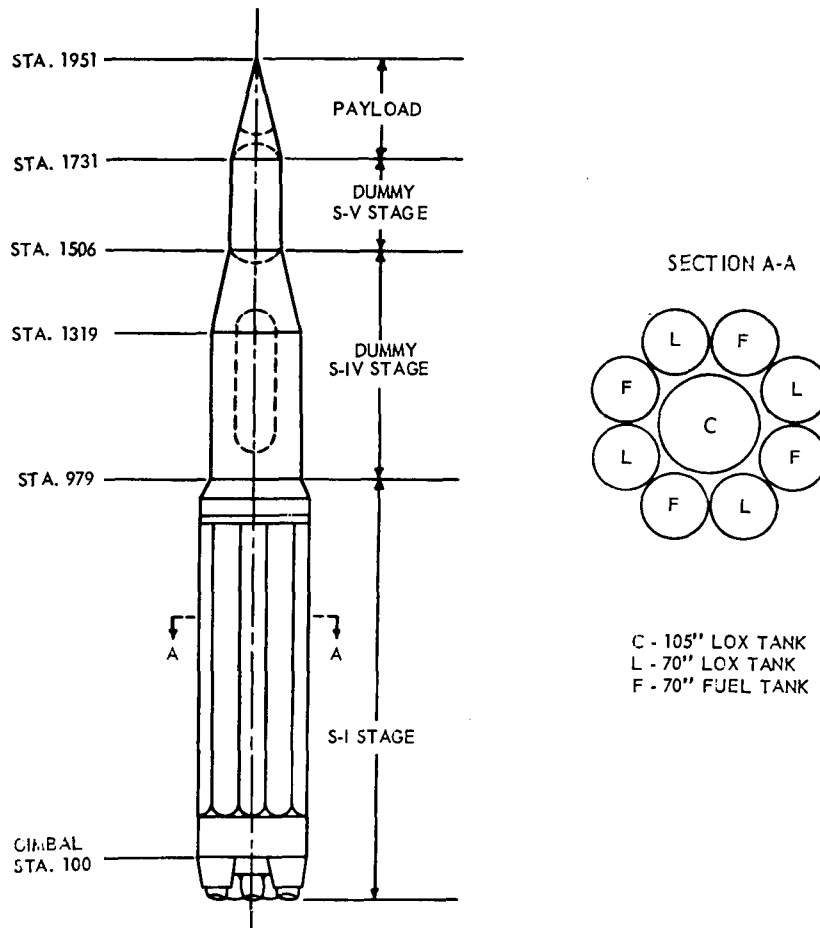


Fig. 1 - Saturn I, Block I configuration

In order to better understand the flight evaluation, some discussion on the analytical and test results to be used is in order.

PREFLIGHT ANALYSIS

Single Beam Model

The first analysis was naturally a simplified model of the actual structure. The model

analysis considerably. Test results showed that for most weight conditions the outer tanks had very little bending for an overall vehicle bending mode shape. A weight breakdown was adopted for the single beam analysis that would represent this effective weight of the outer tanks. The cluster beam analysis illustrates the model selection in Figs. 6 and 11. The weight of the outer tanks in the first mode is effective at the deflection line and therefore,

was distributed to the center tank in the single beam analysis. The weight of the outer tanks is not as effective at the deflection line of the second mode and was, therefore, distributed to the ends of the outer tanks near the node points.

This is a first model and was supplemented by data on the outer tanks as separate pinned end beams with appropriate rotary springs at the ends. The analysis was conducted by a transfer matrix technique.

This first model then gave a first and second bending mode frequency trend as shown in Fig. 2. A typical first and second mode shape is given in Fig. 3 for the flight time of 35 seconds.

Cluster Beam Model

The present analysis for the clustered booster is a coupled beam analysis using the transfer matrix method as the basis for the solution. The transfer matrix routine is begun at the nose of the vehicle and the compatibility

equations are written for the connection at the bottom of the outer tanks. The model considers symmetry and is then defined in terms of vibration planes rather than tanks, as shown in Fig. 5. This complex model includes longitudinal forces in the outer tanks, and spring coupling between the outer tanks. The outer tanks, center tank, and upper stages are distributed as nonuniform beams and the spring constants of the outer tanks attachments are determined from a separate analysis.

The cluster beam analysis was developed by Dr. Rudolph Glaser, of Marshall Space Flight Center, and programmed under his direction. The results of this program have proved to be very good by comparison to a later ground vibration test on the SA-5 vehicle.

A frequency trend curve for this clustered analysis is given in Fig. 4 and typical mode shapes are given in Figs. 5 through 11 for the flight time of 35 seconds. The first and second bending modes can be identified by comparison. The other modes can be called cluster modes since the motion is mainly on the outer tanks.

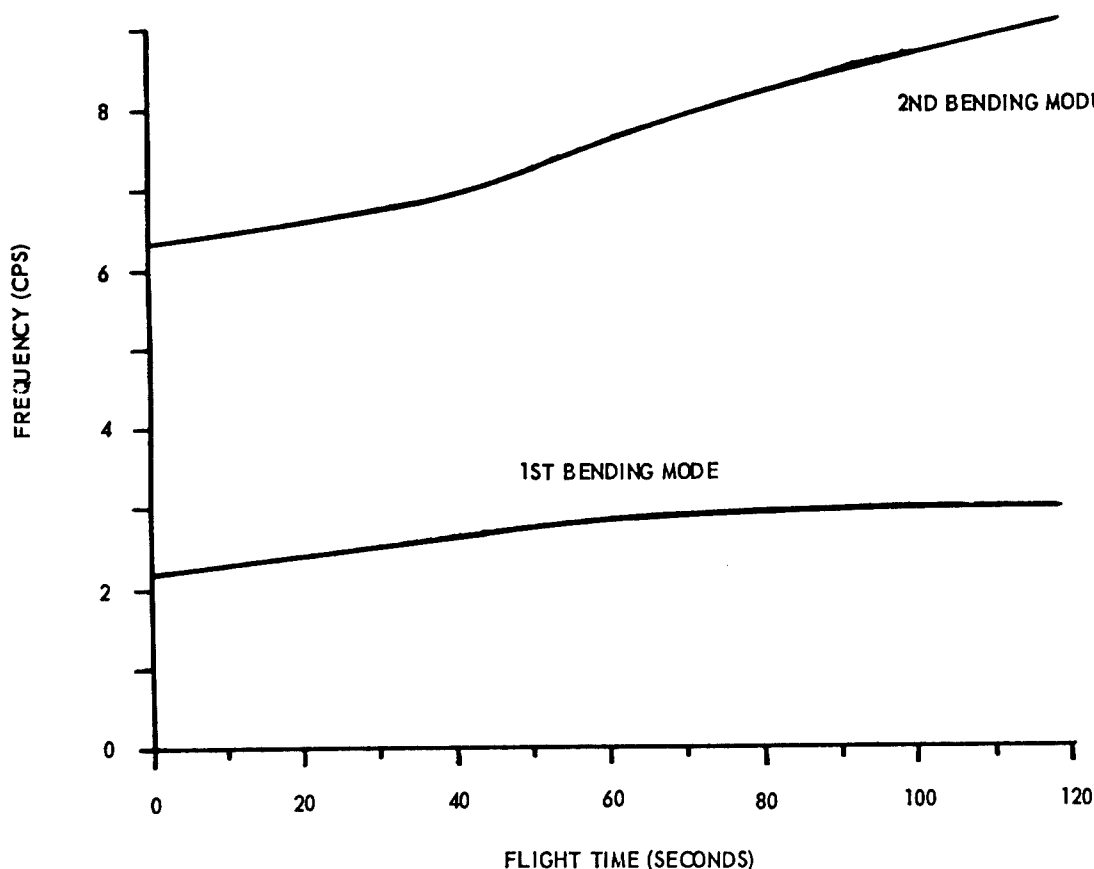


Fig. 2 - Single beam analysis - frequency trend

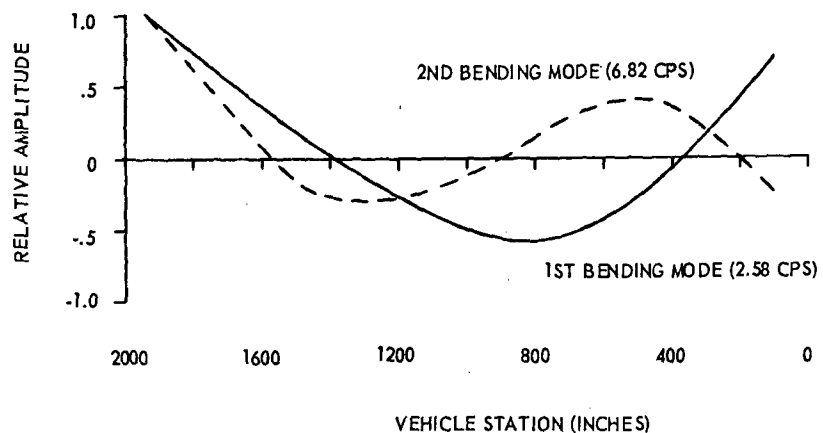


Fig. 3 - Single beam analysis - first and second bending modes (flight time - 35 seconds)

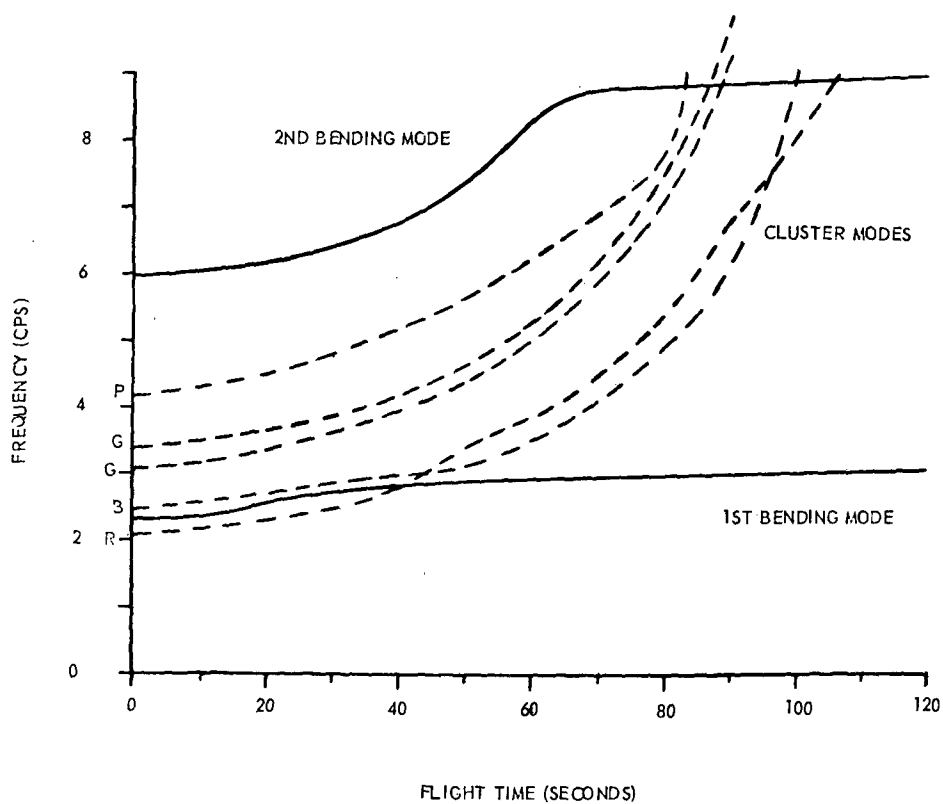


Fig. 4 - Cluster beam analysis - frequency trend

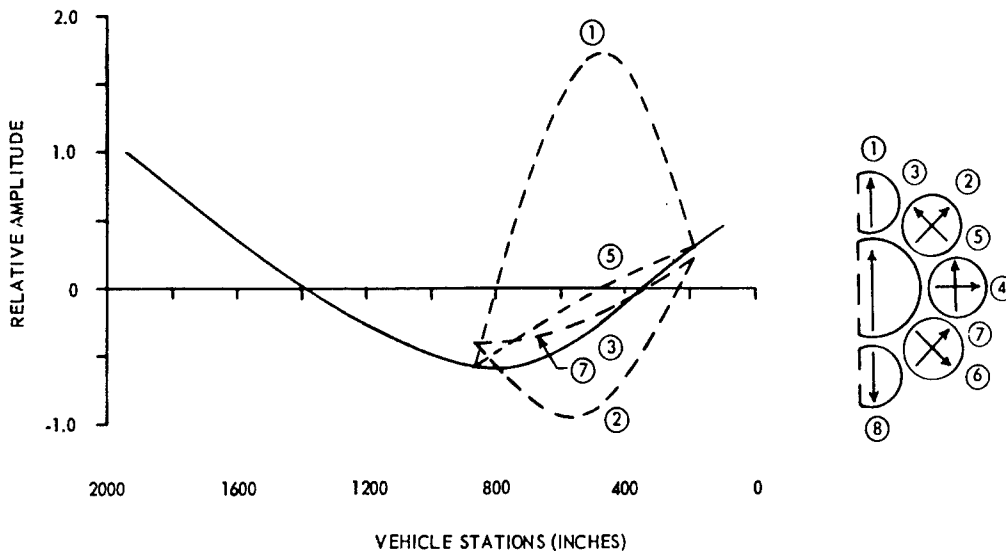


Fig. 5 - Cluster beam analysis - first cluster mode
(flight time - 35 seconds; frequency - 2.56 cps)

Ground Vibration Test

The Saturn I Dynamic Test Vehicle (SA-D1) was subjected to a ground vibration test to determine the lateral bending modes in a simulated free-free condition. To simulate the free-free condition the vehicle was suspended in the dynamic test stand in a vertical position. The suspension system consisted of cables running upward from the outriggers at the tail section of the vehicle through a set of springs to a hydraulic cylinder attached to the tower. The hydraulic cylinder was located at the 72-foot level which is about the top of the booster. The cable attach points at the top are

only slightly outboard of the lower attach points as is indicated by the lateral spring rate of only 626 lb/in. and a vertical spring rate of 625,000 lb/in. This spring rate was varied for the different test fill conditions.

The flight times or fill conditions tested are for 0, 10, 35, 63, and 119 seconds. The tanks were filled with de-ionized water and the correct weight was simulated within 3 percent for each flight time tested.

The rigid body frequencies on the cables were well separated from the lowest natural frequency in bending. The greatest suspension

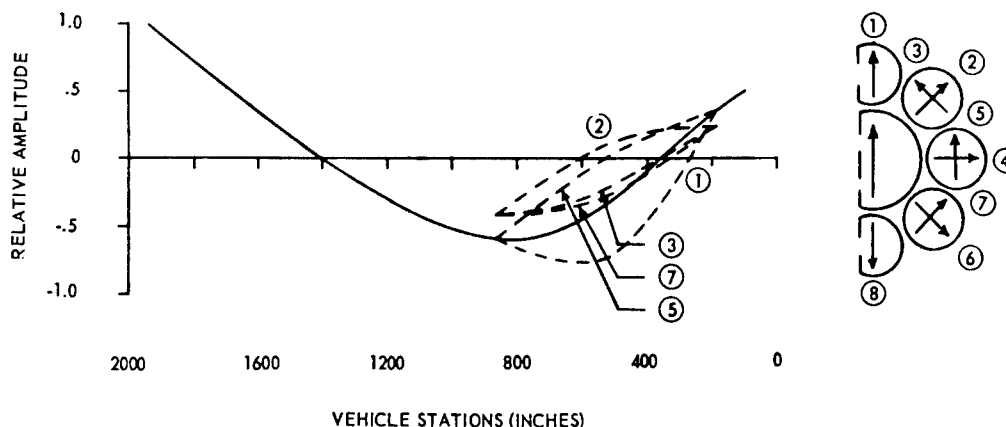


Fig. 6 - Cluster beam analysis - first bending mode
(flight time - 35 seconds; frequency - 2.75 cps)

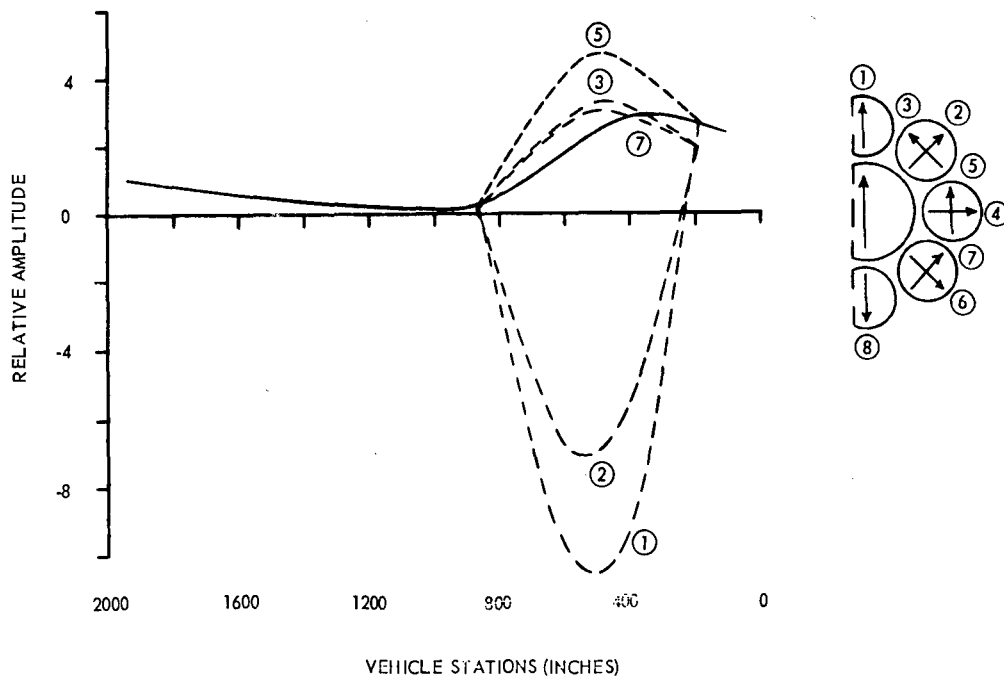


Fig. 7 - Cluster beam analysis - second cluster mode
(flight time - 35 seconds; frequency 2.88 cps)

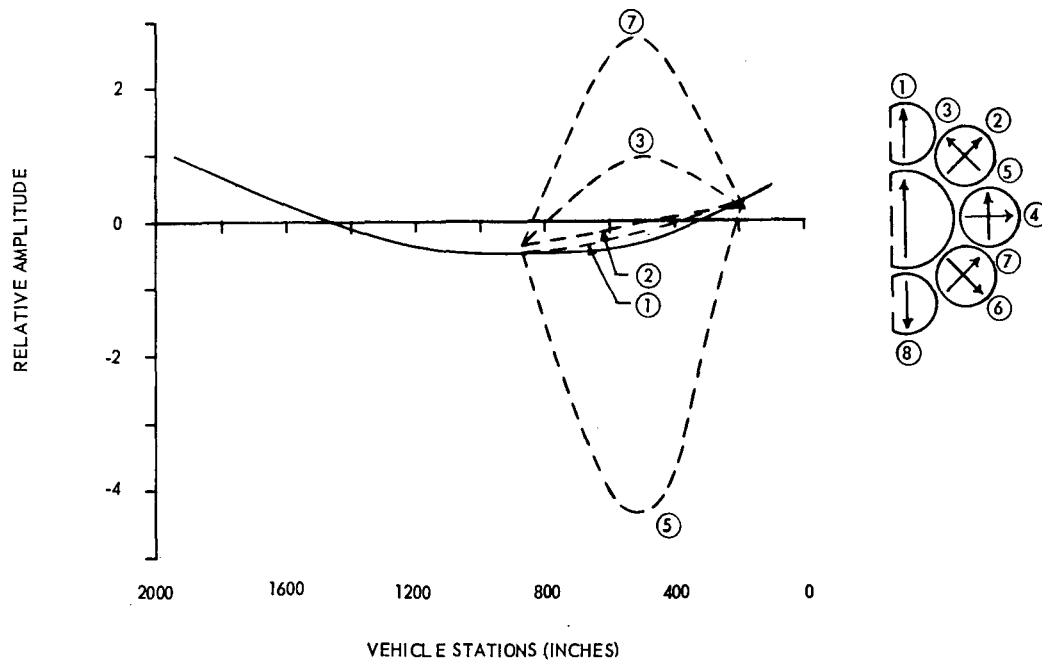


Fig. 8 - Cluster beam analysis - third cluster mode
(flight time - 35 seconds; frequency - 3.75 cps)

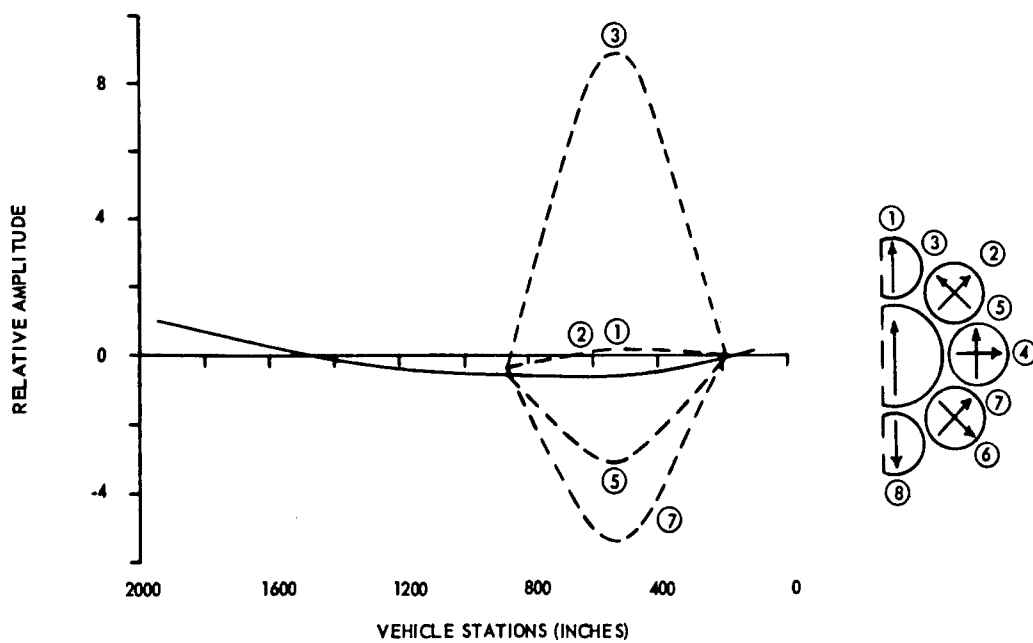


Fig. 9 - Cluster beam analysis - fourth cluster mode
(flight time - 35 seconds; frequency - 3.96 cps)

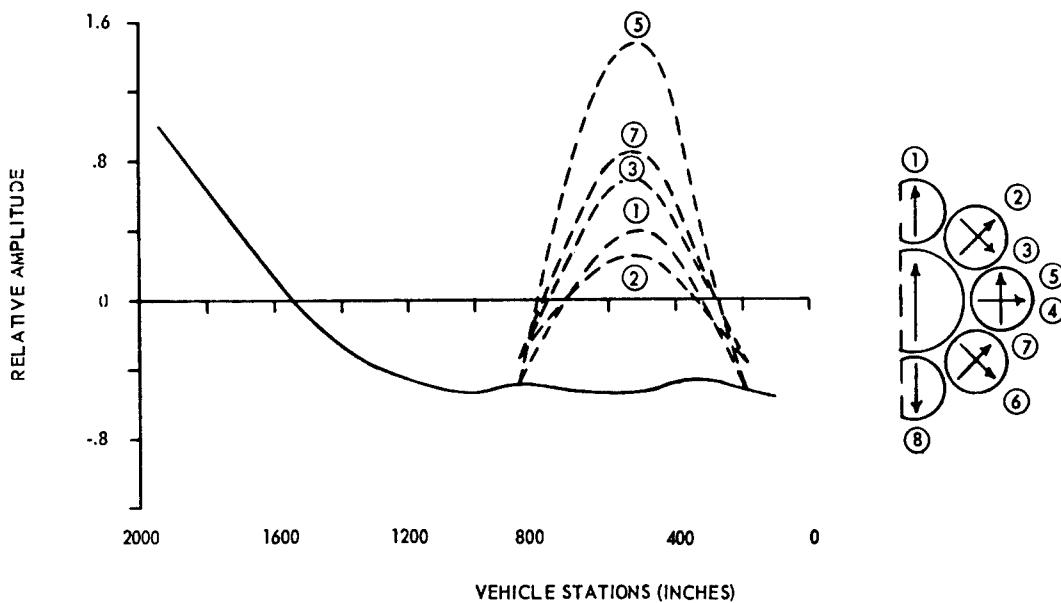


Fig. 10 - Cluster beam analysis - fifth cluster mode
(flight time - 35 seconds; frequency - 4.92 cps)

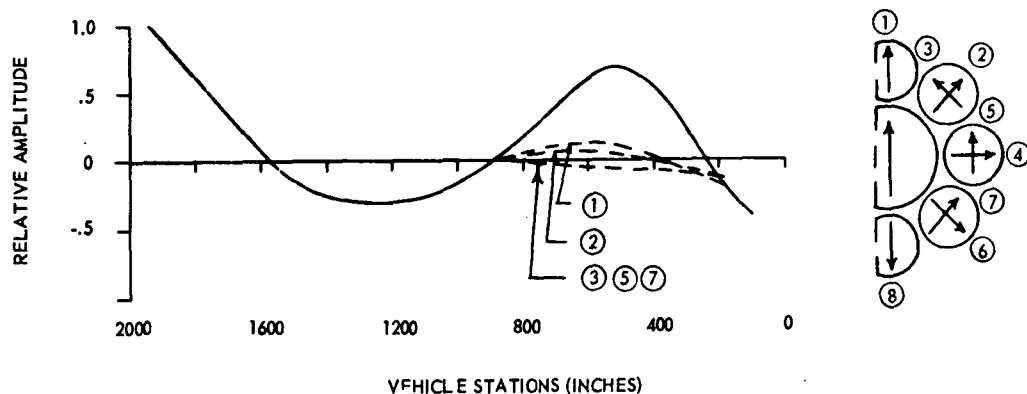


Fig. 11 - Cluster beam analysis - second bending mode
(flight time - 35 seconds; frequency 6.55 cps)

effect was probably on the damping factors determined and is of no great importance to the comparison in this paper.

The tests gave a frequency trend as shown by Fig. 12. Since good comparison exists

between the frequencies (Fig. 13) and the mode shapes for the analytical studies and the test, the test results are used as a comparison in this paper. Some of the mode shapes from the test are given in Figs. 16 through 20 for the comparison to flight evaluation values.

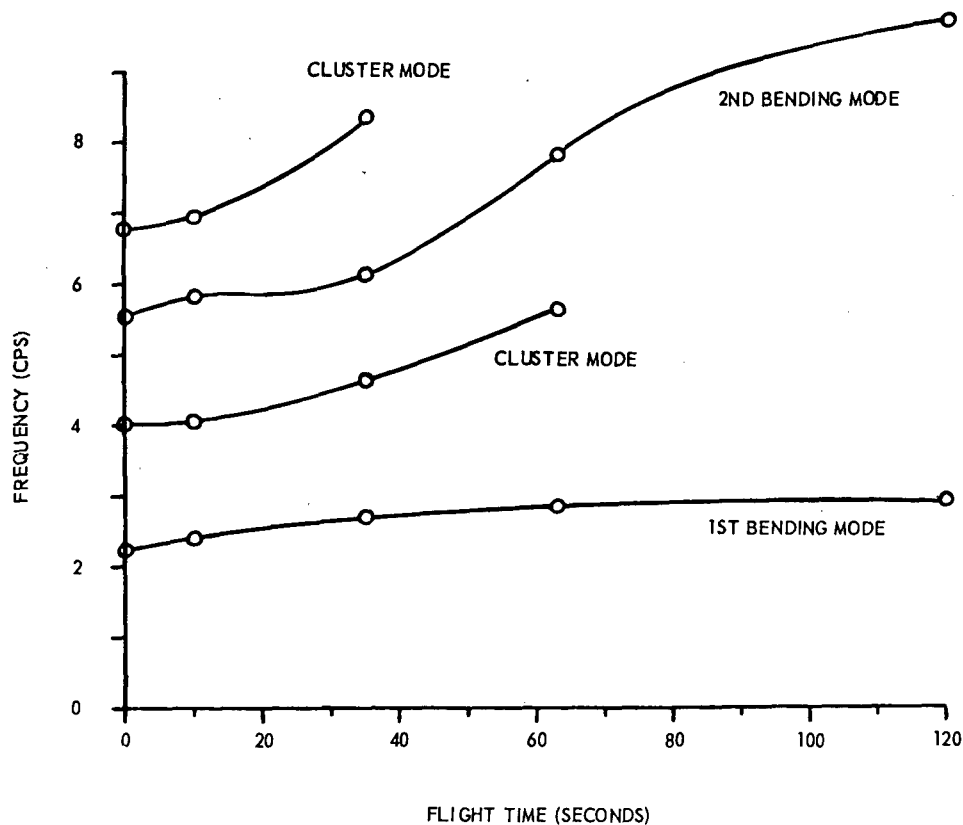


Fig. 12 - Ground vibration test - frequency trend

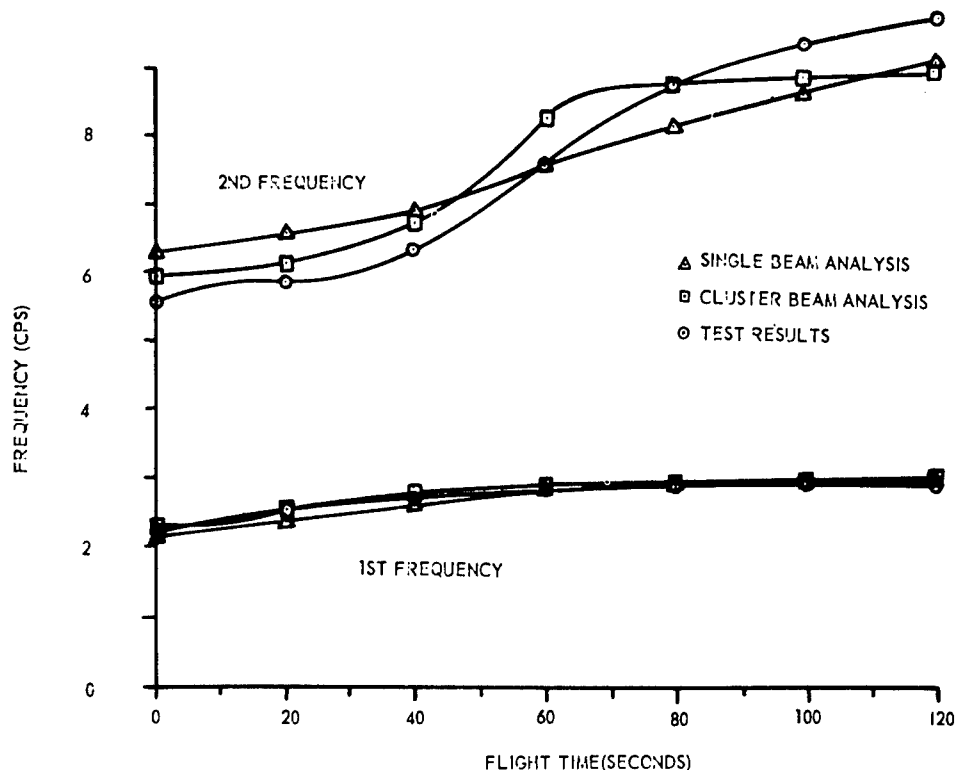


Fig. 13 - Comparison of frequency trends

FLIGHT EVALUATION

Background

A detail flight evaluation of the bending mode accelerometers has been conducted on three Saturn I research vehicles. The data was obtained from low frequency accelerometers which were monitored throughout the powered flight.

The instrumentation for the detection of vehicle bending modes represents a minimum effort in obtaining any information except bending mode frequencies.

The determination of the bending frequency trends of a vehicle can possibly be accomplished with a single accelerometer, although a pitch and a yaw accelerometer would be preferred. If, in addition, torsional frequencies are to be determined, it is necessary to add one more accelerometer in either the pitch or yaw direction. Now by the addition of one more accelerometer, in the longitudinal direction, the vehicle frequencies could be determined for bending in the pitch and yaw plane, for torsion about the longitudinal axis, and for the longitudinal direction. This would be a minimum instrumentation

effort to determine all the frequency trends of the vehicle and probably not very desirable.

The determination of a mode shape associated with a frequency is much more difficult. The determination of a mode shape from a flight test is far beyond the scope of this paper, but identifying a mode by comparison with results of calculations or a ground vibration test is the present effort in flight test evaluation. To accomplish a comparison, it is desirable to have accelerometers at each end of the vehicle and one at each antinode of the mode to be compared. For example, in order to make a comparison to first mode, three accelerometers in the plane of the modal deflections would be required.

Consequently, the instrumentation shown in Fig. 14 for the typical Saturn I flights represent a minimum of instrumentation for a comparison with known first mode shapes and possible comparison with second mode shapes.

Once data is obtained from flight instrumentation, the problems of data reduction and analysis begin. The desired results of bending mode accelerometers are the frequency and amplitude of the response, and the phase relation between the frequency components measured. The problems arise in the separation of

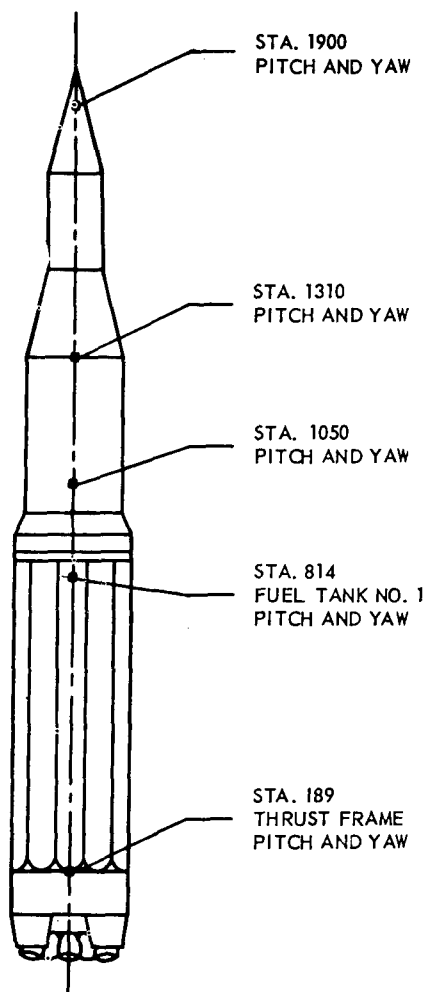


Fig. 14 - Typical instrumentation - bending mode accelerometer locations

this complex signal into the individual frequency responses. A correlation program (using correlation functions to determine power spectral density) to accomplish this separation has been compiled, and is outlined in this section. As stated in the outline of the program, some improvement and refinement are still needed, but the results are satisfactory within certain limitations. The most serious limitations are not inherent in the program, but are in the limited length of data for analysis. Because of the constant change in the flight vehicle weight, the effect of damping, and the continuous input forces on the vehicle, the span of time for a consistent piece of data is short. The length of the data analyzed determines the fundamental frequency, and therefore the resolution of the desired frequency.

With these limitations on the instrumentation and data reduction, the bending mode accelerometer data was evaluated and the typical results for the three flights are presented in this paper in summary form.

Procedure

In order to begin the evaluation, the oscillograph records from each measurement are studied. These records may indicate the presence of trends, and the predominate amplitudes and frequencies. The records of these particular flights were usually covered with high frequency response of 40 cps and up.

From these records time slices are selected for analysis by the digital correlation program. The time slices are usually from 2 to 5 seconds in length, depending upon the length of data considered constant in frequency and amplitude. Several different time intervals may be selected in order to better understand the content and change in the time period of interest. The time slices are selected at times of maximum amplitude, visible low frequency content, or known response times, such as engine gimbaling. Other time slices are selected and analyzed in order to complete frequency versus flight time trends.

The correlation program is used to obtain an amplitude versus frequency spectrum for each measurement. This spectrum shows predominant frequencies present and the amplitude of response at these frequencies. The cross correlation of any two measurements provides the phase relation of these predominant frequencies.

With the frequency, amplitude, and phase relation of the bending accelerometers determined, the mode of response is defined sufficiently for comparison with analytical and test modes.

Correlation Program

There are several approaches to the problem of separation of components of complex signals. The details of any approach may vary depending on the desired end results and experience of processing the particular data of interest. Because of the necessity of a concentrated effort to assure that a working digital vibration analysis program was in operation for the SA-2 flight, the correlation function for obtaining power spectral relations was quickly

selected and the use of the method for other applications was not considered.

The choice of this approach appears to have been a good one, since no better method has been found to obtain comparable results on this type of data. The program now prints a format of amplitude and phase relation for the predominant frequencies in two or more records.

Auto Correlation Function — The auto correlation function can be expressed as the autocovariance, $R(\tau)$, normalized by the autocovariance at lag zero, $R(0)$. Then the auto correlation function is

$$\Psi_{11}(\tau) = \frac{R_{11}(\tau)}{R_{11}(0)},$$

where

$$R_{11}(\tau) = \lim_{T \rightarrow \infty} \frac{1}{2T} \int_{-T}^T f_1(t) f_1(t+\tau) dt,$$

It should be noted that this expression for autocovariance is sometimes called the auto correlation function.

This expression is for the case where the function is a continuous stationary random process $f_1(t)$, and it shows that the auto correlation function $\Psi_{11}(\tau)$ of the function $f_1(t)$ is given by the product $f_1(t) f_1(t+\tau)$ averaged with respect to time. The auto correlation function depends on the interval of time as well as on the function.

Consider the physical meaning of the concept of the auto correlation function. Select a particular random continuously variable quantity $f(t)$. If at the time t the value of $f(t)$ is large, then the probability is small that at the instant $(t+\tau)$, where τ is small, the value of $f(t+\tau)$ will be very small. But if a larger time span is taken for τ then the value of $f(t+\tau)$ may have any value. These values of $f(t)$ and $f(t+\tau)$ may, therefore, be considered as independent random quantities. The behavior of a random function is characterized by the mutual relation between the values of $f(t)$ at t and $t+\tau$ as well as its value at every time t . A measure of the relation between the values of $f(t)$ and $f(t+\tau)$ is the auto correlation function.

The auto correlation function completely defines the Gaussian process. If the signal is random and has no periodic components, then the auto correlation function tends to zero with increasing τ , since the two functions $f_1(t)$ and

$f_1(t+\tau)$ become independent. How fast the function approaches zero is a measure of the randomness of the function. When periodic components are present with no random component, then the auto correlation function is composed of the sum of the individual components. For example, the auto correlation function of a single frequency is a function with a single frequency.

If the signal contains both random and periodic components, then the auto correlation function is a combination of the random function tending to zero and the periodic function. Some properties of the auto correlation function can be seen by considering the autocovariance.

1. The autocovariance at lag zero is the mean value of the function squared or

$$R(0) = f(t)^2 = (\text{S.D.})^2,$$

where S.D. = standard deviation;

2. $R(\tau)$ is an even function or,

$$R(\tau) = R(-\tau);$$

3. Also,

$$R(0) \geq R(\tau).$$

Of course, the real value of the auto correlation function in this program is its use for the generation of the power spectral density function.

Power Spectral Density — The power spectral density (PSD) is obtained by transforming the auto correlation function from a time domain to a frequency domain by means of the Fourier integral

$$\Phi(\omega) = \int_{-\infty}^{\infty} \Psi_{11}(\tau) e^{-i\omega\tau} d\tau,$$

where

$$e^{-i\omega\tau} = \cos \omega\tau - i \sin \omega\tau.$$

Since $\Psi(\tau)$ is an even function,

$$\Phi(\omega) = \text{PSD}_N = \int_{-\infty}^{\infty} \Psi(\tau) \cos \omega\tau d\tau.$$

For periodic signals, the frequencies of the peak values of the PSD represent the frequency content of the input signal. The value of the PSD is normalized by the standard deviation squared, since the auto correlation function was used to compute PSD. The amplitude of

the component at the peak frequencies is determined from the PSD by

$$A_{mp} = \text{S.D.} \sqrt{2\text{PSD}_n}.$$

If the frequency of the signal falls between adjacent resolution bands, splitting of the power between the bandwidths will occur and will give erroneous values of the amplitudes. Since the frequency resolution is completely determined by the length of the data to be analyzed, the splitting can be minimized by increasing or decreasing the length of the data sample. The frequency and amplitude of the periodic components can now be determined from the auto correlation function and auto power spectrum. The cross power must be used to obtain phase relation.

Cross Correlation Function—The cross correlation function is defined as the correlation of two functions in the same way the auto correlation was defined for a single function. The cross correlation function is

$$\Psi_{12}(\tau) = \frac{R_{12}(\tau)}{R_{12}(0)},$$

where

$$R_{12}(\tau) = \lim_{T \rightarrow \infty} \frac{1}{2T} \int_{-T}^T f_1(t) f_2(t+\tau) dt.$$

The important use of the cross correlation function here is in the generation of the cross power spectrum. It should be noted, however, that this is not an even function and will contain the phase relationship.

Cross Power Spectral Density—The cross power spectral density is obtained from the cross correlation function by

$$\Phi_{12}(w) = \int_{-\infty}^{\infty} \Psi_{12}(\tau) e^{-i w \tau} d\tau.$$

This expression may be transformed to

$$\begin{aligned} \Phi_{12}(w) = & 2 \int_0^{\infty} [\Psi_{12}(\tau) + \Psi_{21}(\tau)] \cos w \tau d\tau \\ & + 2i \int_0^{\infty} [\Psi_{12}(\tau) - \Psi_{21}(\tau)] \sin w \tau d\tau, \end{aligned}$$

where the first term is called the cospectrum, C_o , or

$$C_o = 2 \int_0^{\infty} [\Psi_{12}(\tau) + \Psi_{21}(\tau)] \cos w \tau d\tau,$$

and the second term is called the quadrature, Q_i , or

$$Q_i = 2 \int_0^{\infty} [\Psi_{12}(\tau) - \Psi_{21}(\tau)] \sin w \tau d\tau.$$

The importance of the cross power in bending mode analysis is in the real and imaginary parts of the cross power.

Since $\Phi_{12} = C_o + i Q_i$, the phase relation, θ , between the two signals is given by

$$\tan \theta = \frac{Q_i}{C_o}.$$

The frequency and amplitude of the periodic components of a single measurement can now be determined from the auto correlation function, and the phase relation between two or more measurements can now be determined from the real and imaginary parts of the cross power spectrum.

Results and Comparison

Typical instrumentation to detect the vehicle bending frequencies and deflections consisted of five pitch and five yaw accelerometers located at stations 189, 1050, 1310, 1900, and 814 (fuel tank #1) as shown in Fig. 14. The measuring range of these low frequency accelerometers (natural frequency of 18 cps) was ± 0.5 g.

The typical oscillograph trace appears to be more of an indication of the high frequency environment than low frequency bending. The trace has strong response in the 40-cps range with greater response during the noisy times of lift-off, Max q, inboard engine cutoff, and outboard engine cutoff. Much of the higher frequency response is local structure vibration picked up at the lower limit of the accelerometers. Frequencies in the range of first and second vehicle bending were not usually detected on the oscillograph trace because their response amplitude was small and higher frequencies with higher g-level response are predominate. The detection of the correct frequency, phasing, and amplitudes would be impossible without the correlation program.

The flight evaluation results were compared to the ground vibration test results.

This comparison is made since test results have been accepted and the analytical studies compare favorably (Fig. 13).

The frequency trend of the first mode follows the test results throughout flight time. The frequency range is approximately 2.2 cps at lift-off to about 3.0 cps at cutoff as shown in Fig. 15. The trend is substantiated by the mode shapes at several time points throughout the flight. Frequencies in the range of second mode also follow the test results (Fig. 15) but cannot be substantiated with mode shapes due to the low amplitude of response.

Some low amplitude responses were detected in the frequency range of the control system (0.25 to 0.50 cps), propellant slosh (1.25 to 1.50 cps), and local structural mountings.

Typical comparisons to the SA-D1 mode shape and frequencies are given in Figs. 16 through 20 and are summarized as follows:

Fig. 16. At the flight time of lift-off, a single amplitude (S.A.) response of 0.03 g occurred on the nose at 2.2 cps as compared to SA-D1 frequency of 2.19 cps.

Fig. 17. At the flight time of 35 seconds, a frequency of 2.66 cps occurred compared to 2.63 cps for SA-D1.

Fig. 18. At the flight of 63 seconds, a frequency of 2.8 cps was determined as compared to 2.89 cps for SA-D1.

Fig. 19. At the flight time of 119 seconds (empty), a single amplitude response of 0.045 g occurred on the nose at a frequency of 2.9 cps as compared to the SA-D1 frequency of 3.04 cps.

Fig. 20. At the 119-second flight time, a second bending mode comparison was obtained at a frequency of 9.4 cps.

One example may illustrate the usefulness of these accelerometers in determining not only

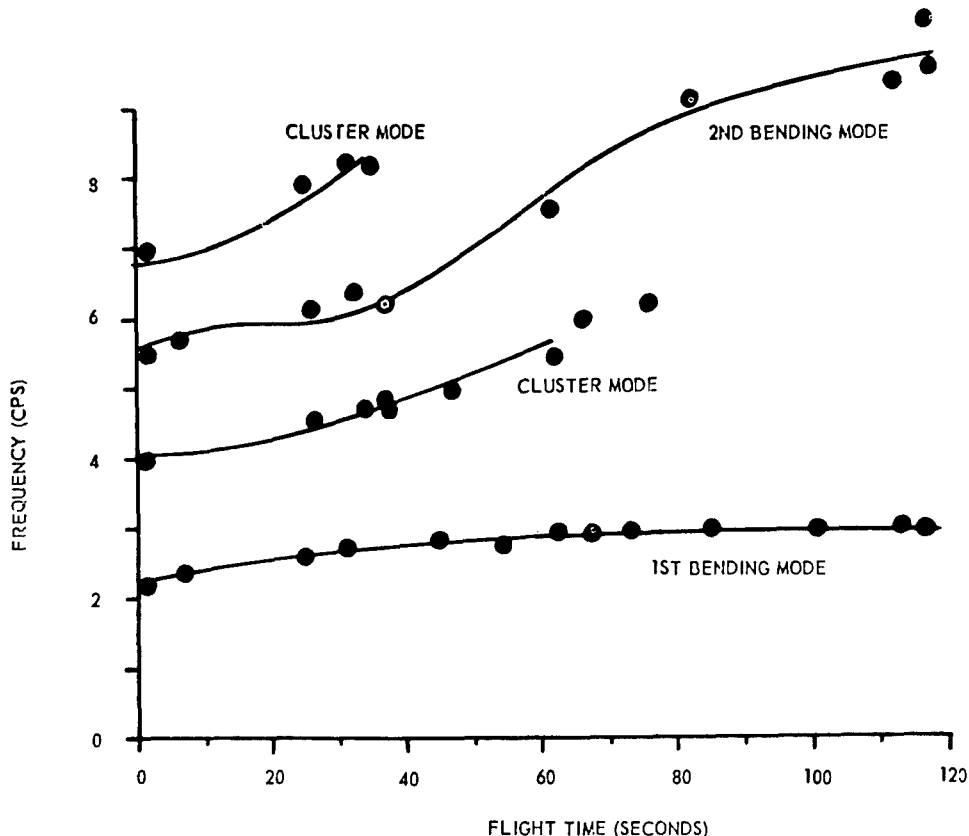


Fig. 15 - Flight evaluation - frequency trend; test results vs flight evaluation

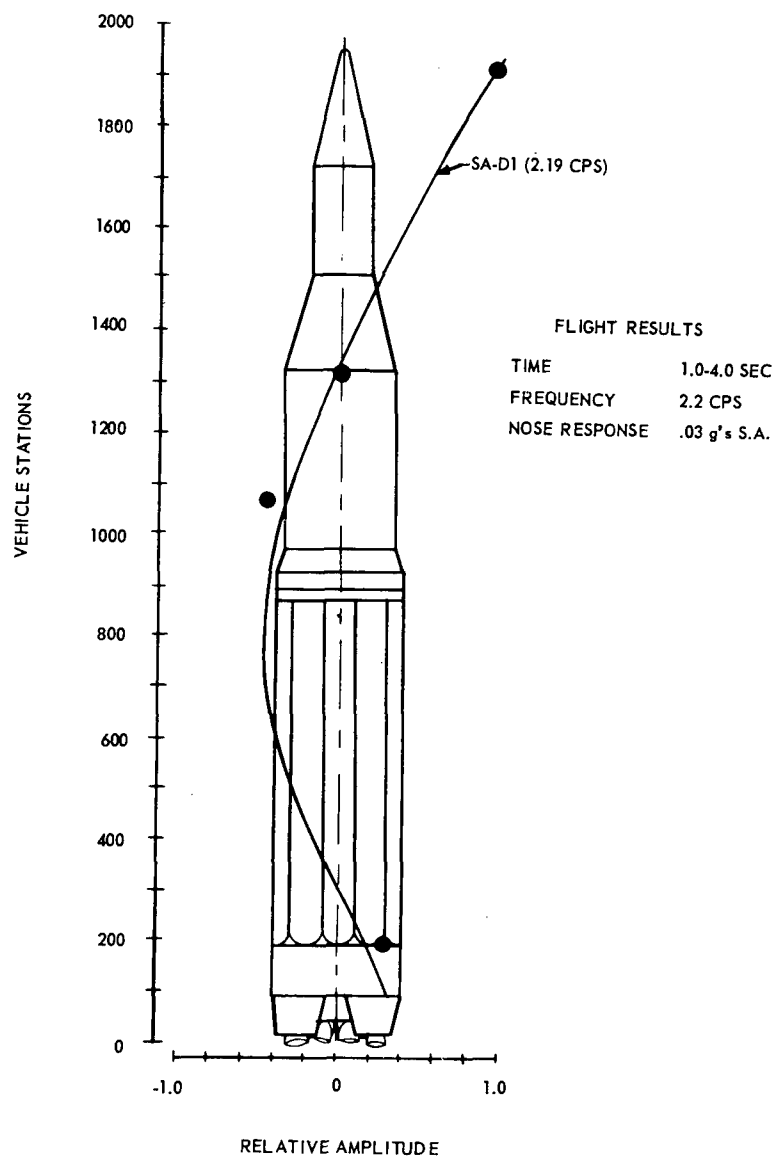


Fig. 16 - Flight evaluation - lift off

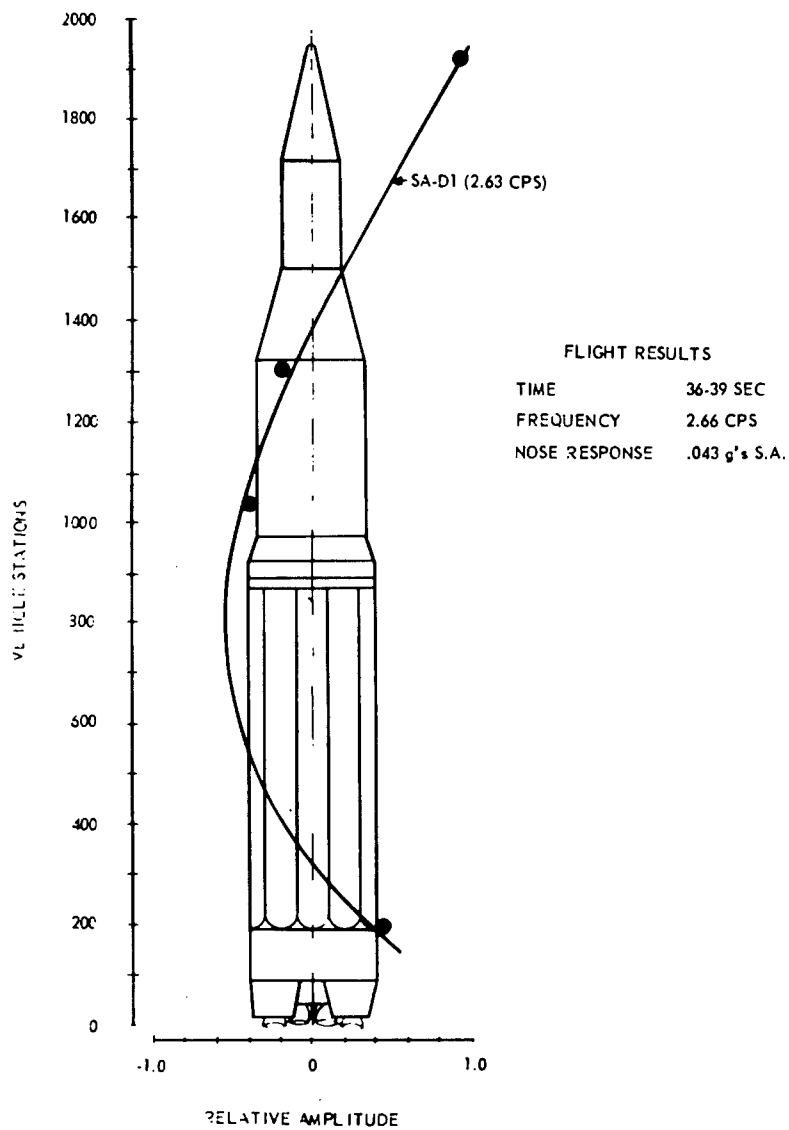


Fig. 17 - Flight evaluation - 35 seconds

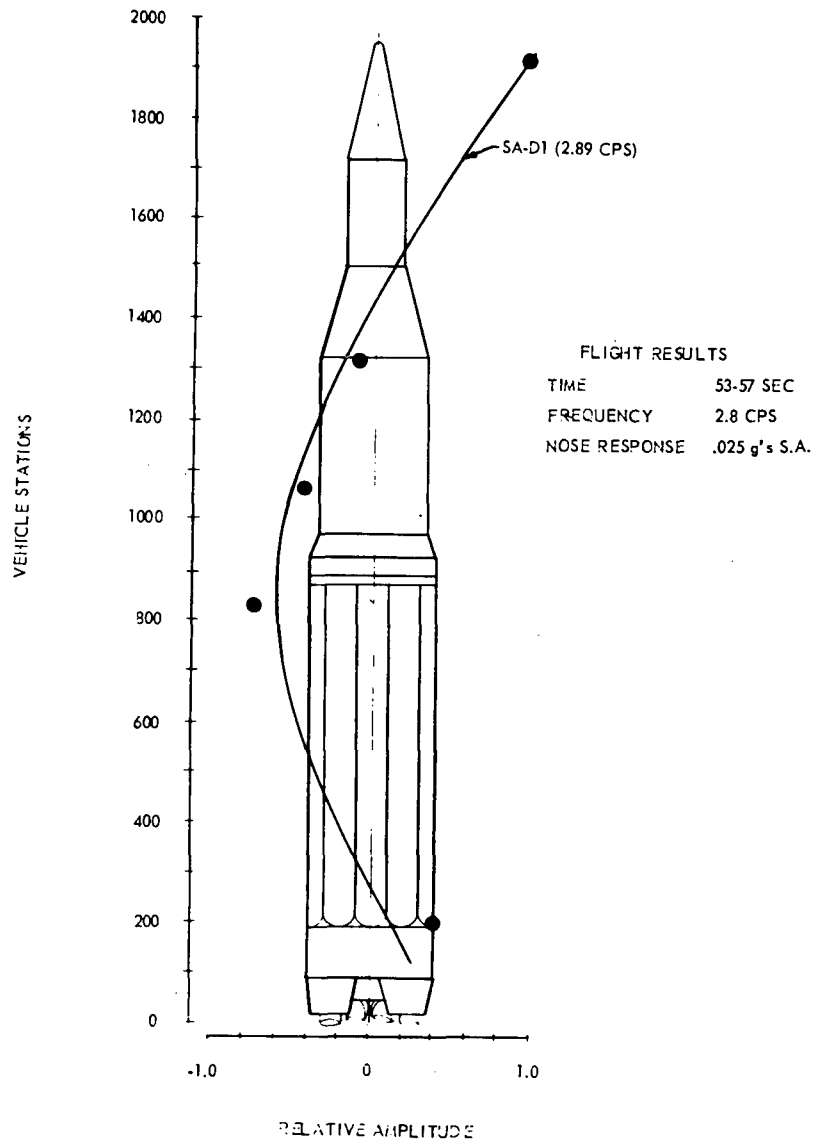


Fig. 18 - Flight evaluation - 63 seconds

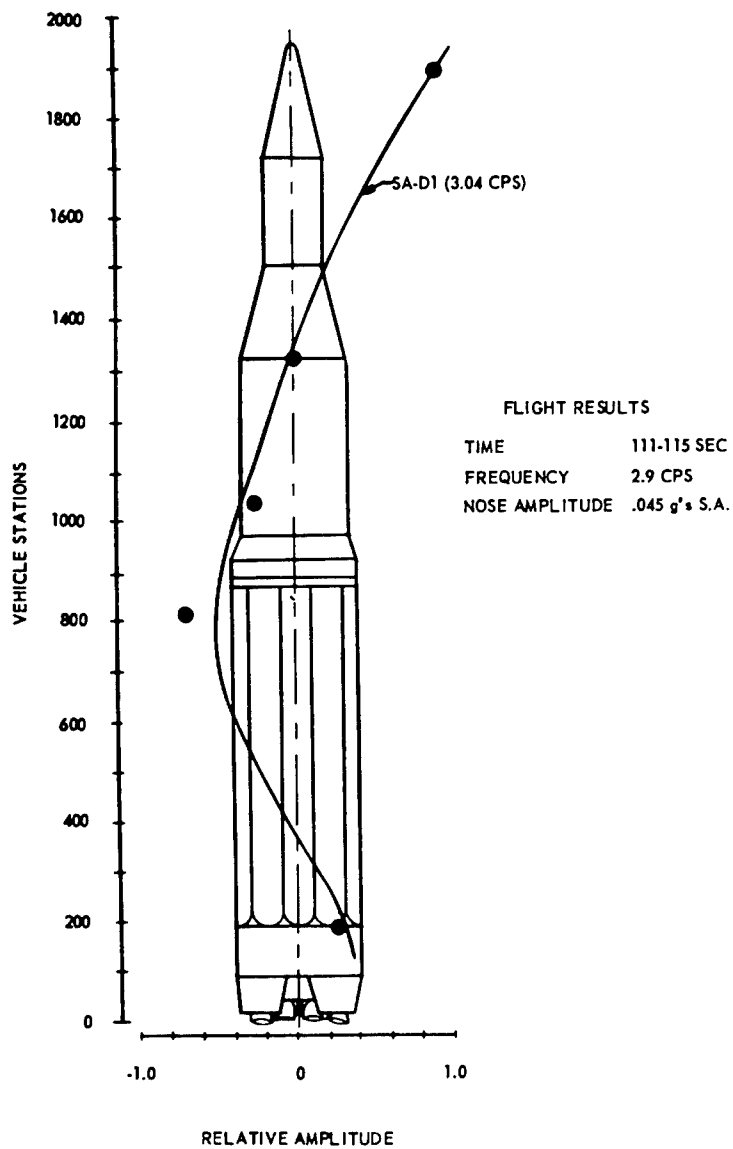


Fig. 19 - Flight evaluation - empty
(frequency - 2.9 cps)

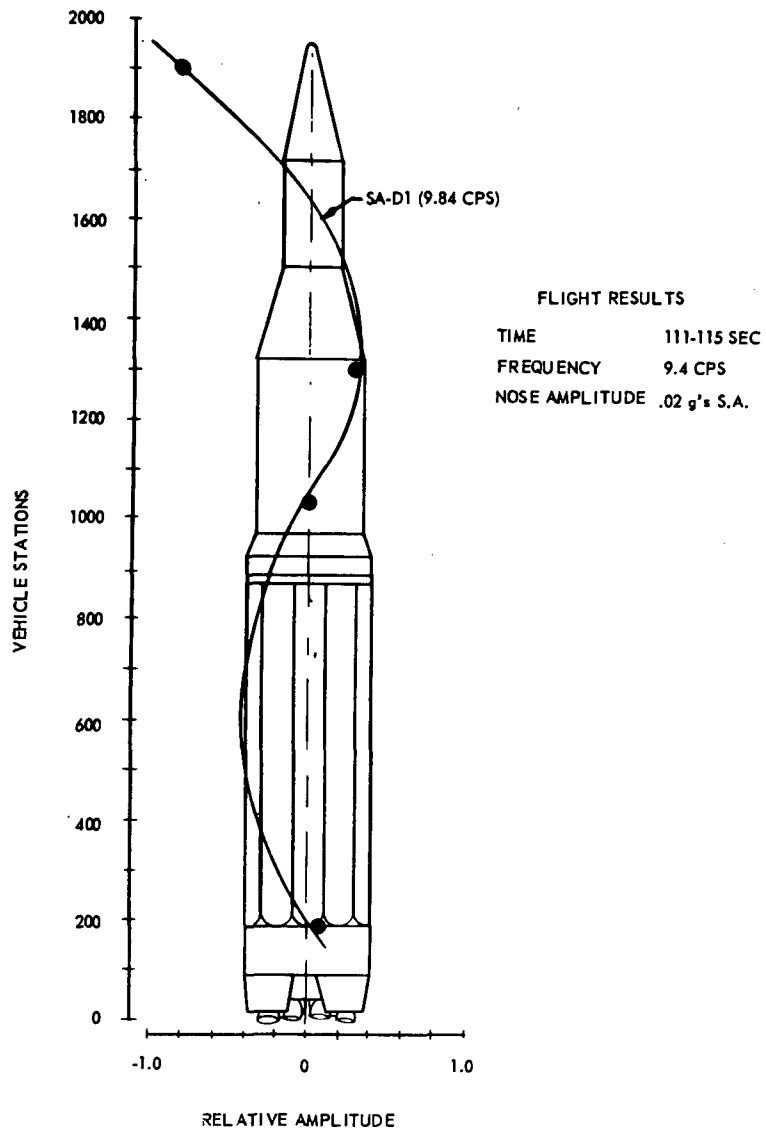


Fig. 20 - Flight evaluation - empty (frequency - 9.4 cps)

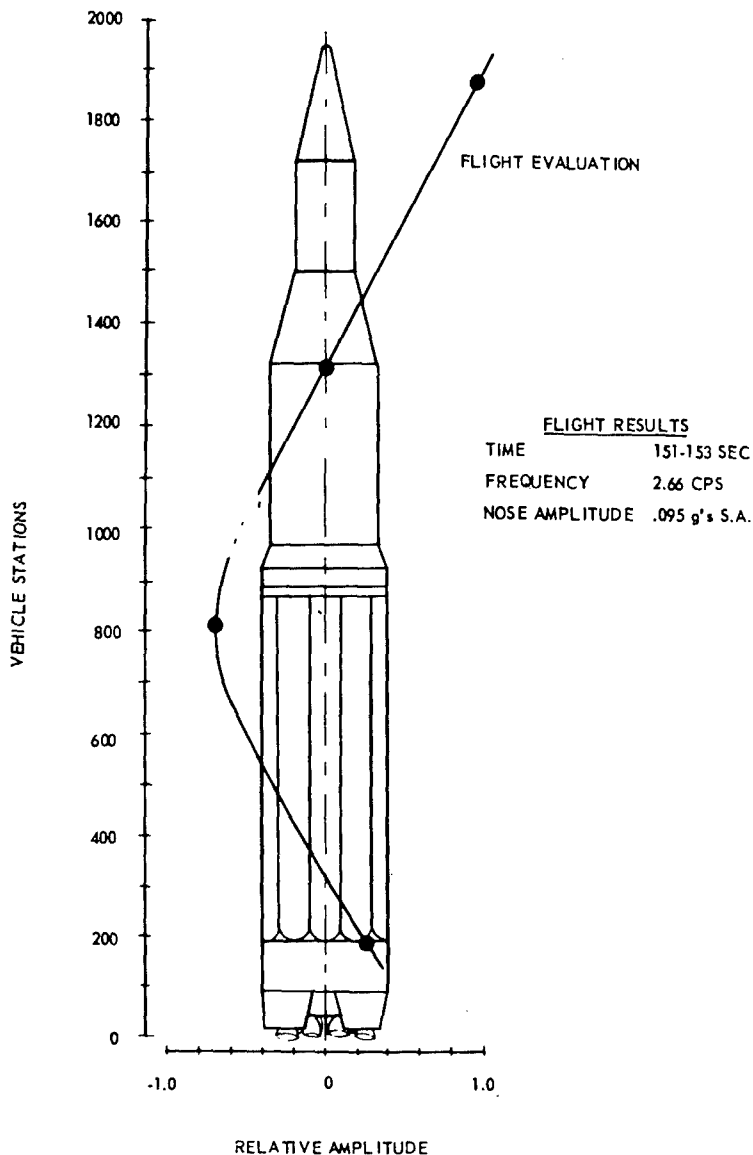


Fig. 21 - Flight evaluation - 151 seconds

structural response but also finding the cause of the response. On one of the early flights there were indications from several types of instrumentation that a large amplitude response occurred immediately after engine cutoff and that it had increased in amplitude before decay occurred. An evaluation produced a mode shape of first bending and a frequency of 2.66 cps (Fig. 21). This frequency is lower than the 3.0 cps first bending mode at cutoff. This response was determined to be due to the engine

gimballing at 2.66 cps with low thrust and the inertia of the engine mass being the driving force.

The accelerometer data and the engine gimbal angle data was used to determine the following: (1) the gimbal angle showed the same frequency (2.66 cps) and did not decay like the accelerometers but showed a step decrease, and (2) the phase relation between the engine angle and the vehicle bending was the proper

relation for inertia forcing. The engine thrust decay curves and the pressure drop in the engine actuators substantiate this result.

The flight evaluation has been satisfactory considering the low level of response. The

instrumentation is considered worthwhile on normal flights and could be important on flights somewhat less than normal.

* * *

CORRELATION BETWEEN MEASURED AND PREDICTED TRANSIENT RESPONSE OF THE TALOS AIRFRAME (IN SHIPBOARD STOWAGE) WHEN SUBJECTED TO A NEARBY UNDERWATER EXPLOSION*

R. G. Alderson
The Bendix Corporation
Mishawaka, Indiana

This paper discusses the development of a mathematical model of the Talos airframe as stowed aboard an ammunition supply ship, the predicted shock response, the experimental test methods and data, and the correlation between predicted and measured shock response.

INTRODUCTION

In a complex engineering study, utilization of analytical methods as an adjunct to experiment is of proven value. Analysis based upon valid techniques not only permits enlightened interpretation of experimental data, but provides a rational basis for interpolation and extrapolation of the data. Analytical extension of data is often essential since the complexity of today's problems frequently does not permit exhaustive experimental work without prohibitive cost. But the validity of a predictive method must be assessed before it can be applied with confidence. The primary objective of this paper is to describe such an assessment as it was conducted by Bendix.

Susceptibility of the Talos 6cl airframe in stowage to damage induced by a nearby underwater explosion is of considerable interest to Bendix and the Navy. A Bureau of Naval Weapons contract, in part, authorized Bendix to develop a mathematical model (simulation) of the missile as stowed aboard an ammunition supply ship (AOE) and to correlate shock responses predicted using this simulation with experimental data.¹ The mathematical model was then used to predict bending moments experienced by Talos during tests in which the missile, in a

simulated stowage configuration, was subjected to nearby underwater explosions. This paper describes the tests from which experimental response data was obtained, and the mathematical simulation used for response predictions. The validity of the simulation is assessed through comparison of measured and predicted responses. Correction of bending moment predictions is discussed in light of this comparison.

SUPPORT CONFIGURATION

In stowage aboard the ammunition supply ship, Talos is supported by a pair of handling bands located forward and aft at structural hard points. A semi-circular steel band forms the upper half of the handling band, while the lower half, supporting the missile weight, consists of several rubber-enclosed, chain-like strands. Two shoes protrude from each of the handling bands, and these shoes are hard mounted to four vertical chocks bolted to the deck. Figures 1 and 2 show two views of a laboratory simulation of the missile mounting configuration. Although only one missile is shown in these figures, missiles may be stowed two high aboard ship. Figure 3 shows the four vertical chocks with the missile removed.

*The study described in this paper was performed under Bureau of Naval Weapons contract, NOW 63-0193.

¹This effort is described in Bendix Mishawaka Division Report No. 5687, "Damage Susceptibility of the TALOS 6cl Airframe (in AOE Stowage) Exposed to Nearby Underwater Explosion--Final Analysis Report."



Fig. 1 - Talos 6cl in simulated AOE stowage configuration, side view

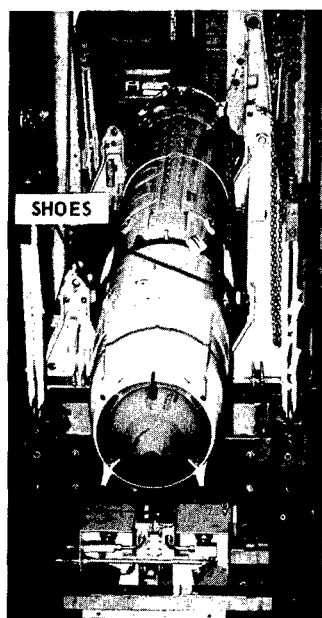


Fig. 2 - Talos 6cl in simulated AOE stowage configuration, front view

DESCRIPTION OF TESTS

A series of underwater explosion tests was performed at the San Francisco Naval Shipyard, in which the missile was mounted aboard a floating platform in a simulated AOE mounting configuration. A one high configuration as shown in the previous figures was used. Although the AOE ship's structure was not simulated, the missile support hardware was quite similar to the anticipated AOE shipboard equipment. The tests consisted of a series of underwater detonations in the vicinity of the floating platform.

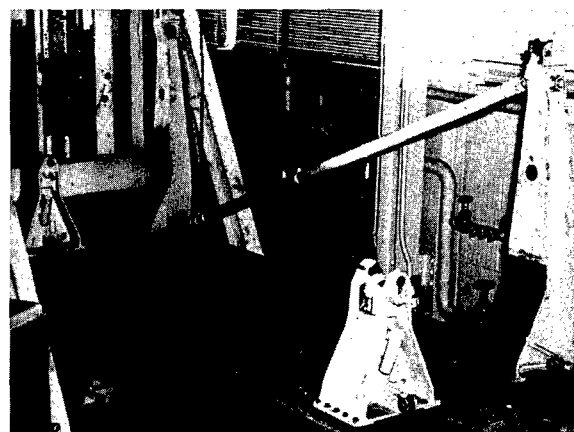


Fig. 3 - Missile support chocks for AOE stowage

Figure 4 shows the platform during one of the tests. Input and response vs time data were obtained for each test from accelerometers mounted throughout the airframe and support structure. Strain gages were also used to monitor deformations in an area thought to be critical from the standpoint of structural integrity. Sensing instrument outputs were amplified and fed to tape recording equipment on shore via cabling.

MATHEMATICAL SIMULATION

A mathematical simulation was desired which would permit predictions of airframe transient response to any arbitrary excitation. This simulation was to find immediate application in the calculation of airframe bending moments experienced during the tests.

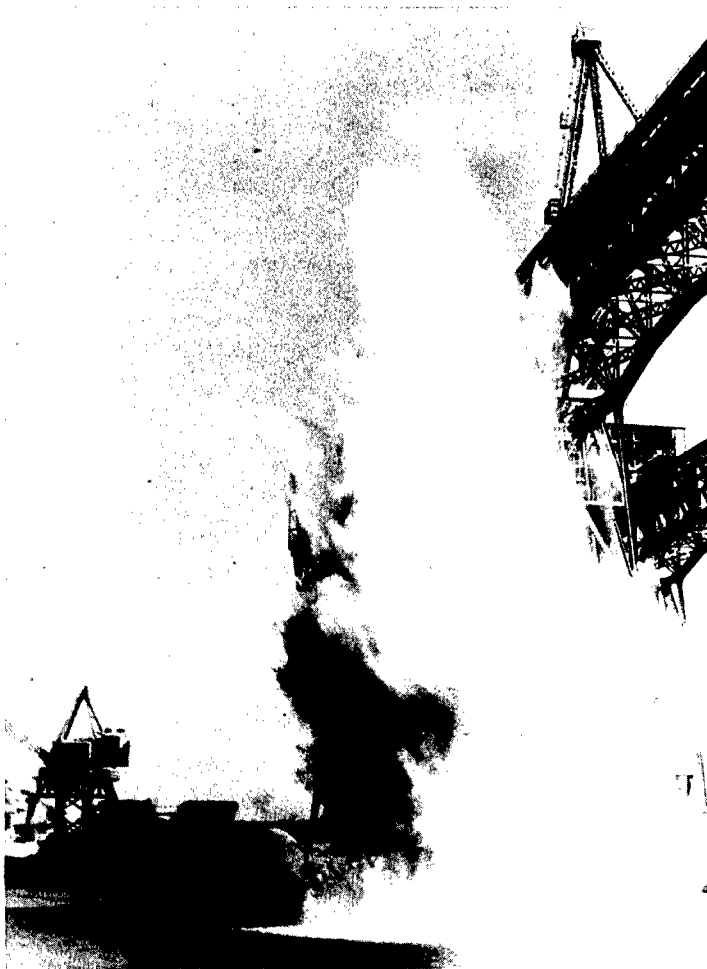


Fig. 4 - Talos 6cl underwater explosion tests, view of floating platform during test

A normal mode analysis was used to predict airframe response to acceleration inputs at the support points. This approach determines the net response by superposition of the airframe response in each of the significant bending modes. The airframe was idealized as a nonuniform, undamped beam, simply supported at the handling points; equations of motion, describing airframe bending in each mode, were derived utilizing the Principle of Virtual Work. Details of this derivation are presented in the appendix. Digital computer solution of the equations of motion was accomplished using the Runge-Kutta numerical integration technique. Solution of the equations of motion yielded predicted deflection and acceleration time histories. Using the predicted accelerations, bending moments were computed at various points on the airframe. These bending moments were derived through consideration of the inertial loading on the

airframe. Moments due to reaction forces at the supports were considered where applicable.

The simulation is capable of utilizing any available support point acceleration data. Acceleration inputs can be accepted either as an analytical function of time or as a set of discrete points giving accelerations at various times. The latter method, used extensively in the investigation, is particularly useful if the input acceleration is an irregular waveform as is encountered frequently in experimental data. The acceleration inputs at the forward and aft supports are treated as separate functions of time which need not be identical.

CORRELATION STUDY

A correlation study was conducted to assess the validity of responses predicted using the

mathematical model. Using measured accelerations at the support points as inputs to the mathematical model, airframe acceleration vs time was predicted and compared with corresponding measured response data.

The input data was obtained from vertical and lateral accelerometers located on the airframe at the support points. Accelerations of the chocks or the deck could not be used as input data since the dynamic characteristics of the support system, although presently under investigation, were not well understood at the time that the analysis was conducted. The input accelerations, having been recorded on tape, were played through a 200 cps low pass filter so that high frequency traces, representing either mechanical or electrical noise, would be eliminated. The "mechanical noise," not likely to threaten airframe structural integrity, arises from such phenomena as looseness throughout the airframe and support structure. The filtered acceleration data was then reproduced on oscillograph records. The acceleration time histories were converted to a digital form using a semi-automatic data reduction device. Acceleration vs time data at 0.001-second intervals over a period of 0.1 second was entered on punched

cards in a format suitable for use as inputs to the digital computer simulation of the system.

Several different calculations were made in which accelerations and bending moments were predicted in either vertical or lateral directions for each of the underwater explosions. Calculations were made using two different versions of the simulation — one in which the first and second bending modes were considered, and one in which the first mode only was considered. The accelerometer location chosen for comparison in all cases was a structural ring 20 inches from the nose of the missile.

In the following discussion of acceleration data, a common normalization factor has been applied to all of the data so that this paper may be kept unclassified. Figures 5 through 8 show the most significant data obtained from the investigation. This data was obtained during a test, denoted "Test A," in which the airframe was on the verge of structural failure. Strain gages indicated that buckling was imminent during this test, but subsequent visual inspection revealed no damage. Evidently the airframe was loaded nearly to its structural limit in this test.

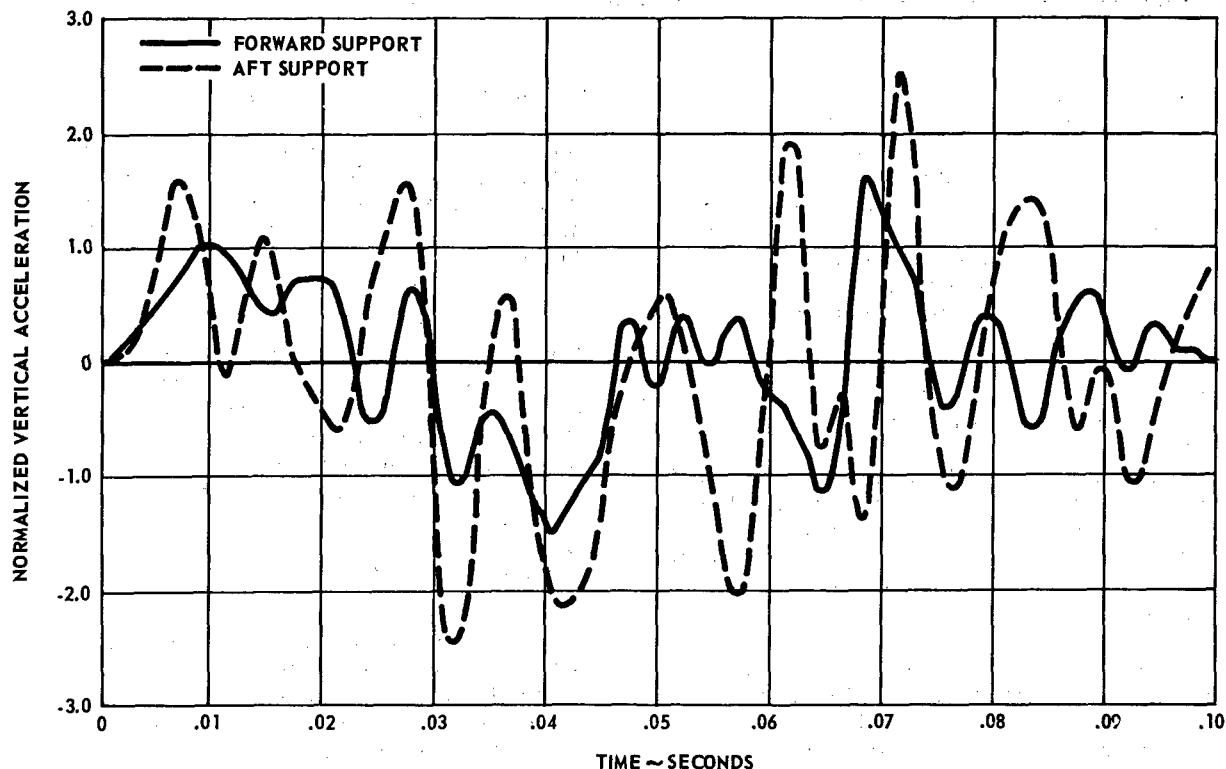


Fig. 5 - Measured vertical acceleration at missile support points. Talos 6cl-SFNS AOE Shock Tests, Test A.

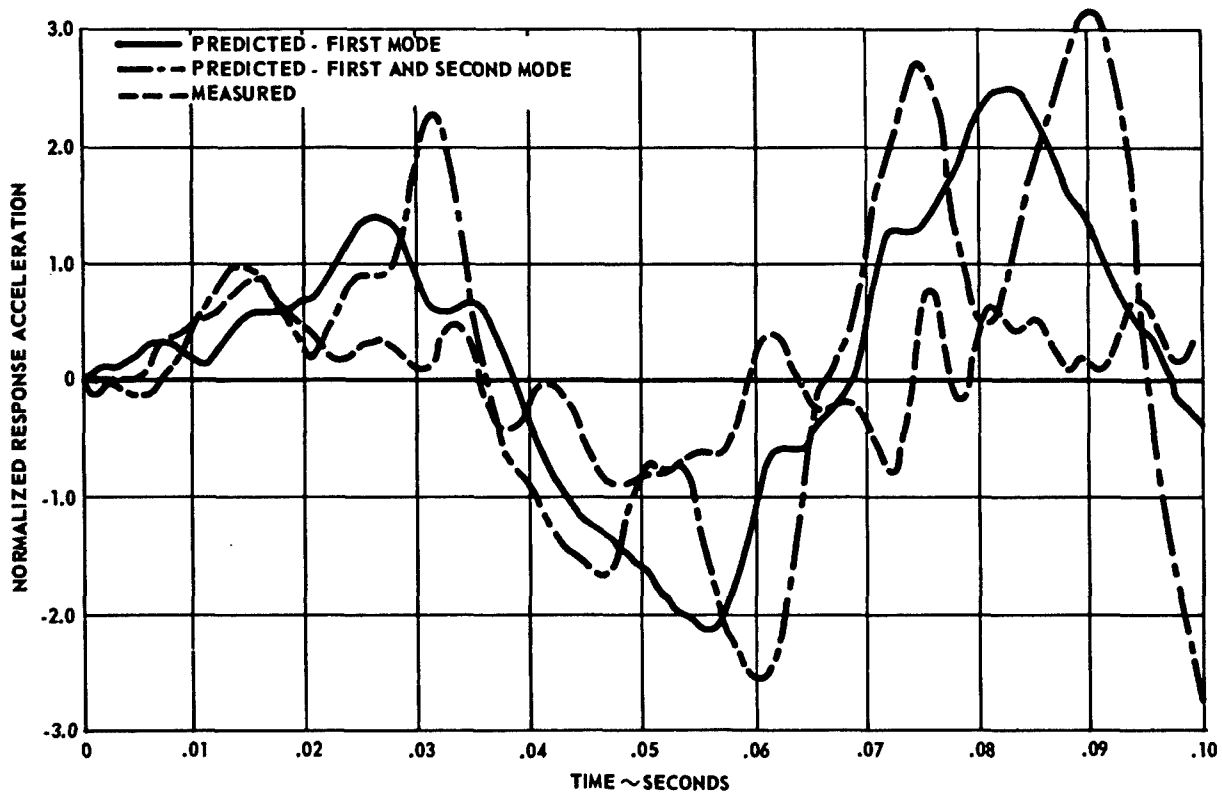


Fig. 6 - Correlation of airframe acceleration. Talos 6c1-SFNS AOE Shock Tests, Test A - vertical acceleration 20 inches from nose.

Figure 5 shows the normalized vertical acceleration inputs experienced in Test A. Figure 6 compares the normalized measured response to these inputs with normalized responses predicted using two different versions of the mathematical model. Predictions were made considering first mode bending alone and also considering both first and second mode bending. Figures 7 and 8 show similar data for Test A in the lateral direction. Reference to Figs. 6 and 8 suggests that except for the first peak, poor correlation exists between experimental data and the corresponding responses predicted by considering both first and second modes. This assertion was confirmed by other test data not presented here. Also, correlation of the data predicted by the first mode only version of the simulation is generally degraded after about 0.05 second, the time at which the first (and most severe) negative peak occurs.

The areas of poor correlation evidently reflect the assumption of negligible damping in the derivation of the mathematical model. As a consequence of this assumption, predicted responses erroneously exhibit large oscillations after a time. This effect is only significant after times comparable to the natural period of

the highest mode under consideration. The conclusion to be drawn is that the best single mathematical representation is the first mode only version of the simulation, since this version should suitably describe the system at the time of maximum acceleration response (about 0.05 second).

Figures 9 through 12 present data from Test B, in which much lower excitation was encountered. Figure 9 shows the normalized vertical input acceleration, while Fig. 10 compares predicted and measured vertical responses. Only predictions based on the first mode only version of the simulation are shown, since this is the preferred version. Corresponding Test B data for lateral inputs is shown in Figs. 11 and 12.

It is of interest to note from the measured input accelerations that the peak values are generally greater at the aft support point than at the forward support point. This is probably due to the mass distribution of the missile which requires that forces applied at the forward support encounter more effective mass than do forces applied aft.

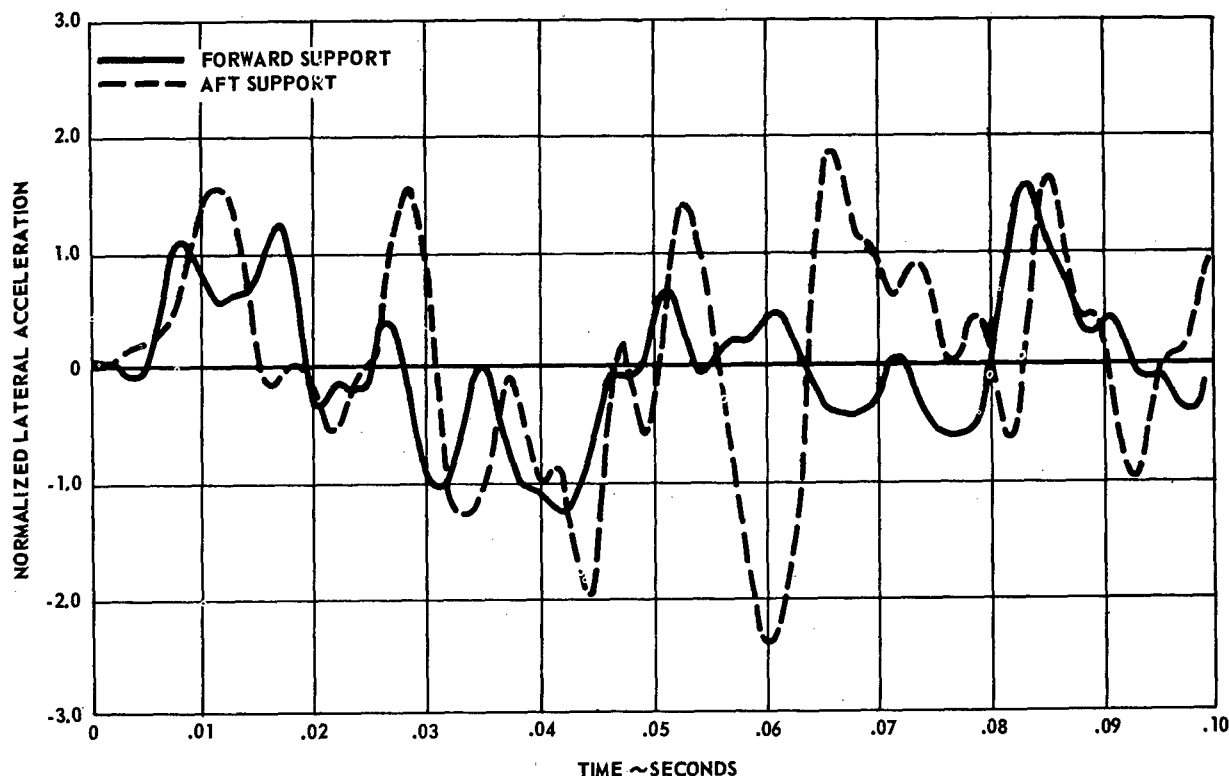


Fig. 7 - Measured lateral acceleration at missile support points.
Talos 6cl-SFNS AOE Shock Tests, Test A.

Although calculations made using the first mode only version of the simulation predict acceleration response vs time histories, which are similar in shape to the measured values, the measured maximum accelerations are generally considerably lower than the predicted values. The measured vertical response from Test A is about 43 percent of the predicted value. Comparison of lateral responses from Test A, as well as both vertical and lateral responses from Test B, reveal that the measured responses are about 68 percent of the predicted values.

Subsequent experimental work has demonstrated that the discrepancy is largely due to the presence of looseness in the missile support structure. Vibration tests have shown that airframe response is actually increased if the handling band shoes are tightly clamped to the support chocks. Since the equations of motion contain the assumption that there is no free play in the supports, the prediction of too-high accelerations is to be expected.

Bending moments induced by inertial loading were computed from predicted acceleration responses. These responses had been obtained using the first mode only version of the simulation. Since the predicted responses were known to be in error, some method of adjusting the predicted maximum bending moments was required. The most obvious adjustment was to diminish the predicted maximum bending moments by a factor obtained from comparison of measured and predicted accelerations. This factor was merely the ratio between maximum predicted and measured accelerations 20 inches from the missile nose.

Some substantiation exists for this admittedly gross bending moment adjustment. Recall that strain measurements from Test A indicate that buckling was imminent. Also, theoretical maximum allowable bending moment data had been obtained previously, using a technique which combined buckling theory and static test results. Comparison of the theoretical maximum allowable bending moments with the

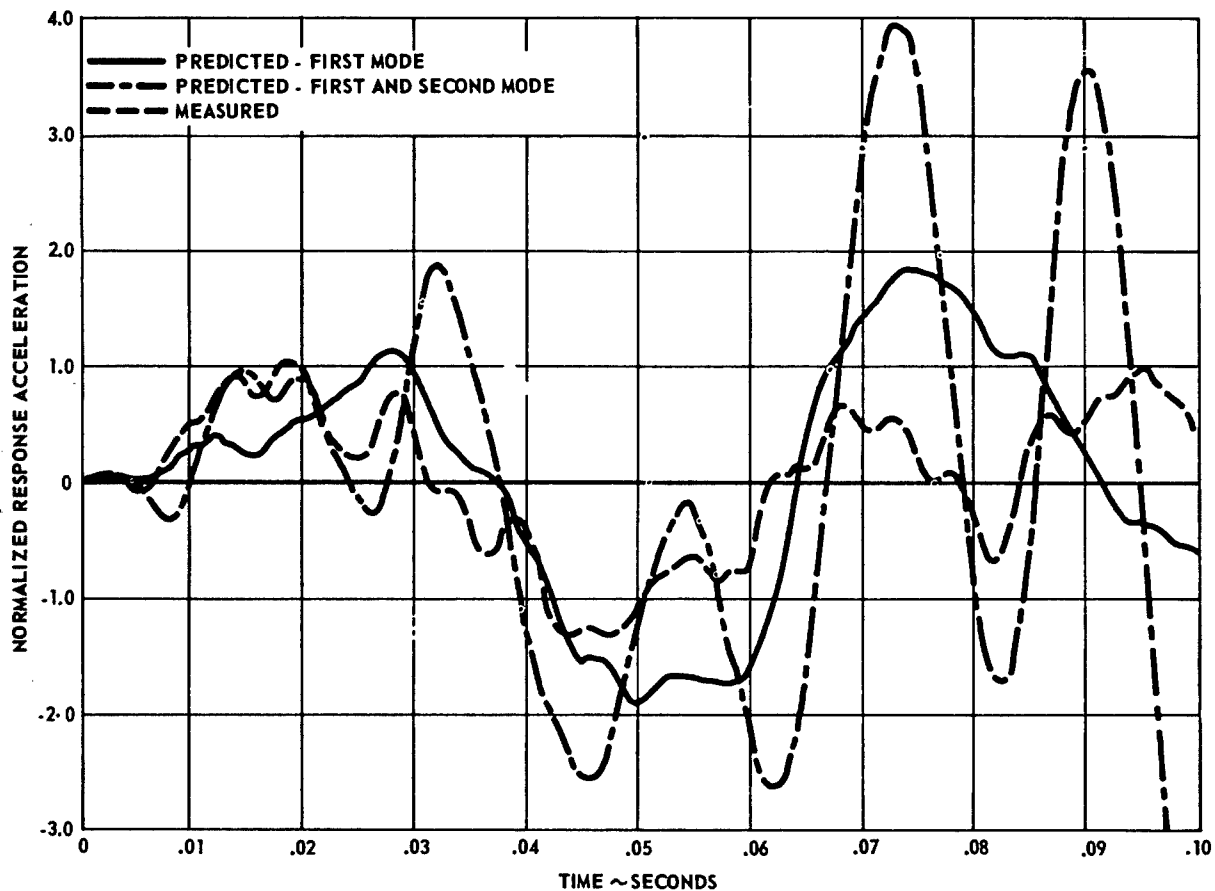


Fig. 8 - Correlation of airframe acceleration. Talos 6cl-SFNS AOE Shock Tests, Test A - lateral acceleration 20 inches from nose.

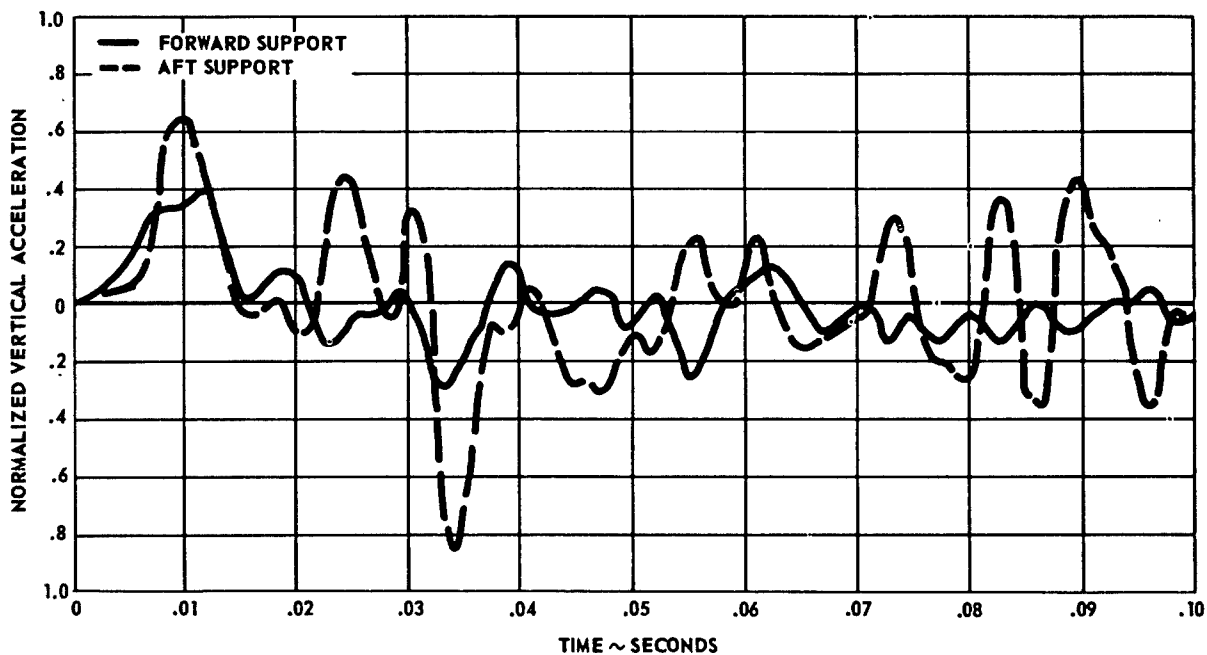


Fig. 9 - Measured vertical acceleration at missile support points. Talos 6cl-SFNS AOE Shock Tests, Test B.

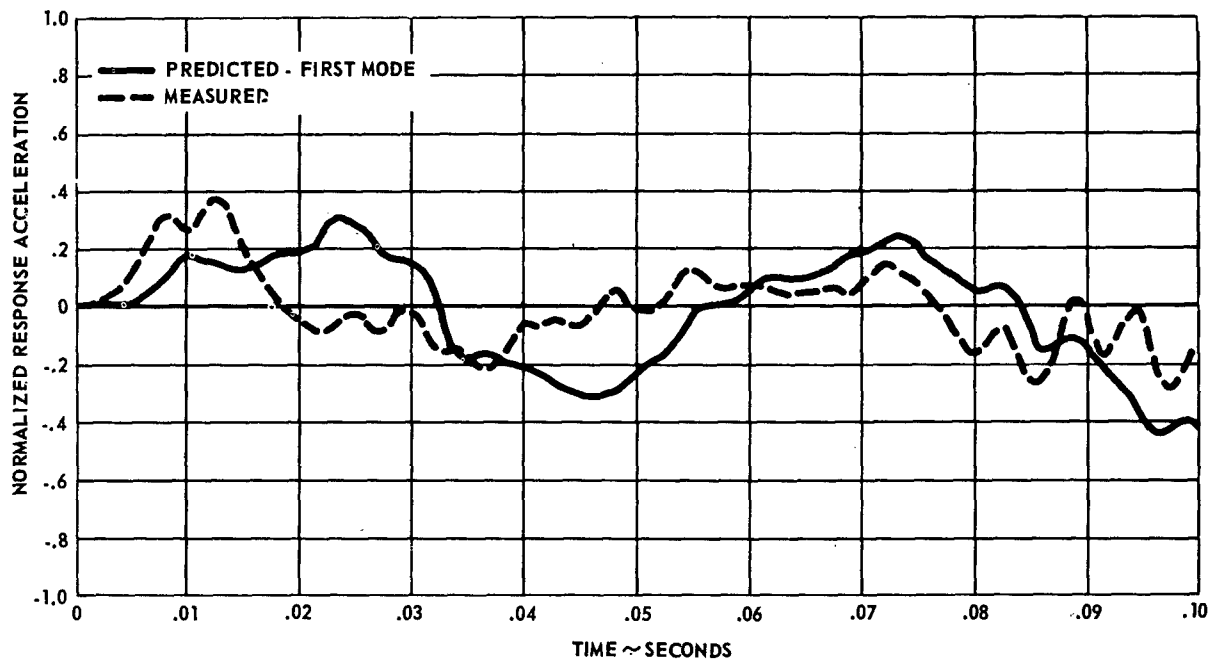


Fig. 10 - Correlation of airframe acceleration. Talos 6cl-SFNS AOE Shock Tests, Test B - vertical acceleration 20 inches from nose.

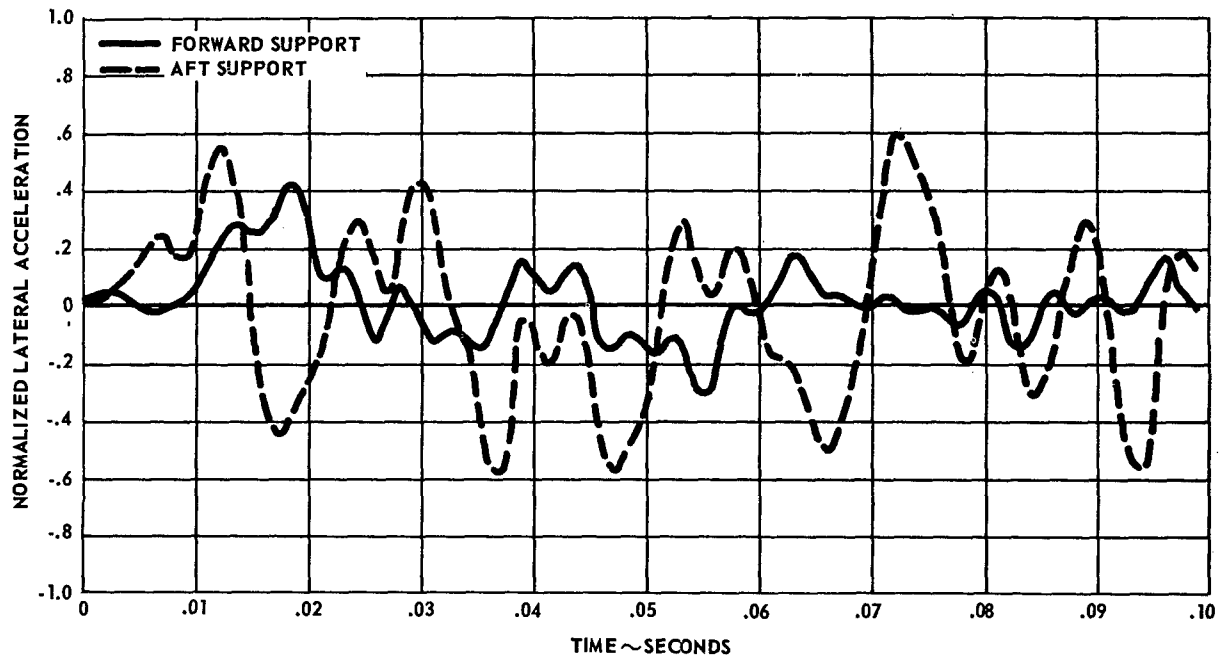


Fig. 11 - Measured lateral acceleration at missile support points. Talos 6cl-SFNS AOE Shock Tests, Test B.

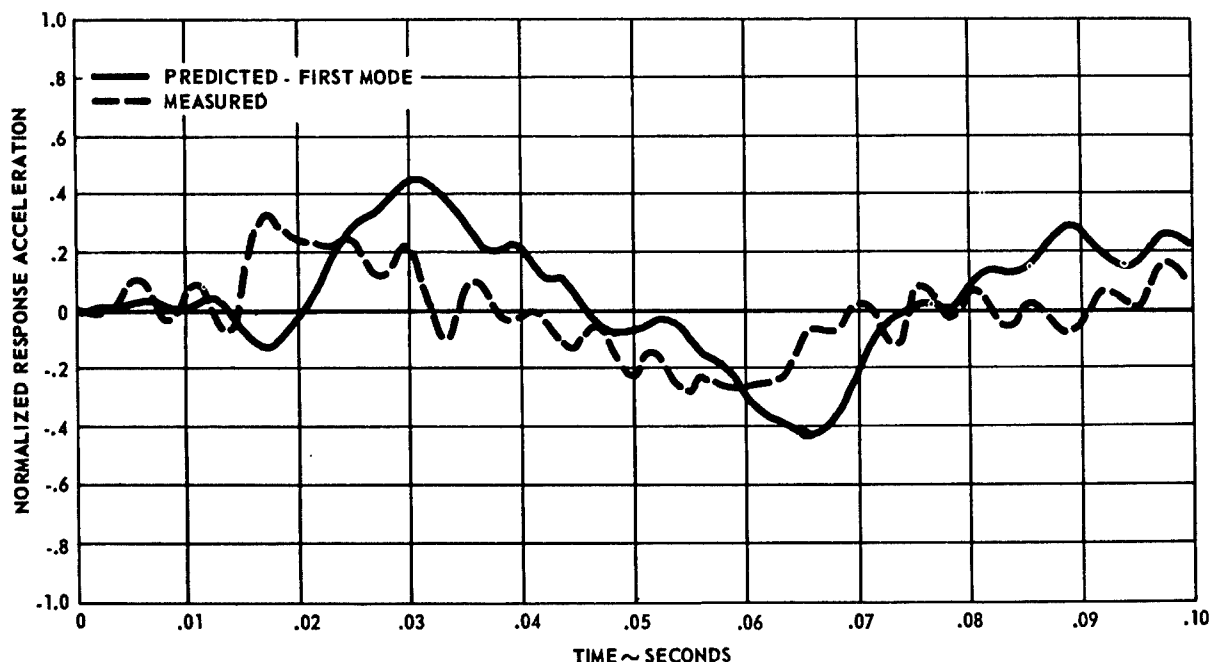


Fig. 12 - Correlation of airframe acceleration. Talos 6cl-SFNS AOE Shock Tests; Test B - lateral acceleration 20 inches from nose.

adjusted bending moments predicted for Test A revealed agreement within 15 percent.

CRITIQUE

In any analysis based upon theoretical considerations, an appraisal of the technique is in order. Of the assumptions made in the development of the mathematical model, the most tenuous is the idealization that the structure is simply supported.

Looseness of the shoes in the chocks is known to produce considerable departure from the predicted response. The neglect of damping in the equations of motion is not unreasonable for transient response calculations, since the

response of a lightly damped system during the first cycle differs little from the response of an undamped system. Errors are known to exist in the airframe stiffness data, but these are probably insignificant compared with looseness effects.

The correlation study has indicated that the simulation is a satisfactory tool for the prediction of responses and bending moments due to either measured or hypothetical inputs. Predictions will naturally be more accurate if looseness effects are not encountered. Inaccuracies due to looseness can, however, be compensated for if any experimental response data is available. In any case, some understanding exists concerning the magnitude of these errors.

Appendix

TRANSIENT DYNAMIC RESPONSE OF A SIMPLY SUPPORTED NONUNIFORM BEAM SUBJECTED TO LATERAL ACCELERATIONS (SHOCK) APPLIED AT THE SUPPORTS

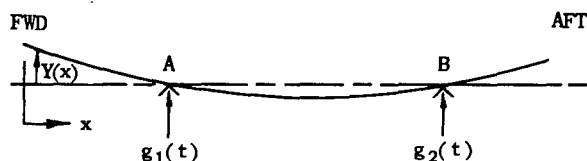
To determine the dynamic response of a simply supported beam, a normal mode analysis is performed. This type of analysis assumes that the overall response of the beam can be obtained from the superposition of response in each of the significant modes of vibration.

The deflection of the beam can be expressed as a function of time and axial position along the beam (deflection station):

$$Y(x, t) = \sum_i \phi_i(t) X_i(x), \quad (1)$$

where the subscript i denotes a particular bending mode and $X_i(x)$ denotes a particular normalized mode shape. $\phi_i(t)$ is a function of time which defines the magnitude of the contribution from each of the significant modes. The determination of $\phi_i(t)$ is the primary product of this analysis.

Define the coordinate system:



$Y(x)$ is the displacement relative to the "rigid body centerline" (centerline of the beam in its undeflected state). $g_1(t)$ and $g_2(t)$ are the accelerations applied at the supports. Note that $Y(x)$ does not represent the absolute motion of the beam, since the support points will experience motion consistent with the applied accelerations.

The absolute acceleration of an element of the beam (ignoring rotation of the element about its own axis) is

$$\ddot{Y} + g_1(t) + \frac{r(x)}{a} \Delta g(t),$$

where a is the distance between supports, and $r(x)$ is the distance from an element to support point A (r is positive for an element forward of A and negative for an element aft of A). The notation \ddot{Y} denotes the second derivative of $Y(t)$ with respect to time and

$$\Delta g(t) = g_1(t) - g_2(t).$$

The inertial force acting on an element is

$$m(x) \left[\ddot{Y} + g_1(t) + \frac{r(x)}{a} \Delta g(t) \right] dx,$$

where $m(x)$ is mass per unit length, and dx is an incremental length. Assume a virtual displacement

$$\delta Y = \delta \phi_i X_i, \quad (2)$$

then the work done by the inertial force through the virtual displacement is

$$dW_1 = -m(x) \left[\ddot{Y} + g_1(t) + \frac{r(x)}{a} \Delta g(t) \right] dx \delta Y. \quad (3)$$

The negative quantity arises since the inertial force applied to the element is in the opposite direction from the motion.

From (1), (2), and (3) the work done by inertial forces on the entire beam is

$$W_1 = - \int_0^{\ell} m(x) \left[\sum_j \ddot{\phi}_j X_j + g_1(t) + \frac{r(x)}{a} \Delta g(t) \right] X_i \delta \phi_i dx,$$

or

$$W_1 = - \delta \phi_i \left[\int_0^{\ell} m(x) X_i \sum_j \ddot{\phi}_j X_j dx + \int_0^{\ell} m(x) X_i g_1(t) dx + \int_0^{\ell} m(x) \frac{r(x)}{a} X_i \Delta g(t) dx \right] \quad (4)$$

Note that the subscript in the summation has been changed from i to j ; this was done for convenience and does not change the original meaning of the subscript. Considerable simplification can be obtained through consideration of the orthogonal nature of normal functions. A thorough discussion of this topic can be found in Advanced Calculus for Engineers, Hildebrand (Prentice-Hall). The normalized mode shapes $X_i(x)$ are normal modes, and are orthogonal with respect to a weighting function $m(x)$. The condition of orthogonality gives

$$\int_0^{\ell} m(x) X_i X_j dx = 0 \quad \text{for } i \neq j. \quad (5)$$

Then (4) becomes

$$W_1 = -\delta \phi_i \left[A_i \ddot{\phi}_i + B_i g_1(t) + C_i \Delta g(t) \right] \quad (6)$$

where

$$A_i = \int_0^{\ell} m(x) X_i^2 dx,$$

$$B_i = \int_0^{\ell} m(x) X_i dx,$$

and

$$C_i = \int_0^{\ell} m(x) \frac{r(x)}{a} X_i dx.$$

The strain energy stored in the beam is

$$V = \frac{1}{2} \int_0^l EI(x) \left(\frac{d^2 y}{dx^2} \right)^2 dx, \quad (7)$$

where E is the modulus of elasticity, and $I(x)$ is the plane moment of inertia.

Rewriting (7),

$$\begin{aligned} V &= \frac{1}{2} \int_0^l EI(x) \left[\frac{d^2}{dx^2} \sum_j \phi_j X_j \right]^2 dx \\ &= \frac{1}{2} \int_0^l EI(x) \left[\sum_j \phi_j \frac{d^2 X_j}{dx^2} \right]^2 dx. \end{aligned} \quad (7a)$$

The work done by the elasticity forces through virtual displacement $\delta \phi_i$ is

$$\begin{aligned} W_2 &= - \frac{\partial V}{\partial \phi_i} \delta \phi_i \\ &= - \delta \phi_i \int_0^l EI(x) \left[\sum_j \phi_j \frac{d^2 X_j}{dx^2} \right] \frac{d^2 X_i}{dx^2} dx. \end{aligned} \quad (8)$$

It has been shown (see Hildebrand) that

$$\int_0^l EI(x) \frac{d^2 X_i}{dx^2} \frac{d^2 X_j}{dx^2} dx = 0 \quad \text{for } i \neq j, \quad (9)$$

as a consequence of the orthogonality property. Then

$$W_2 = - \delta \phi_i \phi_i \int_0^l EI(x) \left[\frac{d^2 X_i}{dx^2} \right]^2 dx. \quad (10)$$

ϕ_i can be brought out of the integrand since ϕ_i is a function of time only.

Although more convenient methods are available, the mode shapes of a vibrating beam can (in principle) be obtained from the solution of

$$\frac{d^2}{dx^2} \left[EI(x) \frac{d^2 X_i}{dx^2} \right] = m(x) P_i^2 X_i, \quad (11)$$

where P_i is the natural frequency (radians/sec) of a particular mode.

For details of the derivation of (11) see Vibration Problems in Engineering, Timoshenko (Van Nostrand). By using (9) and (11), it can be shown that

$$\int_0^l EI(x) \left[\frac{d^2 X_i}{dx^2} \right]^2 dx = P_i^2 \int_0^l m X_i^2 dx = P_i^2 A_i,$$

then (10) becomes

$$W_2 = - \delta \phi_i A_i P_i^2 \phi_i. \quad (12)$$

The network done by the inertia and elasticity forces through the virtual displacement must equal the work done by external forces acting through the virtual displacement. We have ignored dissipative forces in this development, which should be a satisfactory assumption in the study of transient response.

In this formulation of the problem there is no work done by external forces, since the inputs to the beam are given as accelerations rather than forces. The effect of these inputs is reflected in the inertia forces. Then,

$$\begin{aligned} W_1 + W_2 &= 0 \\ - \delta \phi_i [A_i \ddot{\phi}_i + B_i g_1(t) + C_i \Delta g(t)] \\ - \delta \phi_i A_i P_i^2 \phi_i &= 0, \end{aligned}$$

or

$$\ddot{\phi}_i + P_i^2 \phi_i = - \frac{B_i}{A_i} g_1(t) - \frac{C_i}{A_i} \Delta g(t), \quad (13)$$

where

$$A_i = \int_0^l m(x) X_i^2 dx,$$

$$B_i = \int_0^l m(x) X_i dx,$$

and

$$C_i = \int_0^l m(x) \frac{r(x)}{a} X_i dx.$$

The solution of (13) together with (1) determines the deflection of the beam relative to the rigid body centerline.

* * *

PANEL SESSION

PREDICTION OF FLIGHT ENVIRONMENT

Moderator: Mr. John C. New, Goddard Space Flight Center, NASA

Panelists: F. M. Condos, Martin Company
G. L. Getline, General Dynamics/Convair
P. T. Mahaffey, Chance Vought Corporation
G. H. Moore, Lockheed Missiles & Space Co.
H. Runyon, Langley Research Center, NASA

An edited version of the discussion which took place during this panel session follows. Not all comments are included since some were repetitions of statements that were made earlier.

Mr. New opened the session by introducing each of the panelists and asking them to make a brief opening statement.

OPENING REMARKS:

Mr. Condos: "It seems to be the current opinion that vibration prediction has advanced to the point where there are a lot of people who are willing to make comparisons of their predictions and their actual measurements. This is something that no one would do 4 or 5 years ago. I don't believe, however, that we have gone far enough. We are not really predicting the environment; we are still pretty much guessing at it. I think it important that we learn to predict it much more accurately than we have, not so much from the standpoint of perfection, but from the standpoint that we must be able to use vibration predictions and environmental tests as a measure of reliability at a point where we have only hardware, not complete systems. We should, then, be striving for much better reliability predictions very early in the game, so that the systems engineers and the reliability people know where they stand. They should know what kind of margins of safety they have in their equipment and that sort of thing. I think part of the problem of why we are sitting where we are today with respect to prediction is that we haven't in the past really planned our data taking experiments to allow us to predict the environment. We simply have been interested in what the environment was at one location or for one piece of

equipment. I think we are now beginning to plan our measurements for the purpose of finding out what causes the environment, how we can predict it, and that sort of thing."

Mr. Getline: "I am going to spend very little time making remarks now. In a couple of the papers I have heard, however, notably Mr. Mitcheli's just a little while ago, I noticed that the discrepancy of sound pressure as a function of Q seems to be 'bugging' a lot of people. I hope that during the discussions that follow I will get a chance to say a few words on that. I have been working on flow noise for the past few years and, even though it is with respect to underwater vehicles, we have learned quite a bit about it."

Mr. Mahaffey: "It is very gratifying to me to see the progress which is currently being made in this very difficult field of environmental vibration prediction. I can recall that, as recently as 5 years ago, the prediction of environmental vibration levels on any kind of rational basis was generally considered to be beyond the state-of-the-art. From the papers that we have heard today and others that we see on the program, however, it is quite evident that a number of people are making significant strides in this field. This is certainly encouraging because we still have a long way to go. It is particularly important in the space age because the success of an entire mission can depend on how well we have predicted the environmental vibration levels."

Mr. Moore: "I thoroughly agree with some of the observations made by the other panelists as to our advancement over the last 5 years. A significant number of rather discreet vibration and acoustic measurements have been made in flight. Our direction should be toward making planned experiments, rather than observations, where we can fly ground calibrated systems in actual flight vehicles. This approach, I hope, might lead to a better understanding of the true flight environment for the launch as well as other phases of critical flight conditions."

Mr. Runyon: "I feel a little like a maverick here since most of my experience has been in the low frequency spectrum and, perhaps even more restrictively, has dealt with sinusoidal oscillations. The word 'random' has been tossed around here quite a bit. For a few minutes I would like to mention some of the work going on at Langley related to this field."

"For the most part we have been looking at the vehicle as a system, and we are pursuing research on such items as a one-fifth scale dynamic model of the Saturn I. We are now in the process of having a one-tenth scale dynamic model of the Saturn V built. Both of these were a sort of replica-type construction, where we tried to detail almost every nut and bolt in the thing. The one-fifth scale model of the Saturn was about 30 feet high. The Saturn V model will be about 36 feet high. We have worked on the development of analytical methods for determining loads on launch vehicles due to winds. We have been trying to get detailed observations of the winds through the use of smoke trails. Recently, we had a visit from Messrs Jewell and Lifer of Marshall and, as a result, we are now starting to work on this high frequency business. We are applying high frequency sinusoidal oscillations to our Saturn model. We will go to noise eventually, but at this time we are going to try to check out various procedures presented here today, as well as one by Ira Dyer as described in 'Random Vibration' edited by Crandall. Other work at Langley concerns low frequency buffet of the Saturn-Apollo using an experimental dynamic model, high frequency buffet of simple plates, and measurement of acoustic noise. On the Scout, for example, acoustic measurements were made at two positions. This has been published as a TN."

"Measurement of the response of a launch vehicle to ground winds is also an important field right now at Langley. We have two full scale vehicles, the Thor and Jupiter, which are going to be mounted at Wallops Island so that continuous measurements may be made of oscillation and ground winds. Many dynamic

models have been exposed to ground winds in the 16-foot tunnel. As you can see, a lot of work at Langley is directed toward dynamic modeling, and we are of the opinion that this is an important direction to go. I am not an expert in this black box field, but as far as I can see there should be more effort in dynamic modeling."

"I would like to make one last point concerning in-flight measurements. Many of our vehicles, particularly in their first three or four flights, will carry no payload except perhaps dummy weights. It seems that we should be conducting some experiments to measure the environment in the payload in which, I presume, most of you are interested. We should perform a good job of measuring the environment for this payload. In this way, we can then, perhaps, anticipate your problems. As far as I know this has not been done to any extent."

DISCUSSION

Mr. Rice, of Goodyear Aerospace, addressed Mr. Getline. "I have always wondered how you determine your initial skin thickness for fatigue life in these high acoustic and vibration environments. I know that you talked about this some years ago, but what's the latest state-of-the-art? How do you have any confidence that your initial design will pass a fatigue life that's necessary for a mission, particularly in an airplane that has many years to live?"

Mr. Getline answered. "The skin gauges are not set by noise, generally. They are set by either the static or the dynamic load to which the aircraft is being designed. In general, for a high performance aircraft, landing loads at high sink rates will usually control the areas of the fuselage, particularly in a fighter where you would expect a high noise level."

Mr. Rice asked, "Is this adequate to give the required fatigue life?"

Mr. Getline answered, "In general, it is. If you have local areas where there might be a problem, you can treat these by methods other than just going to heavier gauges, such as going to a honeycomb or laminated structure of some sort. On the F-106 which was the last fighter we built, there was no consideration at all given for acoustic fatigue. This was mostly because the noise levels over the structural areas weren't sufficiently high to present a problem when you considered the structural requirements regarding the maneuvering and impact loads to which the aircraft was subjected. On our

commercial aircraft there has been no special treatment on the fuselage except for the closing boat tail where we did have a few problems. These were produced by flow separation causing a very violent oil canning of the skin. This was taken care of merely by laying a couple of layers of glass inside it; there have been no problems since."

Mr. Mahaffey added, "The concern that one has for structural fatigue increases with the decibel level. If the levels are 140 db or lower, perhaps you don't have to worry too much about the structure as long as it is a fairly clean design. On the other hand, if you have a structure exposed to a 160-db level, it's wise to take a good look at the structure on the drawing board. Most designers are currently aware of the fact that 160 db is a high noise level. They have heard of enough cases of sonic fatigue so that they, themselves, think of using honeycomb or some similar type structure. Also, in the high noise levels it is very wise to begin running siren tests or, better yet, jet engine test stand tests on the type of structure which is being proposed. It is a matter of experience for one thing. If you look around you can usually find some test data which gives you some idea of the kind of problems you may run into."

Mr. Griffith, of Chance Vought, mentioned that they had run into this problem on the VTOL type of aircraft, where the weight of the structure is of prime consideration. He didn't know whether noise was used to set the skin gauge, but it did determine the side-wall of the fuselage, say, on one aircraft.

Mr. Getline offered a suggestion on how to provide some cheap insurance for fatigue if the design is pretty well firmed at the time. "What we have done in building the C-141 empennage, as well as our own aircraft, is to lay in a strip of 3M tape of some sort before we lay two fairing surfaces together for riveting. This is a room temperature cure material with a fairly low modulus. Just lay it on and rivet through it. For normal 1-g flight loads the rivets will just be going along for the ride. The most important source of fatigue is the stress raisers where you have rivets, holes, and high local stress concentrations. When you put in the materials that will take these loads, the stress raisers give you no problem and you get a very great extension in fatigue life at practically no cost to weight."

Mr. Moore said that his experience at Lockheed so far had not indicated that structures should be designed for acoustic fatigue, as such. "The primary structure has been

designed for static and dynamic loads—low frequency loads. We have, in recent configurations that we have flown, predicted levels during the transonic phase of flight in excess of 160 db externally. Because of this concern we did go into acoustic sample testing of materials and also sectional testing of the vehicle under acoustic fields. We found no problem along this line for the particular design that was tested."

Mr. Runyon interjected, "You said acoustic fatigue, but it doesn't have to be acoustic. I know on one particular research airplane where certain panels started to fail. It was panel flutter of a limited amplitude that was inducing the cracks, not the acoustics. So it's not always acoustics."

Mr. Getline asked Mr. Runyon what he meant by panel flutter.

Mr. Runyon replied, "We took a panel from the actual airplane and put it in a wind tunnel. We found a point of instability at a particular Q which corresponded to the initiation of vibration in flight. At this point of instability the oscillation suddenly occurred. It didn't build up over a period of time, and it wasn't induced by wind tunnel oscillation."

Mr. Getline said, "We found the same thing, where it looked like an instability, but it really wasn't. You get into a different regime of friction damping in your structure, you break through it, and the stuff will just pop out at you. Every time I hear the term 'panel flutter' I wince, because I get a different definition from every person I talk to."

Mr. Henderson, of the Aeronautical Systems Division, addressed Mr. Getline. "I have heard of your work on the 141 from other sources. Did you go through any optimization process in trying to pick the visco-elastic material for damping on the 141, or was this more or less an ad hoc fix?"

Mr. Getline replied that it wasn't really a fix. "We were sub-contracted to Lockheed on that job and the design was pretty well delivered to us. We had a certain weight budget to meet and they gave us certain ground rules for designing the structure. In addition to that, we sold them on the idea of using this material as additional insurance. The modulus of the material is considerably less than that of the aluminum structure, and we do know it will take the normal 1-g flight load. So, we are saying that we are going to eliminate the stress raisers over a good part of the structure for most of your flight regime.

That is all. It is a cheap bit of insurance which we supplied."

Mr. Bieber, of the Lockheed Missiles & Space Company, said, "In at least one of the papers today we saw the rms of the vibration intensities plotted along with the dynamic pressure. About 2 years ago there was a rash of model testing in tunnels and also reports and papers which indicated that we should take aerodynamic data from transonic tunnel tests and apply scaling to convert this to the pressure field on the full scale vehicle. We get a vibration response more severe than the max Q condition. Today, I haven't heard anything about the transonic buffet problem. We seem to be back to the max Q problem. I am wondering what happened to the transonic buffet problem."

Mr. Moore responded, "In our experience at Lockheed on this problem with the hundred or so configurations that we have flown, we have found that on the booster, where you have a rather thick boundary layer noise from the aerodynamic turbulence, the vibration level inside the vehicle seems to follow Q. However, if you are considering vibration measurement inside or at the forward end of the vehicle, say in or near the nose cone area, both wind tunnel tests and flight tests have shown that the maximum vibration levels are in a range of about mach 0.95 - 0.98, possibly pushing mach 1, and they do not necessarily follow Q. It depends upon the location in the vehicle at which you are making these measurements, and it is also a function of the duration of the levels that you might observe during the flight. The uniqueness of the particular configuration that you are flying strongly influences the vibrational levels that you see during a transonic region of flight, anywhere from a duration of possibly 5 or 10 seconds of flight time, to possibly 40 to 50 seconds."

Mr. Condos continued on the same subject. "The kind of thing that has been discussed in previous papers, to my way of thinking, is in relatively smooth aerodynamic areas where you seem to be Q dependent. If you talk about the area of separated flow and mention some of these things, I think the problem comes out again in transonic regions. There is probably still a big question in the minds of a lot of people as to whether the information that you get out of wind-tunnel testing in this area is directly relatable to vibration response as you generally think of it in terms of the rocket engine noise. If possible, I would like to stimulate some thinking both from the panel and the audience on that subject."

Mr. Runyon commented, "At Langley there has been a model of the Saturn-Apollo configuration, I think in conjunction with the Manned Space Craft Center. This, of course, has a lot of junk out in front creating a lot of buffet. Buffet can be divided into two parts. One is the low frequency buffet which would excite the fundamental modes of the vehicle. At Langley this is more or less the type that they are observing. There is also a high frequency buffet, and I have been trying to figure out the difference between the high frequency buffet and the acoustic noise. There has been a rather large dynamic model tested of the SA-5, and there will be a flight, we hope, in the not too distant future. We will be getting correlation between full scale and model testing for this low frequency buffet."

Mr. Himelblau, of Nortronics, said that he felt a research program was needed in the area of buffet. He asked if any members of the panel knew of any existing program, particularly involving a prediction procedure so that, given a fairly common though arbitrary vehicle shape, one could establish whether there was going to be a problem or not and could predict roughly what the levels might be.

Mr. Moore said that buffet prediction can be broken down into several classes. "As one class, consider that you could fly a configuration which might go into bending mode instabilities during the transonic phase of flight. Along this line, Ames Research Center has conducted rather extensive parameter tests of various configurations over the past few years. I believe they have issued a few reports and that they intend to come out with a few more reports this coming year. They have some preliminary criteria which they intend to issue in the spring which will give some guidelines for configuration constraints.

"A second phase of buffet is that of trying to predict the fundamental response or the bending mode response of the entire vehicle due to buffet loads. This is more or less of a low frequency type buffet loading. There have been various analytical techniques developed to predict this, but very little wind tunnel testing to actually correlate with the analysis. Both Ames and Langley have done some work along this line.

"Finally, we might get into the area of high frequency buffet or boundary layer noise, where we are interested in determining what vibration levels components might be subjected to during the transonic phase. Practically all of the data

is below 100 cycles. Ames Research Center has been working on a one-tenth scale model which has been limited to 1000 cps, whereas full scale is limited to 100 cps. They have issued several reports describing fluctuating pressure coefficients to be used for flight prediction, externally, of course. It does appear from flight experience that most of the energy during transonic flight is about 100 cycles, so there is no good correlation with the tunnel data that has been obtained to date in this higher range. As far as the lower range is concerned, we have one flight named the Ranger V where we measured the external pressures aft of the nose cone shroud and compared them with tunnel data. They agreed very well for the frequency range considered."

Mr. Himelblau asked, "This is all for prediction below 100 cps, then?"

Mr. Moore said it was.

Mr. Himelblau continued, "Is it perhaps possible to extrapolate this type of data into the high frequency range?"

Mr. Moore thought it a little dangerous to do that.

Mr. Himelblau said that he had seen no one else who was willing to try their hand at extrapolation, either.

Mr. Moore replied, "Well, we extrapolate into this area, but we extrapolate from in-flight experience, not from wind tunnel data."

Mr. Kirkley, of Martin-Orlando, said that he had surveyed quite a bit of information regarding the aerodynamic boundary layer disturbance. "It has bothered me quite a bit that most of the information seemed to correlate the overall sound pressure level with free-stream dynamic pressures. Since the disturbances created on the structure appear to be due to the boundary layer pressure fluctuations and are a local condition, I can't understand why local Q's are not used. I'd like to inject this for discussion."

Mr. Getline said he was hoping someone would bring this up. "When the original work on low speed wind tunnels was done and the normal tunnel speed was used, this was fine, but when you get out into an airplane the local flow velocity varies tremendously over the fuselage. When you get up into the transonic and supersonic range, the flow velocity over a good part of the fuselage bears no relation to the free-stream pressure that your boom is

measuring. You're going to get correlation, certainly, but its not going to be correlated with anyone else but yourself. This is why I think Mitchell's data showed coefficients that varied from those of others.

"A number of years ago when we were first flying the F-102, we made some measurements to try to correlate the boundary layer turbulence with noise in the cockpit and that sort of thing. That airplane had normal shock inlets along the side of the cockpit. At about mach 1.2 a strong shock started to form at just about the front edge of the wind screen, and at higher mach numbers it would move back. We took measurements ahead of and behind the shock and correlated the data that was taken behind the shock with a velocity that was subsonic up to free-stream mach numbers of about 1.25. The spectrum and the levels of the noise that we measured correlated exactly with the subsonic data taken at the identical free-stream value. We have also done this little trick on underwater vehicles. We have taken boundary layer measurements up to 60 kc in the water tunnel using appropriate size hydrophones, and we have again gotten correlation as long as we were using the proper local velocity over the hydrophones. People tend to miss the point that just because 300 miles per hour is used in the big tunnel, you don't use it right across the board for supersonic aircraft, particularly in the transonic range."

Mr. Ho, of Aerospace Corporation, was concerned about the vibration of any payload on the top of a booster. The vibration is predominantly in the longitudinal direction, but there is some in the lateral direction, which Mr. Ho called cross modulation. Because of the problem of clearances, he wanted to know whether a figure of 15- to 25-percent cross modulation was a reasonable one, and whether there is any good analytical method of predicting lateral vibration due to longitudinal input.

Mr. Moore responded, "The procedure I like to follow on a problem of this nature is really a combination of test and analysis, not just test alone. I prefer to conduct a survey of the spacecraft combination to find out the dynamics of the spacecraft and then to couple it, for purpose of analysis, with the booster system involved. My analysis shows how the whole system responds and I try to predict from any existing flight experiences what a reasonable response of the entire system would be. For example, you could see what clearances could be obtained on the shroud-spacecraft combination.

"One trouble with testing a spacecraft of these dimensions on a shake table is the fact that the system you test is not the same as the one you have in flight. You must be careful to control your input so that resonances are not excited which do not exist in flight. This problem exists, I know, in a lot of our systems. We do test the spacecraft and normally we try to restrict its response to a strain level which we feel will not be exceeded in flight. This is usually established by analysis. As far as the 15 percent, I really couldn't put a figure like that on any particular application without proper analysis."

Mr. Mahaffey commented, "It strikes me that each case may be different. Your longitudinal vibration, I would hazard a guess, must come from the engine, perhaps thrust variations. On the other hand, lateral vibrations may be arising from some other source and these two would not necessarily have the same relationship from vehicle to vehicle."

Mr. Galletly, of Atomics International, asked, "In describing a structure analytically, do you find that the structural damping mechanism or the viscous damping mechanism is adequate for predicting the structural vibration and frequency range in the acoustical field, say about 500 cycles?"

Mr. Moore answered, "Well, if you are talking about frequency ranges above 500 cycles, we just don't have a model from which we feel we could make accurate predictions to any degree in this range. If we are worried about environment internal to the vehicle in this particular frequency range, we normally try to establish our requirements through tests. There are so many resonances that can exist in a structure which can influence the whole problem. You have to have a sort of trade off of analysis versus the tests. Normally in this range we do go to the tests. Concerning damping, through component testing we do obtain ranges of damping which we feel are reasonable for establishing limits of Q ."

Mr. Galletly then directed a question to Dr. Lyon of Bolt, Beranek, and Newman: "Are we going toward nonlinear analyses? About a year ago we were discussing problems of nonlinear techniques, yet I haven't heard any discussions here, from the point of view of structures, about the possibilities of using, say, nonlinear structural models in helping us to describe some of these problems."

Dr. Lyon answered, "Well, I don't think there is overwhelming evidence that a nonlinear

model would give more accurate prediction than the present uncertainties in the linear estimation. I certainly would hope that we would get a lot closer in linear estimation before we added the complexities of nonlinear studies."

Mr. O'Hearne, of the Martin Company, said, "Mr. Getline has upset me a couple of times this afternoon. First, I couldn't understand why there is a problem distinguishing a limited cycle flutter from the response to a random excitation. Secondly, he said that my free-stream Q was not a good overall parameter for identifying the stochastic process which I am measuring. My particular question is, if I can't use free-stream Q and perhaps mach number as governing parameters, what am I going to use?"

Mr. Getline responded, "I suggested that you use the local free-stream Q . That is the local Q above the boundary layer wherever you are taking your measurements."

Mr. O'Hearne returned, "This will certainly vary along the length of the missile, right?"

Mr. Getline agreed that this was correct.

Mr. O'Hearne continued, "So you have as a governing parameter a big old function instead of just one little number."

Mr. Getline agreed.

Mr. O'Hearne said that this makes things rather difficult.

Mr. Getline said, "Well, if you want to you can relate the local Q 's on the local velocities to your free-stream velocity. This means you are going to get a different function at every measuring station. This is right. If you want to go on, Q is not really the parameter that was used as a relationship."

Mr. O'Hearne asked, "What is?"

Mr. Getline replied, "I understand that they are using friction these days."

Mr. Himelblau of Nortronics said, "Mr. Condos and our own organization has had an opportunity to compare some of the early predictions, at least, with field measurements. I think we are both unhappy about the comparison. Can any of the speakers suggest what we can do in the future to improve the prediction procedures? Perhaps we should scrap them and develop new ones."

Mr. Condos added that he felt there were several major areas where predictions have missed, one of which occurs when an attempt is made to predict what will happen when structural changes are made. As an example, he cited the change in the Titan, from 8 to 10 feet in diameter, as an area where they missed pretty badly. In other areas, where only the skin gauge was changed, they came out pretty good. He suggested that most papers have discussed only changes in mass. It is necessary to find out how to handle the changes in other things.

Mr. Moore, referring to his opening comments, said, "I think that we have reached the point where we must conduct some flight experiments to try to understand better how dynamic systems in vehicles respond to the environments that they see. We might also give better definition to the paths of transmission to the components, acoustically-versus structurally-induced. It is evident to me that if you have a component mounted right on the skin compared with some other internal arrangement, you are going to see quite a difference in the response. The component mounted on the skin might get the full impact of the pressure field actually pounding on the skin adjacent to it. Internally the transmission might be more acoustically induced than structurally transmitted. A good example of this was a recent NASA flight where we had a pickup mounted a few inches from the skin by a heavy ring and another mounted on a rather rigid structure about 1-foot inboard. There was a factor of about five difference in the two rms levels. These are rather difficult to predict. Consequently, I think we should have some further planned experiments where we do make measurements of the internal dispersions of the energy in the launch vehicles with known calibrated systems. Possibly it should be in the nature of reeds or something along this line, where we know exactly the dynamic characteristics of the proposed flight."

Mr. Condos felt that there was a lot that could be done on the ground, too. "We can excite some structures and fairly large sections of other structures acoustically with random sirens. We can also excite them with vibrators. We can trace out some of these transmission paths and define what their characteristics are on the ground. We can also do more by way of establishing what we might call a transfer function between the acoustic sound field and the basic skin itself. We are scratching the surface on a lot of these things from the standpoint of coming up with analytical techniques. At the same time, there is a lot more that can be done than just gathering empirical data for its use in systems."

Mr. Runyon referred again to the one-fifth scale Saturn model. "One of the things we are going to do is to try to impose vibration at the engine mounts and find out how it gets up to the top of the thing. We are going to impose known acoustic fields on it. We will go to an anechoic chamber and blast noise at it. In addition to that, we have recently, at Langley, obtained two complete, full-sized Thor vehicles, one for ground wind tests and one for vibration testing. One of the specific purposes of this vehicle is to introduce known vibration signals at one point and determine what we are going to measure at the top. This is along the line that you are talking about."

Mr. New, just to be controversial, suggested that maybe what we don't need is more data. He asked, "Does a designer really need a better prediction of this environment?"

Mr. Himelblau, an equipment manufacturer, said that the answer is definitely yes, believe it or not. "As soon as we get a little bit of money in the contract, one of the things we do is to go ahead with our structural prototype early in the program. Fortunately, most equipment doesn't require a model. We initiate the design considering what environmental levels we are expecting, so that design problems are foreseen and solved early enough in the program to affect the final drawing which comes considerably later. So, for those who wonder if the designer uses it or not, that prediction is very important to a good design team which consists of a designer and a dynamicist using a combination of analysis and a test."

Dr. Franken, of Bolt, Beranek, and Newman, pursued the point further. "Granted that the designers may need the data, could anyone tell us to what degree of precision they would like the environmental data? Say we are talking about vibration data in g^2/cps or whatever you choose. Is half an order of magnitude close enough? I'm thinking of the results that we got on some statistical studies of data. We found variations of standard deviations of about 2-1/2 expected in nominally identical data. This means that you have about half an order of magnitude of uncertainty right there? Would you like the predictions to be as good as your uncertainty?"

Dr. Cook, of Collins Radio, spoke as the representative of a manufacturer of black boxes. He felt, in general, that the predictions needed to be better and more complete in their definition. For example, when they are given a design requirement of 8 or 10 g, he would like to know whether this load really occurs at the

point of mounting or somewhere else. Unrealistic or excessively conservative prediction of design requirements makes life difficult for the equipment manufacturer.

Mr. New felt that the panel was in sympathy with what Dr. Cook said. "Here's a new system that's coming into being. Since nobody knows exactly what the dynamic characteristics are, we try to predict what the environment is, and usually from that prediction we set a specification. Using that specification, we begin to design configurations and eventually get down to component levels and the black boxes. We begin to pile on factors of safety to get a certain reliability. Then we have factors of ignorance because we want to be safe. Out of all this, at some point the black box manufacturer gets a specification, a set of criteria, or perhaps a test that must be passed to qualify the design. We start assembling parts and pieces and finally get a system which is run off the run-way or boosted off the pad. I think we need to look at the total process that I have described and see where in the various phases we can make the most improvements. Is it in the prediction level or is it in the design level? Is it in the often unrealistic methods of testing on the ground? Is it in removing some of the ignorance from these factors? Is it in reducing the margin of safety? Is it building it quicker, or is it something else?"

Mr. Mahaffey commented as a user of black boxes rather than as a builder of black boxes. "The user of black boxes gets asked very early what the vibration environment is. The builder has to design to something. The user does his best to predict an environment and, usually, what he predicts becomes a qualification test requirement which he feels is necessary to provide equipment that will be satisfactory in service. The difficulty begins when the manufacturer of the black box begins to run into trouble in meeting the specification. I know from my own experience that I've often felt that the requirements given to the black box manufacturer may be conservative, but I don't know how conservative.

"This points up an area where we have got to make some progress. When you are developing a piece of equipment, schedules usually get tight and there is trouble in meeting the specification. The first question arising concerns whether the requirements can be reduced. Here, I think, is really a test of how well we can actually predict the environment to which equipment is subjected. I don't know the answer to this problem. I believe that the man who is making the prediction should, as a first step,

do his best to predict the actual environment without any conservative factors. The second step should be one of incorporating appropriate conservative factors in order to come up with a qualification test requirement. At least if one follows this procedure he will have some idea of how much conservatism there is in the requirements which have been put out for qualification testing."

Mr. Getline directed a question to Dr. Cook of Collins Radio. "Suppose we gave you a number, lets say $0.1 \text{ g}^2/\text{cps}$ from frequency one to frequency two. What do you people do with it in the design stage?"

Dr. Cook responded, "Well, if we knew that that was the exact figure, we would use it as a design figure. Our designers would have to have it converted to an rms number because, generally, they aren't conversant with power spectral density."

Mr. Getline said, "We'll give it to you in rms g or any other form that they can understand. What do they do with it?"

Dr. Cook explained that, in general, designers will make a simplified dynamic analysis using static loads. His group, as consultants, help out in the dynamic design wherever possible, but generally black boxes are not designed to specific dynamic loads. They are built by rule-of-thumb and tested. The specified g-value and frequency range is used as a guide.

Mr. Getline then asked, "Assuming that the accuracy of our predictions with respect to environment was 100 percent, how would you rate your design effort, on the same basis?"

Dr. Cook said that in maybe 10 years they might be able to rate it 100 percent, too. At the present time, some designers would have safety factors on the order of 5 or 10 at times. In other cases they would slip up with a safety factor of $1/2$ and the thing would fail.

Mr. Getline thought this was a pretty wide range when one has a prediction. He cited an example to show why he brought up the subject in the first place. "On the Little Joe II booster we had a component made by a manufacturer, who shall go nameless at the present time. He had a requirement, lets say of 20 g which, because of a change in something, was raised to 22 g. He was ready to guarantee his item at 20 g, but wouldn't do it at 22 g."

Mr. Gray of Space Technology Labs said that he represents a company which both makes

black boxes and provides technical direction to others that make black boxes. "It has been my experience that the failures under environmental exposure in about 9/10 of the cases are due to three things: (1) poor design practice, such as hanging heavy components by their leads. (2) failure to conduct even the simplest type of analysis with a given environmental estimate, and (3) quality control in manufacture, probably the biggest cause. I don't believe that pinning down the environment to the "gnats eyebrow" is going to advance the state-of-the-art all that much. I think the biggest field for future development lies in turning out better modes of analysis with a given environmental criteria."

An unidentified gentleman said, "The environmental specifications that the black box designer gets are exactly the same as the basic loads that booster manufacturers or an airframe manufacturer would use. So, the design of that black box can be no better than those specifications. We use those just as you would use your basic loads. You can say what you will about mechanical design but in the field of analysis we can make as sophisticated a model of a black box as you could of a booster or an airframe. I feel that we can design no better than your prediction. We may not get that good, but we can do no better. If you're off by a certain factor and we use that factor, then we're off at least by that factor."

Mr. Condos felt that there is a difference between an ability to do something and what is done in actual practice. "I agree with you that the ability is there for the mechanical design and analysis of a black box as well as for the entire system. My question is really whether it's done in very many cases. I'd like also to take some exception to Cory Gray's statement implying that we don't need any better predictions. As I mentioned in the beginning, we are extremely interested in reliable systems and we want to find out how reliable these systems are without spending excessive quantities of money in flying them. Our ability to determine a margin of safety from a known environmental distribution and the stress or strength distribution of the part through actual environmental tests on the ground gives us a key to what the reliability can be in relatively cheap fashion. We will never get there when we are off an order of magnitude in our prediction at the beginning."

The unknown man continued, "We are also interested in optimum systems as well as reliable systems. From that point of view we have to have at least realistic environmental conditions to design to. We can't avoid the

problem of having relatively accurate environmental predictions, yet having the designer use a nice healthy number, a safety factor of 10 or so."

Mr. Root, of Collins Radio, commented further on the data problem. "I don't think we need more data. I think we need information from the airframe people as to just what the data means. In other words, when they give us a specification, what factors have they built into it? Our designers now add their own safety factors. They test to it and, given a long enough production run, they eventually trim some of this fat out of the equipment. Once they start trimming some of these safety factors, some of our airborne radios weigh half what they did when they were originally designed. If we knew that you also have a safety factor of 2 to 1 or 1-1/2 to 1, it would allow us to trim these back even further. We can't get this information at present from the airframe people. About all they will do is to tell us that this is the prediction technique and here are the papers that describe it. They won't tell us what additional factors they have put in."

Mr. Moore commented along the same line. "I think that the black box manufacturer has to realize what the user of the black box does. First of all he is handicapped to some degree in not knowing the environment throughout his system the way he would like to. He is limited on every flight by flight measurement restrictions on telemetry. He does not have accurate surveys throughout the whole booster at points where this equipment might be installed. He is required by the customers to have versatility of installation. Very often, when the vendors have the contract to build these components, the bracketry on which the components are going to be installed is not even designed. Frequently, even the area of the vehicle in which the component will be mounted is not known. This often influences, to some degree, the levels of the test requirements that the vendor might receive contractually to which the black box must be built. So it is difficult for the booster manufacturer to predict these things. Discrete observations or measurements from one vehicle to another aids the booster manufacturer in setting test levels, but he has to make sure that the test spec which some black box manufacturer is going to have to use gives him reasonable assurance that he will not have failure in flight. This is a difficult task and requires a little give and take on both sides."

Mr. Kirkley, of the Martin Company, disagreed with Mr. Moore to a certain extent. "I think that we have an obligation as weapons systems contractors to provide good data. We

can't get out of this. We are going to pay for it if we don't give them data which are as close to the actual environment as we can get. I would like to give an example which I think really hits home on why good data are needed. The gyro people have a term which they use called 'drift per g^2 .' They take our g-rms value and some constant derived from tests and in some way determine the drift which the guidance system would have over a period of time. We learned that peak g-rms values over entire flight times was not a desirable form for the data. We had to present a time history of the g-rms, which got us to a truer prediction than we are able to give right now. I hope that in the future some of these things that we are working on such as Q, be it local or free-stream, drag or perhaps some correlation with Reynolds number, will give us the ability to give a better definition of environment."

Mr. Karidakis, of North American Aviation, commented, "I was much interested in hearing Dr. Cook say that he didn't design a black box to a certain figure, yet when he put it on the vehicle it survived the environment. This proves that the environment we are getting is a little overestimated. Perhaps one of the reasons is that we are considering the environment from measurements we have taken on a vehicle in an unloaded condition. We are calling this an infinite impedance input to a black box, when in essence this really isn't so. May we have some comment from the panel on this?"

Mr. Condos said, "I think you would be missing a lot if you only took measurements on an unloaded structure and carried these on as representative component inputs. The majority of our measurements are at points which are loaded with components because that is primarily what we are interested in at that point in the program."

Mr. Karidakis asked Mr. Mahaffey, "In your method, how do you differentiate between structural measurements that are located where components are and where they are not? Do you just lump everything together?"

Mr. Mahaffey responded, "The data which appeared in the paper by Mr. Smith and myself were taken at a large number of locations throughout the aircraft. The emphasis was on getting as much data as possible. The pickups were placed on primary structure as far as possible rather than on skin panels or types of structure which would be influenced radically by changes in component weight. I think that most people try to follow this rule except when they are measuring some specific input into a package."

Mr. Karidakis continued, "In other words, it makes no difference whether we have a component that weighs 6 ounces or 500 pounds?"

Mr. Mahaffey said, "It certainly does, but in my experience that's a little beyond the black box stage. If one is dealing with changes of magnitude of this sort he must be careful in the manner in which he attacks it."

Mr. Kent, of AC Spark Plug, commented on the qualification spec being based on predicted environmental levels. "It would appear that there is a lack of feedback of data from the test to the person predicting the environment, possibly due to the present method of qualifying a device to a certain spec level which is based on the predicted level plus a certain number of unknown safety factors. Using the best predicted level with a number of increasing stress levels during qualification to give us, more or less, a factor of safety involved with the equipment would be possibly a better method. Are there any thoughts on that?"

Mr. Condos agreed that more reliability information should be obtained from the qualification test program than is now obtained.

Mr. Rygelis, of the AVCO Corporation, asked that someone clarify the meaning of "safety factor" from the standpoint of dynamics.

Mr. Runyon said, "In computing the loads on a launch vehicle, for instance, you have static loads for winds, loads from gusts, and the like. You would add all these things up, and on top of this add the safety factor, between the sum of your loads and the capability of the vehicle."

Mr. New asked whether he would feel better if it were called a factor of ignorance.

Mr. Rygelis thought this would be right. "I think many component manufacturers were quite confused about a safety factor which was a field dynamic factor. In this case it was more likely a static load, the maximum capability of a structure."

Mr. Runyon added, "You can compute the stress or a bending moment from the gusts, the fuel slosh, or the dynamics of the engine motion. This is a static type thing."

Mr. Mahaffey commented on the question of safety factor. "I believe that you could classify malfunction under vibration into two general categories—fatigue failure and electrical malfunction. I think that we are concerned with

both of these factors. For airplane usage over long periods of time perhaps fatigue is a more significant factor than in missiles and spacecraft work. In both cases we cannot tolerate electrical malfunction.

"To get rational about the situation in the case of fatigue you expect the equipment to have a certain life. It gets a little sticky when you must decide how you define your safety factor. Should it be a factor on the life itself? Should it be a factor on the stress level? When you get deeper into the question, you are faced with the fact that there is quite a bit of scatter in fatigue. I don't know that there is a real good answer to the question of what a safety factor should be. This is a field that we need to get into. We need to establish, as nearly as we can, what the actual environment is. Then we must set our safety factors on top of this in order to establish qualification tests."

Mr. Dreher, of Wright-Patterson AFB, wanted to go further into the field of safety factor. "The equipment manufacturers are concerned about all these factors of safety and I'd like now to put the discussion into this light. Let us presume that the raw data you have, either measured or predicted, is 100 percent correct. The next step is converting these data into a vibration test specification. The factor of safety, then, is going to involve a number of items. I will list just a few that I would like the panel and the audience to discuss.

"First, if you have measured data, what is the possibility that you have the worst flight? Perhaps these data are from a rather mild flight. Second, usually you only vibrate the item in a single axis when actually the equipment in the aircraft is being vibrated in all three directions. Another factor that we don't usually concern ourselves with is the effect of multi-resonances on causing stresses. We concern ourselves, perhaps, with one resonance, but what effect does another resonance have on this?

"A forth item with which we are concerned is data conversion. Suppose we have a random vibration. How does this random vibration affect the single-degree-of-freedom system, or multi-degree-of-freedom system which our equipment item is? Is it the background random that is giving us problems or is it the peaks, the spikes that come in, that are doing the damage? How do we take account of those factors?

"Finally, suppose you convert it to a sinusoidal test, how do you take nonlinearity into account. Also, how do you take account of the fact that this item is actually going to be exposed to, say 10^9 cycles when you are actually only going to test it for 10^5 cycles?"

Mr. New concluded the session by observing that Mr. Dreher's list of questions might well form the basis for the 34th Symposium.

* * *

Section 2

SHOCK DATA ANALYSIS

DIGITAL SHOCK SPECTRUM ANALYSIS BY RECURSIVE FILTERING

D. W. Lane
Lockheed Missiles and Space Company
Sunnyvale, California

An efficient method of digital shock spectrum analysis employs recursive filtering, a feedback technique which is readily developed using Z transform techniques. By this means, the accuracy, flexibility and production capability of the digital computer are made available without the sacrifice of excessive computer time.

INTRODUCTION

Transient analysis by means of standard shock spectrum calculations has been performed for many years on vibration data at Lockheed Missiles and Space Company, LMSC. Until recently, these calculations were performed by analog methods, passing the transients through a bank of second order analog filters, recording the output on oscillograms, picking off the peak response value of each, and plotting these versus the natural frequency of each filter. The filters simulated the following standard shock response function:

$$F(s) = \frac{\frac{s}{Q\omega} + 1}{\frac{s^2}{\omega^2} + \frac{s}{Q\omega} + 1}, \quad (1)$$

where s , ω , and Q are, respectively, the differential operator, natural radian frequency, and damping factor ($Q = 1/2\zeta$).

Since production high-speed sampling became available, efficient shock spectrum analysis has been performed primarily by digital computation using a technique referred to as recursive filtering. By this method each output point is calculated as a linear combination of one set of weights with the input points along with a linear combination of another set of weights with previous output points. The

result of this use of previous output points is that the number of weights, computer calculations, and, consequently, computer time and cost are minimized. The trick, of course, is to determine those weights which produce the desired system response.

The shock response recursive filter weights are readily calculated by Z transform techniques. Also, a method is available for efficient determination of response peak values which occur in between the sampling times. After these techniques are outlined, the virtues and limitations of digital shock spectrum analysis are then discussed, and applications are suggested which appear to be useful in the shock and vibration area.

DIGITAL SHOCK SPECTRUM ANALYSIS

By means of techniques which have been available for many years, digital shock spectrum analysis is made not only feasible but superior to the analog method. In 1953 it was shown that digital feedback filters, called recursive filters in this discussion, require a minimum number of calculations for a wide range of transformations.¹ Such filters have

¹J. T. Fleck and D. W. Fryer, "Exploration of Numerical Filtering Techniques," Cornell Aeronautical Laboratory, Inc., Report No. XA-869-P-1 (May 1, 1953).

been developed in many ways, but the handiest now seems to be by Z transform techniques, primarily because tables of such transforms are available. Reference 2, for example, includes a thorough treatment of most aspects of the subject, including mathematical techniques for determining Z transforms from Laplace transforms, tables of transform pairs, and various methods of application.

The digital approach is similar in overall technique to the analog method. Transient data is first filtered and the peak response point is then detected for each natural frequency employed. The transformation is made by the following calculation:

$$c(nT) = p_0 r(nT) + p_1 r[(n-1)T] - q_1 c[(n-1)T] - q_2 c[(n-2)T], \quad (2)$$

where

T = sampling increment,

$r(nT)$ = input at the n th point,

$c(nT)$ = output at the n th point, and

p_0, p_1, q_1, q_2 = constants which are designed to effect the desired response (Eq. (1)).

Of the several digital methods which would achieve the same response, Eq. (2) requires a minimum number of calculations and is suitable for the simulation operation required. It will be shown that the constants, p_0, p_1, q_1 , and q_2 can be calculated readily from the main control parameters, ω and Q so as to produce a close approximation to the desired response.

The peak detection operation could be performed by simple comparison if the peak values always occurred at the sampled times. This can be considered the case, however, only when the sampling rate is high relative to the natural frequency. For example, in order to achieve less than 1-percent difference between the peaks of a sampled and continuous function, the sampling rate would have to be more than 20 times greater than the highest significant frequency employed.

As it is generally desirable, or necessary, that the sampling rate be below some maximum value, it is of some importance to incorporate

a technique for extending the frequency range of peak detection relative to the sampling rate. With the recommended technique to be outlined, on the order of 1-percent accuracy is obtained for sampling rates which are as low as five times the highest significant frequency component. It will be obvious that this ratio could be reduced further if desired.

The frequency range of peak detection is extended by the following technique: first, the time increment within which the peak occurs is located; second, in that increment the peak is detected along a suitable interpolation function. The increment containing the peak is located by applying to the response points a simple integrating filter having suitable frequency response characteristics. The narrow band aspect of the response filter is relied on to place the peak value within the interval having the maximum integral. An interpolating function with suitable frequency response is then determined for the increment having the maximum integral. Finally, the peak value of this function is detected. One such point is calculated for the response of each filter employed, and the resultant shock spectrum is plotted on automatic plotters. The three techniques employed in calculating these spectra will be described in greater detail in the following paragraphs. These techniques are: recursive filtering, incremental integration, and interpolation.

RECURSIVE FILTER DEVELOPMENT

The Laplace transform of a continuous system, $G(s)$, could be converted to the Laplace transform of the sampled version of that system, $G^*(s)$, by the following formula:²

$$G^*(s) \triangleq \mathcal{L} \left[g(t) \sum_{n=0}^{\infty} \delta(t - nT) \right] \\ = \frac{1}{T} \sum_{n=-\infty}^{\infty} G \left(s + j \frac{2\pi n}{T} \right) + \frac{1}{2} g(0^+), \quad (3)$$

where $g(0^+)$ is the initial value of the impulse response of the continuous system, and δ is the unit impulse. The response of the sampled system is thus essentially an infinite sum of translations of the continuous system, shifted in the imaginary direction by multiples of the sampling rate.

There are two well-known aspects of Eq. (3) which will be confirmed further on by evaluation of actual filters. First, if the sampling rate is greater than twice the highest frequency

²E. I. Jury, "Sampled Data Control Systems" (John Wiley and Sons, Inc., New York, 1958).

component in the impulse response, $g(t)$, of the system, then the shifted responses will not overlap. The result of the sampling is then merely that a periodic form of the response of the continuous system is produced. Although response functions of continuous systems are not strictly band limited, generally they are effectively so at some finite frequency relative to the error which is allowable in each case.

The second important aspect of Eq. (3) is that when the band limiting conditions described above are obtained, the prime difference between the responses of the sampled and continuous systems is the gain factor $1/T$. Then over the region, $|\omega| < \pi/T$, the following approximation is obtained:

$$T \times G^*(s) \approx G(s) + \frac{T}{2} g(0^+). \quad (4)$$

For many response functions, including those under discussion, the last term of Eq. (4) is negligible.

The infinite summation required by Eq. (3) is generally cumbersome to evaluate. Therefore, another formula is generally employed for conversion of a response function from the continuous to sampled system as follows:²

$$\begin{aligned} G^*(s) &\triangleq \mathcal{L} \left[g(t) \sum_{n=0}^{\infty} \delta(t + nT) \right] \\ &= \sum_{k=1}^K \frac{A(s_k)}{B'(s_k)} \frac{1}{1 - e^{-sT} e^{s_k T}}, \end{aligned} \quad (5)$$

where

$$\frac{A(s)}{B(s)} = G(s),$$

$$B'(s) = \frac{dB(s)}{ds},$$

and

$$s_k = k\text{th (simple) root of } B(s).$$

Applying Eq. (5) to the response function $F(s)$ defined by Eq. (1), and multiplying by T to correct for the gain difference indicated by Eq. (4), the following response function is produced:

$$T \times F^*(s) = \frac{P_0 + P_1 e^{-sT}}{1 + q_1 e^{-sT} + q_2 e^{-2sT}}, \quad (6)$$

where

$$P_0 = \frac{\omega T}{Q},$$

$$\begin{aligned} P_1 &= \frac{\omega T}{Q} e^{-\omega T/2Q} \left\{ \frac{(2Q^2 - 1)}{\sqrt{4Q^2 - 1}} \sin \left[\frac{\omega T}{2Q} \sqrt{4Q^2 - 1} \right] \right. \\ &\quad \left. - \cos \left[\frac{\omega T}{2Q} \sqrt{4Q^2 - 1} \right] \right\}, \end{aligned}$$

$$q_1 = -2 e^{-\omega T/2Q} \cos \left[\frac{\omega T}{2Q} \sqrt{4Q^2 - 1} \right],$$

and

$$q_2 = e^{-\omega T/Q}.$$

Since the operator s always appears as an exponential term in transforms of sampled systems, such transforms are generally written as functions of Z , where $Z = e^{sT}$. Equation (6) thus becomes:

$$T \times F^*(Z) = \frac{P_0 + P_1 Z^{-1}}{1 + q_1 Z^{-1} + q_2 Z^{-2}}. \quad (7)$$

This is the form that is presented in tables of Z transforms. The validity of the digital approach can be evaluated in a standard manner by substituting $i\omega$ for s in Eq. (6) and evaluating gain and phase response over the frequency interval of interest. This frequency response is presented in Fig. 1 for a Q value of 10 and several ratios of natural frequency to sampling rate. Good agreement appears between the responses of the sampled and continuous systems, where the natural frequency is as high as $1/5$ the sampling rate. It is interesting to note that the deviation is imperceptible in the sensitive area of high gain. In the other areas it is noted that as the ratio of natural frequency to sampling rate is increased, so is the deviation increased. This is consistent with Eq. (3).

The errors indicated in Fig. 1 are not due to the recursive filter mode of application but are the effects of operating with the sampled system. The desired response function is not precisely band limited to $1/2$ the sampling rate. These errors could be reduced if necessary by the addition of a simple low-pass recursive filter.

The transformation formulated by Eqs. (6) and (7) can be applied by several programming

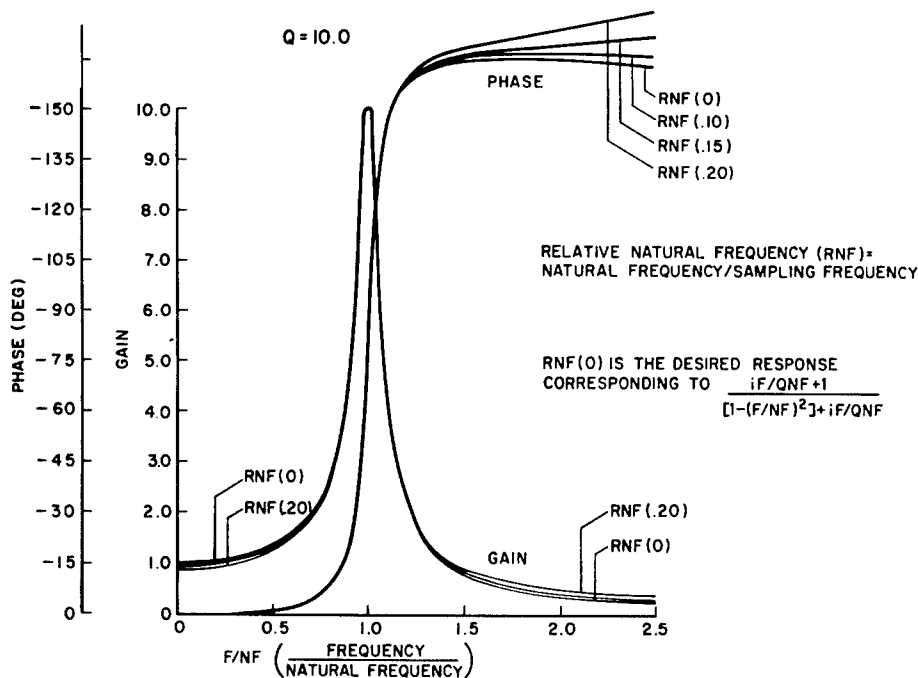


Fig. 1 - Frequency response of digital shock response filters

techniques operating in the sampled time domain as demonstrated in Ref. 2. The method which minimizes the number of calculations is formulated by Eq. (2). The constants p_o , p_i , q_1 , and q_2 are the same as those of Eqs. (6) and (7).

The recurrence operation, which repeatedly makes use of previous output values, requires initial conditions. It is, therefore, important that the calculation be initiated prior to the beginning of the transient in order that the value of the previous input and output points, $r[(-1)T]$, $c[(-1)T]$, and $c[(-2)T]$, may be assumed to be zero. Otherwise, some special calculation would be required to initiate the operation.

One of the prime virtues of the method described is the directness with which the constants are determined and applied. In feedback terminology, a P transformation is made on the input data, and a Q transformation is made in the feedback path on the output data, no transformation being made in the forward path. Equation (2) may thus be interpreted as combining these operations as outlined below:

Modified Input Data,

$$r'(nT) = p_o r(nT) + p_i r[(n-1)T]; \quad (8)$$

Backward Path Modified Output,

$$c'(nT) = q_1 c[(n-1)T] + q_2 c[(n-2)T]; \quad (9)$$

Error "Signal,"

$$\epsilon(nT) = r'(nT) - c'(nT); \quad (10)$$

and

Output,

$$\begin{aligned} c(nT) &= \epsilon(nT) \\ &= p_o r(nT) + p_i r[(n-1)T] \\ &\quad - q_1 c[(n-1)T] - q_2 c[(n-2)T]. \end{aligned} \quad (11)$$

PEAK DETECTION

As indicated above, detection of the peak value of the response is performed in two operations: First, the time increment containing the greatest integral is detected, and then the peak interpolated value within that increment is detected. The aim in each case is to employ a technique which has suitable frequency response characteristics and requires a minimum number of calculations.

An integration technique, which satisfies both the efficiency and accuracy requirements,

consists of applying a numerical integrating filter as follows:

$$i(nT) = \sum_{k=-3}^2 w(k) c[(n+k)T], \quad (12)$$

where

$i(nT)$ = estimate of the integral between $c[(n-1)T]$ and $c(nT)$ and

$w(k)$ = k th weight.

It was found that application of just six weights provides sufficient frequency response, if the weights are determined so as to produce the equivalent to the integral along a 5th-degree polynomial, which is fit through six adjacent points, where the integral is taken over the central increment. The frequency response of this filter is found to be within 1 percent of perfect integration up to frequencies which are $1/5$ the sampling rate. Figure 2 presents this frequency response as the ratio of gain obtained to the gain of perfect integration versus the ratio of frequency to sampling rate. For comparison, Fig. 2 also presents the frequency response of a four-point integrating filter which produces the integral along a 3rd-degree polynomial over the central increment.

The weights of the integrating filter can be determined directly by using the Lagrangian

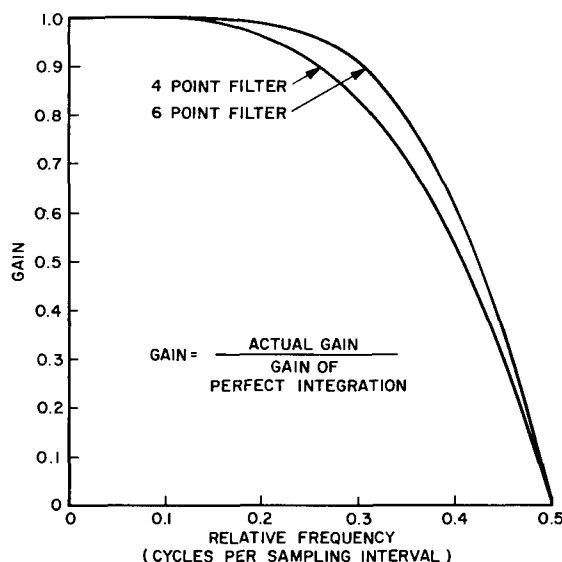


Fig. 2 - Integration filter response

method for polynomial interpolation.³ Each Lagrangian multiplier may be integrated over the central increment to produce a corresponding integration weight as follows:

$$w(k) =$$

$$\int_{-T}^0 \frac{[kT - kT] [(t + 3T)(t + 2T) \cdots (t - T)(t - 2T)]}{[t - kT] [(kT + 3T)(kT + 2T) \cdots (kT - T)(kT - 2T)]} dt. \quad (13)$$

Standard polynomial fitting satisfies the accuracy and efficiency requirements of the interpolation operation which is necessary for peak detection. The 7th-degree polynomial, which is fit through eight consecutive points, provides satisfactory frequency response when the interpolation is restricted to the central time increment. Thus, the peak detection operation begins with calculating the coefficients of the 7th-degree polynomial fit for the eight points which contain the increment having the maximum integral as the central increment. The peak value of that polynomial is then detected within that time increment.

Figure 3 presents the frequency response of the recommended interpolation technique. One complicating factor is that the response of approximation interpolation techniques depends on the time at which interpolation is made relative to the time of the sampled sequence. Consequently, a family of curves is presented, one for each $1/10$ th segment across the increment of interpolation. This family of gain and phase curves shows that the technique provides 1-percent accuracy relative to perfect interpolation up to frequencies greater than $1/5$ th the sampling rate. The parameter ρ signifies the time at which interpolation is made, relative to the beginning and end of the central time increment. Response curves for values of ρ up to 0.5 are indicated in that figure. Because of the symmetry of the fit, the magnitudes of gain and phase are the same for $\rho = 0.5 \pm \Delta\rho$. Only the sign of the phase response is different for these pairs of values. This evaluation, of course, is precisely valid only for sampled functions which are equally spaced in time.

Frequency response of the polynomial interpolation technique was calculated by taking the Fourier transform of the digital impulse

³ L. J. Briggs and A. N. Lowan, "Tables of Lagrangian Interpolation Coefficients" (Columbia University Press, New York, 1944).

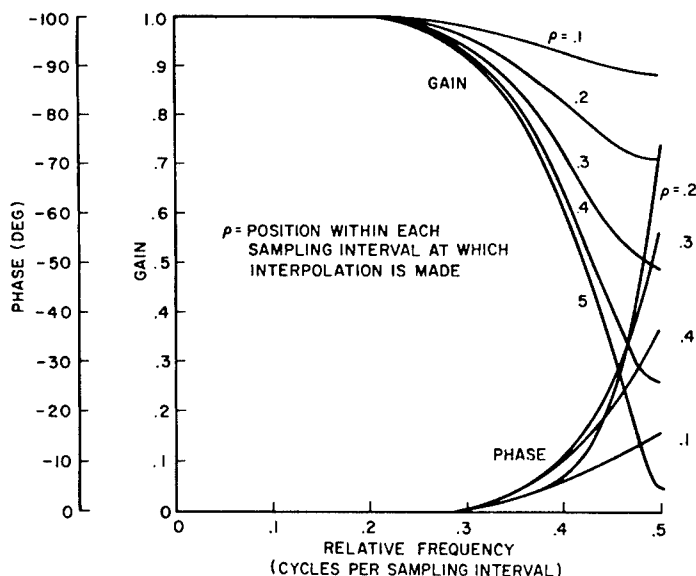


Fig. 3 - Frequency response of eight-point 7th-degree polynomial interpolation

response of the technique for each of the several interpolation points evaluated. First, the set of eight weights was calculated which, if applied to eight consecutive input points, would produce the interpolated point desired. The Lagrangian multiplier technique facilitates this calculation. Each set of weights can be considered to be the impulse response for 7th-degree polynomial interpolation, through eight points, in the central increment, at the point ρ . The standard Fourier transform of each impulse response was then calculated as follows:

$$G(\omega) e^{j\Phi(\omega)} = \sum_{k=-3}^2 w_{\rho}(kT) e^{j\omega Tk} \quad (14)$$

Equation (14) was also used to calculate actual response of the integration filter, described above.

PRODUCTION SHOCK SPECTRUM ANALYSIS

The Shock Spectrum Digital Computer Program, developed at LMSC, is presently employed in the production processing of missile and satellite systems data. The program operates on data which has been digitized at any sample rate. At preselected times it calculates shock spectra consisting of any specified number of natural frequency points over any specified frequency interval. The spectra are recorded on digital tapes for input to automatic plotters.

Less than 0.5 minute of computer time is required for the calculation portion of 150 resonant filters applied to 0.1 second of data which has been sampled at 10,000 samples per second. The analog method consisted of passing the data three times through a bank of 2nd-order filters to produce a 21-point spectrum. Approximately 3 minutes of computer time is required for each complete analysis run including computer setup, input tape search, and output preparation. The frequency range covered in these shock spectra is generally 2000-cps. Figure 4 presents a typical shock spectrum with the special labelling and grid lines removed.

The speed, flexibility, and operational simplicity of the LMSC shock spectrum program have provided economical and quick-turn-around production processing as required for missile and space shock data. The program is presently being modified to correct for dynamic response characteristics of the measurement system on which each data input has been monitored. Further realization of the flexibility of the digital approach will soon be gained with automatic comparison and summary updating of shock spectra over each test series as the testing proceeds.

LIMITATIONS

Several aspects of digital shock spectrum analysis should be considered in the evaluation of this mode relative to the following items:

capability of a particular installation, character of the data to be analyzed, and extent of analysis requirements. First, the installation should have a digital computer and also a high-speed analog-to-digital converter, unless the raw data is in digital form. Then the usual considerations of digital processing must be balanced. These include calculation speed and storage capacity of the computer, sampling rate capability, roll-off characteristics of the low-pass filter which generally must precede sampling, the frequency range, desired accuracy, and production requirements.

Several characteristics of the input data must be considered. First, if there may be signal dropout intervals in the areas of the transients to be analyzed, the value of the digital approach depends on how accurately and easily precise timing control is applied. If precise timing control is available, dropout areas can be avoided and accurate shock spectra obtained in many cases only by the digital method. On the other hand, an analog method, which employs manual selection of peaks, allows for the avoidance of certain signal dropout intervals, when this is possible, without precise time control.

Another important characteristic of the input data is the low-frequency content. Some form of elimination of invalid low-frequency components is generally necessary. When the peak values are detected manually, a form of high-pass filtering is easily, and often unconsciously, performed. With the digital method, however, any form of invalid bias must be extracted. Otherwise, the output of the response filter may be as much a function of an invalid step transient as of the transient to be analyzed. Of the various possible remedies to this situation, the simplest one is to have the computer determine the level of the input data just prior to the transient and subtract that bias from the subsequent data. This has been successful with LMSC data primarily due to the fact that time intervals of the transients analyzed are short relative to variations of the erroneous bias. When this is not the case, high-pass filtering should be employed, by either analog or digital methods, to remove the invalid low-frequency components.

Reliability of the digitizing operation must also be considered, because wild points introduced by the digitization process would cause the calculated spectrum to be invalid. If such

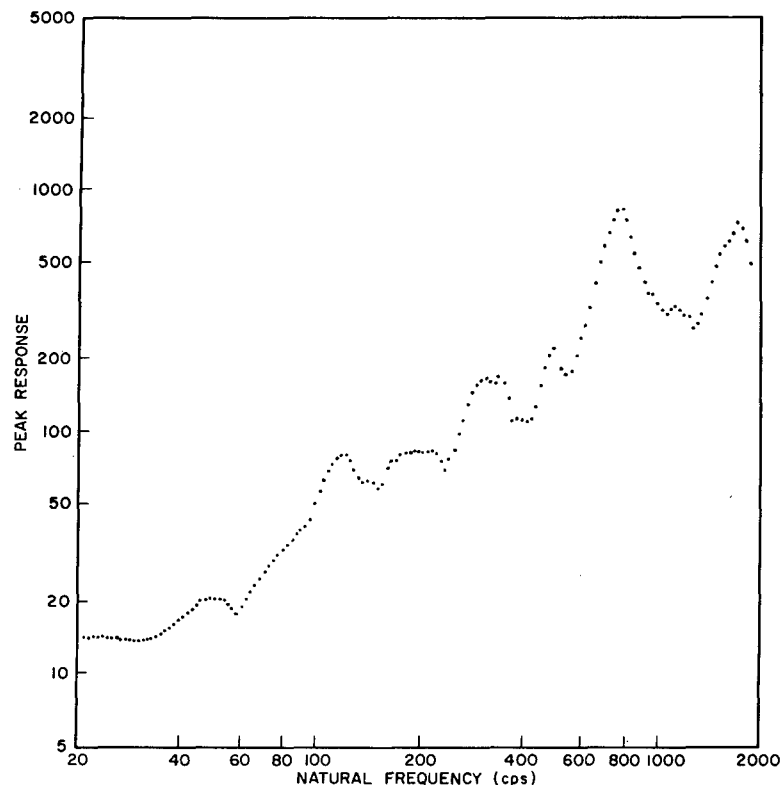


Fig. 4 - Typical digital shock spectrum

wild points were to continue to be a major problem, an automatic detection and correction technique would have to be included in the analysis program. At LMSC, this was a problem only during the checkout stage of the high-speed digitization equipment. The natural solution, which is presently employed, is to rely on maintenance and checking procedures to minimize the number of wild points. This is backed up with automatic detection and correction of extremely wild points, and display of the input data along with the analyzed spectrum to facilitate after-the-fact visual evaluation. The last item is feasible primarily due to the relatively short time intervals of the transients to be analyzed.

The peak detection method described also should be backed up with at least one simple evaluation tool; a list output of the times of each peak response detected. These times are needed to confirm the few cases where the peak detection is apparently not foolproof. Single wild points occur in the final spectrum. These are readily detected during the routine certification of each spectrum, but the time list is helpful in confirming the error, the appearance of which indicates that further development on the peak detection operation is desirable.

To summarize the items of caution noted above, the usual digital processing problems should be expected to occur, but with special effects on spectral analysis. Generally there are simple solutions to these problems, but it is important that they be considered carefully at the initial design stage. Digital programs should be constructed so as to allow for speedy incorporation of new solutions and extensions, a recommendation that appears to have general application.

EXTENSIONS

Recursive filtering has been found to be such a powerful tool in large-scale production analysis that other applications, which could readily be applied, are worth suggesting. It is observed, that the response filtering operation is a form of band-pass separation with a bank of filters. Only minor changes and additions to the constants employed in Eq. (2) would be required to make the operation a true band-pass calculation. Equation (5) shows that any realizable response expressed as a Laplace transform can be converted readily to an extremely efficient recursive filter. In fact, deviations of the response of a sampled band-pass system from the continuous system would be much less than those of the shock response. The latter

deviations are due to the relatively slow roll-off characteristics of the frequency response form of the shock transform defined by Eq. (1).

One important application of a bank of digital recursive filters would be the automatic operation of editing digital data. For example, a relatively few such filters could be applied to cover the frequency range of digital vibration data. Each filter output would be squared and filtered by a simple recursive low-pass filter. These mean square functions would provide a coarse time history type of frequency analysis. This would provide not only a standard quick-look summary, but could also be used to trigger automatic editing of the data prior to detailed analysis. Thus, the time consuming operation of detailed frequency analysis could then be made only over frequency intervals as well as time intervals which contain significant information.

Narrow-band time-history frequency analysis over intervals of interest is also feasible by means of recursive band-pass filtering. The only difference between this type of analysis and the coarse analysis outlined above, is in the number and bandwidth of the filters. This analysis is generally considered valuable when nonstationarity of the data is either significant or in question. The flexibility aspect of digital computation would be especially important in this application. The control required would be as simple as that of the LMSC Digital Shock Spectrum Analysis Program. Input control required for definition of the response filters includes only the following parameters: damping factor (Q), low frequency of the spectrum, high frequency of the spectrum, and the number of natural frequencies desired between the low and high frequencies.

The simulation operation performed by the shock response calculation is of a very simple nature, relative to the wide-range of simulations that can be obtained by recursive techniques. Ironically, there are many cases in which an analog generated by the digital computer is more readily derived than that analogue generated by electrical methods. The main reason for this seems to be that numbers and formulae are employed in the place of amplifiers, capacitors, and the like. The digital application, even though it is of discrete form, more nearly approximates the mathematical model itself, if suitable band limiting is maintained, than does the analogue approach which employs an electrical application of the mathematical model. It is also important to note that the type of recursive filter employed by standard shock analysis (Eq. (2)) is optimum only

for simulation of systems which are already defined. In Ref. 2, this is called the direct programming method. It is also shown in Ref. 2 how cascade and parallel programming are more suitable to transformations which are at least partially developed by trial and error. Thus, a wide range of simulation calculations can be made by these techniques.

Digital calculation also makes possible production application of improved shock analysis. For example, it would be a simple addition to calculate and present parameters such as

the following: density distribution of each response function, density distribution of the peaks of each response function, moments of these distributions, total time over which a specified level is exceeded by each response function, and so on.

In summation, the recursive filter technique has not only been found to provide efficient and accurate shock spectrum analysis of the standard type, but should continue to have other useful applications in the analysis of environmental data.

* * *

AN ANALOG COMPUTER TECHNIQUE FOR OBTAINING SHOCK SPECTRA

J. J. Marous and E. H. Schell
Aeronautical Systems Division
Wright-Patterson Air Force Base, Ohio

A unique method of computing the shock spectra of transient motions on an analog computer has been developed by the Flight Dynamics Laboratory in cooperation with the Directorate of Systems Dynamic Analysis of the Air Force Research and Technology Division. The uniqueness of the method is largely due to controlling the output voltages in such a manner that a direct graphical plot of the shock spectrum is recorded on a strip chart recorder. Another feature is the use of punched tape programming for making automatic frequency and gain changes.

INTRODUCTION

Twenty years ago, M. A. Biot^{1,2} introduced a technique for describing earthquake motions in terms of the maximum response of a simple single-degree-of-freedom system to that motion. The maximum responses of these systems to an input motion can be readily calculated. If the frequency of the simple system is varied over a range of interest (e.g., 0 to 1000 cps) maximum response data for a large number of frequencies can be calculated. Each maximum response calculation (acceleration, velocity, or displacement) and the frequency (cycles or radians per second) for which it is calculated provides the ordinate and abscissa of a data point. These points can then be plotted and connected to each other to form a continuous curve of response versus frequency. Such a plot is known as a "response spectrum" or, more generally, a "shock spectrum." This should not be confused with the Fourier spectrum of a shock which is an entirely different method of reducing shock data to the frequency domain and is not considered here.

The shock spectrum is useful mainly because it gives an indication of the damage

potential of a shock.³ For example, the responses of an equipment which can be assumed to consist of simple uncoupled linear elements of certain natural frequencies can be determined directly by observing the responses in the shock spectrum. Knowledge of the responses tells whether or not the equipment will be damaged. Also, if an equipment is subjected to two or more shocks and a failure occurs in some element of the equipment, examination of the shock spectra of these shocks at the natural frequency of the failing element can indicate which shock is responsible for the failure. This information could not be directly obtained from the time history of the shocks.

The shock spectra might be used in three different ways to overcome this failure. Knowing from the spectrum which shock motion produced the failure, it may be possible to eliminate the source or to isolate it. A further examination of the spectra may indicate certain frequencies common to all the shock motions which act upon the equipment where the response would be low enough to preclude damage. It may then be possible to redesign the element so that its natural frequency coincides with one of these frequencies.

The shock spectrum may also be used as a means of classifying shocks. For example,

¹M. A. Biot, "A Mechanical Analyzer for the Prediction of Earthquake Stresses," *Bull. Seismological Soc. Am.*, 31:151 (1941).

²M. A. Biot, "Analytical and Experimental Methods in Engineering Seismology," *Trans. Am. Soc. Civil Eng.*, 108:365 (1943).

³J. P. Walsh and R. E. Blake, "The Equivalent Static Accelerations of Shock Motions," *NRL Report No. F-3302* (June 21, 1948).

time histories of certain ground motions due to nuclear blasts may bear little resemblance to each other. The shock spectra of these motions, however, resemble each other to such an extent that the shocks can be classified as being in the same category.

In view of the foregoing advantages of the shock spectrum method of studying and interpreting shock phenomena, a unique technique was developed. This capability for analysis has already been of use in studying the variability of MIL-STD-810 shock pulses and in analyzing the responses of equipments located in the X-20 glider when excited by thruster transients. It will also be of use in the future in research studies aimed at understanding the influence of various shock parameters on the failure of equipments. The technique can also be useful in categorizing the shock environment. Control techniques for the shock environment can be studied using this tool. Shock-resistant designs can be created based on the shock spectra. The technique can also be used for several other purposes and in general, it provides a powerful analytical tool for understanding shock motions.

PROBLEM SOLUTION

Several different ways of reducing the data to a shock spectrum are possible and the method should be chosen in accordance with the application of the data. Perhaps the most commonly used spectrum is the maximax spectrum or the spectrum of maximum positive responses attained at any time during the response. Another spectrum of interest may be the spectrum of maximum negative responses. Other spectra are obtained by measuring the maximum responses attained during the shock motion and those attained after the motion is over. The first is termed the primary, initial, or during spectrum, and the latter is termed the residual or after spectrum. Relative response spectra which are useful in determining the maximum strains are also possible. All of these foregoing spectra may be computed with various amounts of damping to form a family of shock spectra for damped systems. The usual practice, however, is to compute the undamped spectra. These provide conservative estimates of the responses of lightly damped systems.

The system simulated is shown in Fig. 1, and the differential equation of motion derived from Newton's second law is as follows:

$$M\ddot{x} + C(\dot{x} - \dot{u}) + K(x - u) = 0,$$

where x is the displacement of the mass at any time (t); u is the displacement of the base at

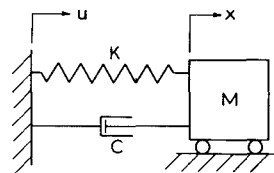


Fig. 1 - Simple system

any time (t); M is the mass; C is the viscous damping coefficient; and K is the stiffness.

Let the relative displacement at any time be: $y = x - u$. Then,

$$M\ddot{y} + C\dot{y} + Ky = -M\ddot{u}$$

and

$$\frac{\ddot{y}}{\omega_n^2} + \frac{2\zeta\dot{y}}{\omega_n} + y = \frac{-\ddot{u}}{\omega_n^2},$$

where ζ is the fraction of critical damping and ω_n is the angular undamped natural frequency. Expressions have also been derived for an excitation force acting on the mass and for displacement, velocity, acceleration, and so forth, acting on the system ground.⁴ Any of these can be expressed in terms of a generalized response (R) and a generalized excitation (E) as follows:

$$\frac{\ddot{R}}{\omega_n^2} + \frac{2\zeta\dot{R}}{\omega_n} + R = E.$$

The generalized form is developed by R. S. Ayre.⁴ Pertinent to this discussion is the table (shown on top of following page) which has been extracted from Ayre's work.

A block diagram of the technique is shown in Fig. 2. The time history of the forcing function (E) is fed into the simulated system. The system is simulated in accord with the generalized equation, and two integrations are performed to determine the generalized response time history (R).

The time history of the response is fed directly to two maximum value memory circuits.

⁴R. S. Ayre, "Transient Response to Step and Pulse Functions," Chapter 8 of "Shock and Vibration Handbook," C. M. Harris and C. E. Crede, Editors (McGraw-Hill Book Co., Inc., New York, 1961).

Alternate Forms of Excitation and Undamped Response*

Excitation (E)		Response (R)	
Force	$F(t)/k$	Absolute displacement	x
Ground displacement	$u(t)$	Absolute displacement	x
Ground acceleration	$-\ddot{u}(t)/\omega_n^2$	Relative displacement	y
Ground acceleration	$\ddot{u}(t)$	Absolute acceleration	\ddot{x}
Ground velocity	$\dot{u}(t)$	Absolute velocity	\dot{x}
nth derivative of ground displacement	$d^n u(t)/dt^n$	nth derivative of absolute displacement	$d^n x/dt^n$

*See corresponding table for damped response on page 194.

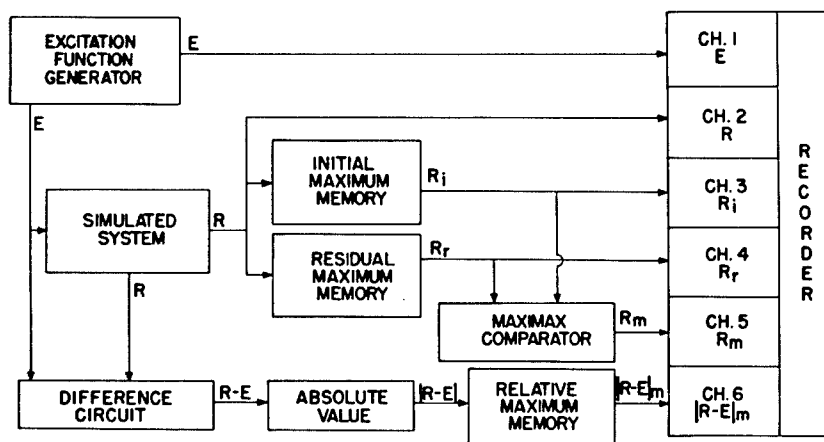


Fig. 2 - Block diagram

One of these circuits operates during the transient input function (E) and holds the maximum response (R_i) which occurs during the pulse. The other is turned on at the instant the pulse is over and holds the maximum positive residual value (R_r) of the response. These values are held until the computation is stopped for each frequency.

The preceding values (R_i) and (R_r) are directed into a third channel where they are compared to determine the maximum of the two responses. This gives us the maximum response (R_m) regardless of whether it occurs in the initial or residual portion of the spectrum.

Concurrently, the response time history (R) is directed into a fourth computation channel where the excitation time history (E) is subtracted from it to provide a relative response time history. The absolute maximum $|R-E|_m$

of this operation is memorized in a third maximum value memory circuit.

The excitation function (E) and the response time history (R) are recorded on channels 1 and 2, respectively. The initial maximum response (R_i), the residual maximum positive response (R_r), the maximax response (R_m), and the maximum relative response $|R-E|_m$ are recorded on channels 3, 4, 5, and 6, respectively. Actual recordings are shown in Figs. 3 through 11, inclusive.

COMPUTER SIMULATION

The simulation was performed on the System Dynamics Simulator, a large scale general purpose analog computer located at Wright-Patterson Air Force Base.

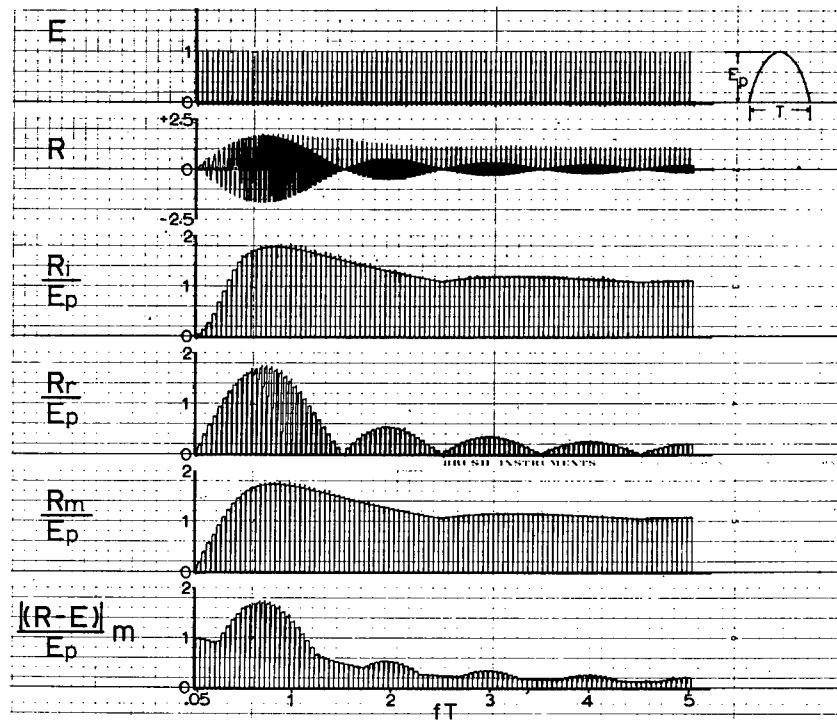


Fig. 3 - Half-sine response spectra, $\zeta = 0$

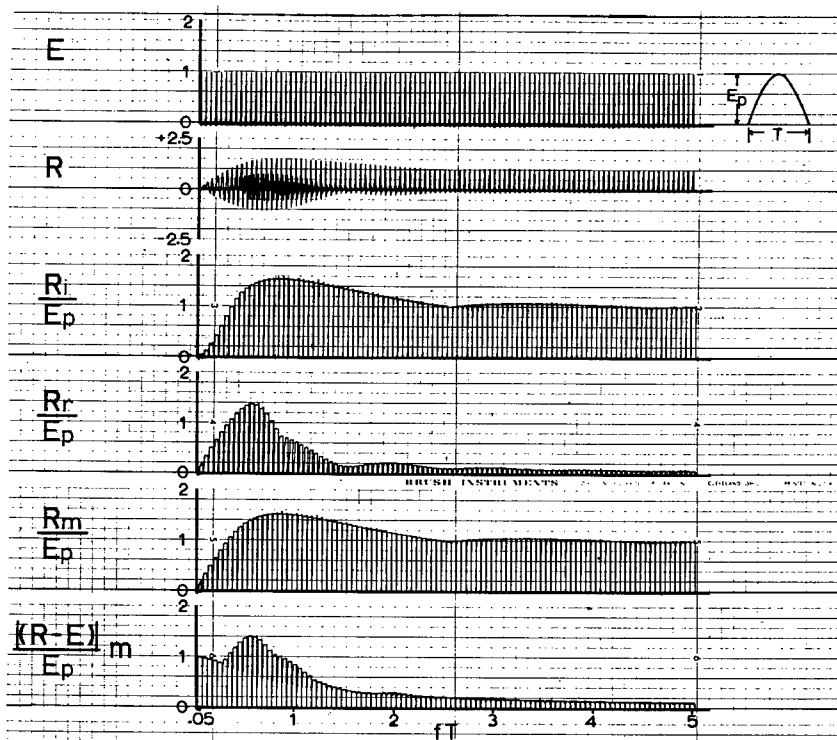


Fig. 4 - Half-sine response spectra, $\zeta = 0.1$

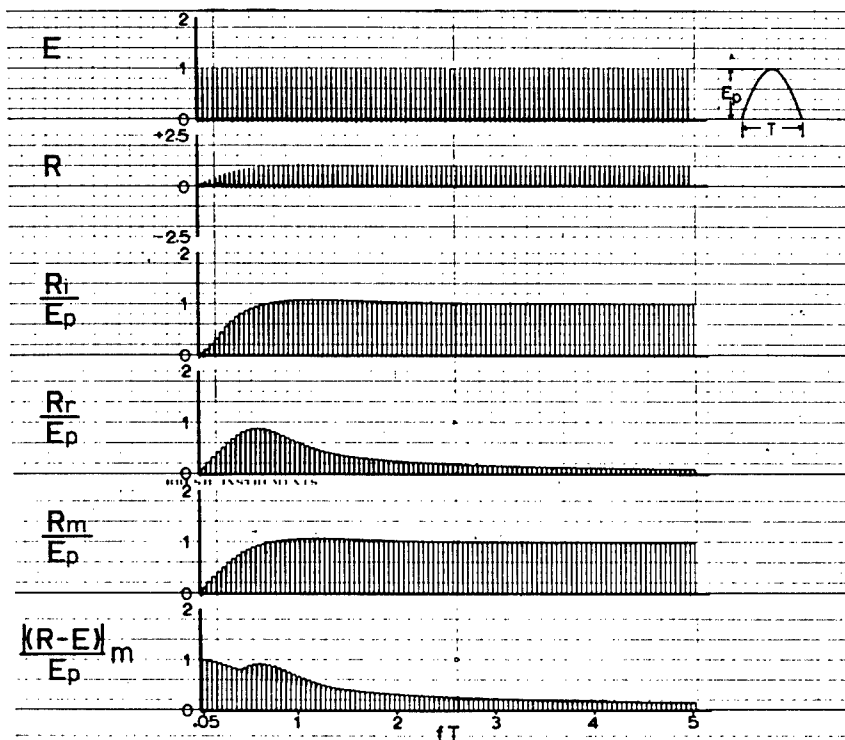


Fig. 5 - Half-sine response spectra, $\zeta = 0.5$

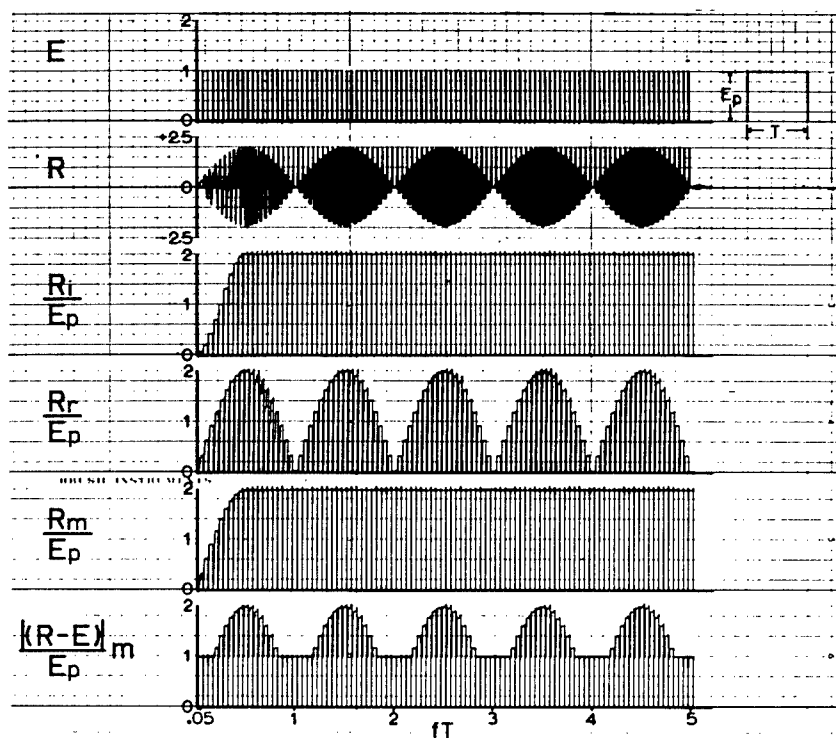


Fig. 6 - Square wave response spectra, $\zeta = 0$

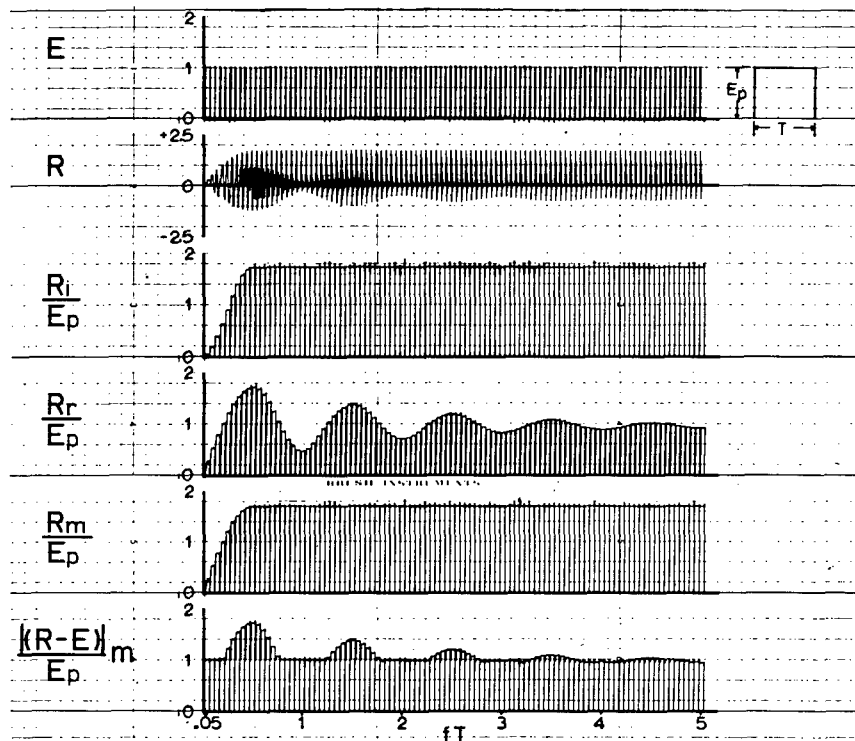


Fig. 7 - Square wave response spectra, $\zeta = 0.1$

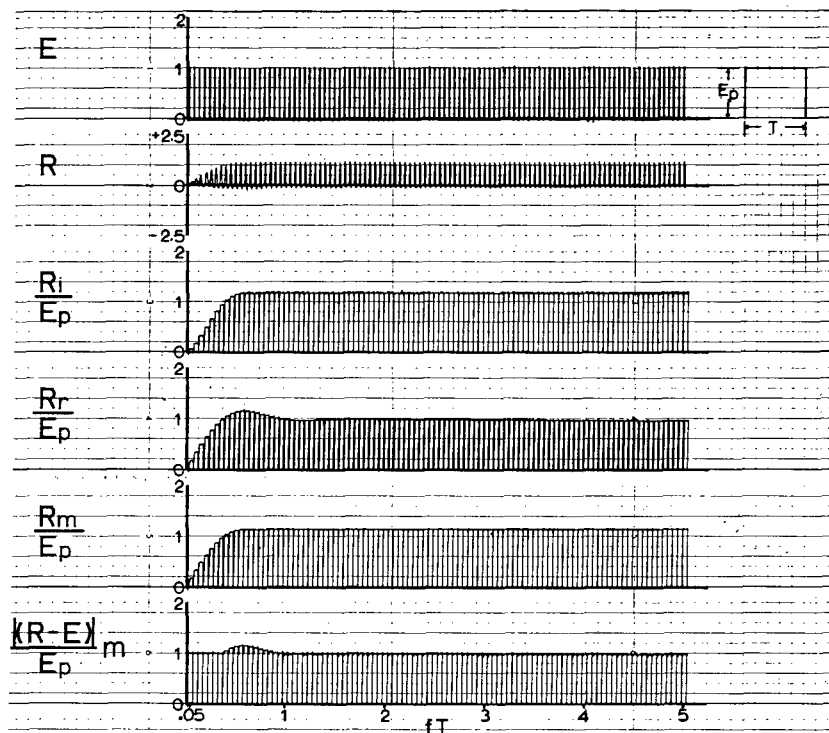


Fig. 8 - Square wave response spectra, $\zeta = 0.5$

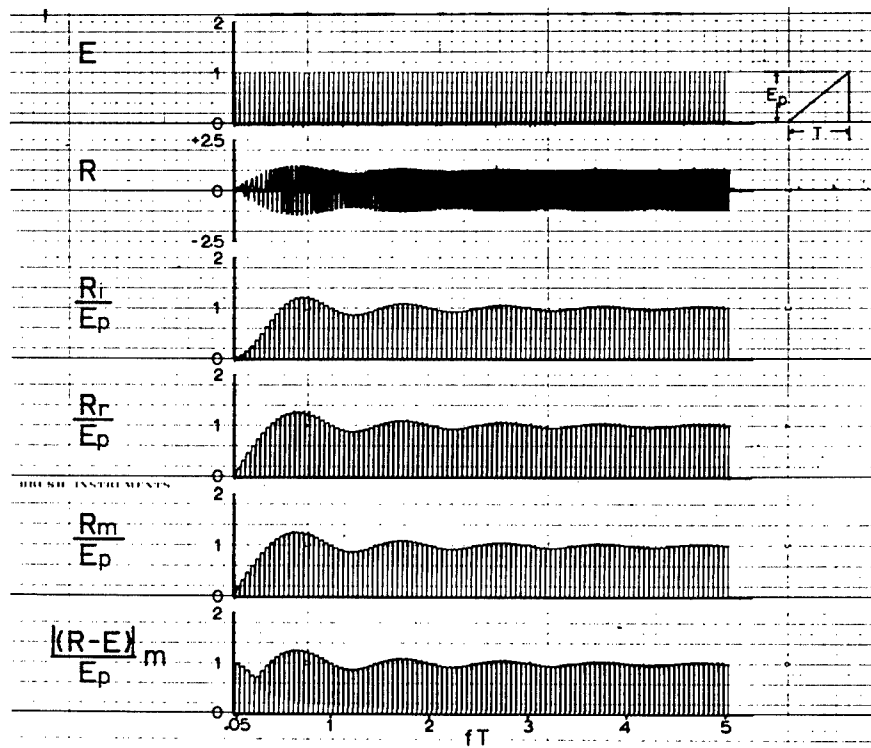


Fig. 9 - Sawtooth response spectra, $\zeta = 0$

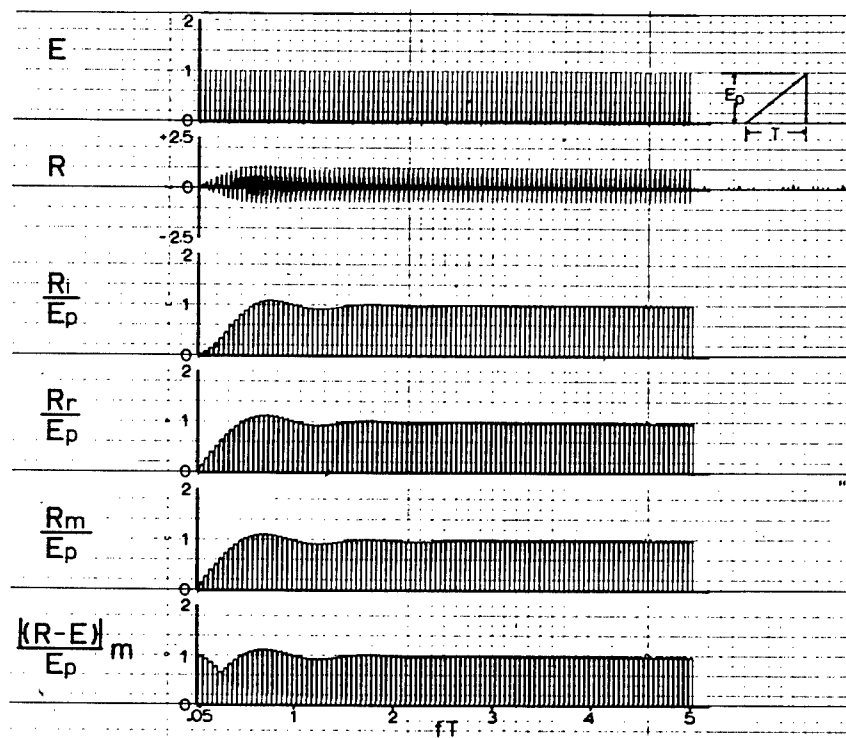


Fig. 10 - Sawtooth response spectra, $\zeta = 0.1$

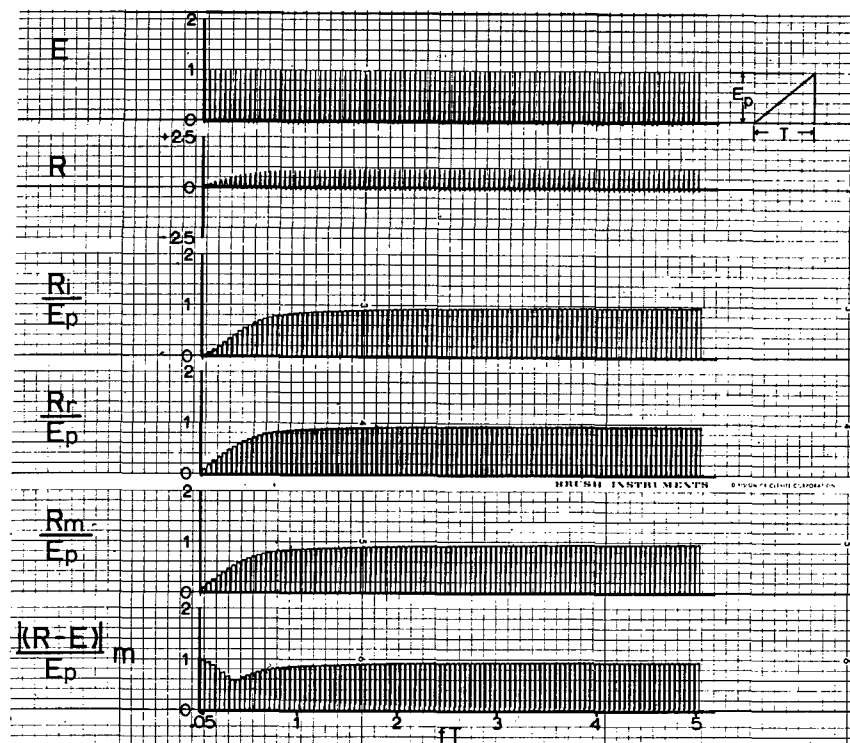


Fig. 11 - Sawtooth response spectra, $\zeta = 0.5$

Although the basic problem itself was very simple, it did present some interesting simulation challenges. One of these arose from the fact that the simple mass, spring, damper system was to be investigated over a range of frequencies too large to permit a single choice of input gains on the amplifiers used to solve the system equation

$$\frac{\ddot{R}}{\omega_n^2} + \frac{2\zeta}{\omega_n} \dot{R} + R = E.$$

The gain changes required to cover the desired frequency range would not pose any difficulty if the problem were to be run in the normal fashion, that is, manually setting in the conditions before each computer run. In this problem, however, many runs were required for each excitation signal with frequency along being changed from run to run. To facilitate the running of such problems the System Dynamics Simulator has a special feature known as autoprogram. It should be pointed out, however, that while the autoprogram feature is desirable it is not necessary in making use of the techniques presented in this paper.

In order to make use of the autoprogrammer, the computer setup must be accomplished in such a manner that the required gain changes

can be made automatically. Two relays whose positions determine the gains of the two integrators used in solving the system equation are used to fulfill this requirement.

The autoprogramming mode of the computer was designed to permit automatic running of a problem. If the problem to be run can be preprogrammed, that is, if the parameter changes to be made are known beforehand, it is possible to use the autoprogram feature.

In order to use the autoprogrammer a criterion for ending the run must be made available. A differential relay is used to sense the occurrence of this criteria and the contacts of this relay should switch +26 volts to the Y line, which places the computer in HOLD, and short the two patchboard holes labeled AP-1 and AP-2 when this criteria is satisfied.

When the computer is in autoprogramming mode it is controlled from a punched paper tape reader. Therefore, it is necessary to prepare an instruction tape. Any of the following operations may be commanded from the tape:

1. Read any amplifier.
2. Set or read any servo set potentiometer.

3. Place the computer into any of its modes. these are:

- a. HOLD (hd)
- b. OPERATE (op)
- c. RESET (re)
- d. BALANCE CHECK (bc). This mode

is often referred to as the pot set mode on many analog computers.

The sequence of events for the tape used in this problem is as follows:

1. The computer is placed in BALANCE CHECK.
2. Potentiometers 10, 11, and 12 or 13 when required are set.
3. A verification that this was obtained correctly is typed on the typewriter next to the command.
4. The computer is placed in RESET.
5. After a brief time delay the computer is placed in OPERATE.
6. The computer remains in OPERATE until the previously described differential relay, which in this problem positions as a function of time, throws it into HOLD, and at the same time instructs the tape reader to look for the next command.
7. This command is a series of amplifier readouts that correspond to the maximum values obtained by R_i/E_p , R_r/E_p , R_m/E_p , and $|(R-E)|_m/E_p$ during the run.
8. The computer is returned to BALANCE CHECK and the whole process repeated as many times as desired.

In this study τ , the duration of the excitation pulses, was 0.005 sec so the system frequency was taken up to 1000 cps to provide a range of

rr up to 5. The frequency was changed in increments of 10 cps thus requiring 100 runs to cover the desired frequency range. By placing these 100 runs on an instruction tape and using the autoprogrammer, the computer could be left unattended while it made the 100 desired runs. The entire process required approximately 90 minutes.

To obtain the rather unique readout of the desired response spectra a Brush Mark 200 strip chart recorder was used. This is an eight-channel rectilinear recorder with a paper speed range of 0.05 mm/sec to 200 mm/sec. By properly adjusting the paper speed to compensate for different computer run times the same paper displacement can be maintained for each of the 100 runs.

The reason different computer run times were required is that for the lower system frequencies the runs were made longer to assure that the desired maximum values were achieved by the system while for higher system frequencies less running time was required. If the paper speed is slow enough, the result appears as a nearly rectangular vertical bar. In this problem each computer run corresponds to 2 mm of paper travel. The result of using this little scheme is that the paper displacement axis becomes proportional to frequency. Since the bar height is proportional to the maximum response, we have a linear plot of response versus frequency.

In order that the desired response spectra could be recorded directly some means of obtaining and storing the desired maximum values associated with each of the four response spectra had to be devised. The circuit used was given the appropriate title of a Maximum Value Memory Circuit. This circuit is shown in Fig. 12.

This circuit requires one integrator and one high gain amplifier which is used in conjunction with the differential relay. The relay operates in the following manner: When the net input

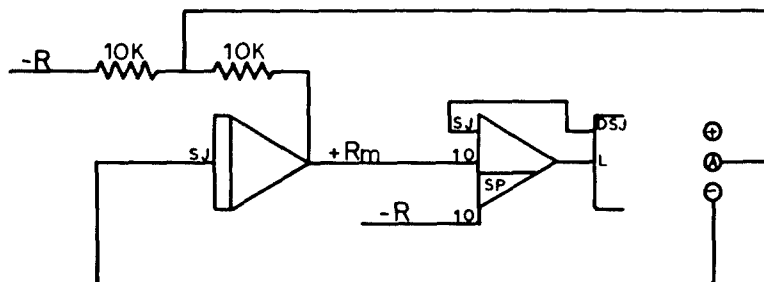


Fig. 12 - Maximum value memory circuit.

voltage to the high gain amplifier is positive, the relay will position in the up direction and when the net input voltage is negative the relay positions down, making contact between the arm and the - terminal.

The operation of the maximum value memory circuit is as follows. The quantity $-R$ is applied to a gain 10 of the relay amplifier and to the 10-K resistor of the tracking integrator. Assuming R starting from zero and increasing in the positive direction, the relay will position in the down direction. This will connect the center point of two 10-K resistors to the summing junction of the integrator which then tracks its input. The output of the integrator, which is another input to the relay amplifier, is very nearly equal to $+R$ at all times. This input to the relay amplifier will lag slightly behind the $-R$ input. As long as R is increasing in amplitude the $-R$ input will be larger in magnitude than the $+R$ input from the tracking integrator. However, once R peaks and begins to decrease the $+R$ input will predominate, causing the relay to throw to the up position, disconnecting the summing junction of the tracking integrator which then maintains this maximum value of R . If at any time the $-R$ input should exceed this retained maximum value of R the summing junction is again connected and the integrator again tracks its input and will move up to the new peak value of R . Thus the final value the integrator assumes will be the peak value R obtained throughout the run. It must be recognized that the circuit as shown only retains the maximum positive value achieved by R . If the maximum negative value were desired, another such circuit hooked up to retain the maximum negative peak would be required. The outputs of these integrators are plotted on the recorder to give the response spectra shown.

In addition to these strip chart recordings a more precise listing of these maximum values was also obtained by securing digital readouts of these values at the end of each computer run. All this information is typed out as hard copy on the typewriter used in conjunction with the computer. The actual printout on the typewriter contains the computer commands from the instruction tape, verification of these commands and readouts of the response values. Figure 13 shows what the printout would look like for one computer run.

A brief list of events as they occur as a function of frequency will serve as a guide in understanding the operation of the computer setup shown in Fig. 14.

COMMANDS	VERIFICATION
BC	
SPT10A +0355/	+0355 10A
SPT11A +1062/	+1062 11A
RE/	
OP	
RIG11A/	+2000 11A
RIG12A/	+3000 12A
RSU21A/	+3000 21A
RIG13A/	+5000 13A

Fig. 13 - Typewriter printout

Frequency

0 - 30 cps	FS 1 UP
	Pot 10 = $10^{-6} \omega_n^2$
	Pot 11 = $20/\omega_n$
	Pot 12 and 13 = 0.0100
40 - 150 cps	FS 1 Center
	Pot 11 = $200/\omega_n$
160 - 790 cps	Pot 10 = $10^{-6}/25 \omega_n^2$
	Pot 11 = $1000/\omega_n$
	Pot 12 = 0.5000
800 - 1000 cps	Pot 10 = $10^{-6}/1000 \omega_n^2$
	Pot 11 = $2000/\omega_n$
	Pot 13 = 0.5000

RESULTS

The spectra of Figs. 3, 6, and 9 are undamped spectra for half-sine, square, and sawtooth driving functions. These were computed to allow comparison with those in the literature. To facilitate this comparison, the ordinate and abscissa are presented as dimensionless ratios consistent with those in the literature. This was accomplished by using a unit peak excitation (E_p). As a result, the actual response and the dimensionless response ratios have the same values. In the abscissa, the product fT provides a dimensionless time ratio in which f is the undamped natural frequency of the responding system in cycles per second and T is the duration of the driving function in seconds.

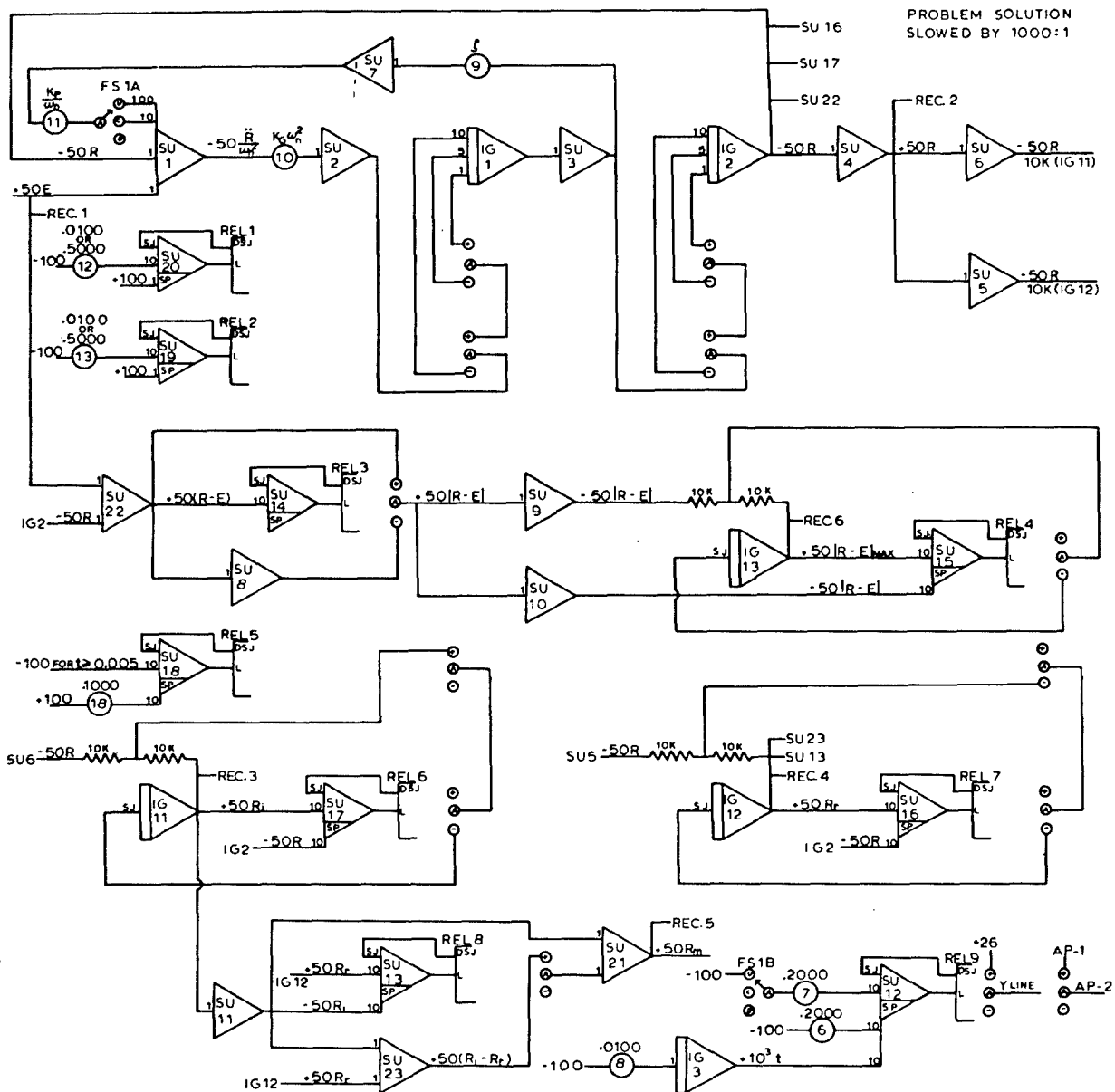


Fig. 14 - Computer circuit diagram

Figures 4 and 5 show the damped spectra of a half-sine excitation function. These can be compared directly with those presented by Mindlin.⁵ It should be emphasized that the residual response spectra are actually the maximum positive residual response spectra. In the undamped case this is not important since the maximum positive, maximum negative, and maximum absolute residual responses are all

equal in magnitude. In the damped case, however, this is not true because the magnitude of each successive positive and negative peak becomes smaller as the oscillation decays due to damping. For this reason, one might compute the negative residual responses or the absolute residual responses depending on how they were to be used.

Figures 7, 8, 10, and 11 show the damped spectra of the square wave and sawtooth. It is interesting to note that the damped residual spectrum of the half-sine and square wave has

⁵R. D. Mindlin, "Dynamics of Package Cushioning," Bell System Technical Journal, 24:353-641 (July-Oct. 1945).

no zeros. It is a characteristic of symmetrical pulses to have zeros in the undamped residual spectrum as shown in Figs. 3 and 6. It is a somewhat unexpected result to find that the addition of damping provides a significant increase in the residual response of simple systems having zero responses in the undamped state. Where maxima occur in the undamped residual spectrum the addition of damping reduces the responses as one would intuitively expect. The fact that the addition of damping does not always reduce the residual response could be an important consideration in the design of equipments subjected to unidirectional shocks. Since most shocks in nature are unidirectional, this is an important case. Examination of the undamped spectra indicates that for values of fT greater than 0.5 the residual spectrum is less severe than the primary spectrum at most frequencies. Since the maximum negative responses occur in the residual era, this means that positive responses are greater than negative responses. A designer can take advantage of this fact by orienting design elements (components, structures, and the like) so that the least sensitive direction is the positive response direction and by designing to have a natural frequency where the residual response is at or near zero. For example, a normally closed relay could be oriented so that positive responses would tend to close the relay. In this case, negative responses would tend to open it causing a malfunction. In view of the fact that damping can either increase or decrease the residual responses, one should be careful in making use of damping to control these responses.

In general, one can say that in any situation where the residual responses are of importance

in determining failure, damping should not be used indiscriminately to reduce response amplitudes.

Figure 9 shows that in a sawtooth pulse the undamped maximax spectrum and the undamped residual spectrum are the same and that they tend to be nearly constant at a response ratio of 1.0 from a very low value of fT out to infinity. This characteristic is desirable from a test standpoint because it provides a nearly constant response over a broad frequency range. Figures 10 and 11 show that the addition of damping enhances the constancy of the response.

CONCLUSIONS

1. Although this paper has been dealing with a simple linear system with pure viscous damping and rather simple excitation functions, the technique itself is virtually unlimited in its application. Any type system, linear or non-linear in nature, can be investigated with any type excitation function desired.

2. Damping can either increase or decrease the residual responses. Thus if responses in the residual era are important, designers should be careful in the use of damping.

3. Observation of the damped responses to a sawtooth excitation pulse shows that the spectrum is even flatter than the undamped spectrum. Since all practical systems have damping, this indicates that the sawtooth spectrum is even more desirable as a test spectrum than one would be able to conclude from the undamped spectrum.

DISCUSSION

Mr. Risse (Sandia Corp.): What method of function generation are you using for arbitrary pulses?

Mr. Schell: In this particular setup, since we are using half-sine, square wave, sawtooth, and what have you; I simply used standard analog components — amplifiers and relays — to generate these. However, if the functions are non-linear, we have various other means of generating them, such as curve following devices. We also have various ways of getting analytic expressions out of approximation functions, so we do have a number of means of generating these things.

Mr. Risse: Can you mention some of the curve follower types that you used?

Mr. Schell: The curve follower that we used most is an 11 X 17 plotter. We actually draw the curve with a conducting ink, or we can lay wire over it. This plotter will then follow the curve, and the output will be proportional to the function that we desire. Then all we have to do is to make the proper scaling adjustments, and we have the function.

Mr. Risse: Thank you very much.

BIBLIOGRAPHY

- L. S. Jacobsen and R. S. Ayre, "Engineering Vibrations" (McGraw-Hill Book Co., Inc., New York, 1958).
- M. V. Barton, V. Chobotov, and Y. C. Fung, "A Collection of Information on Shock Spectrum of a Linear System," Report No. EM 11-9, Space Technology Laboratories, Inc., Los Angeles (July 1961).
- C. T. Morrow, "The Shock Spectrum," Electrical Manufacturing 64:121 (Aug. 1959).
- C. T. Morrow and H. I. Sargent, "Sawtooth Shock as a Component Test," J. Acoust. Soc. Am., 28:959 (Sept. 1956).
- R. Lowe and R. D. Cavanaugh, "Correlation of Shock Spectra and Pulse Shape with Shock Environment," Environmental Engineering, 1 (Feb. 1959).
- I. Vigness, "Navy High-Impact Shock Machines for Lightweight and Medium Weight Equipment," NRL Report No. 5618 (June 1, 1961).
- I. Vigness and E. W. Clements, "Sawtooth and Half-Sine Shock Impulses from the Navy Shock Machine for Medium Weight Equipment," NRL Report No. 5943 (June 3, 1963).

Alternate Forms of Excitation and Damped Response*

Excitation (E)		Response (R)	
Force	$F(t)/k$	Absolute Displacement	x
Ground Acceleration	$-\ddot{u}(t)/\omega_n^2$	Relative Displacement	y
Ground Acceleration [†]	$\ddot{u}(t)$	Relative Displacement	$-\omega_n^2 y$

*This table added subsequent to submission of original manuscript.

[†]In the case where the ground acceleration $\ddot{u}(t)$ is used to excite the system, the response spectrum ordinate is $R/E_p = -\omega_n^2 y/\ddot{u}_p = y/y_{st}$, where y_{st} is the static displacement as defined by Mindlin (6).

* * *

THE USE OF GRAPHICAL TECHNIQUES TO ANALYZE SHOCK MOTIONS OF LIGHTLY DAMPED LINEAR SPRING MASS SYSTEMS*

R. O. Brooks
Sandia Corp.
Albuquerque, New Mexico

INTRODUCTION

Quite often in the area of mechanical shock testing, responsive motions of lightly damped spring-mass systems must be determined or predicted when an actual measurement of the response is lacking. The responsive motions of the systems can be found by several methods. All of the analytical methods require higher mathematics in solving the differential equations of motion. Frequently, however, the input conditions to the system's supports cannot be described easily by a mathematical expression. Sometimes the input shock data are not in a form compatible for an analog or digital computer. At such times, an analytical or computer solution is inconvenient to obtain.

Literature dealing with the study of transient motion has discussed a graphical method of determining responsive displacements of linear spring-mass systems when the support is subjected to a transient displacement. This graphical method is called "Lamoen's Phase-Plane Method." The literature, however, reveals very little information as to whether or not the phase-plane method could be used to solve the transient vibration problem of a lightly damped system of the type encountered in shock testing.

Accordingly, an investigation¹ was conducted to see if the phase-plane method shown in literature could be extended to find acceleration or displacement responses (including spring deflections) of general multidegree damped systems most likely to be encountered

in mechanical shock testing. In these systems, no damper is connected to the ground, and the only external excitations are through the system's supports. This paper presents the results of that investigation. Definition of all terms are listed in the appendix.

DISCUSSION

A general two-degree-of-freedom damped linear spring-mass system mounted on a shock machine is shown in Fig. 1. Support excitation is a known displacement-, velocity-, or acceleration-time history. These quantities are represented by the symbols $\lambda(t)$, $\dot{\lambda}(t)$, $\ddot{\lambda}(t)$. The masses m_1 and m_2 are very small in comparison with the carriage mass. Values for each spring, k_1 , k_2 , k_3 , and each mass, m_1 and m_2 , are known from the physical design of the specimen. The location of each viscous damper, c_1 , c_2 , c_3 , or coulomb (dry friction) damper, f_1 , f_2 , f_3 , is known. The effects of the dampers are either known or would be determined by experiment. The magnitudes of the dissipative forces of the dampers are such that in free vibration at least two complete cycles of each mass in motion will be discernible. If the f 's or c 's of the model are zero, the two-degree viscously- or coulomb-damped model, or both, becomes undamped. Similarly, if one mass is zero, the model becomes a single-degree spring-mass system. The motion of the masses in Fig. 1 can in certain cases be described graphically by means of phase-plane diagrams.

Just what is a phase-plane diagram and how is it used to determine responsive motion of, for example, a simple undamped spring-mass system? Briefly, the motion of a simple system can be shown by the trajectory which a vector makes while rotating at constant angular

¹R. O. Brooks, "Transient Response of Linear Undamped and Lightly Damped Lumped Spring-Mass Systems By Graphical Techniques," Master of Science Thesis, 128 pages, University of New Mexico (June 1963).

*This paper was not presented at the Symposium.

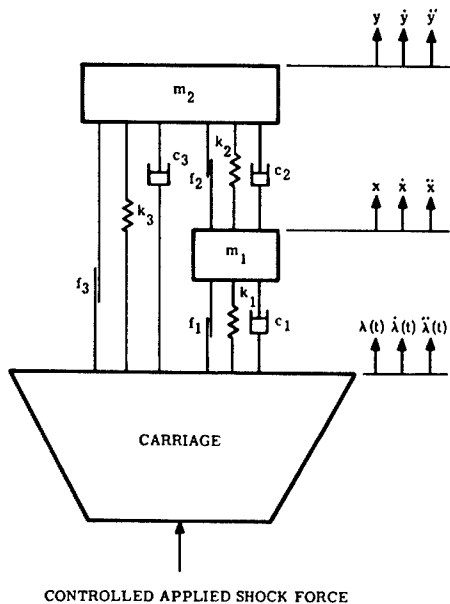


Fig. 1 - General two-degree viscous and coulomb damped spring-mass system under consideration

velocity about a fixed point. The radius and starting point of the vector are functions of the initial conditions of the spring-mass system. The type and amount of damping (when present) affects the radius or the center of arc. The angular velocity represents the natural or resonant frequency of the system. The fixed point (center of rotation) is determined from the known disturbance to the support or carriage.

The construction of the trajectory of the rotating vector makes up the phase-plane diagram. The term "phase" is used because the two coordinates represent a particular motion and the time-derivative of the motion which is 90 degrees out of phase (e.g., displacement and velocity, or velocity and acceleration, and the like); the term "plane" is used because the diagram is always drawn in the plane of the paper. The responsive motion of the mass at any time can be found from the projections of the vector upon the two coordinate axes. The projections can be plotted vs time and the actual responsive motion-time history can be viewed.

Figure 2 shows an example of an undamped spring-mass system in free vibration when the responsive mass, m , has an initial displacement, x_0 , and an initial velocity, \dot{x}_0 . The phase-plane coordinates are in the form to describe either the displacement-velocity conditions, the velocity-acceleration conditions, or the acceleration-jerk conditions at any time. At $t = 0$, the rotating vector, r , is at ①. During the time t_1 , r is rotating at constant angular velocity, p . At the end of time, t_1 , r is at ②. Since there is no support motion, the center of arc ① ② is at the origin. The responsive-time histories for displacement, velocity, or acceleration of m during t_1 are shown by the solid lines; the dotted lines represent the motion as the vector in the phase-plane continues to rotate after t_1 . Generally, all three responses are not desired at once, so the phase-plane coordinate scale may be multiplied by p to find velocity directly and multiplied by p^2 to

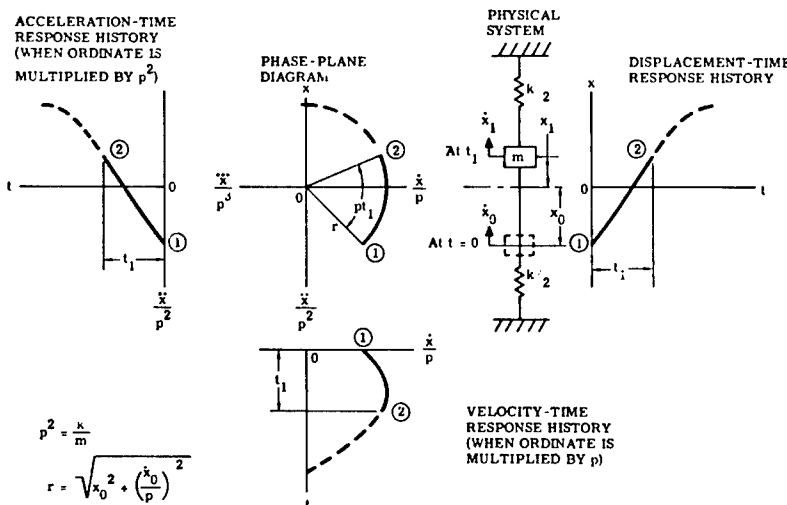


Fig. 2 - Various response-time histories of a simple system in free vibration determined from phase-plane diagram

find acceleration directly. If the support has a disturbance during t_1 , the center of the arc ① ② would shift along the ordinate of the two coordinate axes of interest.

The responses of two-degree spring mass systems can be determined graphically when the problem is broken down into two independent modes of vibration. Each vibration mode behaves as a linear single-degree system.

RESULTS (SINGLE-DEGREE SYSTEMS)

The investigation indicated that responses of three types of single-degree systems — undamped, coulomb damped, and viscously damped — could be solved by graphical methods. The general procedure for constructing the phase-plane diagrams mentioned previously could be used satisfactorily. In the appendix are a list of Guides (1 through 12) which present phase-plane construction details for the undamped, coulomb damped, and viscously damped single-degree system models. They can be used when the types of support excitations and most probable starting conditions are known, and certain types of response histories are desired. The procedures contained in the appendix should assure sufficiently accurate results for most shock testing problems. Very accurate results are possible if the phase-plane diagrams are drawn in greater detail (i.e., more steps are used to construct them).

Undamped System

If only m_1 and k_1 are evident and attached to the carriage in Fig. 1, a single degree undamped model occurs. (The system considered is in translation, but the same procedure holds for a torsional system if mass is replaced by polar moment of inertia, and a linear spring rate by a torsional spring rate.) Figure 3 illustrates an example problem of an idealized system's acceleration response to an acceleration input of its support determined by the phase-plane procedure shown in Guide No. 1, Acceleration Excitation, Acceleration Response. Generally, there is no relative motion between the mass, m , and the carriage before a shock, so the initial acceleration and jerk of the mass are zero, and the phase-plane starts at the origin. The input shape is approximated by a series of steps, each step having the same area during the interval as the actual pulse during the interval. The amplitude of each step input is used to locate the center of arc on the phase-plane diagram. The interval size (t_i) selected for each step is dependent both upon the pulse rise and fall times, and the specimen natural period. The ratio t_r/T (pulse rise time/specimen natural period) governs the time interval of each step when the slope of the input pulse is positive; the ratio t_f/T (fall time/natural period) governs the intervals when the slope of the input pulse is negative. In the guides then, only t_r/T ratios are shown, but t_f/T ratios can be substituted when needed. Symmetrical pulses (e.g., half-sine, triangle, haversine, parabolic cusp) require consideration of both

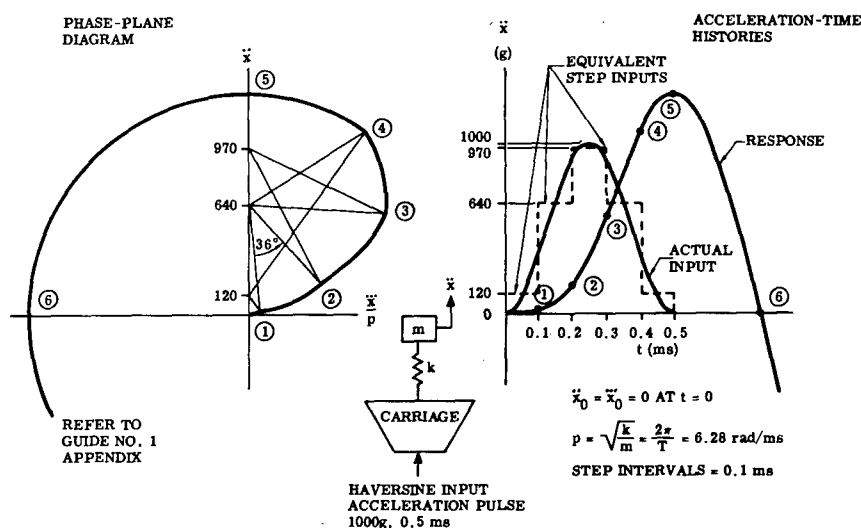


Fig. 3 - Acceleration response of undamped simple system when its support has a transient acceleration input

t_r/T and t_f/T ratios; non-symmetrical shapes such as quarter-sine, terminal peak sawtooth, require consideration of only t_r/T ratios, while quarter-cosine and initial peak sawtooth require consideration of only t_f/T ratios.

When $0.1 \leq t_r/T \leq 1.0$ many steps in the phase-plane construction should be taken. It is in this range that the pulse shape has the most effect upon the maximum response. Generally, interval ratios $t_i/T = 0.1$ should not be exceeded. The arc of the phase-plane step (ρt_i) should therefore be between 18 and 45 degrees. When $t_r/T < 0.1$ only one step interval is necessary regardless of the input pulse shape. When $t_r/T \ll 0.05$ no steps are necessary; it is sufficient to assume a free vibration problem with different starting conditions if time is measured after the pulse is over. (Guide No. 2 could be used in this case.) As t_r/T exceeds 1 and approaches 5, the size of the intervals can be increased until $t_i/T \rightarrow 0.5$. When $t_r/T \geq 5$, the interval size $t_i/T = 0.5$ should always be observed; the response history can be drawn directly without drawing a phase-plane diagram by drawing half cycles or cosine curves for each interval.

In Fig. 4 an undamped system is subjected to a 1000-g, 5-ms, sawtooth pulse. Only the beginning portion of the input and response is shown. A comparison is made of the half-cycle response to the response determined by 36-degree arcs. In this problem, $t_r/T = 5$. The phase planes of both responses are also shown. The greatest error in the half cycle amplitude at any time, while noticeable, is less than 5 percent of the peak value of the input pulse. This error would decrease as $t_r/T \gg 5$.

For an input acceleration pulse, another type of response is possible, that of spring deflection. In this problem, spring compression (-u) has the same sign as the input acceleration. The main difference in the phase-plane construction is that the input acceleration has to be converted into units of displacement.

Guide No. 2 illustrates phase-plane construction details for two free vibration problems likely to occur in shock testing.

Guide No. 3 shows that a displacement response to a displacement shock input is identical in appearance to the same acceleration conditions of Guide No. 1.

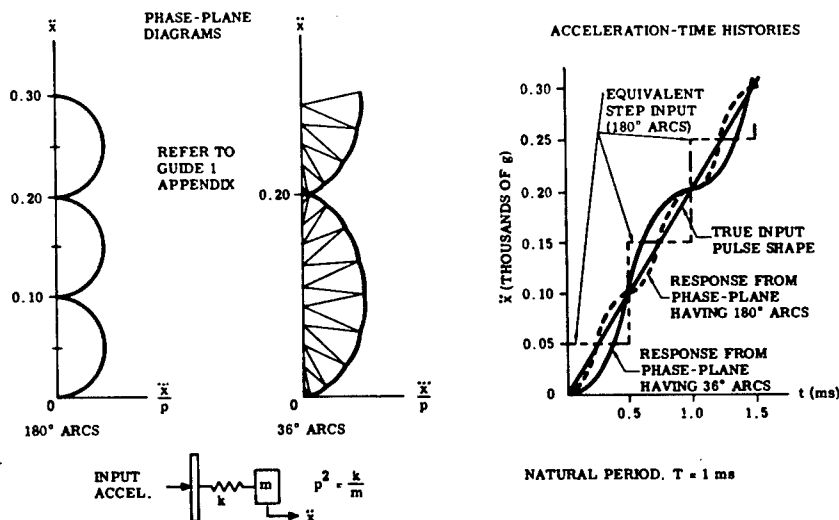


Fig. 4 - Comparison of acceleration-time responses of a simple system using both 36 and 180-degree arcs (half-cycle) in the phase-plane diagram

For the example in Fig. 3 then, the step size would be 0.1 ms since $t_r/T = 0.25$. It should be noted, though, that equal size step intervals are not mandatory, but are generally more convenient.

Coulomb Damped System

If every parameter in Fig. 1 is zero, except m_1 , k_1 , and f_1 , the system becomes an idealized coulomb damped single-degree model in

translation. Note that the damper is fastened to the support (carriage) so now relative motion (specifically the direction of the relative velocity) is important in solving a response problem graphically. When the relative velocity changes direction, the acceleration of the responding mass has a sudden discontinuity. Friction damping thus complicates the problem.

It was mentioned previously that the center of each arc in the phase-plane is determined by the motion of the support. So, when the damper is connected directly to the support, any support action will immediately affect the response of the mass through both the damper and spring. This damping effect can be considered in the phase-plane diagram by applying a correction (a "delta" term) to the center of each arc whenever displacement responses (or spring deflection) is desired.² For an acceleration response, however, the center does not have to be corrected; the radius periodically is corrected because the acceleration discontinuity occurs as the relative velocity changes direction, or when the jerk (\ddot{x}) is zero.

Figure 5 illustrates an example of an acceleration response of a system subjected to an acceleration input of its support. This problem is solved using the phase-plane procedure shown in Guide No. 4. The most probable starting conditions at time $t = 0^-$ are $\ddot{x}_0 = \ddot{x}_s = 0$. Since the first input step λ_1 is greater than Δ_c (the frictional acceleration) at $t = 0^+$, $\ddot{x}_{0+} = \Delta_c$ because force is transmitted only through the damper. If the magnitude of the relative acceleration, $\lambda - \ddot{x}$, had been less than Δ_c , and the spring, k , was not sufficiently deformed, the mass would have responded as though rigidly connected to the support.

The Δ_c discontinuity is always directed to the center of arc when \ddot{x}/p passes through zero. The Δ_c magnitude must be doubled whenever the spring has deformed and transmits enough force to overcome the friction in the damper. In Fig. 5, m has the same instantaneous velocity as the support at points ①, ②, ③, ④, ⑤, ⑦, and so on. This means that the jerk is zero at these points.

In Guide No. 5, Acceleration Response to a Velocity Step Excitation, a free vibration problem occurs. The most probable starting conditions, \ddot{x}_0 and \ddot{x}_s , are not zero because of relative motion existing between mass and support.

For a problem where a displacement response is desired, Guide No. 6 rules must be followed. In this type problem the center of each arc representing the step input magnitude must be corrected by Δ_c (the equivalent frictional displacement). The $\text{sgn}(\dot{\lambda} - \dot{x})$ means "the algebraic sign of" the relative velocity between the mass and its support which determines whether Δ_c is added to or subtracted from λ_i . Figure 6 is an example problem where the support is given a triangle shape displacement, where the t_r/T ratio equals 1.0. In this problem, or any other problem utilizing Guide 6, it should be noted that the spring deflection ($\lambda_i - x_s$) at the start of each step must be greater than Δ_c if the relative velocity ($\dot{\lambda}_i - \dot{x}_s$) is zero, otherwise the system will appear rigid. In Fig. 6, the system appears rigid at point ③. At points ①, ②, ④, ⑤, ⑥, the relative velocity is zero, but the spring is sufficiently deformed, so relative motion must continue. The recommended size of the step intervals, in general, is the same for all ratios of t_r/T as in Guide No. 1 except in the low range where the damper effect on maximum response is more pronounced. It is therefore recommended that $t_r/T = 0.1$ for $0.05 \leq t_r/T \leq 1$. When $t_r/T < 0.05$ a single step can be employed and damping ignored with little error in the phase-plane.

If it is desired to observe the spring deflection directly by means of a phase-plane diagram, it is necessary to know the acceleration-time history of the support (Guide No. 4) or to have a free vibration condition (Guide No. 5). In one case, the center of the phase-plane arcs remains at the origin. In the other cases the centers of the phase-plane arcs have to be corrected by the amount Δ_c until relative motion stops.

Viscously Damped System

If all the parameters in Fig. 1 are zero except m_1 , k_1 , c_1 , the system becomes an idealized viscously damped model with support excitation. The procedure in drawing the phase-plane diagram for the displacement response of a viscously damped system is similar to the procedure followed for displacement response of a coulomb damped system. The main difference is that the damping is now dependent upon the magnitude of the relative velocity of the system as well as its direction. For the viscously damped systems, it can be shown that the rules followed in Guide 7 (Acceleration Excitation and Response) and Guide 9 (Displacement Excitation and Response) are identical if all \ddot{x} 's are replaced by \dot{x} , \ddot{x}_s by \dot{x}_s , Δ_c by Δ_v , and so forth.

²L. S. Jacobsen and R. S. Ayre, *Engineering Vibrations* (McGraw-Hill Book Co., Inc., New York, 1958).

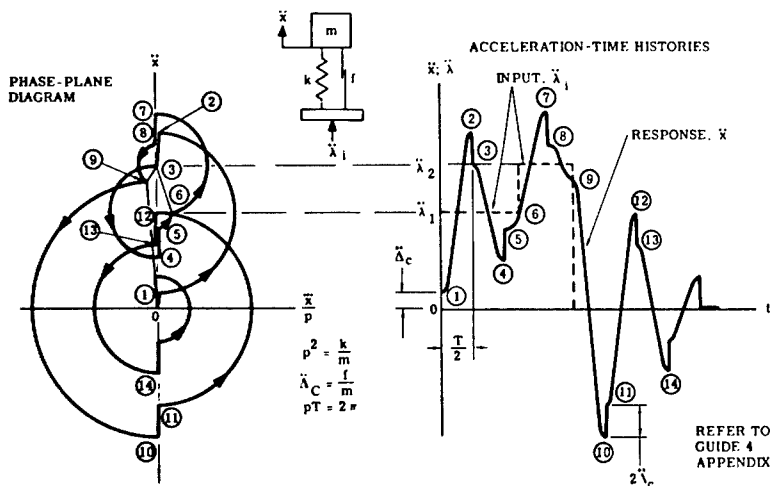


Fig. 5 - Coulomb damped single-degree system having support excitation of acceleration steps (damper attached to support)

Fig. 6 - Response of specimen to transient input displacement when coulomb damper is fastened to movable support

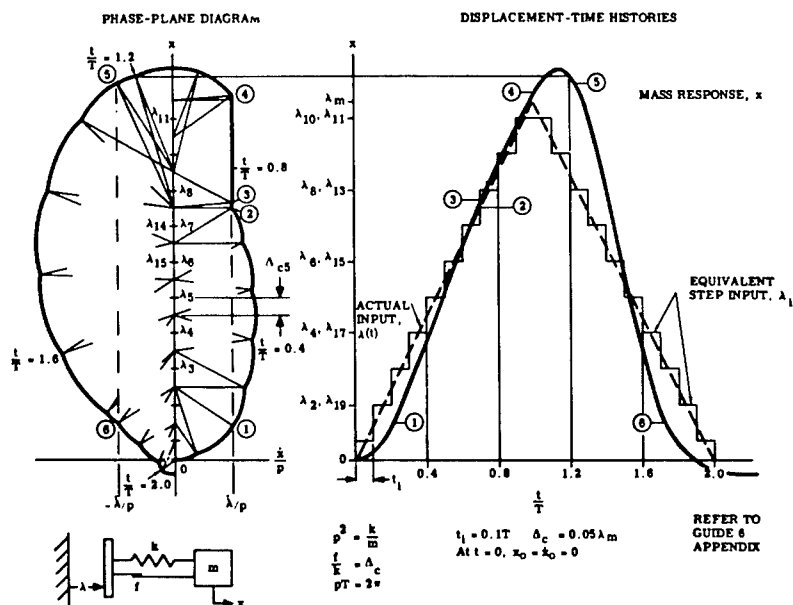


Figure 7 shows an example problem where a viscously damped system (natural period of 1 ms) is subjected to a 1000-g triangle acceleration pulse, 2 ms in duration. The acceleration response is found using the appropriate Guide No. 7. The most probable starting conditions of the mass are zero acceleration and jerk. If each step interval is short enough (true for any pulse shape) the relative jerk (also velocity) between the mass and its support can be considered constant while the support acceleration (also displacement) varies linearly. The center of each arc in the phase-plane can be approximated by the average value ($\bar{\lambda}_i$) of $\lambda(t)$ during the step, while the damping correction to the arc center (Δ_{vi}) is added or subtracted,

depending upon the magnitude and direction of the relative motion. A tabulation for finding Δ_{vi} for the first four steps is shown in Fig. 7. The closer \ddot{x} and $\ddot{\lambda}$ come together, the smaller Δ_v becomes. Thus, the system will never act as though rigidly connected for damping ratios less than 0.2. The ratios of t_i/T for each step used for a coulomb damped system (Guide 4) seem to give good results for the viscously damped system.

A different kind of phase-plane coordinate system is very suitable for solving certain response problems of a viscously damped model. By using oblique coordinates and a logarithmic spiral template (which is dependent only on the

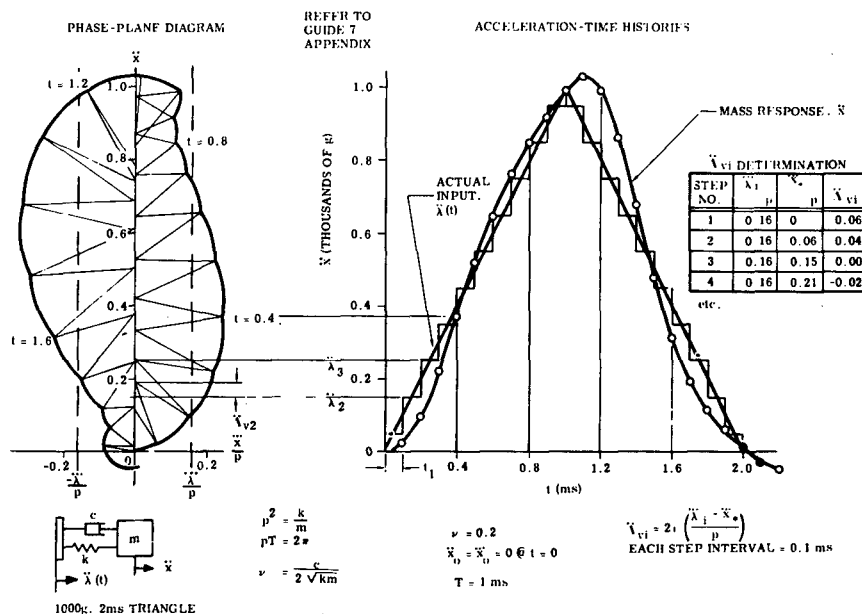


Fig. 7 - Acceleration response of specimen to transient input acceleration when viscous damper is fastened to movable support

damping ratio) the following problems can be solved for damping ratios up to 0.5:

1. A free vibration of the model where the input is a step velocity and the response is absolute acceleration or spring deflection (Guide 8).
2. Spring deflection response to an acceleration input, any shape (Guide 7).
3. Acceleration response to a square pulse acceleration input (Guide 7).

The development of the oblique coordinate system used is found in Ref. 3. The construction of a logarithmic spiral is found in Ref. 2. Figure 8 illustrates how the phase-plane is drawn from spiral templates. The center of the spiral template (shown by dotted lines) is located from a given input acceleration (expressed in units of displacement). The template is pivoted until it intersects the initial conditions of spring deflection at point ①; i.e., $(-u_1)$ and $(-\dot{u}_1/p')$. During the time of the step, t_1 , the phase-plane arc follows along the spiral arc until point ② is reached. The angle σ is dependent only upon the damping ratio, ν . The

spiral template, once drawn for a certain damping ratio, is good for any system having the same damping ratio. The abscissa of the phase-plane can be graduated in $(-\dot{u}/p)$ by multiplying $(-\dot{u}/p')$ by $\cos \sigma$.

Figure 9 shows the solution to a problem where the viscously damped system's support is subjected to a 1025-g, 0.5-ms sawtooth acceleration pulse. The system's natural period is 1 ms. There is no relative motion before the pulse. Guide No. 7 is used to find the maximum spring deflection (tension and compression) as the response history. The maximum compression is found to be 0.0092 inch, while maximum tension occurring after the pulse is 0.0050 inch.

In Guide 8, the derivation of the most probable initial conditions can be found in Ref. 1.

RESULTS (TWO-DEGREE SYSTEMS)

Undamped System

If only m_1 , k_1 , m_2 , k_2 , and k_3 are present in Fig. 1, a general undamped two-degree model occurs. It was found that the methods used in solving for certain response in an undamped single-degree system could be extended to include the general undamped multidegree system.

³R. E. D. Bishop, "On The Graphical Solution Of Transient Vibration Problems," Proc. Inst. Mech. Engrs. (London), Vol. 168, No. 10, pp. 299-322 (1954).

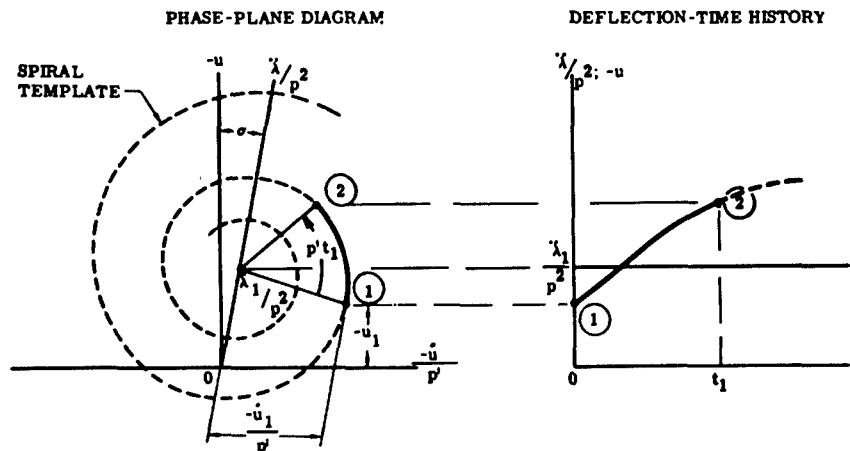


Fig. 8 - Deflection-time response from spiral template on oblique coordinate phase-plane diagram

For support excitation problems, some interesting observations were made, the details of which can be found in Ref. 1. As an example, solving for the response of each undamped mass by phase-plane methods first requires describing the motion and configuration of the system in its natural modes of vibration. Then a phase-plane diagram has to be drawn for each mode, all the conditions of each mode being analogous to conditions of the undamped single-degree system. Data from each mode are then combined in a certain manner to finally describe the motion of each mass separately.

It was found that a single support excitation (Fig. 1) permits phase-plane diagrams to be easily drawn while a two-support excitation permits a phase-plane diagram to be easily drawn only in special cases. The two-support excitations have to have their amplitudes equal to some arbitrary constant ratio which requires the amplitudes to also be either 0 or 180 degrees out of phase. (In Fig. 10, the upper and lower plate of the model disconnected from the rigid frame and subjected to different accelerations would constitute a two-support problem.) Fortunately most controlled shock tests justify

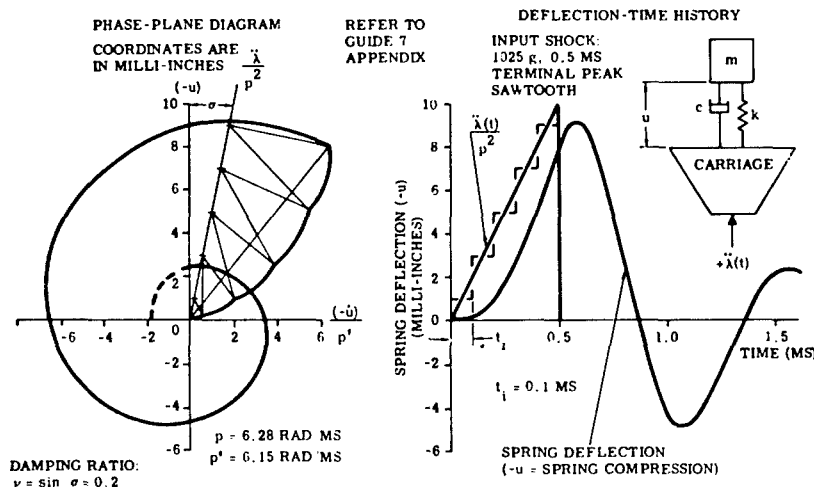


Fig. 9 - Example problem showing responsive deflection-time history of spring when specimen is subjected to sawtooth acceleration pulse

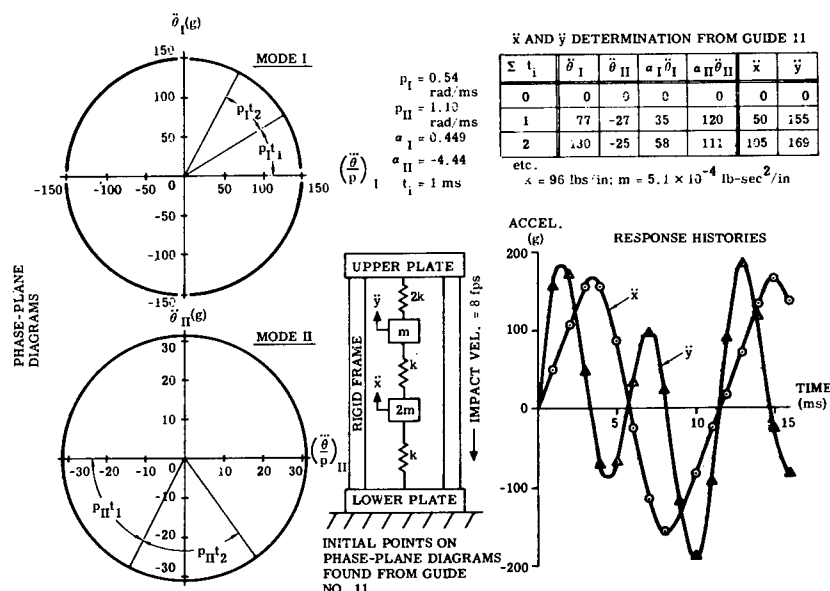


Fig. 10 - Acceleration response of an undamped two-degree system during free vibration

the assumption of single support type excitation, so Guides 10-12 can be used for phase-plane construction.

Figure 10 shows how the acceleration responses of two masses are determined if the framework surrounding them is dropped onto a rigid floor for a sudden velocity change type input. The two masses are in free vibration. When using Guide No. 11 to solve the problem, two phase-planes are needed, one for each mode of vibration. The phase-planes are in principal coordinates. Before impact, the relative motion of each mass to the support is most probably zero. The acceleration of both masses at impact is therefore zero, but the jerks are not. The location of the points representing the initial jerks on the phase-planes have to be found from the equations in Guide No. 11 where $\dot{\lambda}_0 = 0$ and $\dot{x}_0 = \dot{y}_0 = \text{impact velocity}$. (Correct units must be observed.) Each phase-plane can be drawn once the two natural frequencies of the model are known. The response of each mode at any time must then be added together, as shown by Guide No. 11, to get the responsive acceleration of each mass separately.

Spring deflection for this problem can now be found by solving simultaneously the equations of motion to find the displacements of each mass for any determined instantaneous acceleration of each mass. (The displacements of each mass can also be determined from Guide No. 11 when

initial velocities are transformed into principal coordinates and all \ddot{x} 's changed to x 's, and so forth.

Guide No. 10 can be used to find acceleration responses of the two masses when a single support has an acceleration shock pulse. Two phase-planes are again needed, one for each mode, expressed in principal coordinates. A slight problem now arises. If the two coordinate scales are $\ddot{\theta}$ and $\ddot{\theta}/p$ for either mode, then λ_i for each step has to be transformed to principal coordinates for both modes by multiplication of a factor H_I or H_{II} defined in the appendix. However, by dividing the phase-plane coordinates by the appropriate H factor (as shown in Guide No. 10) the center λ_i for each step can be located directly on the phase-plane. In this manner, all phase-plane construction can be completed before any calculations have to be made converting the phase-plane data to response accelerations of each mass. Some time can thus be gained in solving the problem in the manner of Guide No. 10. An example problem using this guide can be found in Ref. 1. Unfortunately, spring deflections cannot be determined easily in two-degree systems when the support is excited by an acceleration shock pulse. If the pulse is integrated twice to obtain a displacement-time input, Guide No. 12 can be used to find displacement responses of each mass. Spring deflections would then be found easily. Guide No. 12 procedure is quite similar to Guide No. 10.

Damped System

The inclusion of either viscous or coulomb damping into a two-degree model, such as shown in Fig. 1, creates many problems. Coulomb friction effects in a two-degree system must be simulated by additional support deflections in phase-plane construction. However, it was mentioned previously that restrictions are necessary when more than one support is involved. So, for friction damping to be included as a condition where a phase-plane solution is possible, only one mode of vibration can be excited, and the friction displacements of the supports have to be identical. The possibility of using phase-planes to find acceleration responses of both masses from a known acceleration input was not investigated.

Viscous damping in a two-degree system also was shown to create problems in that, generally speaking, the two modes of vibration are not independent⁴ unless the magnitudes of the dampers are in the same ratio as the springs (e.g., $k_3/k_1 = c_3/c_1$.) Independence of modes is required for phase-plane construction. Actual damping in two-degree systems are hard to control, so transient responses of such systems were considered impractical for easy solution by phase-plane solutions suitable for single-degree systems.

RESULTS (EXPERIMENTAL INVESTIGATION)

Three different single-degree system models were designed and subjected to shock pulses that would be generated in mechanical shock testing in industry. The three models were undamped, coulomb damped, and viscously damped.

A view of the undamped model is shown in Fig. 11. The design of the model consisted of a single concentrated mass suspended between two sets of four helical coil springs (total of eight springs), each having the same spring rate. One end of each set of springs was held rigid within a very stiff framework. The mass was constrained to move only in either direction of the longitudinal axis by Teflon bushings riding upon four guide rods. The lower plate was fastened to a shock machine carriage during all shock tests. The input shock to each model was monitored by a piezoelectric accelerometer mounted on top of the framework which was the

specimen fixture. The responsive accelerations were monitored by an identical piezoelectric accelerometer mounted directly upon the suspended mass. The output signal of each accelerometer was fed into a cathode follower, the output of which was dc coupled to an oscilloscope.

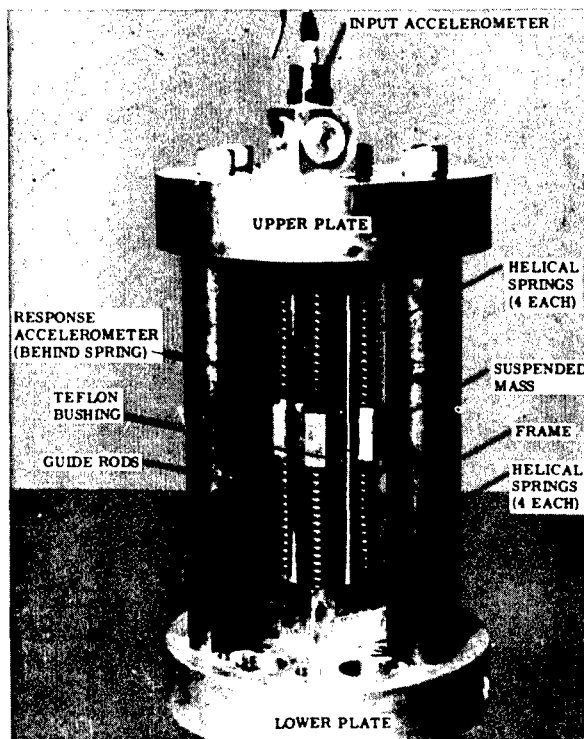


Fig. 11 - Model for experimental investigation

Actually, an undamped model never occurs in reality. However, sometimes the amount of damping is so small that for a few cycles of vibration the amplitude loss is very small. By careful alignment and greasing of the guide rods and by use of a very small contact area between bushings and guide rods, a very lightly damped model (essentially undamped for the time interval of interest during shock) was obtained.

The coulomb-damped model was similar in design to the undamped model shown in Fig. 11. Coulomb friction was introduced by increasing the normal pressure between the bushings and the dry guide rods. The friction damper thus appeared fastened to the support and to the mass of the model.

The viscously damped model design was similar to the model of Fig. 11 with a viscous damper added. The construction and positioning

⁴S. Timoshenko and D. H. Young, *Advanced Dynamics*, 1st Ed. (McGraw-Hill Book Co., Inc. New York, 1948).

of the damper was in the same manner as shown by c_1 in Fig. 1: a piston was fastened to the mass; a cylinder was fastened to the support; and the piston had holes through which oil was metered whenever the piston moved relative to the cylinder. A suitable damping ratio was achieved, so no fine adjustment was incorporated into the design.

Details of each model, such as spring rates, weight of suspended mass, magnitude of dry friction, and viscous forces, could have been measured and then the natural and resonant frequencies of the system calculated. Instead, all parameters needed to solve a transient response problem were found by subjecting each model to a vibration test. A resonant search was conducted to determine the natural frequency for the undamped and coulomb damped models and the resonant frequency for the viscously damped model. (For a damping ratio of 0.2, the resonant frequency is only 2 percent lower than the natural frequency.) Once the natural or resonant frequency had been determined, the type and amount of damping were found by observing the response decay when the input vibration amplitude was suddenly brought to zero.

The three models were subjected to the shock pulses shown in Figs. 12, 13, and 14. The monitored response histories were then compared to the phase-plane constructed response histories. The phase-planes (not shown) were constructed in accordance with the rules in Guides 1, 4, and 7 in the appendix. The shape of the measured response histories in each figure closely resembled the calculated response histories, but were somewhat larger in amplitude than theoretically possible for linear systems. The differences were attributed to non-linearity of the springs. The different natural frequencies of each system were the result of changes in the size of the responding masses. However, the experimental investigation indicated that obtaining response histories from graphical solutions derived from empirical data was feasible.

ACCURACY OF GRAPHICAL SOLUTION

What degree of accuracy can one expect in solving a problem graphically? In Ref. 3 it is pointed out that the question of accuracy of a solution of even a single-degree system problem is difficult to answer, because accuracy can only be determined on an empirical basis. Generally, the more steps taken in a phase-plane construction, the more accurate the

answer, but this is limited by drafting error increase. The type input involved obviously could affect accuracy, especially if a smooth input pulse shape versus a random haphazard pulse shape was involved. Checking of the accuracy can only be done when analytical solutions of a particular problem are available. For practically any engineering problem of transient loading of a single-degree system, the accuracy of phase-plane construction is quite satisfactory.

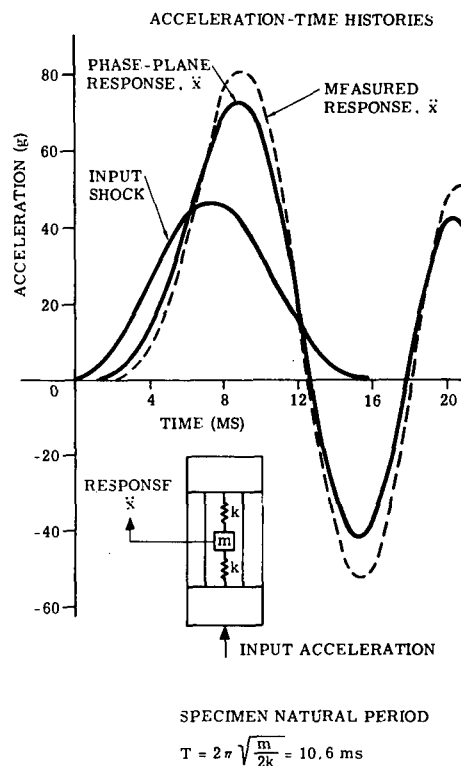


Fig. 12 - Comparison of phase-plane and measured response of a linear system (damping neglected) to an acceleration shock pulse

In multidegree systems, the degree of accuracy decreases while the length of time to solve a problem increases. In any multidegree system the number of phase-plane constructions is proportional to the number of modes of vibration, so the total error is approximately proportioned to the number of modes. It would therefore appear that the accuracy obtained for a single-degree undamped system would be approximately twice that for two-degree undamped systems. It would also appear that the accuracy obtained for a single-degree undamped

Fig. 13 - Comparison of phase-plane and measured response of a linear coulomb damped system subjected to an acceleration shock pulse

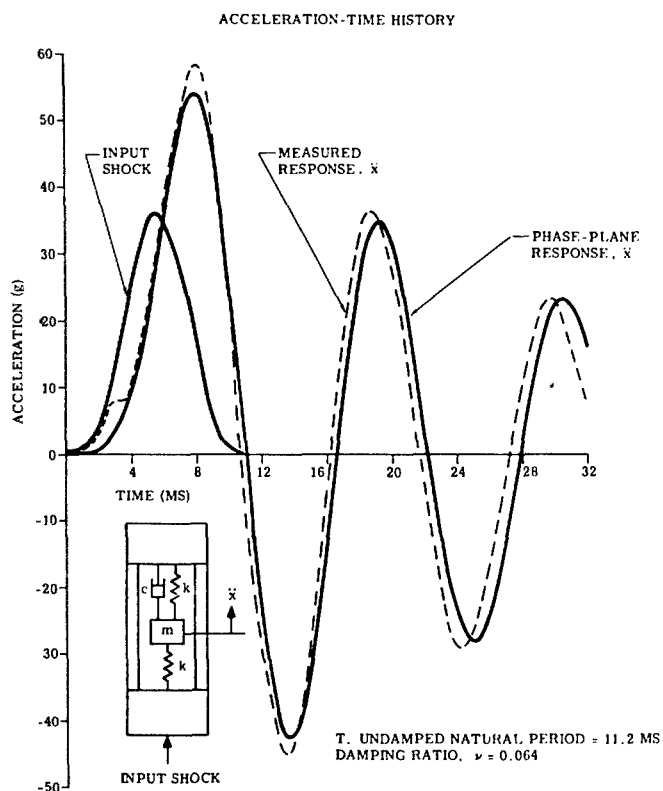
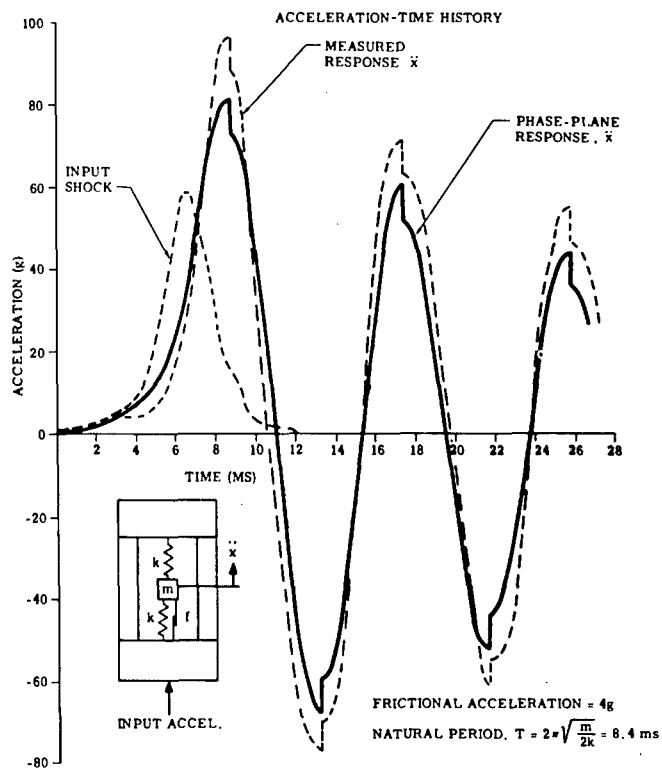


Fig. 14 - Comparison of phase-plane and measured response of a linear viscously damped system subjected to an acceleration shock pulse

system would be approximately three times the accuracy obtainable for a three-degree system solved by similar techniques. This statement is qualified to the extent that phase-plane construction follows the guidelines set forth in the appendix. The amount of tabular work that needs to be done in converting principal coordinate values to rectangular coordinate values increases directly as the type of degree system. It is therefore estimated that solving a two-degree system problem would take two and one-half times as long as a single-degree problem, while a three-degree system problem would take four times as long as a single-degree system problem. Again, this statement is dependent upon the type of phase-plane construction needed for each mode of vibration. It would thus appear that solving a three-degree system problem by graphical techniques would not be too satisfactory; computers could solve the problem more quickly and accurately.

CONCLUSIONS

The graphical solution of responsive motion of certain models subjected to a controlled mechanical shock test has its place in the field. The phase-plane-delta method would most probably be used in situations where a model representing the specimen is known and a computer not available, or where the input data is not immediately suitable for computer use and the responsive information needed in a few hours. The method is a useful education tool in understanding the theory of shock motion. A trained technician can solve a problem by selecting the correct Guide in the appendix and using graph paper, protractor, compass, straightedge, and french curve. He only needs to know the following: the specimen's natural period; type and amount of damping which can be found from a simple vibration test where a response can be measured; initial starting conditions; and type of support excitation.

APPENDIX

Guides 1 - 12, developed from Ref. 1, summarize conditions that are needed to construct phase-plane diagrams for transient response of linear, undamped, single- and two-degree lumped spring-mass systems; and linear, single-degree viscous- and coulomb-damped systems. The type of excitation and initial conditions selected are those that are most generally found in mechanical shock testing of inert specimens. Other starting conditions, however, are possible if a specimen is functioning. Displacement excitation has been included since some solutions of response need it, and because acceleration-time data of the input pulse can be graphically integrated easily to obtain it. The velocity input and velocity response determination of a system by phase planes can easily be an extension of the list. However, the information is more generally obtained by the integration of acceleration-time histories or by the differentiation of displacement-time histories.

A list of the symbols used in the guides are shown below:

- $\lambda(t);$ - Input displacement- or acceleration-time disturbance, respectively, of the support
- $\lambda_i; \ddot{\lambda}_i$ - Equivalent step input of support disturbance for time interval, t_i

- p - Natural frequency of responding system
- p' - Resonant frequency of viscously damped system
- T - Natural period of responding system
- $x, \dot{x},$ - Motion of responding mass, m_1
 $\ddot{x}, \ddot{\ddot{x}}$
- $\dot{\lambda}_0, \dot{x}_0,$ - Initial condition at $t = 0$
etc.
- t_r - Rise time of support disturbance (nonsymmetrical pulses might require substitution of t_f , fall time)
- $(-u),$ - Spring compression
etc.
- Δ_c - The ratio f_1/k_1 from Fig. 1; the delta correction term for the phase-plane center of any time interval of a coulomb damped system
- $\ddot{\Delta}_c$ - The ratio f_1/m_1 from Fig. 1; the correction term for the phase-plane radius vector of a coulomb damped system
- $x_*, \ddot{x}_*,$ - Responding mass starting conditions
etc. at beginning of the i th step interval

GUIDES FOR GRAPHICAL SOLUTION OF LINEAR SINGLE-DEGREE
UNDAMPED SYSTEM PROBLEM - SUPPORT EXCITATION

Guide No.	Type Support Excitation	Type Response	Phase-Plane Construction Details
1	Acceleration $\ddot{X}(t)$	Absolute acceleration, \ddot{X} (Forced vibration)	Coordinates: rectangular, \ddot{X} , and \ddot{X}/p . Most probable starting conditions: ¹ $\ddot{X}_0 = \ddot{X}_0/p = 0$. Suitable step intervals: $t_i/T = 0.5$ for $t_i/T \geq 5$; $t_i/T = 0.1$ for $0.1 \leq t_i/T < 1$; Interpolate $0.1 \leq t_i/T < 0.5$ for $1 \leq t_i/T < 5$; use single step for $t_i/T \leq 0.1$. Center of arc: \ddot{X}_i . Angle of arc = $(360 t_i/T)$ deg. $pT = 2\pi$ rad.
		Relative displacement of mass to support; $(-u)$, spring compression (Forced vibration)	Coordinates: rectangular, $(-u)$, and $(-\dot{u}/p)$. Most probable starting conditions: ¹ $(-u_0) = (-\dot{u}_0/p) = 0$. Suitable step intervals: ratios of t_i/T under Guide No. 1 absolute acceleration apply. Center of arc: \ddot{X}_i/p^2 . Angle of arc: $(360 t_i/T)$ deg. $pT = 2\pi$ rad.
2	Velocity step \dot{X}_0 (Sudden change in velocity might go to zero)	Absolute acceleration, \ddot{X} (Free vibration)	Coordinates: rectangular, \ddot{X} and \ddot{X}/p . Most probable starting conditions: ¹ $\ddot{X}_0 = 0$; $\ddot{X}_0/p = p(\ddot{X}_0 - \dot{X}_0)$. Center of arc: origin. Angle of arc: $(360 t_i/T)$ deg. $pT = 2\pi$ rad.
		Relative displacement of mass to support; $(-u)$, spring compression (Free vibration)	Coordinates: rectangular, $(-u)$, and $(-\dot{u}/p)$. Most probable starting conditions: ¹ $(-u_0) = 0$; $(-\dot{u}_0/p) = (\ddot{X}_0 - \dot{X}_0)/p$. Center of arc: origin. Angle of arc: $(360 t_i/T)$ deg. $pT = 2\pi$ rad.
3	Displacement $\dot{\lambda}(t)$	Absolute displacement, x (Forced vibration)	All details same as under Guide No. 1 absolute acceleration response, except for replacing \ddot{X} by x , \ddot{X}_i by $\dot{\lambda}_i$, etc.

¹Other starting conditions are possible. They can be derived from equations in Ref. 1.

Guides 1, 2, and 3

GUIDES FOR GRAPHICAL SOLUTION OF LINEAR SINGLE-DEGREE
COULOMB-DAMPED SYSTEM PROBLEM - SUPPORT EXCITATION
(Damper Tied to Support; Friction Permits Two or More Cycles of Free Vibration)

Guide No.	Type Support Excitation	Type Response	Phase-Plane Construction Details
4	Acceleration $\ddot{X}(t)$	Absolute acceleration, \ddot{X} (Forced vibration)	Coordinates: rectangular, \ddot{X} , and \ddot{X}/p . Most probable starting conditions: ¹ $\ddot{X}_0 = \ddot{X}_c$, $\ddot{X}_0/p = 0$ if $\ddot{X}_1 > \ddot{X}_c$. Suitable step intervals: See under Guide No. 1. Center of arc: \ddot{X}_i . Angle of arc: $(360 t_i/T)$ deg. $pT = 2\pi$ rad. Note: Discontinuity in \ddot{X} occurs every time $\text{sgn } \ddot{X}/p$ changes; jump is always toward \ddot{X}_1 . If $\ddot{X}_0 = 0$ and $\ddot{X}_1 - \ddot{X}_0 \leq \ddot{X}_c$, then \ddot{X}_1 will parallel $\ddot{X}(t)$ curve for the interval.
		Relative displacement; $(-u)$, spring compression (Forced vibration)	Coordinates: rectangular, $(-u)$, and $(-\dot{u}/p)$. Most probable starting conditions: ¹ $(-u_0) = (-\dot{u}_0/p) = 0$. Suitable step intervals: ¹ $t_i/T = 0.5$ for $t_i/T \geq 5$; $t_i/T = 0.1$ for $0.05 \leq t_i/T \leq 1$; Interpolate $0.1 \leq t_i/T < 0.5$ for $1 \leq t_i/T < 5$; use single step for $t_i/T < 0.05$ (damping ignored). Center of arc: $(\ddot{X}_i/p^2) - \ddot{X}_c \text{sgn } (-\dot{u})$. Angle of arc: $(360 t_i/T)$ deg. $pT = 2\pi$ rad. Note: If $\dot{u}_0 = 0$ and $(\ddot{X}_i/p^2) - (-\dot{u}_0) \leq \ddot{X}_c$, then \dot{u}_1 will parallel $\ddot{X}(t)/p^2$ curve for the interval.
5	Velocity step \dot{X}_0 (Sudden change in velocity might go to zero)	Absolute acceleration, \ddot{X} (Free vibration)	Coordinates: rectangular, \ddot{X} , and \ddot{X}/p . Most probable starting conditions: ¹ $\ddot{X}_0 = \ddot{X}_c \text{sgn } (\ddot{X}_0 - \dot{X}_0)$; $\ddot{X}_0/p = p(\ddot{X}_0 - \dot{X}_0)$. Center of arc: origin. Angle of arc: $(360 t_i/T)$ deg. $pT = 2\pi$ rad. Note: \ddot{X} reduced by $2\ddot{X}_c$ every time $\text{sgn } \ddot{X}/p$ changes.
		Relative displacement; $(-u)$, spring compression (Pseudo free vibration)	Coordinates: rectangular, $(-u)$, and $(-\dot{u}/p)$. Most probable starting conditions: ¹ $(-u_0) = 0$; $(-\dot{u}_0/p) = (\ddot{X}_0 - \dot{X}_0)/p$. Center of arc: $-\ddot{X}_c \text{sgn } (-\dot{u})$. Angle of arc: $(360 t_i/T)$ deg. $pT = 2\pi$ rad.
6	Displacement, $\dot{\lambda}(t)$	Absolute displacement, x (Forced vibration)	Coordinates: rectangular, x , and \dot{x}/p . Most probable starting conditions: ¹ $x_0 = \dot{\lambda}_0/p = 0$. Suitable step intervals: ratios of t_i/T under Guide No. 4 relative displacement apply. Center of arc: $\dot{\lambda}_i + \ddot{X}_c \text{sgn } (\dot{\lambda} - \dot{x})$. Angle of arc: $(360 t_i/T)$ deg. $pT = 2\pi$ rad. Note: If $(\ddot{X}_0 - \dot{X}_0) = 0$ and $\dot{\lambda}_1 - x_0 \leq \ddot{X}_c$, then x_1 will parallel $\dot{\lambda}(t)$ curve for the interval.

¹Other starting conditions are possible. They can be derived from equations in Ref. 1.

Guides 4, 5, and 6

GUIDES FOR GRAPHICAL SOLUTION OF LINEAR SINGLE-DEGREE
VISCOUSLY DAMPED SYSTEM PROBLEM - SUPPORT EXCITATION
(Damping Tied to Support; Damping Ratio, $\mu \leq 0.2$)

Guide No.	Type Support Excitation	Type Response	Phase-Plane Construction Details
7	Acceleration, $\ddot{\lambda}(t)$	Absolute acceleration, \ddot{x} (Forced vibration)	Coordinates: rectangular, \ddot{x} and \ddot{x}/p . Most probable starting conditions: ¹ $\ddot{x}_0 = \ddot{x}_0/p = 0$. Suitable step intervals: ratios of t_i/T under Guide No. 6 relative displacement apply. Center of arc: $\ddot{x}_i + \ddot{x}_{vi}$, where $\ddot{x}_{vi} = 2\sqrt{\frac{\ddot{x}_i - \ddot{x}_0}{p}}$. Angle of arc: $(360 t_i/T)$ deg. $pT = 2\pi$ rad. Note: Spiral diagram is used when amplitude of input pulse does not change for a time. Then angle of spiral diagram arc = $p\sqrt{1 - \mu^2}(t_i)$ rad.
		Relative displacement of mass to support; $(-u)$, spring compression (Forced vibration)	Coordinates: oblique, $(-u)$, and $(-\dot{u}/p')$. Most probable starting conditions: ¹ $(-u_0) = (-\dot{u}_0/p') = 0$. Suitable step intervals: ratios of t_i/T under Guide No. 6 relative displacement apply. Center of arc: \ddot{x}_i/p^2 (on \ddot{x}/p^2 oblique axis). Note: Spiral diagram needed. Angle of arc = $p\sqrt{1 - \mu^2}(t_i)$ rad. $pT = 2\pi$ rad. $p' = p\sqrt{1 - \mu^2}$ rad/mm
8	Velocity step $\dot{\lambda}_0$ (Sudden change in velocity might go to zero)	Absolute acceleration, \ddot{x} (Free vibration)	Coordinates: oblique, \ddot{x} and \ddot{x}/p' . Most probable starting conditions: ¹ $\ddot{x}_0 = 2\mu p(\dot{x}_0 - \dot{x}_0) = \ddot{x}_0/p' = (\dot{x}_0^2/p^2)(1 - \mu^2)(\dot{x}_0 - \dot{x}_0)$ Center of arc: origin. Note: Spiral diagram used. Angle of arc = $p\sqrt{1 - \mu^2}(t_i)$ rad. $p' = \sqrt{1 - \mu^2}$ rad/mm $pT = 2\pi$ rad.
		Relative displacement; $(-u)$, spring compression (Free vibration)	Coordinates: oblique, $(-u)$, and $(-\dot{u}/p')$. Most probable starting conditions: ¹ $u_0 = 0$; $(-\dot{u}_0/p') = (\dot{x}_0 - \dot{x}_0)/p'$ Center of arc: origin Note: Spiral diagram used; angle of arc = $p\sqrt{1 - \mu^2}(t_i)$ rad. $p' = \sqrt{1 - \mu^2}$ rad/mm $pT = 2\pi$ rad.
9	Displacement $\lambda(t)$	Absolute displacement, x (Forced vibration)	All details same as under Guide No. 7 absolute acceleration, except for replacing \ddot{x} by x , \ddot{x}_i by λ_i , etc.

¹Other starting conditions are possible. They can be derived from equations in Ref. 1.

Guides 7, 8, and 9

GUIDES FOR GRAPHICAL SOLUTION OF TWO-DEGREE LINEAR UNDAMPED
SYSTEM PROBLEM - SINGLE-SUPPORT EXCITATION

Guide No.	Type Support Excitation	Type Response	Phase-Plane Construction Details
10	Acceleration $\ddot{\lambda}(t)$	Absolute acceleration, \ddot{x} and \ddot{y} (Forced vibration)	Coordinates: principal, $\ddot{\theta}_I/p_I$ and $\ddot{\theta}_{II}/p_{II}$ for mode I phase-plane. $\ddot{\theta}_{II}/p_{II}$ and $\ddot{\theta}_I/p_I$ for mode II phase-plane. Most probable starting conditions: ¹ $\ddot{x}_0 = \ddot{y}_0 = \ddot{\lambda}_0 = 0$; therefore each phase-plane starts at origin. Suitable step intervals: Steps t_i/T_I of mode I and t_i/T_{II} of mode II each follow rules under Guide No. 1. Centers of arcs: \ddot{x}_i for both mode I and II. Angles of arcs: $(360 t_i/T_I \text{ or } T_{II})$ deg. Note: Principal coordinates transformed to rectangular coordinates by $\ddot{x} = \ddot{\theta}_I + \ddot{\theta}_{II}$ and $\ddot{y} = \alpha_I \ddot{\theta}_I + \alpha_{II} \ddot{\theta}_{II}$.
11	Velocity step $\dot{\lambda}_0$ (Sudden change in velocity might go to zero)	Absolute acceleration, \ddot{x} and \ddot{y} (Free vibration)	Coordinates: principal, $\ddot{\theta}_I$ and $\ddot{\theta}_{II}/p_I$ for mode I phase-plane. $\ddot{\theta}_{II}$ and $\ddot{\theta}_{II}/p_{II}$ for mode II phase-plane. Most probable starting conditions: ¹ $\ddot{x}_0 = \ddot{y}_0 = 0$; $\ddot{\theta}_I = \ddot{\theta}_{II} = 0$; initial jerk \ddot{x}_0 and \ddot{y}_0 expressed in principal phase-plane coordinates are $\ddot{\theta}_I/p_I = p_I \left[\frac{(\ddot{x}_0 - \ddot{y}_0) - \alpha_{II}(\ddot{x}_0 - \ddot{y}_0)}{\alpha_I - \alpha_{II}} \right]$ $\ddot{\theta}_{II}/p_{II} = p_{II} \left[\frac{\alpha_I(\ddot{x}_0 - \ddot{y}_0) - (\ddot{x}_0 - \ddot{y}_0)}{\alpha_I - \alpha_{II}} \right]$ Center of arcs: origin. Angles of arcs: $(360 t_i/T_I \text{ or } T_{II})$ deg. $p_I T_I$ and $p_{II} T_{II} = 2\pi$ rad. Note: Principal coordinates transformed to rectangular coordinates by $\ddot{x} = \ddot{\theta}_I + \ddot{\theta}_{II}$, $\ddot{y} = \alpha_I \ddot{\theta}_I + \alpha_{II} \ddot{\theta}_{II}$.
12	Displacement $\lambda(t)$	Absolute displacement, x and y (Forced vibration)	All details same as in Guide No. 10 except replacing $\ddot{\theta}_I$ by θ_I , \ddot{x} by x , etc.

¹Other starting conditions are possible. They can be derived from equations in Ref. 1.

Guides 10, 11, and 12

sgn - "algebraic sign of"

ν - Damping ratio (viscously damped system)

Δ_{vi} ,
etc. - Delta correction term for phase-plane center of ith step interval of viscously damped system

$\theta, \ddot{\theta}$,
etc. - Principal coordinates of multidegree spring mass systems

Subscript

I, II - Particular mode of vibration

y, \ddot{y} ,
etc. - Motion of responding mass, m_2

σ - Angle of obliqueness for ordinate axis in viscously damped model phase-plane diagram ($\sin \sigma = \nu$)

a_n - Ratio of amplitudes of nth mode of vibration. For Fig. 1 configuration

$$a_I = \frac{k_1 + k_2 - m_1 p_I^2}{k_2}; \quad a_{II} = \frac{k_2}{k_2 + k_3 - m_2 p_{II}^2}$$

H_n - Conversion factor to describe response from support disturbance in terms of nth mode of vibration. For Fig. 1 configuration

$$H_I = \frac{\frac{k_3}{m_2} - a_{II} \left(\frac{k_1}{m_1} \right)}{p_I^2 (a_I - a_{II})}; \quad H_{II} = \frac{a_I \left(\frac{k_1}{m_1} \right) - \frac{k_3}{m_2}}{p_{II}^2 (a_I - a_{II})}$$

p_n - Natural frequency of nth mode of vibration. For Fig. 1 configuration

$$\left. \begin{matrix} p_I^2 \\ p_{II}^2 \end{matrix} \right\} = \frac{1}{2} \left\{ \left(\frac{k_1 + k_2}{m_1} + \frac{k_2 + k_3}{m_2} \right) \right.$$

$$\left. + \left[\left(\frac{k_1 + k_2}{m_1} + \frac{k_2 + k_3}{m_2} \right)^2 \right. \right.$$

$$\left. - 4 \left(\frac{k_1 k_2 + k_2 k_3 + k_1 k_3}{m_1 m_2} \right) \right]^{1/2} \left. \right\}$$

* * *

SHOCK SPECTRA FOR A GENERAL FORCING FUNCTION

A. F. Todaro
Lawrence Radiation Laboratory
University of California
Livermore, California

Shock spectra, which are the maximum responses of many one-degree-of-freedom systems to a particular shock force or motion, can be helpful in the understanding of the general motion of elastic bodies subjected to shock forces or motions. While shock spectra for well-defined analytic functions are available, those for non-analytic forcing functions are not so easily found. A method for determining these spectra is described.

INTRODUCTION

The object of this paper is to familiarize engineers with the concept of shock spectra, its mathematical development, and finally the only reason for its existence — its use.

The general motion of elastic bodies when subjected to shock forces or motions is extremely complicated and often leads to frustration when a reasonably concise understanding is attempted. Shock spectra, however, do indeed shed some light and can be a useful tool.

Shock spectra are the maximum responses of many one-degree-of-freedom (ODF) systems to a particular shock force or motion. The responses can be displacement, velocity, or acceleration (absolute or relative). The spectra representations can be plotted as the ratio of the maximum displacement response (A_{\max}) divided by the maximum displacement input (U_g) versus the natural frequency of each ODF system. Shock spectra are also plotted with velocity and acceleration ratios versus the ratio of the pulse duration (τ) divided by the natural periods of the ODF system (T).

The conceptual definition of shock spectra will be illustrated with the following example: Suppose that attached to the mounting plane of a shock machine are many ODF systems, each with a different natural frequency. To each ODF system an accelerometer is mounted, and the mounting plane is suddenly accelerated. If the ensuing maximum acceleration response for each ODF system is plotted versus its

natural frequency, the result would be an acceleration shock spectra. The response motion is generally divided into two subdivisions. The "primary response" is in the direction of the applied motion only, while the "residual response" is in two directions and symbolizes the system in free vibration.

Shock spectra for well-defined analytic functions such as half-sine, sawtooth, square, and so on, are available;¹ however, the spectra for non-analytic forcing functions are not generally available, and therefore a method for determining these spectra will now be discussed.

MATHEMATICAL DEVELOPMENT²

Assume $U_g > X$,

$$X_r = U_g - X = \text{relative displacement,}$$

$$\ddot{X}_r = \ddot{U}_g - \ddot{X} = \text{relative acceleration,}$$

$$m\ddot{X} = kX_r,$$

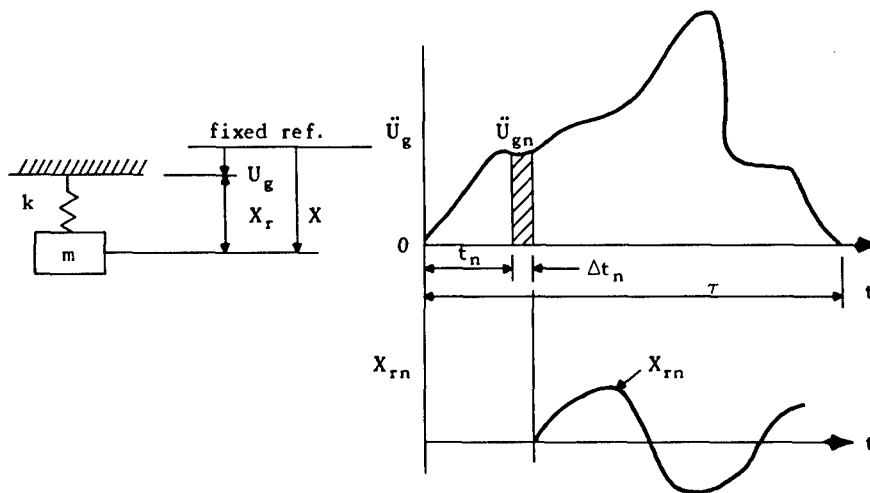
$$m(\ddot{U}_g - \ddot{X}_r) = kX_r,$$

and

$$\ddot{X}_r + \frac{k}{m} X_r = \ddot{U}_g(t). \quad (1)$$

¹C. M. Harris and C. E. Crede, editors, *Shock and Vibration Handbook* (McGraw-Hill Book Co., Inc., New York, 1961), Vol. 1, Section 8.

²Method of superposition using the Duhamel integral.



To solve the differential equation, Eq. (1), divide the $\ddot{U}_g(t)$ function into Δt_n strips, the areas of each being a velocity change $\ddot{U}_{gn} \times \Delta t_n$. Since the system is linear, the theory of superposition is valid and therefore for each velocity change the system can be described as independent of the motion that has taken place before or after each impulse. Summing over each velocity change is all that remains for a description of the system.

The solution to Eq. (1) is

$$X_{rn} = A \sin \omega_a [t - (t_n + \Delta t_n)], \quad \omega_a^2 \equiv \frac{k}{m}.$$

This characterizes an ODF system in free vibration due to a sudden velocity change applied to its foundation and starting at time $(t_n + \Delta t_n)$. Taking the first derivative,

$$\dot{X}_{rn} = A \omega_a \cos \omega_a [t - (t_n + \Delta t_n)],$$

with boundary conditions at $t = t_n + \Delta t_n$ and $\dot{X}_{rn} = \ddot{U}_{gn} \times \Delta t_n$. Therefore,

$$A = \ddot{U}_{gn} \times \Delta t_n / \omega_a,$$

$$X_r = X_{r1} + X_{r2} + \dots + X_{rn},$$

and

$$X_r = \frac{\Delta t}{\omega_a} \sum_{n=1}^{n=t/\Delta t} \ddot{U}_{gn} \sin \omega_a [t - (t_n + \Delta t)] \quad (2)$$

for equal Δt_n .

From $\ddot{X} = \omega_a^2 X_r =$ absolute acceleration,

$$\ddot{X} = \omega_a \Delta t \sum_{n=1}^{n=t/\Delta t} \ddot{U}_{gn} \sin \omega_a [t - (t_n + \Delta t)] \quad (3)$$

Equation (3) is maximized for each of many ω_a , thus yielding shock spectra, or solved for a particular ω_a , yielding the time response of the absolute acceleration.

DIGITAL COMPUTER METHOD

Should digital computers be available, codes are in existence to solve Eq. (1) directly when the non-analytic forcing function is digitized.¹ This is the method the author used. Care should be taken so that Δt strips are small in width compared to both the nature of the forcing function and the top frequency of interest. In addition, choose many frequency points or τ/T ratios so that interpolation is minimized. Forcing functions with known shock spectra were used as a check on the computer code. Various shock spectra are shown in Figs. 1 through 5. When the forcing function goes to zero, Eq. (1) reduces to

$$\ddot{X}_r + \frac{k}{m} X_r = 0. \quad (4)$$

In other words, the system is in the free vibration mode and the solution to Eq. (4) is

$$X_r = A \sin \omega_a t + B \cos \omega_a t \quad t > \tau, \quad (5)$$

with A and B to be determined.

From the computer, $X_r(\tau)$ and $\dot{X}_r(\tau)$ at the end of the pulse are known quantities. By

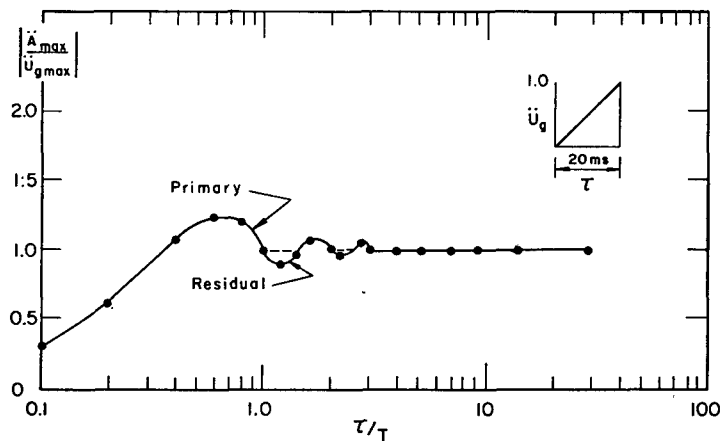


Fig. 1 - Primary and residual shock spectra for a sawtooth forcing function

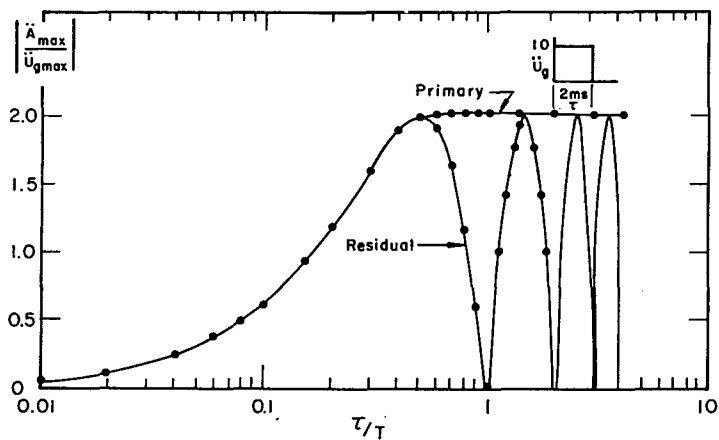


Fig. 2 - Primary and residual shock spectra for a square wave forcing function

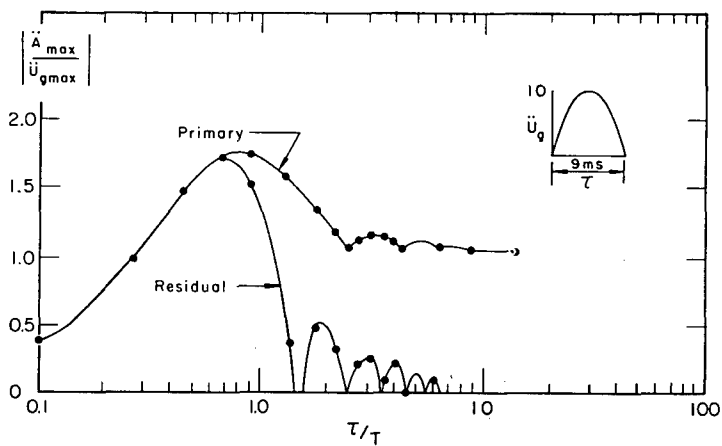


Fig. 3 - Primary and residual shock spectra for a half-sine forcing function

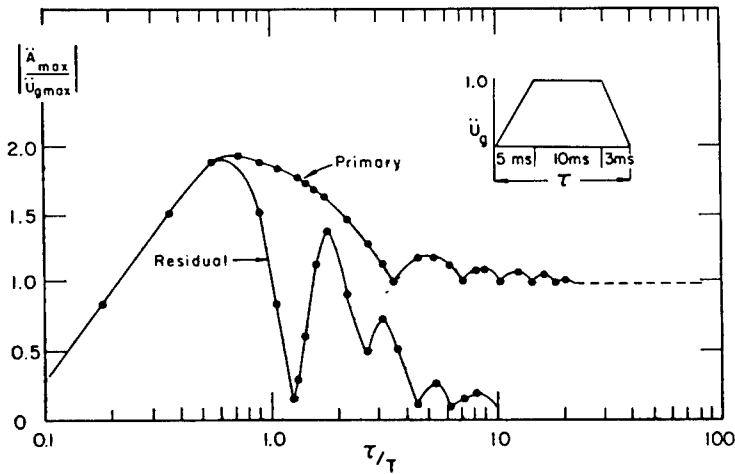


Fig. 4 - Primary and residual shock spectra for a trapezoidal forcing function

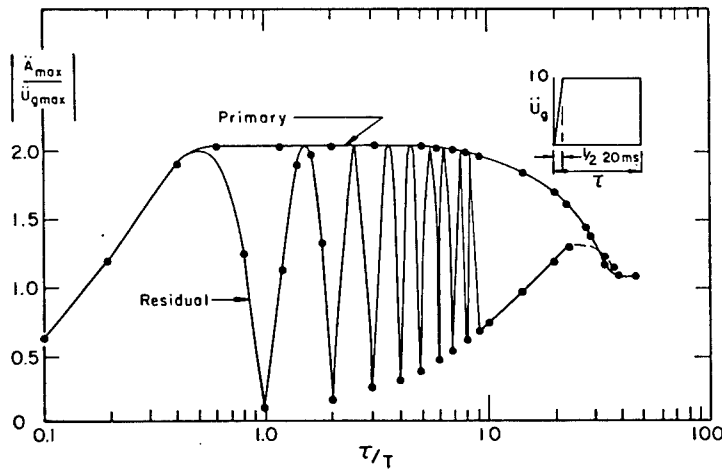


Fig. 5 - Primary and residual shock spectra for a square wave forcing function with a finite rise time

taking the first derivative of Eq. (5), X_r has a maximum value when

$$\tan^{-1}\left(\frac{A}{B}\right) = \omega_a t.$$

$$\begin{aligned} X_{rmax} &= A \sin\left(\tan^{-1}\frac{A}{B}\right) + B \cos\left(\tan^{-1}\frac{A}{B}\right) \\ &= [A^2 + B^2]^{1/2}. \end{aligned} \quad (6)$$

Solving for the constants A and B from the boundary conditions at $t = \tau$, namely $X_r(\tau)$ and $\dot{X}_r(\tau)$, yields

$$A = X_r(\tau) \sin \omega_a \tau + \frac{\dot{X}_r(\tau)}{\omega_a} \cos \omega_a \tau,$$

$$B = X_r(\tau) \cos \omega_a \tau - \frac{\dot{X}_r(\tau)}{\omega_a} \sin \omega_a \tau.$$

Substitution into Eq. (6) yields

$$X_{rmax} = \left[\overline{X_r(\tau)}^2 + \left(\frac{\dot{X}_r(\tau)}{\omega_a} \right)^2 \right]^{1/2}, \quad (7)$$

which is the maximum response in the free vibration mode. Thus the computer can stop

solving Eq. (1) at time $t = \tau$, and with the use of Eq. (7) the primary and residual shock spectra are totally determinant.

USE OF SHOCK SPECTRA

It is important to note that when $\tau/T \leq 1/4$ the pulse shape is of little significance in determining the system response.

1. A designer can approximate the response of his design knowing the natural frequency and the forcing function. The response can be either velocity, acceleration, or displacement.

2. Given a shock spectra as an environmental criteria, transformation to a response-

time function is made by simply comparing the desired spectra to the spectra associated with each forcing function.

3. The response-time signatures from an experimental test can now be transformed to its equivalent shock spectra.

ACKNOWLEDGMENTS

The author would like to express his sincere appreciation for the help of Prof. Joseph Penzien, Engineering Consultant to the Laboratory and to Joe Brady of the Computation Division. This work was performed under the auspices of the U. S. Atomic Energy Commission.

* * *

SOLUTION OF STRUCTURAL RESPONSE PROBLEMS

BY ANALOG COMPUTERS*

R. Pittman and R. W. Wheeler
McDonnell Aircraft Corporation

INTRODUCTION

Of significant importance to the engineer in the analysis of various equipment packages and aircraft structural components in today's high performance aircraft is the dynamic response of the structure to both continuous random and impulsive exciting phenomena. These excitations may be produced by such varied sources as engine exhaust noise, rotating unbalances, gun fire, air turbulence, aerodynamic buffeting, and dynamic loads such as developed during landing and takeoff, particularly in carrier operations. Since these exciting forces are often random in occurrence or impulsive in nature and the structure is redundant and sometimes nonlinear, analysis by conventional methods becomes very difficult, if not impossible. Therefore, operational and direct analog computers are of increasing importance in the solution of such problems. Both types of analog computers allow solution of either linear or nonlinear differential equations and rapid parameter variation. They can also supply the solution directly in plotted form. With reference to structural problems, the operational analog computer (also known as a differential analyzer) is best suited for solving modal problems, i.e., equations which may contain variable (during a problem) or nonlinear springs, masses, and damping. In the direct analog computer, all of the major structural components are represented by their electrical equivalents. In this manner, any structural redundancies are simulated directly by electrical redundancies. Rapid changes may be made in structural components and the stress in a structural component may be easily monitored under any external excitation, which may be of any form desired. It is the purpose of this paper to demonstrate the use of analog computers by showing how such computers were used on two separate and entirely different problems. Either of these problems

would have been virtually impossible to solve on digital computers.

OPERATIONAL ANALOG COMPUTER

The first problem to be discussed is the fuselage response study of a high performance reconnaissance aircraft subjected to random atmospheric turbulence. This study was initiated to determine the effects of turbulence-induced fuselage motion on camera resolution. The operational analog computer was chosen for this problem because of the inclusion of a nonlinear control system and because mode shapes were previously available. The equations of motion could therefore be written. The operational analog computer essentially solves these equations electrically. To demonstrate the fundamental concepts of the operational analog computer, let us take a simple spring-mass-damper system as shown in Fig. 1. This figure shows how the equation of motion governing this system is set up on the computer. It should be noted that each integration gives a sign inversion so that, e.g., when we feed $(-\ddot{x})$ in, the output is $(+x)$. As can be seen, the input into the summing integrator is,

$$\frac{F(t)}{M} - \frac{c}{M} \dot{x} - \frac{k}{M} x,$$

as shown in Fig. 1, is equal to \ddot{x} . The computer-signals may be monitored anywhere along the line so that any parameters may be read out during problem-solution.

For this analysis, the aircraft was considered to be operating within the proposed low altitude, high-speed flight regime during which the maximum effects due to turbulence are expected to occur.

*This paper was not presented at the Symposium.

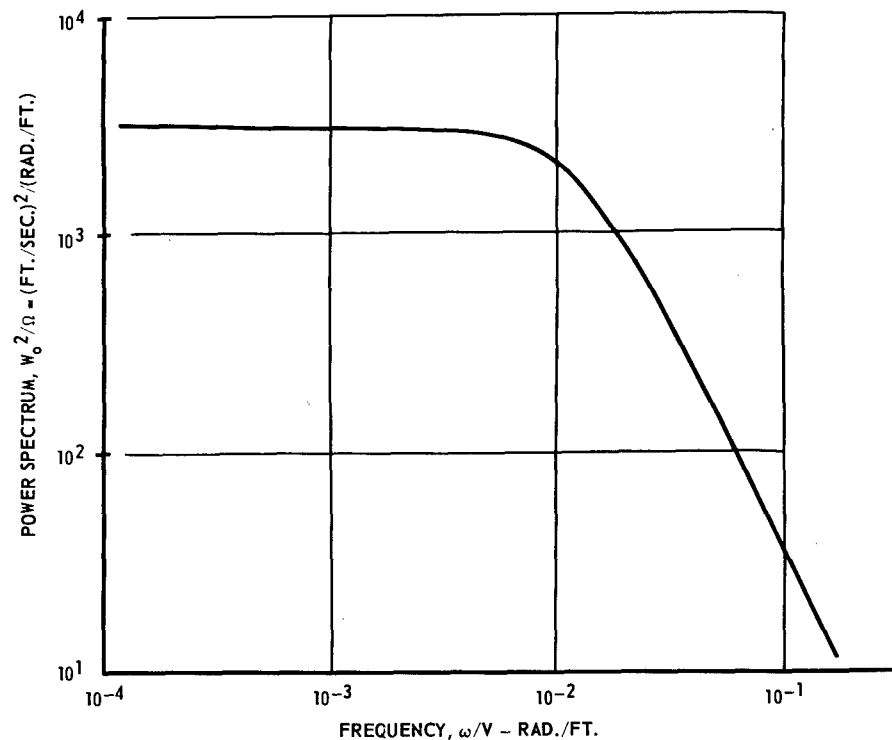


Fig. 4 - Extreme gust spectrum, low altitude, clear skies

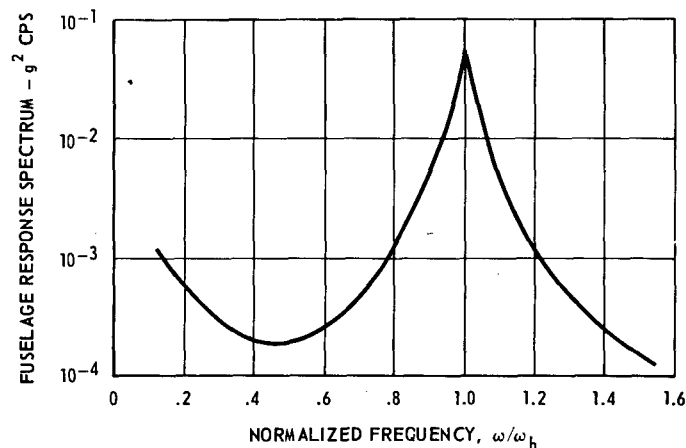


Fig. 5 - Fuselage response spectrum, at nose

The power spectral density plot of Fig. 5 shows the energy distribution peaking at the fuselage fundamental bending frequency. This tuned response is caused by the single elastic degree of freedom considered in the analysis. The inclusion of additional elastic degrees of freedom would show the effective energy level being fed into the airframe through each of the various modes.

Figure 6 presents the results of a statistical analysis in the form of a frequency-distribution. As can be seen, the distribution of peaks is quite close to that of a Rayleigh-distribution.

Comparison of the results of this study with experimental flight data for several high performance aircraft shows the analog solution to

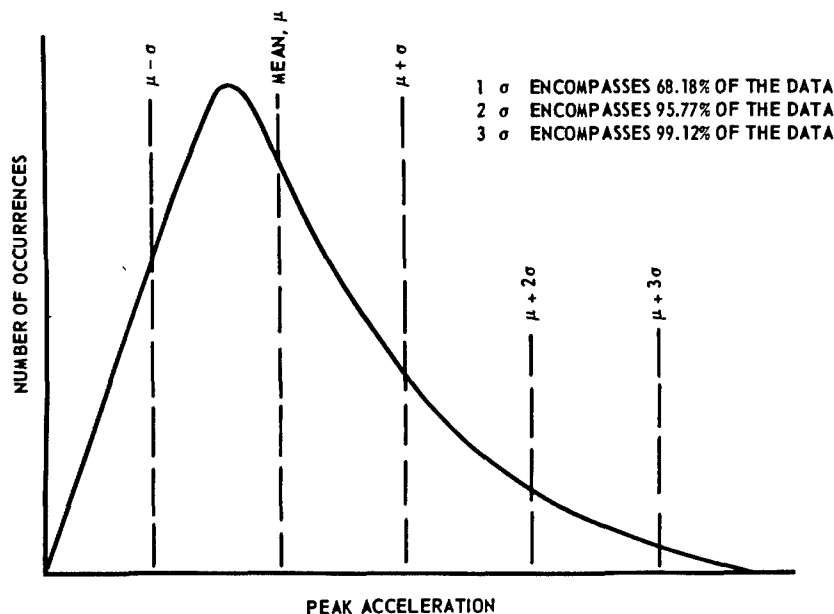


Fig. 6 - Acceleration distribution

be representative of the aircraft structural response in the frequency region investigated. The inclusion of additional elastic degrees of freedom is easily accomplished by adding the necessary transfer functions as indicated in Fig. 4 by dashed blocks, and should adequately define the vibration environment throughout the frequency range encompassed by those elastic modes. The number of elastic modes that may be considered is limited only by the analog computer's capacity.

DIRECT ANALOG COMPUTER

The second problem, the dynamic response of a low aspect ratio aircraft wing to a carrier landing, was solved on the direct analog computer. This computer was chosen for this problem for several reasons:

1. The direct analog computer has an electrical equivalent for each member of the structural system, and therefore structural redundancies pose no special problem;
2. Rapid stiffness and mass changes of wing components can be made; and
3. By monitoring voltages and currents in appropriate locations, the bending moment, shear, or torque in a wing structural member can be readily obtained as a function of time.

The operational analog computer is not suitable for this type of problem because shears, bending moments, or torques of individual wing members are not inherently obtained from a modal approach. A digital computer is quite cumbersome for this type of problem. The only satisfactory alternative to performing the analysis on the direct analog computer from an analysis standpoint would be a test program which, naturally, would be quite expensive and also questionable from a test-article availability standpoint.

The direct analog computer is distinguished from the operational analog computer by the fact that passive circuit elements, namely inductors, capacitors, transformers, and resistors are employed in the direct analogy circuitry, as well as amplifiers and other electronic devices. The computer's passive elements are used to represent the analogous elements of the mechanical system. For purposes of illustration, let us look at a simple mass-spring-damper system and its electrical equivalent, Fig. 7. As can be seen from this example, the passive electrical elements represent physical properties of the mechanical system. In addition, currents as well as voltages take on physical significance in the direct analog computer as opposed to the operational analog computer in which only voltages are used as outputs. Transformers are the only passive circuit elements not covered in the mass-spring-damper system. They are used to represent distances, sign changes,

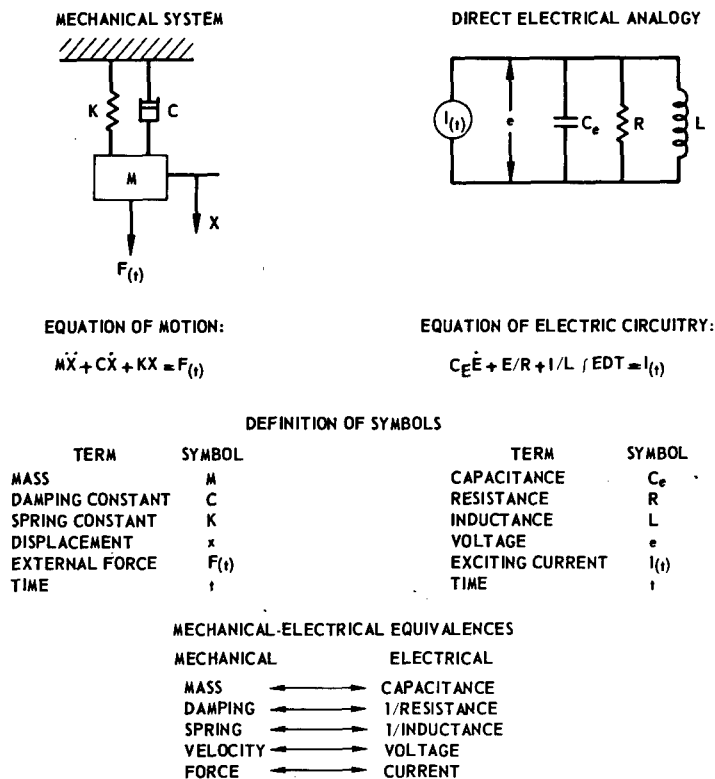


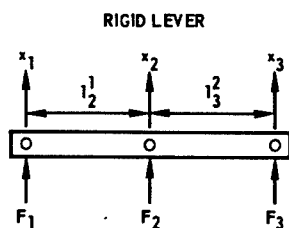
Fig. 7 - Analogy between mass-spring-damper system and electrical equivalent (direct analog)

and coordinate transformations, the mechanical equivalent being a rigid lever as illustrated in Fig. 8.

This general concept, illustrated in Figs. 7 and 8, can then be applied to much more complex structures. The structure analyzed in this problem is shown in Fig. 9. As can be seen, we have a rather complex structure, especially inboard of the wing-fold. The electrical equivalents of this structure are presented in Figs. 10 through 12. (Note that three circuits are used, one for each deflection coordinate.) The following are representative examples of how the mechanical-electrical analogy applies: the bending flexibility of the spar between nodes 8 and 9 (see Fig. 9) is represented by inductor L9 in the roll circuit; the twisting flexibility of the torque box between spars 2-3-4-5 and 7-8-9-10 and ribs 2-7 and 3-8 is represented by inductor L18 in the pitch circuit; the distance between the midpoint of spar 7-8 and the midpoint of spar 8-9 is represented by the primary winding of transformer 6 (or P6) shown in the plunge circuit; and the mass associated with node 8 is represented by capacitor C₈ in the plunge circuit.

The fighter aircraft wing shown in Fig. 9 was represented on the direct analog computer as a built-up structure analogy and a beam-rod analogy inboard and outboard of the wing-fold, respectively. In a built-up structure analogy, inductors are used to represent the flexibility of each rib, spar, and torque box segment, and the masses, represented by capacitors, are located at rib-spar intersections. The beam-rod representation requires that the stiffness of all spars and torque boxes be "lumped" into one beam in bending and one rod in torsion, respectively, and that "lumped" inertias and masses must be associated with points along the beam-rod.

The coupling between the three circuits required to fully describe the electrical circuitry of the analog representation can be seen if one considers the deflection of a point on the wing planform. The total deflection of any point consists of rigid body pitch, roll, and translation motions in which no bending or twisting of any wing element takes place, deflection due to bending of ribs and twisting of torque boxes (pitching), and deflection due to bending of spars



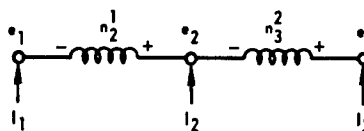
EQUILIBRIUM RELATIONSHIPS:

$$\frac{\dot{x}_3 - \dot{x}_2}{l_3^2} = \frac{\dot{x}_2 - \dot{x}_1}{l_2^1}$$

$$F_3 l_3^2 = F_1 l_2^1$$

$$F_1 + F_2 + F_3 = 0$$

TRANSFORMER



EQUATIONS EXPRESSING VOLTAGE AND CURRENT LAWS OF AN IDEAL TRANSFORMER AND KIRCHHOFF'S CURRENT LAW:

$$\frac{e_3 - e_2}{n_3^2} = \frac{e_2 - e_1}{n_2^1}$$

$$i_3 n_3^2 = i_1 n_2^1$$

$$i_1 + i_2 + i_3 = 0$$

DEFINITION OF SYMBOLS			
TERM	SYMBOL	TERM	SYMBOL
FORCES	F_1, F_2, F_3	CURRENTS	i_1, i_2, i_3
VELOCITIES	$\dot{x}_1, \dot{x}_2, \dot{x}_3$	VOLTAGES	e_1, e_2, e_3
LEVER ARMS	l_2^1, l_3^2	TRANSFORMER TURNS	n_2^1, n_3^2

MECHANICAL-ELECTRICAL EQUIVALENCES	
MECHANICAL	ELECTRICAL
FORCES	←→ CURRENTS
VELOCITIES	←→ VOLTAGES
LEVER ARMS	←→ TRANSFORMER TURNS

Fig. 8 - Rigid lever and electrical equivalent

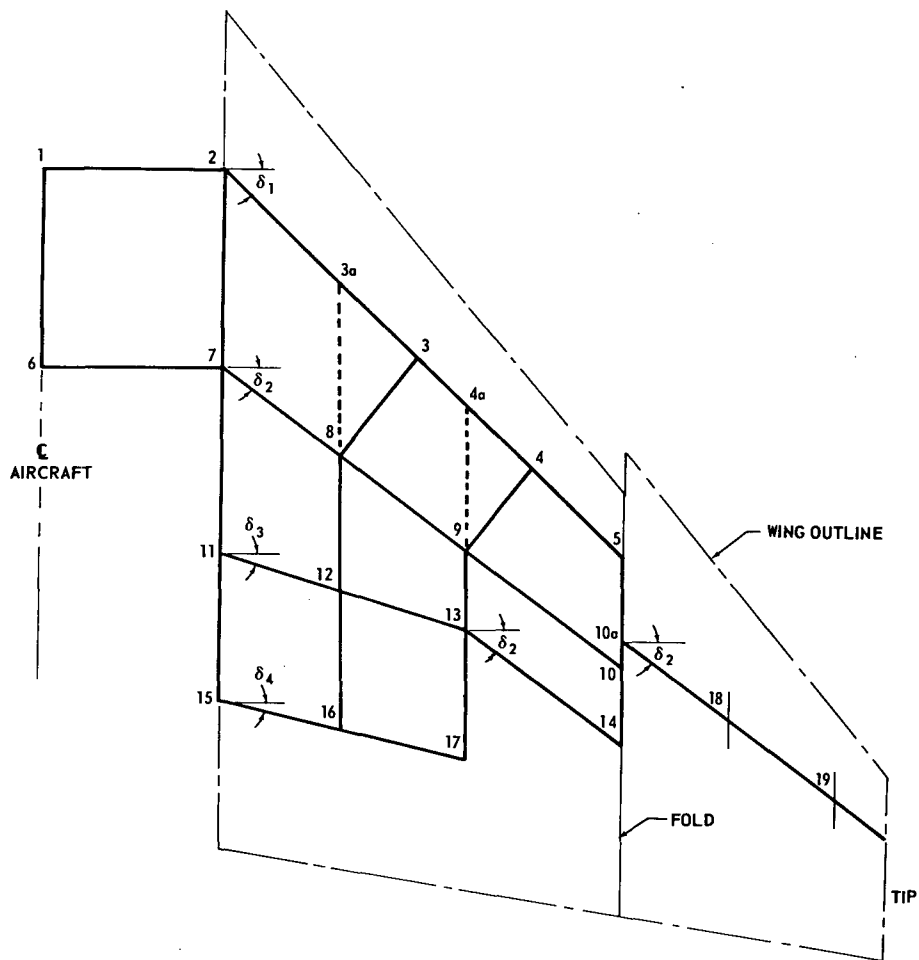


Fig. 9 - Layout of idealized fighter wing

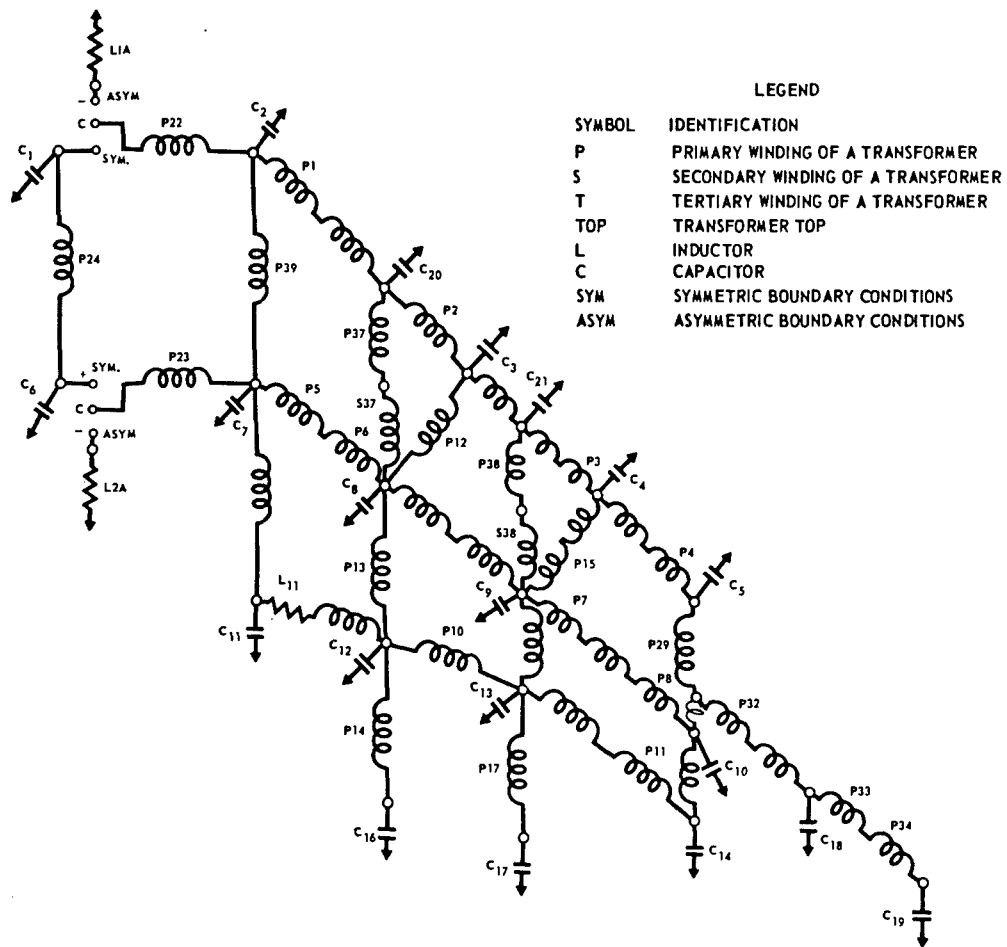


Fig. 10 - Idealized fighter wing plunge circuit

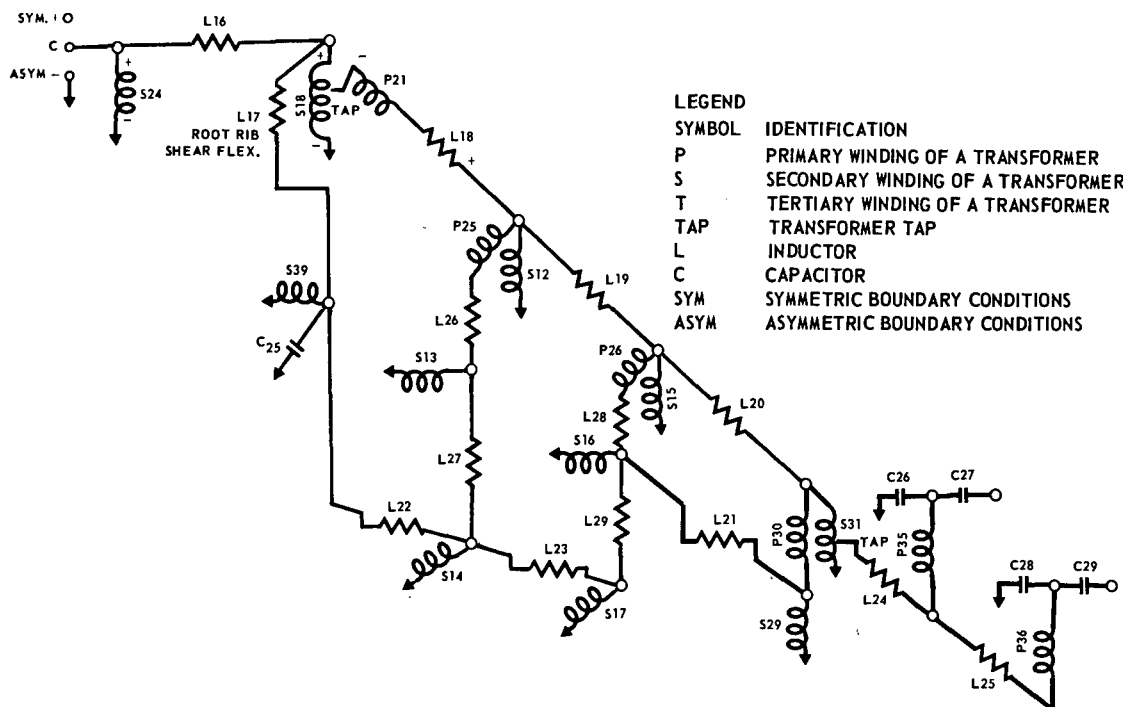


Fig. 11 - Idealized fighter wing pitch circuit

(rolling). Therefore, to fully describe the total motion of a point all three circuits are coupled together by having common nodes.

In this dynamic response study, the main gear loads impressed during hard landings were determined from a series of airplane drop tests. The gear loads are considered to consist of axial, lateral, and longitudinal components applied at the axle of the wheel. The lateral loads result from the aircraft touching down in a rolled attitude and the longitudinal loads are caused by a combination of wheel spin-up and aircraft pitched attitude at touchdown. These gear loads were introduced into the analog by diode function generators at the wing chord plane above the main landing gear (between points 9 and 13 in Fig. 9) as vertical, pitching moment, and rolling moment forcing functions.

Dynamic response studies of the wing were performed for several combinations of sink speed and aircraft roll and pitch attitudes at touchdown. Very early in the study, lateral and longitudinal gear loads were found to have minor effects on the fundamental wing response for realistic values of roll and pitch attitude at touchdown. This leaves the axial gear load as the major determinant for the wing dynamic response and thus the factors which determine

the magnitude and shape of the axial load vs time histories dictated the maximum wing response. These factors were aircraft roll and pitch attitudes and sink speed at touchdown (pitch attitude having a very minor effect). With all other factors remaining constant, a higher sink speed resulted in larger axial gear loads which in turn produced larger wing response. The rolled attitude of the aircraft at touchdown was found to be an extremely important factor in determining the dynamic response of the wing.

When an aircraft lands with a rolled attitude, one main landing gear touches down before the other, thus producing two separate axial gear load vs time curves, one for the low gear and one for the high gear. Typical axial load vs time curves for both gears are presented in Fig. 13. As can be seen from the curve for the low gear, there are two peaks, the phasing of which is determined by the aircraft roll angle (i.e., the period between touchdown of the main-gears). When this phasing coincides with the period of a fundamental wing bending mode of vibration, the wing response will be amplified. To illustrate this let us consider the two dynamic axial strut load curves in Fig. 14. Presented in Fig. 14 are the axial gear load vs time curves for two different aircraft rolled attitudes (2 and 7 degrees) at touchdown. From

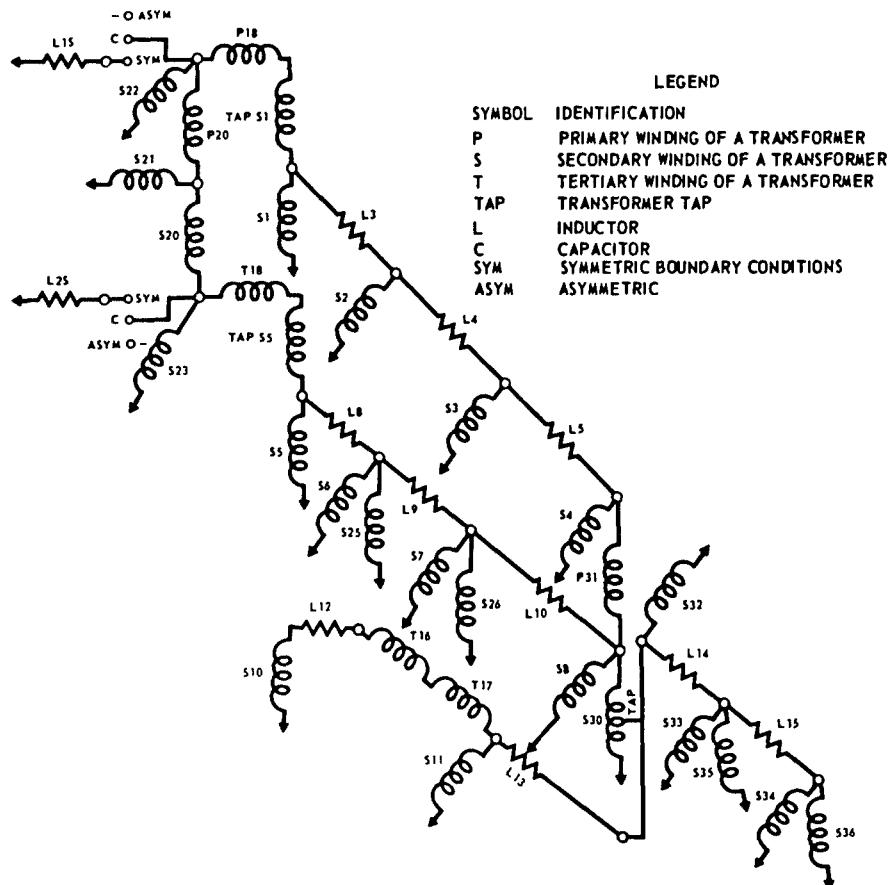


Fig. 12 - Idealized fighter wing roll circuit

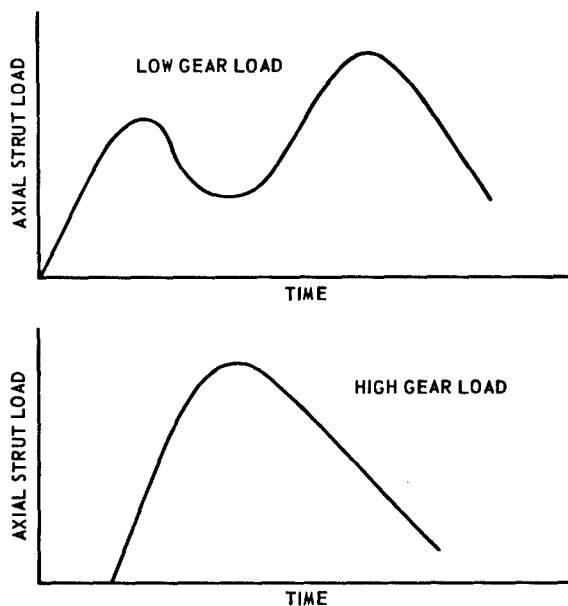


Fig. 13 - Typical axial strut load vs time curve for an aircraft landing at a rolled attitude

a work concept, work being expressed as

$$\int_0^{t_e} F \dot{q}_w dt ,$$

where t_e is the time at which the dynamic axial strut force, F , reduces to zero; a 2-degree roll would result in more work being done on the wing than would a 7-degree roll for the particular fundamental-wing frequency considered in the illustration. Since the work done on the wing or the kinetic energy imparted to it determines the response, the rolled attitude with peak load phasing coincident with a fundamental wing mode results in maximum wing response in that mode. Figure 15 illustrates this by presenting the bending moment responses in the spar between point 13 and the midpoint of the segment between points 13 and 14 for 2- and 7-degree aircraft roll attitude at touchdown. It can be seen that because of the dynamic effects, the lower roll-angle actually results in higher loads on the wing.

In the dynamic response studies the maximum accelerations of wing points, dynamic bending moments and shears in ribs and spars, and dynamic twisting moments in torque boxes for various landing conditions were determined to provide a complete carrier landing loads environment. A wing pylon with stores could have been incorporated in the analog circuitry with little difficulty and the environment to which the stores would be subjected during carrier landings could have been easily determined.

CONCLUSIONS

It has thus been shown on two representative examples that analog computers, operational and direct, are ideally suited for the solution of structural response problems. Operational analog computers are particularly suited to structures which can be represented by a modal approach, and direct analog computers are especially well suited to analyze highly redundant structures. Parameter

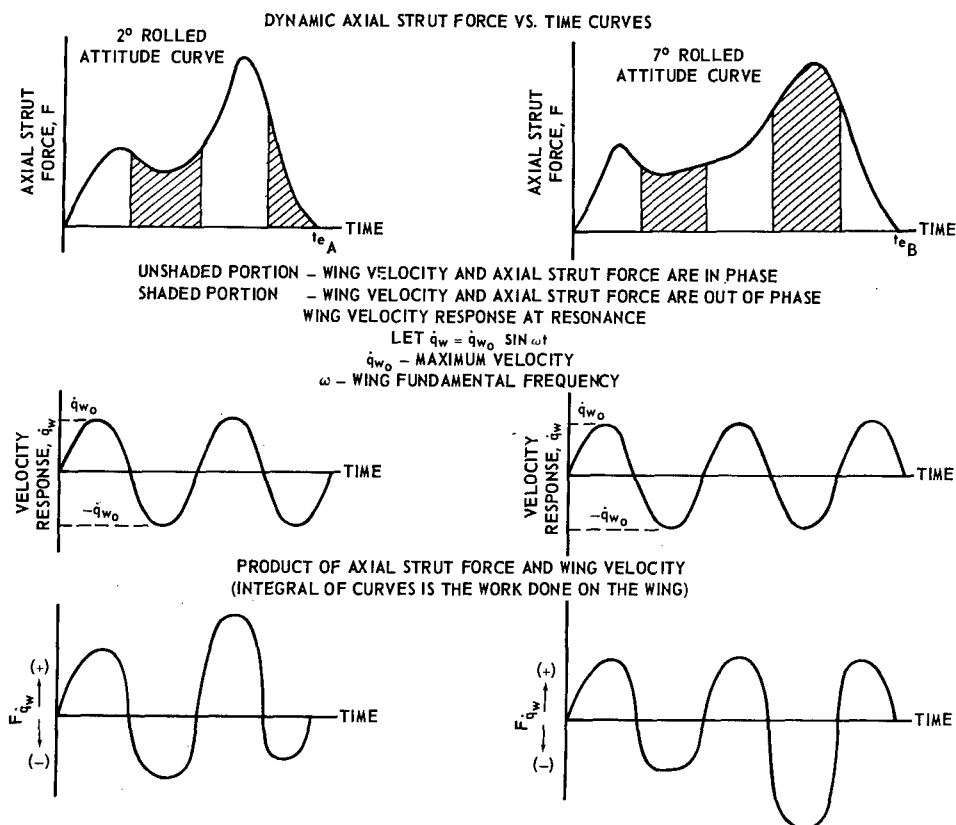


Fig. 14 - Graphical analysis of two dynamic axial strut forces for wing response at resonance

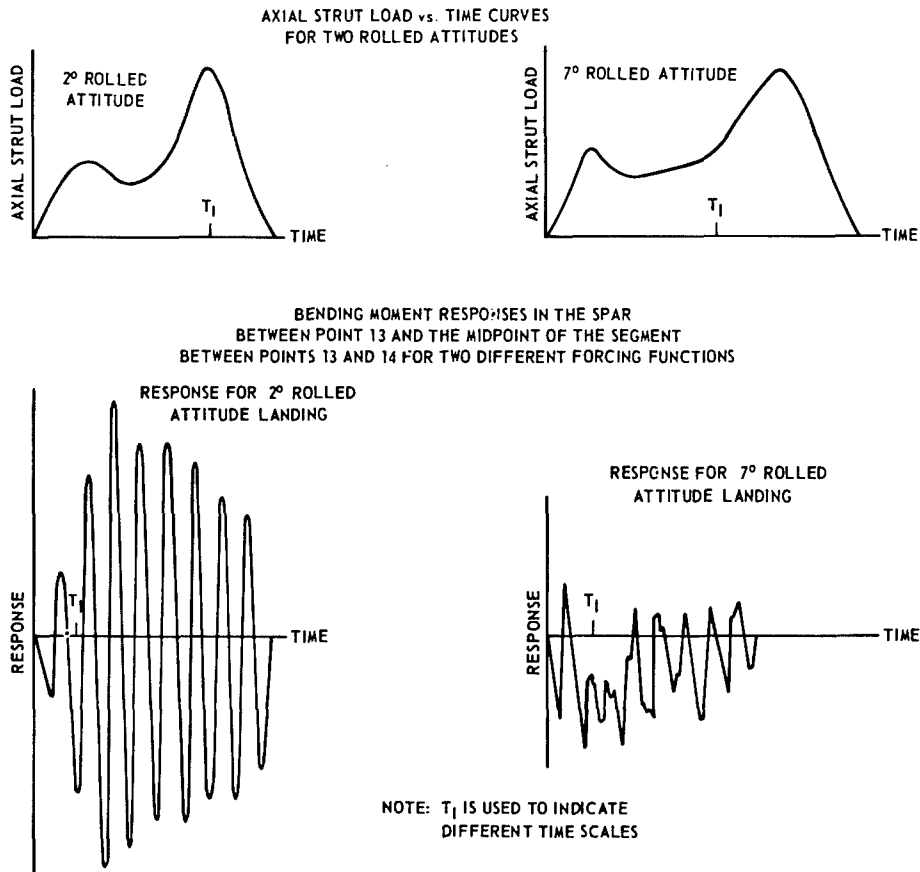


Fig. 15 - Typical wing responses to two separate forcing functions

changes are easily made and the solution is readily obtained in a plotted form. Non-linear and highly redundant structures and the various forms that forcing functions take do not represent obstacles in the determination of a structure's dynamic response characteristics.

LIST OF SYMBOLS

One and two dots over symbol indicate first and second differentiation with respect to time, i.e., velocity and acceleration:

Symbol Definition

c coefficient of damping

F axial strut force

I_p total airplane pitch moment of inertia about c.g.

$K_1, K_2, K_a, K_a',$
and K_q autopilot constants dependent on speed and altitude

M_A total mass of airplane

M_E equivalent mass, $= \sum M_i q_i^2 / q_\phi^2$

M_i mass of airplane section associated with fuselage station i

q_a total displacement of airplane c.g.

q_h displacement of airplane c.g. due to airplane vertical translation

q_i displacement due to fuselage bending at fuselage station i

q_w displacement of wing at gear

q_ϕ displacement at fuselage reference station due to fuselage bending

q_θ displacement at fuselage reference station due to airplane pitch

S Laplace operator

V forward velocity

w_o	upwash velocity	θ	airplane pitch angle
α_A	total airplane angle of attack	μ	mean
α_{ϕ_T}	pitch slope at tail due to fuselage bending	σ	standard deviation
δ	total stabilator angle of attack	ω	frequency
$\delta_{A/P}$	stabilator angle due to autopilot	ω_h	fuselage first bending natural frequency
		Ω	ω/V

* * *

AN ANALYTICAL SIMULATION OF THE DYNAMIC RESPONSE OF AN IMPACTING ELASTIC SYSTEM*

R. E. Hess and W. L. Kammer
North American Aviation, Inc.
Columbus, Ohio

INTRODUCTION

A common operational requirement of certain modern-day military equipment is that it must be capable of being delivered to forward field units by means of a parachute-retarded air drop from a cargo airplane. This type of delivery frequently imposes critical loading conditions on the equipment during opening of the parachute system and, more significantly, during the impact at landing. The nature of some equipment, such as heavy vehicles and artillery pieces, is such that ruggedness is inherent in the basic design, and the shock loadings associated with ground impact are inconsequential. Other equipment, such as electronic instruments and their spare parts, are extremely delicate, but their relatively small size permits careful packaging to prohibit shock damage. However, one particular class of equipment, the mobile, field-operated tactical missile, presents a significant design problem when air-drop delivery is required.

Since it is usually required that the missile and its transporter-launcher vehicle be ready for operation and missile launchings shortly after ground impact, it is mandatory that the total system be dropped intact in its operational configuration. This precludes fancy tie-downs and elaborate shock-isolation of the missile itself if the system is to be activated in a short time. On the other hand, the missile itself represents a design which is extremely weight-critical and which cannot afford excessive design margins to cover loading contingencies such as extreme shock loads. Several alternatives are open to the missile system designer faced with this problem.

First, the designer must provide a basic means for absorbing or reducing the impact shock transmitted to the entire system, such as

the use of crushable honeycomb, retro-rockets, or hydraulic shock absorbers. Second, in designing the method of supporting the missile on its launcher mechanism, he must position the supports such that they allow a minimum of missile airframe dynamic response due to excessive unsupported lengths of the missile body. Third, having minimized the input loads and dynamic response loads which the missile airframe feels, the designer is obligated to predict these response loads as accurately as possible so that the missile structure may be designed efficiently and not conservatively.

True, the designer could adopt an experimental cut-and-try method of designing his impacting system. Reference 1, for instance, presents a comprehensive discussion of the current state-of-the-art in cushioning system design, including the conclusion that drop-testing of full-scale hardware is the most effective method of investigating the design of an impacting system since "there are no analyses for the data to be compared with, nor are there any analytical methods which would use the data to predict results under different test conditions." This design approach might be economically used when relatively small, inexpensive equipment or material is concerned. For large systems, however, such as the mobile tactical missile system involving six and seven-digit cost figures for each full-scale hardware unit, the cut-and-try approach cannot be justified and the designer must resort to extensive design analysis of the impact condition prior to hardware fabrication.

This paper presents a discussion of an analytical simulation of an impacting elastic

¹M. P. Gionfriddo, "Design of Cushioning Systems for Air Drop," paper presented at the 30th Symposium on Shock, Vibration, and Associated Environments (Oct. 1961).

*This paper was not presented at the Symposium.

system such as could be used to furnish design parameters for the air-dropped missile system introduced above. The particular simulation described here was accomplished during the preliminary design of a mobile field-artillery surface-to-surface missile system and as such, was carried out under limitations in schedule and computer equipment. As a result, many simplifications in the mathematical representation of the system were necessary and will be noted in subsequent paragraphs. The basic approach used, however, is typical of that which would be used in a more extensive analysis, and its simplicity will serve to facilitate its illustration.

The primary purpose in accomplishing the simulation was to determine the missile airframe dynamic loads resulting from the impact conditions. Simple preliminary analyses had predicted that this condition would produce critical loads for the design of portions of the missile airframe. Therefore, a more extensive analysis was required to establish the dynamic load values for structural design.

DESCRIPTION OF THE SYSTEM

The missile system which was simulated is shown in Fig. 1. The system consisted of a tracked transporter vehicle to provide operational mobility, a launcher unit mounted on the rear deck of the transporter vehicle, and the missile. The launcher unit consisted of a rotary platform to control azimuth, and a set of launch rails whose elevation was controlled by a hydraulic actuator. During an air-drop the rails were positioned at zero elevation and were supported at their forward end by a vertical post, thus eliminating the elevation

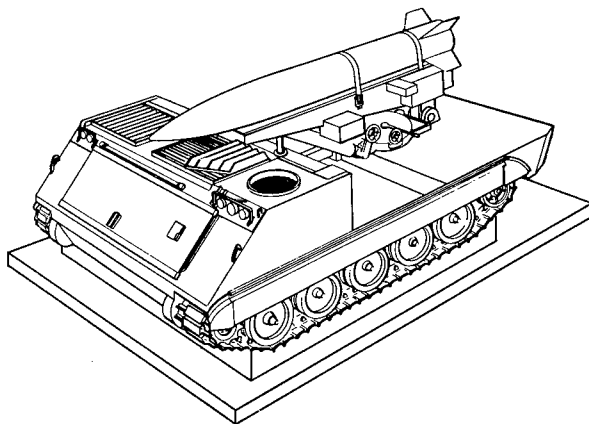


Fig. 1 - Mobile missile system

actuator as a load-bearing member for this condition. For the air-drop delivery the entire transporter-launcher-missile system was mounted on a rectangular pallet to which a multi-parachute system was attached. A layer of crushable paper honeycomb installed between the pallet and the bottom surfaces of the transporter vehicle provided the main cushioning to absorb much of the ground impact shock load. Prior studies of the primary cushioning system had indicated that a reduction in overall impact loading could be achieved through the use of a dual cushioning system employing both retro-rockets and crushable paper honeycomb. Excessive cost and complexity eliminated this concept, however, and the simulation therefore reflected the single cushioning system of crushable honeycomb.

THE MATHEMATICAL MODEL

The mathematical model of the missile system developed for this simulation was limited in complexity and completeness by (1) a compressed time schedule in which the work had to be completed, and (2) the availability of only one 80-amplifier analog computer console for the study. (The selection of an analog computer as the simulation tool is discussed in a later section of this paper.) Nevertheless, the final model contained sufficient detail to qualify as a valid representation of the actual system.

Figure 2 shows a schematic of the transporter-launcher-missile system resting on the crushable honeycomb cushioning system. The missile itself was assumed to be an elastic body represented by the first two body-bending vibration modes. In a more complete analysis, it would be desirable to include at least one or two additional vibration modes in representing the missile body. The missile is shown in Fig. 2 with its launch shoes, represented by stiff springs, resting on the aft end of the forward and aft rails of the launcher unit. Figure 2

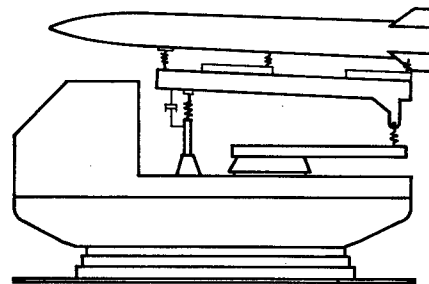


Fig. 2 - System schematic

also shows a third stiff spring support under the missile nose section. A secondary objective of the simulation was to study the effect of this third support in reducing missile airframe dynamic loads due to the excessive cantilevered length of missile body forward of the forward launch shoe.

The launcher unit is shown consisting of two major parts—the elevation platform containing the launch rails, and the rotatable azimuth platform mounted to the rear deck of the transporter vehicle. The elevation platform was assumed to be a rigid body, whereas in a more extensive analysis one might consider representing its characteristics by the first several significant vibration modes of the platform. The elastic characteristics of the aft extension of the rotatable azimuth platform were represented by a simple spring. The forward post support of the elevation platform was assumed to be equivalent to a stiff spring. Another secondary objective of the simulation was to investigate the effect of adding a hydraulic shock absorber to the post, and therefore a viscous damper was added to the representation of the post. The transporter vehicle was

assumed to be a rigid body capable of vertical translation only.

Figure 3 represents an exploded view of Fig. 2, and shows the various coupling forces and degrees of freedom associated with each component. A summary of the seven degrees of freedom allowed in representing the system is as follows:

Missile

1. Two elastic vibration modes
2. Rigid-body vertical translation
3. Rigid-body pitch rotation

Launcher (elevation platform)

1. Rigid-body vertical translation
2. Rigid-body pitch rotation

Transporter Vehicle

1. Rigid-body vertical translation

The exploded schematic of Fig. 3 facilitated the writing of the equations of motion for each degree of freedom. These equations, along with

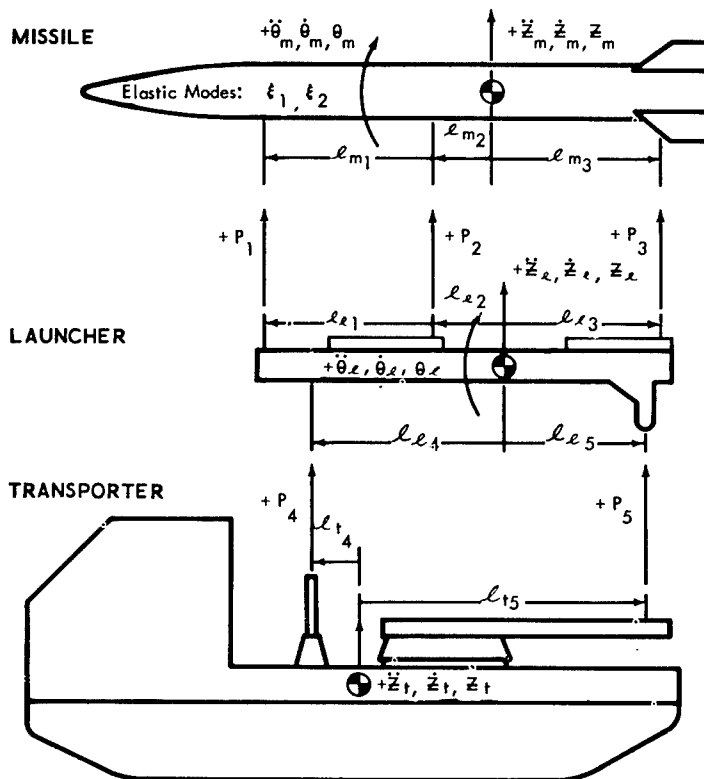


Fig. 3 - Exploded schematic

the flow of coupling data between each equation, are shown in Fig. 4. Also shown in Fig. 4 are the equations used to provide missile body bending moment data at three body stations.

Note in Fig. 4 that the forcing function for the total system is shown by the variation of total system vertical acceleration, \ddot{Z}_{TOT} , with time. This parameter was developed by considering the stress-strain characteristics of the crushable honeycomb cushioning system shown in Fig. 5. It can be seen that the honeycomb cushioning stress abruptly rises early in the strain cycle, and then becomes reasonably

constant until near the end of the strain cycle where the crushing stress rapidly diverges due to the bottoming of the honeycomb cushion. The dotted curve indicates the manner in which a typical recovery stress cycle occurs following removal of the crushing load. The area under the solid curve represents absorbing energy and the area under the dotted curve rebound energy due to spring-back of the honeycomb. The deceleration of the system was determined from the data of Fig. 5 by (1) establishing a time zero with the system at an initial constant vertical velocity immediately prior to ground contact, (2) integrating this

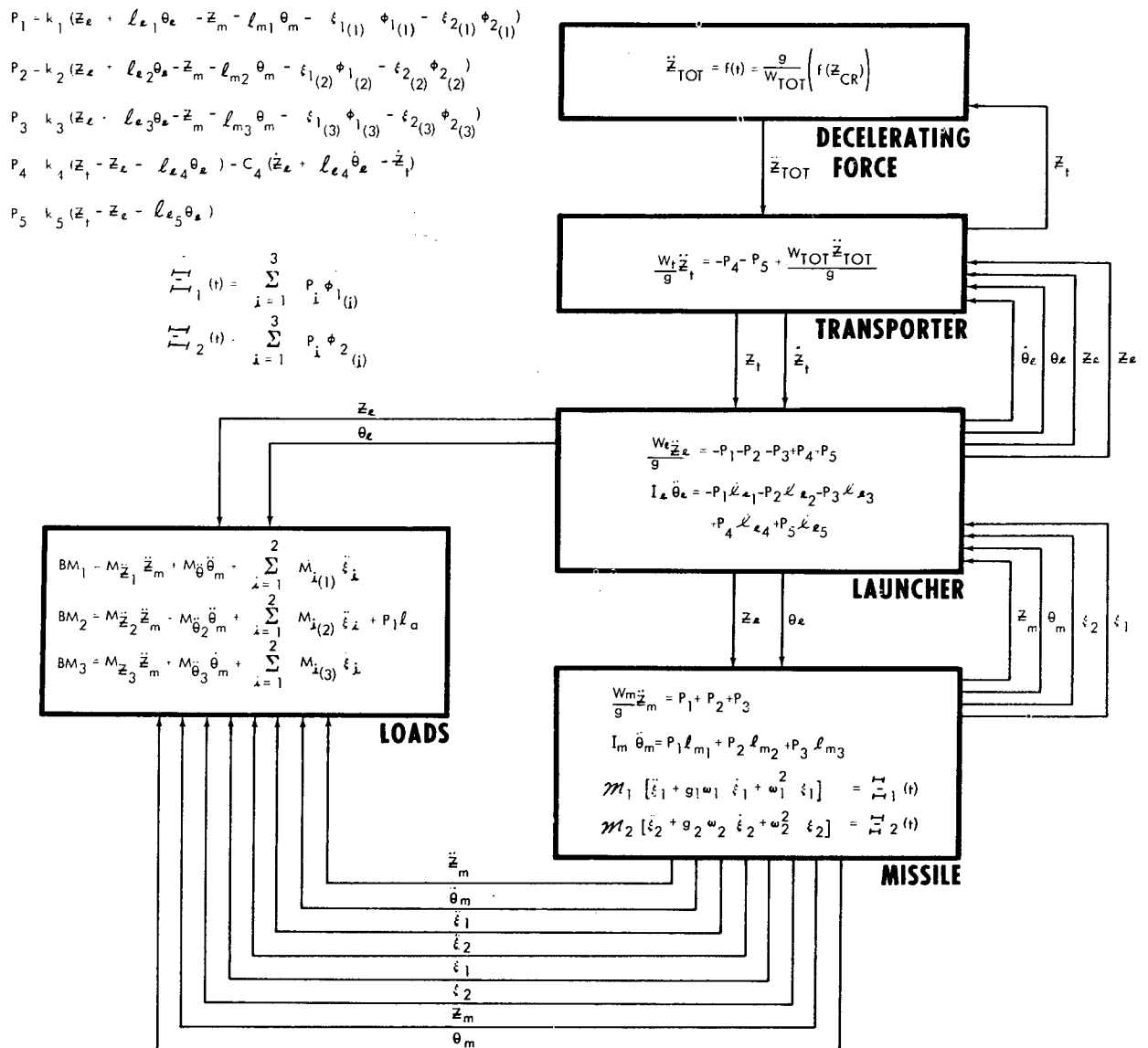


Fig. 4 - Data flow diagram

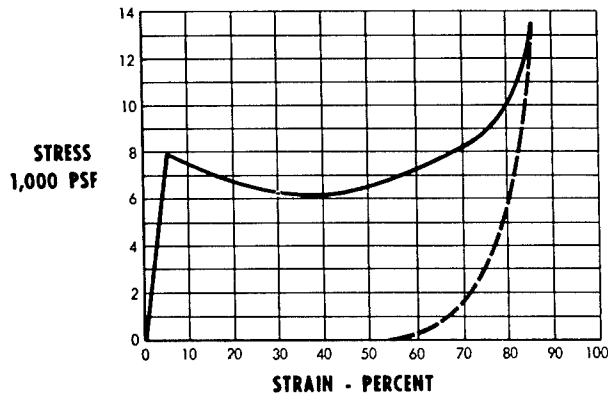


Fig. 5 - Honeycomb stress-strain characteristics

velocity to yield a crushing distance (and hence a crushing strain), and (3) obtaining a decelerating force as a function of crushing strain and crushing area. The system deceleration can therefore be determined from the decelerating force. This computation cycle is shown by the two blocks "Transporter" and "Decelerating Force" and their data exchange (Fig. 4). Another analytical simplification was made in setting the decelerating force equal to zero at the instant the transporter vertical velocity became zero, thereby neglecting the rebound energy available to the system.

COMPUTER MECHANIZATION

Prior to mechanizing the problem for an automatic computer, consideration was given to the question of whether to perform the computations on an analog or a digital computer. While the dynamic response problem can conceivably be mechanized for either type of computer, several significant aspects of this particular problem made the analog computer a much more attractive choice. The operational analog computer is an extremely useful tool in that the solution of ordinary differential equations, a feature of most dynamic load problems, lends itself directly to the continuous integration capability of the analog computer, as opposed to the discrete time interval integration process necessary on a digital computer. The problem of whether or not to neglect certain parameters or effects may be studied efficiently on the analog computer by successive elimination of the electrical circuits representing those parameters in the total mechanization, and determining their influence on the problem solution. On the analog computer, solution results are immediately available in the form of plotted time-histories or parameter

crossplots, while digital computer results normally require an extensive plotting process; hence, parameter surveys such as those conducted during the simulation are more easily performed on the analog computer.

The analog computing facility at North American's Columbus Division is an integral part of the Engineering Department, thus insuring maximum coordination between computing engineers and problem originators. There are no rental charges involved, hence the cost to a given program of using the analog computer are significantly lower than those of the digital computer. For these reasons, the analog computer was selected as the computing tool for this simulation.

As was mentioned earlier, the analog computing facility scheduling was such that the mathematical model and the computer mechanization of the problem were tailored to the equipment available on one fully-expanded Electronic Associated PACE 231-R console. A tabulation of the equipment used is as follows:

- 72 amplifiers
- 99 potentiometers
- 12 function switches
- 2 relays
- 1 six-channel recorder
- 1 eight-channel recorder
- 1 diode function-generator

An accurate non-linear representation of the honeycomb stress-strain variation was accomplished by the use of a diode-function generator as shown in Fig. 6. A relay, sensing the vertical velocity of the system, caused the crushing stress, and hence the decelerating force, to become zero instantaneously when the vertical velocity became zero.

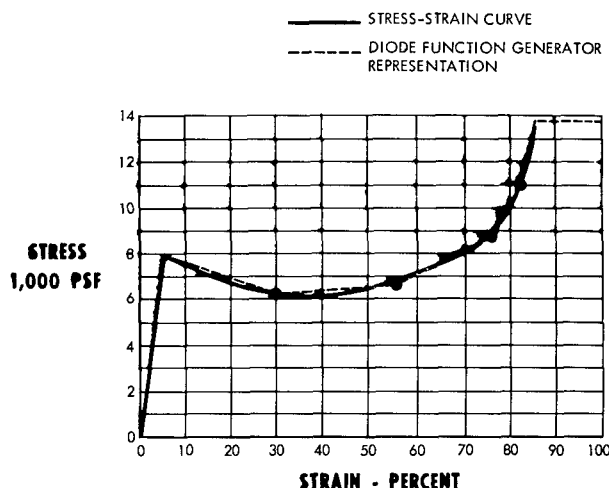


Fig. 6 - Computer representation of honeycomb stress-strain

A checkout procedure was employed to insure correct equation simulation and problem solution. An electrical static check was made of the entire mechanization by applying static voltages to various amplifiers, measuring the output of other amplifiers, and comparing these results to hand-calculated values. A static check of missile loads was made by applying a constant acceleration to the system and measuring the resulting bending moments applied to the missile. These values checked to within 2 to 3 percent of hand-calculated results. Finally, a dynamic check was performed on the uncoupled missile elastic-body modes by applying an impulse input to each mode, measuring the frequency and damping ratio of the resulting oscillation, and comparing these results to the input frequency and damping for each mode.

Two significant problems arose during checkout of the mechanization. One was an electrical circuit instability in the missile elastic-body modes resulting in an oscillatory divergence of each mode whenever an excitation was applied. This problem was caused by a combination of the number of amplifiers in the electrical loop of each mode coupled with the time scaling selected. This problem was never completely eliminated during the simulation, but a change in the mechanization of these modes reduced the amplitude and rate of divergence of the instability to where it was no longer significant in the early portion of the system response time history where critical responses occurred. Another problem encountered was the need for scaling the variables for a wide range of values, thus requiring

high amplifier gains at various points in the mechanization. This problem was partially circumvented by a time scaling of two-hundred-times slow. Also, in cases where the small difference of two large numbers was required, the difference was taken before integrating, thus yielding more accuracy.

PRODUCTION RUNS AND RESULTS

As was stated before, the primary objective of the simulation was to determine missile air-frame dynamic loads due to the ground-impact condition. However, with the problem already mechanized, studies of the effect of varying several significant problem parameters were accomplished with little additional cost and effort. The following is a summary of the parameter surveys accomplished during the course of the simulation:

1. Determination of the effectiveness of a third support at the nose of the missile to reduce missile dynamic response loads during impact. The stiffness of this support was varied from zero to that of an extremely stiff spring.
2. Determination of the effectiveness of adding a viscous damper to the forward launcher support post in reducing missile loads.
3. Determination of the effect of varying impact velocity on missile loads. This survey provided data for considering changes in impact velocity due to system weight changes, impact altitude variations, and a partially-damaged parachute system.
4. Determination of the effect on missile loads of changes in honeycomb cushion thickness.

Following a complete checkout of the mechanization, initial impact runs were made with (1) a rigid missile and (2) an elastic missile simply to study the results and gain confidence in the simulation. Then, with a nominal value of impact velocity and the third missile support set at maximum stiffness, the viscous damper in the launcher post support was varied from zero to nominal value to five-times nominal value with no appreciable effect in missile loads. It was therefore concluded that the viscous damper was of no consequence and was eliminated from further consideration.

A study of the effect of the third support at the missile nose was then undertaken. With a nominal value of 25 fps impact velocity, the value of the spring stiffness of this support was set at zero, one-quarter, one-half, three-quarters, and one times the maximum scaled value of 10^6 pounds per inch. Typical time histories of the forcing function, \ddot{Z}_{TOT} , along with accelerations of the various system degrees of freedom for one of the runs in the above set of runs is shown on Fig. 7. Figure 8 shows time histories of missile support loads and missile body bending moments for the extreme values of zero and maximum stiffness of the nose support. Note the behavior of the bending moment at missile load station 2. With

zero stiffness, or no nonsupport, the airframe loads were high in magnitude as expected. When the nose support was added at maximum spring stiffness, airframe loads were reduced by a factor of 7.

A plot of maximum missile support loads versus the stiffness value of the nose support is shown in Fig. 9, and, as expected, shows that as the support stiffness decreases, the nose support load eventually drops to zero while the middle support picks up virtually all the load. Based on the data shown on Fig. 9, a nominal (not optimum) value for the nose support spring stiffness of 0.2 times the maximum value was selected for the remainder of the study. Shown in Fig. 10 is the variation of missile c.g. vertical acceleration with spring-stiffness of the nose support. Figure 11 shows the variation of missile bending moments with nose support stiffness, clearly showing the sharp reduction of the moment at station 2 with increasing support stiffness.

Next, a study was made of the effect of varying impact velocity on missile support loads and bending moments. Runs were made at impact velocities of 20, 22.5, 25, 27.5, and 30 fps. Shown in Fig. 12 are time histories of the forcing function, missile c.g. acceleration,

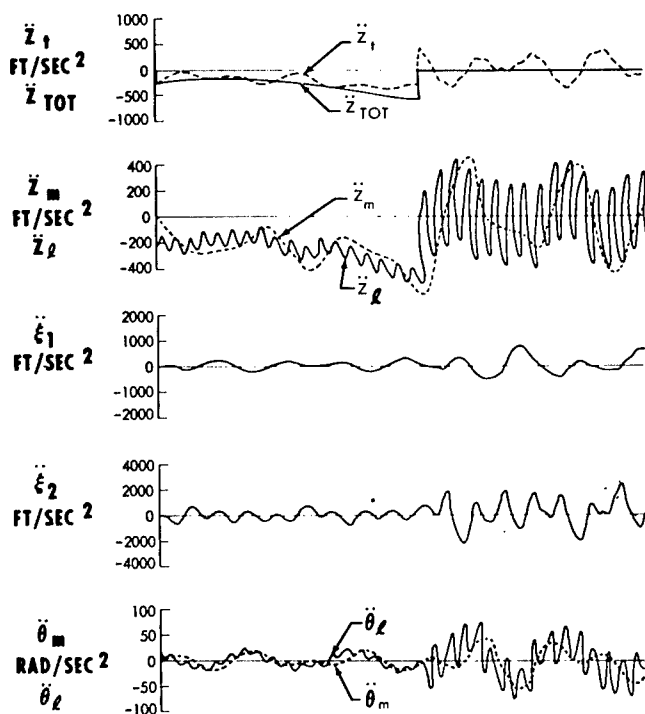


Fig. 7 - Typical time histories

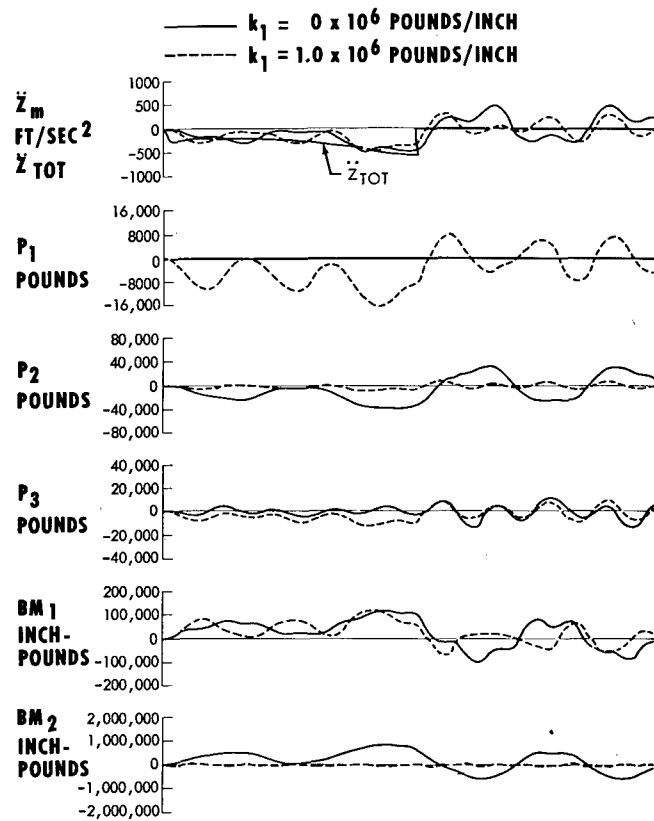


Fig. 8 - Time histories with varying forward support stiffness

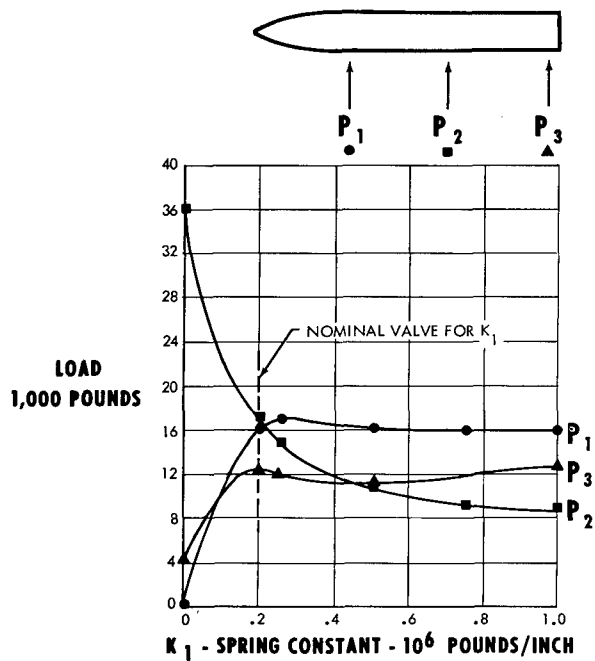


Fig. 9 - Support reactions vs forward support stiffness

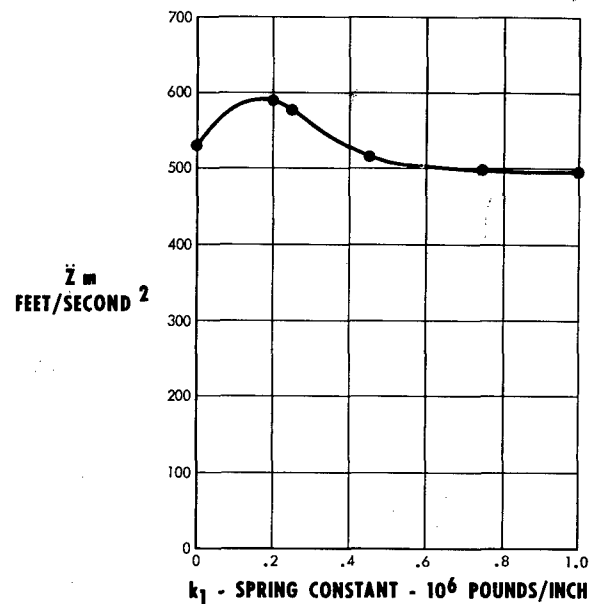


Fig. 10 - Missile acceleration vs forward support stiffness

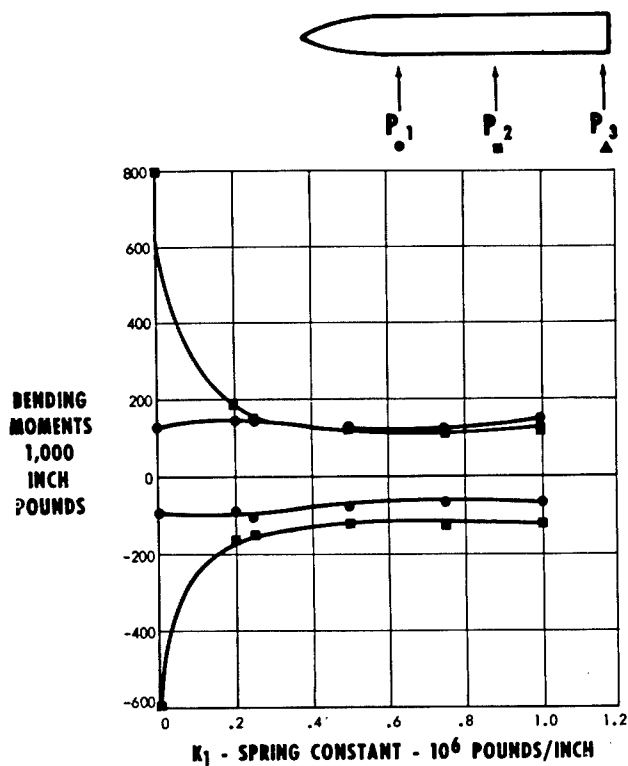
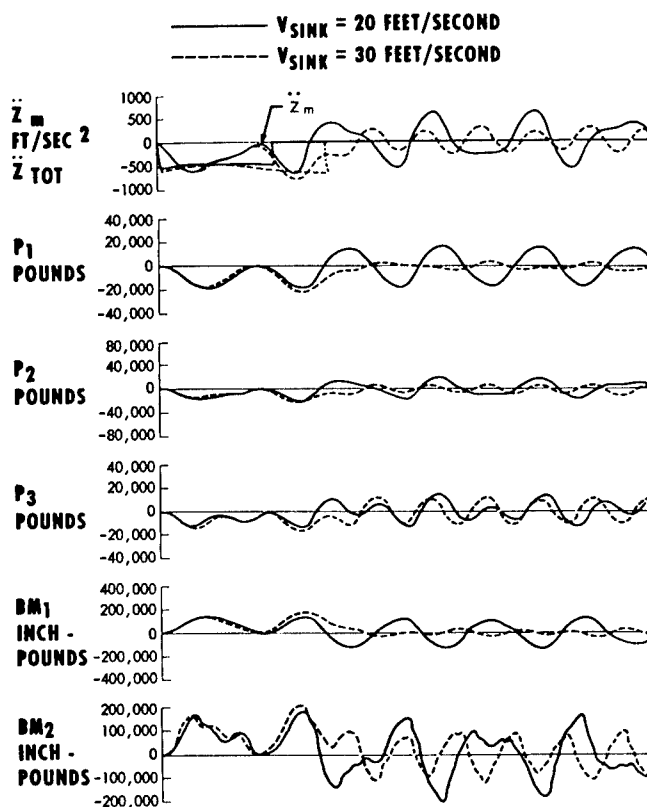


Fig. 11 - Bending moments vs forward support stiffness

Fig. 12 - Time histories with varying impact velocity



support loads, and bending moments for the minimum and maximum impact velocities studied. Note the increased area under the \dot{Z}_{TOT} curve, reflecting an increase in the total energy absorbed by the system with increasing impact velocity. Figures 13, 14, and 15 show the variation of support loads, missile c.g. acceleration, and bending moments, respectively, with impact velocity. As anticipated, the trends show increasing loads and accelerations with increasing impact velocity.

The final runs made during the simulation were an attempt to vary the thickness of the honeycomb cushion downward from its design value of 1.5 to 0.6 feet. Successful runs were made at thicknesses of 1.5 feet and 1.25 feet. However, the load data during the run at thickness of 1.0 foot exhibited a rapid divergence during the latter part of the honeycomb crushing cycle and resulted in overloading several amplifiers of the computer. This data, along with the nominal run at a thickness of 1.5 feet, is shown in Fig. 16. The honeycomb stress-strain curve of Fig. 17 shows why the rapid divergence of loads occurred. Points are shown on the curve indicating the maximum amount of strain experienced during each

impact. The drop at 1.0-foot thickness caused a strain which entered the "bottoming" end of the stress-strain curve and produced a rapid increase in the decelerating force.

CONCLUSIONS

The analytical simulation described in this paper was satisfactorily accomplished; and it produced significant numerical results from which design decisions could be made. From a description of the development of the mathematical model and the computer mechanization, it can be seen that this simulation may readily be extended in complexity, by the simple addition of computing equipment, to provide a very comprehensive representation of a complex dynamic system.

The entire significance of the study, however, does not only lie in the values and trends of the numerical data produced during the investigation. It also points out still another facet of hardware design problems where analytical simulation provides the design engineer with a relatively inexpensive method of establishing his critical design parameters. The design of air-dropped impacting systems in the

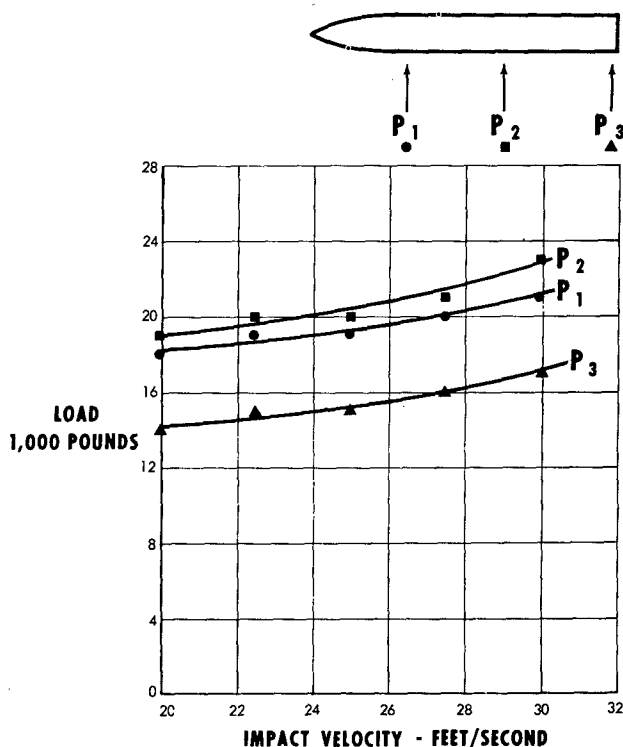


Fig. 13 - Support reactions vs impact velocity

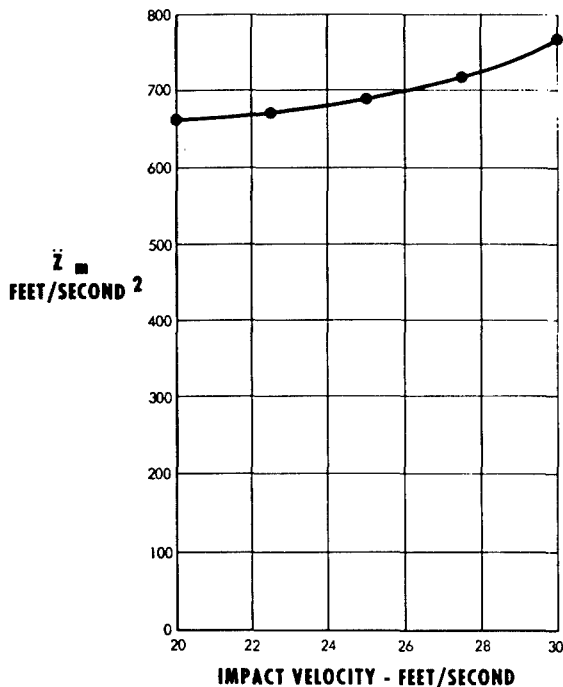


Fig. 14 - Missile acceleration vs impact velocity

past has frequently been based initially on a somewhat crude numerical analysis followed by an extensive and expensive full-scale drop test program using either prototype hardware or boilerplate mockup units. By using analytical simulation, the designer may conveniently investigate not only critical loading conditions, but also subcritical buildup conditions, and therefore he can generate a spectrum of loads and response data for correlation with the results of experimental drop-test data. With the analytical data available, the drop-test program may be more efficiently planned and will result in a more logical starting point and a fewer number of drops in the total program. Correlation of analytical, experimental, and design data will provide prediction of premature failures before they occur. At the same time, results of early experimental drops may be used to check the accuracy of the simulation and to refine the mechanization if necessary.

In summary, analytical simulation is a powerful tool in the design of impacting complex elastic systems in that it provides accurate loading data early in the engineering design effort, and also aids in the economical planning and executing of development testing.

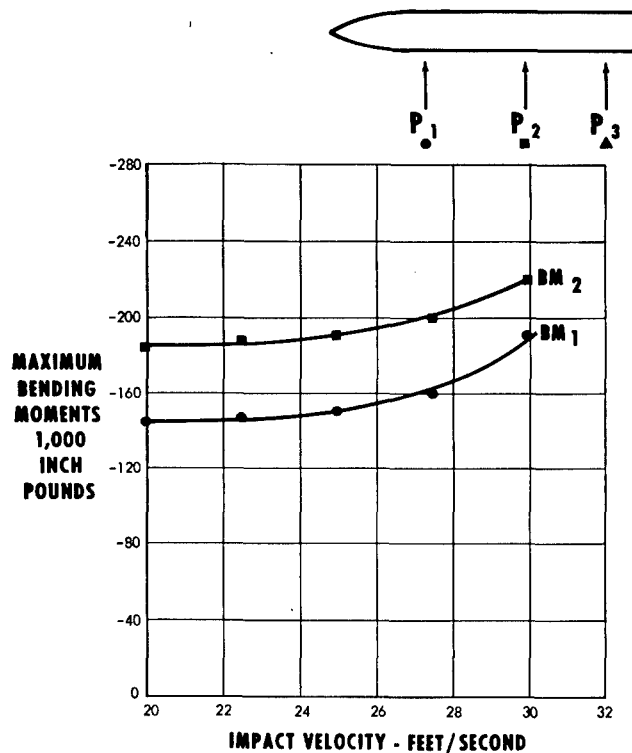


Fig. 15 - Bending moments vs impact velocity

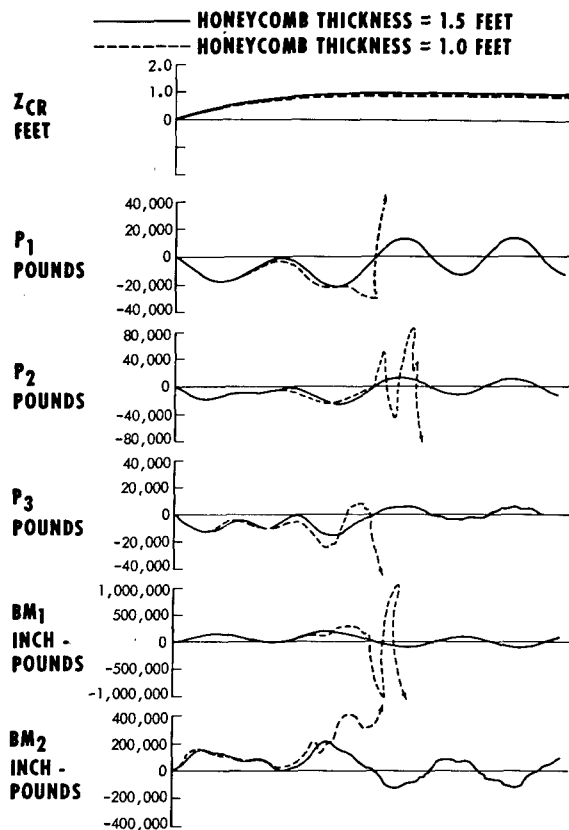


Fig. 16 - Time histories for varying honeycomb thickness

LIST OF SYMBOLS

BM Bending moment (inch pounds)

c dashpot damping coefficient (pounds/ft/sec)

g gravity (32.2 ft/sec²)

g structural damping (N.D.)

I Moment of Inertia (slug-ft²)

k Spring constant (pounds/inch)

l length (inches)

M Unit inertial bending moments (inch-pound/ft/sec²) or (inch-pound/rad/sec²)

m Generalized mass (slugs)

P Spring load (pounds)

(t) Time (seconds)

W Weight (pounds)

z Vertical translation (feet)

θ Pitch angle (Radians)

ϕ Elastic mode deflection (in./in.)

ξ Generalized coordinate (feet)

Ξ Generalized force (pounds)

ω Elastic mode frequency (radians/second)

Superscripts

· First derivative with respect to time

'' Second derivative with respect to time

Subscripts

1, 2, 3, Used to denote point of interest or mode number

CR Crushable material

l Launcher

m Missile

t Transporter

TOT Total system

z Translational

θ Rotational

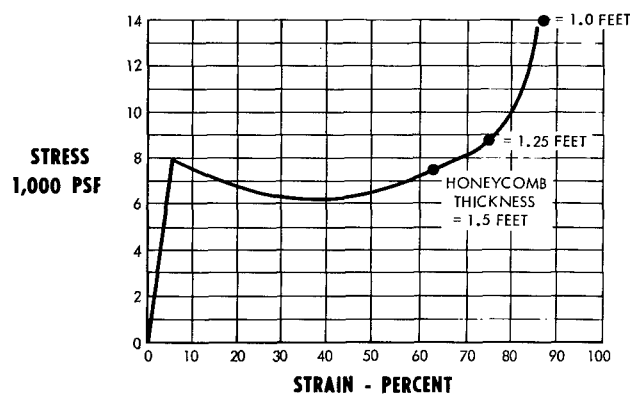


Fig. 17 - Honeycomb bottoming

Section 3

VIBRATION DATA ANALYSIS

MODEL BASIN PROCEDURE FOR THE ANALYSIS AND PRESENTATION OF VIBRATION DATA

E. Buchmann and R. G. Tuckerman
David Taylor Model Basin
Washington 7, D. C.

Procedures used at the David Taylor Model Basin to analyze and present vibration data obtained from trials of surface ships and submarines are discussed. These procedures were developed to assist engineers in understanding the vibration phenomena on ships and to meet the objectives which prompted the vibration surveys. Samples of presentations include power and amplitude spectra, statistical distribution histograms, transient analysis of impulse loadings, mode shapes, and damping values.

INTRODUCTION

Since World War II, ship builders and ship owners have become increasingly concerned with vibration problems aboard ships. This concern has grown because of the greater speed of ships, their high-powered propulsion systems, and the use, especially on naval vessels, of shipboard equipment which is sensitive to its vibratory environment. In most cases, the safety of the ship itself is not endangered by these vibrations except on rare occasions where large vibration amplitudes may occur due to impulsive loadings resulting from slamming or explosions. The welfare of the crew and their inability to operate complex instrumentation in a vibratory environment are factors which also require sound knowledge of vibratory effects.

The knowledge gained in the vibration field has followed two paths, namely experimental investigations of ships and development of ship vibration theory. Work in both fields has led to remarkable findings during recent years. The refined knowledge of the vibration of such complex structures as ships has, on the one hand, opened new avenues of experimental investigations and, on the other hand, emphasized the need for a better understanding and knowledge of the actual physical phenomena. Only a few areas may be mentioned such as sprung masses,

hull-appendage effects, nonuniform-beam theory, resiliently mounted equipment, virtual mass associated with hull vibrations, hull damping, hull stiffness parameters, and the like. The work done at the Model Basin is reflected in numerous publications; a list of the unclassified reports is available through January 1962.¹

The experimental study of ship vibration phenomena becomes increasingly complicated when the areas mentioned above are to be investigated. Continual refinement and improvement of methods for recording and analyzing data are required to ensure the most economical approach for each case. There is a mutual interchange of ideas among the Model Basin, other naval activities, and agencies outside the Navy. The Basin is in constant contact with the Maritime Administration and with vibration experts in other areas, and the station is represented on the International Ship Structure Congress. The increasing emphasis placed on vibration work at the Basin is demonstrated in Fig. 1 which indicates the number of reports published in recent years.

¹F. F. Vane, *et al.*, "A Bibliography of Vibration Reports and Ship Dynamics Division Reports Issued by David Taylor Model Basin," DTMB Report 1608 (Apr. 1962).

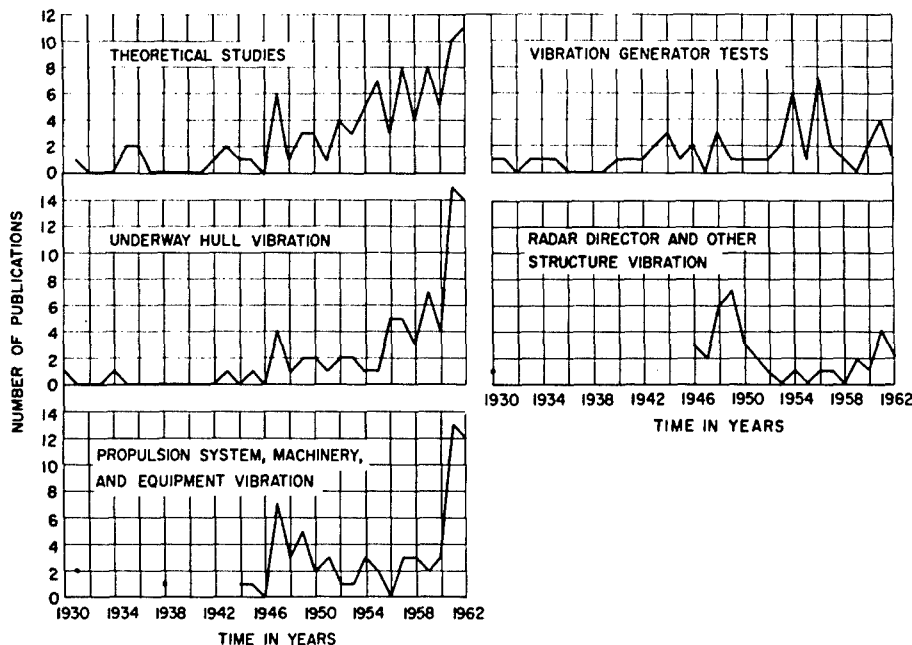


Fig. 1 - Model Basin publications on ship vibration

This paper restricts itself to methods of data analysis now used at the Model Basin. These methods should not be considered as fixed procedures for they are being continually reviewed and improved. The frequency range of primary interest is from 0 to 100 cps and, although in only a few cases, this work has involved frequencies up to a few thousand cps.

DATA ANALYSIS

General Remarks

It is not intended to discuss all possible means of data analysis obtained from various methods of recording. The analysis methods described herein refer to the evaluation of oscillogram and magnetic-tape records. Signals, such as a displacement, velocity, acceleration, and force or pressure, are obtained from transducers and transmitted to a recording system. The recorder either makes a paper recording of the variation of a measured value versus time or magnetizes a moving tape according to the measured value. In most cases, the data obtained from reducing these recordings are in the form of frequencies, peak, mean, rms amplitudes, or phasing between the signals obtained from various locations. The importance of calibrating the recording system in order to obtain correct values of the quantities should be mentioned in passing.

Data Reduction from Oscillograms

The ship structure has an infinite number of natural frequencies and mode shapes. They are usually analyzed into components of vertical, horizontal, longitudinal, and torsional hull vibration, coupled to each other to some degree due to asymmetry of mass distribution and of forces. The ship responds to any excitation force like a large mechanical filter. This response is similar to that of a complex electric circuit to a forcing voltage. Evaluation of paper records, therefore, would seem hopeless unless the transducers are so arranged and selected that certain frequencies are predominant in the oscillograph trace. If predominant frequencies are sufficiently separated and limited to two or three significant values, the envelope methods described in detail by Manley^{2,3} may be used. Envelopes are faired by hand and the procedure requires good engineering judgment. These methods are quite successful in evaluating vibration-generator-excited vibrations where the applied frequency is known. A ship, however, is never a quiet structure and even under ideal conditions, many frequencies

²R. G. Manley, "The Analysis and Interpretation of Vibration Records and Similar Traces in Engineering," Transaction North East Coast Inst. Vol. 64 (1948).

³R. G. Manley, "Wave Form Analysis" (Chapman and Hall, 1945).

are present in a trace due to operation of auxiliary machines, surface wave actions, wind effects, etc. Any trace, therefore, usually shows a rather high noise level which may affect the amplitudes of interest. In some cases vibration generator tests can be arranged so that the noise level is measured with the generator inactive to allow for a correction. Tests under ideal conditions result in accuracies of about 3 percent for frequency, ± 10 degrees for phase angle degrees, and 10 percent for amplitude.

The actual vibration records due to ship operation, however, are much more complex, as can be seen from Fig. 2 which presents two traces obtained from a vibration generator test and one from an underway trial. The evaluation of a trace from an underway trial poses many difficulties. A trained analyst may detect individual frequencies he desires to evaluate which may correspond to shaft, propeller blade, double-blade frequency, and so on. Since some of these frequencies are usually separately recorded on special channels for identification, a transducer trace in a particular test run can be evaluated for their presence. The amplitudes of these frequencies vary considerably with time even when ship operating conditions are kept as steady as possible. The evaluation is then usually restricted to those parts of the trace where certain frequencies are predominant and easily separated. The amplitude values are derived from the largest excursions at a particular frequency. Recording various

transducer outputs simultaneously permits evaluating not only the amplitude but also the phasing between various channels.

Measured amplitude values may vary as much as 30 percent and phasing as much as ± 20 degrees. Even with this inaccuracy, the method allows the detection of resonance frequencies by the known change of phasing when the exciting frequency passes through a resonance. This permits determination of a natural frequency with an accuracy of from 1 to 5 percent, depending on the damping value.

The data thus obtained are presented in the form of tables or graphs. The graphs usually present an amplitude versus a selected frequency over the whole speed range of the ship. Such a graph is shown in Fig. 3 where vibration amplitudes from various selected machinery components are plotted versus rotation frequency. The three peaks occur at resonances which correspond to different modes of vibration. A good example of the use of oscillograms to evaluate the vibration characteristics of a modern destroyer is given in Ref. 4.

In cases where vibration characteristics at selected frequencies are of interest, an electronic filter is inserted in the system and only

⁴A. R. Paladino, "Vibration Survey of USS DECATUR (DD 936)," DTMB Report 1271 (Mar. 1960).

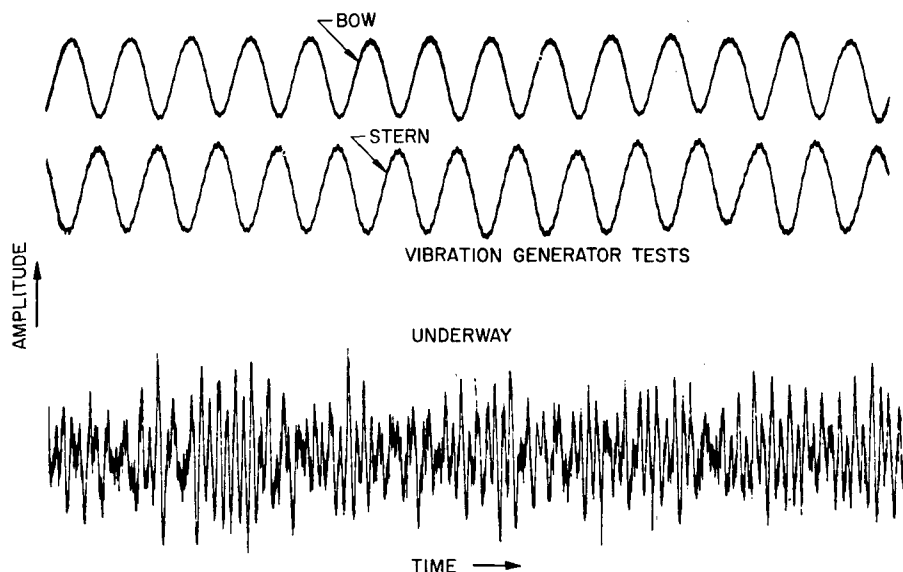


Fig. 2 - Typical oscillograms of vertical velocities

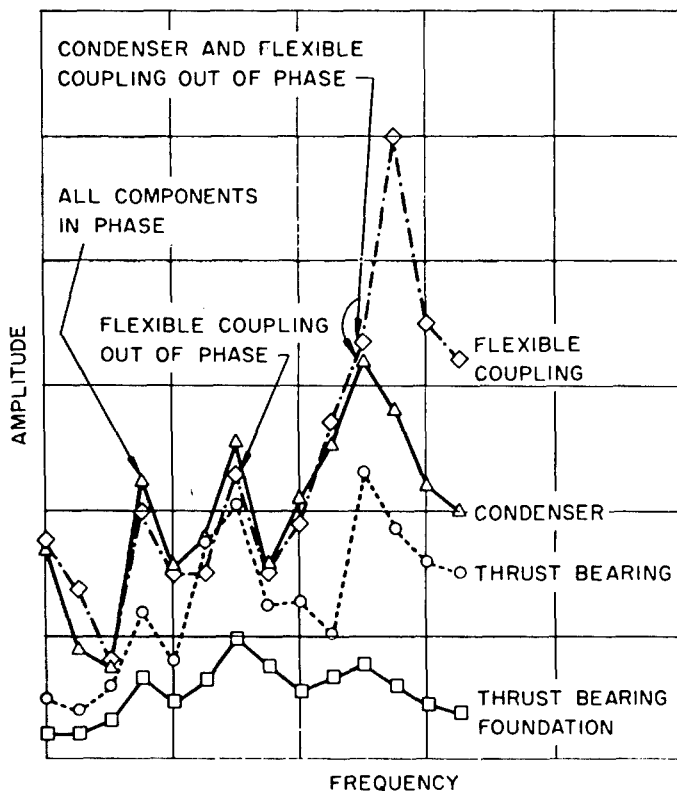


Fig. 3 - Vibration of machinery parts versus frequency

the desired frequency is recorded. This is useful when the measurements are for specific purposes, e.g., to check machinery balance, shaft alignment, and so forth.

Relatively clean records with a low noise level can also be evaluated by a Fourier analysis which is coded for a digital computer. By starting at the same chosen zero time base, each trace is digitized by use of a mechanical-optical oscillograph reader up to a selected time t . The evaluation of each trace $f(t)$ gives the in-phase component a and the out-of-phase component b of a frequency, ω ;

$$a = \frac{2}{t} \int_0^t f(t) \sin(\omega t) dt,$$

$$b = \frac{2}{t} \int_0^t f(t) \cos(\omega t) dt,$$

with the amplitude A ,

$$A = a^2 + b^2,$$

and the phasing,

$$\phi = \tan^{-1} \left(\frac{a}{b} \right).$$

The evaluation of oscillograms from actual vibration trials is rather cumbersome and time consuming. It requires well trained personnel who must consider in the evaluation the characteristics of the transducers, the effect of the recording system on the signal, and the characteristics of the excitation forces and their time variations. The results give maximum values of amplitudes during the recording time and allow for a restricted evaluation of mode shapes and frequencies. The results, however, can often be misleading due to lack of resolution.

The use of the oscillograph is intriguing to the engineer because it produces a frequency trace during the testing period and indicates any radical changes in the vibration that may occur during trial variations. It should, therefore, not be neglected as an auxiliary tool for relatively simple vibration problems. For complex problems, however, it is surpassed by the possibilities offered by magnetic-tape recording.

For additional information see also Ref. 5 and DTMB Report 715 (listed in Ref. 1).

DATA REDUCTION FROM MAGNETIC TAPE

General Remarks

The recording of transducer signals on magnetic tape allows a storage of signals obtained from many channels. Recording of up to 10 data signals on the same track by means of a multiplex, provides a total of 140 data channels on a single 14-track tape recorder. The Model Basin makes use of these possibilities. Figure 4 shows a recording system installed on a ship.

The analysis of magnetic tape records by electronic wave analyzers and digital systems is independent of individual judgment. Both analytical methods, the electronic wave and digital analysis, are used extensively. Figure 5 shows the vibration data wave analysis systems (VIDA) which is used at the Model Basin.

⁵J. J. Francis, et al., "Marine Vibrations Diagnosis," New England Section, Society of Naval Architects and Marine Engineering (Oct. 1960).

The advantage of using magnetic tape for recording lies not only in the storage of many data obtained during a short test period available, but allows the versatility of combining traces in the laboratory. Signals from various transducers can be added or subtracted to obtain the six possible motions (velocities, or accelerations) of certain structural units in translation and rotation. Signals of several transducers can be filtered at selected frequencies to obtain the patterns of vibrations. Furthermore, magnetic tape can be stored and additional analysis undertaken at a later date should other findings or theoretical developments need verification.

Analysis of Predominant Frequencies

A record $f(t)$ of ship vibration is usually taken for a condition when ship course, speed, and the like, are not changed, i.e., at steady speed runs. The tape recording obtained during this condition is then transferred to a loop-tape. This loop is used for analysis either at the original or at higher or lower tape transport speeds. A filter with a fixed bandwidth and adjustable center frequency scans the loop to obtain average amplitudes \bar{A} per unit frequency over the frequency range of interest.

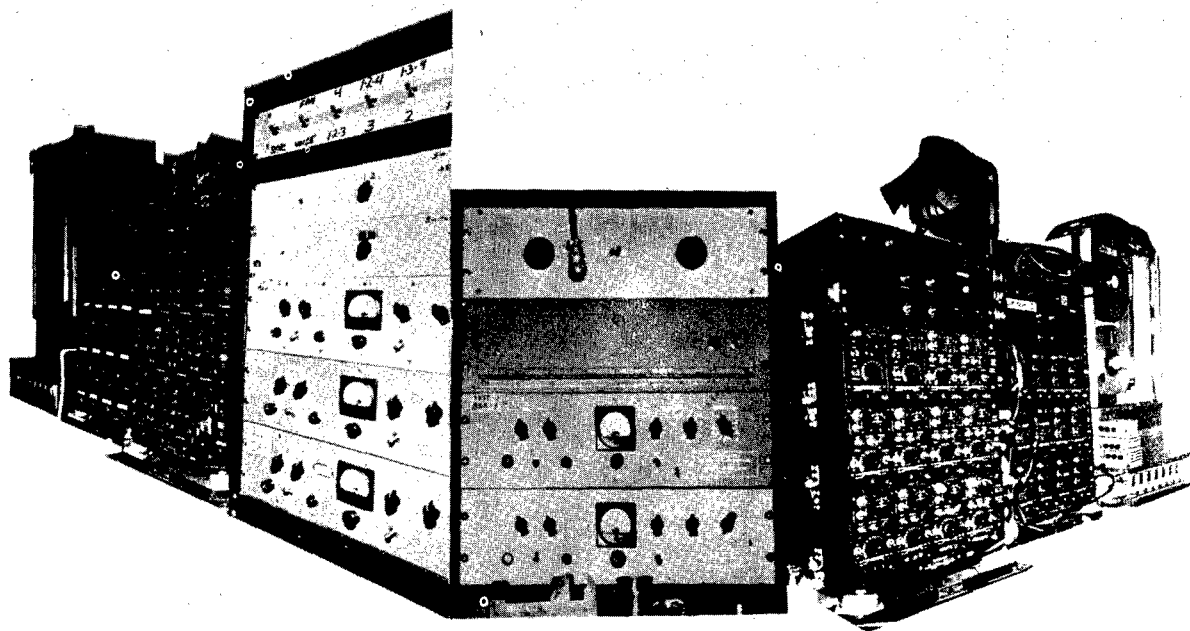


Fig. 4 - Vibration recording system installed aboard a ship

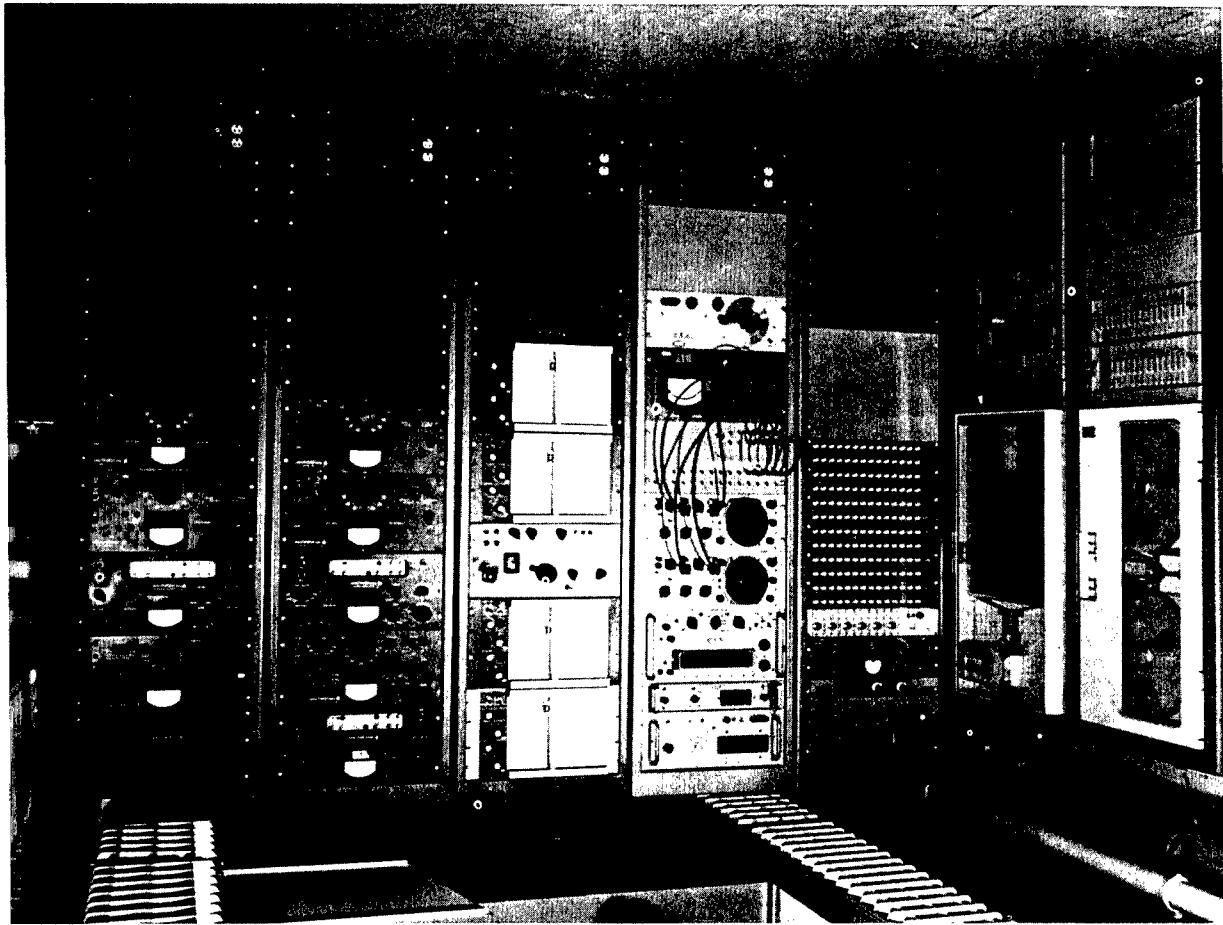


Fig. 5 - Vibration data wave analysis system

$$\bar{A}(\omega) = \frac{1}{t_1} \int_0^{t_1} |f(t)| dt,$$

$$\int_0^{\omega_m} G_{11}(\omega) d\omega.$$

where t_1 is the time and is so adjusted according to the filter bandwidth that each part of the loop is once scanned. The result is automatically plotted by use of a x-y plotter; see Fig. 6. This plot shows the investigator the presence of frequencies with relatively large amplitudes. The power spectral density $G(\omega)$ can be obtained during the same evaluation process and gives the mean square amplitude per unit bandwidth. It shows the energy distribution over the frequency range under certain conditions. Figure 7 presents such a power spectrum where

$$G_{11} = \frac{1}{t_1} \int_0^{t_1} f(t)^2 dt$$

is plotted versus frequency. This graph also shows the time integral of this function

Certain vibrations with relatively large amplitudes relating to specific excitation frequencies are usually of great interest as to their amplitude and transmission in structures. These frequencies can be singled out and analyzed further. Figure 8 shows a filtered frequency typical for ship vibrations and exhibits a time-variable amplitude.

A mean value of this amplitude can be obtained over various time periods. The vibration shown in Fig. 8 is integrated over 2, 4, 6, and 8 seconds and the results thus obtained for the mean amplitude

$$\bar{A}(t) = \frac{1}{t} \int_0^t |f(t)| dt$$

are shown in Fig. 9.

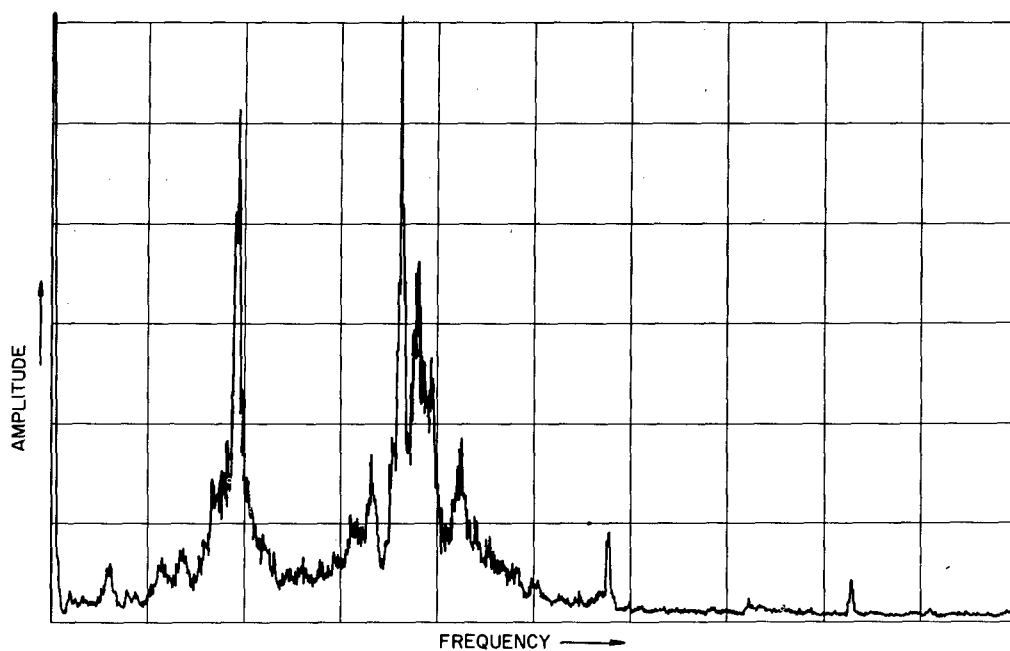


Fig. 6 - Amplitude spectrum of vertical velocity

Fig. 7 - Power spectrum and its integration of vertical velocity

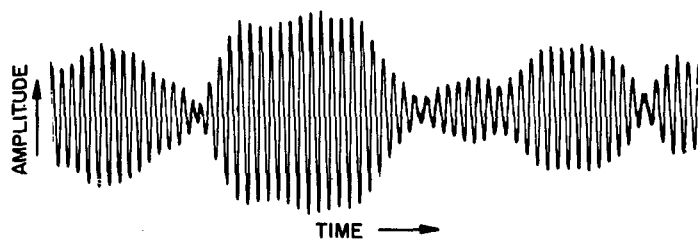
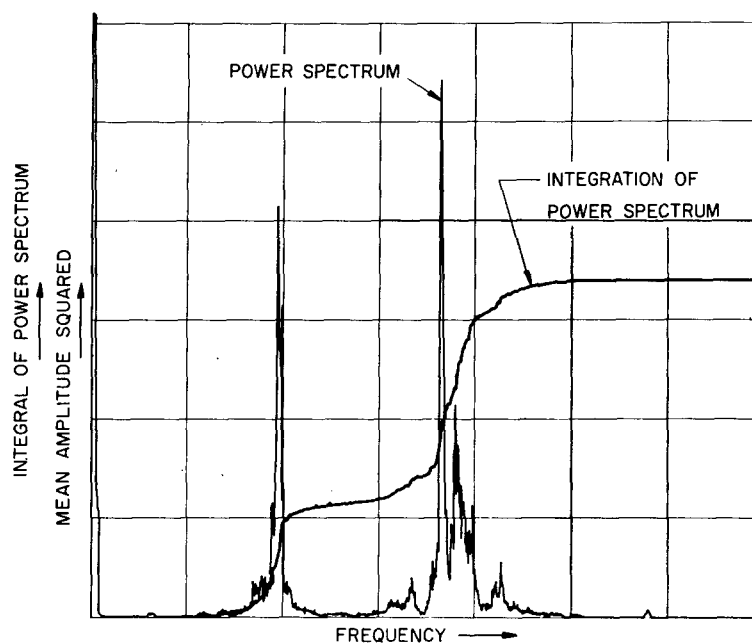


Fig. 8 - Oscillogram of filtered frequency of interest

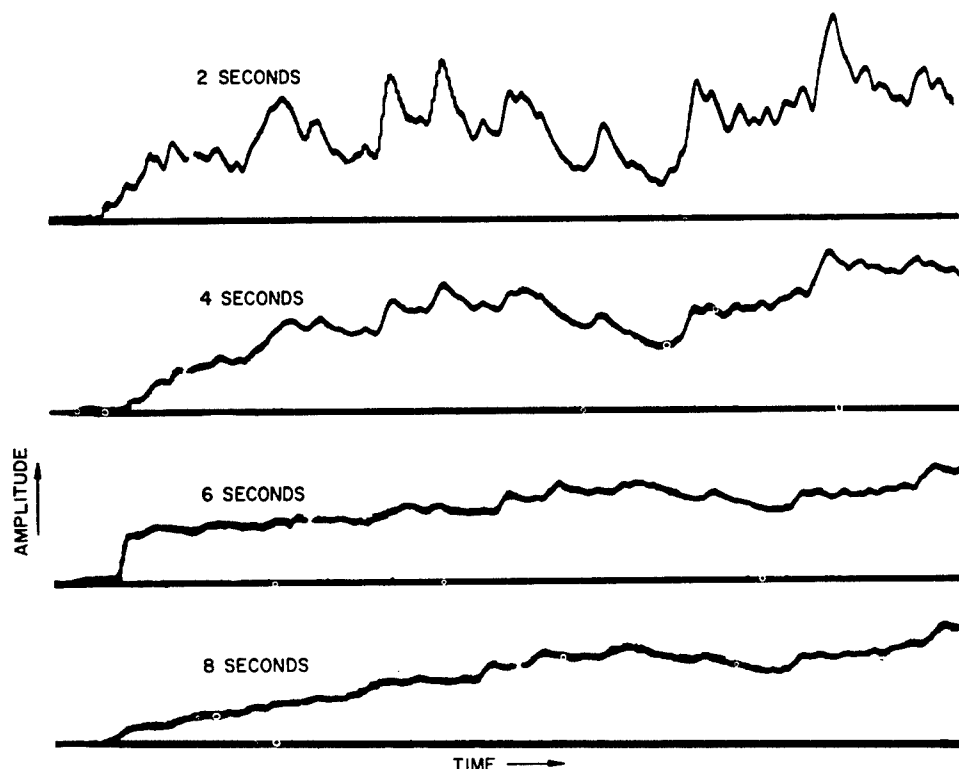


Fig. 9 - Mean amplitude of a filtered frequency over various time intervals

The maximum values that may occur during a recording period are obtained by rectifying the filtered frequency and integrating over a short time period. The result of this operation shows that the envelope of the vibration and peak values can easily be read from such a graph. Figure 10 presents the envelope curve of the vibration shown in Fig. 8.

The mode of vibration of a structure at a particular frequency is obtained by defining the amplitudes at that frequency at various locations of the structure 1, 2, ... i, and by obtaining the phasing of the vibration at the locations with respect to the vibrations at a selected reference location. Amplitudes are obtained in the method mentioned before. The phasing is derived from the in-phase and out-of-phase correlation functions,

$$G_{12}(\text{Co.}) = \frac{1}{t} \int_0^t f_1(t) f_2(t) dt$$

and

$$G_{12}(\text{Quad.}) = \frac{1}{t} \int_0^t f_1(t) f_2\left(t + \frac{\pi}{2}\right) dt.$$

The phase angle ϕ between $f_1(t)$ and $f_2(t)$ at the selected frequency is

$$\phi = \tan^{-1} \frac{G_{1,2}(\text{Quad.})}{G_{1,2}(\text{Co.})}.$$

An example of a mode shape thus obtained is shown in Fig. 11 which presents the measured longitudinal mode shape of a cylinder and compares it with the calculated mode shape. This process is especially successful in cases where the amplitudes are not too large and where many other frequencies are present.

The analysis system can also be used to obtain the frequency domain transfer function $T(\omega)$ from the power spectrum of the input function G_i , and the power spectrum of the output G_a .

$$G_a(\omega) = |T^2(\omega)| G_i(\omega),$$

where $T(\omega)$ is a complex function.

Data obtained by the above methods are usually presented in a form where selected frequency amplitudes are plotted versus shaft

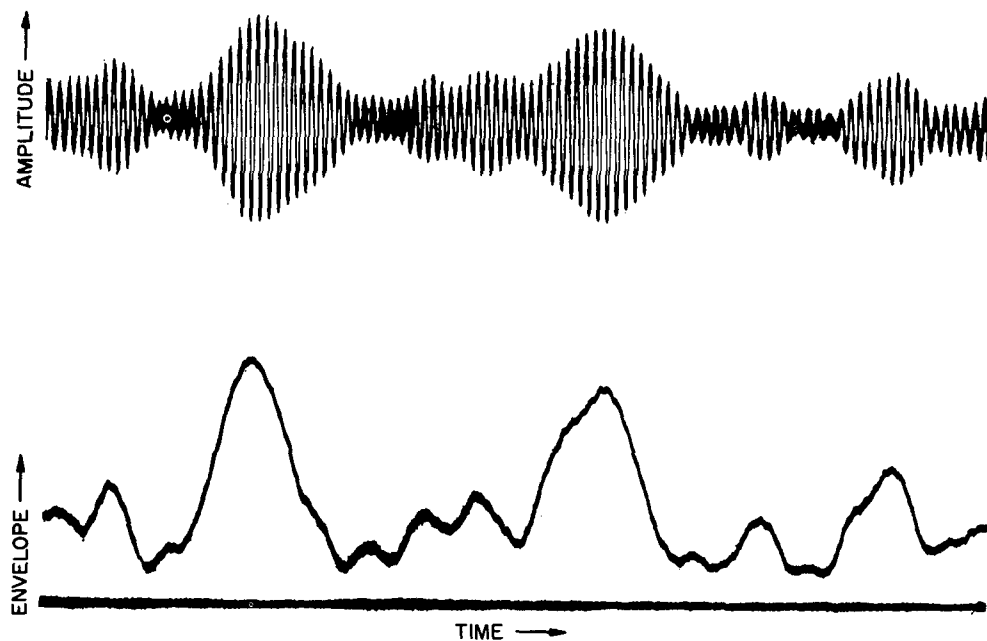


Fig. 10 - Amplitude envelope of a filtered frequency

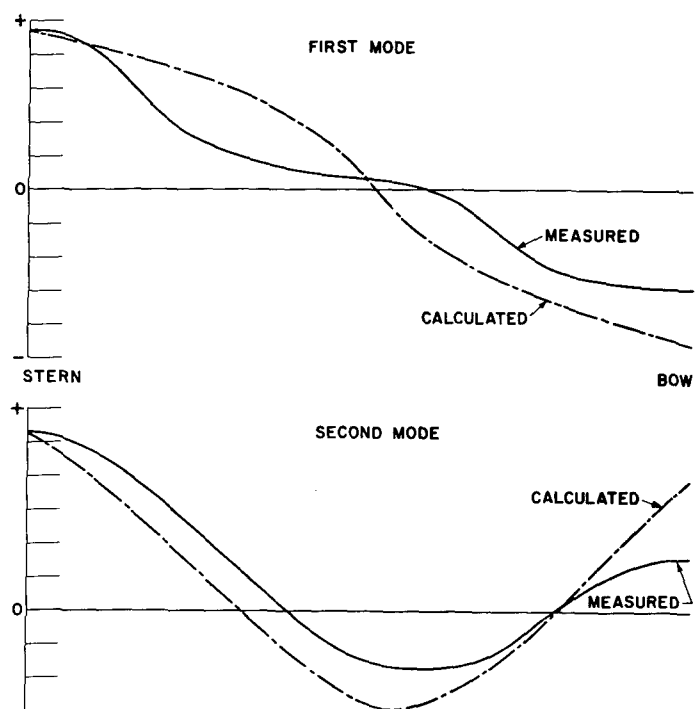


Fig. 11 - Calculated and measured mode shape

rpm. Additional information is given on mode shapes and phases. The bulk of the information is used in the laboratory to obtain a better insight into the phenomena that cause the vibration and into the response characteristics of the ship structure. Figure 12 serves as an example where the vertical response of a ship hull at the stern due to sinusoidal input forces is compared with the calculated response. It is hoped that this approach not only helps to develop the applicability of theoretical work to actual ships but also will eventually give an understanding of the various forces acting on a ship.

Most of the evaluation processes described before are also coded for digital analysis. A similar process will also be described by Mr. Collier in a paper to be presented later.⁶

STATISTICAL AMPLITUDE DISTRIBUTION

In certain cases, it is desired to obtain not only an average or maximum amplitude of a measured quantity but also the amplitude distribution function. This is particularly true in cases where the presence of relatively large random amplitudes may cause relatively large stresses or forces. Furthermore, the

presentation has thus far dealt with steady speed runs. It is certainly of interest to know vibration distribution functions which express quantities for a broader range of operation or for all possibilities of vibrations of a ship during all occurring courses, sea states, wind, and so forth. A statistical representation for all these conditions seems to be the only way of representing a maximum of information in a concise form.⁷⁻⁹

Two instruments have been developed to further this approach; one is an automatic vibration recorder which can be installed on a ship to record data in a random way and the other is a statistical analyzer which evaluates the vibrations. These instruments are shown in Figs. 13 and 14, respectively.

The statistical analyzer counts up to 4000 amplitude values at a selected frequency. The amplitudes may be subdivided into 16 increments. The analyzer then counts the number of amplitudes that fall within these increments. Furthermore it automatically records the total number of counts, the total first moment, and

⁶R. D. Collier, "An Automatic System for Shipboard Vibration Data Acquisition and Integrated Analog-Digital Analysis," Shock, Vibration, and Associated Environments Bulletin No. 33, p.

⁷J. Bendat, et al., "The Application of Statistics to the Flight Vehicle Vibration Problem," Aeronautical Systems Division Technical Report No. 61 - 162 (Dec. 1961).

⁸R. Kennard, "Shock and Vibration of Standard Military Vehicles," Journal of Environmental Sciences (Dec. 1961).

⁹V. Hardy, "Statistical Analysis of Missile Vibration Data," NRL Report No. 1018 (Jan. 1960).

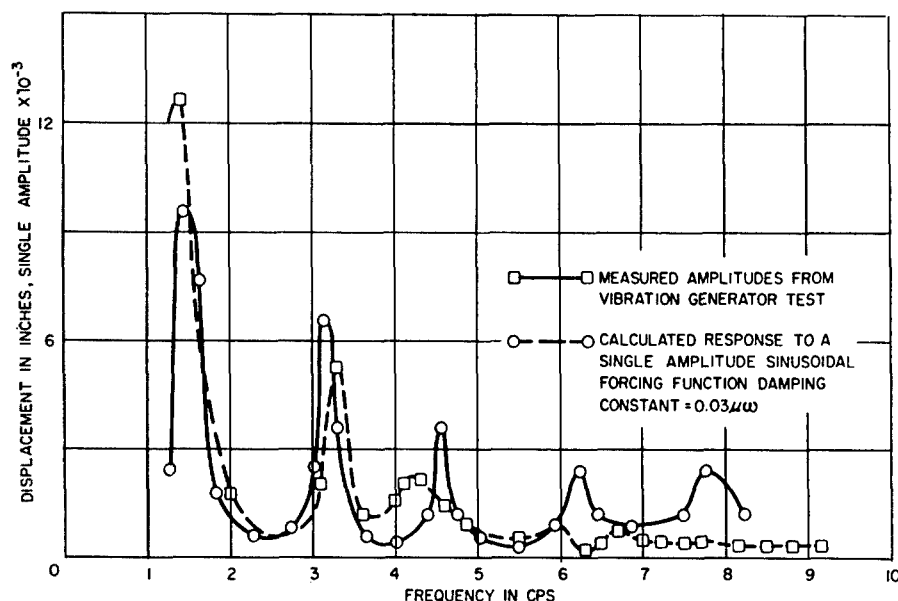


Fig. 12 - Comparison of measured and calculated response

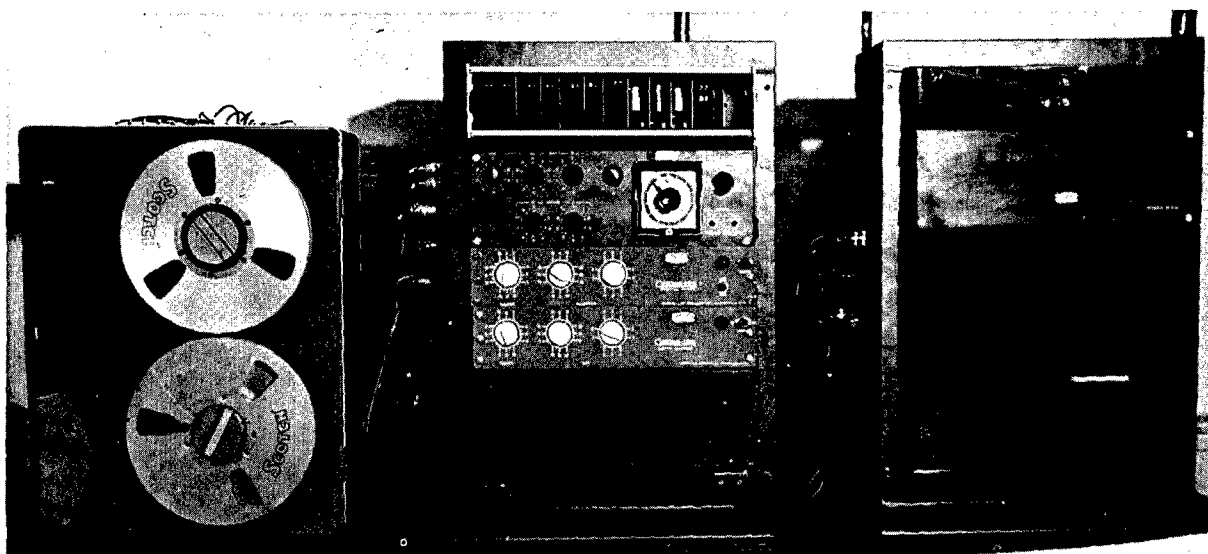


Fig. 13 - Unattended shipboard vibration recorder

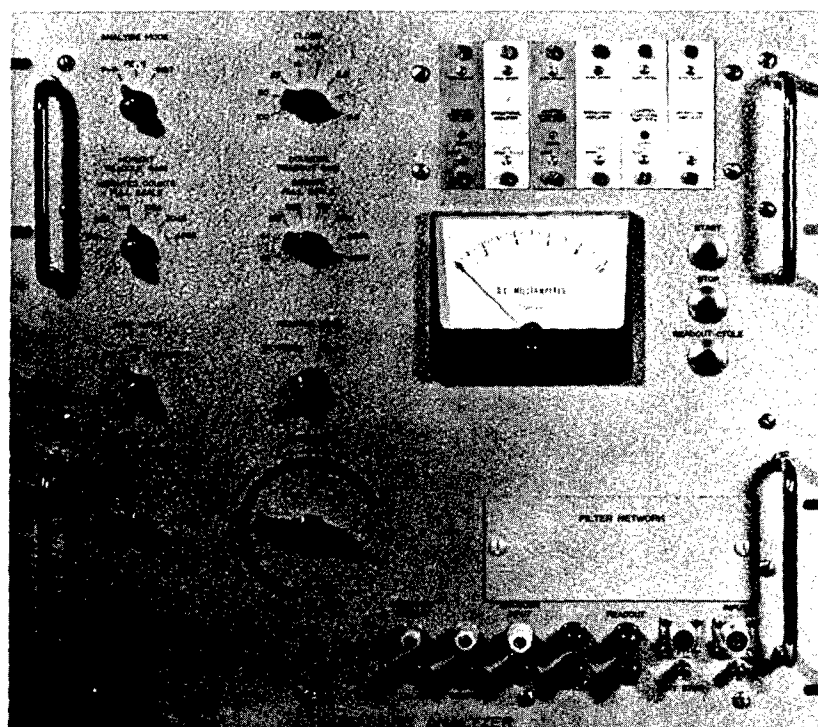


Fig. 14 - Statistical analyzer

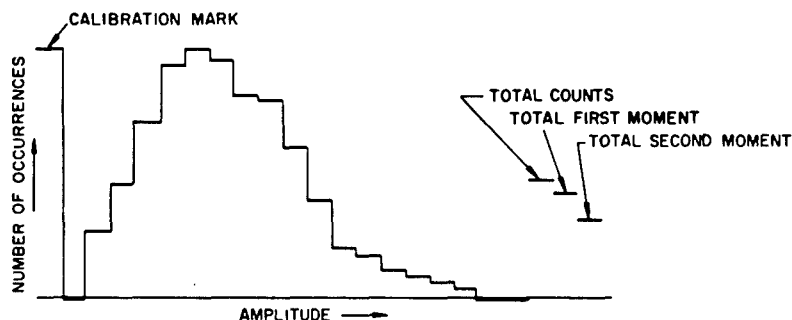


Fig. 15 - Histogram of velocity amplitude of a filtered frequency

the total second moment, from which the standard deviation may be obtained. Figure 15 shows such a histogram. The evaluation of amplitudes obtained over a speed range of from 140 to 174 shaft yielded the histogram shown in Fig. 16.

The vibration amplitudes for a small range of ship speeds can best be presented in the form of a truncated normal distribution, Fig. 17. The truncated probability curve for the histogram shown in Fig. 16 is given in Fig. 18; the line was calculated with the parameters obtained from the histogram, and the measured values are indicated by circles. This approach appears to be promising. It is expected, however, that the probability function for the presentation of all vibration amplitudes obtained under any operational condition may not follow a normal distribution. On some applications interest is mainly directed towards extreme values of vibrating amplitudes. Observed extreme values here are to be analyzed so that further extremes can be predicted. The extreme values are new random variates which belong to a special statistical distribution, that has been defined in recent years as the distribution of extreme values.

ANALYSIS OF TRANSIENTS

Excitation of transient hull and equipment vibration has been used for a long time to obtain characteristic hull frequencies. Some excitation means that have been used are the anchor-drop test where the free fall of an anchor is suddenly stopped, the preload method, in which a unit such as a mast is forcefully bent and suddenly released, and the bump test where a suitable ram hits a unit.

From a visual evaluation of oscillographs, the natural frequencies and the decay of the amplitudes due to damping could be obtained for only a few low frequencies. Difficulties

have been encountered because of the superposition of many frequencies with decaying amplitudes at relatively low frequencies and the short record length.

Recording on magnetic tape and using active analogs with no damping and narrow frequency filtering, however, make the evaluation of transient responses a powerful tool.¹⁰⁻¹³ The condition still remains that two frequencies should not be too close together. Two analytical methods are applied:

1. The measurement of the amplitude versus frequency curve.
2. The amplitude versus time record of a measured natural frequency.

Figure 19 shows the result of a bump test made on the rudder of a ship.

To obtain the amplitude response of this record at a frequency, the tape record signals are used as input into an undamped active filter with the time reversed. The result of such a process is shown in Fig. 20.

The output of the filter shows the amplitude increasing to a maximum value, and then

- ¹⁰R. H. Stringham, Jr., "A Method for Measuring Vibration Modes of a Transiently Heated Structure," Paper presented at SAE-ASNE National Aeronautical Meeting, Washington, D. C. (Apr. 1963).
- ¹¹J. E. Anderson and W. Comley, "Transient Response Data Reduction and a Unique Transient Wave Analyzer," National Telemetering Conference (May 1960).
- ¹²AGARDO graph 56, "Several Techniques for Flight Flutter Testing," NATO Advisory Group for Aeronautical Research and Development (Sept. 1960).
- ¹³R. Mozet, "Some Aspects of Ground and Flight Vibration Tests," NATO Report 40-T (Apr. 1956).

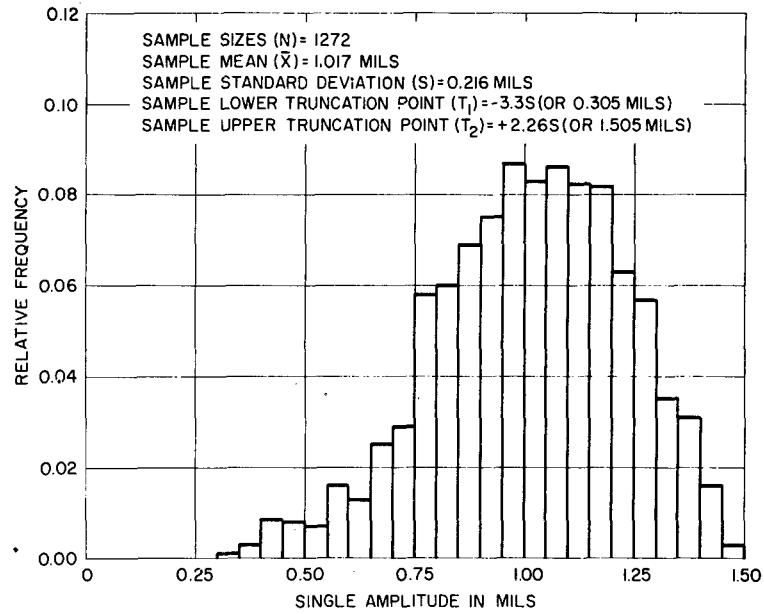
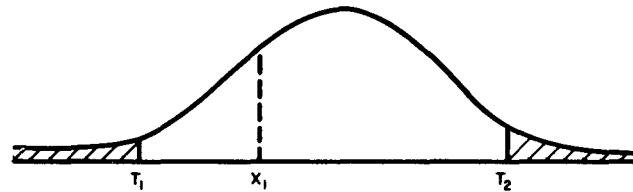


Fig. 16 - Histogram of longitudinal vibrations



$T_{(1)}$ = Lower Truncation Point

$T_{(2)}$ = Upper Truncation Point

A = Area of Normal Curve from $-\infty$ to $+\infty$

$A(T_1)$ = Area of Normal Curve from $-\infty$ to $T_{(1)}$

$A(T_2)$ = Area of Normal Curve from T_2 to $+\infty$

$A_{(3)} = A - (A(T_1) + A(T_2))$ = Area under Truncated Curve

$A(X_1)$ = Area of Normal Curve from $-\infty$ to X_1

$A(X_1 - T_1)$ = Area of Normal Curve from T_1 to X_1

$$P\{X\} = \frac{A(X_1 - T_1)}{A - (A(T_1) + A(T_2))} = \text{Probability } T_1 < x < X_1$$

Fig. 17 - Truncated normal theory

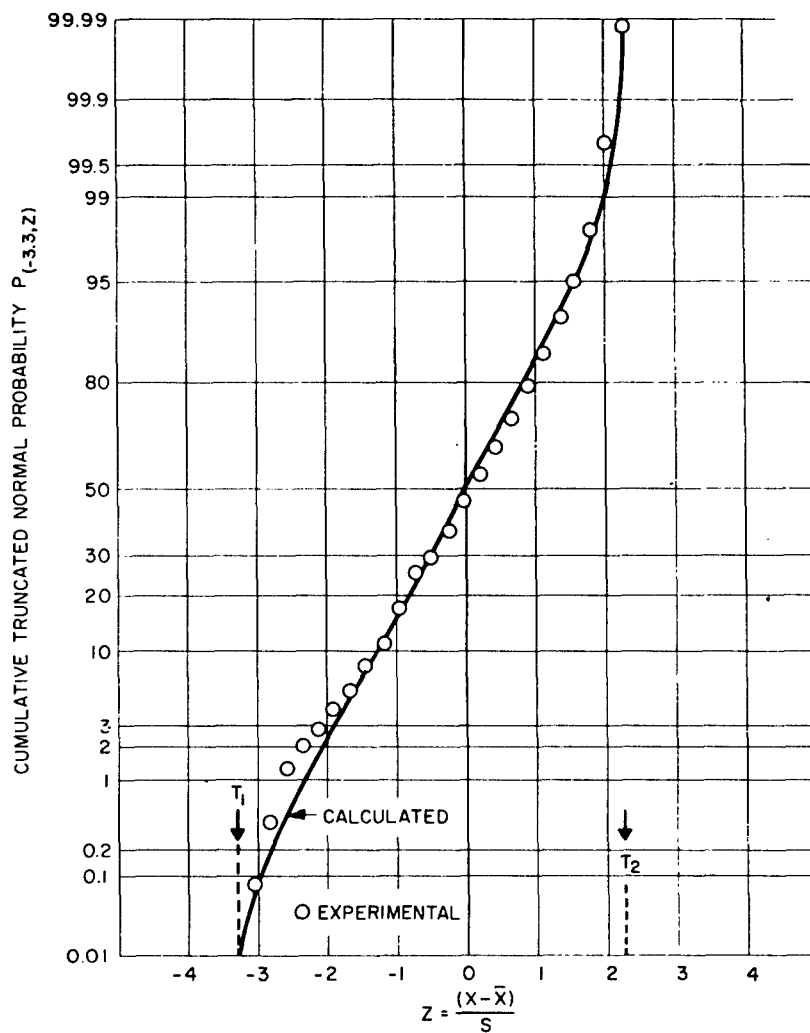


Fig. 18 - Probability curve for longitudinal vibrations

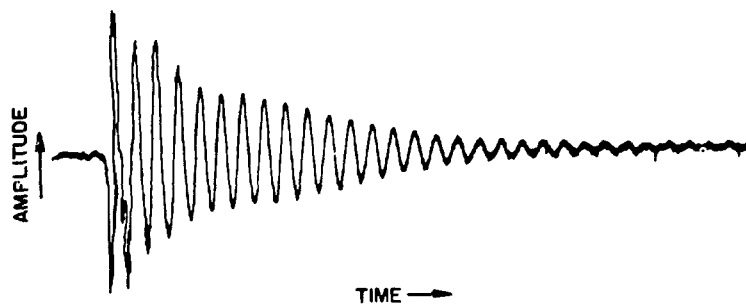


Fig. 19 - Transient response of a structure

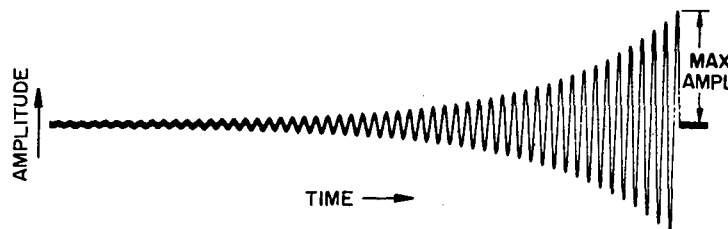


Fig. 20 - Analysis of a transient response to obtain a frequency response curve

continuing at this maximum value. Increasing selected filter frequencies gives the amplitudes at these frequencies over the desired frequency range. Such a frequency response curve is shown in Fig. 21. It is the result of the analysis of the transient response curve shown in Fig. 19.

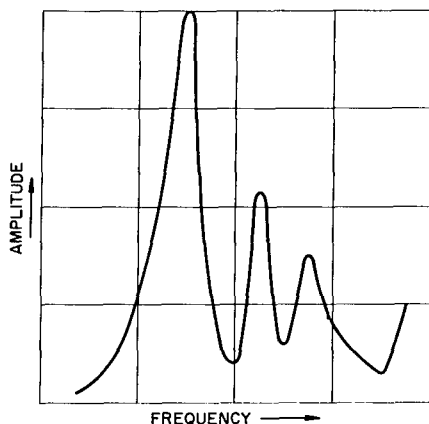


Fig. 21 - Frequency response curve of a transient

This frequency response curve defines the natural frequencies of the structure under investigation and the damping values associated with the various frequencies. The peaks at the natural frequencies correspond to the

damping.¹⁴ The importance of damping in naval vessels is summarized in Ref. 15.

CONCLUSION

Information on vibration characteristics of ships is needed to insure (1) structural suitability during service life, (2) habitability and operability, and (3) silent operation. These objectives can be met only if the data obtained confirm existing theories of ship vibration and their useful application to actual structures.

Important parameters that enter into the calculations include stiffness factors, virtual masses, damping, and correct simulation of the structure by the mathematical model. Increasing demands on shipboard equipment require the accurate presentation of vibratory environment.

Most of the work in the development of experimental measuring techniques and corresponding analytical methods is directed towards a better understanding of the vibration mechanism and a refinement of present vibration theories. This should enable the naval architect to predict vibration characteristics of a ship and to detect the structures that may need redesign.

¹⁴G. M. L. Gladwell, "A Refined Estimate for the Damping Coefficient," *J. Roy. Aeronaut. Soc.*, Vol. 66 (Feb. 1962).

¹⁵R. C. Leibowitz, "A Proposed Study of Vibration Damping Associated with Naval Vessels," *Proceedings of the Structural Vibration Damping Conference at Mare Island Naval Shipyard* (Oct. 1962).

BIBLIOGRAPHY

Breslin, J., "Ship Vibration, Part I, Propeller-Generated Excitations," *Applied Mechanics Revision*, Vol. 13, No. 7 (July 1960)

Forkois, H. M. and Woodward, K. E., "Design of Shock and Vibration Resistant Electronic

Equipment for Shipboard Use," *NAVSHIPS 900*, 185A (Apr. 1957)

Kanazawa, T., "A Proposal for the Vibration Limits of Ships," *Schiff und Hafen*, Heft 7 (1961)

McGoldrick, R. T., "Ship Vibration," DTMB
Report 1451 (Dec. 1960)

"Military Standard Mechanical Vibrations of
Shipboard Equipment," MIL-STD-167
(SHIPS) (Dec. 1954)

Miller, N. S. and Kno, C., "Main Hull Vibration
of Ships," paper presented at the Interna-
tional Ships Structure Committee (1961)

Suetsugu, I., "The Effects of the Bottom Vibra-
tion on the Hull Natural Frequencies,"
paper presented at the Kansas Society of
Naval Architects (May 1963)

Todd, F. H., "Ship Hull Vibration," Edward
Arnold Limited, London (1961)

Voight, H., "Recent Findings and Experimental
Data Obtained in the Field of Ship Vibra-
tions," DTMB Translation 268 (Feb. 1958)

* * *

TECHNIQUES FOR ANALYZING NONSTATIONARY VIBRATION DATA

P. T. Schoenemann
Sandia Corporation
Livermore, California

This paper reviews the theory and problems associated with the analysis of nonstationary random vibration data. A practical method using comb filters is described. The results, when translated into vibration tests, tend to overtest in terms of rms value but assure that each frequency band represents the extremes of the environment.

INTRODUCTION

In most instances the in-flight vibration environment endured by a missile warhead is a nonstationary random process. However, most current methods of random vibration data analysis assume that the data represents stationary, ergodic random phenomena, which is generally true only for laboratory shaker tests and most shipping environments. If a process is nonstationary, the standard methods do not apply with assurance, and the resulting analysis must be treated with care.

Considerable theoretical work on nonstationary random phenomena has been published during the last decade. Little of this theory has been applied to the task of analyzing missile flight vibration data other than assuming that the data is piecewise stationary and then treating each piece in the conventional manner. It is possible and sometimes quite practical, however, to treat the data as nonstationary to derive a more meaningful representation of the actual environment.

THEORETICAL BACKGROUND

Various investigators¹⁻⁷ have developed expressions which describe the spectrum of a

nonstationary process as a function of both time and frequency. Some of their relationships are particularly applicable to missile vibration analyses. Although many of the developments differ in detail, a common factor to the various theoretical treatments is a time varying expression for the power spectrum, $P(t, f)$, where f is frequency in cps and t is the time in seconds.

These expressions are derived in the following general manner. Consider a general signal $s(t)$. The correlation function is defined as usual by

$$R(t, \tau) = E [s(t) s(t + \tau)], \quad (1)$$

where E represents the mathematical expectation.

For stationary, ergodic processes $R(t, \tau)$ is constant with t so it can be represented as a function of τ only,

$$R(t, \tau) = R(\tau) \quad (2)$$

¹A. A. Kharkevich, *Spectra and Analysis* (translated from Russian) (Consultants Bureau, New York, 1960).

²C. H. Page, "Instantaneous Power Spectra," *J. Appl. Phys.*, Vol. 23, No. 1 (Jan. 1952).

³C. H. M. Turner, "On the Concept of an Instantaneous Power Spectrum and its Relationships to the Autocorrelation Function," *J. Appl. Phys.*, Vol. 25, No. 11 (Nov. 1954).

⁴P. G. Lampard, "Generalization of the Wiener-Khinchine Theorem to Nonstationary Processes," *J. Appl. Phys.*, Vol. 25, No. 6 (June 1954).

⁵R. M. Fano, "Short-Time Autocorrelation Functions and Power Spectra," *J. Acoust. Soc. Am.*, Vol. 22, No. 5 (Sept. 1950).

⁶N. A. Zheleznev, "Some Problems of the Spectral Correlation Theory of Nonstationary Signals," *Radiotekhnika i Elektronika*, Vol. 4, No. 3 (1959), pp. 359-379.

⁷J. Kampe de Fariet and F. N. Frenkiel, "Estimation de la Correlation d'une Fonction Aleatoire non Stationnaire," *Comptes Rendus, Acad. Sciences, Paris*, Vol. 249 (1959), pp. 348-351.

and the familiar manipulations can be made⁶ to obtain the power spectrum.

$$\begin{aligned} P(f) &= \int_{-\infty}^{\infty} R(\tau) e^{-j2\pi f\tau} d\tau \\ &= 2 \int_0^{\infty} R(\tau) \cos 2\pi f\tau d\tau. \end{aligned} \quad (3)$$

$P(f)$ is the Fourier transform of $R(\tau)$.

For the nonstationary case, a parallel expression can be obtained,

$$p(t, f) = 2 \int_0^{\infty} R(t, \tau) \cos 2\pi f\tau d\tau. \quad (4)$$

This is the spectrum of the instantaneous power of $s(t)$, as shown in Refs. 1 and 6. There is, in general, a different spectrum for every instant t .

This expression for $p(t, f)$ is for only one sample function of the random process. Other sample functions will yield, in general, different functions for $p(t, f)$. For stationary ergodic processes one sample function is statistically representative of all sample functions, and one time interval of the sample function is statistically representative of the whole sample function, so the data analysis problem is greatly eased. This, unfortunately, is not the case for nonstationary processes.

The vibration environment of a missile flight is by no means stationary, but it is essentially repeatable from flight to flight for a given set of launch and re-entry parameters. Over the ensemble of similar missile flights, averaging yields an estimate for the power spectrum of the nonstationary process at a given time t .

$$E[p(t, f)] = \frac{1}{n} \sum_{i=1}^n p_i(t, f) = \overline{p(t, f)}, \quad (5)$$

where p_i is the spectrum of the i^{th} flight and n is the number of flights.

$p(t, f)$ then is the expected spectrum of the instantaneous power at time t . The desired quantity, however, is the expected spectrum of the power averaged over some interval T ,

$$P(t, f) = \frac{1}{T} \int_{t-T}^t \overline{p(t, f)} dt. \quad (6)$$

The length of the averaging interval T affects the value of $P(t, f)$ at any time t , since it determines the degree of time smoothing afforded to the spectrum. A correct choice of T depends upon engineering compromises between the degree of time resolution desired, the response characteristics of the system under vibration, and the severity of the nonstationarity.

It is shown in Ref. 1 that the time averaging and statistical averaging can be performed in any order. This is important for data analysis where time averaging on a single flight is usually performed before all the flights are averaged together. In mathematical terms

$$\begin{aligned} P(t, f) &= \frac{1}{T} \int_{t-T}^t \frac{1}{n} \sum_{i=1}^n p_i(t, f) dt \\ &= \frac{1}{Tn} \sum_{i=1}^n \int_{t-T}^t p_i(t, f) dt. \end{aligned} \quad (7)$$

SEPARABLE RANDOM PROCESSES

There are some specialized forms of nonstationary processes of frequent practical interest that have been studied by several investigators^{6,8-10}. Most of these fall into the so-called "separable class" where the correlation function can be represented as

$$R(t, \tau) = R_1(x) R_2(y), \quad (8)$$

where x and y are related in some specific way to t and τ .

Of particular interest are signals separable with respect to t and τ .

$$R(t, \tau) = R_1(t) R_2(\tau). \quad (9)$$

($R_1(t)$ is constant for wide-sense stationary processes.) For many practical situations (Refs. 6 and 10) a good approximation to the physical situation is

$$R(t, \tau) \cong R_1(t) R_2(\tau),$$

where $R_1(t)$ is proportional to the instantaneous power.

⁸A. H. Nuttall, "Theory and Application of the Separable Class of Random Processes," MIT Res. Lab or Elect., Rept. 343 (May 1958).

⁹R. A. Silverman, "Locally Stationary Random Processes," IRE Trans. on Information Th., IT3, No. 3 (Sept. 1957).

¹⁰L. I. Gudzenko, "On Periodic Nonstationary Processes, Radio Engineering and Electronics," Vol. 4, No. 6 (1959), pp. 220-224.

This is particularly applicable in the case where some wide-sense stationary random signal is slowly amplitude-modulated. The power spectrum can then be approximated by

$$p(t, f) \cong R_1(t) P_2(f), \quad (10)$$

where $P_2(f)$ is the Fourier transform of $R_2(\tau)$.

In many cases, even though a nonstationary process is not strictly separable, the assumption of separability yields useful approximations.

APPLICATION

Various practical problems arise in the application of the nonstationary theory. Most important of these are:

1. The complexity of the equipment needed to perform the necessary mathematical operations;
2. The assigning of statistical meaning to data samples taken from the nonstationary environment; and
3. The interpretation of the resulting data for use in component or system design and for developing meaningful laboratory environmental test specifications.

In some cases there are no practical solutions for all these problems. There are many physical situations, however, where useful information can be obtained.

The experimental determination of $P(t, f)$ at a point on the (t, f) plane is impossible (Ref. 6) since only averages are considered. The average value over an area $\Delta t \Delta f$ can be estimated by taking a time average over some frequency band.

Equipment suitable for the spectral analysis of nonstationary random signals must measure all the spectrum of interest all of the time. The analysis can be performed on a digital computer but this is a formidable task

even for a computer with a large memory. For installations with large computing facilities, however, computer time may be less expensive than the installation and operation of some special-purpose equipment.

One practical method of estimating $P(t, f)$ is to use a set of comb filters with continuous frequency bands to separate the data in the frequency domain and then use squaring and appropriate averaging on the output of each filter to produce real-time analysis. A generalized block diagram of one channel of such a device is shown in Fig. 1.

The output of each channel can then be represented as a time varying function $A_j(t)$, which represents the squared signal distributed over some frequency band Δf_j and averaged over some time interval Δt .

The multiple filter device similar to Fig. 1 but with an integrator for a time averager is described in Ref. 11. The device does not yield a continuous $A_j(t)$ for each channel but gives samples every n seconds, where n is variable in discrete steps from 1 to 10 seconds. A device yielding a continuous $A_j(t)$ would utilize a low-pass filter for the time averaged. Fano⁵ examines the case for RC filters. An RC filter gives an exponentially-weighted time average. To perform the averaging indicated in Eq. 6 requires complex circuitry using delay lines to produce the transfer function

$$\frac{1 - e^{-sT}}{sT}$$

where s is the Laplace variable. Such transfer function realization is uneconomical at present for multi-channel real-time analog analyzers.

The output of each analyzer channel can be represented as a time varying function $A_j(t)$,

¹¹P. T. Schoenemann, "Real Time Analysis of Random Vibration Power Density Spectra," OSD/R&E, Shock, Vibration, and Associated Environments Bulletin No. 31, Part III (Apr. 1963).

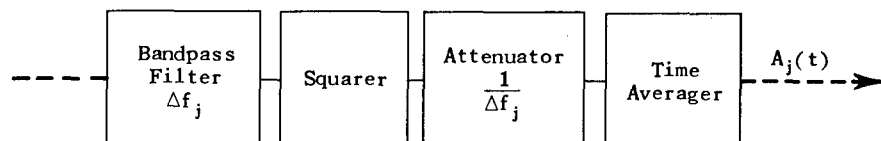


Fig. 1 - One channel of a multiple channel analyzer

which represents the squared signal averaged over some finite time interval T . Now, if we have data from n similar flights, the representation of $P(f, t)$ becomes

$$P(f, t) = \frac{1}{n} \sum_{i=1}^n A_{ij}(t), \quad (\text{All } t, f \text{ in } \Delta f_j) \quad (11)$$

where $A_{ij}(t)$ is the output of the j^{th} channel for the i^{th} flight.

In order to analyze the statistics of the collection of $A_{ij}(t)$ we must consider the ensemble at some $t = t_0$, a constant. $P(f, t_0)$ is the expected value for any given flight datum at t_0 . The variance for the ensemble is estimated by

$$\sigma_j^2 = \frac{E \sum_{i=1}^n [A_{ij}(t_0) - P(f, t_0)]^2}{n - 1}, \quad (12)$$

which is the formula for the unbiased estimate of the variance of a random variable. This means that the $A_{ij}(t_0)$ for the $(n+1)^{\text{th}}$ flight will have an expected value estimated by Eq. (11) and a variance estimated by Eq. (12).

If $s(t)$ is a Gaussian variable at all t_0 , the output of the averaging circuits will be something between chi-square and Gaussian depending on the averaging time T . Usually the determination of the distribution is done empirically. The determination of the distribution of the output of a linear system for non-Gaussian inputs is covered in a paper by Mazelsky.¹² In practice, the empirical approach is easier.

$P(f, t)$ as defined will be a variable for stationary processes as well as nonstationary processes. However,

$$\lim_{n \rightarrow \infty} P(f, t_1) = \lim_{n \rightarrow \infty} P(f, t_2)$$

holds for stationary cases but not for nonstationary cases. The statistics for the stationary case have been treated thoroughly in the literature. As a measure of nonstationarity, a

statistical confidence test can be made on a succession of time samples.

The third problem is to develop a sensible environmental test specification for electrodynamic shaker systems. The average environment can, with a lot of expense and complication, be represented by some artificial nonstationary process. However, most, if not all, testing laboratories utilize a stationary process for environmental simulation. The problem, then, is to derive a stationary process that in some meaningful way represents the nonstationary process of the missile environment. One method is to construct a composite spectrum with the level in each frequency band Δf_j greater than some arbitrary percentage of the $A_{ij}(t)$. This can be, in general, an overtest since maxima in the different frequency bands do not necessarily coincide in time. However, such a specification does assure that each frequency band is tested to a significant level.

Often in practice this method of deriving a specification is not an overtest. When the environment can be closely approximated by a separable process described by Eq. (10)

$$p(t, f) = R_1(t) P_2(f),$$

then the test specification can be

$$P(f) = [\max R_1(t)] P_2(f). \quad (13)$$

The rms value of the test environment will then coincide with the maximum of the real environment.

One method of reducing the overtest if Eq. (10) does not hold is to break the environment into sections where separate tests can be specified. For example, if the launch phase has predominantly low frequencies and the re-entry phase predominantly high frequencies, two separate tests can be run. This method increases testing time and costs, but may be worthwhile if appreciable component weight savings are affected.

CONCLUSIONS

Methods are available for the analysis of nonstationary vibration data. The resulting analysis is more voluminous than that for stationary environments since two variables, frequency and time, are important, rather than just frequency. For many missile flight environments where the statistics are time variable but repeatable, a stationary test specification can logically be derived from the nonstationary environment.

¹²B. Mazelsky, "Extension of Power Spectral Methods of Generalized Harmonic Analysis to Determine Non-Gaussian Probability Functions of Random Input Disturbances, and Output Responses of Linear Systems," J. Aeronaut. Sci., Vol. 21, No. 3 (Mar. 1954).

DISCUSSION

Mr. O'Hearne (Martin Co.): I'd like to ask a brief question about these functions which are functions both of frequency and of time, or functions of both variables when one is more or less the inverse of the other. I just can't quite understand what they are. Is that a real mathematical function, or is it some kind of an approximation?

Mr. Schoenemann: It is a real function. I've loaded the bibliography on this subject as an exercise-to-the-reader kind of thing. The τ was the usual delay time and the T was the instant of concern. In a stationary case, you can hope that regardless of where you take a correlation function, you're going to get the same answer. If it is nonstationary, you take a correlation function one time and then take it another time and they're not the same. The power spectrum generally is the Fourier transform of a correlation function with respect to τ , the delay time, and you just ignore the T . There are some treatments where a double transform is taken, that is, with respect to T and with respect to τ , and you get a correlation function in the frequency domain. That is in one of the references also. Yes, it is a real function and you do get some meaningful data out of it. As

I did mention, you're going to get a little bit of time variation in your spectrum where, in the stationary case in the limit, you're not supposed to.

Mr. Bieber (Lockheed Missiles and Space Co.): If you assume that this correlation or covariance has several properties, essentially aren't you normalizing the signal by the variance? When you get your τ or whatever you call it, it seems to me that then all the methods of estimation of the spectra for the stationary case could be brought to bear. Is that right?

Mr. Schoenemann: Yes, actually one of the authors that I quoted in the references developed this particular spectrum as something that is the power X the time varying g^2X a spectrum that doesn't change. This is very closely related to the stationary case, but the separable cases do not exactly happen in reality. For many of our particular components, which are isolated far away from the original forcing function and mounted on all kinds of ducts, we're just seeing something that is a resonant response of some mounting for it. It looks very much like this at all times; tends to be a narrow band kind of thing.

BIBLIOGRAPHY

Batkov, A. M., Generalization of the Shaping Filter Method to Include Nonstationary Random Processes, Automation & Remote Control (USSR), Vol. 20, #3 (1959), 1049-1062.

Borford, T. M., "Nonstationary Velocity Estimation," Bell Syst. Tech. Journ., Vol. 37, No. 4 (July 1958).

Lampard, P. G., "The Response of Linear Networks to Suddenly Applied Stationary

Random Noise," IRE Trans. Circuit Theory, Vol. CT-2 (Mar. 1955).

Nuttal, A. H., "Theory and Application of the Separable Class of Random Processes," MIT Res. Lab. of Electronics, Tech. Report 346 (May 26, 1958).

Schoenemann, P. T., "Measurement of Power Spectra for Nonstationary Random Signals," Sandia Corp. SCTM 311-62-81 Apr. 1962).

* * *

THE APPLICATION OF A COMPONENT ANALYZER IN DETERMINING MODAL PATTERNS, MODAL FREQUENCIES, AND DAMPING FACTORS OF LIGHTLY DAMPED STRUCTURES

F. E. Hutton
General Electric Company
Re-Entry Systems Department

A system is described in which the quadrature and in-phase responses of acceleration are plotted versus frequency to determine modal frequencies and damping factors. An accelerometer is moved from station to station on the structure to plot out a graph of quadrature response versus station for each modal frequency selected, directly obtaining the modal patterns of the structure.

INTRODUCTION

A method of vibration testing has been adopted at The Re-Entry Systems Department of The General Electric Company whereby modal patterns, frequencies, and damping factors of space vehicles can be determined with a component analyzer (see Fig. 1).

The system is comprised of a force gage to couple the test specimen to the shaker, an accelerometer attached to the test specimen, and a servo system to control the shaker force. Signals from the force gage and the accelerometer are coupled to the component analyzer, where the acceleration signal is presented as a vector quantity using the force signal as the reference. Typical test setups are shown in Figs. 2 to 5.

The presentation of this vector is in four forms: (1) the amplitude of the acceleration component that is in-phase with the force signal, or the in-phase response, (2) the amplitude of its component that is 90 degrees from the force signal, or the quadrature response, (3) the total amplitude of the acceleration signal and the force link, and (4) the phase angle.

The system employs essentially the same technique discussed by Stahle.¹ The quadrature

¹C. V. Stahle, Martin Company, Baltimore Division, "A Phase Separation Technique for the Experimental Determination of Normal Vibration Modes of Flight Vehicles."

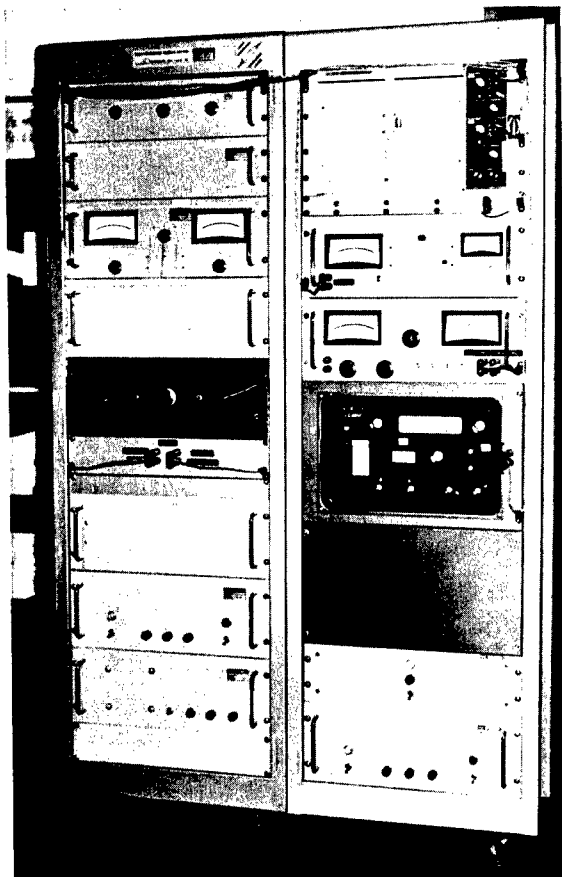


Fig. 1 - Component analyzer

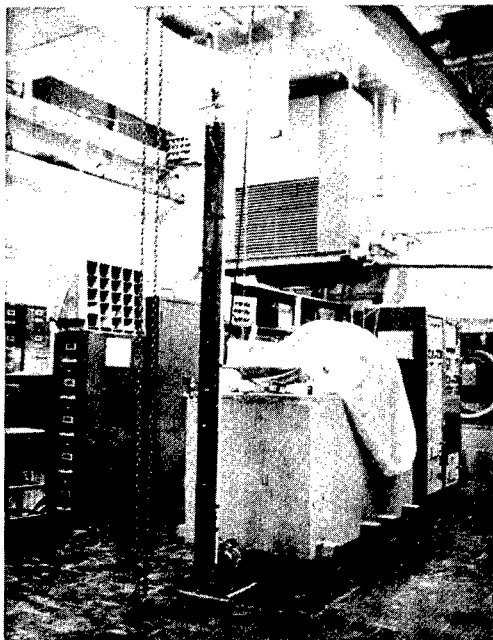


Fig. 2 - Free-free beam
and suspension system

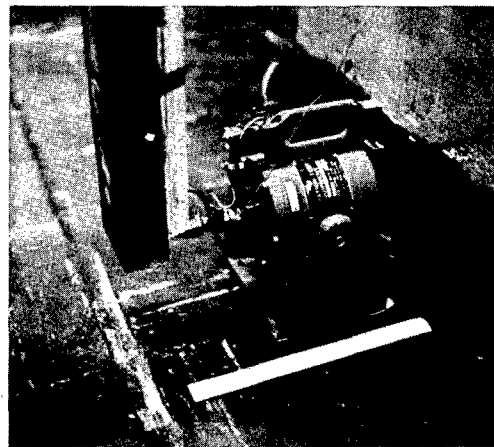


Fig. 3 - Shaker, force-gage,
beam configuration

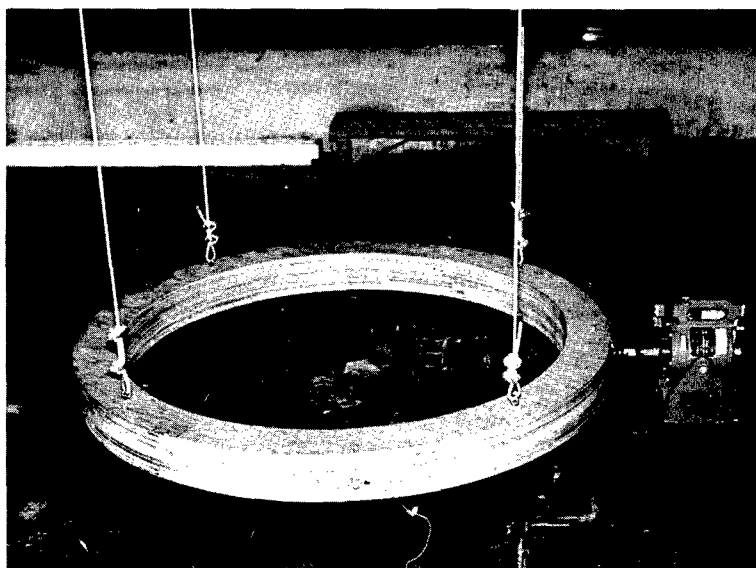


Fig. 4 - Wooden hoop and suspension system

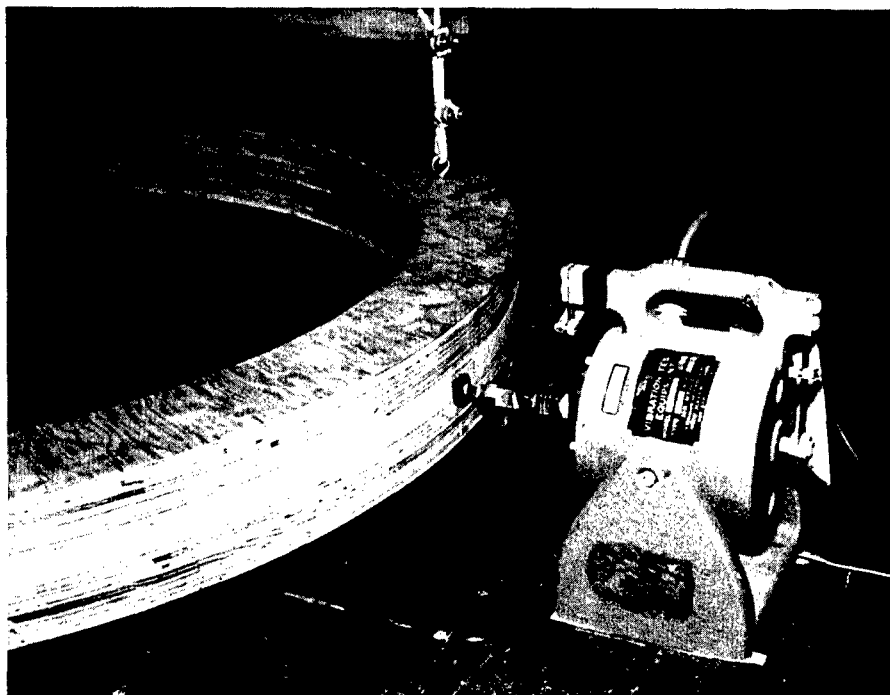


Fig. 5 - Shaker, force-gage, hoop configuration

and in-phase responses of acceleration are plotted versus frequency to determine modal frequencies and damping factors, and then the accelerometer is moved from station to station on the structure to plot out a graph of quadrature response versus station for each modal frequency selected, directly obtaining the modal patterns of the structure.

THE COMPONENT ANALYZER

The component analyzer presently employed is a model 711A-4 manufactured by the Boonshaft & Fuchs Company. It is shown in block diagram form in Fig. 6 along with the additional equipment necessary for its operation for structural measurements.

The technique of multiplying the force signal by the acceleration signal is used for obtaining the separated components of the acceleration vector. The in-phase response of the acceleration signal is obtained in the following manner. The acceleration signal, $A \sin(\omega t + \theta)$, is multiplied by the force signal, $F \sin \omega t$, in the return signal analyzer section of the component analyzer, yielding the following expression:

$$F \times A = [A \sin(\omega t + \theta)] [F \sin \omega t],$$

or

$$F \times A = \frac{FA}{2} \cos \theta - \frac{FA}{2} \cos 2\omega t \cos \theta + \frac{FA}{2} \sin 2\omega t \sin \theta,$$

where

A = Acceleration (g),

F = Force (lb),

ω = Angular Frequency (rad/sec),

t = Time (sec), and

θ = Angle between the Acceleration and Force

The last two terms of the expression are removed with a low pass filter and the first term, $FA/2 \cos \theta$, is obtained in the form of a dc-voltage. The coefficient, F , is held constant by controlling the force into the specimen, and the scale factor of the in-phase meter is doubled so that the first term is read out as $A \cos \theta$, the in-phase response of the acceleration signal.

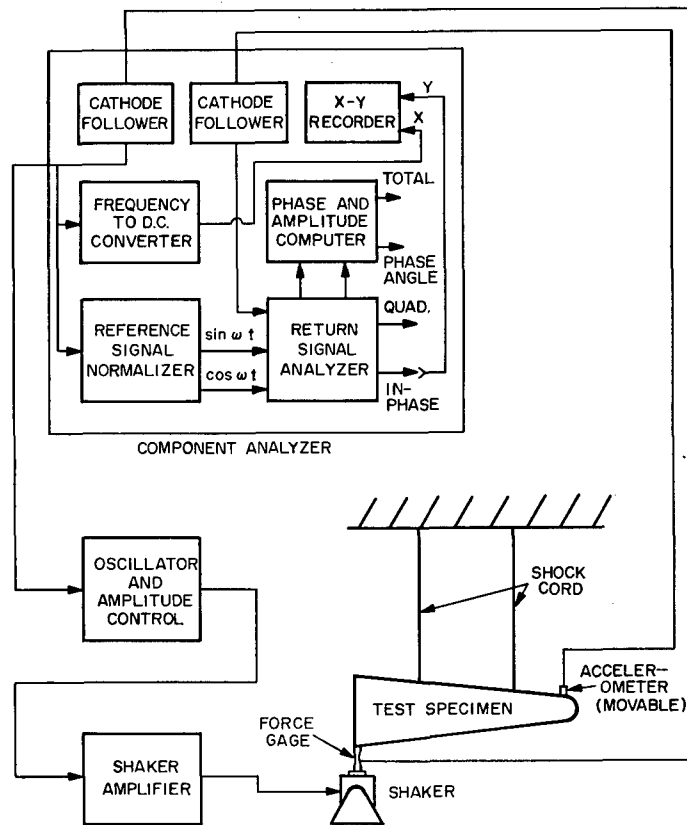
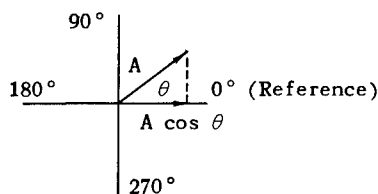


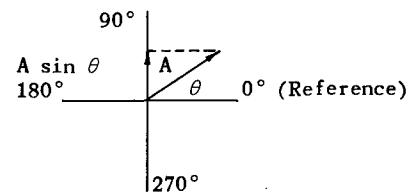
Fig. 6 - Typical test setup, block diagram



The quadrature response of the acceleration signal is obtained in a similar manner. The force signal, $F \sin \omega t$, is phase shifted by 90 degrees in the reference signal normalizer section of the component analyzer so that it becomes $F \cos \omega t$. Multiplication of this signal with the acceleration signal in the return signal analyzer yields

$$F \times A = \frac{FA}{2} \sin \theta + \frac{FA}{2} \sin 2\omega t \cos \theta + \frac{FA}{2} \cos 2\omega t \sin \theta.$$

The last two terms are filtered out and the first term is read out as $A \sin \theta$, the quadrature response of the acceleration signal.



The component analyzer has the additional feature of being able to recombine these two dc-voltages (in-phase and quadrature responses) as the square root of the sum of the squares for measuring the total acceleration response, and the phase angle between the force and acceleration signals.

Each of the four measurements (in-phase response, quadrature response, total amplitude, and phase angle) are presented on meters for a quick readout and also in the form of dc-voltages for use with X-Y plotters or other recorders.

THE VIBRATION SYSTEM

A block diagram of the vibration system is shown in Fig. 6.

The signal from the force gage is coupled via a cathode follower in the component analyzer to (1) the oscillator to serve as the feedback signal to control the shaker, (2) the frequency to dc-converter to drive the x axes of the x-y plotters, and (3) the reference signal normalizer of the component analyzer to serve as the signal to which the acceleration signal is referred.

The acceleration signal is fed via the other cathode follower into the return signal analyzer of the component analyzer where it is multiplied by the force signal.

X-Y plotters are used for recording the in-phase response, quadrature response, total response, and phase angle outputs of the component analyzer as a function of frequency. In addition, one of the X-Y plotters is used for recording quadrature response versus predetermined locations on the test specimen.

A Bruel & Kjaer Model 1018 Oscillator is utilized for its control features to drive the shaker and maintain the force at a constant level for obtaining the frequency response plots. A Wayne Kerr Model S121 Oscillator, having good frequency stability is used when obtaining the modal pattern plots.

Endevco crystal force transducers are used for coupling the shakers to the test specimens and Endevco crystal accelerometers are used for measuring the acceleration.

The shakers used for these tests have relatively light moving elements compared to the weight of the specimen being driven. An MB Model SDA Shaker having an armature weight

of 0.6 pounds and a maximum rated force of 10 pounds was used for tests with a solid steel beam weighing 230 pounds and a wooden hoop weighing 50 pounds. An MB Model C-10 Shaker having an armature weight of 17 pounds and a maximum rated force of 1200 pounds was used for vibrating a re-entry vehicle.

Each specimen is usually suspended with elastic shock cord so that the natural frequency of the suspension system-specimen combination is about 1 cps.

TEST PROCEDURE

The modal frequencies of the specimen are determined first. The accelerometer is attached to the specimen at an anti-mode. (At the extreme end of the specimen for beam bending modes, and opposite the force gage for hoop modes.) The specimen is then vibrated through the frequency range of interest at a very slow sweep rate. The amplitude of the force input to the specimen is maintained at a constant level with the Bruel & Kjaer Oscillator.

Plots of frequency versus in-phase response, quadrature response, total response, and phase angle of the acceleration signal with reference to the force signal are recorded with the component analyzer (see Figs. 7 to 9). These plots are studied in order to determine the resonant frequencies of the specimen. Each resonant frequency is selected at the point where the quadrature response peaks in a positive or negative direction.

Damping factor at each resonant frequency of the specimen is obtained from the in-phase response plots using the formula,¹

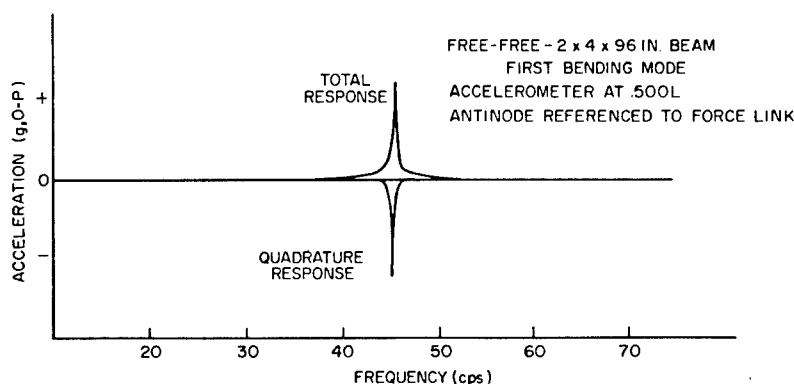


Fig. 7 - Total and quadrature response versus frequency of a steel beam

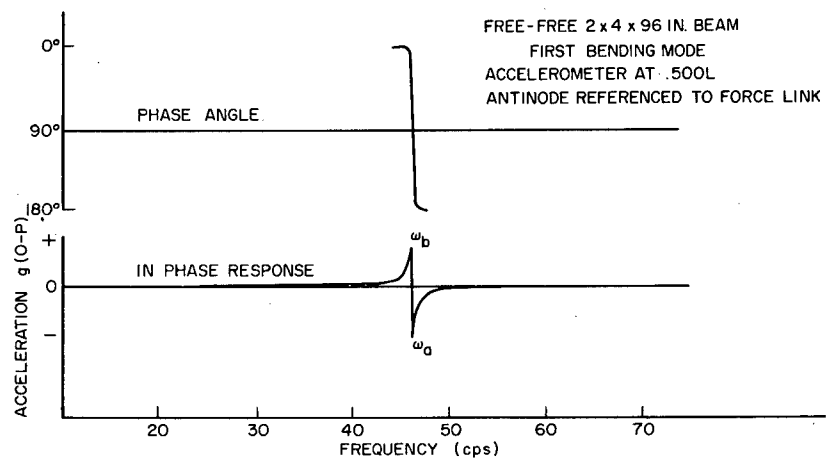


Fig. 8 - Phase angle and in-phase response versus frequency of a steel beam

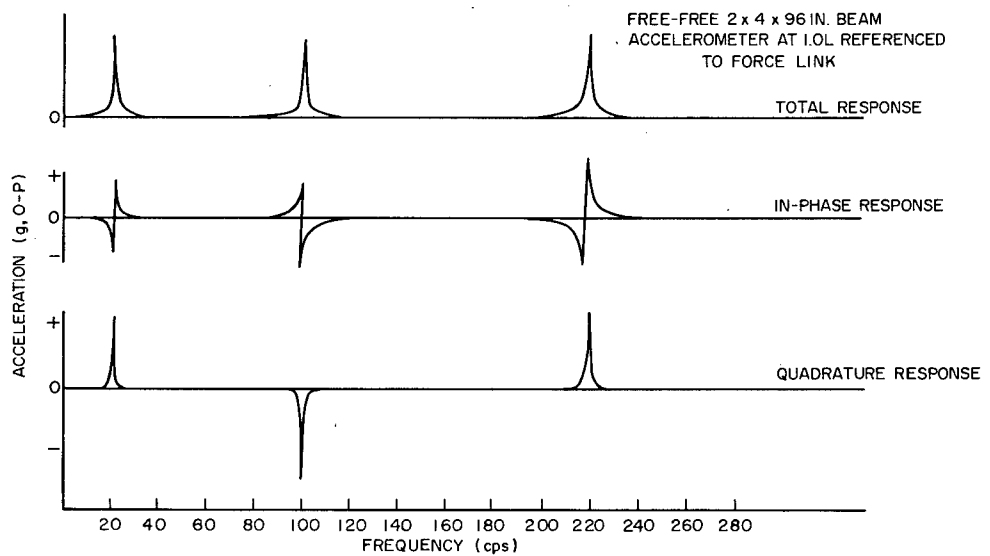


Fig. 9 - Quadrature, in-phase, and total response versus frequency of a steel beam

$$\zeta = \frac{\left(\frac{\omega_a}{\omega_b}\right)^2 - 1}{\left(\frac{\omega_a}{\omega_b}\right)^2 + 1},$$

where

ζ = Damping Factor, and

ω_a and ω_b are the frequencies where the in-phase response peaks (Fig. 8).

The system is used next for determining the modal patterns of the specimen. The oscillator is adjusted to the resonant frequencies determined from the quadrature response plots, and the force is applied to the specimen. The X axis of the X-Y plotter is adjusted so that it can be manually made to correspond to pre-determined locations on the specimen. The Y axis of the recorder is used for recording the quadrature response of the accelerometer. The accelerometer is then attached to each location on the specimen and the quadrature responses of these locations are plotted. Since the quadrature response can have both positive and negative amplitudes, the modal pattern of the specimen is plotted (see Figs. 10 to 15).

CONCLUSIONS

The component analyzer is an effective and relatively simple device for performing these tests. The analyzer may be used with various types of transducers provided that their phase characteristics are known and may be used in conjunction with magnetic tape recorders, although it is most effective when used directly at the test site.

Vibration sweep rates must be necessarily slow since accurate control of the shaker force is required. The shaker should be selected for having a light moving element rather than a high force rating since it becomes part of the vibration system under test and since the only force requirements are those in overcoming damping forces. The shaker linkage to the specimen should be designed for a resonance well above the modal frequencies to be explored.

The modal patterns obtained were found to conform within reason to those outlined in Ref. 2 for the wooden hoop and Ref. 3 for the steel beam.

²D. Hartog, *Mechanical Vibration* (McGraw-Hill Book Co., Inc., New York, 1947) p. 205.

³C. M. Harris and C. E. Crede, *Shock and Vibration Handbook* (McGraw-Hill Book Co., Inc., New York, 1961) Vol. I, pp. 1-14.

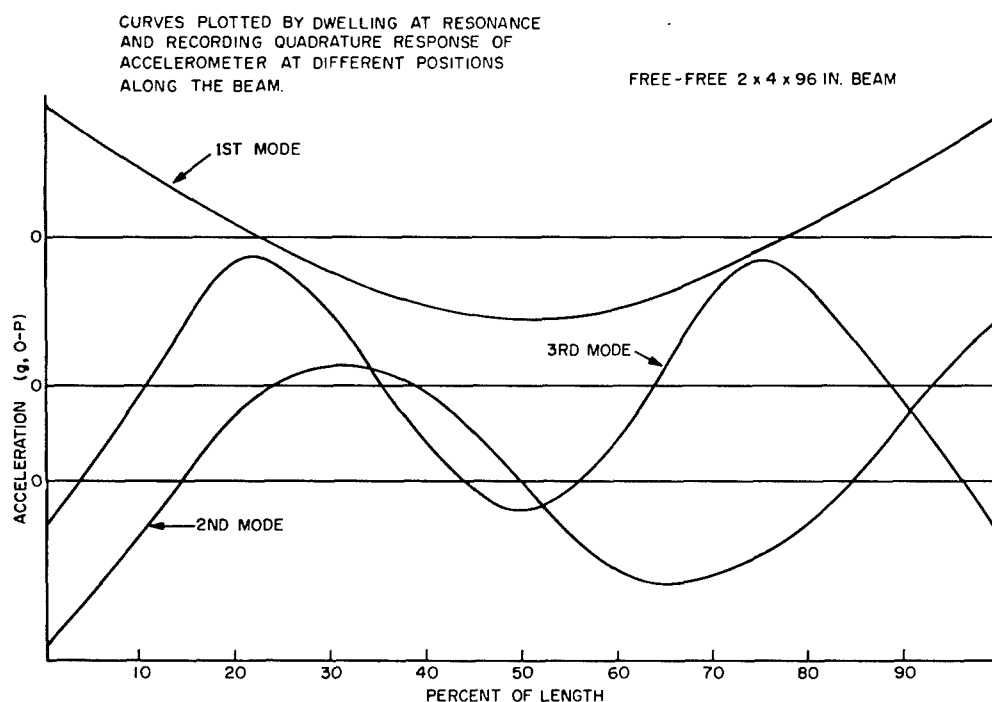


Fig. 10 - First three bending modes of a steel beam

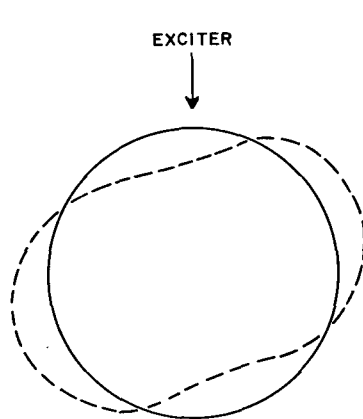


Fig. 11 - First mode of the wooden hoop

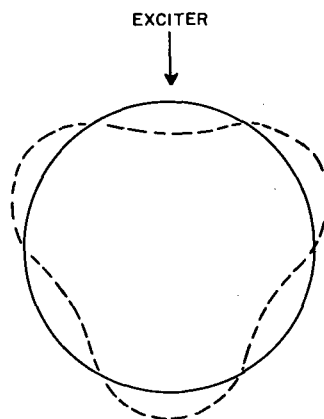


Fig. 12 - Second mode of the wooden hoop

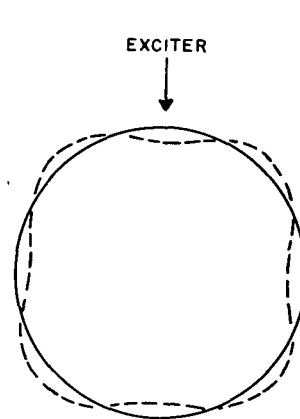


Fig. 13 - Third mode of the wooden hoop

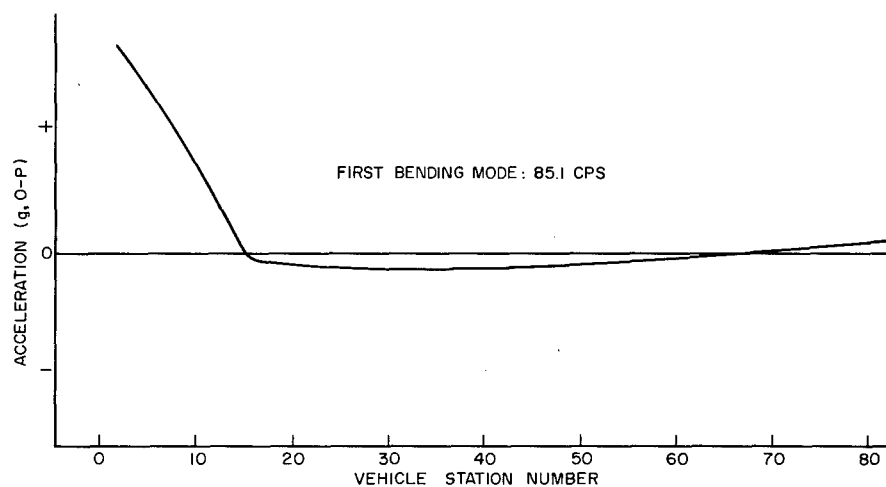


Fig. 14 - First bending mode of the re-entry vehicle

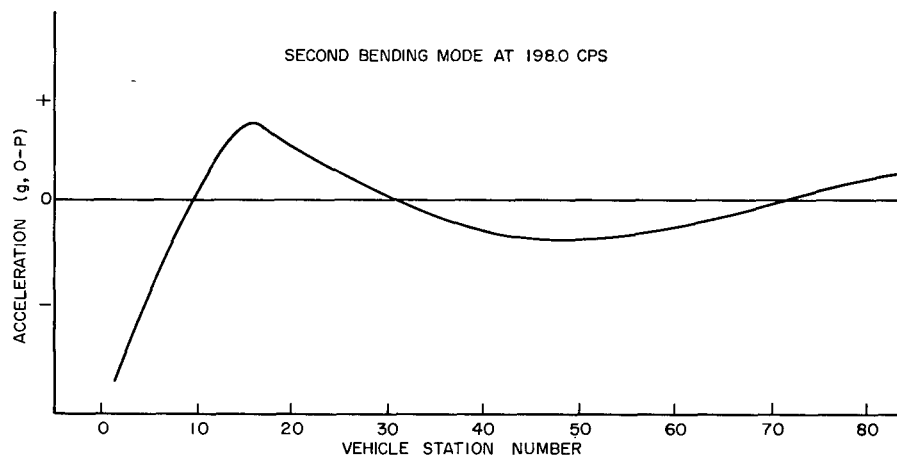


Fig. 15 - Second bending mode of the re-entry vehicle

DISCUSSION

Mr. Jacobi (AC Spark Plug): I'd like to know if you use demodulators to get the components? Also, if you use filters to clean up the wave form?

Mr. Hutton: As far as using demodulators, we multiply the two signals together inside the analyzer, and there is a filtering circuit to read out our in-phase and quadrature responses. Now as to using filters going into the analyzer, when we use our force signal as a reference, we always get a clean reference signal. You can then have a dirty acceleration signal going into the analyzer but still come out with valid results. If, however, we use a dirty acceleration signal as the reference, we have to filter the first channel of the analyzer so that we do not have any phase shift between the two channels.

Mr. Otts (Sandia Corp.): I asked this question earlier. What kind of luck do you have with your phase measurements? Do you have any feeling for your accuracy on that?

Mr. Hutton: Well, our phase measurements are of less accuracy than our quadrature and in-phase response measurements, due to the nature of the analyzer. It takes our in-phase response and our quadrature response and recombines these as the square root of the sum of the squares to come out with both the total amplitude and the phase angle. So you have a second step here which can give you an additional error out of the analyzer. We rely strictly on our in-phase response and our quadrature response, mainly.

Mr. Otts: What kind of percent would you say? Have you any feeling for that?

Mr. Hutton: For phase angle?

Mr. Otts: Yes.

Mr. Hutton: I'd say 10 percent.

Mr. Otts: Is this signal also filtered? The phase angle?

Mr. Hutton: If we use the force signals as reference, no, it is not filtered.

Mr. Clevenston: I'd like to comment that the instrument gives phase angles better than the 10 percent because the accuracy of the quadrature component is much better than 10 percent

and the phase angle is determined from the component. I think Mr. Hutton was being conservative in his estimate of the accuracy of the phase angle.

Mr. Dranetz (Dranetz Eng. Labs.): It's also possible to resolve the vector components by a technique other than the one that's been described. The technique is one of basically synchronous detection followed by integration. Again, you can talk about the accuracy in terms of a reconstructed amplitude and vector phase. Now, from experience it would appear, at least over many of the frequencies one is interested in for vibration work, that one could probably get phase accuracy in the neighborhood of 1 degree. Now, this means, of course, that your minor component will have a much greater error than the major component. In fact, if the minor component is, say, less than 10 percent of the major component, it may have an error due to say, 1 degree or 2 percent of full scale, which is, say, 20 percent of the minor component. But I think that it is possible to get down to perhaps somewhat better than even the 1 degree. There are ways of getting rid of this error to a substantial extent.

Mr. Hutton: I believe also that the method you describe is one that gives better low frequency response characteristics.

Mr. Dranetz: It has one advantage compared to a lot of systems in that being a synchronous detection system, a lot of noise disappears if the noise is of sufficient frequency for the filter to integrate.

Mr. Hutton: Yes, this analyzer works on nearly the same principle, it uses general filters to filter out the double frequencies which occur when two signals are multiplied together. They do have another analyzer that can go to a lot lower frequency, down to the order of a tenth of a cycle. This is of no importance to us but it uses this technique where the signal is integrated over a period of time.

Mr. Dranetz: The only problems that we have seen in this regard are very low frequency noises that don't get filtered out, or if you have a lot of waveform distortion, the third, fifth, and other odd harmonics, will come through the system, so you need some broad filtering.

Mr. Hutton: Right.

* * *

THE EFFECTS OF FILTER BANDWIDTH IN SPECTRUM ANALYSIS OF RANDOM VIBRATION

W. R. Forlifer
Goddard Space Flight Center
Greenbelt, Maryland

The problem is treated both theoretically and experimentally and the results obtained show excellent agreement. Curves are presented for the errors in both the width and magnitude of a resonant peak in terms of the ratio of measured resonant peak bandwidth to the analyzer filter bandwidth.

INTRODUCTION

The techniques and equipment for the determination of power spectral density under random vibration have been highly developed over the past 5 years. There presently exist accurate methods for performing this type of analysis using both analog and digital data reduction techniques. Most of the sources of error in the data collection and spectrum analysis process have been well documented in the literature.¹⁻⁴

However, the problem of reduced spectral resolution or "blurring" caused by the use of excessive analyzer filter bandwidth has not received any detailed treatment in the literature. It is the purpose of this paper to present the results of an analytical and experimental investigation into the effects of analyzer filter bandwidth on spectral resolution.

In many cases, especially those involving flight vibration measurements, the short data sample time and the lack of stationarity of the

random process prohibit obtaining high spectral resolution. This results because of the conflicting requirement on filter bandwidth due to the statistical uncertainty inherent in the sampling procedure. The standard error (e) associated with a measured spectrum estimate is:

$$e \approx \frac{1}{\sqrt{BT}}$$

where B is the filter bandwidth in cps and T is time duration of the data sample in seconds.

It is apparent from the above equation that, for short sample times, the filter bandwidth must be relatively large to reduce this error to a reasonable value. However, where the random process is stationary and long time data samples can be collected and analyzed the statistical uncertainty becomes small and high spectral resolution can be obtained by the use of a sufficiently narrow filter. A reasonable criterion for proper resolution — that the filter bandwidth be one-fourth the bandwidth of the narrowest peak in the power spectrum — has been proposed.^{3,4}

Laboratory vibration testing is one example of a case where the random input can be controlled and long duration data samples can be obtained. In this case, when a flat or "white" input spectrum is used, the response power spectral density curve provides a measure of the magnitude of the transfer function or the transmissibility between the input and the response point. This information, however, is only of value if the spectral resolution is such as to provide an accurate measure of the

¹C. M. Harris and C. E. Crede, Editors, *Shock and Vibration Handbook - Volume II* (McGraw-Hill Book Company, Inc., New York, 1961).

²S. H. Grandall, Editor, *Random Vibration* (Technology Press of M.I.T., Cambridge, Mass., 1958).

³J. S. Bendat, L. D. Enochson, G. H. Klein, and A. G. Piersol, "The Application of Statistics to the Flight Vehicle Vibration Problem," ASD Technical Report 61-123 (Dec. 1961).

⁴J. S. Bendat, L. D. Enochson, and A. G. Piersol, "Analytical Study of Vibration Data Reduction Methods," NASA-Marshall Space Flight Center (Sept. 1963).

half-power bandwidths and the maximum values of the peaks in the power spectral density curve.

ANALYTICAL APPROACH

Consider a true or actual power spectral density curve which is the result of applying a unit spectral density white noise input to a single-degree-of-freedom damped mechanical system:

$$S_A = |H_s|^2 S_I, \quad (1)$$

where

S_A = actual power spectral density (g^2/cps),

H_s = SDF system transfer function (g/g), and

S_I = input power spectral density ($1 g^2/\text{cps}$);

and

$$|H_s| = \frac{1}{\sqrt{\left(1 - \frac{f^2}{f_n^2}\right)^2 + \left(2D \frac{f}{f_n}\right)^2}}, \quad (2)$$

where

f = forcing frequency (cps),

f_n = natural frequency of the system (cps), and

D = ratio of damping to critical damping.

The actual spectrum is then:

$$S_A(f) = \frac{1}{\left(1 - \frac{f^2}{f_n^2}\right)^2 + \left(2D \frac{f}{f_n}\right)^2}. \quad (3)$$

Assume an analyzer filter which is a rectangular window with unit height and variable width:

$$\left. \begin{aligned} H_F &= 1 \quad \text{for } f_c - \frac{\Delta f_F}{2} \leq f \leq f_c + \frac{\Delta f_F}{2} \\ H_F &= 0 \quad \text{otherwise} \end{aligned} \right\}, \quad (4)$$

where

H_F = filter transfer function (g/g),

f_c = filter center frequency (cps), and

Δf_F = filter bandwidth (cps).

At a particular value of the filter center frequency, the measured power spectral density is

$$S_M = \frac{1}{\Delta f_F} \int_0^{\infty} |H_F|^2 S_A df, \quad (5)$$

where S_M = measured power spectral density (g^2/cps).

The process described above is shown in Fig. 1 for a typical example. The parameters used in this example are:

$f_n = 100 \text{ cps}$, $D = 0.05$, and

$\Delta f_F = 20 \text{ cps}$, $f_c = 90 \text{ cps}$.

The upper curve is the actual power spectral density of the response of the mechanical system to a white noise input. The actual half power bandwidth (Δf_A) is 10 cps. The middle curve shows the assumed rectangular transfer function of the filter which is the equivalent of the noise bandwidth of the actual filter shown in the dashed curve. The bottom curve presents the product of the squared filter transfer function and the actual power spectral density outlined in solid lines. This is an instantaneous picture when the sweeping filter center frequency is at 90 cps. The circled point at 90 cps is the result of integrating the solid area and dividing by the filter bandwidth as described by

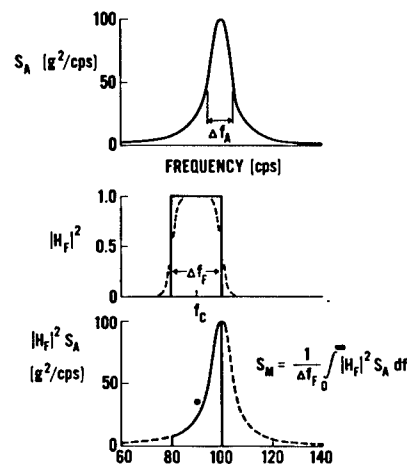


Fig. 1 - Spectrum analysis process

the equation on the figure and corresponds to the measured power spectral density at 90 cps.

By carrying out this process analytically by substituting Eqs. (3) and (4) into (5), we have

$$S_M(f_c) = \frac{1}{\Delta f_F} \int_{f_c - \frac{\Delta f_F}{2}}^{f_c + \frac{\Delta f_F}{2}} \frac{df}{\left(1 - \frac{f^2}{f_n^2}\right)^2 + 4D^2 \frac{f^2}{f_n^2}} \quad (6)$$

By using approximations valid in the neighborhood of the natural frequency and carrying out the integration, Eq. (6) becomes:

$$S_M(f_c) = \frac{f_n}{4D\Delta f_F} \times \left[\tan^{-1} \left(\frac{f_c - f_n + \frac{\Delta f_F}{2}}{Df_n} \right) - \tan^{-1} \left(\frac{f_c - f_n - \frac{\Delta f_F}{2}}{Df_n} \right) \right] \quad (7)$$

Figure 2 presents the curve of Eq. (7) for the example described in Fig. 1. The solid curve is the actual power spectral density and the dashed curve is the measured power spectral density. It can be seen that, for this example, the half-power bandwidth of the measured curve is over twice that of the actual curve and the measured peak is almost half the actual peak.

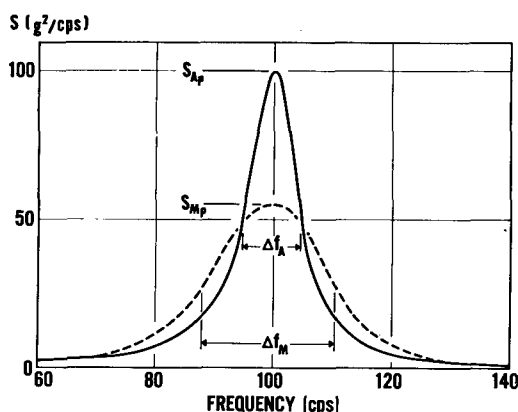


Fig. 2 - Comparison of actual and measured power spectra

By continuing with the analysis, the peak value of the measured spectral density occurs when the filter center frequency coincides with the system natural frequency:

when $f_c = f_n$,

$$S_{M_P} = \frac{f_n}{4D\Delta f_F} \left[\tan^{-1} \left(\frac{\Delta f_F}{2Df_n} \right) - \tan^{-1} \left(\frac{-\Delta f_F}{2Df_n} \right) \right]$$

Since the arctangent is an odd function,

$$S_{M_P} = \frac{f_n}{2D\Delta f_F} \tan^{-1} \left(\frac{\Delta f_F}{2Df_n} \right) \quad (8)$$

The bandwidth of the half-power points on the actual spectrum is

$$\Delta f_A = 2f_n D \quad \text{or} \quad D = \frac{\Delta f_A}{2f_n} \quad (9)$$

By substituting Eq. (9) into Eq. (8),

$$S_{M_P} = \frac{f_n^2}{\Delta f_A \Delta f_F} \tan^{-1} \left(\frac{\Delta f_F}{\Delta f_A} \right) \quad (10)$$

At the half power points on the measured spectrum,

$$S_M = \frac{1}{2} S_{M_P} \quad \text{and} \quad f_c - f_n = \frac{\Delta f_M}{2}$$

where Δf_M = half-power bandwidth of the measured spectrum (cps).

At $f_c = f_n + (\Delta f_M/2)$,

$$S_M = \frac{f_n^2}{2\Delta f_A \Delta f_F} \times \left[\tan^{-1} \left(\frac{\Delta f_M + \Delta f_F}{\Delta f_A} \right) - \tan^{-1} \left(\frac{\Delta f_M - \Delta f_F}{\Delta f_A} \right) \right] \quad (11)$$

$$\frac{1}{2} S_{M_P} = \frac{f_n^2}{2\Delta f_A \Delta f_F} \tan^{-1} \left(\frac{\Delta f_F}{\Delta f_A} \right) \quad (12)$$

Equating (11) and (12), we get an equation relating the actual, measured, and filter bandwidths:

$$\tan^{-1} \left(\frac{\Delta f_F}{\Delta f_A} \right) = \tan^{-1} \left(\frac{\Delta f_M + \Delta f_F}{\Delta f_A} \right) - \tan^{-1} \left(\frac{\Delta f_M - \Delta f_F}{\Delta f_A} \right) \quad (13)$$

This equation has been solved numerically and is shown on Fig. 3 as the solid curve. The ratio of the bandwidth of the measured curve to the actual bandwidth is plotted versus the ratio of

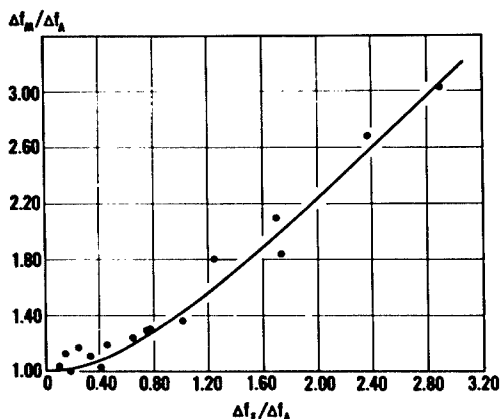


Fig. 3 - Effect of filter bandwidth on the width of the measured spectral density curve

filter bandwidth to the actual bandwidth. It can be seen that the measured bandwidth errors start exceeding 10 percent when the filter bandwidth exceeds about one-half the actual bandwidth.

Another important effect of spectral resolution is on the peak value of the measured spectral density. The peak value of the actual spectral density occurs at $f = f_n$ and is

$$S_{A_P} = \left(\frac{1}{2D} \right)^2 = \left(\frac{f_n}{\Delta f_A} \right)^2. \quad (14)$$

Taking the ratio of the measured peak value (10) to the actual peak value (14) we have:

$$\frac{S_{M_P}}{S_{A_P}} = \frac{\Delta f_A}{\Delta f_F} \tan^{-1} \left(\frac{\Delta f_F}{\Delta f_A} \right). \quad (15)$$

This equation is plotted in Fig. 4. A comparison of Figs. 3 and 4 shows that the magnitudes of the error in both bandwidth and peak value of the measured curve are approximately the same at a given filter bandwidth. Applying the previously mentioned criterion of filter bandwidth equal to one fourth the actual bandwidth results in errors no greater than 3 percent in both measured bandwidth and peak value.

EXPERIMENTAL APPROACH

Figure 5 presents a block diagram of the experiment performed to confirm the analytical results. A random noise generator was used to provide a flat or "white" power spectrum input to an electrical analog of a damped single-

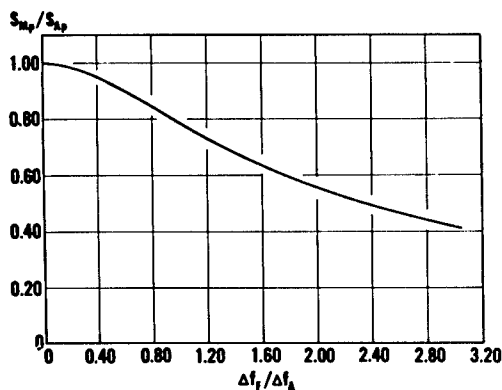


Fig. 4 - Effect of filter bandwidth on the peak value of the measured spectral density curve

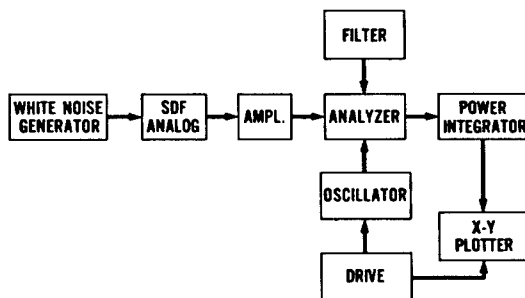


Fig. 5 - Experiment block diagram

degree-of-freedom system. The output from the analog was then amplified and fed into a heterodyne type analyzer, in conjunction with a power integrator, and the resulting power spectral density curve was reproduced by an x-y plotter.

Before proceeding with the experiment, the frequency response of each of the analyzer filters was carefully measured and the filter noise bandwidth (Δf_F) was determined by numerical integration of the frequency response curve. The nominal values of the filter bandwidths used were 5, 10, 20, 50, 100, and 200 cps.

The single-degree-of-freedom analog circuit is shown in Fig. 6. This analog represents the relative motion between the mass and the input rather than the absolute motion of the mass as used in the previous analysis. These two parameters, however, are nearly identical in the neighborhood of the resonant frequency. The resonant frequency of the analog was 3380 cps and nominal Q values of 10, 40, 50, and 90 were used. For each case, the frequency

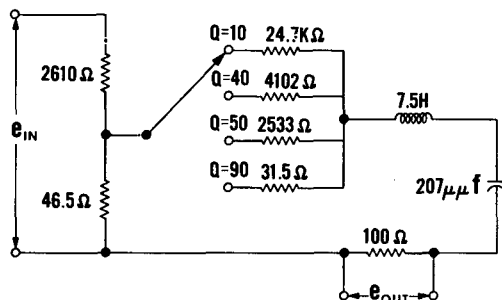


Fig. 6 - Single-degree-of-freedom analog circuit

response of the analog was measured with a sine wave input in order to determine accurately the actual bandwidth (Δf_A).

The test procedure consisted of measuring the response power spectral density curve for each of the Q values of the analog using various filter bandwidths. A total of 16 response power spectra were obtained in this manner. The half-power bandwidth (Δf_M) was determined for each of the measured spectral density curves. In order to generalize the data, the measured bandwidth and the filter bandwidth were both ratioed to the actual bandwidth and the resulting values are plotted as the circles in Fig. 3.

Although there is considerable scatter in the experimental data, it is apparent that these results verify the analytical curve. This data scatter is attributable to the insufficient averaging time used with the narrow bandwidth filters resulting in significant statistical errors in the measured spectra for these cases.

DISCUSSION

The effect of filter bandwidth on the width and peak value of the measured spectral density curve is shown in Figs. 3 and 4, respectively. A potentially more useful form of these results, however, is shown in Fig. 7. Here, the ratio of filter bandwidth to measured bandwidth is plotted versus the ratio of filter bandwidth to actual bandwidth.

By making a preliminary spectrum analysis of random vibration data using a relatively wide filter, the ratio of filter to measured bandwidth can be determined for each of the significant peaks in the spectrum. Using this ratio, in conjunction with the curve of Fig. 7, the actual bandwidth of the spectral peaks can be estimated and a suitable filter can be selected for the final spectrum analysis. However, the filter bandwidth

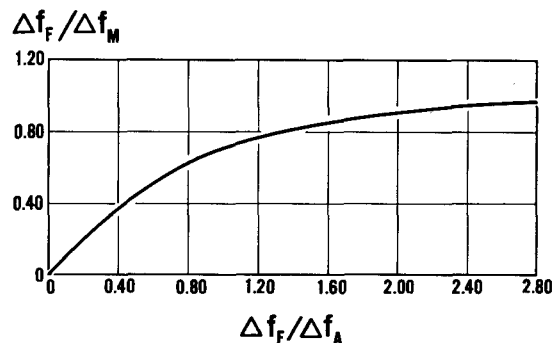


Fig. 7 - Relationship between bandwidth ratios

selected for final analysis must be based on statistical uncertainty errors as well as resolution errors.

The conflicting filter selection requirements generated by these two sources of error are shown in Fig. 8. Here, the same actual spectrum is used as in the example of Fig. 1 and the data sample time duration is assumed to be 4 seconds. The solid curve is the error in the peak value of the measured spectrum caused by lack of resolution, and the dashed curve is the statistical uncertainty associated with the filter bandwidth and the sample time. In this case, the optimum analyzer filter bandwidth to minimize the combined spectrum measurement error is about 5 cps.

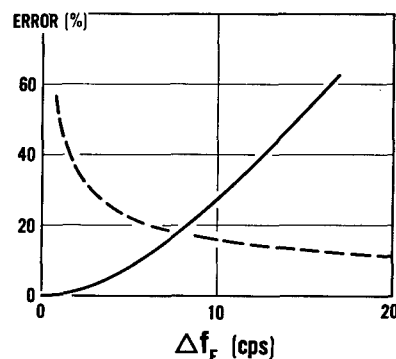


Fig. 8 - Comparison of errors

CONCLUSIONS

1. Significant errors in both width and magnitude of spectrum peaks can result from lack of resolution in the analyzing filter.

2. From the results of a preliminary spectrum analysis using a relatively wide filter, the actual bandwidth of significant spectral peaks may be estimated.

3. By considering both the statistical uncertainty and the resolution error, an optimum filter bandwidth can be selected for final analysis to minimize the combined error.

ACKNOWLEDGMENT

The author wishes to acknowledge the valuable contributions of Messrs. D. Thomas and M. Matrullo of Martin-Baltimore in carrying out the experimental portion of this investigation.

* * *

RANDOM-SINE FATIGUE DATA CORRELATION

L. W. Root
Collins Radio Company
Cedar Rapids, Iowa

This paper presents the results of a study to verify a technique suggested in [2] for predicting the random fatigue curve from the sine fatigue curve by making use of the Palmgren-Miner hypothesis of fatigue damage accumulation. Resonant cantilever beams were used to obtain the sine and random fatigue curves. The predicted curve was found to give a conservative estimate of life which was within less than one order of magnitude of the measured life. This result is in contrast to previous studies which gave nonconservative estimates of the measured random fatigue life.

INTRODUCTION

The problem of predicting structural response to random loads has received considerable attention during the past decade.¹⁻³ General analyses of one- and two-degree-of-freedom systems subjected to loads having a Gaussian distribution are available. The state-of-the-art is such that the designer can predict, in many cases, the statistical parameters of the stress distribution. In general, however, an accurate fatigue life analysis cannot be performed due to the lack of random fatigue data.

Only a limited portion of the results of the extensive research in this area have been published.⁴⁻⁷ Until more random fatigue data are published, it will be necessary to use the extensive sine fatigue data in conjunction with theoretical or experimental techniques, or both, to estimate random fatigue damage. Several prediction techniques^{1,2,7} have been proposed, although none as yet lead to consistently accurate estimation of random fatigue damage.

Engineering design seldom has sufficient time to wait for complete theoretical treatment of its problems, and it must use the best available hypotheses in solving its problems within the allotted time. Design for random fatigue damage must proceed with one or more of the proposed prediction techniques until more satisfactory theories are developed. The present study was undertaken to become familiar with one such technique² and to define its limitations.

THEORETICAL PREDICTION OF RANDOM FATIGUE DATA

Consider the ergodic random process, $\phi(T)$, representing the instantaneous stress at a point. Associated with $\phi(T)$ is a probability distribution function, $p(a)$, representing the maximum peak between consecutive zero crossings. It is assumed that peaks smaller than the maximum peak in any interval between zero crossings make a negligible contribution to the fatigue damage accumulation. Let the fatigue damage

¹J. W. Miles, "On Structural Fatigue Under Random Loading," J. Aeronaut. Sci. (Nov. 1954), pp. 753-762.

²S. H. Crandall and W. D. Mark, Random Vibration in Mechanical Systems (Academic Press, 1963).

³S. H. Crandall, Editor, Random Vibration (Technology Press MIT and John Wiley and Sons, 1958).

⁴A. K. Head and F. H. Hooke, "Random Noise Fatigue Testing," Proceedings of the International Conference on the Fatigue of Metals (1956), pp. 301-303.

⁵P. W. Smith, Jr. and C. I. Malme, "Fatigue Tests of a Resonant Structure with Random Excitation," J. Acoust. Soc. Am. (Jan. 1963), pp. 43-46.

⁶S. R. Swanson, "An Investigation of the Fatigue of Aluminum Alloy due to Random Loading," University of Toronto Institute of Aerophysics Report No. 84 (Feb. 1963).

⁷J. R. Fuller, "Research on Techniques of Establishing Random Type Fatigue Curves for Broad Band Sonic Loading," National Aeronautical Meeting, Washington, D. C., April 8-11, 1963, Paper No. 671C.

be represented by $A(a)$. The mathematical expectation for the fatigue damage per individual interval between consecutive zero crossings is given by Eq. (1),

$$E [A(a)] = \int_{-\infty}^{\infty} A(a) p(a) da. \quad (1)$$

The expected damage accumulation as a function of time is of more interest than Eq. (1). Assuming the total zero crossings during time, T , may be represented by a function, $P_o(T)$, the expected damage accumulation is given by Eq. (2),

$$E [D(T)] = P_o(T) \int_{-\infty}^{\infty} A(a) p(a) da. \quad (2)$$

Several damage accumulation hypotheses have been proposed.⁸⁻¹¹ The simplest of these

and probably the most widely used is the Palmgren-Miner hypothesis.^{8,9} It represents the damage accumulation as a linear summation of individual damage increments and is given by Eq. (3),

$$D(T) = \sum_{i=1}^n \frac{n_i}{N_i}. \quad (3)$$

In order to relate Eq. (3) to the peak stress amplitude, a , the sine fatigue curve will be approximated by a straight line fit of the log-log data. This requires an equation of the form (4),

$$NS^b = c. \quad (4)$$

Figure 1 is a typical plot (log-log) of fatigue data with the significance of b and c as shown.

The typical stress process due to a resonant response may be assumed to be narrow band which allows one to represent the probability distribution function of the peaks as the Rayleigh distribution. The zero crossings of a narrow-band process are relatively uniform in spacing and may be represented by a characteristic frequency v_o . By using Eqs. (3) and (4), the Rayleigh distribution, and v_o , it is possible to evaluate Eq. (2). Reference 2 gives complete details. Following integration, Eq. (2) may be written as Eq. (5),

$$E [D(T)] = \frac{v_o T}{c} (\sqrt{2} \sigma)^b \Gamma(1 + b/2). \quad (5)$$

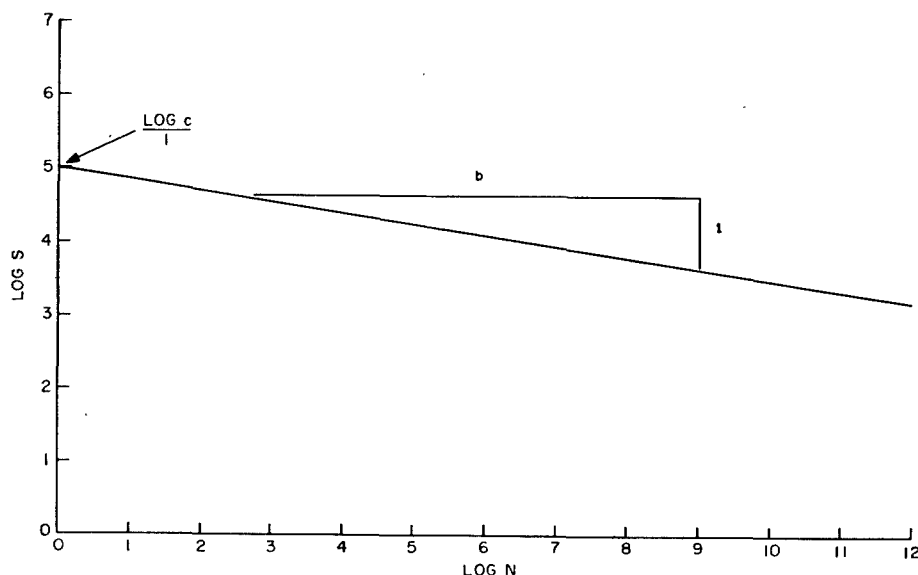


Fig. 1 - Typical straight line representation of fatigue curve on log-log plot

⁸A. Palmgren, "Die Lebensdauer Von Kugellagern," *Zeitschrift des Vereines Duetscher Ingenieure* (1924).

⁹M. A. Miner, "Cumulative Damage in Fatigue," *J. Appl. Mech.* (Sept. 1945), pp. 159-164.

¹⁰H. T. Corten and T. J. Dolan, "Cumulative Fatigue Damage," Proceedings of the International Conference on the Fatigue of Metals (1956), pp. 235-246.

¹¹S. R. Valluri, "A Theory of Cumulative Damage in Fatigue," California Institute of Technology Aeronautical Research Laboratory Report 182 (Dec. 1961).

Failure is considered to occur when $E[D(T)]$ becomes equal to unity. Since $v_o T$ is just the total number of cycles of stress, it is possible to rewrite Eq. (5) at failure as Eq. (6).

$$N_o^b = \frac{c}{2^{b/2} \Gamma(1 + b/2)} \quad (6)$$

All of the parameters on the right side of the equality are known from the sine fatigue data. Therefore, Eq. (6) is identical in form to

and stresses. The material selected was aluminum (6061-T6).

During a previous fatigue study,¹² it was determined that a one-half percent shift in the natural frequency corresponded closely to the

¹²M. Vet, "Dwell-Sweep Correlation," Proceedings of the Institute of Environmental Sciences (1963), pp. 433-443.

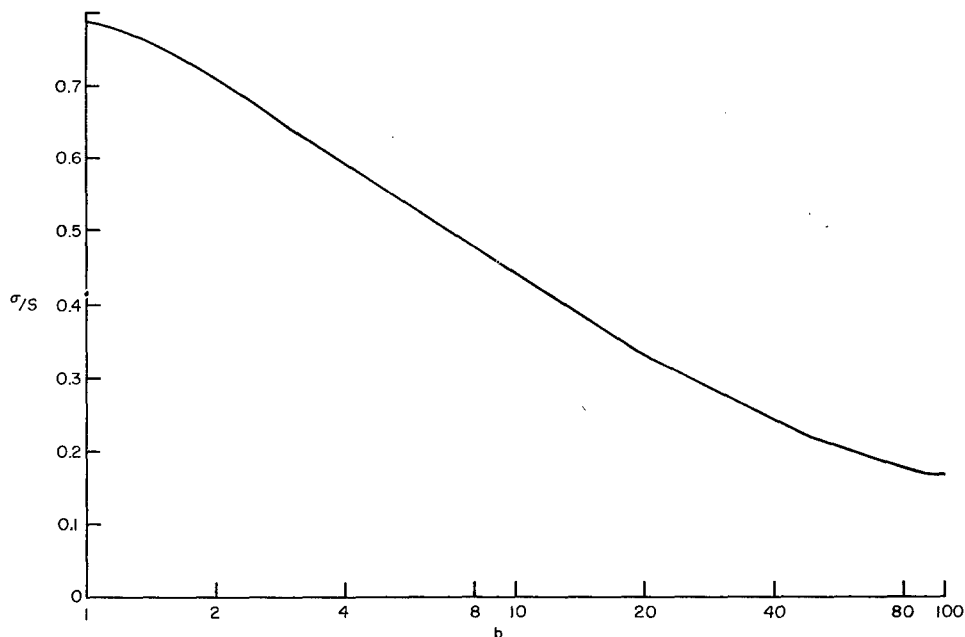


Fig. 2 - Relationship between σ and s as a function of the parameter, b

Eq. (4) with the exception of the constant representing the log stress intercept.

Since c is common to both Eqs. (4) and (6), the denominator of the right side of Eq. (6) can be evaluated as a function of b , allowing the prediction of the random fatigue curve once b is known from the sine fatigue data. Figure 2 is a plot of the ratio of the rms random stress to the peak sine stress versus the parameter b .

TEST SETUP AND PROCEDURES

A simple cantilever beam, Fig. 3, with a natural frequency of 300 cps was selected to check the results of theoretical predictions of random fatigue data. The reasons for this particular configuration are high Q attainable (300 to 1100) and ease of computing responses

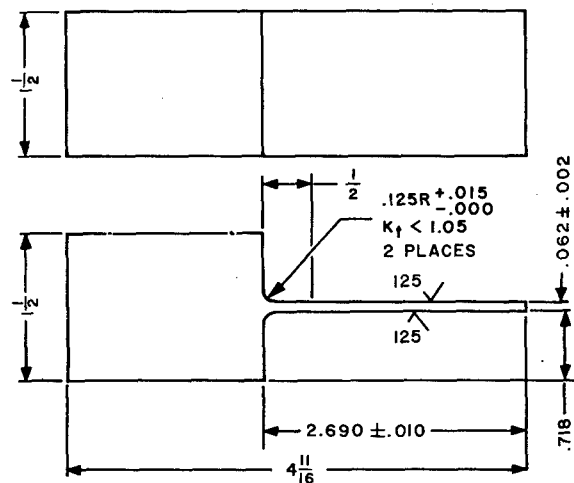


Fig. 3 - Simple cantilever beam test specimen (Aluminum 6061-T6)

appearance of surface cracks visible to the naked eye. The one-half percent frequency shift (1.5 cps) was selected as the failure criteria in the present study.

The response frequency of the beam was obtained by using the beam as one plate of a capacitor. This allowed accurate determination of the frequency and a relative measurement of the amplitude of the beam response.

Initially the output of the capacitance transducer was put through a narrow filter tuned to the initial natural frequency of the beam, and the shift in natural frequency was observed as a reduction in signal amplitude. This procedure was discontinued due to a 0.2-cps spread in the measured frequency shift of the beams monitored in this way during the sine tests. The final test setup consisted of the capacitance transducer and a frequency counter as shown in Fig. 4.

The sine tests consisted of the following procedures:

1. Establishing an input level at a low frequency.
2. Locating the frequency of maximum response.
3. Manually maintaining the input frequency so that the maximum response was maintained.
4. Timing until the frequency shifted 1.5 cps.

The random tests consisted of the following procedures:

1. Locating the frequency of maximum response with a 0.5-g sine input.
2. Centering the input shaping filter (20-cps bandwidth) at frequency determined in the first procedure.
3. Vibrating the beam to band-limited white noise.
4. Sampling the frequency of the beam response for one-second intervals.
5. Locating frequency as in the first procedure after frequency sampling indicated approximately a 1.5-cps frequency shift.

TEST DATA

Several beams were strain-gaged to verify stress computations and to obtain a curve of input level versus stress. Subsequent sine tests were run at measured input levels and it was assumed that the stress was identical to that in the strain-gaged beams. This assumption was verified on some of the beams by observing the end displacement of the beam by using a microscope.

A total of 25 beams were tested at six stress levels (three to seven per level). The

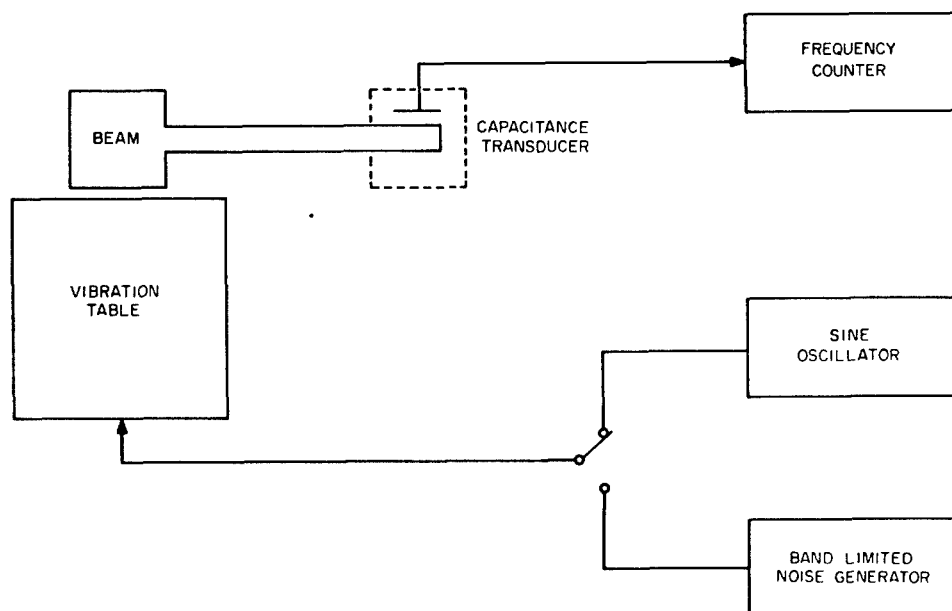


Fig. 4 - Schematic of test setup

data were reduced to the median life at each stress level and a least squares straight line was fitted to the log S versus log N data. This curve is represented by Eq. (7).

$$NS^{6.87} = 9.918 \times 10^{35}. \quad (7)$$

The deviation of Eq. (7) from the measured data may be seen in Table 1 which contains the stress levels and lives (measured N, and computed N_c).

TABLE 1

S	$\bar{\sigma}$	No. of Points	N	N_c
33,000	23,300	3	1.03×10^5	0.9×10^5
30,000	21,200	5	1.78×10^5	1.73×10^5
27,800	19,650	3	2.80×10^5	2.92×10^5
24,800	17,550	7	4.68×10^5	6.41×10^5
22,600	15,950	3	1.40×10^6	1.21×10^6
19,650	13,900	4	3.26×10^6	3.17×10^6

The random fatigue data were obtained in essentially the same manner. Initial beams were strain-gaged with subsequent random tests made at measured input levels. It was not possible to obtain a frequency shift of exactly 1.5 cps, so the failure times were corrected to reflect the measured frequency shift. The correction factors were obtained from sine tests at different input levels. The fatigue data were obtained from a total of 20 beams which were tested at four stress levels (one to eight per level). Again, the median corrected lives were used in obtaining Eq. (8) by a least squares fit of the log σ - log N data. The stress levels and lives (measured and computed) are contained in Table 2.

TABLE 2

σ	No. of Points	N	N_c
19,880	8	7.23×10^4	7.87×10^4
17,040	8	2.45×10^5	2.20×10^5
14,200	3	6.42×10^5	7.40×10^5
11,360	1	3.22×10^6	3.27×10^6

$$N\sigma^{6.66} = 3.337 \times 10^{33}. \quad (8)$$

Both Eqs. (7) and (8) are plotted in Fig. 5.

CORRELATION OF RESULTS

Figure 2 and Eq. (7) are used to obtain the predicted random fatigue curve given by Eq. (9) and plotted in Fig. 5.

$$N\sigma^{6.87} = 8.624 \times 10^{33}. \quad (9)$$

This result is to be compared to Eq. (8), representing the measured random fatigue data. Considering stress levels corresponding to predicted lives of 10^4 and 10^7 cycles, the respective measured lives are 3.2 and 2.3 times longer than the predicted lives. This conservative estimation of the fatigue life applies to the complete life range normally considered in structural design.

The preceding result is contrary to previously published results^{4,5,7} in that measured lives were 0.5 to 0.1 times the predicted life in the comparable predicted life range for the published studies. Essentially, a common approach was taken in the past studies and the present one; that is, (1) the stress was due to

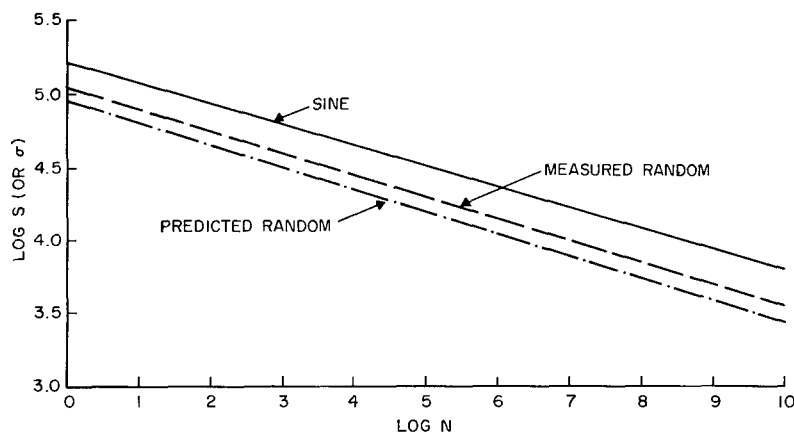


Fig. 5 - Least squares fit of log-log fatigue data

bending, (2) the sine fatigue curve was obtained for the given test specimen, (3) the Palmgren-Miner hypothesis was used in predicting the random fatigue curve, and (4) the random fatigue data were measured in the range 10^4 to 10^7 cycles. Two differences between the present study and the past studies are as follows:

1. Test specimen material (2024 in past studies and 6061 in present study).
2. Grain direction (longitudinal direction in past studies and lateral direction in present study).

The differences are not considered sufficient to explain the major disagreement between the present study and the past studies.

At present, no explanation can be offered for the conflicting conclusions. The present study is to be extended in an attempt to clarify the reason for the differences.

RECOMMENDED FUTURE STUDY

The first efforts in extending the present study should be to clarify the reasons for the conflicting conclusions of the present study and the past studies. This can be done by:

1. Improving present instrumentation and test procedures to minimize error.
2. Simplifying data analysis procedures to allow handling larger quantities of samples

which will improve statistical significance of the data.

3. Checking effect of material and the grain direction on the correlation of measured and predicted random fatigue curves.

A second area for further study is the representation of the probability distribution function for peak stresses in a high Q structural test specimen. Nonlinear damping in test specimens and truncation of the Gaussian probability distribution function representing the input at ± 3 to 4 standard deviations require modification of the Rayleigh distribution.

A third area is in the selection of an appropriate damage accumulation hypothesis. Recent studies^{7,13} indicate currently used hypotheses suffer certain shortcomings. Evaluation of the present hypotheses should be undertaken, and studies to formulate improved hypotheses should be continued.

Efforts in these three areas should be used in improving the present random fatigue data prediction techniques. The large expense of obtaining random fatigue data will necessitate the continued use of sine fatigue data in the design for random loads.

¹³H. L. Leve, "The Utilization of Random Response Information in the Determination of Structural Integrity," The 63rd Meeting of the Acoustical Society of America, New York, May 23-26, 1962, Paper No. 1353.

LIST OF SYMBOLS

a = peak amplitudes of random stress process	M = number of individual stress levels in Palmgren-Miner summation of fatigue damage
$A(a)$ = fatigue damage due to stress amplitude a	n_i = total applied stress cycles at i^{th} stress level
b = stress exponent in S-N equation	N = number of cycles to failure at a constant stress from either random or sine fatigue data
c = constant in S-N equation	N_c = number of cycles to failure computed from least squares fit of measured fatigue data
$D(T)$ = fatigue damage accumulation at time T	N_i = number of cycles to failure associated with i^{th} stress level
$E[]$ = mathematical expectation of quantity within brackets	
K_t = stress concentration factor	

$p(a)$ = probability distribution function of peak stress amplitudes

$P_o(T)$ = total zero crossings of stress process at time T

Q = amplification factor

S = peak stress from sine fatigue data

T = time

v_o = expected frequency of narrow-band process

$\Gamma(\)$ = gamma function

σ = root mean square stress from random fatigue data

$\bar{\sigma}$ = root mean square stress from sine fatigue data

$\phi(T)$ = instantaneous stress at time T

ACKNOWLEDGMENT

The research work upon which this paper is based has been sponsored by Collins Radio Company as a part of a continuing program to improve the environmental design of its products. The author wishes to acknowledge the valuable assistance and suggestions received

ACKNOWLEDGMENT

from S. Marshall and other personnel in the Environmental Testing Department regarding the experimental portions of the study, and to acknowledge suggestions from M. Vet and P. Francis regarding the theoretical portions of the study.

* * *

THE DEVELOPMENT OF DIGITAL TECHNIQUES FOR THE STATISTICAL ANALYSIS OF RANDOM INFORMATION*

Charles L. Pullen
Martin Company

INTRODUCTION

The purpose of the author in writing this paper is to describe the development of a system for processing random digital data. This system is designed to incorporate a high speed digital computer in the evaluation of the desired statistical parameters. Auto-correlation, cross-correlation, and power spectral density may be computed using this system.

The data considered in this report are taken from rocket engine noise measurements, but other types of data with similar statistical properties could be used. Large amounts of these data have been accumulating because of inadequate methods of evaluating the data rapidly. This fact and the increased number of measurements being taken in random environments has stimulated interest in the development of better data processing methods.

The data are originally recorded on an F.M. analog tape, and then a loop is made from a section of this tape. This loop is processed by the analog to digital converter which produces a digital tape. The digital tape is used as the input data for the digital computer.

For the purpose of determining the quality of the digital program, the data were analyzed as shown in Fig. 1. This allowed comparison of the power spectral density calculated by the digital computer and the direct band pass filter method. In actual analysis this would be omitted and only the faster digital method would be employed.

The use of statistical concepts and methods in the handling of random data is widely accepted. There are problems inherent in any statistical analysis that must be considered. Basic problems encountered in the development

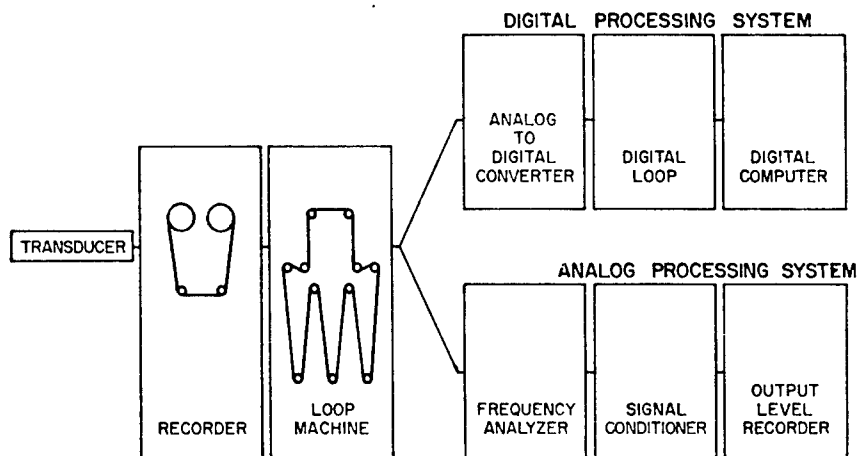


Fig. 1 - Digital analysis procedures and analog power spectrum check, block diagram

*This paper was not presented at the Symposium.

of the analysis program include both the limitations of the mathematical models and the limitations imposed by the approximation methods of integration. These problems will be discussed in more detail in the section on theoretical considerations.

THEORY

An important consideration in the analysis of random data (see Fig. 2) is the quality of the data acquisition technique. The maximum frequency which can be detected is a function of the sampling rate, the degree of stability in the sampling rate, and how well the assumptions of the statistical analysis are met. If we assume that the data perfectly represent the actual situation, the maximum frequency that we can uniquely define is given in the formula derived by Nyquist:¹

$$f_N = \frac{1}{2} t,$$

where

f_N = Nyquist frequency, and

t = time between digital samples in seconds.

This may also be written:

$$f_D = 2f_N,$$

where

f_D = digital sampling rate, and

f_N = Nyquist frequency.

It is extremely desirable that the sampling rate be as low as possible and still give high statistical reliability to the analysis. An excessive sampling rate would not result in increased accuracy and would unnecessarily lengthen the computer time required for analysis. Because of distortions in the data caused by the data acquisition process, the highest frequency which can be uniquely defined is lower than the Nyquist frequency. The criterion used for this analysis was that the maximum frequency will be given by the relation:

$$f_D = 8f_M,$$

where

f_M = maximum frequency detected, and

f_D = digital sampling frequency.

This provides greater statistical reliability to the analysis procedure. All of the frequencies below f_M will be sharply defined. All frequencies above f_M , however, will be indistinguishable. Therefore, all of the energy in the frequency bands above f_M must be filtered out. This implies that the sampling rate must be high enough to distinctly define the highest frequency containing significant energy.

The calculation of correlation and power spectral density functions for discrete, equally spaced data involves considerations that do not arise in the analysis of continuous data. All integrations must be replaced by their summation equivalents. The average value $\overline{X(t)}$ of a data function $X(t)$ is given by:

$$\overline{X(t)} = \lim_{T \rightarrow \infty} \frac{1}{T} \int_0^T X(t) dt,$$

whose summation equivalent for discrete data is:

$$X(t) = \frac{1}{n} \sum_{i=1}^n x_i(t),$$

where $T = n\Delta t$.

The following notation has been adopted. The function composed of discrete data points is called $X(t)$ and contains data points $x_i(t)$.

The correlation function may be called the lagged-mean-squared value of the data function $X(t)$. It is given by:

$$X(t) X(t+i) = \frac{1}{n-i} \sum_{j=1}^n x_j(t) x_{j+i}(t).$$

Only time lags (τ) which are multiples of the time increment (Δt) have any meaning for discrete data. This additional consideration may be expressed:

$$\tau = 0, 1h\Delta t, 2h\Delta t, \dots mh\Delta t,$$

where $h = 1, 2, \dots k$.

Since the data are discrete, we will make the following notational change:

$$R_{xx}(i) = \overline{X(t) X(t+i)}.$$

¹J. S. Bendat, *Principles and Applications of Random Noise Theory* (John Wiley & Sons, Inc., New York, N. Y., 1958), p. 51.

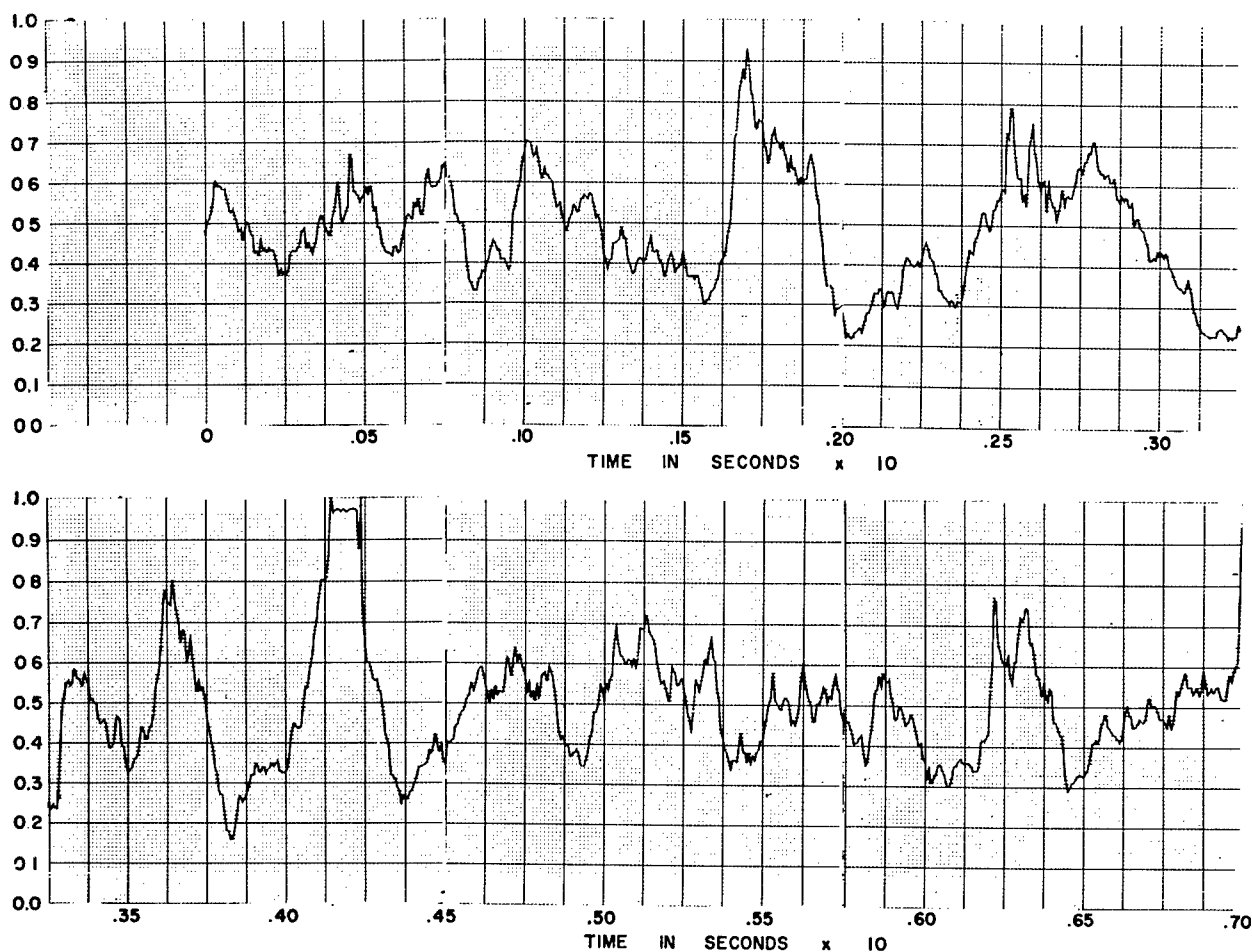


Fig. 2 - Normalized digital input data

The cross-correlation function of two functions $X(t)$ and $Y(t)$ is often of interest in phase correlation measurements and may be calculated according to the relation:

$$R_{xy}(i) = \frac{1}{n-i} \sum_{j=1}^{n-i} x_j(t) y_{j+i}(t).$$

The assumption has been made that the data are stationary and ergodic random data. The auto-correlation function is therefore symmetric about $\tau = 0$. This method is justified even if the data do not meet these conditions.² Since it is difficult to determine if a physical process is ergodic or not, this is encouraging.

The power spectral density function may be calculated by taking the Fourier transform

of the auto-correlation function. It becomes a finite cosine series transformation for the discrete record data function and is expressed as:

$$P_{xx}(\omega) = \frac{\Delta\tau}{\pi} \left[R_{xx}(0) + 2 \sum_{j=1}^{n-1} R_{xx}(j) \cos(\omega j h \Delta t) + \cos(\omega n h \Delta t) \right].$$

It might be erroneously assumed from a quick glance that the power spectrum could be determined arbitrarily precisely according to the formula given. This is not the case, however. In a Fourier transform pair of time and frequency it is not possible to determine frequency precisely without an infinite time period. An exact determination of time in the inverse transformation would require an infinitely broad frequency band. This is analogous to the quantum mechanical problem of determining both the energy and position of a particle.

²Laning and Battin, *Random Processes in Automatic Control* (McGraw-Hill Book Company, New York, N. Y., 1956), p. 134.

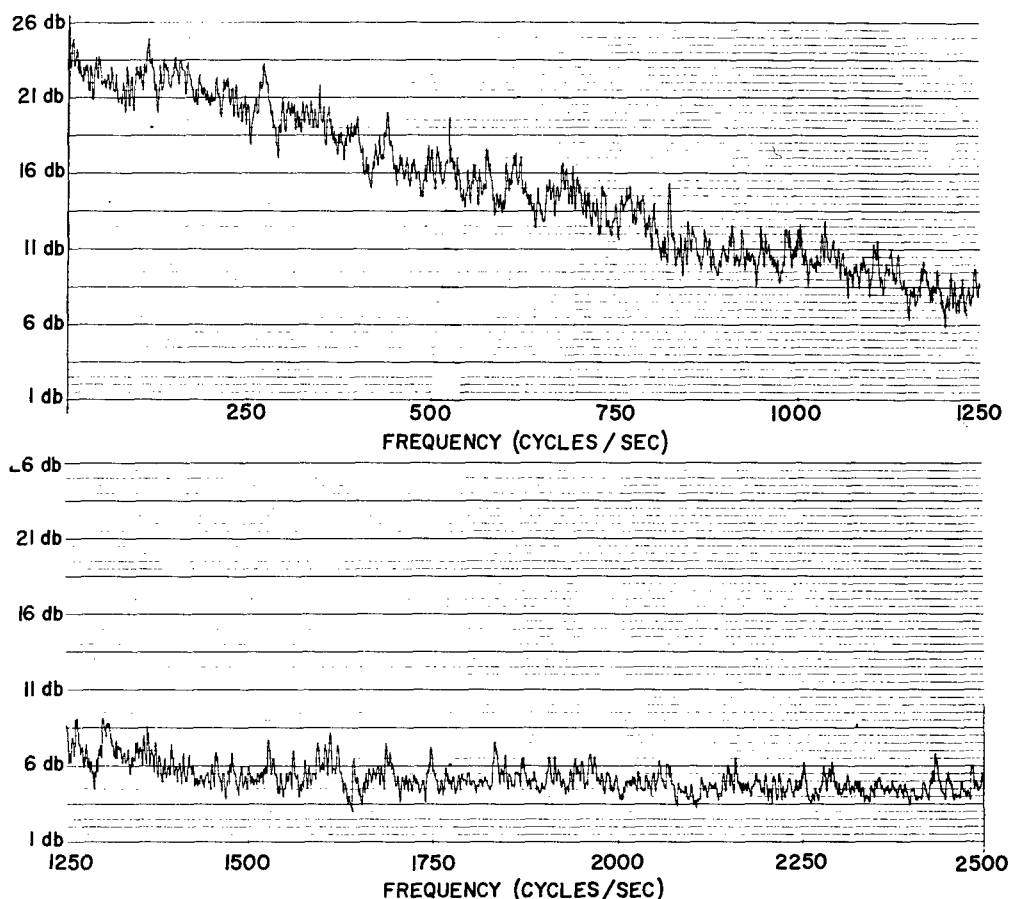


Fig. 3 - Analog filter method power spectral density

TEST PROCEDURES AND RESULTS

The testing procedure outlined in Fig. 1 is designed to give a comparison of the power spectral density as calculated by the digital computer with the direct band pass filter method. The results of the analog method (see Fig. 3) were obtained using a constant bandwidth filter whose bandwidth was 5 cps. To allow direct comparison of the power spectrum obtained in this manner with the digital results, bandwidth considerations must be made. Bandwidth corrections were made and the results are given for 10 frequencies (see Table 1).

A tape has been constructed with several sinusoids of different frequencies and this will provide another check on the quality of the program.

CONCLUSION

The methods outlined in this paper appear to provide a feasible system for the analysis of random information. Further experimental verification would be desirable to determine more accurately the validity of this approach.

TABLE 1
Digital Power Spectral Density Results

Frequency (cps)	Power Level (db) (Bandwidth Corrected)
250	22.8
500	18.6
750	13.1
1000	9.4
1250	10.2
1500	6.7
1750	7.9
2000	5.8
2250	5.9
2500	6.1

BIBLIOGRAPHY

- Blackman and Tukey, The Measurement of Power Spectra (Dover Publications, Inc., New York, N. Y., 1959).
- Davenport and Root, Random Signals and Noise (McGraw-Hill Book Company, New York, N. Y., 1958).
- Deutsch, R., Nonlinear Transformations of Random Processes (Prentice-Hall, Inc., Englewood Cliffs, N. J., 1962).
- Helstrom, C. W., Statistical Theory of Signal Detection (Permagon Press, New York, N. Y., 1960).
- Laning and Battin, Random Processes in Automatic Control (McGraw-Hill Book Company, New York, N. Y., 1956).
- Yerkes, J. W., "The Application of Digital Acquisition Techniques to the Analysis of Shock and Vibration Data," Shock, Vibration and Associated Environments Bulletin No. 31, Part III (1963), p. 225.

* * *

RANDOMNESS TESTER FOR ACOUSTIC SIGNALS

E. D. Griffith
LTV Vought Aeronautics
Dallas, Texas

INTRODUCTION

Band limited random noise with reasonably flat power spectral density distribution has a predictable number of zero crossings per second (N_0), which is a function only of the upper and lower frequency limits.¹ However, the addition of periodic signals to this noise usually causes a deviation in N_0 , and measurements of the percentage deviation (N_0) can be used to determine the randomness or non-randomness of unknown signals under data analysis.² In this case a nonrandom signal is defined as any signal with periodic components. At LTV Vought Aeronautics, during the last year, a randomness tester, which is based on

the measurement of ΔN_0 , has been used to separate the random and nonrandom parts of a broadband acoustic signal when the amplitudes of the periodicities in the nonrandom component were not large enough to be detected by either routine power spectral density or amplitude probability density analysis.

THE PROBLEM

Figure 1 shows a PSD plot of a typical unknown acoustic signal recorded on an LTV test program. With the exception of slight dips at F_D^I , F_D^{II} , and F_D^{III} , this distribution is fairly flat. One of these low points is thought to indicate the division between a higher-frequency band of random noise under investigation in the test program and a lower-frequency band of nonrandom background noise.

At no point in the spectrum, however, do sharp peaks exist that might indicate the presence of periodic components that would aid in

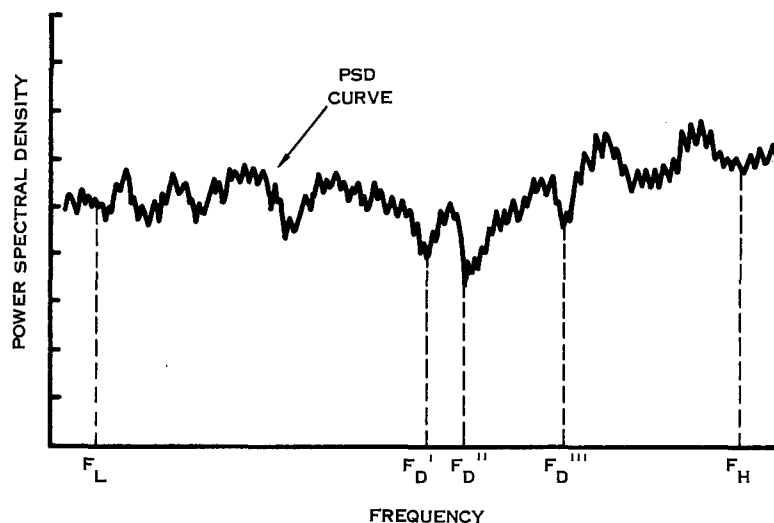


Fig. 1 - Power spectral density plot of typical unknown acoustic signal

¹S. O. Rice, "Mathematical Analysis of Random Noise," Bell System Technical Journal, Vols. 23 and 24.

²J. S. Bendat, L. D. Enochson, G. H. Klein, and A. G. Piersol, "The Application of Statistics to the Flight Vehicle Vibration Problem," ASD Technical Report 61-123 (June 1963).

identifying the nonrandom background noise and in locating the true F_D .

Amplitude probability density plots were also made on both the overall signal and on selected bandwidths, but this type of analysis produced only normal (Gaussian) amplitude density curves as shown in Fig. 2. Since neither of these methods produced evidence of periodicities, it was assumed that any that existed in the background noise were of small magnitude.

RANDOMNESS TESTER

To provide a third type of data analysis that might have the resolving power to detect

the presence of these small magnitude periodic signals within the strong random noise field, the so called "randomness tester" shown in block diagram in Fig. 3 was assembled from commercial electronic instruments and checked out under a company sponsored R and D program. The basic instrument in this system is the Technical Products Probability Analyzer that provides an amplitude "window" or "filter" near zero amplitude as shown in the sketch. The width of this amplitude window (ΔX) was 0.067σ , where σ is the root-mean-square amplitude of the signal under investigation.

Each time the signal passes through ΔX the event is counted, and over a given time interval (T) the total number of events or zero crossings

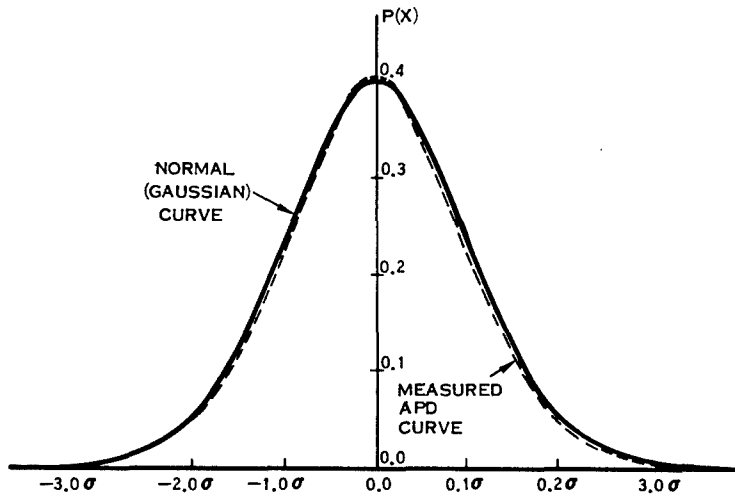


Fig. 2 - Amplitude probability density plot

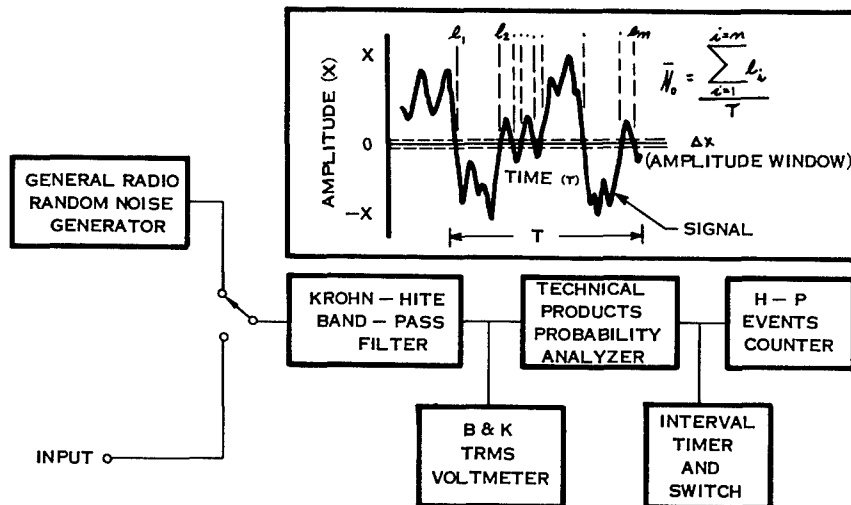


Fig. 3 - Randomness tester for acoustic signals

is registered on the electronic counter. N_0 , the number of zero crossing per second, is then determined by:

$$N_0 = \frac{\sum e_i}{T}$$

To obtain an indication of the statistical confidence in N_0 , this measurement may be repeated for several samples.

Since laboratory band-pass filters do not have ideal frequency cutoff characteristics and since N_0 is a function of band limits of these filters, a technique is required for eliminating filter cutoff slope effects. This is done by establishing N_0 for any band-pass setting of the filter using a standard electronic noise generator. Any subsequent measurements of N_0 in unknown signals passed through this filter setting are compared to this standard N_0 to determine ΔN_0 , the percentage deviation in N_0 .

MEASURED DATA

We are mainly concerned with a fixed sine wave mixed with random noise. This problem has been solved analytically by Rice.¹ The equation for the number of zero crossings per unit time (N_0) is given in Fig. 4. N_0 is seen to be a function of the sine wave amplitude; Q , the autocorrelation function; R , of the noise for zero time lag; and T , the second derivative of R with respect to T at $T = 0$ and the noise frequency band limits. Even discounting the problem of laboratory filter cutoff characteristics, the solution of such an equation to determine ΔN_0 for typical sine waves is impractical.

Fortunately, with the randomness tester it is not difficult to use electrical analogs of typical sine waves and the random noise to measure ΔN_0 .

This measurement was made for various fixed sine waves added to band limited random noise and a family of curves produced in Fig. 5. Here, ΔN_0 is plotted as a function of sine wave frequency (f) using the S/N ratio (r), the ratio of the respective root-mean-square amplitudes of the sine wave to the noise, as the parameter. Notice that just above the center frequency of the random noise frequency band limits, a frequency (f_0) exists at which no change in N_0 occurs when a sine wave is added. Otherwise, ΔN_0 is directly proportional to the S/N ratio (r) and has negative values for $f < f_0$ and positive values for $f > f_0$.

These data show that large percentage deviations in N_0 are possible when sine waves are added to random noise; however, in our problem at LTV no peaks were noted in the PSD plots. Considering the analyzer filter bandwidth employed, this indicates that any hidden periodicities are of small magnitude, perhaps with S/N ratios of under 0.2 for noise bandwidths convenient to analyze. For this S/N ratio, the maximum ΔN_0 is about 2 or 3 percent. This is a small measurement, but more than one sine wave may be present.

To determine the magnitude of ΔN_0 that can be expected with addition of several sine waves to the noise, the laboratory instrument setup shown in Fig. 6 was used to mix up to five fixed sinusoidal components to random noise. A family of curves for ΔN_0 as a function

$$N_0 = \frac{1}{\pi} \left(\frac{D_0}{R_0} \right)^{\frac{1}{2}} \left\{ e^{-\alpha} I_0(\beta) 2b \int_0^{\pi} \psi(-a \cos \theta) \sin \theta \left[\int_0^b \psi(x) dx \right] d\theta \right\}$$

WHERE: SINE WAVE = $Q \sin(\omega_0 t + \phi)$
RANDOM NOISE = $G(\omega) = \begin{cases} \text{POSITIVE CONSTANT,} & 0 \leq a \omega_0 \leq (\omega) \leq b \omega_0 \\ 0 & \text{OTHERWISE} \end{cases}$

$$a = \left(\frac{Q}{R_0} \right)^{\frac{1}{2}} \quad b = \omega_0 \left(\frac{Q}{D_0} \right)^{\frac{1}{2}}$$

$$R_0 = \text{AUTOCORRELATION FUNCTION FOR ZERO TIME LAG} = \int_0^{\alpha} G(\omega) d\omega$$

$$D_0 = - \left. \frac{d^2 R}{dT^2} \right|_{T=0} = \int_0^{\alpha} \omega^2 G(\omega) d\omega$$

$$I_0(\beta) = 2A e^{\alpha}, \alpha = (a^2 + b^2)/4, \beta = (a^2 - b^2)/4$$

$$2A = \int_0^{\pi} \psi(-a \cos \theta) \psi(b \sin \theta) d\theta, \pi(x) = \frac{1}{2\pi} e^{-x^2/2}$$

Fig. 4 - Number of zero crossings, N_0 , for a fixed sine wave added to band limited random noise (Ref. 1)

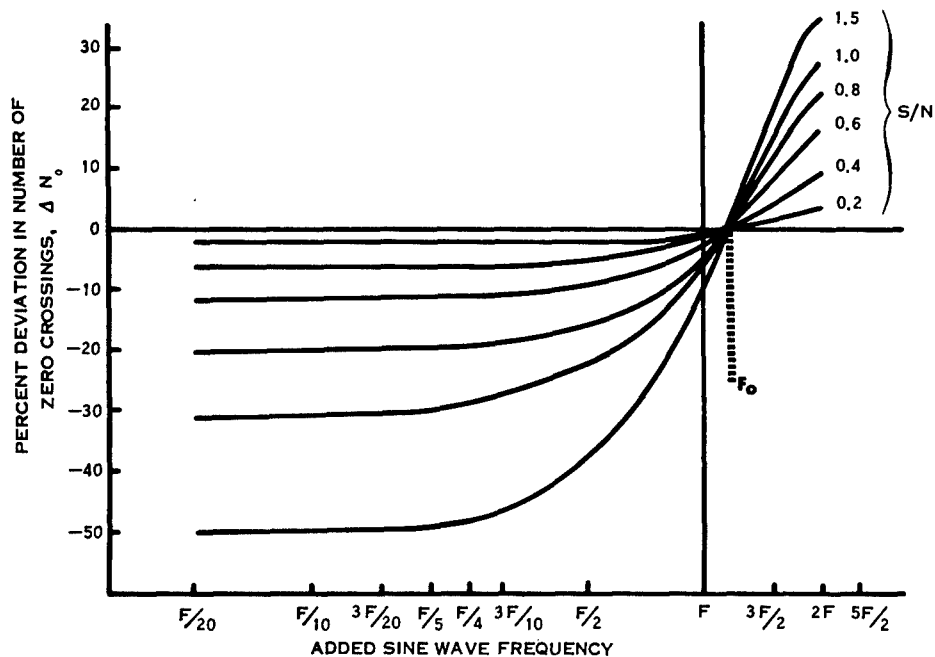


Fig. 5 - Fixed sine wave plus band limited random noise

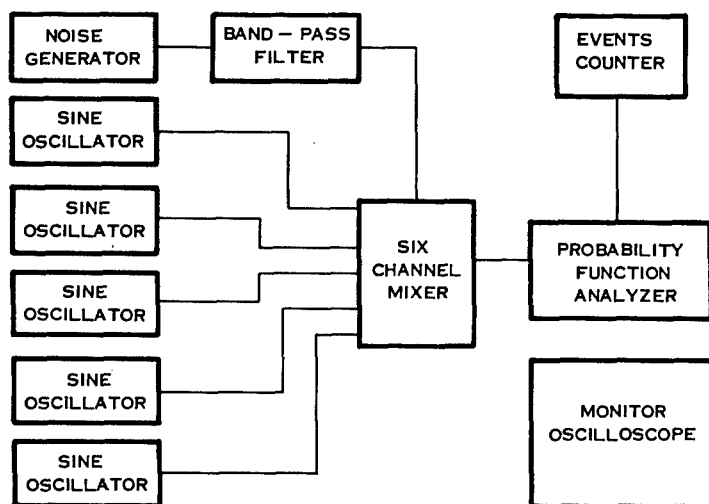


Fig. 6 - Laboratory instrument setup

of S/N ratio (r), using the number of added sine waves in the frequency range from $f_0/10$ to $3f_0/10$, is shown in Fig. 7. For this example, ΔN_0 increased from 2 percent with one sine wave to 6 percent with five sine waves when the S/N ratio was held at 0.2.

RESULTS

Measurements in ΔN_0 were made on selected frequency bandwidths of the unknown acoustic noise signal. Indications of hidden periodicities were obtained for the frequency

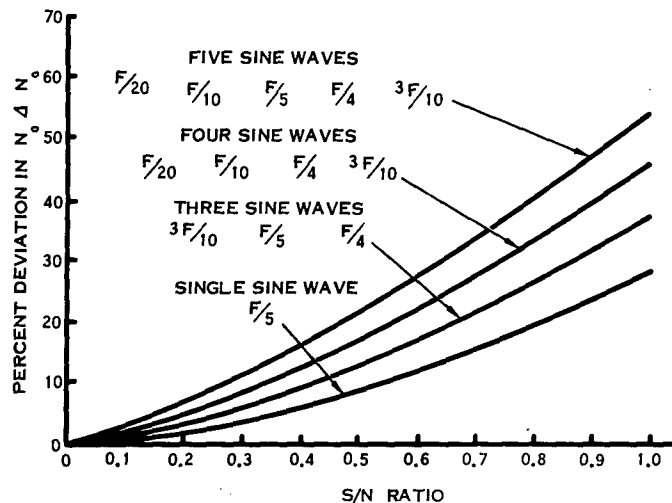


Fig. 7 - Deviation in N_0 with addition of several sine waves

band below the frequency designated F_D^{11} on the PSD curve in Fig. 1. These indications included some ΔN_0 's of up to 15 percent. Measurements on the band above F_D^{11} showed zero or very small ΔN_0 's.

CONCLUSIONS

The acoustic spectrum above F_D^{11} was taken as the random noise energy under investigation while the lower part of the spectrum was discarded as nonrandom background noise. It was assumed that the large ΔN_0 's were caused

by many small amplitude periodicities in this background noise signal.

The presence of these small amplitude periodicities could have been detected just as well by very narrow band spectral analysis; but, at acoustic frequencies, this process would require a very long data analysis period to obtain complete results, while this method using the so called "randomness tester" will detect hidden periodic components in broad selected band limits of random noise in a convenient and minimum time process.

* * *

RESPONSE OF A SINGLE-DEGREE-OF-FREEDOM SYSTEM TO EXPONENTIAL SWEEP RATES*

P. E. Hawkes
Lockheed Missiles and Space Co.
Sunnyvale, California

The peak response and the number of cycles of a single-degree-of-freedom system is plotted for several damping conditions. The results are shown as functions of a dimensionless parameter which can be considered to be a measure of the sweep rate of the system. The results are related to vibration tests.

INTRODUCTION

Many laboratory vibration testing programs specify that components be subjected to sinusoidal sweep tests to qualify either the component itself or the support structure to which the component is mounted. Although this type of test has long been used, little information is available concerning the response of a system subjected to a forcing function characterized by a sinusoidal sweep rate.

Lewis¹ solved the problem of the response of a single-degree-of-freedom system subjected to a linear sweep rate in terms of dimensionless parameters. The linear sweep rate is characterized by a constant rate of change of frequency with respect to time. Most types of sweep tests presently conducted, however, use an exponential-type sweep rate (commonly referred to as octave- or logarithmic-type sweep tests). The mathematics involved in Lewis' solution becomes a formidable obstacle in applying his method of solution to exponential-type sweep rates

This paper will present in terms of dimensionless parameters a method for solving the envelope response of a single-degree-of-freedom system subjected to a harmonic forcing function of variable frequency. Specifically discussed will be the results of solutions of

systems subjected to octave sweep rates. Although only octave sweep rates are discussed in detail, the method presented is general and can be applied to other types of sweep rates.

LIST OF SYMBOLS

- y - instantaneous value of response
- η - damping factor
- ω_n - natural frequency (rad/sec)
- t - time (sec)
- ω - instantaneous value of forcing frequency (rad/sec)
- h - slope of linear sweep frequency-time curve (rad/sec²)
- ω_o - initial octave sweep frequency (rad/sec)
- $1/K$ - time for one octave (sec)
- ω_f - final sweep frequency (rad/sec)

EQUATIONS

Consider the familiar vibration equation,

$$\ddot{y} + 2\eta\omega_n\dot{y} + \omega_n^2 y = F(t), \quad (1)$$

and assume we are interested in a solution of the response "y" extending over a large number of oscillations. In the case of constant

*This paper was not presented at the Symposium.

¹F. M. Lewis, "Vibration During Acceleration Through a Critical Speed," paper presented at the Second National Meeting of the A.S.M.E. Applied Mechanics Division, New Haven, Connecticut, June 23-25, 1932.

coefficients where the right hand side of the equation is equal to zero or $A \sin \omega t$, a closed form solution can be found by the substitution,

$$y = Y(t) e^{i\omega t}. \quad (2)$$

Unfortunately, this simple substitution does not suffice in the case of variable coefficients or where the right hand side of Eq. (1) is a periodic function of varying frequency. For these cases few closed solutions exist, and it often becomes necessary to use a computer solution.

Instead of solving for the instantaneous value of response, it would be helpful to solve the response in terms of an "amplitude" and "frequency" as is done in Eq. (2). This type of solution should reduce the number of integration steps necessary for computer solution and also improve the accuracy. A solution of this type was derived by Harvey² and is discussed in the following sections.

Assume that the response can be represented by a function

$$y(t) = Y(t) e^{if(t)}. \quad (3)$$

The unique characteristic of this function is that $f(t)$ is completely arbitrary and can be used for other than periodic functions. Some of the forms of $f(t)$ are as follows:

$f(t)$	$e^{if(t)}$
constant	constant
ωt	harmonic function of constant frequency
$(h/2)t^2$	harmonic function of linearly varying frequency (linear sweep rate)

$Y(t)$ is arbitrary and represents the amplitude or "envelope" of the response. In most cases, it is the amplitude and phase angle of $Y(t)$ that must be evaluated.

Derivation of Equations

By substitution of Eq. (3) into (1), the equations to be solved on the computer can be obtained. By differentiating Eq. (3) with respect to time to obtain \dot{y} and \ddot{y} ,

$$\dot{y} = \frac{d}{dt} [Y(t) e^{if(t)}] = e^{if(t)} (\dot{Y} + i\dot{f}Y),$$

and

$$\ddot{y} = \frac{d^2}{dt^2} [Y(t) e^{if(t)}] = e^{if(t)} \times [\ddot{Y} + 2i\dot{f}\dot{Y} + Y(i\ddot{f} - \dot{f}^2)]. \quad (4)$$

Substitution of Eq. (4) into (1) yields

$$\ddot{Y} + \dot{Y}(2i\dot{f} + 2\eta\omega_n) + Y(i\ddot{f} - \dot{f}^2 + 2\eta\omega_n i\dot{f} + \omega_n^2) = E, \quad (5)$$

where $E(t)$ is defined as

$$F(t) = E(t) e^{if(t)}.$$

Equation (5) can be nondimensionalized by selecting $\tau = \omega_n t$ such that

$$\dot{Y} = \omega_n Y',$$

$$\ddot{Y} = \omega_n^2 Y'',$$

$$\dot{f} = \omega_n f',$$

and

$$\ddot{f} = \omega_n^2 f'',$$

where the prime denotes differentiation with respect to dimensionless time, $\omega_n t$. Equation (5) then becomes

$$Y'' + Y'(2if' + 2\eta) + Y(if'' + 2i\eta f' + 1 - f'^2) = E/\omega_n^2. \quad (6)$$

For the solution of Eq. (6) for a constant ω_n and η and non-zero right hand side, Y is taken to consist of a real and imaginary part such that

$$Y = u + iv. \quad (7)$$

It is necessary to take a complex Y because the coefficients of Eq. (6) are complex and the right hand side is real.

Differentiating Eq. (7) to obtain Y' and Y'' and substituting into Eq. (6) yields

$$u'' + u'(2\eta) + u(1 - f'^2) - 2v'f' - v(f'' + 2\eta f') = E/\omega_n^2 \quad (8)$$

²T. J. Harvey, "A New Technique for Solution of Transient Dynamic Oscillation Problems," Lockheed Missile and Space Company Report SS-269 (Apr. 17, 1961) (unpublished).

and

$$u'(2f') + u(f'' + 2\eta f') \quad (8)$$

$$+ v'' + v'(2\eta) + v(1 - f'^2) = 0, \quad (\text{Cont.})$$

where the real parts of the left hand side are equated to E/ω_n^2 and the imaginary parts are set equal to zero.

Equations (8) can then be solved for the envelope by specifying f' and f'' in terms of dimensionless time, $\omega_n t$. The additional complexity of Eqs. (8) over Eq. (1) poses no problem for high speed digital computers. Reduction in the number of integration steps and increased accuracy of solution are the primary advantages of this approach. Equations (8) were solved on a computer for the case of a linear sweep rate, and the results were compared to Lewis' solution;¹ agreement was excellent.

Change of Variable

Equations (8) can be used to study response as a function of dimensionless time $\omega_n t$, where $\omega_n t$ is the independent variable. For a forcing function of varying frequency, however, response is actually a function of the instantaneous frequency ratio f' , where $f' = \omega/\omega_n$. It would therefore be advantageous to change the independent variable in Eqs. (8) to f' . This can be accomplished in the following manner:

$$u' = \frac{du}{d(\omega_n t)} = \frac{du(f')}{d\omega_n t} = \frac{du}{df'} \quad (9)$$

$$\times \frac{df'}{d(\omega_n t)} = f'' \times \frac{du}{df'}$$

$$u'' = \frac{d^2 u(f')}{d(\omega_n t)^2} = f''' \times \frac{du}{df'} + (f'')^2 \frac{d^2 u}{df'^2}$$

Letting

$$\frac{du}{df'} = u^I$$

and

$$\frac{d^2 u}{df'^2} = u^{II}$$

yields

$$u' = f'' u^I$$

and

$$u'' = f''' u^I + (f'')^2 u^{II} \quad (10)$$

Substituting Eqs. (10) into (8) yields

$$(f'')^2 u^{II} + (2\eta f'' + f''') u^I$$

$$+ (1 - f'^2) u - 2f' f'' v^I - v(2\eta f' + f'') = E/\omega_n^2 \quad (11)$$

and

$$(2f' f'') u^I + (2\eta f' + f'') u + (f'')^2 v^{II}$$

$$+ (2\eta f'' + f''') v^I + (1 - f'^2) v = 0.$$

The envelope, $Y = u + iv$, can now be obtained for solution of Eqs. (11) by specifying f'' and f''' as functions of the independent variable f' .

Octave Sweep Rate Equations

The frequency equation specified by an octave sweep rate is

$$\omega = \omega_0 2^{Kt} \quad (12)$$

In order to obtain f'' and f''' as functions of f' for an octave sweep, the following operations are performed. Integrating Eq. (12) from time 0 to time t yields the total angular displacement at any time. Performing this integration yields

$$f(t) = \omega_0 \int_0^t 2^{Kt} dt = \frac{\omega_0}{K \ln 2} (2^{Kt} - 1).$$

Converting $f(t)$ to dimensionless time

$$f(\omega_n t) = \frac{\omega_0}{K \ln 2} [2^{(K/\omega_n)(\omega_n t)} - 1].$$

Differentiating with respect to $\omega_n t$

$$f' = \frac{\omega_0}{\omega_n} \times 2^{(K/\omega_n)(\omega_n t)}.$$

Differentiating f' with respect to $\omega_n t$ to obtain f'' and f'''

$$f'' = (K/\omega_n) \times \ln 2 \times \frac{\omega_0}{\omega_n}$$

$$\times 2^{(K/\omega_n)(\omega_n t)} = (K/\omega_n) \times \ln 2 \times f'$$

and

$$f''' = (K/\omega_n \times \ln 2)^2 \times \frac{\omega_0}{\omega_n}$$

$$\times 2^{(K/\omega_n)(\omega_n t)} = (K/\omega_n \times \ln 2)^2 \times f'.$$

The quantities f'' and f''' are now specified as functions of the independent variable f' . Substitution of these quantities into Eqs. (11) will yield the quantities necessary to solve the envelope response for an octave sweep rate. Equations (11) were programmed for solution on a computer using Newmark's Beta method³ as the integration method of solution.

The quantity ω_n/K can be considered as a measure of the sweep rate in the following manner: Let the number of oscillations of the forcing function between any two times be represented by

No. of cycles = N

$$= \int_{t_1}^{t_2} [\text{sweep frequency } (t)] dt.$$

In the case of an octave sweep

$$N = \frac{1}{2\pi} \int_{t_1}^{t_2} \omega_o \times 2^{Kt} dt$$

$$= \frac{\omega_o}{2\pi K \ln 2} (2^{Kt_2} - 2^{Kt_1}). \quad (13)$$

Nondimensionalizing Eq. (13) in the manner

$$N = \frac{\omega_o}{2\pi K \ln 2} \left[2^{(K/\omega_n)(\omega_n t_2)} - 2^{(K/\omega_n)(\omega_n t_1)} \right],$$

and substitution of the relationship

$$2^{(K/\omega_n)(\omega_n t)} = (\omega_n/\omega_o) f'$$

into Eq. (13) yields

$$N = (\omega_n/K) \times \frac{1}{2\pi \ln 2} (f'_2 - f'_1). \quad (14)$$

Equation (14) states that the number of oscillations which the system makes between any two frequency ratios is proportional to the value of ω_n/K . As the value of ω_n/K is increased, the response can also be expected to increase reaching a limiting value of the steady-state response. For a value of ω_n/K equal to ∞ , the classical steady-state response

curves would be obtained since this would mean that the sweep frequency is changing at an infinitely slow rate. The above equations indicate that octave sweep rates can be characterized by a single nondimensional parameter, ω_n/K . In a similar manner, other types of sweep rates can also be solved and characterized by a single nondimensional parameter.

DISCUSSION

Computer solution results of Eqs. (11) for an octave sweep rate will be discussed in this section.

As previously mentioned, the octave sweep rates can be characterized by a single nondimensional parameter ω_n/K . This is in contrast to Lewis' solution where the characteristic nondimensional parameter " q " is equal to the number of free undamped oscillations the system would make from time zero to resonance.

Requirements for laboratory sweep testing are commonly specified in terms of test time per octave or total test time for a specific range of frequencies. As an aid in obtaining values of the parameter K for these laboratory sweep rates, Fig. 1 is included. This figure gives K values as a function of the ratio of the final to initial sweep frequency versus sweep time. For example, an octave sweep rate of 5 to 3000 cps in 15 minutes would have a K value of 0.103×10^{-1} . For a constant final to initial sweep frequency ratio, an increase in sweep time corresponds to a decrease in the value of K .

Some typical plots of the resonance envelopes obtained from computer solutions are shown in Figs. 2 and 3. The plots shown for 5- and 1-percent damped systems bear a close resemblance to the classical steady-state curves. The pulsations seen in Fig. 3 are typical of lightly damped systems before the response has attained amplitudes near the steady-state values. As the value of ω_n/K increases with a corresponding increase in response, these pulsations disappear and the resonance envelope begins to resemble the steady-state curves.

The frequency ratio at which the peak steady-state amplitude occurs is equal to $\sqrt{1 - 2\eta^2}$. For the octave sweep rate, the peak amplitude occurs after the steady-state value and approaches the steady-state value from the right as ω_n/K increases.

Plots of the percentage of the maximum steady-state response versus ω_n/K for various

³N. M. Newmark, "Computation of Dynamic Structural Response in the Range Approaching Failure," paper published in Proceedings of the Symposium of Earthquake and Blast Effects on Structures, University of California, Los Angeles, California, June, 1952.

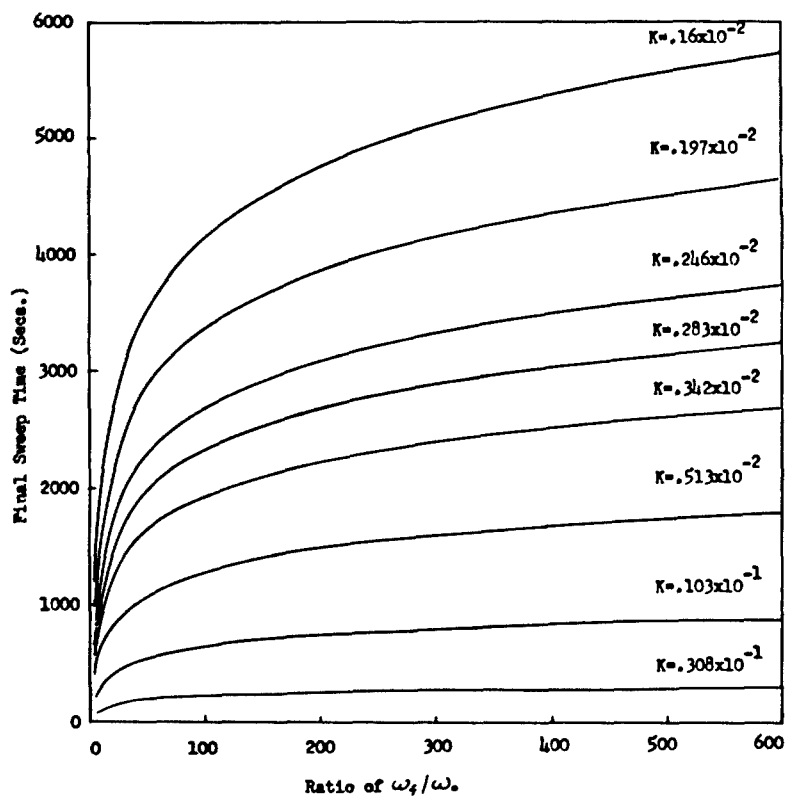


Fig. 1 - K values for various sweep times and ratios of final-initial sweep frequencies

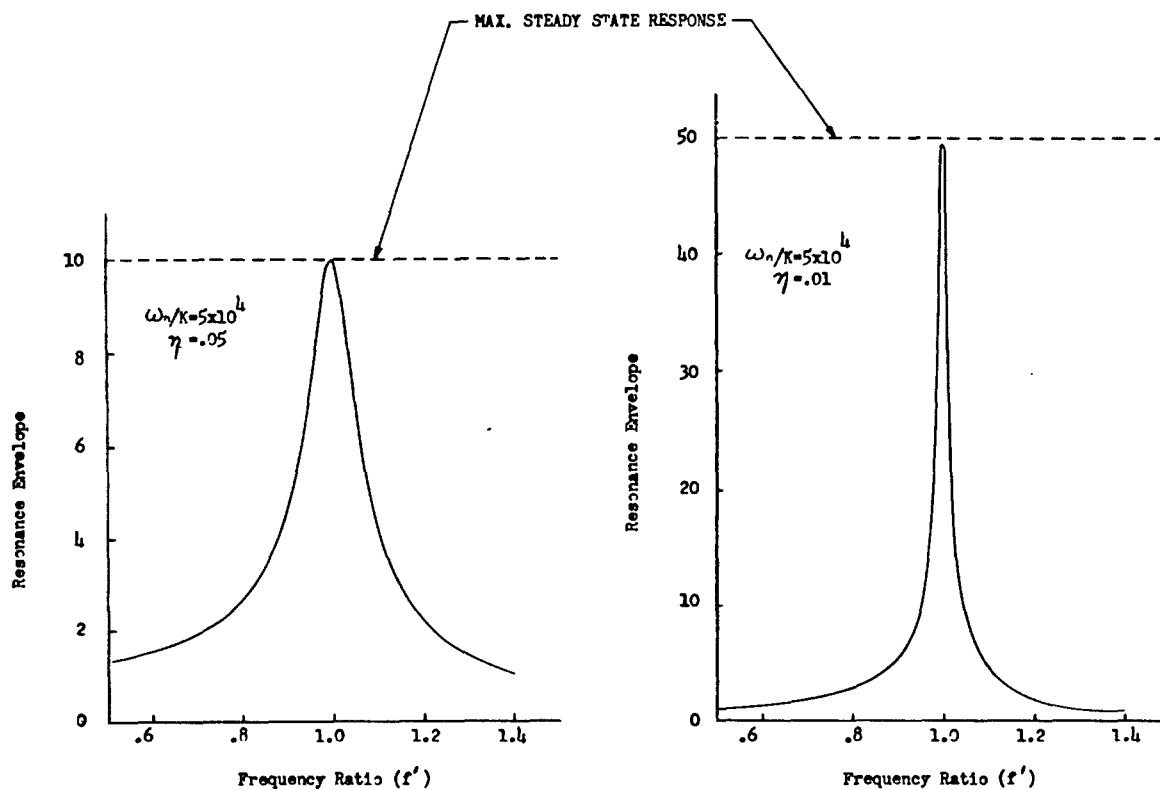


Fig. 2 - Typical resonance envelopes for 5- and 1-percent damped systems

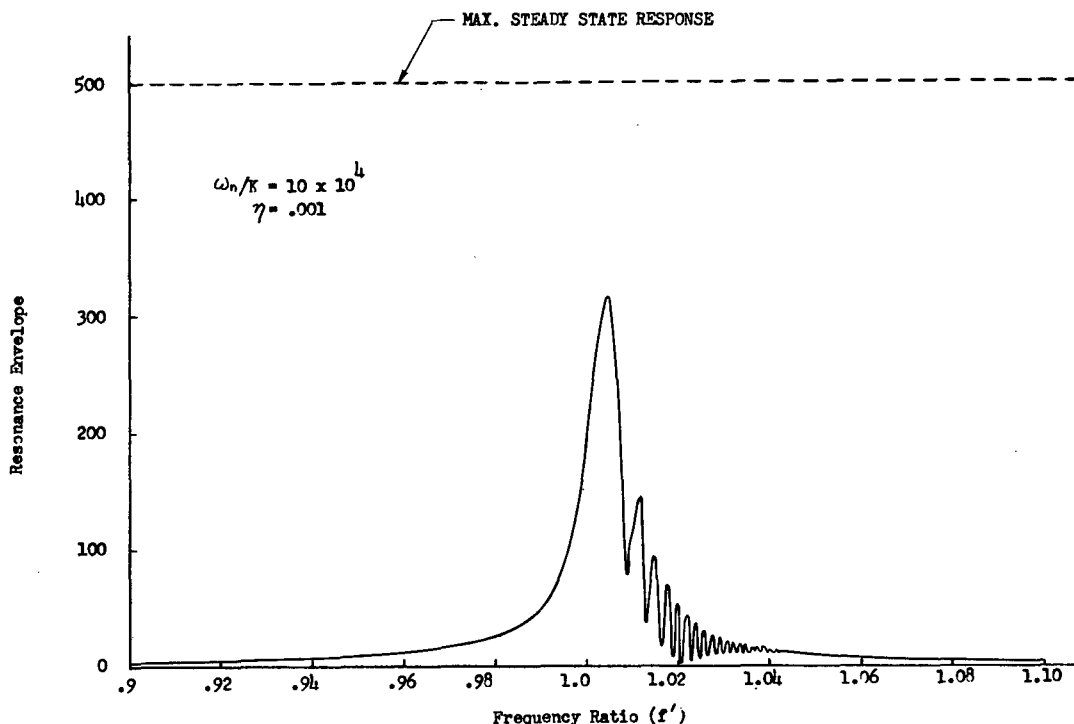


Fig. 3 - A response envelope for a 0.1-percent damped system

damped systems are shown in Figs. 4 and 5. These curves indicate that as damping of the system is decreased, the value of ω_n/K must be increased in order to maintain the same percentage of peak steady-state response. This is to be expected. Under steady-state conditions as the damping is decreased, the number of cycles necessary to obtain the steady-state amplitude increases. For the systems studied with damping factors greater than 1 percent, the response is practically the same as the steady-state response.

As some idea of the number of high amplitude cycles that occur during a sweep test, Fig. 6 is included. This figure is a plot of the number of cycles lying between the half-power points versus ω_n/K for the various damping factors studied. An inconsistency may seem to exist for this plot in that a linear relationship seems to exist for all the damping factors except the 0.1-percent damped system. An explanation for this is as follows:

"From Eq. (14), the number of cycles within the bandwidth is proportional to $(\omega_n/K)\Delta f'$ where $\Delta f'$ is the bandwidth. When the system response builds up to values approximately 90 percent of or greater than the maximum steady-state value, $\Delta f'$ approaches a constant. The number of cycles then becomes directly proportional to

the value of ω_n/K . For all the damped systems except the 0.1-percent system, the response is greater than 90 percent of the steady-state value, and a linear relationship exists between the value of ω_n/K and the number of cycles. Higher values of ω_n/K would have to be used for the 0.1-percent damped system before linearity is established.

"The number of cycles within the half-power points versus frequency for a 2.5-percent damped system subjected to a commonly used laboratory sweep test rate are shown in Fig. 7. This figure indicates that the number of cycles is proportional to frequency for K equal to a constant. In a similar manner, if the system frequency and ratio of the final to initial sweep frequency were constants, the number of high amplitude cycles would be proportional to sweep time."

SUMMARY

One should be careful in applying the results obtained to actual tests where an idealized single-degree-of-freedom system does not exist. However, the following conclusions can be made. The response is dependent on the sweep rate, package frequency and damping. If the system damping is decreased, then either the

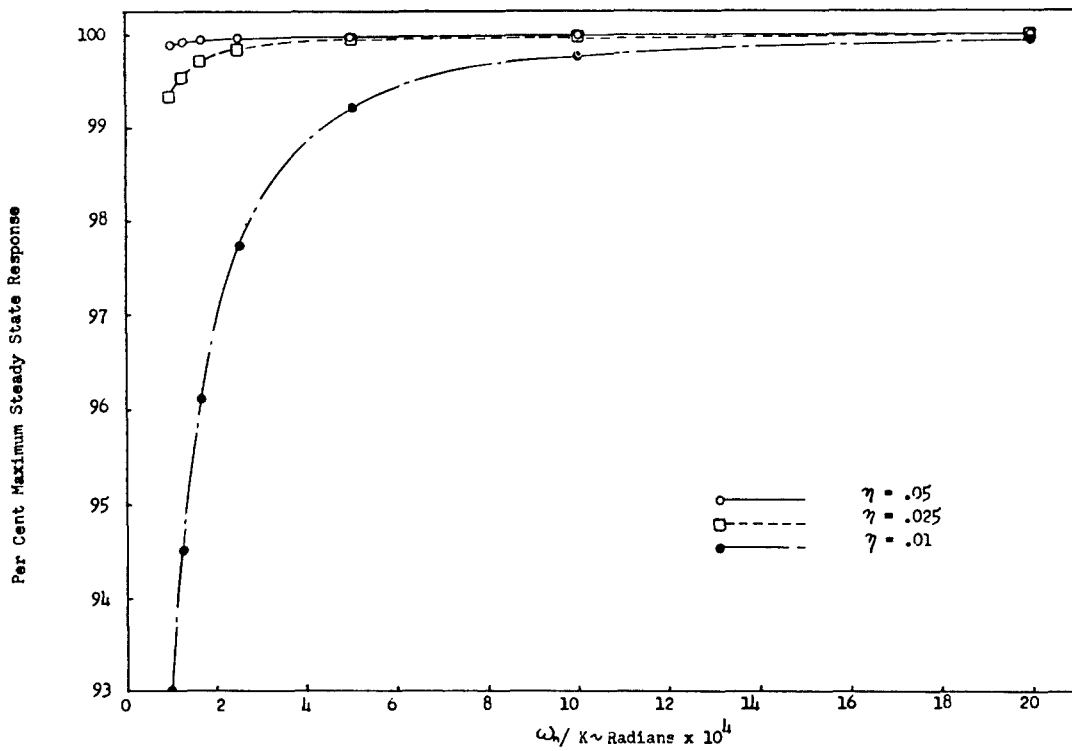


Fig. 4 - Maximum response to applied sweep rate, $\eta = 0.5, 0.025$, and 0.01

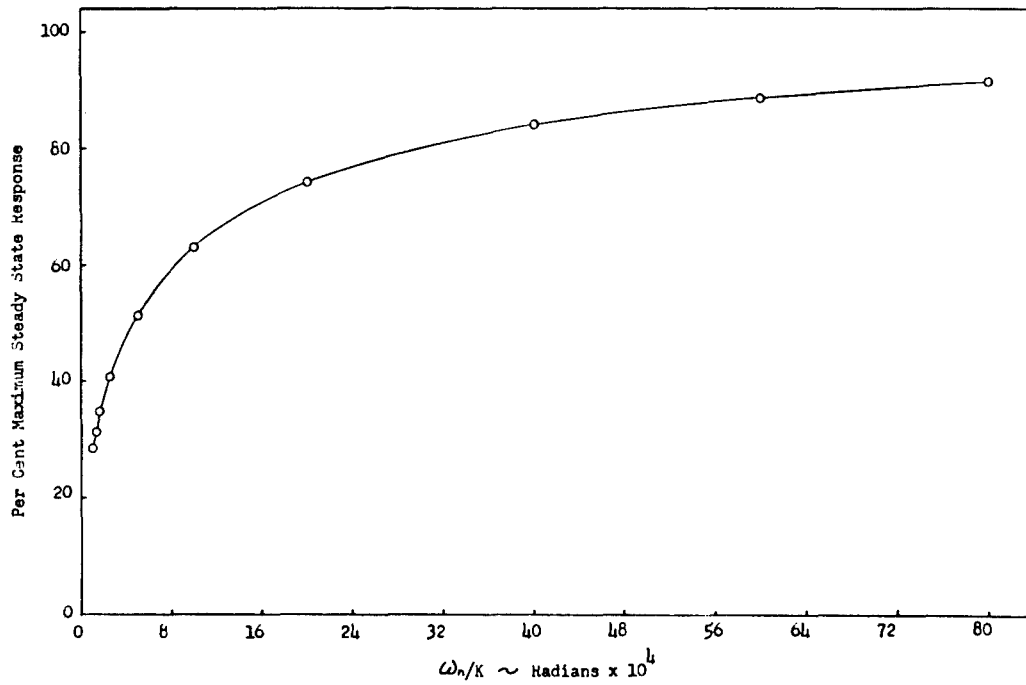


Fig. 5 - Maximum response to applied sweep rate, $\eta = 0.001$

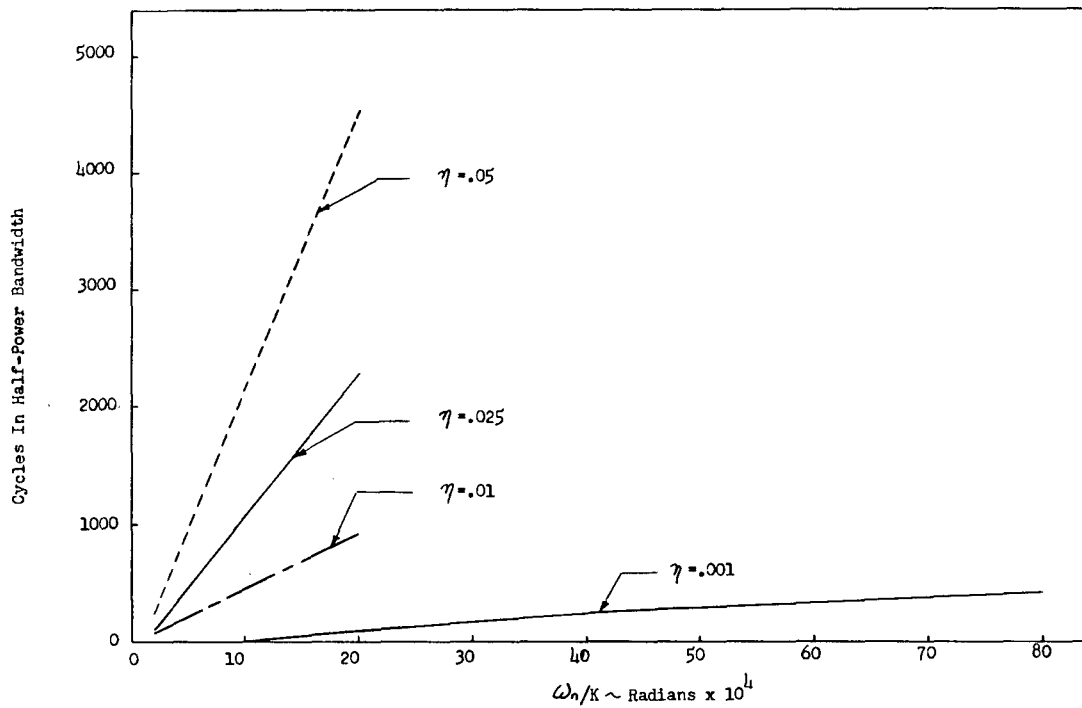


Fig. 6 - Number of cycles for applied sweep rates

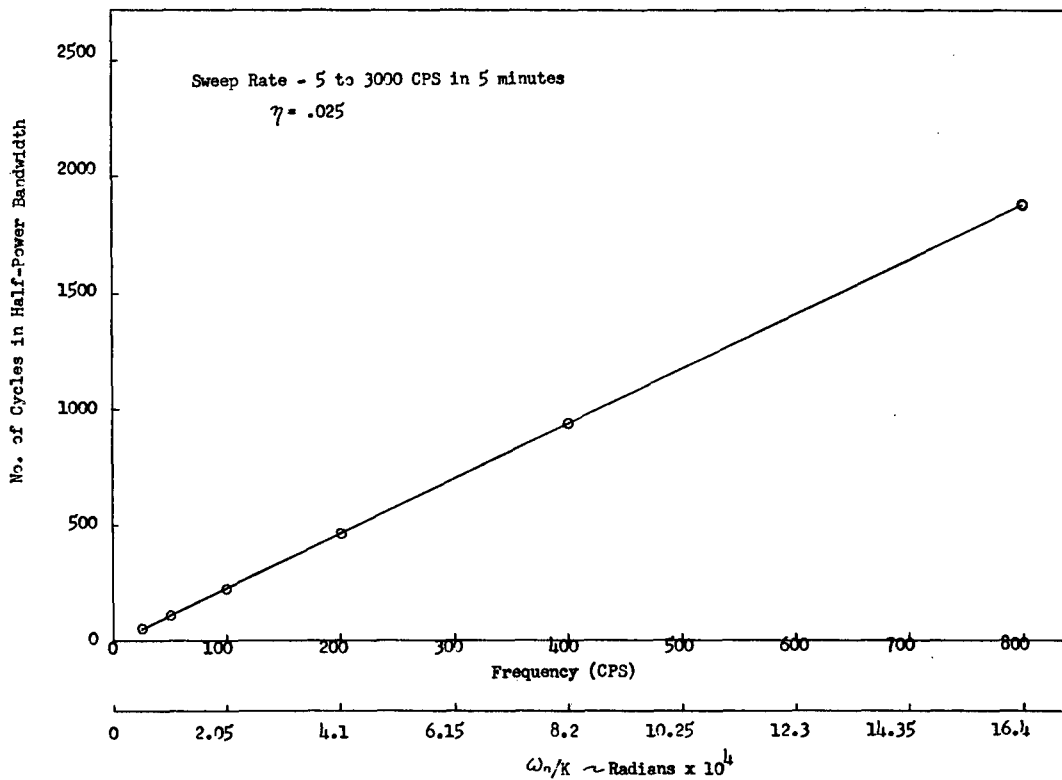


Fig. 7 - Cycles vs frequency for a specified sweep rate

package frequency or duration of sweep time must be increased to maintain the same percentage of peak steady-state response.

For normal package frequencies of 25 cps and above and damping factors approximately equal to or greater than 1 percent, commonly specified laboratory sweep rates of 5-minutes duration and longer should for all practical purposes give the steady-state response. Very low frequency packages or very lightly damped systems (less than 1 percent) may require a

slower sweep rate to obtain values near the steady-state response.

Solution of the equations shown can be used to study other forms of sweep rates besides the exponential type. One may possibly obtain a sweep rate in which the response and number of high amplitude cycles are independent of frequency. Whether the fact that the response and number of high amplitude cycles are frequency dependent is a deterrent or advantage to the use of exponential type sweep rates depends on the specific test purpose.

* * *

THE INTEGRATED CORRELATION SYSTEM

B. K. Leven
Trials and Analysis Branch
U. S. Navy Marine Engineering Laboratory

An integrated correlation system is described which is designed to provide the data necessary to discern and identify noise propagation paths in mechanical structures. The requirement, development, and present capabilities of the system are described.

The integrated correlation system consists of electronics designed to perform spectral analyses and to determine the correlation between two noise processes. It is the purpose of this paper to describe the correlation system developed at the U. S. Navy Marine Engineering Laboratory and to show that such a system provides data applicable to the solution of problems involving airborne, waterborne, and structural noise propagation.

In past years, the emphasis in the noise reduction field has been on spectral analysis techniques. This approach has utilized Fourier analysis techniques and mechanical or electronic filtering to describe the "character" or "shape" of a noise process. It is important to note that these methods provide neither the means for detecting discrete frequency components buried below the ambient noise level nor the ability to compare, other than visually, the character of noise processes detected at physically separated points. The necessity for defining the noise propagation paths between discrete points in mechanical systems (submarines and destroyers, for example) led to the development of the integrated correlation system.

The theoretical basis for the applicability of the correlation function to the aforementioned type of problems is well documented.^{1,2} It will be instructive, however, to list briefly some of the more significant properties of the

function. The correlation function is defined mathematically as

$$R_{xy}(\tau) = \lim_{T \rightarrow \infty} \frac{1}{T} \int_0^T x(t) y(t - \tau) dt,$$

where

τ = time delay, and

T = integration time.

When $x(t)$ and $y(t)$ are identical processes, the function is known as the autocorrelation function (R_{xx}). This function possesses several important properties:

1. The function, $R_{xx}(\tau)$, is even with a maximum at $\tau = 0$;
2. The function, $R_{xx}(\tau)$, contains all the past periodicities in $x(t)$; and
3. The function, $R_{xx}(\tau)$, for $x(t)$ some bandwidth limited random function takes the form

$$R_{xx}(\tau) = R_{xx}(0) e^{-\pi B |\tau|} \cos \omega_0 \tau;$$

where

B = Bandwidth, and

ω_0 = center frequency of band,

and therefore decays to some negligible value for $\tau > 1/B$ (see Fig. 1).

The last two properties admit the possibility of detecting discrete buried signals (see Fig. 2).

¹A. G. Ratz, "Use of a Time Delay Correlator in Solving an Acoustic Multipath Problem," Proc. Inst. Radio Engrs. (Jan. 1963), p. 239.

²J. S. Bendat, Principles and Applications of Random Noise Theory (John Wiley and Sons, Inc., New York, 1958), Chapter 2.

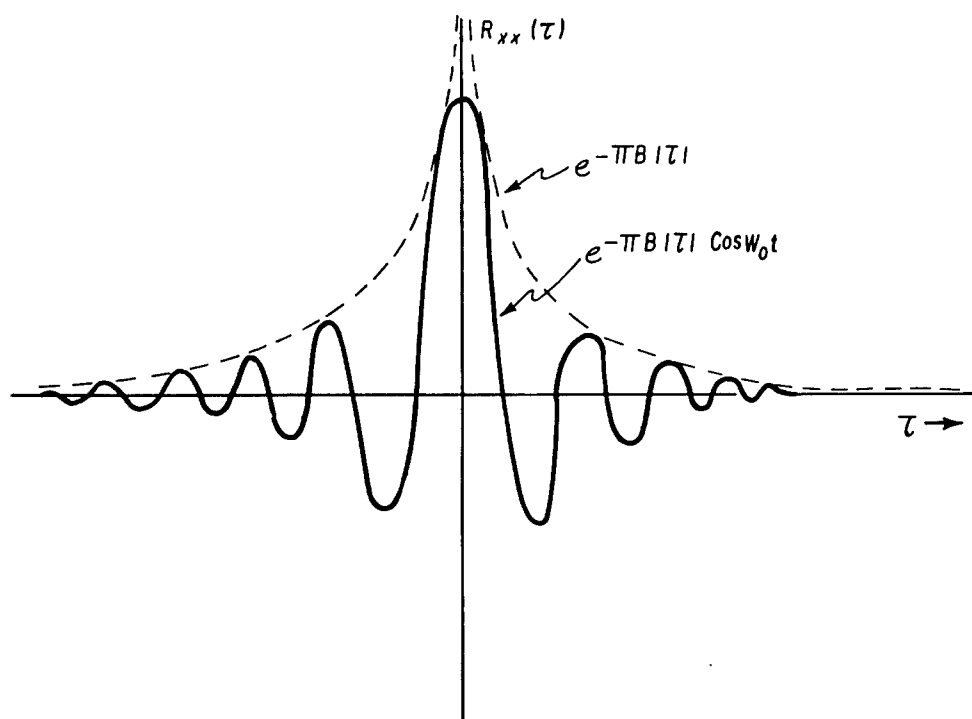


Fig. 1 - Autocorrelation function for random noise of bandwidth B and center frequency W_0 .

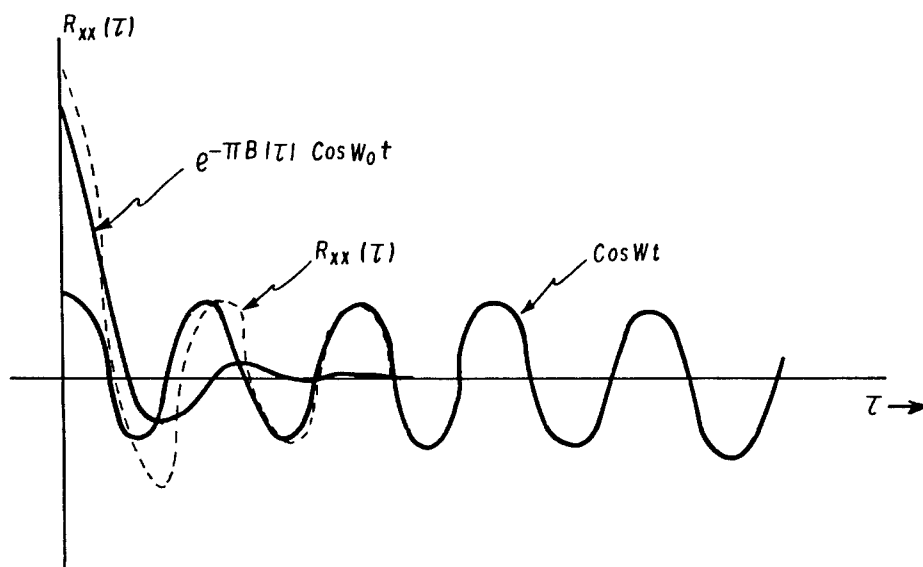


Fig. 2 - Autocorrelation function for discrete signal of frequency W buried in bandwidth limited random noise

When $x(t)$ and $y(t)$ are dissimilar signals, the function is known as the cross correlation function. Application of the cross correlation function to noise processes can determine the interrelationship between the two processes as a function of the time delay (τ) introduced between them. Thus, the correlation function can provide the data necessary to ascertain transmission times between two points in a mechanical system.

Correlators are not new; they were built as early as 1949.³ The integrated correlation system developed at the Marine Engineering Laboratory is an analog system which is composed of state-of-the-art components and capabilities; and is, therefore, able to provide high accuracy, flexibility, and applicability.

Mechanizing the correlation function presents few difficulties. One must only implement a time delay, a multiplication, and an integration (see Fig. 3). The following is a description of the components designed to produce these effects.

The time delay unit consists of a 3-inch magnetic drum and associated modulation and servo control circuitry. The system utilizes fixed read- and write-heads and obtains a time delay by varying the speed of rotation of the drum. The rotational speed is closely controlled by a servo system. The speed of rotation is varied by switching two of the three phases of the 400-cycle power supply which drives the drum. Reversing the two phases tends to reverse the direction of drum rotation.

³K. W. Goff, J. Acoust. Soc. Am., Vol. 22 (1955), pp. 223-236.

In the interest of smooth control, the switching occurs at a 60-cycle rate over a variable duty cycle. This method of operation allows continuously variable time delays over a reasonably wide range with high delay stability. For example, with associated ramp generating circuitry, the true closed loop servo system provides delays from 0 to 60 milliseconds with ± 10 -microsecond accuracy. The time delays may be controlled manually or swept automatically at 0.1, 0.25, 0.5, 1, 2.5, 5, and 10 milliseconds per minute. This circuitry, in conjunction with a fixed delay line (10 ms) in one of the data channels, provides relative delay between channels from -10 to +50 milliseconds. Time delays of this magnitude are sufficient for studies of acoustic energy propagation in water for paths as long as 250 feet and in steel for paths as long as 750 feet (longitudinal).

The time delayed signal and undelayed signal are multiplied together as the next step in the operation. The multiplier uses a modulation technique (not the quarter-squares approximation) to produce highly accurate results. For example, the multiplier provides accuracy within ± 1 percent of full scale for any combination of input signals up to full scale values and drift less than ± 1 percent of full scale per day. The magnitude of multiplier error is an important consideration since it is multiplier error which limits total system accuracy and repeatability.

The final step in the realization of the correlation function is the integration of the delayed signal-undelayed signal product. The integrated correlation system has provision for both long- and short-term integration. The short-term integration mode uses RC networks

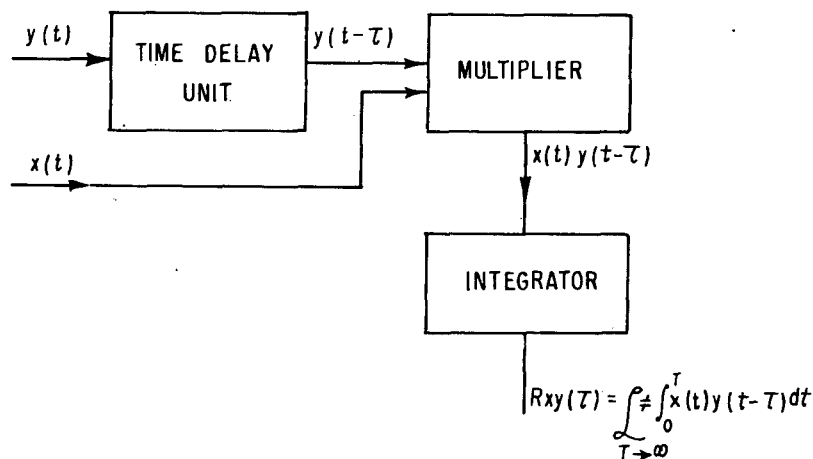


Fig. 3 - Correlator system, block diagram

to provide averaging over 0.3, 1, 3, 10, 30, and 100 seconds. The long-term integration mode is implemented by a cycling operational amplifier circuit. The cycle is triggered by the splice on a circulating data tape loop. Thus, long-term integration is carried out stepwise over the entire delay range. The output of the integrator is applied to the y-axis of an xy recorder for display.

The system also includes a two-channel synchronous spectrum analyzer. This heterodyne-type analyzer operates over a range of 3 to 30,000 cps with filter bandwidths of 1, 5, 50, and 200 cps. The heterodyne modulator oscillator is voltage controlled and can be operated either manually or swept automatically over the analysis range. In all, 10 sweep times, ranging from 10 to 3000 seconds, are provided.

The correlator and spectrum analyzer may be used independently or the spectrum analyzer may be used to supplement the operation of the correlator. Experience has shown that it is often opportune to utilize the spectrum analyzer as a filter to select specific portions of the data sample for correlation analysis. This technique assumes particular importance when common periodicities to cross correlated data samples mask significant correlations due to actual transmission. Moreover, some additions to the present

system will make possible the presentation of cross power spectra and transfer functions.

To date, the correlator has been used to institute preliminary investigations into such topics as the determination of sound velocities in compliant piping systems (to verify predicted values from a modified form of Van Der Weg's equation) and detection of vane frequencies for a sea water pump which were undiscernible using normal analysis techniques. At the present time, the correlator is being used to study the propagation paths on the guided missile destroyer, HARRY E. YARNELL, in an attempt to find the major paths for self noise to the sonar dome (see Fig. 4). Cross correlation techniques should make it possible to determine transmission times between the vibration transducers strung out along the ship's hull. In the interest of this experiment, data will be recorded with only single machinery items operating so that noise contributions can be pinpointed.

One can see that the application of correlation techniques to the investigation of acoustic energy transmission in complex mechanical structures can make possible the gathering of information which cannot, due to the complexity of the physical situation, be collected in any other way.

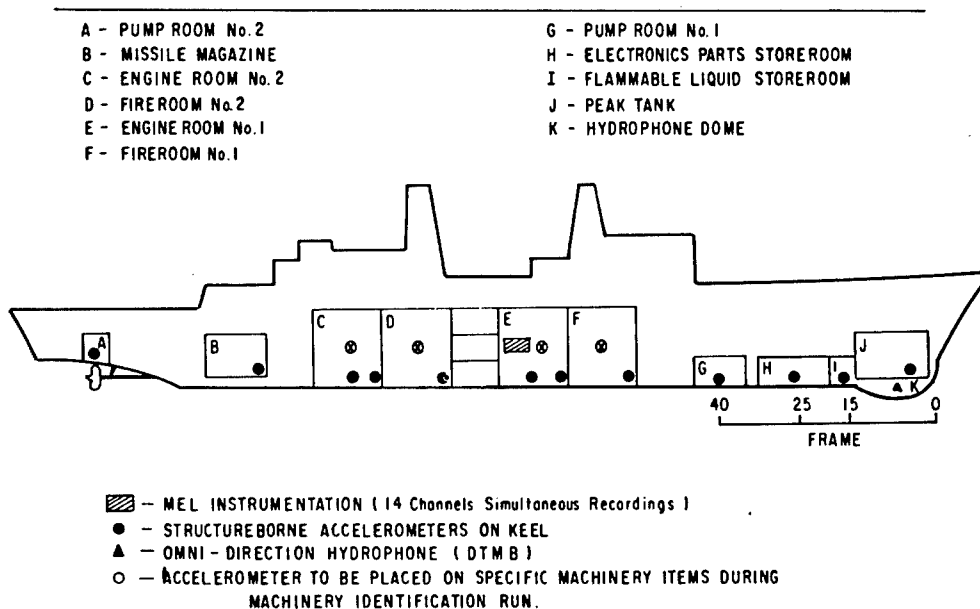


Fig. 4 - USS YARNELL (DLG-7); US Navy Marine Engineering Laboratory pickup location for special correlation study

BIBLIOGRAPHY

Blackman, R. B. and Tukey, J. W., The Measurement of Power Spectra (Dover Press, New York, 1958).

Wainstien, L. A. and Zubakov, V. D., Extraction of Signals from Noise (Prentice-Hall, New York, 1962).

Harris, C. M. and Crede, C. E., Shock and Vibration Handbook, Vol. II (McGraw-Hill Book Co., Inc., New York, 1961).

* * *